PIERS 2010 Xi'an

Progress In Electromagnetics Research Symposium

Abstracts

March 22–26, 2010
Xi'an, CHINA

www.emacademy.org
www.piers.org

PIERS 2010 Xi'an Abstracts

Published by

The Electromagnetics Academy
777 Concord Avenue, Suite 207
Cambridge, MA 02138

www.emacademy.org
www.piers.org

ISSN: 1559-9450
ISBN: 978-1-934142-11-0

Progress in Electromagnetics Research Symposium

March 22–26, 2010

Xi'an, CHINA

PIERS 2010 XI'AN ORGANIZATION

PIERS Founding Chair

J. A. Kong, MIT, USA

PIERS Chair

L. Tsang, University of Washington, USA

PIERS 2010 Xi'an General Chair

C. Jiang, Northwestern Polytechnical University, CHINA

PIERS 2010 Xi'an Organizing Committee Chair

J. Xu, Northwestern Polytechnical University, CHINA

PIERS 2010 Xi'an International Advisory Committee

S. Barmada
L. C. Botten
C.-H. Chan
W.-C. Chew
C-K. Chou
H.-T. Chuah
S.-T. Chun
N. Engheta
A. K. Fung
Z.-H. Gu
L. Gurel
T. M. Habashy
M. Hallikainen
Y. Hara
H.-C. Huang
A. Ishimaru
E. Jakeman
K. Kobayashi
L.-W. Li
I. V. Lindell
S.-G. Liu
K.-M. Luk
S. Mano
G. D. McNeal
K. K. Mei
Y. Miyazaki
P. Pampaloni
A. Priou
K. Senne
R. Shin
M. Tateiba
K. Yasumoto
W.-X. Zhang

PIERS 2010 Xi'an Technical Program Committee

S. J. Anderson
A. Baghai-Wadji
G. Berginc
W. M. Boerner
H. Braunisch
C.-T. Chan
H. W. Chang
H.-S. Chen
K.-S. Chen
T.-J. Cui
Y. Du
A. Elsherbeni
H. T. Ewe
H. C. Fernandes
S. He
W. Hong
Y.-Q. Jin
Q.-H. Liu
S. Lucyszyn
J. T. Lue
A. Massa
M. Moghaddam
Z.-P. Nie
Y. Okuno
M. Oristaglio
J. Pribetich
R. Ramer
L.-X. Ran
C. M. Rappaport
A. K. Sarychev
C. Seo
X.-Q. Sheng
Y. V. Shestopalov
J.-C. Shi
A. Sihvola
M.-S. Tong
S. Tjuatja
D. P. Tsai
J. Vrba
M. Y. Xia
G. Xie
T. S. Yeo
B.-I. Wu
C. J. Wu
X.-M. Zhang
J. Zhou

PIERS 2010 Xi'an Organizing Committee

G. Chen
H.-S. Chen
X. Gao
S. Gong
J. T. Huangfu
Q. Jiang
S. Lee
B. Li
P. Li
Y. Li
Z.-Y. Li
G. Wei
B. I. Wu
P.-L. Xie
S. Xie
L. Ye
X. M. Zhang
K. Zheng

PIERS 2010 XI'AN SESSION ORGANIZERS

D.-C. Chang
C-K. Chou
H. T. Ewe
S. A. Gredeskul
R.-B. Hwang
J.-H. Jou
R. Kubacki
C.-F. Li
Y. Lu
M. Oristaglio
I. M. Pinto
S. Tjuatja
S. D. Wall
Z.-S. Wu
Y. Yu
H. Zhang
H.-W. Chang
X.-L. Ding
D. Felbacq
B. Guizal
K. Iwatsuki
Y. S. Kivshar
Y.-C. Lan
J. Li
J. T. Lue
P. Osmokrović
C.-W. Qiu
M. S. Tong
G. Wang
G. Xie
P. P. Yupapin
X. Zhang
K.-S. Chen
Y. Du
G. Franceschetti
M. Han
G. V. Jandieri
K. Kobayashi
J. F. László
Z. Li
A. Michette
K. Ouchi
Y. V. Shestopalov
D. P. Tsai
H. Wang
T.-J. Yang
Q. Zeng
X. Zheng
W. C. Chew
B. Elouadi
E. Gescheidtová
G. Hu
L. K. Jian
C. Kostov
J.-F. Lee
P. Liu
H. O. Moser
Z. Peng
J. Shi
J. Vrba
C.-J. Wu
W.-Y. Yin
Z. Zeng

PIERS 2010 XI'AN EXHIBITOR

- ATK National Capital Region (www.magictoolsuite.com, www.lspsuite.com)
- Wavenology EM (www.waveadvance.com.cn)

PIERS 2010 XI'AN SPONSORS

- Northwestern Polytechnical University
- National Key Laboratory of Space Microwave Technology
- Zhejiang University
- The Electromagnetics Academy at Zhejiang University
- MIT Center for Electromagnetic Theory and Applications/Research Laboratory of Electronics
- The Electromagnetics Academy

PIERS 2010 SESSIONS

Session 1A1
Advanced Interferometric SAR Techniques and Their Engineering and Geophysical Applications

Subsidence Detection by PSInSAR Based on High Resolution TerraSAR-X Images

Guoxiang Liu, **Hongguo Jia**, **Rui Zhang**, **Minyi Cen**, **and Tonggang Zhang**
Department of Surveying Engineering, Southwest Jiaotong University
Chengdu 610031, China

Abstract— Land subsidence is a major concern for land use planning and geological risk assessment. Here we describe a persistent scatterer interferometric synthetic aperture radar (PSInSAR) method for subsidence detection. The Jinghai County in Tianjin (China) is selected as the study area, which has been sinking due to the overuse of groundwater. The time series of high resolution SAR images collected by the X-band radar sensor onboard the satellite TerraSAR-X (TX) are utilized for the PS detection, PS networking and subsidence estimation. The test results show that the high resolution of TX SAR images can dramatically increase the PS density, especially in the built-up areas. Subsidence information can be extracted on the individual objects like buildings, street lamps and manhole covers, and on the linear engineering structures like the Jinghu high speed railway. The TX PSInSAR with short radar wavelength (3.1 cm) is quite sensitive to vertical motion, and the derived subsidence measurements are in good agreement with the *in situ* data taken by optical leveling.

Deformation Rate Estimation with Small SAR Data Sets: Case Study for Shanghai Region

Lei Zhang[1], **Xiaoli Ding**[1], **and Zhong Lu**[2]

[1]Department of Land Surveying and Geo-Informatics, The Hong Kong Polytechnic University
Hung Hom, KLN, Hong Kong, China
[2]U. S. Geological Survey, Vancouver, Washington, USA

Abstract— We present a new InSAR method for estimating deformation rate based on a small number of SAR images and results from a case study for the Shanghai region. Our method for identifying temporarily coherent points (TCP) which does not need to appear in the whole time span is based primarily on the spatial characteristics of offset consistency in both the range and azimuth directions. The method involves connecting the identified TCP using local Delaunay triangulation that ensures the distance between connected points under the required length, then solving the parameters by a least squares estimator from wrapped double-difference phases in interferograms with short baselines. The method focuses only on using arcs without phase ambiguities so that the need of phase unwrapping can be eliminated. A technique based on the theory of outlier detections is used to detect the small number of arcs that happen do have phase ambiguities. Results shown in terms of comparison with GPS data in Shanghai region indicate that the proposed method is particularly well suited for areas with moderate ground deformation rates and reasonable point density.

Datong Land Subsidence Monitoring with Short Baseline Subsets (SBAS) InSAR Techniques and MODIS Data

Chaoying Zhao[1, 2], **Qin Zhang**[1, 2], **Chengsheng Yang**[1], **and Jing Zhang**[1]

[1]College of Geology Engineering and Geomatics, Chang'an University
126 Yanta Road, Xi'an 710054, China
[2]Key Laboratory of Western China's Mineral Resources and Geological Engineering
Ministry of Education, 126 Yanta Road, Xi'an 710054, China

Abstract— Datong is a city in the northern Shanxi Province in China, and is located a few hundred kilometers west by rail from Beijing with an elevation of 1090 meters. Datong is an old fashioned coal mining city in China, and still sits on significant reserves of this commodity. On the other hand, Datong city has been suffering serious land subsidence, ground fissures, mine collapse and earthquake hazards, which give rise to serious damages to building, roads, and large economic losses.

In order to monitor and mitigate and predict these natural hazards, ten Envisat ASAR data are collected and Short Baseline Subsets (SBAS) InSAR technique is applied to achieve the surface deformation covering thousands of square kilometers areas. Meanwhile, several MODIS data are introduced and paired to check the atmospheric effects for the InSAR interferograms. Finally, nine stages of the nonlinear land subsidence time series results during Sep. 2004 to Feb. 2008 are obtained.

From these series deformation maps, we can clearly detect several kinds of land subsidence including the deformation from mine collapse, ground water withdrawal, new economical zones construction, and the annual mean subsidence velocity amounts to 1 to 2 cm. As investigated, the designed express way with 350 km/h velocity will get through 2 land subsidence regions, so special measures should be taken for the long safe run of this express way. Secondly, the mine collapses and landslips are well monitored, and reasonable inversion should be followed. Lastly, as for the relations among the ground fissures, land subsidence and earthquake duration need to be researched in details.

D-InSAR and PS Technology Monitoring Tianjin Urban Subsidence

Tao Li[1], **Tingchen Jiang**[1], **Sichun Long**[1],
Jingnan Liu[1], **and Ye Xia**[2]

[1]GNSS Research Center of Wuhan University, 129 Luoyu Road, Wuhan 430079, China
[2]GeoForschungsZentrum Potsdam, Germany

Abstract— Due to the fast economy developing, urban subsidence turned to be one serious environmental hazard in many China cities. Tianjin city has been suffered form significant subsidence caused by huge quantities of underground water extraction for many years. The leveling history data showed that the largest subsidence had accumulated to over 1 m since 1985. D-InSAR technique was able to monitoring urban subsidence within 1 mm in vertical and 20 m horizontal resolution. Time and baseline decorrelation are main reasons affected InSAR results, which caused misunderstanding and wrong information. This paper use stacking method to decrease time decorrelation and atmosphere effect in interferograms. The temporal filtering and the spatial filtering by various stacking interferograms eliminated most of the noise and kept the correlated phase signal. More than 40 SAR images have been used to make the stacking pairs. Leveling data were introduced into the final results as a check. The D-InSAR results showed that a continuous subsidence cone lies in YI XINGBU town from 2003 to 2009. D-InSAR results showed highly consistent with leveling surveys in this region. The comparing between D-InSAR results and leveling points showed that only this method could find out the real subsidence cone center. The stacking method derived InSAR results showed that interferogram became more reasonable and reliable. It also showed that only in urban area with many buildings could we get the continuous fringes. Therefore, subsidence in these areas can be monitored by InSAR monthly or yearly.

With enough ENVISAT SAR images, the PS method was applied to survey the subsidence cone in urban area. However, due to the human control for the water pumping in Tianjin area, most of the subsidence cones in Tianjin urban area did not subsidize linearly. Without nonlinear model in PS data processing, the results are not reliable in the testing area. Comparing the PS results and D-InSAR results of Tianjin subsidence area, only the stacking method D-InSAR results were closer to the leveling data, which means it is more robust. The errors that contaminated the PS and D-InSAR results need to be studying in the future.

InSAR Time Series with Atmospheric Estimation Model for Mapping City Subsidence in the Wuxi-Changzhou Region, Eastern China

Zhenhong Li[1], **Jianqiang Wu**[2], **Xiaojun Yuan**[2], **Huogen Chen**[2], **Dengming Zhang**[2], **Jun Yu**[2], **Yulin Xu**[2], **Shuliang Wu**[2], **Wei Li**[2], **and Yefei Zhu**[2]

[1]Department of Geographical and Earth Sciences, University of Glasgow, UK
[2]Geological Survey of Jiangsu Province, Nanjing, China

Abstract— Using small baseline interferograms, an advanced InSAR time series technique, InSAR Time Series with Atmospheric Estimation Model (InSAR TS + AEM), has been developed with the following two notable features: (1) partially coherent pixels are explored in time series analyses, together with fully coherent pixels over time; (2) no deformation model is required to separate deformation signals from atmospheric effects, as the latter are estimated based on their turbulence and (partly) topography-dependent features.

The InSAR TS + AEM was employed to process ERS and Envisat SAR images collected during the period between 1992 and 2008 over the Wuxi-Changzhou region, Eastern China. Validation with precise levelling and GPS data suggested: (1) the accuracy of the InSAR-derived mean velocity map was 3.7 mm/yr; (2) InSAR-derived deformation agreed to precise levelling with root mean squares ranging from 2.4 mm to 6.7 mm; (3) the accuracy of InSAR-derived atmospheric signals was 6.5 mm. It is evident that InSAR TS + AEM can be used to image the evolution of the deformation patterns of the Wuxi-Changzhou region over time: the maximum mean velocity decreased from 6–15 cm/yr during the period of 1992–1993 to 2∼3 cm/yr in 2003–2008. This is believed to be a result of the prohibition of groundwater use carried out by Jiangsu provincial government.

Multi-mode SAR Interferometry Processing Research and Implementation

Cunren Liang[1, 2], **Qiming Zeng**[1, 2], **Jianying Jia**[1, 2], **Xiao Zhou**[1, 2], **Jian Jiao**[1, 2], **and Xi'ai Cui**[1, 2]

[1]Institute of RS & GIS, Peking University, Beijing 100871, China
[2]Beijing Key Laboratory of Spatial Information Integration and 3S Application Beijing 100871, China

Abstract— Current operation mode of SAR can be roughly divided into two types: strip-map mode and burst mode. The most conventional mode is strip-map mode, in which the swath width is quite limited. The other type is burst mode, which is an active option to overcome this limitation by cyclically scanning several subswaths, known as ScanSAR. In addition, Envisat ASAR has another type of burst mode, that is, Alternating Polarization mode. ALOS PALSAR and Radarsat-1 also have their own ScanSAR operation modes, but each of them is distinctive from the others in implementation. Numerous theoretical results and applications of interferometry using strip-map data have been published before. Interferometry with burst mode data, however, is much rarer and different from the case of the traditional strip-map mode from raw data focusing to interferogram generation because of its burst nature of data acquisition pattern. In our study, we put our emphasis on each kind of burst mode interferometry and mixed mode interferometry. Until now, our successful research work includes Envisat ASAR WS-WS, IM-WS and ALOS PALSAR WB1-WB1 Interferometry. Other development activities including Envisat AP-AP and Radarsat-1 SNA-SNA interferometry are still on going. In the following paper, we will present our results and give an overview of multi-mode SAR interferometry for the present spaceborne SAR sensors.

Mitigation of Atmospheric Water-vapour Effects on Spaceborne Interferometric SAR Imaging through the MM5 Numerical Model

D. Perissin[1], **E. Pichelli**[2], **R. Ferretti**[2], **F. Rocca**[3], **and N. Pierdicca**[4]

[1]ISEIS, Chinese University of Hong Kong, Hong Kong, China
[2]CETEMPS, University of L'Aquila, Italy
[3]DEI, Politechnic of Milan, Italy
[4]DIE, Sapienza University of Rome, Italy

Abstract— Synthetic Aperture Radar (InSAR) imaging is a well established technique to derive useful products for several land applications. One of the major limitations of InSAR is due to atmospheric effects, and in particular to high water vapour variability.

In this work we make an experimental analysis to research the capability of Numerical Weather Prediction (NWP) models as MM5 to produce high resolution (1km-500m) maps of Integrated Water Vapour (IWV) in the atmosphere to mitigate the well-known disturbances that affect the radar signal while travelling from the sensor to the ground and back. Experiments have been conducted over the area surrounding Rome using ERS data acquired during the three days phase in '94 and using Envisat data acquired in recent years. By means of the PS technique SAR data have been processed and the Atmospheric Phase Screen (APS) of Slave images with respect to a reference Master have been extracted. The MM5 NWP model is a non hydrostatic model at primitive equations with a terrain following vertical coordinates system and multiple nesting capabilities; in this work it has been driven by archived European Centre for Medium-Range Weather Forecast (ECMWF) data, by local physical parameterization (topography, land cover, etc.) and by Planetary Boundary Layer (PBL) parameterization derived by the wide experience of the atmospheric research group of L'Aquila. MM5 provides realistic water vapour distribution fields that can be converted into electromagnetic slant delays. PSInSAR APS's have then been compared to MM5 IWV maps revealing interesting results. MM5 IWV maps have a much lower resolution than PSInSAR APS's: the turbulent term of the atmospheric vapour field cannot be well resolved by MM5, at least with the low resolution ECMWF inputs. However, the vapour distribution term that depends on the local topography has been found quite in accordance. Whilst archived data taken in '94 match just in 50% of cases, the height-IWV linear trends estimated in Envisat data agrees well with MM5 ones. Unfortunately, the cases in which the topography-dependent APS term is stronger than the turbulent one are not predominant. Therefore, at the moment MM5 cannot be used yet as an operational tool for mitigating atmospheric delays. Further research and development are needed to improve non-SAR APS estimates. In this work we will present experimental results as well as discussions over the adopted processing strategy.

MERIS Water Vapour Correction Model for WS InSAR

Zhenhong Li[1], **Paolo Pasquali**[2], **and Alessio Cantone**[2]

[1]Department of Geographical and Earth Sciences, University of Glasgow, UK
[2]Sarmap s.a., Cascine di Barico, Purasca, Switzerland

Abstract— At the expense of its spatial resolution, Wide Swath (WS) InSAR provides much wider coverage than Image Mode (IM) InSAR, e.g., 400 km vs 100 km for ENVISAT WS and IM images. Therefore, WS InSAR has obvious advantages over IM InSAR: (1) it better controls long-wavelength deformation signals; (2) it allows for a more frequent revisit-time deformation monitoring.

Being a unique geodetic tool, repeat-pass WS InSAR is limited by a major source of error: the phase delay in radio signal propagation through the atmosphere; the part due to tropospheric water vapour only could cause errors as large as 10–20 cm in deformation retrievals. Reduction of atmospheric water vapour effects on IM InSAR derived deformation maps using the ESA MEdium Resolution Imaging Spectrometer (MERIS) has been successfully demonstrated: the order of water vapour effects on IM interferograms can be reduced from ~ 10 mm to ~ 5 mm [Li et al., 2006; 2009]; however, no water vapour correction model on WS InSAR has been reported to date.

Scientists in the University of Glasgow and Sarmap are working closely to incorporate MERIS correction models into the SARScape package, and the first result on WS InSAR water vapour correction model will be reported in this paper.

Determination of Fault Slip of 2008 Ms8.0 Wenchuan China Earthquake Using Coseismic Displacements by GPS and DInSAR

Jicang Wu[1], **Guoxiang Liu**[2], **Yongqi Chen**[3], **Shouchao Hu**[1], **and Guojie Meng**[4]

[1]Department of Surveying and Geo-informatics, Tongji University, Shanghai 200092, China
[2]Department of Surveying Engineering, Southwest Jiaotong University, Chengdu, Sichuan, China
[3]Department of Land Surveying and Geo-informatics, The Hong Kong Polytechnic University Hong Kong, China
[4]Institute of Earthquake Science, China Earthquake Administration, Beijing 100036, China

Abstract— In May 21, 2008, a disaster earthquake with magnitude of Ms8.0 occurred in Wenchuan, Sichuan province, southwest of China, with huge lost of life and property. According to the geological investigation and earthquake mechanism analysis, the earthquake was predominantly thrusting with minor dextral striking on the Yingxiu-Beichuan fault and resulting from the collision between Indian plate and Eurasian plate. Determination of fault geometry and slips are very important for understanding of earthquake processes and estimation of the recurrence of such a huge earthquake, so as to mitigate the seimic hazards. In this paper, coseismic displacements obtained by GPS and DInSAR of ALOS PALSAR data are inversed to determine a curve shaped fault geometry and slips, a Bayesian inversion method is used to combine different sources of information and to enhance the resolution of model parameters, and to assess the contributions of different data sources. At initial stage, the rectangular plane fault geometry and only GPS data are included in the inversion and the results obtained are used as a start model for the following inversion analysis. The spatial sampling rate of the DInSAR LOS displacements and improvements of including these data on the inversion results will be explored. At last an optimization inversion method for combining GPS and InSAR displacements for fault geometry and slips is developed. The obtained inversion results are compared with geological investigations and seismological exploration results in this area, so as to understand the earthquake mechanism of this huge earthquake. And the recurrence time of earthquake on the Longmengshan fault zone is estimated based on the inversion results obtained and some preferred assumptions.

Postseismic Deformation Following the Yutian Earthquake, China, March 21, 2008

Yangmao Wen[1], **Caijun Xu**[1], **and Zhenhong Li**[2]

[1]School of Geodesy and Geomatics, Wuhan University, Wuhan, Hubei 430079, China
[2]COMET, Department of Geography and Earth Sciences, University of Glasgow
Glasgow, G12 8QQ, UK

Abstract— The March 21, 2008 (Mw 7.2) Yutian earthquake is one of the largest continental normal faults to have occurred in recent years. The event occurred in the southern edge of Yutian country, 150 km due south of Yutian, on the Xinjiang-Xizang border, China. Here we use the multitemporal SAR interferometry to map the postseismic deformation following the Yutian event. The radar data from two Envisat descending orbits are used to calculate the displacement time series within 1.5 year after the event. We then use the postseismic displacements to compute a single afterslip model. Results of inversions show that the observed LOS displacements are consistent with deep afterslip occurring underneath the coseismic rupture area.

Session 1A2a
Fields Coupling and Integrated Design of Electromagnetics, Temperature and Structure for Antennas and Electronic Equipments

Electromechanical Coupling Optimization Design of Large Reflector Antennas Include Feed (Sub Reflector) Support Structure

P. Li, **D. W. Yang**, **and F. Zheng**
Research Institute on Mechatronics, Xidian University, Xi'an, China

Abstract— The structure design of large reflector antennas is a typical electromechanical multidisciplinary optimization process, and both main reflector back frame and feed/sub reflector support structure should be include. From electromechanical coupling angle, a new coupling formula is presented by introducing the distortion of main reflector and position/angle error of feed/sub reflector into antenna's far field patterns formula. So the structure parameters (include back frame and feed support structure) is related to electrical parameter (include gain, side lobe, beam width and pointing accuracy). Based on the coupling formula, a coupling optimization model is proposed with design variable of feed/sub reflector support structure parameters besides back frame, and with constraint conditions of electrical parameter besides structure conditions. A numerical example has been done for an 8 m reflector antenna. Results of the example show that the coupling optimization model is more efficient than tradition structure optimization model. Finally the coupling optimization model is applied to a 40 m reflector antenna with good results.

Updating Methods for Antenna Servomechanism Structures

Hong Bao, **Congsi Wang**, **and Jun Cheng**
Key Laboratory of Electronic Equipment Structures Design of Ministry of Education
Xidian University, Xi'an, China

Abstract— A new updating method is presented based on the model condensation technique and frequency response function (FRF) for antenna servomechanism dynamic structures. As a result of the introduction of the ratio of damping to stiffness, this method reduce the numbers of parameters than the traditional FRF updating methods. The finite element model (FEM) condensation technique is used to overcome the disadvantage of the traditional FRF updating methods that the testing mode dimension is too large, it decrease the request of the testing model dimension. Finally the numerical result shows the validity and feasibility of the method.

Improved Coupling Matrix Extracting Method for Chebyshev Coaxial-cavity Filter

Hongbo Ma, **Daiwen Yang**, **and Jinzhu Zhou**
Key Laboratory of Electronic Equipment Structure Design (Xidian University), Ministry of Education
Xi'an 710071, China

Abstract— In this thesisa kind of coaxial-cavity tunable filter is presented. When the passband of such filters moves in the mobile communications frequency bands, the stopband suppression gradually decreases while the passband insertion loss increases. Thus, it makes more difficult to tune the filters. Coupling matrix is an important means for design and analysis to such filters. In addition, it is also an effective method for improving the efficiency and precision of the microwave filters tuning. Therefore, the accurate coupling matrix extracting method is important for the procedure. In this thesis, an improved coupling matrix extraction method was developed based on the combination of the inverse eigenvalue method for Jacobian matrices and the optimization method. The method gets the initial matrix from the solutions of the inverse eigenvalue of Jacobian matrices. Then the matrix is utilized as the initial value of the iterative optimization. Finally, the accurate coupling matrix could be obtained by optimization. This method has the advantages that both the methods have and can avoid the defects such as the low searching speed or inaccuracy of optimization approaches. To obtain the initial coupling matrix, experiments about coupling matrix extracting for coaxial-cavity tunable filter is designed and carried out. The characteristic S parameters are measured in the experiment. And zeros and poles are measured as the coaxial terminal is shorted. According to the experimental data, the initial coupling matrix is obtained for optimization algorithm. Proved by engineering experiments and analysis, the method presented in the thesis is feasible and rational.

Analysis of Integrated Structure-electromagnetic Wave Basing on the Same Discrete Meshes

Li-Wei Song
Research Institute on Mechatronics, Xidian University, Xi'an, Shaanxi 710071, China

Abstract— With the rapid development of science and technology, the urgent needs are not only the farther study in single discipline, but also the detail research of cross-disciplines. The higher frequency, density and performance of the electronic equipments are developed, the more complicate relations among disciplines result that the performance of them can not be improved fundamentally. For example, electronic equipment is the combination of its structure and electromagnetism. The electromagnetic performances depend on its structural accuracies. The errors exist in the process of manufacture or assembly and also in the working cases due to loads, such as selfgravitation, wind, vibration etc, which result in decreasing the EM performance. So the relation between the structure and electromagnetism of electromagnetic equipments is necessary to be studied for the integrated analysis between them, in order to understand the effect of the deformation of structure on EM performance.

Then, a novel method of analysis of integrated structure-electromagnetic wave is developed for use with the electro-mechanical system and other metallic and composite engineering structures. To satisfy the computational precision, the same discrete meshes are used in the analysis of structure and electromagnetism. A finite element method is used for structural analysis and the method of moment basing on the EFIE is employed to analyse the EM performances of distorted structure. A criterion of their discrete meshes is given to account for the meshes size of structural deformation by iterative methods. Finally, the above method is applied in an electromagnetic scattering and an antenna's radiation. The obtained results prove that the effect of the structural distortion on electromagnetism is negligible. This study can be considered in the design of structure and electromagnetism.

Subreflector Real-time Compensation for Main Reflector Deformation of Shaped Cassegrain Antenna

W. Wang, G. J. Leng, and H. P. Li
School of Electromechanical Engineering, Xidian University, Xi'an, Shaanxi 710071, China

Abstract— Shaped Cassegrain antennas are widely used in many fields, such as radar tracing, satellite communication and deep space exploration, due to their advantages of higher illumination efficiency and lower side loss. The main and sub-reflector are both shaped for the uniform distribution of phase in aperture, which will improve the efficiency of the antenna system. There are many loads, such as gravity, wind, rain and so on, which drive the antenna structure deform from their design shape. Moreover, the influence of these coefficients changes with the variation of elevation angles. The surface accuracy gets down which results in gain loss and beam distortion. To change the relative position of dual reflectors via subreflector motion may eliminate some phase error in aperture.

On the degradation of electromagnetic performance of large shaped Cassegrain antennas by the main reflector deformation, a method for compensation by moving subreflector is presented. A group of best-fit paraboloids are found by least-square fitting the theoretical discrete data. The group of paraboloids are used to fit the deformed main reflector, with the constraint of all these focuses being in line. The best-fit parameters are optimized and the adjustments of subreflector are derived with the ratio of main reflector and subreflector. The adjustments at various attitudes are saved in a look-up table to real-time compensate for main reflector deformation. From the experimental verification on a 64 m reflector antenna, satisfactory results are obtained and will be used in practice.

Performance of Planar Slotted Waveguide Arrays with Surface Distortion

Li-Wei Song
Research Institute on Mechatronics, Xidian University, Xi'an, Shaanxi 710071, China

Abstract— Since the slotted waveguide arrays antenna have the advantage of compact configuration, stable mechanical characteristics, low loss and perfect efficiency, it is widely used in communication and radar systems. Evaluation of antenna performance under the influence of distortion is an important part of the engineering work in the course of design and development of a new antenna system. This is especially true for large radar antennas of slotted waveguide arrays type, for which antijam performance is critical, and no similar work can be done yet for this kind of antennas.

So the performance of planar slotted waveguide arrays with distortion was investigated in this paper. Errors in array element (radiating slot) positions as a result of structural deformation are considered as predictable. Practically discrete points on the front plate containing the radiating slots were measured with the help of API measurement system. But these points are too few to determine the radiation slot positions by the methods of interpolation or fitting accurately. So the finite element method was used to settle out the radiation slot positions with ANSYS according to the given points. The slot voltages were obtained from antenna measurement system in an anechoic chamber and assumed to be unchangeable for the distortional antenna used in the calculation of far-field pattern. The pattern for distortion and undistortion antenna was obtained by an analytical formula. Finally, measurements were found to be in a good agreement with the calculation results.

Session 1A2b
Electromagnetic Modeling, Inversion, and Applications 1

Performance Enhancement of FDTD-PIC Beam-wave Simulations Using Multi-core Platforms

Andrew J. Woods, Lars D. Ludeking, and David L. Rhoades
Alliant Techsystems (ATK), 8560 Cinderbed Road, Suite 700, Newington, VA 22122, USA

Abstract— The MAGIC electromagnetic (EM) finite difference time domain particle-in-cell (FDTD-PIC) code has been tested for performance speed on typical large-scale electro-energetic calculations. Computer systems employed were the ATK and University of Miami (UMIA) Linux clusters and several single platforms including Windows and Linux dual quad core Intel and AMD machines. A gain of a factor of $10x$ over 2006 state-of-the-art personal computers (PCs) was also achieved on the ATK cluster, and $27x$ on the larger UMIA system. The AMD server achieved up to a $6x$ speedup for parallel processing compared to only $1.6x$ for Intel-based platforms resulting in a $2x$ best rate for AMD compared to Intel. Computer science analysis of the low-latency AMD platform compared to the less expensive Intel architecture explains the enhanced AMD performance for EM FDTD-PIC.

Performance Enhancement of FDTD-PIC Plasma-wave Simulations Using GPU Processing

Lars D. Ludeking and Andrew J. Woods
Alliant Techsystems (ATK), 8560 Cinderbed Road, Suite 700, Newington, VA 22122, USA

Abstract— Present-day computers equipped with powerful graphics processing units (GPUs) show considerable promise of increased performance for the electromagnetic (EM) modeler. In order to determine the degree-of-performance gain at the ground level of electro-energetic physics computation, the MAGIC EM finite difference-time domain (FDTD) particle-incell (PIC) plasma code [1] is undergoing testing for parallel performance speedup on typical large-scale plasma-wave EM calculations using GPU processing. The results of the tests should be of great interest to the EM community because the MAGIC code suite is widely employed and implements the methods common to many large scale IO-intensive computing applications. The performance data obtained will quantify the benefits of GPUs to the EM modeller, and aid in selecting the proper system including GPUs potentially critical to effectiveness with EM codes. Calculation times often run into days due to small zone and timestep requirements, and every method of significant potential speedup is worthy of consideration. GPUs promise a relatively low cost boost which leverages the vast development driven by the computer game industry.

Our approach is to first develop simple models of major CPUintensive code portions using the freely-available CUDA language. [See the NVIDIA corporation website [2]: "The NVIDIA® Compute Unified Device Architecture™ (CUDA™ software platform for massively parallel highperformance computing. CUDA™ hosted on the company's powerful GPUs, enables the user to take maximum advantage of the processors using a high-level language. GPUs are becoming versatile devices suitable for much more than electronic games and 3-D graphics. NVIDIA® CUDA™ is a general purpose parallel computing architecture that leverages the parallel compute engine ... to solve complex ... problems in a fraction of the time required on a CPU. ... To accommodate the program to the CUDA™ architecture, developers can also use C. Other languages will be supported in the future, including FORTRAN and C++.] [2].

The major challenge of this performance testing exercise is to recast the particle and field update schemes in MAGIC into vector forms such that large blocks of data are shipped to the GPU for processing in parallel. This of course requires the data vectors to be independent of one another during the time advance. The CPU-intensive code portions are: The Lorentz equation particle updates, the Maxwell equations EM-fields, and ultimately, the particle allocation onto the finite-difference grid. The last (particle accumulation into current density arrays on the grid) is perceived to be the greatest challenge for GPU effectiveness. Locating considerable data at points surrounding each particle and the accompanying transfer time to the GPU may cancel benefits of the accelerated processing speed.

Our implementation of a simple particle update scheme uses a Fortran main program calling the C-based GPUlib [3], which has been developed to interface the higher level language with CUDA™. It provides needed math functions not yet available directly in CUDA. As can be seen in [3], the GPUlib developers have performed various investigations of the potential of GPUs.

Our implementation employed a Dell 64-bit quad-core processor with Windows Vista and a Quadro FX 3700 GPU (800 on the NVIDIA website). As seen in Table 1, the computing speed was a disappointing 2.3x compared to the same calculation using the conventional CPU for a 100 k particle vector with 100 k time steps. This GPUlib evaluation version-based case was extrapolated to 6x for a Tesla GPU, and is potentially much faster with optimization [4]. A similar Fortran-C combination particle update, calling available CUDA routines directly, yielded a more desirable computing rate 5.1x as fast.

Table 1: CPU speed enhancement for simple particle position/velocity update scheme on GPU vs. CPU.

# Particles (k)	# Time Steps (k)	Case	CPU Time (s)	Case	CPU Time (s)	**CPU Speed (GPU/CPU)**
100	100	C only	45	C-GPU	19.6	**2.3**
100	100	Fortran only	41	Fortran-C-GPU	8	**5.1**

Based on the results obtained to date, we are encouraged that MAGIC will benefit from GPU use, particularly in the particle update and (hopefully) accumulation on the Maxwell equations grid. Prudent selection of particles can keep them independent of one another, enabling parallel updates of large blocks. An intriguing prospect is that efficient, shared memory usage of the GPU can potentially enable the simultaneous, massively parallel update of very large blocks without detailed particle selection. This method will deal with the most CPU-intensive portion of many typical user simulations. Speedup on Windows is the current focus, as this OS has the largest customer base and is slower than parallel Linux [5].

REFERENCES

1. Goplen, B., et al., "User-configurable MAGIC for electromagnetic PIC calculations," *Computer Physics Communications*, Vol. 87, 1995, http://www.mrcwdc.com.
2. http://www.nvidia.com/object/cuda_home.html#.
3. http://www.txcorp.com/products/GPULib/index.php.
4. Messmer, P., "Re: GPULib particle push C GPU vs. CPU speed," *Private Comm.*, Oct. 7, 2009.
5. Woods, A. and L. Ludeking, "Performance enhancement of FDTD-PIC beam-wave simulations using multi-core platforms," *Progress In Electromagnetics Research Symposium Abstracts*, Xi'an, China, March 22–26, 2010.

The Method of Fundamental Solutions for Helmholtz Equation

Tzon-Tzer Lu and Zi-Cai Li
Department of Applied Mathematics, National Sun Yat-sen University, Kaohsiung 80424, Taiwan

Abstract— In the paper, the error and stability analysis is made for the Helmholtz equation by the method of fundamental solutions (MFS) using both Bessel and Neumann functions. The bounds of errors in bounded simply-connected domains are derived, while the bounds of condition number are derived only for disk domains. The MFS using Bessel functions is more efficient than the MFS using Neumann functions. Interestingly, for the MFS using Bessel functions, the radius of the source points is not necessarily larger than the maximal radius of the solution domain. This is against the traditional assumption for MFS. Numerical experiments are carried out to support the analysis and conclusions made.

Analysis of Electromagnetic Transients by Corona in Transmission Lines: Proposal of an Alternative Frequency-dependent Model by Lumped Elements and State Equations Representation

Sérgio Kurokawa[1], **Eduardo Coelho Marques Da Costa**[2], **Germano Ferreira Wedy**[1], **José Pissolato Filho**[2], **and Afonso José Do Prado**[1]

[1]School of Engineering of Ilha Solteira, University of São Paulo State
Avenida Brasil Centro 56, Caixa Postal 31, CEP 15385-000, Ilha Solteira, SP, Brazil
[2]School of Electric Engineering and Computation, State University of Campinas
Caixa Postal 6101, CEP 13081-970, Campinas, SP, Brazil

Abstract— The corona effect is a phenomenon described by an electrostatic discharge due to intense electric field in transmission lines. The critical value of the electric field associated to electric discharge by corona is determined by experimental methods or from formulation developed by empiric data.

The experimental procedure to evaluate the critical electric field consists in the energization of a conductor sample, in arrangement where it is possible to determine, in analytical form, the electric field. The empiric formulation, used to describe the critical electric field, is based on several values and constants obtained by experimental procedures, considering Peek's formula one of the most utilized.

The corona performance in transmission lines is defined by corona losses, audible noises and radio interference. The occurrence of discharges by corona effect is greatly influenced by climatic and atmospheric conditions. Generally, rainy weather and drizzle contribute to occurrence of corona effect and increase the possibility of discharges by corona one or two times.

Overhead transmission lines are frequently submitted to surge voltages due to atmospheric discharges and switching operations. When these surge voltages reach great peaks of magnitude, occurring corona effect, the behavior of currents and voltages on transmission line are distorted and attenuated. These transient phenomena were studied, in 1937, by Skilling and Dykes. The alterations on voltage wave form through transmission line due to corona effect must be considered in transmission line projects and respectively protection systems.

The corona effect is characterized from the line transversal parameters (shunt capacitance and conductance) in function of the magnitude of voltage through the transmission line. This variation on transversal parameters has a nonlinear behavior, making more complex the line modeling.

In line models including corona, from line representation by a cascade of π nominal elements, the currents and voltages through transmission line can be evaluated by statespace technique. However, usually, the representation by π circuits is not used as an alternative to introduce the frequency influence on line longitudinal parameters, as described by several authors. Therefore, the purpose of this paper is to associate the frequency influence on longitudinal parameters and corona effect in a modeling based on lumped parameters and estate-space representation. The state equations are obtained from a cascade of modified π elements that represents, approximately, the distributed nature of frequency-dependent longitudinal parameters.

To improve the lumped parameters model, the line longitudinal parameters are approximated by a rational function and then associated with an equivalent RL circuit. Subsequently, this equivalent circuit is inserted in each π circuit. Then, from this procedure it is possible to describe the state equations for currents and voltages along the cascade of π nominal elements.

The corona effect is inserted by modifications in transversal lumped elements of respectively π circuits, applying the Skilling-Umoto model for corona effect.

This work presents the electromagnetic transients from a typical switching operation, considering and not the corona effect, for a single-phase transmission line. Finally, it describes a possible procedure to insert corona effect in three-phase lines modeling and its eventual problems in implementation by lumped elements and modal analysis.

Analysis of Electromagnetic Transients in Transmission Lines by a Frequency-dependent Three-phase Modeling based on State-space Representation: Numerical and Analytical Solution

Sérgio Kurokawa[1], **Eduardo Coelho Marques Da Costa**[2], **José Pissolato Filho**[2], **and Afonso José Do Prado**[1]

[1]School of Engineering of Ilha Solteira, University of São Paulo State
Avenida Brazil Centro 56, Caixa Postal 31, CEP 15385-000, Ilha Solteira, SP, Brazil
[2]School of Electric Engineering and Computation, State University of Campinas
Caixa Postal 6101, CEP 13081-970, Campinas, SP, Brazil

Abstract— Overhead transmission line models, applied to simulate electromagnetic transients, are frequently classified as lumped or distributed parameters model.

In lumped parameters model, a given transmission line is represented by n nominal π circuits connected in cascade. Considering the transient frequency range, line length and a sufficient number of nominal π circuits connected in cascade, the distributed nature of the transmission line parameters can be synthesized adequately.

When a lumped parameters line model is adopted, it is very common to use state space techniques to evaluate currents and voltages through the line. Therefore, it is possible for the model to carry out simulations directly in time domain without explicit use of inverse transforms and it can be easily implemented. These characteristics are the same as those used to simulate electromagnetic transients on lines with nonlinear components, such as corona effects and fault arcs, or when a detailed voltage and current profile is needed.

The state space representation presents several advantages, as to extend the methodology to time-variable and nonlinear systems. Furthermore, the transmission line is represented by a system composed by first order differential equations and can be easily solved by numerical or analytical integration methods.

However, several papers present lumped parameters model without take into account the frequency dependence of line longitudinal parameters and then limiting the model performance.

Therefore, this paper proposes a three-phase modeling by lumped elements considering frequency-dependent longitudinal parameters and developing the state matrices that represent the transients of current and voltage through the line.

To improve the lumped parameters model, the line longitudinal parameters are approximated by a rational function and then associated with an equivalent RL circuit. Subsequently, this equivalent circuit is inserted in each π circuit. Then, from this procedure it is possible to describe the state equations for currents and voltages along the cascade of π nominal elements. Finally, the state matrices are evaluated from numerical and analytic integration methods. To validate the proposed model, results are compared to transients simulated from software MICROTRAN (EMTP).

The proposed frequency-dependent model is used to represent a non transposed 440 kV three-phase line.

Ill-Conditioning of Finite Difference Equations for Singularly Perturbed Differential Equations

Zi Cai Li[1], **Song Wang**[2], **H. T. Huang**[3], **and Yimin Wei**[4, 5]

[1]Department of Applied Mathematics and Department of Computer Science and Engineering
National Sun Yat-sen University, Kaohsiung 80424, Taiwan
[2]Department of Mathematics and Statistics, The University of Western Australia
35 Stirling Highway, Crawley, Western Australia 6009, Australia
[3]Department of Applied Mathematics, I-Shou University, Kaohsiung 80424, Taiwan
[4]School of Mathematical Sciences, Fudan University, Shanghai 200433, China
[5]Key Laboratory of Mathematics for Nonlinear Sciences (Fudan University) Ministry of Education
Shanghai 200433, China

Abstract— Consider singularly perturbed differential equations (SPDE),

$$-\varepsilon\Delta u + \alpha u_x + \beta u_y + cu = f \text{ in } S,$$
$$u = g \text{ on } \partial S,$$

where $\Delta = \frac{\partial^2}{\partial x^2} + \frac{\partial^2}{\partial y^2}$, and S is the rectangle: $S = \{(x, y)|0 < x < a, 0 < y < b\}$. The parameter ε may be very small, $0 < \varepsilon \ll 1$. The finite difference methods, such as the upwind difference scheme and the fitted difference method, are used, and local refinements of grids are adopted in the singular layer regions, where the meshspacing is infinitesimal as $h_{\min} = O(h\varepsilon)$. The traditional condition number in 2-norm is given by $C_{ond} = O(h^{-2}\varepsilon^{-1}))$, to provide the bounds of relative errors from rounding errors. Such a bound is huge for the given h and the infinitesimal ε. To follow the effective condition number in Li et al. (2007), we will provide a better bound of relative errors of the solutions by the upwind difference scheme. For Dirichlet problems in a rectangle, when the Dirichlet boundary condition on the downwind side is homogeneous, the effective condition number is obtained as $C_{ond\_eff} = O\left(\frac{1}{\sqrt{h}}\right)$, where h is the maximal boundary length of meshspacings. Also when the entire Dirichlet boundary conditions are homogeneous, the extraordinary bound, $C_{ond\_eff} = O(1)$, is obtained. For comparisons, based on the maximum principle, we also derive the bounds of relative errors, $C_{ond\_actual} = O\left(\frac{1}{\sqrt{h}}\right)$ and $C_{ond\_actual} = O\left(\frac{1}{h}\right)$ for the homogeneous and the non-homogeneous SPDE, respectively. Hence, the effective condition number as $C_{ond\_eff} = O(1)$ or $O\left(\frac{1}{\sqrt{h}}\right)$ is a better criteria for stability analysis of the upwind scheme of SPDE. Note that the bounds of effective condition number do not depend on ε; this is distinct from the traditional condition number.

Session 1A3
X-Ray Sources, X-Ray Optics and Applications of Focused X-Ray Probes

Focused X-ray Probes for Studies of Radiation-induced Cancers

Alan Michette
King's College London, London WC2R 2LS, England, United Kingdom

Abstract— This talk will present a case study in x-ray source/optics integration, with an exemplar application in the study of radiation-induced cancers. The development of a new microfocus source, with x-ray emission from a spot of diameter $\sim$1 μm, will be described, as will active array x-ray optics.

X-ray Microbeams for Radiobiological Studies: Current Status and Future Challenges

G. Schettino[1], **M. Folkard**[2], **B. Vojnovic**[2], **A. Michette**[3], **and K. M. Prise**[1]

[1]CCRCB, Queen's University Belfast, 97 Lisburn Road, Belfast BT9 7BL, UK
[2]Gray Institute for Radiation Oncology and Biology, Old Rd. Campus, Oxford OX3 7DQ, UK
[3]King's College London, Strand, London WC2R 2LS, UK

Abstract— Recent technological advances and new radiobiology challenges are behind the great interest in the use of microirradiation techniques for radiobiological studies. Radiobiological microbeams are facilities able to deliver precise doses of radiation to preselected individual cells (or part of them) *in vitro* and assess their biological consequences on a single cell base. They are therefore uniquely powerful tools to address specific problems where very precise targeting accuracy and dose delivery are required. The majority of radiobiological microbeams are centred on particle accelerators in order to irradiated biological samples with an exact number of ions. Currently there are only three microbeam facilities in routine use which employ focused X-rays: two based on laboratory bench X-ray sources (Queen's University Belfast and Nagasaki University) and one developed using synchrotron X-ray beams (Photon Factory in Tsukuba, Japan). While low dose rates limit laboratory bench sources to a few keV, micronsize X-ray probes of a few tens of keV are achievable using synchrotron sources. Each facility has however their own benefits and draw back points. Techniques for focusing X-rays are well established and continuously improving with focal spots down to 50 nm achievable for ultrasoft X-rays using circular diffraction gratings known as "zone plates". Reflection X-ray optics such as Kirkpatrick-Baez mirrors and polycapillary systems are also used to produce micron size X-ray spots. Combined with nano-positioning accuracy of the new generation of stages, improved optics and image analysis algorithms, X-ray microbeams are able to address radiobiological issues in an unprecedented way.

Microbeams have contributed significantly to the discovery and characterization of important new findings regarding the mechanisms of interaction of ionizing radiation with cells and tissues. In particular, they have played a fundamental role in the investigation of non-targeted effects where radiation response is induced in samples whose DNA has not been directly exposed. The exquisite resolution offered by focused X-ray probes has allowed important questions regarding the locations and mechanisms of subcellular targets to be precisely addressed. Evidences of the critical role played by the cytoplasm have been collected and radio-sensitivity across the cell nucleus itself is attracting considerable interest. Moreover using the microbeam single cell approach, it has been possible to study the mechanisms underpinning the bystander effect where radiation damage is expressed in cells which have not been directly irradiated but were in contact or shared medium with directly exposed samples. As a result, microbeam facilities are regarded as a main tool for the formulation of a new radiobiological paradigm where direct damage to cellular DNA is not a requirement. Additionally, the implications of the non-targeted effects in *in vivo* systems and ultimately humans have still to be fully understood. The new generation of X-ray microbeams equipped with 3D image stations and higher X-ray energies offers the perfect approach to extend targeted studies to complex biological models. Finally, the single-cell approach and the high spatial resolution offered by the microbeam provide the perfect tool to study and quantify the dynamic processes associated with the production and repair of DNA damage. Using green fluorescent protein (GFP), it is now possible to follow the spatio-temporal development of the DNA damage sites which is currently of great interest in order to monitor the remodelling of chromatin structure that the cell undergoes to deal with DNA damage.

Design of Narrowband Multilayer for Cr K_α X-rays

H. Jiang, **A. G. Michette**, **S. J. Pfauntsch**, **D. Hart**, **and M. Shand**
Department of Physics, King's College London, Strand, London WC2R 2LS, UK

Abstract— Narrowband multilayer mirrors have been designed for monochromatization of a soft x-ray microfocus source, selecting a narrow band around the Cr Kα line. The reflected beam from the multilayer mirror can be focused by a zone plate in a microprobe to study the pathological changes of cells. The design, taking into account fabrication limitations, was based on theoretical analysis and a local optimal algorithm. The results show that Cr/B_4C and Ni/B_4C multilayer mirrors working in high-order Bragg reflection can provide high reflectivity (above 70%) and sufficient resolution to satisfy the requirement of the zone plate. Potential problems in fabrication are also discussed briefly.

A W/B4 C Transmission Multilayer as an Achromatic Phase Shifter for XUV Polarization Measurements

Franz Schäfers[1], **Andreas Gaupp**[1], **and Michael A. MacDonald**[2, 3]

[1]BESSY GmbH, Albert-Einstein-Strasse 15, D-12489 Berlin, Germany
[2]STFC Daresbury Laboratory, Daresbury, Warrington, WA4 4AD, UK
[3]Canadian Light Source Inc., 101 Perimeter Road, Saskatoon, SK S7N 0X4, Canada

Abstract— Soft x-ray synchrotron radiation with variable polarisation is a sophisticated probe of the physical properties of matter. Many of the most advanced experiments take advantage of the inherently high degree of linear and/or circular polarisation of such a source which is in general an elliptical undulator. Polarimeters designed to deliver the four Stokes parameters of a source rely on a phase retarder and analyser in combination [1]. Because of the enhancement of the multilayer performance near absorption edges most multilayer phase retarders have been designed to be used near the 2p absorption edges of the constituting materials (Mo/Si, Cr/C, Cr/Sc, Ni/Ti, and Ni/V) [1]. Thus these optical elements are monoenergetic in the range between 100 eV and 600 eV. At best they can operate at two distinctive energies (e.g., Sc 397 eV and Cr 550 eV) [2]. Here we show the performance of a new W/B4C phase retarder designed to work from ~ 600 eV to ~ 1000 eV. This range was previously not accessible for circular polarisation analysis without further modelling [3]. The measured phase shift is slowly variing and sufficiently large over this photon energy range to enable quantitative and self-calibrating soft x-ray polarimetry in the range of the 2p edges of Fe, Co and Ni, where most of the polarisation-sensitive magneto-optical investigations are being carried out.

REFERENCES

1. Schaefers, F., H.-Ch. Mertins, A. Gaupp, W. Gudat, M. Mertin, I. Packe, F. Schmolla, S. Di-Fonzo, G. Soullie, W. Jark, R. P. Walker, X. le Cann, R. Nyholm, and M. Eriksson, "A soft soft x-ray polarimeter using multilayer optics: Complete analysis of the polarization state of light," *Applied Optics*, Vol. 38, 4074–4088, 1999.
2. Kimura, H., T. Hirono, Y. Tamenori, Y. Saitoh, N. N. Salashchenko, and T. Ishikawa, *J. Electron Spectrosc. Relat. Phenom.*, Vol. 144, 1079, 2005.
3. MacDonald, M. A., F. Schaefers, R. Pohl, I. B. Poole, A. Gaupp, and F. M. Quinn, "A W/B4C multilayer phase retarder for broad-band polarisation analysis of soft x-ray radiation," *Rev. Sci. Instrum.*, Vol. 79, 1025108, 1–4, 2008.

Progress in the X-Ray Free-Electron Laser Research — Tutorial Review

Toshiyuki Shiozawa
Department of Electronics and Information Engineering, Chubu University, Japan

Abstract— The free-electron laser is expected to play an important role for the radiation source in the region of X-ray wavelengths. In this range of the spectrum, it is extremely difficult to get coherent radiation with the conventional quantum laser. This is because radiation absorption in the lasing medium becomes drastically large in the region of X-ray wavelengths. In the X-ray wavelength region, the free-electron laser can generate radiation with much higher coherence and brightness than existing synchrotron light sources. With its short and coherent pulses carrying enormous peak power, the X-ray free-electron laser will open a whole new field of scientific research, such as new medical and life sciences, solid-state physics, and fabrication of nano-scale structures.

First, starting from the discussion of synchrotron radiation, we briefly review the basic principles of the X-ray free-electron laser, from the viewpoint of classical electrodynamics [1–3]. Specifically, an electron bunch undergoing a zigzag motion with relativistic velocity in transverse periodic magnetic field produces powerful coherent synchrotron radiation through the stimulated emission. Thus the operation principle of the free-electron laser can be explained purely classically, as opposed to the conventional laser which resorts to the quantum-mechanical treatment. Having in mind the basic principles of the X-ray free-electron laser, we review the progress in the X-ray free-electron laser research at the major research facilities in the world, such as SLAC [4] (the United States), DESY [5] (Germany), and Spring-8 [6] (Japan).

REFERENCES

1. Saldin, E. L., E. A. Schneidmiller, and M. V. Yurkov, *The Physics of Free Electron Lasers*, Springer, Berlin, 2000.
2. Shiozawa, T., *Classical Relativistic Electrodynamics — Theory of Light Emission and Application to Free-Electron Lasers*, Springer, Berlin, 2004.
3. Schmuser, P., M. Dohlus, and J. Rossbach, *Ultraviolet and Soft X-Ray Free-Electron Lasers*, Springer, Berlin, 2008.
4. www.slac.stanford.edu.
5. www.desy.de.
6. www.spring8.or.jp.

Generation of X-rays Based on Quantum Coherence

Yuri Rostovtsev
University of North Texas, Denton, TX 76203, USA

Abstract— Using quantum coherent effects provides effective techniques to control nonlinear optical processes in various media. In this talk we extend approaches based on induced quantum coherence in media to the generation of X-rays. The objective of the current approach is to show that such coherence can improve nonlinear generation as well as lasing in the X-ray region. We present study of new methods of generation of coherent X-ray radiation based on coherence induced in quantum systems. Effects of the CEP is also considered.

Nanoscale Imaging and Diffraction with Ultrafast XUV Radiation

R. T. Chapman[1], **B. E. Mills**[2], **C. F. Chau**[2], **J. G. Frey**[1], **and W. S. Brocklesby**[2]

[1]School of Chemistry, University of Southampton, UK
[2]Optoelectronics Research Centre, University of Southampton, UK

Abstract— XUV diffraction and imaging of nanostructures with lab-based sources is facilitated by the use of high harmonic generation (HHG) to provide a spatially coherent source. Results are presented showing diffraction and imaging with sub-micron resolution in the spectral region around 30 nm.

High harmonic generation (HHG) is a useful lab-based source of ultrafast pulses of XUV radiation. Its output is typically in the form of short (< 10 fs) pulses of spatially coherent radiation in well-collimated beams. The combination of short wavelength and spatial coherence opens up areas of diffraction from periodic nanostructures [1], and scattering from individual nanostructures [2] with a view to nanoscale imaging, and also determination of other physical properties such as the dielectric constant. In this talk we describe how diffraction from nanostructures can be used for dielectric constant measurement, and how the same experimental setup can be used for XUV microscopy via coherent diffractive imaging (CDI).

XUV pulses are produced in our experiments by HHG from an argon gas target, using either gas jet or gas-filled capillaries as appropriate for particular experiments. The XUV is focused using a Mo/Si spherical mirror onto targets supported by a 50 nm Si_3N_4 substrate. XUV scattering is collected using a CCD camera.

Examples of diffraction and scattering are shown in Figure 1. Figure 1(a) shows the diffraction pattern from a self-assembled array of 200 nm nanospheres. The array period is small enough not to diffract visible light, but XUV light shows several diffraction orders, which allow extraction of the period, and the dielectric constant of the sphere material. Figure 1(b) shows the reconstructed image of a small test object consisting of several micron-sized holes. The image is reconstructed from the measured scattering pattern shown in the inset using CDI, in which an iterative algorithm is used to reconstruct the missing phase of the image from the measured scattering. The talk will describe scattering from nanoscale objects, and progress toward nanoscale imaging of biological objects using CDI.

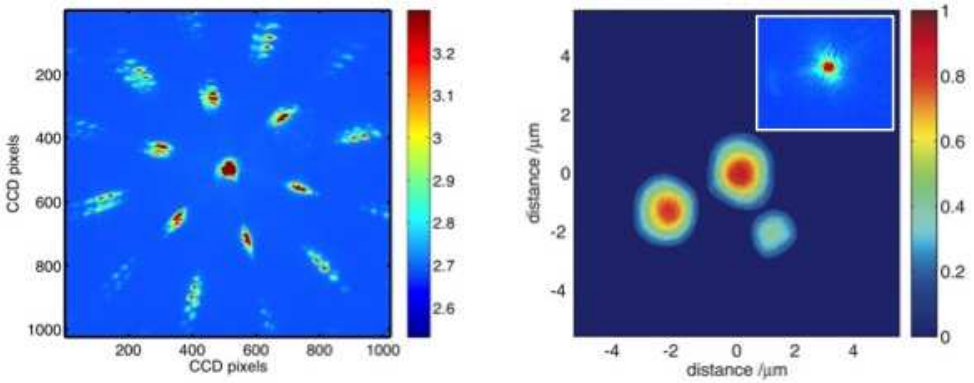

Figure 1: (a) Scattering from an array of self-assembled 200 nm polymer spheres. (b) Reconstructed image and scattering pattern (inset) of an object consisting of three 2 μm holes.

REFERENCES

1. Mills, B., C. F. Chau, E. T. F. Rogers, J. Grant-Jacob, S. L. Stebbings, M. Praeger, A. M. de Paula, C. A. Froud, R. T. Chapman, T. J. Butcher, J. J. Baumberg, W. S. Brocklesby, and J. G. Frey, "Direct measurement of the complex refractive index in the extreme ultraviolet spectral region using diffraction from a nanosphere array," *Appl. Phys. Lett.*, Vol. 93, 231103, 2008.
2. Sandberg, R. L., A. Paul, D. A. Raymondson, S. Hadrich, D. M. Gaudiosi, J. Holtsnider, R. I. Tobey, O. Cohen, M. M. Murnane, and H. C. Kapteyn, "Lensless diffractive imaging using tabletop coherent high-harmonic soft-X-ray beams," *Phys. Rev. Lett.* Vol. 99, 098103, 2007.

Session 1A4a
Electromagnetic Theory

Relaxation and Resonance as Dispersion Mechanisms in Mixtures

Ari Sihvola and Jiaran Qi
Department of Radio Science and Engineering, Helsinki University of Technology
Box 3000, FI-02015 TKK, Espoo, Finland

Abstract— Present-day electromagnetics research is focusing much attention on research on complicated material responses and metamaterial in general [1]. By embedding artificial resonating "molecules" as elements in a matrix environment, the global response of the composite can be engineered to follow unexpected and sometimes even desirable dispersion behavior. In this presentation, the objective is to show that also "ordinary" mixtures (meaning heterogeneous media which are not called metamaterials) can display interesting dispersive characteristics.

The basic mechanisms in the temporal dispersion in dielectric mixing are Debye (e.g., polar liquids), Lorentz (solid-state media), and Drude (conductors). As shown in [2], mixing such media with non-dispersive materials may change the dispersion character very strongly (and if two dispersive media are mixed, the behavior of the composite becomes even less predictable).

The important mechanisms in the dielectric response of matter are relaxation and resonance. The fundamental principle of causality leads to the strong restriction on the spectral behavior of the complex permittivity of materials, the so-called Kramers-Kronig relations [3], which connect the real and imaginary parts as global broadband functions.

This study will generalize some of the earlier results on the effect of mixing on dispersion. Also the question of precursors [4] in composites media will be discussed. In particular, the following relaxationCresonance permittivity model in the frequency domain will be analyzed:

$$\epsilon(\omega) = \epsilon_\infty + \frac{1}{2}\left(\epsilon_s - \epsilon_\infty\right)\left[\frac{1 + j\omega_0\tau}{1 + j(\omega + \omega_0)\tau} + \frac{1 - j\omega_0\tau}{1 + j(\omega - \omega_0)\tau}\right] \tag{1}$$

with ϵ_s and ϵ_∞ being the low- and high-frequency permittivities, τ the relaxation time, and ω_0 the resonant frequency (the engineering-type convention $\exp(j\omega t)$ is followed for time-harmonic fields). If the frequency ω is much higher than the resonant frequency ω_0, this model reduces to the classical relaxation-type Debye model. The model (1) was suggested by Van Vleck and Weisskopf for a collection of dipolar molecules whose orientations change rapidly. It is also known as the Fröhlich model [6, 7].

REFERENCES

1. Sihvola, A., "Metamaterials in electromagnetics," *Metamaterials*, Vol. 1, No. 1, 2–11, 2007.
2. Sihvola, A., *Electromagnetic Mixing Formulas and Applications*, IEE Publishing, London, UK, 1999.
3. Jackson, J. D., *Classical Electrodynamics*, 3rd Edition, Wiley, New York, 1998.
4. Qi, J. and A. Sihvola, "Truncation effect on precursor field structure of pulse propagation in dispersive media," *Progress In Electromagnetics Research B*, Vol. 14, 65–86, 2009.
5. Van Vleck, J. H. and V. F. Weisskopf, "On the shape of collision-broadened lines," *Reviews of Modern Physics*, Vol. 17, 227–236, 1945.
6. Fröhlich, H., *Theory of Dielectrics*, 2nd Edition, Clarendon Press, Oxford, UK, 1986.
7. Scaife, B. K. P., *Principles of Dielectrics*, Clarendon Press, Oxford, 1989.

Energies in Electromagnetic Field and Gravitational Field

Zi-Hua Weng
School of Physics and Mechanical & Electrical Engineering, Xiamen University, Xiamen 361005, China

Abstract— In current electromagnetic theory and gravitational theory, there are some kinds of energies, including the kinetic energy, potential energy, work, and proper energy, etc. Rephrasing the electromagnetic theory and gravitational theory with the octonions, the paper claims that there are a few new kinds of energies besides the existing sorts of energies we found before. The new energy can be considered as one candidate for the quasar's energy source.

The quaternion was first used by J. C. Maxwell to describe the properties of electromagnetic field in 1861. Two quaternions can be combined together to become an octonion. The latter can be used to rephrase the gravitational field and electromagnetic field simultaneously, although these two fields are quite different from each other. In the octonion space, we can study the features of field potential, field strength, field source, angular momentum, and energy, etc.

To incorporate various kinds of energies within a single definition, the angular momentum and energy will both be extended to apply within electromagnetic field and gravitational field. In the octonion space, the angular momentum can be defined from the linear momentum, the radius vector, and one new physical quantity. The last is similar to Hertz vector in the electrodynamics, and its derivation will yield the electromagnetic potential and gravitational potential.

Defining from the angular momentum, the energy involves the existing sorts of energies, and some new kinds of energies. The latter is total different from the former, and is related with above new physical quantity. In general, this new physical quantity is much less than the radius vector, and then we may neglect the new energy. The results state that when the radius vector is almost equal to zero, the influence of new energies will become powerful obviously.

ACKNOWLEDGMENT

The author is grateful for the financial support from the National Natural Science Foundation of China under grant number 60677039.

Electromagnetic Sources and Observers in Motion I — Evidence Supporting the EM Propagation Medium for the Transmission of Light

S. E. Wright
Moor Lane Laboratory, ECASS Technologies Ltd., Kirkburton, Huddersfield, HD8 0QS, UK

Abstract— A propagation medium (ether) has long been thought essential to facilitate the transmission of light. Conflicting scientific evidence both substantiated and contradicted the medium's existence. Einstein's ether-less universe was reluctantly accepted by the establishment, although the controversy was never resolved. This study concludes that there is extensive data supporting the medium, challenging Einstein's special relativity (SR). Measurements on and above the Earth, through satellite and space communications show that away from gravitational matter, the medium is basically at rest in space. Close to a gravitational body the medium appears to be attracted to and moves with the body. Einstein was not aware of this detail in developing his SR, which now appears to be in error. It is confirmed that Lorentz's time and space contraction is in fact a direct result of motion with respect to the medium, as Lorentz predicted. And that clear distinction is found between source and observer motion relative to the medium, which SR cannot distinguish between. These medium distinctions appear to restore causality and remove paradox present in Einstein's relativity. *Experimental methods an order of magnitude more sensitive than that of Michelson and Morley, are described, that can now finally investigate in detail claims that the propagation medium exists.*

It appears that there is irrefutable data supporting the medium, which Einstein did not often refer to. Sagnac established that the medium exists and moves with the surface of the Earth. Michelson and Gale showed that the medium rotates with the surface relative to a 'stationary' medium surrounding and orbiting with the Earth. This data was well documented and available in Einstein's time. With modern technology, Hafele and Keating in a high flying aircraft, using atomic clocks confirmed the medium orbits with the Earth. This moving medium model has been confirmed further through satellite communications across the Pacific, Saburi et al. and through satellite Global Positioning Systems (GPS). The 'stationary' medium orbiting with the Earth, in turn, is shown to move relative to a 'stationary' medium surrounding and moving with the Sun and Solar System through space, measured in the Viking-Mars Lander project by Reasenburg et al. It appears that Einstein's concept of relativity, based on no propagation medium, has never been verified theoretically or confirmed experimentally. *Researchers claiming to have verified Einstein's special relativity have usually verified the kinematic aspects of SR, not relativity or the absence of the propagation medium.* Removing the medium, as Einstein attempted to do, besides making light propagation appear impossible, creates fundamental analytical difficulties. Without the medium's presence, Einstein could not solve the electromagnetic (EM) motional wave equation. Without its solution, there can be no predictability of an observed sequence of events, no formal definition of time, no causality.

SR, without a medium, can predict only relative motion between projectiles. Without satisfying the solution of the motional wave equation, SR apparently cannot describe observations of motion of any kind, whether relative or absolute. The description of observed motion, complete with emission, reception and retarded time, appears to be absent. To predict observations, one should acknowledge the existence of the medium and use the full solution of the motional wave equation reflected through Lorentz's medium based transform (LT). *The LT is a complete observational theory, it does not depend on SR. Whereas, SR is based on LT, but without its medium, SR appears incomplete, it is unobservable and cannot be supported by LT.* This new medium based theory supports Fresnel's light convection, transverse Doppler, changes in time, space, mass, momentum and Einstein's energy equation. Relativistic quantum mechanics, which is Lorentz invariant, quantum electrodynamics and the Standard Model in particle physics, all appear to be in agreement with this medium based theory. The new theory is also in accord with general relativity; here the medium inclusion leads to Schwarzschild metric and event horizon. Assuming the medium to be homogeneous and isotropic, the Robertson-Walker metric in cosmology is obtained. There appears to be nothing in any of the above theories to doubt the existence of the propagation medium and the exact application of the LT with respect to this medium. Therefore, this new medium based approach is not rewriting history, but offers a more robust, physical understanding of electromagnetic sources and observers in motion relative to their propagation medium.

Electromagnetic Sources and Observers in Motion II — Einstein's Ether-less Relativity Versus Lorentz's Medium Based Theory

S. E. Wright
Moor Lane Laboratory, ECASS Technologies Ltd., Kirkburton, Huddersfield, HD8 0QS, UK

Abstract— For regular media movement, such as air and water, it is expected that the upstream and downstream wave propagation times will be different and change with propagation medium speed (simultaneity not upheld), similar to water waves viewed from the bank on a rapidly moving river. If the water speed, for example, equals the wave speed, the waves would appear stationary upstream relative to the river bank, giving half the downstream and an infinite upstream propagation time. This asymmetric propagation time, caused through the propagation medium, is predicted by solving the classical wave equation. This equation predicts the whole process of generation transmission and reception for all kinds of rational (causal) wave motions. In the case of electromagnetic (EM) waves the wave equation predicts the source events (light) as seen by an observer. However, Einstein believed the asymmetric propagation time upstream and down does not apply to EM waves, light. Without any definitive proof, and against basic physics, it was thought there is an unidentified light propagation mechanism, not requiring a medium. As a result of the apparently missing medium, and supposedly equal propagation times up stream and down, Einstein proposed his concept of special relativity (SR).

In spite of Einstein's belief, considerable data is shown to exist in support of an EM propagation medium (ether) in a companion paper: Evidence Supporting the EM Propagation Medium for the Transmission of Light. As a consequence, it was thought appropriate to revisit Einstein's SR. It was found that having no medium appears to disqualify SR from being a solution of the motional wave equation, and therefore gives a non causal sequence of events (prediction of time). This was understood by Lorentz, who had already established causality in his medium based transform, and Sagnac, who had actually measured motion relative to the medium, confirming the asymmetric propagation time. Many in the scientific community including Maxwell, Poincar and Lorentz fervently resisted the medium's abandonment. Even so, Einstein's SR was still considered to account for the Michelson and Morley experiment and its implied missing medium. Aware that light propagation was not straight forward, but having no suspicion of the medium velocity gradients produced by the body's motion, discussed in the companion Paper I, Einstein decided to remove the propagation medium altogether. This was attempted through using Einstein's inertial frame, where without a medium he assumed that stationary and constantly moving frames are indistinguishable. Mathematically this was equivalent to simulating the medium removal through an oblique time and space axes transform. *It appears that Einstein's non-causal, ether-less, oblique axes transform cannot be supported by Lorentz's causal, medium based, rectangular axes transform, these oblique axes have not been verified theoretically or confirmed experimentally.*

Based on Maxwell's wave equation, a new transform extends Lorentz's theory, for both source and observer motion, not only confirming Lorentz's original motional optics, but predicting additional motional properties for individual source and observer motion relative to the medium. It explains observations in the universe quite naturally, removing optical simultaneity and reciprocity, predicted by SR, neither of which appears to have been observed. Researchers claiming to have verified Einstein's relativity have usually verified the kinematic aspects of SR. These kinematic aspects are basically Lorentz's time and space contraction leading to $E = mc^2$, which appear to have nothing to do with relativity or the absence of the propagation medium. Having no medium, besides the obvious effect of making light impossible, also appears to restrict SR to describing a positional sequence of events, creating fundamental observational difficulties. Without accepting the medium's presence, Einstein could not solve the motional wave equation. Without its solution, there appears to be no predictability of an observed sequence of events, no formal definition of time, no causality. This appears to take Einstein's unobservable relativity into a metaphysical, realm, whereas, light propagation is an observable and predictable phenomenon. As a consequence, SR appears not to be able to describe observations of motion of any kind, whether relative or absolute. The description of observed motion, complete with emission, reception and retarded time appears to be absent. *To predict observations one should acknowledge the existence of the medium and use the medium based Maxwell's wave equation, with motion being included through Lorentz's medium based transform (LT). Einstein's SR, not being based on a propagation medium, is an unobserved theory and is not supported by the LT.*

On 3D Cherenkov Wave Calculation from Split-quaternion Space

Geert C. Dijkhuis
Convectron N.V., Rotterdam, the Netherlands

Abstract— For regions with space charge we calculate coherent 3D wave fronts by adapting 4D function theory for static potential field solutions [1]. Analogous to elliptic quaternions for static fields we regularize hyperbolic split-quaternions for 3D wave propagation. But now relativistic light cones separate regular split-quaternion regions from an inaccessible "elsewhere" absent from static field solutions. Parametric plots of split-quaternion functions reveal wave propagation converging on conical wave front envelopes as seen in Cherenkov radiation.

Charged particles moving in transparent media excite coherent Cherenkov radiation when their velocity exceeds the local speed of light. Collectively the eye observes such radiation as a bright blue glow around nuclear reactors submerged in water. Unseen Cherenkov emission comes from air molecules excited by highly relativistic charges in energetic cosmic ray showers. Research and health care exploit Cherenkov radiation in advanced particle detectors and medical radiology.

Without any velocity threshold moving charges also excite coherent waves upon transition of refractive interfaces and photonic crystals. In square photonic lattices Bloch waves solve 2D Maxwell equations for Cherenkov radiation converging on wedge-like envelopes [2]. Numerical results include velocity regimes with reversed wedge orientation and wave propagation as expected for materials with negative index of refraction. Our regular split-quaternion format enables similar 3D analysis for conical Cherenkov radiation envelopes.

For smooth functions in 4D space the split-quaternions require twelve symmetry conditions on their sixteen partial derivatives, moments and eigenvalue equations analogous to quaternions [1]. Our real matrix format now extends symmetric Cauchy-Riemann conditions for split-complex planes into split-quaternion space. Accordingly we find some sign changes in the six local gradient en rotation symmetries, and none in the six non-local moment and eigenvalue symmetries. This regularization scheme ensures smooth closure of 4D functions in split-quaternion space.

Inspection readily verifies regularity for split-quaternion versions of standard polynomial and cyclometric functions. We plot their wave front surfaces in parametric form, and likewise field lines for the wave vectors as intersection of two complementary sets of field surfaces. Thus we find that the exponential split-quaternion function draws coaxial hyperbolic wave fronts converging on a conical envelope as shown in Fig. 1. Projections of such wave envelopes spread as rings in special gas-filled particle detectors, and possibly in our atmosphere as short-lived ionospheric elves.

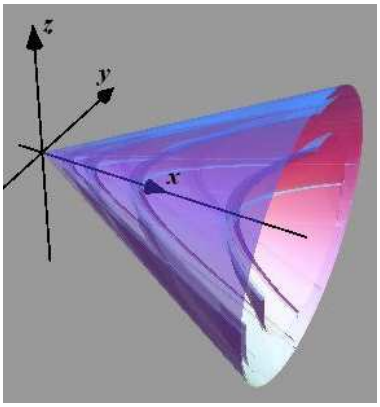

Figure 1: Split-quaternion exponential converges hyperbolic wave fronts on a conical envelope as in Cherenkov radiation.

REFERENCES

1. Dijkhuis, G. C., "On potential flow solutions from the division algebras," *Proc. of the 6th European Symposium on Aerothermodynamics of Space Vehicles*, Versailles, France, Nov. 3–6, 2008 (ESA-SP659, Jan. 2009).
2. Luo, C., et al., "Cerenkov radiation in photonic crystals," *Science*, Vol. 299, 368–371, 2003.

On the A, B, C Numbers and Their Application in the Theory of Circular Waveguide with Azimuthally Magnetized Ferrite

Mariana Nikolova Georgieva-Grosse[1] and Georgi Nikolov Georgiev[2]

[1]Meterstrasse 4, D-70839 Gerlingen, Germany
[2]Faculty of Mathematics and Informatics
University of Veliko Tirnovo "St. St. Cyril and Methodius", BG-5000 Veliko Tirnovo, Bulgaria

Abstract— The A, B, C numbers have been advanced in the theory of azimuthally magnetized circular ferrite waveguides, propagating normal TE_{0n} modes, based on the complex confluent hypergeometric functions, as a means for computation of the differential phase shift produced by these structures [1, 2]. Finding the quantity mentioned is important in view of the possible application of geometries in the development of nonreciprocal digital phase shifters for microwave frequencies [1–6]. This requires knowledge of the numbers, the information for which still is scarce [1, 2]. In this work the discussion is confined to the circular waveguide, entirely filled with ferrite that supports normal TE_{01} mode ($n = 1$). An iterative technique is elaborated, yielding the quantities A, B, C in the whole area of phase shifter operation of configuration [3]. The numbers of interest are determined from the definiens: $A = A_- - A_+$, $B = B_- - B_+$, $C = C_- - C_+$ where $A_\pm = \sigma_{1\pm}/\sigma_{2\pm}$ or $A_\pm = \sigma_{2\pm}/\sigma_{1\pm}$, $B_\pm = \sigma_{1\pm}\bar{r}_0$, or $B_\pm = \sigma_{2\pm}\bar{r}_0$ and $C_\pm = (\sigma_{1\pm}/\sigma_{2\pm})\bar{r}_0$ or $C_\pm = (\sigma_{2\pm}/\sigma_{1\pm})\bar{r}_0$ with $\sigma^2_{1\pm,2\pm} = 0.5[(1-\bar{\beta}^2_{2\pm}) \pm \sqrt{(1-\bar{\beta}^2_{2\pm})^2 - 4\times 4\bar{\beta}^2_{2\pm}k^2_\pm}]$ in that $1-\bar{\beta}^2_{2\pm} \geq 4\bar{\beta}_{2\pm}|k_\pm|$, $(1 > \sigma_{1-} \geq \sigma_{1+} \geq \sigma_{2-} \geq \sigma_{2+} \geq 0)$ [2]. If $\bar{\beta} = \beta/(\beta_0\sqrt{\varepsilon_r})$, $\bar{\beta}_2 = \beta_2/(\beta_0\sqrt{\varepsilon_r})$ and $\bar{r}_0 = \beta_0 r_0\sqrt{\varepsilon_r}$ are the normalized phase constant, radial wavenumber and guide radius, resp., $\beta_0 = \omega\sqrt{\varepsilon_0\mu_0}$, $k = \alpha\bar{\beta}/(2\bar{\beta}_2)$, $\bar{\beta}_2 = (1-\alpha^2-\bar{\beta}^2)^{1/2}$ and α and ε_r are the off-diagonal permeability tensor element and the relative permittivity of the ferrite, then $\sigma_{1\pm}$ and $\sigma_{2\pm}$ stand for $\bar{\beta}_\pm$ ($|\alpha_\pm|$) and $|\alpha_\pm|$ ($\bar{\beta}_\pm$), resp. and the term $\bar{\beta}_{2\pm} = \zeta^{(c)}_{k_{\pm,n}}/(2\bar{r}_0)$ specifies the eigenvalue spectrum of the fields ($\zeta^{(c)}_{k_{\pm,n}}$ — roots of the structure's characteristic equation, written by complex Kummer function, $n = 1, 2, 3, \ldots$) [1–4, 7]. (The subscripts "+" and "−" relate to positive ($\alpha_+ > 0$, $k_+ > 0$) and negative ($\alpha_- < 0$, $k_- < 0$) magnetization, resp.) For fixed $\bar{r}_0$ the parameter k is varied until $\sigma_{1\pm}$ (or $\sigma_{2\pm}$) coincides with the chosen $|\alpha_\pm|$. An analysis is made of the influence of quantities $\bar{r}_0$ and $|\alpha_\pm|$ on the numbers. The employment of the latter in the exact calculation of the differential phase shift produced by the configuration is demonstrated.

REFERENCES

1. Georgiev, G. N. and M. N. Georgieva-Grosse, "Formulae for differential phase shift computation in an azimuthally magnetized circular ferrite waveguide," *Proc. Millenn. Conf. Antennas Propagat., AP-2000*, 1002, in CDROM, Davos, Switzerland, April 9–14, 2000.
2. Georgieva-Grosse, M. N. and G. N. Georgiev, "The A, B, C numbers and their application in the theory of waveguides," *PIERS Proc.*, 1043–1047, Moscow, Russia, August 18–21, 2009.
3. Georgiev, G. N. and M. N. Georgieva-Grosse, "A new property of the complex Kummer function and its application to waveguide propagation," *IEEE Antennas Wireless Propagat. Lett.*, Vol. 2, 306–309, December 2003.
4. Georgiev, G. N. and M. N. Georgieva-Grosse, "A theorem for the properties of some classes of numbers, connected with the zeros of complex Kummer function and its application in the theory of circular ferrite waveguides with azimuthal magnetization," *Proc. XXIX URSI General Assembly*, in CDROM, D05.4(182), Chicago, IL, USA, August 7–16, 2008.
5. Georgiev, G. N. and M. N. Georgieva-Grosse, "An application of the complex Tricomi function," *Proc. Eleventh Int. Conf. Electromagn. Adv. Applicat., ICEAA'09*, 819–822, in CDROM, Turin, Italy, September 14–18, 2009.
6. Georgiev, G. N. and M. N. Georgieva-Grosse, "Effect of the dielectric filling on the phase behaviour of the circular waveguide with azimuthally magnetized ferrite toroid and dielectric cylinder," *Proc. Asia-Pacific Microwave Conf., APMC-2009*, in CDROM, WE4B-4(1680), Singapore, December 7–10, 2009.
7. Tricomi, F. G., *Funzioni Ipergeometriche Confluenti*, Edizioni Cremonese, Rome, Italy, 1954.

Session 1A4b
Electromagnetic Detectors of Gravitational Waves

Very High Frequency Gravitational Wave Detectors

A. Mike Cruise
University of Birmingham, Birmingham, UK

Abstract— As with electromagnetic waves, gravitational waves may be expected to span a very wide range of frequencies. At present the search for cosmic signals using gravitational waves is limited to the audio frequencies — 50–3000 Hz though studies of lower frequency detectors (0.1–100 milli Hz) in space are well advanced. These frequency choices have been based on the initial practicality of the detector construction and the emission frequencies expected from identified astronomical objects such as neutron stars, black holes and white dwarfs. A major advantage of using gravitational waves to study the universe is the fact that they are neither absorbed nor scattered in astronomical situations, even at the densities pertaining at the Planck Time in the early universe. Gravitational waves will carry information to us directly from the earliest moments after the big bang as well as during the period of inflation and re-ionisation. They will allow us to study energetic processes even at the Grand Unified Transition. These kinds of sources will have to be studied at very high frequencies, certainly above 10 MHz, and most likely by detectors that employ electromagnetic signatures of various kinds. The paper will outline the practical issues associated with detectors at these frequencies and explore the most promising development paths. New data from detectors operating at 10 GHz and in the optical region will be presented.

Detection of High-frequency Gravitational Waves by a Coupling Electromagnetic Resonance System

Fang-Yu Li and Nan Yang
Department of Physics, Chongqing University, Chongqing 400044, China

Abstract— We consider an electromagnetic (EM) detection scheme to high-frequency gravitational wave (HFGWs) in the microwave band ($\sim 10^8$–10^{10} Hz) by a coupling EM resonance system, and analyze the perturbative photon flux, background noise, signal accumulation time, phase matching and displaying condition of the HFGWs in the coupling EM system. In addition, we review the huge challenge we are facing, difficulty and possible opportunity in this subject.

Cosmic Deceleration Parameter $q(Z)$ Dependence upon Gravitons? Implications for DM Models, DE, and the Search for Gravitons as Measured via E and M Interactions in Detectors

Andrew Walcott Beckwith
American Institute of Beamed Energy Propulsion, USA

Abstract— In this paper, the author asks if DM and gravitons could also impact the cosmic acceleration of the universe, leading to an increase of acceleration one billion years ago, in a manner usually attributed to DE. Following Alves et al. (2009) the author will high light what KK style gravitons, with a slightly different mass profile could mean in terms of DM. The consequences are from assuming that axions are CDM, and KK gravitons are for WDM, then up to a point, $\rho_{Warm\text{-}Dark\text{-}Matter}$ would dominate not only structure formation in early universe formation. Further efforts in obtaining data for such suppositions would lie in electro magnetic-graviton interactions contributing toward $h_0^2\Omega_{gw}(f)$ being appropriately measured.

Session 1P1
Remote Sensing, GPR, and SAR

A Comparison of Genetic Algorithm and Differential Evolution Methods for the Estimation of Low Atmospheric Refractivity Profiles from Radar Sea Clutter

Bo Wang[1], **Zhen-Sen Wu**[1], **Zhen-Wei Zhao**[2], **and Hong-Guang Wang**[2]

[1]School of Science, Xidian University, Xi'an, Shanxi 710071, China
[2]China Research Institute of Radio-wave Propagation, Qingdao, Shandong 266107, China

Abstract— A comparison between differential evolution algorithm and genetic algorithm based optimization methods applied to the estimation of low atmospheric refractivity profiles is presented in this paper. Differential evolution (DE) algorithm is a very effective method for global optimization. And it is firstly applied to estimate low tropospheric refractivity profiles in this paper. Evaporation duct is the main consideration in this work. All conclusions are arrived at by comparing the results obtained from Differential evolutionary (DE) algorithm with that from genetic algorithm (GA). The objective functions, which are used to evaluate the fit of simulated and *measured* power in estimation procedures, are also investigated under different wind speeds and frequencies such as L-, S-, C- and X-frequency. The results show that all the objective functions are multi-peak functions, which call for the algorithms should take measurements to avoid the local extremum such as enhancing the population size. An Adjusted Barton Model of radar cross section (RCS) is adopted which is different from previous work that took radar cross section (RCS) as a constant. The characteristics of the objective functions are analyzed by comparing estimating results obtained from genetic algorithm (GA) and differential evolutionary (DE) with different population size. The performances of DE and GA in estimating evaporation and surface-based duct parameters are investigated from 200 Monte Carlo simulations. Both DE and GA use the same population size and number of iteration. The content of analyze includes probability distributions, mean values and RMS of results.

Underground Diseases Identification of Airport Runway Using GPR

Xuejing Song, **Renbiao Wu**, **and Jiaxue Liu**
Tianjin Key Laboratory of Advanced Signal Processing, Civil Aviation University of China, China

Abstract— This paper proposes an automatic identification method of the underground diseases from ground penetrating radar (GPR) imagery of airport runway. Cracks and voids (which have two type: air voids and water voids) are the most common diseases underneath the airport runway. In GPR B-scan images, the crack appears as a linear shape, while the apparent shape of void is a hyperbola. The entire process is subdivided into three steps. Firstly, the B-scan images are processed in the order of mean filtering, morphological image processing, and thresholding. After a preprocessing step, Hough transform is introduced in GPR B-scan images to detect and classify the two kinds of diseases. The classical Hough transform is used to identify linear segments in the B-scan images, while a generalized Hough transform is proposed to identify hyperbolic segments. The crack images are focused on one point after being transformed to the parametric space of straight line. A hyperbolic equation with a time-delay factor is introduced in void images, in order to locate the position of the hyperbolic apex accurately. Finally, a windowing operation centered at the apex is applied for intercepting the most efficient signal fragment, which is used to identify the void type by the least squares curve fitting method.

To illustrate the performances of proposed method, we conducted a thorough experimental study based on GPR images generated by a GPR simulator based on the finite-difference time-domain method. The simulation results demonstrate that the method has advantages of small calculation quantity, fast-speed and high-accuracy. It is good at real-time predicting tracking.

Satellite Thermal Monitoring of Arctic Ice Front in Relation to Dynamics of a Polar Orbital Ocean Circulation

Shigehisa Nakamura
Kyoto University, Japan

Abstract— In order to show an evaluation of a satellite monitoring of the ice front in the Arctic Sea, a ocean water intrusion from the Bering Sea to the Arctic Sea through the Bering Strait is studied on the basis of the knowledge on geophysical aspect of fluid dynamics applied in meteorological research field. First, an illustration reduced referring to the satellite data is introduced the ice front evolution during 1997 to 2008 for the season of September. The Arctic Sea is covered by a sea ice sheet in the cold season, for. example, in December, January and February. So that, the author considers it better to introduce a September ice front evolution in the Arctic Sea. The September ice front evolution in the Arctic Sea can be found by a mapping of the ice front location in a several years interval monitoring, for example, in 1980, in 2005 and in 2007. This time interval is too short to see the trend of the September ice front in the Arctic Sea. One of the specific patterns in the September ice front evolution is the sea water intrusion from the Bering Sea into the Arctic Sea through the Bering Strait is clearly found a chart of the polar zone where the satellites have had monitored the earth surface. At present, most of the scientists might call its pattern as a typical example of the global earth Warming effect. Nevertheless, this effect is only in the twenty years history though the earth has spent for more than several thousand years. Then, the author has felt it now what is necessary is what dynamical effect could be the driving force for the September ice front evolution. Now, the author may introduce a spherical coordinate at the center of the earth. Then, the equation of motion for the sea water covering the earth surface can be described in a mathematical form. With several assumption, a solution can be obtained. Introducing several parameters, an approximated solution can be obtained to demonstrate several patterns can be possible motion of the interested sea waters. Some bold illustration gives us that one of the several solutions may be supporting actively what process found around the Arctic September ice front evolution. This process may be a scale of longer time than the global climate changing process, because the sea water inertia rhotion can not be easily changed as the atmospheric inertia motion. In this work, a simplified linearized model is introduced for the purpose of seeing what is an essential factor is for driving the ice front evolution. The author is considering a meridional motion of the sea water could be a part of the actual sea water motion in the interested sea area. This motion could be a polar orbital ocean circulation, which could be take part of the three dimensional ocean circulation.

Satellite Thermal Monitoring of Ocean Water Front Formation after an Intruding Bering Sea Water into the Arctic Sea

Shigehisa Nakamura
Kyoto University, Japan

Abstract— The author has had several reports on satellite thermal monitoring of ocean front evolution in a mid latitude zone. It was the site of the Northwest Pacific so that satellite thermal mentoring had been undertaken after directly receiving the satellite signal and processing the signal for obtaining a series of the ocean front evolution by utilizing a desk top personal computer. In this work, an example of ocean front in,the Arctic Sea formed by an intrusion of the Bering Sea water. This intrusion might have been appeared many times in some other scientific publications. For example, Shimada et al. [1] in 2006 noticed on the Pacific Ocean inflow as an effective factor for influence on catastrophic reduction of sea ice cover. Stroeve et al. [2] in 2007 have noted on the Arctic Sea ice decrease, that was greater than forecast. Stroeve et al. [3] in 2008 noted about Arctic sea ice content plummets in the year of 2007. Gasaard et al. [4] in 2008 noted the Arctic trans-polar drift during dramatic sea ice retreat. These notes on phenomenological process seem to suggest the author to promote a research on the specific process in the Antarctic Sea in a scope of hydrodynamics. The author found in this time a review on the driving processes of the Atlantic meridional overturn circulation. These works are simply notices on the phenomenological process. Then, the author tend to consider what is the way to have a key to a dynamical understanding on a Bering sea water intruding into the Arctic sea to form a ocean front. In this case, the ocean front could be identified as a maximum of thermal gradient on the sea surface during the satellite monitoring. An illustration for a thermal pattern on the sea surface in a global scale must be constructed by a set of coarse pixel units in a scale of 100 km when the satellite thermal data is taken as a reference. In order to see the Bering Sea water intrusion in relation to a global ocean circulation, a dynamical model is introduced under some bold assumption in the field of the earth's gravity and the earth's rotation. This might be helpful at considering what part of the intrusion is the natural process and how is the rest part. The author has wish to distinguish it clarify what weight should be considered for the effect of man-made anomaly in the global ocean circulation. Some note is introduced in order to have a dynamical background of this intrusion and a dynamical process of the ocean front evolution.

Satellite Thermal Monitoring of Ocean Front Evolution in Relation to Ocean Climate in the North Atlantic, Pacific and Arctic Sea

Shgehisa Nakamura
Kyoto University, Japan

Abstract— A possible model of ocean front evolution is studied in relation to ocean climate in the North Atlantic. For this, the satellite monitoring and the oceanographic observations are taken as the references. As is well understood, the meridional ocean circulation system is effective to see the global ocean circulation as a three dimensional process. This process could be possible to consider the two layers of the ocean, i.e., the surface layer and the deep layer with the down flows surface to the deep in Labrador Sea and Nordic Sea. In the ocean water circulation updated, the deep water flow is suggesting to get to the Philippine Basin of the northwestern Pacific through the Southern Circum Polar Current. Some of the recent reports tell us that the oldest water has been found in the deep sea of the Philippine Basin after aging of the dissolved oxygen. The water from the North Atlantic might have got to the Basin after dissipating the original dissolved oxygen. This oldest ocean water might be there to raise the sea level of the Basin. The author here considers that this water in the tropical zone forms a stable deep layer. This could affect the ocean front evolution in the northwestern Pacific which had been monitored well by the recent satellites. As well known, the ocean front evolution process in the northwestern Pacific is not so simple. Considering several other related factors, one of the factors controlling the ocean front evolution process in a longer time scale than the age of the oldest water could be the deep water mass transported from the Atlantic. An additional note is about the decreasing trend of the Arctic Sea ice for these two hundreds years, i.e., between 1900 to 2100. A part of this decreasing must be caused by the human-made climate change.

Evaluation of the Local Standard Deviation Method for SNR Estimation on Remotely Sensed Optical Imagery

Xinhong Wang, **Bo Zhu**, **Lingling Ma**, **Lingli Tang**, **and Chuanrong Li**
Academy of Opto-Electronics, Chinese Academy of Sciences, Beijing, China

Abstract— Signal-to-Noise Ratio (SNR) is one of the basic and commonly used statistic parameters to evaluate the imaging quality of optical sensor. In quite a few algorithms to calculate SNR, the Local Standard Deviation (LSD) method may be the most widely used one. However, we found that although the LSD method may behave well to uniform surface, it doesn't have the same good effect on complicated image. In the condition of complicated image, changes of land cover in spatial will also be considered as part of imaging noise in each sub-image blocks, so the eventual SNR result is often to be underestimated. In this paper, a lot of pure noise images and imitated true scene images have been simulated to examine the capability of the LSD method. The pure noise images have various mean values and standard deviations, and they can be regarded as uniform images. Besides the pure noise images, a set of relative variety images, which show changes of grey level due to natural transition of land surfaces in spatial, is also generated with different texture patterns. Then plenty of imitated true scene images can be produced by overlaying certain percent of pixels of the variety image on corresponding part of the pure noise image. The overlaying rate may vary from 0% to 100%. Afterwards corresponding to each imitated true scene image, SNR estimation can be obtained by using the LSD method, and comparing it with the SNR true value, the estimation error will be work out. Then we can easily see the effects of the LSD method under various conditions. This paper designed a scheme to validate performance of the LSD method for retrieving SNR parameter of optical sensor, and achieved the rules of SNR estimation errors of this method, which would be useful on those applications needing SNR parameter.

Cross-calibration of HJ-1B/CCD with Terra/MODIS

Lingling Ma[1], **Lei Xu**[1, 2], **Xinhong Wang**[1], **Lingli Tang**[1], **and Chuanrong Li**[1]

[1]Academy of Opto-Electronics, Chinese Academy of Sciences, Beijing 100190, China
[2]Graduate University of Chinese Academy of Sciences, Beijing 100049, China

Abstract— The radiometric performance of onboard sensor will decline with the time's going, therefore the update of calibration coefficients periodically is very important to those precise remote sensing applications. For lack of onboard calibration instrument, and for vicarious calibration is expensive, the updates of calibration coefficients to Chinese earth observing satellites are usually once a year, which is difficult to satisfy the requirements of quantitative remote sensing. With cross-calibration method, a dedicated sensor can be calibrated on a certain spectral channel to another sensor which has high accurate calibration coefficients. The advantage of cross-calibration method is more economical since radiometric stable site and simultaneous ground measurements are no longer necessary. In this paper, the visible and near-infrared spectral bands of HJ-1B/CCD were calibrated by the cross-calibration method based on the corresponding bands of EOS/MODIS. The paper addresses the cross-calibration of the visible and near-infrared CCD onboard Chinese satellite HJ-1B against corresponding channels of the MODerate resolution Imaging Spectroradiometer (MODIS) onboard satellite Terra. Two types of cross-calibration methods, including the Ray-Matching (RM) method, and the Radiative Transfer Modeling (RTM) method, were introduced in a desert region nearby the city of Dunhuang, using the HJ-1B/CCD and Terra/MODIS images acquired on August of 2009. The synchronous vicarious calibration was carried out and the calibration coefficients were calculated, which is considered to be the criterion to measure the accuracy of cross-calibration method. Results were compared between the two cross-calibration methods, RM method and RTM method, and the validity of cross-calibration was proved. Uncertainties in cross-calibration were analyzed at last, mainly including discrepancies of spatial resolution, and spectral differences between the two sensors.

A Comparison of LSD Method and SSDC Method for Estimating SNRs of Imaging Spectrometer Data

Bo Zhu, **Xinhong Wang**, **Lingling Ma**, **Lingli Tang**, **and Chuanrong Li**
Academy of Opto-Electronics, Chinese Academy of Sciences
Beijing 100190, China

Abstract— Up to now, many methods have been developed to calculate the signal-to-noise ratio (SNR) of a remote sensing image, and each method has its own applicability and precision level. Not all methods are suitable for images observed by imaging spectrometer, and more often than not different methods will derive different results of SNR even on the same imaging spectrometer data. It is necessary to estimate the applicability and precision of each method, and the estimation will help us to get more explicit and implicit information about a remote sensing image and deal with it better. Some noises are often brought into a remote sensing image when an imaging spectrometer is normally working. They will determine the level of the signal-to-noise ratio of a remote sensing image. There are two typical methods, i.e., the Local Standard Deviation (LSD) method proposed by Gao and the Spectrally and Spatially Dimensional Correlation (SSDC) method proposed by Roger et al, which are often used when people want to know the SNR of each band in an imaging spectrometer data. This paper will estimate the convenience, computing speed, applicability and precision of these two methods in virtue of simulated and measured images. Through calculating the SNRs of a simulated uniform image added by different types of simulated noise, the precision of each method can be estimated, for the real values of SNR of the simulated images are known. Do the SNR calculation on the measured images similarly, in that the measured images are more complex and more helpful to show applicability, precision and other attributes of various methods. By comparison and analysis between the two methods, it is known that the SSDC method in which some little flaws exist, only fit for hyperspectral image but can not be applied to panchromatic image. It has a fairly good computing speed and usually induces high numerical SNR values of the bands in an hyperspectral image. The LSD method, however, fits for not only panchromatic image and multispectral image, but also hyperspectral image. It has a faster computing speed, and when the scene of the image is homogeneous it will also get a good SNR estimation. If the scene is rather heterogeneous, the results of LSD method will be worse to some extent. So the stability of SSDC is better than that of LSD. In general, the LSD method and the SSDC method each has its own virtues and restrictions.

Possible Abnormal Phenomenon of the Atmospheric Water Vapor before Hengchun Earthquake

Yuntao Ma[1, 3], **Yiyang Zhao**[1], **Shanjun Liu**[1], **and Lixin Wu**[1, 2]

[1]Institute for Geoinformatics & Digital Mine Research, Northeastern University
Shenyang 110004, China
[2]Academe of Disaster Reduction and Emergency Management, Beijing Normal University
Beijing 100875, China
[3]School of Civil Engineering, Shenyang Jianzhu University, Shenyang 110168, China

Abstract— Earthquake is the major natural disaster that human beings are facing. The complexity of the earthquake pregnancy remains the earthquake prediction a unresolved problem. Low density of observation stations and small coverage of observation do not provide the necessary information for earthquake predictions. But satellite space monitoring techniques, which have such advantages as wide coverage, rich information, dynamic and high resolution, can provide more comprehensive seismic precursor information. There have been many studies and achievements on satellite thermal infrared, cloud, geoelectricity, gravity and magnetism abnormities before earthquakes, yet there has been little concern about the atmospheric water vapor abnormity before earthquakes.

A M7.2 earthquake (21.9°N, 120.6°E) occurred in Hengchun of Taiwan at 12 : 26 hrs on December 26, 2006 (UTC). Another M6.7 earthquake occurred after eight minutes at the same region. In this paper we analyzed the atmospheric water vapor anomaly before Hengchun earthquake by use of the MOSIS satellite data. The information of the atmospheric water vapor was extracted out by two channels of MODIS, 2nd and 19th bands. It was converted into the color maps of the water vapor content by the density slice. We analyzed space-time evolution of the atmospheric water vapor around the epicenter before Hengchun earthquake through the combination of manual interpretation, mathematical statistics. The analytical results show: In the non-seismic period, the water vapor content in the South China Sea was mostly about $2\,\mathrm{g/cm^2}$. However, the water vapor content was far less than $2\,\mathrm{g/cm^2}$ several days before Hengchun earthquake, even reached minimum value of $0.801\,\mathrm{g/cm^2}$ on December 17, 2006. The phenomenon of low-value water vapor content lasted from December 17th to 29th, 2006. Farther mathematical statistic also show similar results.

The study results indicated that there was possible water vapor anomaly to appear before Hengchun earthquake, but further studies are still needed to conduct.

The Time-space Relationship between Strain, Temperature and Acoustic Emission of Loaded Rock

Yingwei Shi[1], **Qun He**[1], **Shanjun Liu**[1], **and Lixin Wu**[1, 2]

[1]Institute for Geo-informatics & Digital Mine Research, Northeastern University, Shenyang 110004, China
[2]Academe of Disaster Reduction and Emergency Management, Beijing Normal University
Beijing 100875, China

Abstract— The tectonic activity and rock fracture will cause many physical phenomena, including strain, temperature change and acoustic emission (AE). In theory these physical variables exist determinate relationships because they are the results of stress activity of curst. How to obtain the relationship between them is the key to monitor the tectonic activity and rock cataclysm (including geological disasters, earthquake and mine disasters and so on) by use of remote sensing technology.

In this paper the tortuously non-connected fault and the hole-rock samples were loaded to simulate the tectonic activity and rock engineering failure in the real world. In the process of loading, an infrared thermal imager was used to detect the temperature field change of the loaded models, and a digital CCD camera and the digital speckle correlation method (DSCM) were used to collect and analyze images to obtain the evolution processes of displacement and strain fields. Meanwhile, an AE instrument was used to obtain the data of acoustic emission, and the AE field change were also simulated with RFPA software. Some experimental results were found: there are two kinds of thermal effects control the temperature field change pattern in the loading process, thermoelastic effect and frictional-heat effect. They have different features at the different loading stages; high strain, high temperature and strong AE signals appear simultaneously in the same area. The three physical fields existed nice relationship between them.

The research was beneficial to early warning of tectonic activity and the monitoring of rock fracturing.

Session 1P2
Electromagnetic Modeling, Inversion, and Applications 2

Modelling the Effect of a Defect on Crosstalk Signals under the Weak Coupling Assumption

M. Franchet, **M. Olivas**, **N. Ravot**, **and L. Sommervogel**
Embedded Systems Reliability Laboratory, CEA, LIST
Point Courrier 94, Gif-sur-Yvette, F-91191, France

Abstract— Nowadays automotive electronic systems rely on intricate wire networks. The reliability of the system depends on the health and the quality of the cables used for communication or power supply. It is all the more important to monitor and predict the network's state as a simple defect, such as short or open circuit on a wire can have heavy consequences such as failure breakdown.

Most of the time it is implicitly assumed that only the wire, where the fault is located, is sensitive to it. One method commonly used to locate this defect is called Time Domain Reflectometry (TDR). It is based on the injection of probe signal(s) into the wire network and the analysis of the reflected signals at the injection point. This method can be extended to on line diagnosis thanks to SSTDR [1]. However the presence of such a fault on a wire can also have an impact on the neighbouring wires and can significantly change crosstalk signals. As a consequence it can disrupt the performances of the other wires. In order to quantify the level of this deterioration, the impact of a defect on induced signals needs to be well understood and modelled.

This paper proposes an analytical model for near-end voltages in the case of a three-conductor line under the weak coupling assumption. The line is supposed to be lossless, uniform and symmetric. We will consider the case where a defect is located on the generator circuit (where the probe signal is injected) and focus on its impact on time domain signals.

In this paper, we adapt a model initially proposed by S. Bazzoli [2]. In this first reference, a theoretical model for the crosstalk voltage in the frequency domain is developed in the case of a three-conductor, with no defect, under the weak coupling assumption. In reference [3], Paul presents a similar model in the time domain, for the same configuration.

In order to illustrate this work and point out the accuracy of the model, a comparison will be made between the proposed model and the computed results obtained with CST Microwave Studio.

REFERENCES

1. Lelong, A., M. Olivas, V. Degardin, and M. Lienard, "On line wiring diagnosis by modified spread spectrum time domain reflectometry," *PIERS Proceedings*, 182–186, Cambridge, USA, July 2–6, 2008.
2. Bazzoli, S., "Caractérisation et simulation de la susceptibilité des circuits intégrés face aux risques d'inductions engendrés par des micro-ondes de forte puissance," Ph.D. thesis, Université des Sciences et Technologie de Lille, 2005.
3. Paul, C. R., "Solution of the transmission-line equations under the weak-coupling assumption," *IEEE Transactions on Electromagnetic Compatibility*, Vol. 44, No. 3, 413–423, August 2002.

A Theoretical Study of Transition Probabilities for Rare Gas Atoms in an Alternating Electric Field

E. V. Koryukina
Tomsk State University, Lenin avenue 36, Tomsk 634050, Russia

Abstract— In this work, the influence of an external electric field on the behavior of transition probabilities between energy levels was investigated, and dependences of these characteristics on frequency and strength of the electric field were obtained. Rare gas atoms under the effect of the circular polarized electric field (electric fields of such polarization are generated in a high-frequency discharge and under laser excitation) were chosen as subjects for study. Rare gases are widely used in plasma physics, therefore, this problem is topical both from a theoretical point of view and for practical applications of the calculation results.

In the circular polarized electric field, the non-stationary Schrödinger equation, the energies and wave functions of atoms in the electric field are determined from, can be reduced to the stationary one. In traditional works, the stationary Schrödinger equation is solved in the framework of perturbation theory. However, it is much more convenient to solve this equation by the method of the energy matrix diagonalization [1]. This method, free from limitations inherent in perturbation theory, is suitable for a wide range of frequency and strength of the electric field. The wave functions and energies of atoms in the electric field obtained from the energy matrix diagonalization are used for calculating the transition probabilities between the Stark levels. According to [1], the probabilities of the $JM \to J'M'$ transitions are calculated using the formula

$$A(JM \to J'M') = \frac{4\omega^3_{JM,J'M'}}{3\hbar c^3}|D_{JM,J'M'}|^2,$$

$$|D_{JM,J'M'}|^2 = \sum_q \left| \sum_{ij} C_i^{(JM)*} C_j^{(J'M')} (-1)^{J_i - M_i} \begin{pmatrix} J_i & 1 & J_j \\ -M_i & q & M_j \end{pmatrix} \cdot \langle \gamma_i J_i \| D \| \gamma_j J_j \rangle \right|^2,$$

where $C_i^{(JM)}$ and $C_j^{(J'M')}$ are the expansion coefficients of the wave functions for an atom in the electric field in terms of the unperturbed wave functions. Suggested theoretical approach was realized in a special software package written in FORTRAN.

Based on the calculation results, a number of regularities was revealed in the behavior of the transition probabilities under a change in the frequency and strength of the electric field. It was shown that for the transitions with $J, J' \leq 1$ the behavior of spectral lines and transition probabilities essentially depends on the core type (for the Ne, Ar, and Kr atoms). At $J, J' > 1$, the interaction of atomic energy levels in the electric field plays a key role in the behavior of transition probabilities. This interaction leads to anomalies in the emission spectra and unequiprobable filling of atomic levels. Moreover, it was found that the transition probabilities have a polynomial dependence on the electric field strength, and the higher the electric field frequency is, the bigger the polynomial degree is.

The obtained theoretical results allow us to explain the processes taking place in plasma, clarify the mechanism of filling of the excited levels and reasons for changes in spectral line intensities. The transition probabilities can be used as input data for calculations of lifetimes, spectral line intensities, and for solution of the population density balance equations. In addition, the calculation results are very useful for plasma diagnostics. And, finally, the revealed regularities can be used for construction of new devices.

REFERENCES

1. Koryukina, E. V., "Modelling of the dynamic stark effect and calculation of the transition probabilities for an Ar atom," *J. Phys. D: Appl. Phys.*, Vol. 38, 3296–3303, 2005.

Influence of Carbon Coatings on the Breakdown Threshold for an S-band Pillbox Output Window

Fang Zhu, **Zhaochuan Zhang**, **and Jirun Luo**
R & D Center for High Power Microwave Device, Institute of Electronics
Chinese Academy of Sciences, Beijing 100190, China

Abstract— An S-band klystron with average output power of larger than 50 kW has been developed in the Institute of Electronics, Chinese Academy of Sciences (IECAS). The research process showed that the RF output window of the klystron was frequently cracked in the center of its ceramic disk when the RF output average power was less than 50 kW, and the crackle was always along the diameter of the disk on the H-plane, and there were two fawn elliptic spots on both side of the crackle on the vacuum side of the disk. The cracked disks were sampled and analyzed, the results demonstrated that the elliptic spots belong to organic matter pollution, and the ingredient of the organic matter is mainly carbon, whose thickness is in the range of nanometers. In addition, the thicker the thickness, the lower the average RF power cracking the window. In order to find the reason of the window breakdown, the electromagnetic field distribution in the window had been calculated with MAFIA code. The simulations suggested that the longitudinal electric field component of the resonant mode TM_{11} in the pillbox is distributed in two symmetrical elliptic areas on the transverse section of the disk, similar to the two fawn elliptic spots, besides the direction of the maximum electric field of the TE_{11} cylindrical guide mode is in good agreement with that of the crackle appearing on the disk. So the longitudinal electric field of the TM_{11} mode may be the reason that the organic matter is deposited on the surface of the disk. After a new window structure design is used for decreasing the effect of TM_{11} mode and vacuum baking system is improved for decreasing organic matter pollution, the klystron can stably operate with the average power of larger than 50 kW without breakdown.

Adaptive Finite Element Methods for Time-dependent and Time-harmonic Eddy Current Problems

Weiying Zheng
Academy of Mathematics and System Sciences, Chinese Academy of Sciences, China

Abstract— In this talk, I will talk about adaptive finite element computations for both time-dependent and time-harmonic eddy current problems with multiply-connected conductors. Fully discrete schemes are developed for the time-dependent problem and reliable and efficient a posteriori error estimates are derived in terms of time and spatial errors. We also obtained the a posteriori error estimates for the time-harmonic problem. The competitive performances of the time-domain method and the frequency-domain method are demonstrated by an engineering benchmark problem, Team Workshop Problem 7. Our numerical results agree very well with the experimental data.

Resistance to Earth of Grounding Grids in Tow-layer Soil Structure Using FEM and GA

P. Hajebi, **A. A. Heidari**, **and A. Mirzaei**
Electrical and Computer Engineering Department, Yazd University, Yazd, Iran

Abstract— Numerical Methods such as finite element method (FEM) are the most accurate methods for computing of grounding grids resistance. Generally, these methods are complex and time consuming. Therefore, simple expressions have been proposed for estimating the earthing grids resistance. In [1], resistance to earth of grounding grids in two-layer soil has been expressed as:

$$R(\rho_1, \rho_2) = C_{2/1} R(\rho_1) \tag{1}$$

where $R(\rho_1)$ represents the resistance to earth of the grid in uniform soil with the soil resistivity equal to the top layer resistivity and $C_{2/1}$ is the correction factor incorporating the effect of the actual tow-layer soil. Under assumption that the earthing grid is in the top layer, the following expression has been suggested for $C_{2/1}$:

$$C_{2/1} = \left(\frac{\rho_2}{\rho_1}\right)^x \text{ where : } x = a_1 \log_{10}\left[a_2 N \left(\frac{A}{A_0}\right)^{\frac{1}{2}} \left(\frac{h_0}{h}\right)^2\right] \quad \text{for } \rho_2/\rho_1 < 1 \tag{2}$$

$$x = b_1 \log_{10}\left[b_2 N \left(\frac{A}{A_0}\right)^{\frac{1}{2}}\right] - b_3 \log_{10}\left(\frac{h}{h_0}\right) \log_{10}\left[b_4 \left(\frac{A_0}{A}\right)^{\frac{1}{2}}\right] \quad \text{for } \rho_2/\rho_1 > 1$$

h is the thickness of the top layer, $A_0 = 1\,\mathrm{m}^2$ and $h_0 = 1\,\mathrm{m}$. The parameters in these equations are:

$$a_1 = 0.14,\ a_2 = 44,\ b_1 = 0.12,\ b_2 = 3160, b_3 = 0.2,\ b_4 = 1000 \qquad \text{P.1}$$

In this paper, these parameters are optimized using the FEM results and genetic algorithm (GA) in order to increase the accuracy of the above expression. Considering results of different experiments for different grounding grids in two-layer soil (in terms of width, length, soil resistivity of layers and depth of top layer soil), the optimized parameters are obtained using the FEM. Objective function of GA is: $F_g = \sum_{i=1}^{N} \frac{|C^i_{FEM} - C^i_C|}{C^i_{FEM}}$, where $C^i_{FEM}$is the ith measurement of correction factor for tow-layer grounding grid resistance using FEM and C^i_C is the Computed value of correction factor for the same grid by GA. The optimized parameters were obtained as:

$$a_1 = 0.25148,\ a_2 = 3.335,\ b_1 = 0.12369,\ b_2 = 9975.5,\ b_3 = 0.32395,\ b_4 = 1937.2 \qquad \text{P.2}$$

Table 1 shows the objective function values for different parameters. For investigating accuracy

Table 1: Objective function values.

F_g (Objective Function)	P.1	P.2
$\rho_2 > \rho_1$	3.3645	1.3876
$\rho_2 < \rho_1$	0.9405	0.7425

of the proposed method, the obtained results using P.1 and P.2 parameters are compared with the FEM results for various types of grounding grids. Simulation results show that more accurate results are obtained using the optimized parameters P.2 than P.1.

REFERENCES

1. Nahman, J. and V. Djordjevic, "Resistance to earth of substation earth electrodes in uniform and two layer-soils," *Electrical Eng.*, Vol. 80, No. 5, 337–342, Springer, 1997.

Analysis for the Stability of Hughes-type Coupled Cavity in an Extended-interaction Klystron

Jian Cui, **Ji Run Luo**, **Min Zhu**, **and Wei Guo**
Institute of Electronics, Chinese Academy of Sciences, Beijing 100190, China

Abstract— Extended-interaction klystron (EIK) is invented to achieve a large power, wide frequency bandwidth and high gain in the millimeter/sub-millimeter wave length range. Multi-gap coupled cavity in it is a key technique for enhancing the gain-bandwidth product and power capability. However, the modes causing parasitical oscillation may increase and is difficult to suppress with the increase of the coupled cavity numbers. In this article, the analytical expressions for the beam-wave coupling coefficients and the beam-loaded conductance of the coupled cavity with n gaps in the EIK are derived based on the space-charge wave theory. The stability of the circuit was discussed through calculating the quality factor of the multi-gap coupled cavity. The multi-gap coupled cavity can be considered as a shorted slow wave circuit at its two ends, the interaction of the beam with wave depends on the difference between the longitudinal velocity of the beam and the wave phase velocity in the circuit. The difference will directly affect the variation of the beam-wave coupling coefficients and the beam-loaded conductance. The variation will become more acute with the increase of the gap numbers. When the increase of the maximum absolute value of the beam-loaded conductance makes that the overall loaded quality factor of the coupled cavity becomes infinite, the unstable oscillation will occur. Because the velocity of the beam depends on the beam voltage and the phase velocity of the wave is mainly relative to the spacing between the adjacent gaps, the stability of the multi-gap coupled cavity is very sensitive to the beam voltage and the spacing between the adjacent gaps with the increase of the gap number n. There are n cavity modes and n-1 slot modes in the n-gap coupled cavity. The instability of each mode can be judged by calculation of the loaded quality factor with the combination of the electromagnetic field around the gaps, the beam-wave coupling coefficients and the beam-loaded conductance.

Experimental Study on the Microwave Monitoring of Rock Stress and Fracture

Zhongyin Xu[1], **Shanjun Liu**[1], **Lixin Wu**[1, 2], **and Zhe Feng**[1]

[1]Institute for Geo-informatics & Digital Mine Research, Northeastern University, Shenyang, China
[2]Academe of Disaster Reduction and Emergency Management, Beijing Normal University
Beijing, China

Abstract— Recent years many authors reported thermal anomaly change around epicenter before earthquake. Some researchers tried to predict the earthquake based on the analysis on the temperature anomaly feature by using satellite thermal infrared data. However the infrared radiation can not pass through the thick-layer cloud, so as to hardly achieve the earthquake monitoring. Microwave is also a kind of thermal radiation and some scholars have found microwave radiation anomaly appearing before earthquake. To explore the feature of microwave emission anomaly before earthquake, a group of physical simulation experiments were carried out. In the experiments, a hydraulic loader (YGA-3000), whose maximum vertical load is 3000 kN, was applied as loading machine for the granite samples. A microwave radiometer was used for microwave emission detection in the loading process of rock. Its detection wavelength is 8 mm, temperature sensibility 0.01°C. The experimental results showed that microwave emission energy changed along with the change of stress. The microwave emission energy varied little in the beginning loading stage, increased in the elastic loading stage, decreased in the crack appearing stage and increased again in the fracturing stage. The average infrared radiation temperature (AIRT) increased with the increase of the load from the loading beginning to the crack appearing stage, and decrease in the fracturing stage. The AIRT had the close relationship with the load, but the brightness temperature of microwave emission had the close relationship with the AE energy. Both AIRT and brightness temperature of microwave emission exist the precursors of rock failure, but the microwave emission precursor for rock failure is more obvious than the AIRT precursor. These experiment results indicated that it was possible to use the microwave remote sensing for monitoring the stress variation and fracturing of rock masses, including earthquakes.

Time-domain Electromagnetic Surveying: 3D Modeling and Interpretation

Chow-Son Chen[1], **Ganquan Xie**[2], **and Jianhua Li**[2]

[1]Institute of Geophysics, National Central University, Taiwan
[2]GL Geophysical Laboratory, USA

Abstract— The idea of using time-domain electromagnetic measurements (TEM) in geophysics is that signals are measured in the absence of the primary field. A studying survey using three component TEM receiver was undertaken at a test site of buried waste, in particular, detection and location of underground metallic objects. This case TEM survey revealed the existence of anomalous zones in the analyzed region. Outcrops in some of the selected areas confirmed that the anomalies were generated by underground conducting material. Modeling of the data using the program PLATE (Dyck et al., 1980), which gives first approximation of a theoretical plate-style buried conductor in air. It is apparent that the *Hz* data, which displays only uni-polar, positive anomalies, are usually the strongest, cleanest data, and provide the best indication of target location, while *Hx* and *Hy* data are by nature weaker, but can be used to determine direction to off-line 3D targets. Results from the three component data are unambiguous as to the location and orientation of conductors. Measuring adding of the horizontal components of the secondary magnetic field leads to more confidence in the interpretation of azimuth, orientation and size of the conductor. Although this was a metal detection survey, it was particularly useful to the characterization of the layered subsoil.

Analysis of Saturation Effects on the Operation of Magnetic-controlled Switcher Type FCL

Faramarz Faghihi and Homa Arab
Young Researchers Club, Islamic Azad University South Tehran Branch, Iran

Abstract— With the extensive application of electrical power system, suppression of fault current limiter is an important subject that guarantees system security. The superconducting fault current limiters (SFCL) have been expected as a possible type of power apparatus to reduce the fault current in the power system. The results shown that under normal state, the FCL has no obvious effect on the power system; under fault state, the current limiting inductance connected in the bias current will be inserted into the fault circuit to limit the fault current. By regulating the bias current, the FCL voltage loss under normal state and the fault current can be adjusted to prescribed level. This kind of SFCL used the nonlinear permeability of the magnetic core for create a sufficient impedance and the transient performance considering the magnetic saturation is analyzed by Preisach model. Preisach model that intrinsically satisfies nonlinear properties is used as the numerical method for analysis of saturation effects. It is able to identification isotropic and no isotropic behaviour. The main idea is to compute the magnetization vector in two steps independently, amplitude and phase. The described model yield results in qualitative agreement with the experimental results.

Modeling and Analysis of Magnetostatic Field Disturbed by an Elliptic Cavity

Xiaoqing Jin, **Qian Wang**, **and Leon M. Keer**
Center for Surface Engineering and Tribology, Department of Mechanical Engineering
Northwestern University, Evanston, IL 60208, USA

Abstract— Electromagnetic loading can significantly influence the fracture behavior in a cracked conductor. The present study considers the distribution of the electromagnetic fields in an infinitely extended iron-free conductive plate, which contains an elliptic hole and is subjected to remote electric current of uniform density. The analytical solution to the steady current field is obtained in the elliptical coordinates. The concentration effect of the current density at the vertices of the elliptic hole is examined. To investigate the perturbation of the magnetic field resulting from the disturbed electric current, a two dimensional (2D) model by employing certain simplified assumptions is attempted, where the governing Maxwell's equations are able to be solved in closed-form. In view of the linearity of the problem, a three dimensional (3D) computational method is proposed by superposing a hierarchy of rectangular parallelepiped elements. To improve the efficiency of the 3D calculation, an adaptive mesh refinement algorithm is implemented in the numerical discretization. Finally, through a comparative study, the validity of the introduced simplifications in the 2D analysis is benchmarked with the 3D computational results. The present study shows that the 2D solution predicts the upper bound for the out-of-plane component of the magnetic field perturbed by the elliptical hole. When the thickness of the plate is about one order of magnitude larger than the major axis of the elliptical hole, the disturbance of the in-plane magnetic components is negligible.

Session 1P3
Vectorial Properties and Physical Effects of Finite Light Beams and Their Applications in Optical Trapping and Manipulation

Optically Coherent Manipulation of Spin Dynamics in CdTe Crystal at Room Temperature

Hong Ma[1], **Zuanming Jin**[1], **Guohong Ma**[1], **Weiming Liu**[2], **and Sing Hai Tang**[2]

[1]Department of Physics, Shanghai University, 99 Shangda Road, Shanghai 200444, China
[2]Department of Physics, National University of Singapore, Singapore 117542, Singapore

Abstract— In the last few decades spin dynamics down to subpicosecond time domain in semiconductors and semiconductor nanostructures have attracted intense interest because of the potential applications in emerging areas such as "spintronics" and quantum information processing. The popular method studying spin dynamics is the time resolved pump probe reflectivity (TRPPR) technique, which has proved to be one of the simple and powerful means to study the dynamical behavior of carriers in semiconductor, especially in thick and nontransparent samples such as GaAs, CdTe.

In this study, carrier density and photon energy dependence of electron spin relaxation in CdTe crystal were investigated by femtosecond TRPPR technique at room temperature. With photon energy increases from 1.48 to 1.51 eV, the spin relaxation time continuously decrease from 7.78 to 3.08 ps. By varying carrier density, it is found that the spin relaxation time increases initially, reaching a maximum value of $\sim$7 ps at carrier density of $3 \times 10^{11}\,\mathrm{cm}^{-2}$, then it shows continuously decrease with carrier density. These results reveal that both D'yakonov-Perel (DP) and Elliot-Yafet (EY) mechanisms take equal important role for spin relaxation in CdTe crystal at room temperature. This conclusion is also supported by the fact that the measured spin relaxation time is 4-fold smaller than the theoretical prediction based on DP mechanism. The opposite dependences on momentum relaxation time τ_p of EY and DP mechanism makes the spin relaxation tendency of theory coincide with that of the experimental data.

REFERENCES

1. Sabbah, A. J. and D. M. Riffe, "Femtosecond pump-probe reflectivity study of silicon carrier dynamics," *Phys. Rev. B*, Vol. 66, 165217, 2002.
2. Hall, K. C., S. W. Leonard, H. M. van Driel, A. R. Kost, E. Selvig, and D. H. Chow, "Subpicosecond spin relaxation in GaAsSb multiple quantum wells," *Appl. Phys. Lett.*, Vol. 75, 3665, 1999.
3. Tackeuchi, A., H. Otake, Y. Ogawa, T. Ushiyama, T. Fujita, F. Takano, and H. Akinaga, "Nanosecond excitonic spin relaxation in cubic GaN," *Appl. Phys. Lett.*, Vol. 88, 162114, 2006.
4. Kikkawa, J. M. and D. D. Awschalom, "Resonant spin amplification in n-type GaAs," *Phys. Rev. Lett.*, Vol. 80, 4313, 1998.
5. Lai, T., X. Liu, H. Xu, Z. Jiao, J. Wen, and W. Lin, "Temperature dependence of electron-spin coherence in intrinsic bulk GaAs," *Appl. Phys. Lett.*, Vol. 88, 192106, 2006.

Radiation Force of a Focused Stochastic Electromagnetic Beam

Chengliang Zhao and Yangjian Cai
School of Physical Science and Technology, Soochow University, Suzhou 215006, China

Abstract— Propagation of a stochastic electromagnetic Gaussian Schell-model beam through a focusing optical system is formulated. Radiation force of a focused stochastic electromagnetic GSM beam on a Rayleigh dielectric sphere is investigated. It is found that the radiation force of a stochastic electromagnetic GSM beam is closely related to its twist phase, degree of polarization and correlation factors. The trapping stability is also discussed. By raising the absolute value of the twist factor it is possible to increase both transverse and longitudinal trapping ranges at the focus.

Radiation Forces for Cosine-Gaussian Beams on a Rayleigh Particle

Yunfeng Jiang and Xuanhui Lu
Department of Physics, Zhejiang University, Hangzhou 310027, China

Abstract— The radiation forces of highly focused cosine-Gaussian beams on a particle in Rayleigh scattering regime is theoretically investigated in this paper. The cosine-Gaussian beams with the parameter $\alpha = 2.7$ has been studied in trapping Rayleigh particles. The distribution in the whole space of the gradient force and the scattering force exerted on the particle is obtained in the research, which shows that it is feasible to utilize cosine-Gaussian beams in optical trapping system. Besides, with this special beam, the optical trap could attain a good stability as well. Above all, this special beam could simultaneously trap the particles whose refractive index is lower or larger than the ambient. So it is possible that the cosine-Gaussian beams will be widely used in the optical tweezers or the other physical and biological field. For this beam is unable to manipulate the particles longitudinal, we could use three orthotropic beams to form a three-dimensional potential well if needed.

Energy Flux Method for Goos-Hänchen Shift in Frustrated Total Internal Reflection and Its Applications

Xi Chen[1, 2], **Tao Duan**[3], **and Chun-Fang Li**[1]

[1]Department of Physics, Shanghai University, Shanghai 200444, China
[2]Departamento de Química-Física, UPV-EHU, Apdo 644, Bilbao 48080, Spain
[3]State Key Laboratory of Transient Optics and Photonics
Xi'an Institute of Optics and Precision Mechanics of CAS, Xi'an 710119, China

Abstract— It is well known that a finite light beam totally reflected from an interface between two dielectric media undergoes lateral displacement from the position predicted by geometrical optics [1]. This phenomenon is referred to as the Goos-Hänchen (GH) effect. The investigations of the GH shifts have been extended to frustrated total internal reflection, partial reflection and to other areas of physics, such as acoustics, quantum mechanics, atom optics, spintronics, and graphene.

Historically, the phenomena of GH shifts are usually believed to be associated with the evanescent wave in optically thin medium, and are explained in terms of energy flux conservation [2–4], meanwhile, Artmann's stationary phase approach [5] is extensively used to calculate the GH shift, according to the reshaping effect due to the interference between each plane wave components undergoing different phase shift after the total internal reflection. Until 1983, Yasumoto and Ōishi [6] have established new energy flux method, which confirms the consistency of the predictions by the stationary phase method from the point of view of the conservation of energy. However, they only discussed the energy flux for GH shift in a single interface. As a matter of fact, recent investigations show that the energy flux is of importance in better understanding of negative or positive GH shifts [7, 8].

In this paper, we will investigate the GH shift frustrated total internal reflection based on the energy flux method. According to Yasumoto and Ōishi's method, the GH shift s_E, which is equal to the GH shift given by Artmann's stationary phase method, satisfies

$$s_E = s_R + s_I, \tag{1}$$

where s_R is the GH shift given by Rernard's energy flux method and s_I results from the interference between the incident and reflected energy fluxes. More interestingly, the interference terms s_I due to the interference between the incident and reflected beams can be applicable to the explanation of the saturation of GH shifts [9]. In addition, the relation mentioned above can also be generalized to calculate the GH shifts in frustrated total internal reflection containing absorbing or nonlinear materials.

ACKNOWLEDGMENT

This work is supported by the National Natural Science Foundation of China (Grants No. 60806041, 60907026, and 60877055), the Shanghai Rising-Star Program (Grants No. 08QA14030), the Science and Technology Commission of Shanghai Municipal (Grants No. 08JC14097), the Shanghai Educational Development Foundation (Grants No. 2007CG52), and the Shanghai Leading Academic Discipline Program (Grants No. S30105). X. C. is also supported by Juan de la Cierva Programme of Spanish MICINN.

REFERENCES

1. Goos, F. and H. Hänchen, "Ein neuer und fundamentaler versuch zur totalreflexion," *Ann. Phys.*, Vol. 1, 333, Leipzig, 1947; Vol. 5, 251, 1949.
2. Renard, R. H., *J. Opt. Soc. Am*, Vol. 54, 1190, 1964.
3. Pillon, F., H. Gilles, and S. Girard, "Experimental observation of the imbert-fedorov transverse displacement after a single total reflection," *Appl. Opt.*, Vol. 43, No. 9, 1863–1869, 2004.
4. Chen, J. J., T. M. Grzegorczyk, B. L. Wu, and J. A. Kong, "Role of evanescent waves in the positive and negative Goos-Hanchen shifts with left-handed material slabs," *J. Appl. Phys.*, Vol. 98, 094905, 2005.
5. Artmann, K. V., "Berechnung der seitenversetzung des totalreflektierten strahles," *Ann. Phys.*, Vol. 2, 87, Leipzig, 1948.

6. Yasumoto, K. and Y. Ōishi, "A new evaluation of the Goos-Hänchen shift and associated time delay," *J. Appl. Phys.*, Vol. 54, No. 5, 2170–2176, 1983.
7. Lai, H. M., C. W. Kwok, Y. W. Loo, and B. Y. Xu, "Energy-flux pattern in the Goos-Hänchen effect," *Phys. Rev. E*, Vol. 62, 7330–7339, 2000.
8. Zhang, Z.-M. and B. J. Lee, "Lateral shift in photon tunneling studied by the energy streamline method," *Opt. Express*, Vol. 14, No. 21, 9963, 2006.
9. Chen, X., C.-F. Li, R.-R. Wei, and Y. Zhang, *Phys. Rev. A*, Vol. 80, 015803, 2009.

Guided Modes in a Composite Left-handed Material Waveguide

Ying He, **Yanfang Yang**, **and Chunfang Li**
Department of Physics, Shanghai University, 99 Shangda Road, Shanghai 200444, China

Abstract— The guided modes are investigated in a four-layer slab waveguide with two composite layers made of a left-handed material (LHM) and a normal dielectric as the cores surrounded by two traditional media as the substrate and cladding. We select a system where the left-handed material layer is made of the artificial metamaterial with negative permittivity and negative permeability for the gigahertz range of frequency, and the cladding are made of normal materials differing from solid to gas. The solutions to the guided modes are obtained by the graphical method. A theory of the guided modes in the four-layer composite LHM waveguides is developed indicating that a light wave can propagate either in the LHM layer only or in both the composite layers simultaneously. The LHM core supports both oscillating guided modes and surface guided modes. The surface modes in the left-handed material propagate along the interface with their evanescent fields localized near the interface. The coupling between the modes in the LHM and in the dielectric core results in two types of fundamental modes. Mode double degeneracy appears. Some high-order modes are absent. With evanescent fields in the dielectric core the four-layer composite waveguide is reduced to a three-layer left-handed waveguide. The coupling between the modes in the RHM and LHM results in some new phenomena about the guided modes in a composite LHM waveguide. It may provide bases for applications in integrated optics as the fabrication technology of a LHM progresses.

Real-time Generation the Non-uniformly Polarized Beams with the Liquid Crystal Retarder

Yan-Fang Yang, **Kai Xu**, **Ying He**, **Xiao-Hong Han**, **and Chun-Fang Li**
Department of Physics, College of Sciences, Shanghai University, Shanghai 200444, China

Abstract— Polarization of a laser beam is one of its fundamental characteristics. The laser beams with special polarization distribution have been attracted more and more attentions for their interesting properties especially when been tightly focused. In this paper, Firstly, we obtain a radially polarized and an azimuthally polarized beam from a linear polarized Gaussian beam by using a liquid crystal polarization converter, and then make them pass through a Liquid Crystal Variable Retarder (LCVR), which can be modulated real-time by varying the applied voltage, to obtain non-uniformly elliptically polarization distribution beams. The results show the local polarization states analyzed by the Stokes parameters strongly depend on the spatial position and the phase retardation angle of the LCVR. And angular momentum of such beams is varying in different space quadrant, in which the polarization rotated direction of a radially polarized beam after passing through the LCVR is right-handed direction in the first and the third quadrants, while the polarization rotated direction is left-handed direction in the second and fourth quadrants. However, there is just opposite rotated direction for the azimuthally polarized beam after passing through the LCVR. The emphases we investigated are how to real-time modulate and generate non-uniformly polarized beams and to estimate ellipticity and polarization rotated direction at each point across the transverse section of beam in different spatial positions. The aim of this paper is to further detect the polarization states changing from point to point across transverse section of non-uniformly polarized beam in later experiment that we are putting up according to the Stokes polarization parameters.

The Electron Spin Polarization Degree Measured by Femtosecond Pump-probe Reflection Spectroscopy

Zuanming Jin, **Hong Ma**, **Guohong Ma**, **and Qibiao Zhu**
Department of Physics, Shanghai University, Shanghai 200444, China

Abstract— The electron spin-relaxation processes in direct gap bulk and low-dimensional semiconductor have attracted the attention for past three decades. The understanding of the physics of spin relaxation processes is still a very active field of research. Dependence on the optical orientation theory, we used the circular pump-probe polarization reflection spectroscopy with femtosecond resolution to measure the dynamics of electron spin polarization ($\wp(t)$), which provides a direct picture of the evolution of the two kinds of electronic spin populations in the excited state. Specifically, after the pump pulsed injection of nonequilibrium spin-polarized carriers in the conduction band, they progressively flip their spin towards a spin balanced situation. Fitting with the experiment results of the dynamics of electron spin polarization ($\wp(t)$) by theory model, we get the spin relaxation time with different carrier densities. The electron spin relaxation time increases with increasing the electron density, which suggests that the D'yakonov-Perel' mechanism dominants the electron spin relaxation in CdTe at low temperature (about 30 K).

There Does Not Exist the Paradox about the Spin of Circularly Polarized Plane Wave

Chun-Fang Li
Department of Physics, Shanghai University, Shanghai 200444, China

Abstract— A rigorous approach is put forward to separate the total angular momentum of an electromagnetic field in free space into spin and orbital AM by examining the property of its momentum density. It is shown that the momentum density splits into two parts. One does not have any contribution to the net momentum due to the transversality condition. The other produces all the momentum. The angular momentum that comes from the former part is shown to be the spin, and the angular momentum that comes from the latter part is orbital angular momentum. The spin angular momentum defined this way is applied to show that there does not exist the paradox on the spin of circularly polarized plane wave.

ACKNOWLEDGMENT

The author would like to thank Masud Mansuripur of the University of Arizona for his constructive suggestions. This work was supported in part by the National Natural Science Foundation of China (60877055 and 60806041), the Science and Technology Commission of Shanghai Municipal (08JC1409701 and 08QA14030), the Shanghai Educational Development Foundation (2007CG52), and the Shanghai Leading Academic Discipline Project (S30105).

Self-trapping of Necklace-ring Vector Beam in Nonlocal Media

Ming Shen, **Jielong Shi**, **and Chunfang Li**
Department of Physics, Shanghai University, 99 Shangda Road, Shanghai 200444, China

Abstract— We introduce the self-trapping of optical vector solitons that consist of incoherently coupled self-trapped "necklace" beams carrying zero, integer, and even fractional angular momentum in nonlocal media. We show that the nonlocality can effectively improve the stabilization of such incoherently coupled beam. Such stationary localized structures exhibit quasistable propagation for much larger distances than the corresponding scalar vortex solitons and expanding scalar necklace beams.

Formation of the Optical Spatial Comb by the Reflections and Transmissions on the Surfaces of the Weakly Active Slab

Tao Duan[1] **and Chun-Fang Li**[1, 2]

[1]State Key Laboratory of Transient Optics Technology
Xi'an Institute of Optics and Precision Mechanics, Academia Sinica
Xi'an 710119, China
[2]Department of Physics, Shanghai University, 99 Shangda Road, Shanghai 200444, China

Abstract— There are a series of diminishing discrete amplitude of the reflected and transmitted beam emerges on each side of the slab when the thickness of the slab is much beyond the restricted condition. The amplitudes are continuously divided by the surface, so the amplitude of the reflection beams diminish and become about zero quickly. The condition retains the same shape of the reflected and transmitted beam as that of the incident beam. If the plane-parallel dielectric slab is the isotropic weakly active medium and all the physical parameters, including incident angle, slab thickness and the active index of the active dielectric slab, is satisfied some conditions, the optical spatial comb that is a series discrete reflected and transmitted beams of the same amplitudes and the same spacing distance between adjacent beams emerge on each side surfaces.

The Representation of the Beams with $e^{il\phi}$ Phase Factor for Two Special Cases of the Characteristic Unit Vector

Yan Zhang[1], **Wen-Jun Zhang**[2], **and Chun-Fang Li**[3]

[1]School of Communication and Information Engineering, Shanghai University
149 Yanchang Road, Shanghai 200072, China
[2]School of Film and TV Arts Technology, Shanghai University
149 Yanchang Road, Shanghai 200072, China
[3]Department of Physics, Shanghai University, 99 Shangda Road, Shanghai 200444, China

Abstract— We present the integral transformation solutions for the beams with phase factor $e^{il\phi}$ to the Helmholtz equation and transversality condition. These beams are considered to be closely related to the orbital angular momentum of light, which have aroused much attention recent years. As the vectorial property of a finite beam can be described by a characteristic vector which determines the azimuthal angle θ_I of a fixed unit vector with respect to the wave vector, we consider two specific cases of θ_I correspond to $|\theta_I| = \frac{\pi}{2}$ and $\theta_I = 0$, respectively. When $|\theta_I| = \frac{\pi}{2}$, we have the uniformly polarized beams in the zeroth-order approximation. When $\theta_I = 0$, the case corresponds to the cylindrical vector beams under the paraxial condition. If the scalar amplitude of the plane-wave component is chosen properly, a large family of the beams with $e^{il\phi}$ phase factor can be derived and some of them are believed to be reported for the first time. Further, the influence of the generalized Jones vector and the azimuthal factor l on the vectorial structure of the cylindrical vectors beams are discussed.

Electron Spin Dynamics in Bulk InP Crystal by Pump Probe Reflectivity Spectroscopy

Hong Ma, **Zuanming Jin**, **Dong Li**, **and Guohong Ma**
Department of Physics, Shanghai University, 99 Shangda Road, Shanghai 200444, China

Abstract— In the last few decades spin dynamics in semiconductors and semiconductor nanostructures have attracted intense interest because of the potential applications in emerging areas such as "spintronics" and quantum information processing. However, most studies of spin dynamics have been carried out in GaAs compound materials at low carrier density, where the behavior of the carrier is independent of many body effects and simple to describe. In this article, electron spin dynamics was studied by time resolved pump probe reflectivity (TRPPR) technique using the same and oppositely circularly polarized 100 fs, 80 MHz pulses at 12 K in bulk InP crystal. The sign of reflectivity changes at the pump photon energy of about 1.476 eV at high carrier density. Carrier density dependence of electron spin dynamics were studied at 1.425 eV and 1.512 eV respectively. The results show that the electron spin relaxation time decreases with increasing the carrier density. These phenomena were interpreted by spin-dependent band filling effect (BF), band gap renormalization (BGR) and free carrier absorption (FCA). These effects contribute positively or negatively to the signal and changed with increasing the carrier density and photon energy. Therefore, the sign of reflectivity signal changed at certain photon energy and carrier density.

Giant Bistable Shifts in a One-dimensional Photonic Crystal Containing Indefinite Metamaterials

Wei Zhang, **Yuan-Yuan Chen**, **and Jie-Long Shi**
Department of Physics, Shanghai University, Shanghai 200444, China

Abstract— Usually, the fabricated materials, such as negative-index materials which can be constructed by thin metallic wire and metal split-ring resonators, are intrinsically anisotropic because of the orientations of the rings and rods in space. One of the anisotropic metamaterials, the so-called indefinite metamaterial (IMM), in which not all the principal components of the electric permittivity and magnetic permeability tensors have the same sign, has recently received increasing attention. The dispersion relation for such a material may be hyperbolic or elliptic, significantly different from those for left-handed materials, single negative materials, and conventional medium. In this study, nonlinear wave propagation is investigated theoretically in a one-dimensional photonic band gap structure containing indefinite metamaterials. Using the transfer matrix method and the stationary-phase method, we investigate the transmission property in such composite structure for four kinds of indefinite metamaterials in detail. It is found that there exists a typical S-shape curve of the normalized input-output intensity when the indefinite metamaterial is a cutoff, anti-cutoff or never cutoff medium. The hysteresis response between the incident light intensity and the lateral shift for the transmitted beams, resulting from the reshaping effect (constructive and destructive interferences of each plane wave components undergoing different phase shifts) is strongly dependent on the nonlinear defect, the refractive index of indefinite metamaterials, and the incident angle. All these phenomena lead to potential applications in integrated optics and optical switches.

Session 1P4
Metamaterial, Properties, and Applications

Broaden the Bandwidth of Patch Antenna by Using Inhomogeneous Metamaterial Substrate

Lei Xing, **Qian Xu**, **Jing Li**, **Zhixia Wei**, **Jun Ding**, **and Chenjiang Guo**
School of Electronic and Information, Northwestern Polytechnical University, Xi'an 710129, China

Abstract— Inhomogeneous substrate has proven to be an efficient approach to broaden the bandwidth of the patch antenna. Because of its inhomogeneity, it is very difficult to manufacture it by using ordinary materials. In this paper, we first optimize the inhomogeneity of the substrate with physical insight and then use nonresonant metamaterial elements to realize it. By tuning the geometrical parameter of the metamaterial element, the effective constitutive parameters can be controlled; the permittivity and permeability are well designed to optimize the bandwidth of the antenna. As the working frequency is far from the resonant region of the element, it is expected to exhibit stable effective constitutive parameters in a large frequency range. Our results have shown that the metamaterial substrate broadened the bandwidth of the antenna from 10.5% to 20.6% (−10 dB).

Dust Removal from Processing Plasmas by a Traveling Plasma Modulation

Yangfang Li, **H. Thomas**, **and G. Morfill**
Max-Planck-Institute for Extraterrestrial Physics, Garching 85741, Germany

Abstract— The dust particle contamination in plasma processing plays a crucial role in the quality and the yield of the products [1]. To avoid the contamination from the dust particles, a favorable way is to remove the dust particles actively from plasma reactors.

Our recent experiments in the striped electrode device showed that a traveling plasma modulation allows for a systematic particle transport independent of the reactor size [2]. Different from the normal industrial reactor, a striped electrode, which consists of 100 electrically insulated narrow strips, is introduced into the plasma chamber besides a radio frequency powered electrode. The potential profile above the segmented electrode is modulated by the voltage signals on the strips, the dust particles are trapped in the potential well and they are transported across the strips with the traveling of the potential profile.

The particle-in-cell simulations on the potential modification above the segmented electrode indicate that the traveling plasma modulation can be produced by applying on the strips either low-frequency (LF, 0.1–10 Hz) voltage signals with a fixed phase difference between two neighboring strips or high-frequency (HF, 10 kHz–100 MHz) signals with the amplitudes modulated by a low-frequency envelope (See Figure 1). The case by using LF signals has been verified experimentally and the removal efficiency of dust particles is controllable by adjusting the amplitude, frequency, phase shift, and as well waveform of the applied LF signals on the strips. The experiment by using the HF modulation on the strips is in preparing which should be more applicable to the industrial reactor since the modulation signal must be capable to penetrate the processing wafer placed above the electrode.

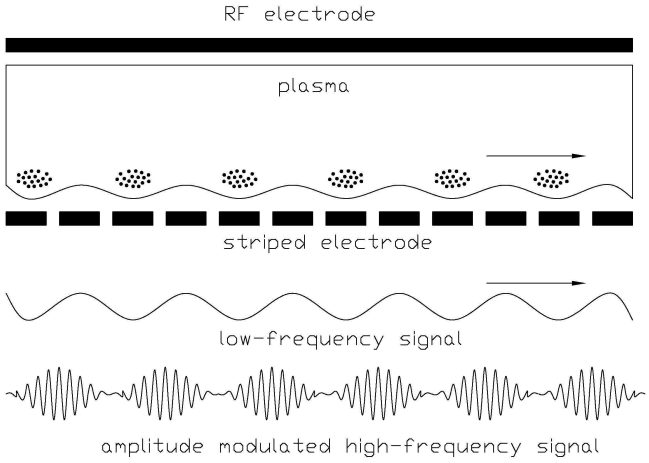

Figure 1: The physical mechanism of dust transport is sketched for the striped electrode device.

REFERENCES

1. Bouchoule, A., ed., *Dusty Plasmas: Physics, Chemistry and Technological Impacts in Plasma Processing*, J. Wiley & Sons, 1999.
2. Li, Y.-F., U. Konopka, K. Jiang, T. Shimizu, H. Höfner, H. M. Thomas, and G. E. Morfill, "Removing dust particles from a large area discharge," *Appl. Phys. Lett.*, Vol. 94, 081502, 2009.

Application of Periodic Structure on the Isolation and Suppression for Notebook Multi-antennas Coupling

Han-Nien Lin, **Ching-Hsien Lin**, **Chun-Chi Tang**, **and Ming-Cheng Chang**
Department of Communications Engineering, Feng-Chia University
100 Wen-Hua Rd., Taichung 40724, Taiwan, R.O.C.

Abstract— Due to the increasing add-on functions demand for consumer electronics, currently multi-radios, such as WLAN, WWAN, GPS, Bluetooth, and even DVB-H modules, have all been crowdedly embedded and highly integrated in a tiny space of wireless communications platform. Nowaday notebook computers or PDA phones usually have been equipped with more than one antennas, the purpose is to fit for different communication system such as Cellular mobile communications, wireless local area networking, and personal area networking. Under this situation, the performance of various kinds of wireless communications is usually degraded by the mutual coupling and interference of closely arranged antennas inside the mobile device. Since the RF modules co-existence has become a critical design problem for wireless communications, the isolation technique has gained increasing attention recently. We will investigate the coupling effect between 2.4 GHz antennas not only because Bluetooth and 802.11b/g WiFi share the same frequency band, but they also have been widely adopted for ubiquitous wireless networking, wireless headphone, wireless mouse, and wireless keyboard. Since the isolation requirement is relatively stringent for both WiFi and Bluetooth concurrent operation, therefore we will in this paper investigate the coupling of Bluetooth and 802.11b/g WiFi antennas placed inside the prototype mold of notebook computer. Then, we will utilize the distance, orientations between antenna, and application of periodic structure to provide the isolation between antennas and resolve the problem of mutual interference.

Directivity Enhancement of Line Source by Parabolic Cylinder Made of Left-handed Metamaterials

Da-Yong Zou, **Rui-Xin Wu**, **Min Liu**, **and Ping Chen**
Department of Electronic Sciences and Engineering
Nanjing University, Nanjing 210093, China

Abstract— We have studied radiation of a line source within a parabolic cylinder made of left-handed metamaterials. The parabolic cylinder is ended with a semicircle and the line source is located at the focus of the parabola. Fig. 1 gives a schematic view of the cross section of the cylinder. We calculate far field radiation patterns of a line source and find that the metamaterials parabolic cylinder can greatly enhance the directivity of the line source radiation. Fig. 2 shows the far field radiation patterns of a line source when the feature length OO_1 of the parabola is $5\lambda_0$ and the focus length p is $1.25\lambda_0$. We also studied the effect of the focal length p and the feature length OO_1 of the parabolic cylinder on the directivity of the line source. We found that the directivity increased with the increase of focal length and the feature length of the parabolic cylinder. Finally, in order to suppress the back slob and improve the directivity of a line source, we use a metallic circular arc to connect the parabolic end instead of a metametarials semicircle. The center of the metallic circular arc is located at the focus F of the parabola. The metallic arc reflects the ray on it to the focus point of parabola, and reradiated. So, the directivity is enhanced further and the back slob is suppressed. The new ending of the parabolic cylinder not only improves the overall radiation pattern but also reduces the whole size of the parabolic cylinder. The metamaterials parabolic cylinder may be used to design antennas with high directivity.

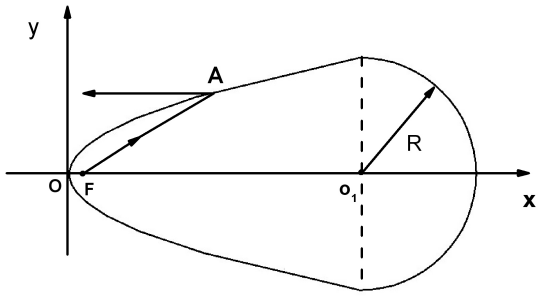

Figure 1: Schematic diagram of a line source within a parabolic cylinder of left-handed metamaterials.

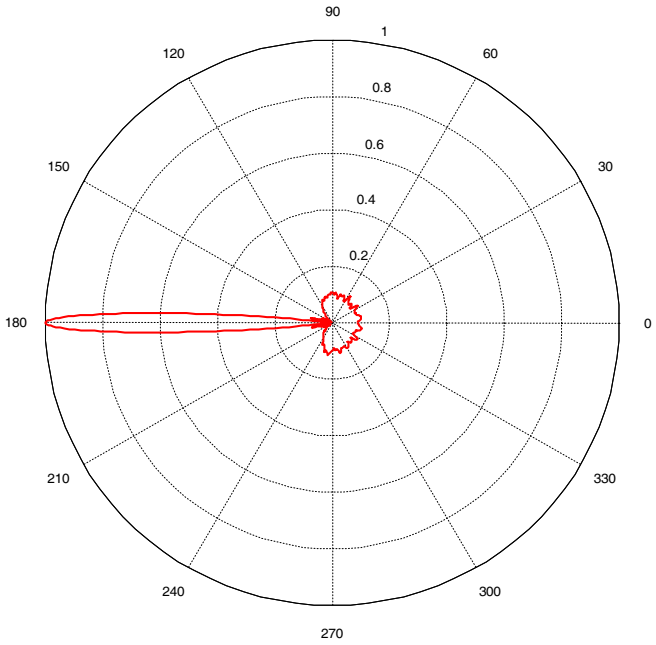

Figure 2: Normalized field radiation pattern of the line source when the feature length OO_1 of the parabola is $5\lambda_0$ and the focus length p is $1.25\lambda_0$.

Dynamical Green's Function Theory to Study the Optical Phenomena Related to Metamaterials

Weihua Wang, Xueqin Huang, and Lei Zhou
Surface Physics Laboratory (State Key Laboratory) and Physics Department, Fudan University
Shanghai 200433, China

Abstract— We combine a space-time Lorentz transformation with a dyadic Green's function technique to establish a general and rigorous dynamical theory, which can be employed to study the optical phenomena occurring in a moving environment. As the applications of this method, we studied the Doppler effects of a source moving near a metamaterial slab and the super imaging effect achieved by a moving metamaterial lens. Many interesting anomalous phenomena were discovered, induced typically by the interplays between the source and the surface waves of the metamaterial slab. For example, the figure on the left depicts the frequency spectrum of a radiating source measured by a receiver, with both the source and receiver moving on a metamaterial surface. The figure on the right compares the super imaging effects of a static lens and a moving lens. All of these intriguing phenomena can be interpreted with the dispersion of surface waves on the metamaterial and the spectra of the moving source.

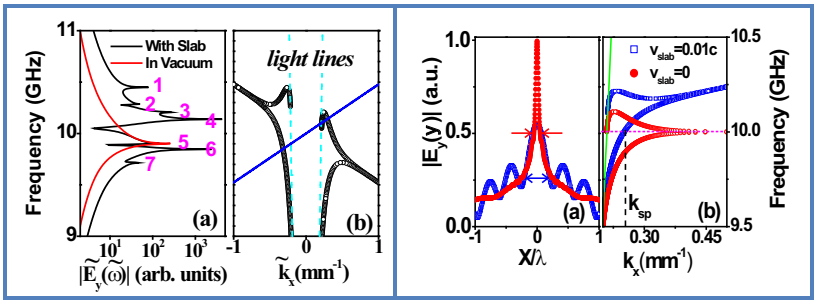

REFERENCES

1. Wang, W., X. Huang, and L. Zhou, "Photonics and nanostructures: fundamentals and applications," submitted.
2. Wang, W., X. Huang, L. Zhou, and C. T. Chan, *Opt. Lett.*, Vol. 33, 369, 2008.

Resonance and Anomalous High Transmission through Metallic Mesh Structures

Zhengyong Song, Qiong He, and Lei Zhou
Surface Physics Laboratory (State Key Laboratory) and Department of Physics
Fudan University, Shanghai 200433, China

Abstract— It is well know that metallic meshes with subwavelength hole size are opaque for electromagnetic waves, since the EM wave solutions are intrinsically evanescent inside such media. However, we recently found that EM waves of a particular polarization can perfectly transmit through an appropriately arranged stacking of metal mesh structures, although each individual metallic mesh is opaque for EM waves. We demonstrate that such unusual high transparencies are induced by an EM resonance generated in a specifically arranged metallic mesh structure, with governing mechanism different from previous established ones, such as the surface-plasmon and Fabry-Perot resonance induced transparencies [1, 2]. We performed microwave experiments to realize such an anomalous phenomenon, and discussed the potential applications of the discovered effect.

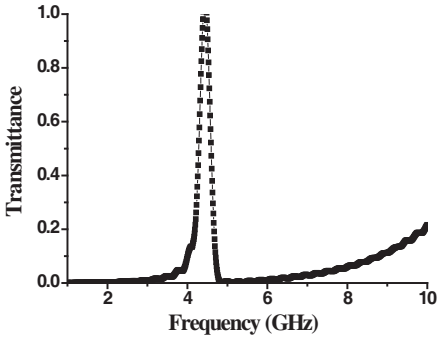

Figure 1.

REFERENCES

1. Ebbesen, T. W., H. J. Lezec, H. F. Ghaemi, T. Thio, and P. A. Wolff, *Nature*, Vol. 391, 667, London, 1998.
2. Porto, J. A., F. J. García-Vidal, and J. B. Pendry, *Physical Review Letters*, Vol. 83, 2845, 1999.

Tight Binding Studies of the Coupling Effects in Metamaterials

Hao Xu, **Qiong He**, **Shiyi Xiao**, **Jiaming Hao**, **and Lei Zhou**
Surface Physics Laboratory (State Key Laboratory), Department of Physics
Fudan University, Shanghai 200433, China

Abstract— We employ a tight binding method (TBM) [1] to explore the underlying physics behind the unusual transparency in metamaterial-loaded waveguides [2]. Adopting appropriate hopping parameters, we find that the TBM quantitatively explained many interesting phenomena discovered previously by brute-force numerical simulations (FDTD) and experiments, including the number and positions of the transmission peaksthe parities of wave functions, the band width, dispersion and the group velocities of the transmission bandsand the defect modes, etc. For example, the following figure is the dispersion which is calculated by Transfer matrix method (TMM), FDTD and TBM, showing that they match each other very well.

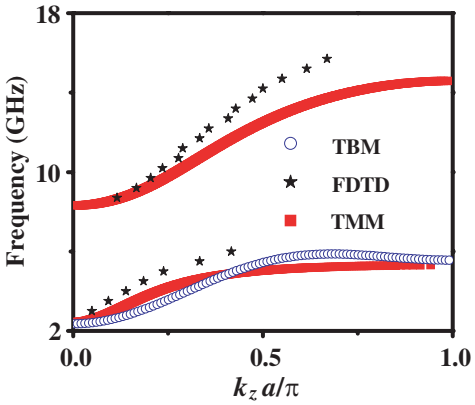

Figure 1.

REFERENCES

1. Xu, H., J. M. Hao, and L. Zhou, unpublished.
2. Xu, H., Z. Y. Wang, J. M. Hao, J. J. Dai, L. X. Ran, J. A. Kong, and L. Zhou, "Effective-medium models and experiments for extraordinary transmission in metamaterial-loaded waveguides," *Appl. Phys. Lett.*, Vol. 92, 041122, 2008.

Tunable Metamaterial Ferrite Stepped Impedance Resonator (SIR)

S. Karimian[1], **M. Abdalla**[2], **and Z. Hu**[1]

[1]MACS Group, School of EEE, University of Manchester, UK
[2]EEE Department, University of Cairo, Cairo, Egypt

Abstract— A novel tuneable microstrip metamaterial ferrite $\lambda_g/4$-type stepped impedance resonator (SIR) is introduced for the first time. The presented resonator has been designed over ferrite substrate in left-handed configurations. The tunability theoretical concepts of its operation are discussed. Also, its performance has been validated using the numerical electromagnetic full-wave simulations. The results show that the operating resonant frequency can be tuned from 4.6 GHz to 5.65 GHz by changing the applied DC magnetic bias.

a-b Plane Dielectric Discussion on Layered Multiferroic Oxides

Yalin Lu and R. J. Knize
Laser Optics Research Center, United Air Force Academy, CO 80840, USA

Abstract— A remarkable coexistence of ferroelectricity and ferromagnetism above room temperature in a new layer-structured ceramics was discussed. Magnetic moment increases more than 3 times by substituting half Fe sites by Co ions. The material exhibits an Aurivillius phase with a four-layer unit cell structure. The potential to be an intrinsic metamaterial was also discussed.

Realization of Negative Refraction via Overlapping Ferroelectric and Ferromagnetic Oxides

Yalin Lu and R. J. Knize
Laser Optics Research Center, United Air Force Academy, CO 80840, USA

Abstract— In this paper, two possible physical mechanisms toward realizing negative refraction will be discussed. When using the superlattice structure through overlapping two ferroelectric and ferromagnetic oxides together, the phonon spectrum coupling among the electromagnetic waves, dielectric dipoles and magnetic moment vibrations is used to obtain both negative permeability and negative permittivity in a short frequency range after the resonance. When using the multilayer structure, new frequency-tuning techniques will be used to fine-tune both dielectric and magnetic resonances to concurrence, from which the negative refraction could be obtained after the concurred resonance frequency. Further material selection for the two configurations are discussed, and the research focus will be the realization of such superlattices for optical frequencies, and multilayers for long wavelengths from terahertz to RF frequencies.

Electromagnetic Tunneling in Nonconjugated Epsilon-negative and Mu-negative Metamaterial Pair

Yaqiong Ding[1, 2], **Yunhui Li**[1, 2], **Haitao Jiang**[1, 2], **and Hong Chen**[1, 2]

[1]Pohl Institute of Solid State Physics, Tongji University, Shanghai 200092, China
[2]Shanghai Key Laboratory of Special Artificial Microstructure Materials and Technology, China

Abstract— As is known, reflection is a common and inevitable optical phenomenon for interfaces with notable impedance contrast. To enhance the transmission, many methods are introduced. For instance, in optics, quarter-wavelength antireflective coatings are widely used to reducing the reflection of optical devices. As well as in microwave region, tapered transmission line (TTL) is often employed to avoid reflection caused by the impendence contrast between different transmission lines. Theoretically, in order to achieving perfect transmission efficiency, the length of TTL must be much longer than the wavelength, which greatly restricts the possibility to design compact microwave communication devices with high transmission efficiency. Metamaterials, which have attracted wide interests recently, may be a solid candidate to solve this problem. Metamaterials include double negative (DNG) materials (both the permittivity and the permeability are negative) and single negative (SNG) materials (only one of the permittivity or the permeability is negative). In SNG materials, the EM waves are evanescent since their wave vectors are complex. In particular, a tunneling scenario will emerge when a pair of lossless epsilon-negative (ENG) and mu-negative (MNG) slabs is conjugated matched between two similar half spaces. In this paper, we investigate the tunneling phenomenon occurring at the interface between two different materials with great impendence contrast by numerical calculation. It is shown that, when a nonconjugated sub-wavelength ENG-MNG pair is introduced between two different materials with great impendence contrast, perfect transmission can still be achieved theoretically. The tunneling condition of the nonconjugated ENG-MNG pair in above case is also figured out. Moreover, the calculated electromagnetic field distributions show clearly that, by choosing proper parameters we can even amplify only one component of the tunneling mode (either the electric or the magnetic field), suppressing another one at the same time. Therefore, the nonconjugated ENG-MNG pair is promising to be applied in modern optic and microwave communication systems for less reflection, compact device volume and flexible control of EM field distribution.

Session 1P5a
Computational Electromagnetics

FDTD Study of a Novel Terahertz Emitter with Electrical Field Enhancement Using Surface Plasmon Resonance

Shuncong Zhong, Yao-Chun Shen, Hao Shen, and Yi Huang
Department of Electrical Engineering and Electronics, University of Liverpool
Liverpool L69 3GJ, UK

Abstract— Much of the recent interest in terahertz radiation stems from its ability to penetrate deep into many organic materials without the damage associated with ionizing radiation such as X-rays. Terahertz radiation can also help scientists understand the complex dynamics involved in condensed-matter physics and processes such as molecular recognition and protein folding. Recently terahertz pulsed imaging (TPI) has also been adopted by the pharmaceutical industry for non-destructive and quantitative characterization of pharmaceutical tablet coatings [1]. The most common device for generating broadband terahertz radiations is a biased photoconductive antenna, pumped with high-power laser pulses from a femtosecond laser [2]. However, this photoconductive emitter, though widely used for terahertz spectroscopy and imaging systems, has limited terahertz power. This prohibits some important applications of the terahertz technology.

In this work, finite-difference time-domain (FDTD) technique was used to study a number of novel terahertz emitter structures. We found that our proposed terahertz antenna requires less pump power of the femtosecond laser pulse whilst provides higher output power of the generated terahertz pulse. Our FDTD simulations revealed that this was achieved by the enhancement of the localized electric field in the terahertz emitter, as shown in Fig. 1. This electric field enhancement was found to have two origins: one is owing to the enhancement of the static electric field of the bias voltage, and the other is the enhancement of the electric field of the incoming femtolaser pulse. The latter enhancement is caused by the interaction of the pump laser and the surface plasma resonance at the conical gold structure of the photoconductive emitter. We believe that this new terahertz emitter could lead to new applications where high-power and broadband terahertz sources are needed.

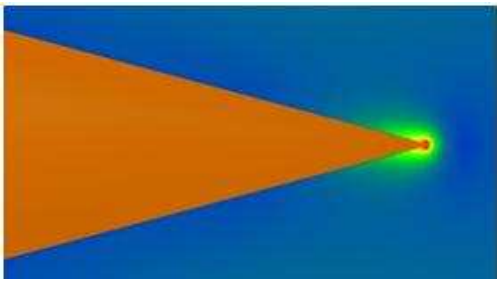

Figure 1: Intensity (|E|) enhancement around the tip of the novel Terahertz emitter.

REFERENCES

1. Shen, Y. C. and P. F. Taday, "Development and application of terahertz pulsed imaging for non-destructive inspection of pharmaceutical tablet," *J. Selected Topics in Quantum Electronics*, Vol. 14, 407–415, 2008.
2. Shen, Y. C., P. C. Upadhya, H. E. Beere, E. H. Linfield, A. G. Davies, I. S. Gregory, C. Baker, W. R. Tribe, and M. J. Evans, "Generation and detection of ultrabroadband terahertz radiation with photoconductive emitter and receiver antennas," *Appl. Phys. Lett.*, Vol. 85, 164–166, 2004.

PML-FDTD Method in Prolate Spheroidal Coordinates

Maoyu Zhang and Jianguo Wang
Northwest Institute of Nuclear Technology
P. O. Box 69-12, Xi'an, Shaanxi 710024, China

Abstract— This paper presents a three-dimensional (3-D) finite-difference time-domain (FDTD) formulation of Maxwell's equation and perfectly matched layer (PML) in three dimensional prolate spheroidal coordinates. The perfectly matched layer formulation relies on the complex stretching coordinates approach. Numerical simulation result of the perfectly matched layer-finite-difference time-domain (PML-FDTD) method shows very good agreement with reference solution computed on an extremely large space.

In order to calculate the electromagnetic pulse generated by a nuclear burst of low or middle altitude in the presence of a finitely conducting earth and the geomagnetic fields, we solve Maxwell's equation in three dimensional prolate spheroidal coordinates by the FDTD method. This coordinate system was chosen because it is suitable for the ground/air boundary problem better than the common orthogonal coordinate systems.

First of all, we introduce the definition of the prolate spheroidal coordinates. The transformation equations from Cartesian coordinates to prolate spheroidal coordinates and the scale factors of prolate spheroidal are presented. Then, the three-dimensional FDTD schemes in prolate spheroidal coordinates are formulated. At last, the unsplit-field PML absorbing boundary conditions of three-dimensional prolate spheroidal coordinates for the FDTD schemes are derived. The formulation is based on the complex stretched coordinates approach.

In order to validate the FDTD schemes and test the property of the PML, the field radiated from a point current source that has the time signature of a Gaussian pulse is calculated. Numerical simulation results show good agreement with analytic solutions. And the maximum relative error between the PML-FDTD result and reference solution computed on an extremely large space due to outer boundary reflections is less than $-40\,\mathrm{dB}$.

Investigation of UPML in the FDTD Analysis of Planar Microstrip Structures

Junjun Wu, **Huiling Zhao**, **and Nakun Jing**
Northwestern Polytechnical University, Xi'an, Shaanxi 710072, China

Abstract— Planar microstrip structures are analyzed with a three dimensional finite difference time domain method (FDTD). Uniaxial anisotropic perfectly matched layer (UPML) absorbing boundary condition is utilized to truncate the FDTD lattices. In order to validate the numerical model, scattering parameters of a line-fed rectangular patch antenna and a low-pass filter are investigated. Simulation results are compared with measurements given by published works. Moreover, efficiency and convergence of FDTD-UPML are also compared with Mur's absorbing boundary condition. Simulation results demonstrated that FDTD-UPML needs less total mesh and convergences faster than Mur's ABC. The method presented in this paper is valid for arbitrary microstrip geometries, such as microstrip circuits and microstrip antennas.

Application of Moving Coordinate FDTD Method on Electromagnetic Pulses Propagation

Yong Li and Jianguo Wang
Northwest Institute of Nuclear Technology, P. O. Box 69-12, Xi'an, Shaanxi 710024, China

Abstract— With the increase applications on communication and detection, there is an ever-increasing interest in the propagation of pulses over long distance. Finite-Difference Time-Domain (FDTD) method is widely used in electronmagnetic simulation. Because FDTD method is a full-wave method, when simulating propagation of electomagnetic pulses over long distance, the computational burden quickly becomes too large. This is the major diffcultly why FDTD method can not be applied to simulating long distance propagation of pulses directly. In order to overcome these diffculities, moving coordinate is combined with FDTD method, the coodinate system is 'frozen' with pulses, and the pulses are in small calculation zones when simulating. The computational grid size is limited to the order of the pulse length, and it and moves along with the pulse. The FDTD meshes (in the dimension along the propagation path) need only to be large enough to contain the pulses while using this methid to simulate propagation of pulses.

The moving coordinate frame FDTD method is developed to simulate the propagation of electromagnetic pulses over large distances. In this work, this method is extended to three dimension case. The discretized form of moving coordinate frame FDTD in three dimensions is given, and is used in propagation of waves of different frequencies in rectangular waveguides. After comparing the results of both FDTD method and moving coordinate frame FDTD method, this method is numerically validated. The simulation results are shown to be accurate and physically appealing. The feasibility of moving coordinate FDTD are proved in this work. This method can be widely used for simulating propagation of electromagnetic pulses.

An Efficacious Computational Procedure to Solve Electromagnetic Transients on Transmission Lines Represented by State Equations

E. C. M. Costa[1], **S. Kurokawa**[2], **A. J. Prado**[2], **and J. Pissolato**[1]

[1]School of Electric Engineering and Computation, State University of Campinas, Brazil
[2]School of Engineering of Ilha Solteira, São Paulo State University, Brazil

Abstract— Overhead transmission line models, applied to simulate electromagnetic transients, are frequently classified as lumped or distributed parameters model.

In lumped parameters model, a given transmission line is represented by n nominal π circuits connected in cascade. Considering the transient frequency range, line length and a sufficient number of nominal π circuits connected in cascade, the distributed nature of the transmission line parameters can be synthesized adequately.

When a lumped parameters line model is adopted, it is very common to use state space techniques to evaluate currents and voltages through the line. Therefore, it is possible for the model to carry out simulations directly in time domain without explicit use of inverse transforms and it can be easily implemented. These characteristics are the same as those used to simulate electromagnetic transients on lines with nonlinear components, such as corona effects and fault arcs, or when a detailed voltage and current profile is needed.

The state space representation presents several advantages, as to extend the methodology to time-variable and nonlinear systems. Furthermore, the transmission line is represented by a system composed by first order differential equations and can be easily solved by numerical or analytical integration methods.

The integration method known as Trapezoidal Rule for lumped parameters is widely used in computational algorithms for transients simulation and commercial softwares based on *Electromagnetic Transients Program* (EMTP).

The simulation precision is intrinsically dependent of the procedure applied to solve the state equations and emphasizing that Trapezoidal Rule as well as other numerical methods are incremental procedures and largely dependent of integration step Δt, thus the simulation results are also directly dependent of Δt.

However, numerical solutions have an ideal performance when Δt is significantly small otherwise the simulation presents numerical oscillations hence several inaccuracies. Another limitation is associated to the great number of lumped elements used to represent adequately long transmission lines, thus this fact associated to a very small Δt results in a hard computational processing and sometimes it results in numerical errors and computational faults. Therefore it is important emphasize that the consideration of these factors is not restricted to numerical procedures but also it is directly related to the reliability of electromagnetic transients simulation. Based on this assertion, this paper proposes an analytical procedure to solve the state equations, less dependent of Δt and then less computational cost.

The computational procedure, presented in this work, is based on matrix diagonalization for non-homogenous systems and Eigensystem-Based Solution.

The results are obtained by numerical solution based on trapezoidal integration method, by analytical solution and from MICROTRAN (EMTP) and then all results are compared and analyzed in function of integration step Δt.

Session 1P5b
Recent Progresses in Time Domain Electromagnetics

Transient Analysis of Ultra Wideband (UWB) Pulse Propagation in Dispersive Media

Qingsheng Zeng[1] and Gilles Y. Delisle[2]

[1]Communications Research Centre Canada, Government of Canada
Ottawa, Ontario, Canada
[2]Technology Integration Center, Technopôle Defense & Security
Quebec City, Quebec, Canada

Abstract— The advent of ultra wideband (UWB) pulse sources has generated renewed interest in the studies of pulse propagation in dispersive media. When one is trying to numerically simulate transient wave propagation through a dispersive medium, the main difficulties are encountered in attempting to transform from frequency domain to time domain. In recent years, we have developed an efficient time domain technique on the basis of numerical inversion of Laplace transform for characterization of electromagnetic pulses propagating in plasma and a lossy dielectric slab and pulses reflected from a conductive, Debye and Cole-Cole interfaces. In this paper, this technique is extended and applied to transient analysis of UWB pulse propagation in other dispersive media than plasma. Its correctness and effectiveness are validated by comparing our results with those published in the literature.

Characterization of Pulse Distortion and Performance Analysis for Indoor Ultra Wideband (UWB) Communication Systems Using a Time Domain Multipath Model

Qingsheng Zeng[1] **and Gilles Y. Delisle**[2]

[1]Communications Research Centre Canada, Government of Canada, Ottawa, Ontario, Canada
[2]Technology Integration Center, Technopôe Defense & Security, Quebec, Canada

Abstract— Recently a new theoretical framework has been set up, making it possible to predict ultra wideband (UWB) system performances directly from propagation environment parameters. In a multipath channel, normally reflected waves have most significant impacts on pulse distortion. In the new framework, the impulse response of a lossy interface is utilized, and then reflected waves are evaluated in time domain by convolving the incident field waveform with the impulse response. This impulse response contains an infinite sum of modified Bessel functions that evaluates the response term persisting in time. In order to apply this expression to practical problems, truncation of the infinite sum of modified Bessel functions is needed. Few terms permits a simple evaluation but makes the accuracy degrade, while many more terms are required to approach an acceptable accuracy but makes calculation complicated and time-consuming. Furthermore, this impulse response was derived from the approximate Fresnel reflection coefficient, which holds under the conditions that the relative dielectric constant ε_r is on the order of 10 or more and that the incident angle θ with the interface is large. Hence, the accuracy of the evaluation of reflected waves is questionable for incident angles less than 10° and/or ε_r less than 10, particularly for vertical polarization.

In this contribution, a time domain multipath model is utilized to characterize indoor UWB signal propagation. Transient waves reflected from conducting interfaces for both vertical and horizontal incidence are calculated through numerical inversion of Laplace transform. It is shown that the wave-based method using numerical inversion of Laplace transform is simple and accurate. With the evaluation of direct and reflected waves in time domain, the performance analysis is conducted for binary UWB communications, and the impacts of propagation environment parameters on pulse distortion and UWB system performance are discussed. This approach does not need the conditions on the relative dielectric constant ε_r and the incident angle θ, and can achieve satisfactory accuracy in both late and early time.

The significance of this contribution is threefold: First, the methodology combines the time domain electromagnetics and the UWB system theory, and lends us the powerful methods and rich solutions already available to gain insight into UWB problems. Second, the conditions on the relative dielectric constant and the incident angle are removed, and the efficiency of the methodology is improved, leading to simple implementation, low computation cost and easy estimation and control of errors. Third, the methodology connects the meaningful system performance parameters such as bit error rate (BER) and signal-to-noise (SNR) with propagation environment parameters such as incident angles and wave polarizations.

Characterization of Time Domain Surface Impedances of a Lossy Dielectric Half Space

Qingsheng Zeng[1] and Gilles Y. Delisle[2]

[1]Communications Research Centre Canada, Government of Canada
Ottawa, Ontario, Canada
[2]Technology Integration Center, Technopôle Defense & Security
Quebec City, Quebec, Canada

Abstract— In many electromagnetic compatibility (EMC) and antenna problems, accurate numerical analysis of interaction between electromagnetic field and lossy dielectric objects is essential, which often requires a very fine spatial grid and then leads to a large number of cells for moderately sized objects. A surface impedance boundary condition (SIBC) that is a function of material parameters can accurately model the skin effect of a lossy body and replace a conducting or lossy dielectric object. So a SIBC reduces the overall size of the solution domain not only by eliminating cells inside the dielectric object, but also by allowing larger cells to be used in the exterior region. A numerical technique that reduces the solution domain and number of unknowns is always welcome.

It is the purpose of this paper to develop an efficient technique for solving the inverse transform of exact closed form representations of frequency domain surface impedances without pursuing tedious and complicated mathematical manipulations. This technique is based on numerical inversion of Laplace transform and has several advantages. The numerical results are illustrated with an excellent agreement between our results and those published in the literature, validating the correctness and effectiveness of this technique. Furthermore, the time domain surface impedances with some incident angles neither close to 0° nor 90° are also presented.

Transient Electromagnetic Topology and Its Validation

Haiyan Xie[1], **Jianguo Wang**[1, 2], **Dongyang Sun**[3], **Ruyu Fan**[1, 2], **and Yinong Liu**[1]

[1]Department of Engineering Physics, Tsinghua University, Beijing 100084, China
[2]Northwest Institute of Nuclear Technology, P. O. Box 69-12, Xi'an, Shaanxi 710024, China
[3]Institute of Nuclear Technology, P. O. Box 69-10, Xi'an, Shaanxi 710024, China

Abstract— This work presents the concept and the validation of the transient electromagnetic topology (TEMT) method. The concept of the TEMT method is introduced first, and then the results of several models obtained by the TEMT method are compared with those obtained by the experiments and a three-dimensional finite difference time domain (FDTD) method. The primary goal of this work is to study whether the TEMT method can be used to analyzed electromagnetic interference (EMI) on systems.

Due to the geometrical and electronic complexity of electronic systems, electromagnetic topology (EMT) method has been proposed in the analysis of EMI on systems. First, the excitation fields of wiring in systems are obtained by numerical methods or experiments. Then, the responses at the nodes of wiring are obtained, usually via the Baum-Liu-Tesche (BLT) equation. However, the BLT equation is a frequency-domain equation and implicitly assumes that the systems studied are linear and time invariant. But many systems are nonlinear and time-varying. Consequently, we use SPICE models of wiring to compute the responses of the loads. All the computations are done in time domain, so the EMT when the SPICE models are used can be called the TEMT, which can be used for nonlinear and dynamic loads.

Several models, which consist of lines, shielded cables, cavities, and transient voltage suppressor diodes, illuminated by a plane-wave electromagnetic pulse (EMP), are studied by using the TEMT method. To validate the TEMT method, these models are also studied by using the FDTD method and the experiment. In the experiment, a bounded-wave simulator, which can produce a perpendicular polarized EMP, is used and the current of the loads are measured. The results show that solutions of different methods are in a good agreement and the TEMT method is more efficient than the FDTD method, which is because that the lines and cables have not to be meshed in the phase of excitation field computations in the EMT method.

Neural Network Techniques for Efficient Modeling of Microwave Circuits

Qi-Jun Zhang, Lei Zhang, and Humayun Kabir
Department of Electronics, Carleton University
1125 Colonel By Drive, Ottawa, ON K1S 5B6, Canada

Abstract— The demand for faster, more accurate and automated tools in designing today's RF/microwave circuits and systems becomes more and more urgent to meet the challenges of increasing design complexity, tighter component tolerances, and shorter design cycles. At RF/microwave frequency, the electromagnetic effects in circuits are significant. Therefore, it becomes important to use electromagnetic/physics based simulations to achieve design accuracy. However, such simulations are in general computationally expensive. Modeling with electromagnetic/physics level accuracy as well as circuit level speed has become an important research direction. This paper presents an overview of emerging artificial neural network (ANN) techniques for linear and nonlinear microwave modeling. Artificial neural networks (ANN) are recognized as an important vehicle in the microwave computer-aided design (CAD) area in addressing the growing challenges of designing next generation microwave devices, circuits, and systems [1–3]. ANN is capable of modeling multidimensional nonlinear behaviors of microwave circuits/devices. The evaluation of an ANN model is also fast [1, 2]. ANN models are trained by component data to learn electromagnetic and physics behaviors. The trained ANNs are used in high-level circuit and system design allowing fast optimization including electromagnetic and physics effects in components. ANN techniques and their applications have been applied in a variety of circuit modeling and design such as modeling microstrip lines, vias, spiral inductors, transistors, VLSI interconnects, coplanar waveguide discontinuities, printed antennas, and embedded passives for circuit synthesis, optimization, and yield analyses. Research and developments in the area are still continuing in developing ANN based methodologies for advanced linear/nonlinear microwave modeling and circuit optimization. More recently, ANN techniques for analysis of multilayered shielded microwave circuits [4], effective design of waveguide dual mode filter [5], large-signal statistical modeling of nonlinear devices [6], and state-space DNN modeling for high-speed IC applications [7] have also been proposed. ANN based modeling and design techniques have been found advantageous over conventional EM based approach in terms of computational expenses with comparable accuracy. ANN based modeling techniques have become highly capable alternatives in microwave modeling area. It aims to develop accurate models from component and circuit data based on neural network training. Trained ANN models can be incorporated into high-level simulators to increase the speed and accuracy of RF/microwave circuit and system design.

REFERENCES

1. Zhang, Q. J. and K. C. Gupta, *Neural Networks for RF and Microwave Design*, Artech House, Boston, MA, 2000.
2. Zhang, Q. J., K. C. Gupta, and V. K. Devabhaktuni, "Artificial neural networks for RF and microwave design: From theory to practice," *IEEE Trans. Microwave Theory Tech.*, Vol. 51, No. 4, 1339–1350, 2003.
3. Burrascano, P., S. Fiori, and M. Mongiardo, "A review of artificial neural networks applications in microwave computeraided design," *Int. J. RF and Microwave CAE*, Vol. 9, No. 3, 158–174, 1999.
4. García, J. P., F. Q. Pereira, D. C. Rebenaque, J. L. G. Tornero, and A. A. Melcón, "A neural-network method for the analysis of multilayered shielded microwave circuits," *IEEE Trans. Microwave Theory Tech.*, Vol. 54, No. 1, 309–320, 2006.
5. Kabir, H., Y. Wang, M. Yu, and Q. J. Zhang, "Neural network inverse modeling and applications microwave filter design," *IEEE Trans. Microwave Theory Tech.*, Vol. 56, No. 4, 867–879, 2008.
6. Zhang, L., Q. J. Zhang, and J. Wood, "Statistical neuro-space mapping technique for large-signal modleing of nonlinear devices," *IEEE Trans. Microwave Theory Tech.*, Vol. 56, No. 11, 2453–2467, 2008.
7. Cao, Y., R. Ding, and Q. J. Zhang, "State-space dynamic neural network technique for high-speed IC applications: Modeling and stability analysis," *IEEE Trans. Microwave Theory Tech.*, Vol. 54, No. 6, 2398–2409, 2006.

Parametric Time-domain Neural Network Models for Microwave Modeling

Qijun Zhang
Department of Electronics, Carleton University
1125 Colonel By Dr., Ottawa, Ontario K1S 5B6, Canada

Abstract— The drive for first-pass success, coupled with stringent design specifications demands higher and higher accuracy in component models. Electromagnetic (EM)-based modeling and design is essential. For EM based design optimization with physical/geometrical parameters as design variables, the EM structure has to be solved repetitively with changing values of geometry. This expensive computational problem remains a challenge in microwave CAD. Neural Network techniques are recent developments addressing such challenges [1]. Neural networks can be trained to learn EM data with varying geometrical parameters, and trained neural networks become fast models for circuit design with geometrical optimization.

Time-domain parametric model for EM-behavior is useful for time-domain simulation and design of high-speed integrated circuits, interconnects, and packaging. We describe two approaches, one based on state-space equation/neural network (SSE-NN) [2], and another based on direct time-domain recurrent neural network (RNN) [3]. The SSE-NN model consists of two levels of submodels. At the higher level, we use a set of linear state equations to provide the EM response in time domain. At the lower level, a neural network maps the geometrical parameters of the EM structure into the coefficients of the state equations. To train such SSE-NN models, we first extract the state-space coefficients from EM data, for different values of geometrical parameters. We then train a neural network to learn the extracted coefficients w.r.t. the geometrical parameters. An example SSE-NN model for embedded passives in multilayer circuits is trained from EM data, and used for time-domain signal integrity based design of VLSI interconnect networks. The second method, i.e., the RNN method, provides a direct time-domain model trained from time-domain EM data. The output of the RNN is the time-domain signal $y(t)$, which is expressed as a function of the time-domain input signal at the present moment $u(t)$, its history $u(t-\tau)$, $u(t-2\tau)$, ..., $u(t-N\tau)$, and the history of the y signal $y(t-\tau)$, $y(t-2\tau)$, ..., $y(t-N\tau)$, as well as physical/geometrical inputs. The RNN is trained using a recurrent-backpropagation algorithm learning the time-domain EM data. An example RNN model for waveguide filter is trained with time-domain EM data from a time-domain EM simulator. The techniques allow fast and accurate model for EM behavior of passive microwave components. They can be used for efficient microwave design with physical/geometrical parameters as design variables.

REFERENCES

1. Zhang, Q. J. and K. C. Gupta, *Neural Networks for RF and Microwave Design*, Artech House, Boston, 2000.
2. Ding, X., V. K. Devabhaktuni, et al., "Neural network approaches to electromagnetic based modeling of passive components and their applications to high-frequency and high-speed nonlinear circuit optimization," *IEEE Trans. Microwave Theory Tech.*, Vol. 52, 436–449, 2004.
3. Sharma, H. and Q. J. Zhang, "Transient electromagnetic modeling using recurrent neural networks," *IEEE MTT-S International Microwave Symposium Digest*, Long Beach, CA, June 2005.

Session 1P6a
Extended/Unconventional Electromagnetic Theory, EHD (Electro-hydrodynamics)/EMHD (Electro-magneto-hydrodynamics), and Electro-biology

Processing of MR Slices of Human Liver for Volumetry

J. Mikulka[1], **E. Gescheidtova**[1], **and K. Bartusek**[2]

[1]Department of Theoretical and Experimental Electrical Engineering, Brno University of Technology
Kolejni 2906/4, Brno 612 00, Czech Republic
[2]Institute of Scientific Instruments, Academy of Sciences of the Czech Republic
Kralovopolska 147, Brno 612 64, Czech Republic

Abstract— This article deals with a segmentation of MR images of human liver. The aim of the segmentation is bounding of tumors in MR images of the human liver in each slice. It is possible to reconstruct the original shape of the tumor from these bounded areas and if we know the thickness of each slice the volume can be solved. This method is suitable to monitoring the development of tumor volume during the treatment. The volume reducing means successful treatment. There was chosen an active contour method based on level set partial differential equation for the MR image segmentation [1, 2]. There was found the boundary of the liver tumor in the noised image of low contrast with suitable parameters and initial curve without any kind of preprocessing. The article shows our results of the segmentation of some MR slices with visible liver tumors. These results are poised to following postprocessing which will be the 3D model creation and the volumetry of the tumor.

REFERENCES

1. Li, C., C. Xu, C. Gui, and M. D. Fox, "Level set evolution without re-initialization: A new variational formulation," *Proceedings of the 2005 IEEE Computer Society Conference on Computer Vision and Pattern Recognition, CVPR'05*, 430–436, San Diego, USA, ISBN 0-7695-2372-2, IEEE Computer Society, Washington, DC, USA, 2005.
2. Aubert, G. and P. Kornprobst, *Mathematical Problems in Image Processing: Partial Differential Equations and the Calculus of Variations*, 2nd Edition, ISBN 0-387-32200-0, Springer Science + Business Media, LLC, New York, 2006.

Detection of Magnetization of 6 Hz, 10 μT Magnetic Field Applied Water Using PT-MI Sensor

K. Mohri[1, 2], **M. Fukushima**[3], **Y. Mohri**[4], **and Yu. Mohri**[5]

[1]Nagoya Industrial Science Research Institute (NISRI), Nagoya 464-0819, Japan
[2]Aichi Micro Intelligent Co., Tokai 476-8666, Japan
[3]TRI, Foundation for Biomedical Research and Innovation, Kobe 650-0047, Japan
[4]Graduate School of Eng., Meijo Univ., Nagoya 468-8502, Japan
[5]Graduate School of Arts, Meijo Univ., Nagoya 468-8502, Japan

Abstract— Possibility of magnetization of water has been discussed for a long time, which may change the water structure and improve the water function on physical and bio-chemical operations. We constructed an extremely sensitive magnetic sensor having one pico-Tesla resolution using single amorphous wire core CMOS IC magneto-impedance sensor with dc selective negative feedback circuitry ("pT-MI sensor") for detection of the water residual magnetization. 1 pico-Tesla resolution for magnetic field detection is realized by suppression of the magnetic noises in the amorphous wire with some tension annealing and the electronic circuit noises using some notched filtering in the magneto-impedance sensor (MI sensor) [1].

Detection of water residual magnetization M_r is carried out using a pendulum oscillation sample magnetic measurement method (POSM), in which a water sample bottle of 100 ml oscillates as a pendulum with 1.5 Hz over the pT-MI sensor head at 5 cm apart position showing 3 Hz magnetic field sinusoidal wave. Sample water (public drinking water) with 6 Hz, 1 μT magnetic field applied through more than 1 hour showed a clear 3 Hz sinusoidal wave output of around 1 nT amplitude ($M_r = 12$ pT-m^3) during at least 30 min. and not for samples without magnetic field application and also magnet dc field application. Mechanism of water magnetization has been proposed with an assumption of the cyclotron resonance of the water cluster ($H_3O^+(H_2O)_n$) which activates the proton transport in water [2].

REFERENCES

1. Mohri, K. and Y. Honkura, "Amorphous wire and MOS IC based magneto-impedance sensors — Origin, topics, and future," *Sensor Letters*, Vol. 5, 267–270, 2007.
2. Mohri, K. and M. Fukushima, "Milligauss magnetic field triggering reliable self organization of water with long range ordered proton transport through cyclotron resonance," *IEEE Trans. Magn.*, Vol. 39, No. 5, 3328–3330, 2003.

An Optimized Universal Adaptive ARC Filter Block

Martin Friedl, Lubomír Fröhlich, and Jiří Sedláček
Brno, FEEC BUT, UTEE, Kolejní 2906/4, Brno 612 00, Czech Republic

Abstract— Active RC filters designed using cascade synthesis method are in practise used very often. Each selective building biquads can be designated using many different circuits. There are divided most often according number of active elements (OA — operational amplifier) to different groups. These circuits with three or four active elements exhibit some advantages. Their outputs enable concurrently to obtain all required kinds of filter types (Low pass LP, highpass HP, bandpass BP, all pass AP). The flexibility of above mentioned biquads also allows it to be used in some special applications — As tuning requirements or switchable-filter options.

This paper deals with comparison of an universal biquad blocks with modern active elements, which are usable for many special filter applications. Here are presented some optimization methods and achieved parameters of realized tuneable and switchable blocks with modern operational amplifier too. Briefly here are also discussed and presented possible tuning circuits realized using microprocessor technique. An example of main parameters and frequency characteristics of optimized universal tuneable building biquad including microprocessor control circuit for all kinds of outputs (LP, HP, BP, AP) in wide frequency range of frequencies is here also presented.

REFERENCES

1. Daryanani, G., *Principles of Active Network Systems and Design*, Bell Lab. Inc., USA, 1976.
2. Hájek, K. and J. Sedláček, *Kmitočové Filtry*, Vydavatelství BEN Praha, 2002.
3. Hájek, K. and J. Sedláček, "Lossy LC ladder prototypes and their use for ARC filter optimization," *Wseas Transactions on Electronics*, Vol. 2, No. 3, 94–99, July 2005.
4. Martinek, P. and T. Daša, "Evolutionary algoritmes by ARC filter synthesis," *ECCTD 05*, 155–159, Cork, 2005.

Processing of MR Slices of Temporomandibular Disc for 3D Visualization

J. Mikulka[1], **E. Gescheidtova**[1], **K. Bartusek**[2], **and Z. Smekal**[3]

[1]Deptartment of Theoretical and Experimental Electrical Engineering, Brno University of Technology
Kolejni 2906/4, Brno 612 00, Czech Republic
[2]Institute of Scientific Instruments, Academy of Sciences of the Czech Republic
Kralovopolska 147, Brno 612 64, Czech Republic
[3]Department of Telecommunications, Brno University of Technology
Purkynova 118, Brno 612 00, Czech Republic

Abstract— This article deals with a segmentation of MR images in temporomandibular joint (TMJ) area. The TMJ belongs to small but the most overloaded joint of the human body. It consists of the head of the mandible and articular fossa [1]. Between them is the mandibular disc. The mandibular disc is a cartilage for a force transmission. The physiological placement of the disc is on the top of the mandibular head. One of the frequent diseases is the disc dislocation from the physiological placement therefore there is a blocking of the mandibular head movement. In the worse case it can come to the total disc deformation [2]. The aim of this work is to obtain the most exact image or model of the mandibular disc for the right assessment of a treatment in order to minimize the invasive surgery. There was chosen an active contour method based on level set partial differential equation for the MR image segmentation [3, 4]. There was found the boundary of the mandibular disc in the noised image of low contrast with suitable parameters and initial curve without of any kind of preprocessing. The article shows our results of the segmentation of some MR slices with visible mandibular disc. These results are poised to following postprocessing which will be the 3D model of the mandibular disc creation. There are described some methods for this kind of preprocessing.

REFERENCES

1. Cihak, R., *Anatomie 1*, ISBN 80-7169-970-5, Grada Publishing, 2001.
2. Machon, V., *Onemocneni Celistniho Kloubu* [online], Superservis.cz, c2006 [cit. 2009-04-15], available on WWW: <http://www.webclient.cz/klouby/index.php?action=obsah&id=28>.
3. Li, C., C. Xu, C. Gui, and M. D. Fox, "Level set evolution without re-initialization: A new variational formulation," *Proceedings of the 2005 IEEE Computer Society Conference on Computer Vision and Pattern Recognition CVPR'05*, San Diego, USA, ISBN 0-7695-2372-2, 430–436, IEEE Computer Society, Washington, DC, USA, 2005.
4. Aubert, G. and P. Kornprobst, *Mathematical Problems in Image Processing: Partial Differential Equations and the Calculus of Variations*, 2nd Edition, ISBN 0-387-32200-0, Springer Science + Business Media, LLC, New York, 2006.

Modeling of Saturation Characteristic of an Aspiration Condenser

Z. Roubal, **M. Steinbauer**, **and Z. Szabó**
Faculty of Electrical Engineering and Communication, Brno University of Technology
Kolejní 2906/4, Brno 612 00, Czech Republic

Abstract— It was confirmed that light air ions have positive influence on the human health. For its appraisal it is necessary to know the concentration of air ions and air ion mobility spectrum. This spectrum is usually found out using the saturation characteristic measurement with gerdien tube, another possibility propose the aspiration condenser with segmented inner electrode. The second method is faster, but their resolution of air ion mobility spectrum is worse. This paper deals with a mathematic analysis and numerical modeling of saturation characteristic evaluation for this aspiration condenser with segmented inner electrode. Using combination of both methods may increase the resolution of air ion mobility spectrum when speed of measurement is still higher than with gerdien tube. Modeled and measured saturation characteristic of aspiration condenser with segmented inner electrode will be compared. The estimation of mobility spectrum obtained from condenser with segmented electrode will be compared with the one obtained from gerdien tube, as well.

REFERENCES

1. Charry, J. M. and R. Kavet, *Air Ions: Physical and Biological Aspects*, CRC Press, Inc., Boca Raton, Florida, 1987.
2. Tammet, H. F., *The Aspiration Method for Determination of Atmospheric-Ion Spectra*, IPST, Jerusalem, 1970.
3. Vojtek, T., T. Skoupil, P. Fiala, and K. Bartušek, "Accuracy of air ion field measurement," *PIERS Online*, Vol. 2, No. 4, 412–415, 2006.
4. Steinbauer, M., P. Fiala, K. Bartušek, and Z. Szabó, "Experiments with accuracy of air ion field measurement," *PIERS Proceedings*, 1062–1066, Hangzhou, China, March 24–28, 2008.

Integrated Programming and Application of Genetic Algorithm and Conjugate Gradient Method

Wei Xie and Jian-Xin Liu
School of Info-physics and Geomatics Engineering, Central South University
Changsha 410083, China

Abstract— The power of dealing with matrix operations in MATLAB write this paper, the procedure of hybrid genetic algorithm has great advantages. Because of the characteristics: Partly depending the primary estimation and having the global convergence, it can be used to solve different complex applications, such as the optimal design of projects, artificial intelligence, strategic system, geo-physical, inversion and so on. Although the genetic algorithm is an efficient global-optimization method, from the simulation results the defaults of time-consuming and vain local-researching ability can be detected. But the conjugate gradient algorithm belongs to a non-heuristic global-optimization search method, with the characteristics of swift convergence, easily dumping into local extreme value and severely depending on the primary estimation. This essay adopts a hybrid genetic algorithm of geo-physical inversion, according to the properties of the genetic algorithm and the conjugate gradient algorithm. The method has the attributes of the global-convergence of the genetic algorithm and the swift convergence of the conjugate gradient. Finally in accordance with procedures to test simulation algorithm and analysis with examples to prove that the procedure has good practicability.

Session 1P6b
Education of Electromagnetic Theory

Student Projects of Extended Study in Introductory Electromagnetics

Y. Du, **X. M. Zhang**, **S. L. Zheng**, **X. F. Ye**, **and K. S. Chen**
The Department of Information Science and Electronic Engineering
Zhejiang University, Hangzhou 310027, China

Abstract— Electromagnetics is one of the most important bases of our modern life, upon which lay the life style enhancing technologies such as communication, RFID, wireless sensor network, antenna, and other electronic systems. Understanding the principles of Electromagnetics is thus required for undergraduate students majoring in Electrical Engineering to prepare them for a smooth and successful career. However, since electromagnetics is a strongly mathematical subject, it is often the case for a student to find it very difficult to apply advanced mathematical techniques while maintaining a physical comprehension.

In the literature it is observed that incorporating real-world examples of applications serves to improve student learning and to bring a colorful course material presentation. This is undoubtedly an effective way of teaching electromagnetics. However, there might also be some limitations of this approach: the chosen real-world examples may have to be simple and the applicable principles from electromagnetics may be restricted considering the limited knowledge span and mathematical skills of the average student. For instance, the real world examples taken from one study were almost associated with electrostatics or magnetostatics. The very nature of electromagnetics, that is, time varying aspect, is unwantedly de-focused in this approach.

In this work, we propose an approach that is complementary to the real-world examples one. In our approach, we encourage the students to extend the material from what has been covered in the class. For instance, after learning the reflection and transmission of a plane wave at the interface of two homogeneous media in the conventional setting, the students may proceed to work out with the help of the instructors the reflection and transmission phenomena when one of the media is anistropic. In this way, the comprehension of the material, the employment or even improvement of mathematical skills can be greatly boosted, which will in turn help build up the confidence and further curiosity of the students.

The proposed extended study is not introduced as a mandatory part of the fundamental EM course; rather, it is based on voluntary participation. The feedbacks from the participants have been positive in majority.

Discussion on Teaching Electromagnetic Field and Wave Course

Xianfeng Ye, **Xianmin Zhang**, **Shilie Zheng**, **and Yang Du**
Department of Information and Electronics Engineering
Zhejiang University, Hangzhou 310027, China

Abstract— The course Theory of Electromagnetic Field and Wave is one of the most important technical foundation courses in electronic engineering. With the recent great advances in electronics and information technology, particularly in the internet technology as the representative of the network and communication technologies, the course teaching methodology should keep pace with them. We have already launched certain teaching reform, where we combined the course Theory of Electromagnetic Field (including the antenna) and the course Microwave and Optical Guided Wave Technology into a single course, Electromagnetic Fields and Electromagnetic Wave. Although the depth and coverage of the course has increased, the course hours have been compressed. This requires teachers to make greater efforts and take more effective measures.

First, we strengthen the foundations of mathematics and seize the heart of vector and field theory. This course is abstract and difficult for students to understand, mainly because students can not combine mathematical tools with the physical concepts. It is necessary to clear mathematical obstacles. The main mathematical tool of the course is vector and field theory. For a vector field, divergence and curl are core concepts. The vector dot product and cross product have a wonderful correspondence with them. By clarifying these relationships, the difficulty of students on mathematics is resolved.

Second, we have analyzed electromagnetic theory systematically and rigorously to cultivate innovative thinking ability of students. Maxwell extracted from the essential characteristic of electromagnetic phenomena the concept of electric and magnetic fields from the Faraday line force, and using these two concepts he rewrote Coulomb's law, Ampere's law and Faraday's law. By conjecturing the displacement current, Ampere's Law was rewritten into the Ampere's full current law, and finally the construction of electromagnetic theory system was completed. Maxwell's electromagnetic theory predicted the existence of electromagnetic waves. Electromagnetic wave is not a result through perception but a logical reasoning one. It is a sure existence which was confirmed by the German physicist Hertz in the experiment. The establishing process of electromagnetic theory could make students to recognize the logic of the relationship in the electromagnetic theory, and appreciate the power of logical reasoning and Maxwell's creative spirit.

Finally, we introduce electromagnetic theory by combining it with practice applications. Electromagnetic theory is abstract, but the application is extensive. During the course we select the content and problems about new technologies, such as communication, networking, radar, navigation, remote sensing, integrated circuits, integrated optical circuit and so on. In these application examples, students' interest is stimulated. They appreciate the importance of electromagnetic theory, and their understanding is greatly deepened.

In short, we have focused on three aspects of EM teaching. We have seized the keys of vector field theory to clear students' obstacles about mathematics, made students to understand the rigorous logic system of electromagnetic theory which deeply enhances the students' sense of innovation, and combined the theories with practical applications to improve their capabilities of applying knowledge and solving engineering problems.

Perspective of Electromagnetics Education

X. M. Zhang, S. L. Zheng, Y. Du, X. F. Ye, and K. S. Chen
Department of Information Science & Electronic Engineering
Zhejiang University, Hangzhou 310027, China

Abstract— Electromagnetic Field and Wave is the backbone of the foundation courses of electrical profession. The course involves a large number of field theory and vector analysis relying on mathematical knowledge. Compared with the application-oriented courses, it covers wider contents and requires more theoretical analysis. The subject is very abstract, and is difficult to learn for most students.

Electromagnetic problems arise in diverse areas such as radar systems, antennas, communication systems, EMC, RFIC, RFID, and other electronic systems. The electromagnetic applications in everyday life can be used as a vehicle to explain fundamental theoretical concepts. With the extensive use of simulation tools, rigorous analytical methods and their engineering approximations for these application examples can be omitted, and the role of basic electromagnetic theory in engineering practice can be clearly presented. The abstract theories are shown in realistic existence so that students can deepen their understanding of the course contents.

How to make students not only feel the latest developments and applications in the field of electromagnetics, but also with great interest to learn the basic theory is the key to success of teaching, which requires teaching contents to be constantly updated. The integration with the modern science and technology ensures the advanced nature of teaching contents. The introduction to the hot electromagnetic issues in recent years can greatly enhance the student's enthusiasm, and arouse their curiosity to explore the unknown world, which also lays the foundation to learn the basic theory.

Students tend to become best motivated to learn something when they can see its relevance. Integrated with scientific research and achievements, the teaching conducts undergraduates to research and training programs. Many students will relate topics into their own research projects, and present the corresponding small research reports in the end of course. This process helps students understand the abstract theories deeply. Students have also gained self confidence and improved interest in electromagnetics. Some students will set it to be one of their directions for future efforts.

Architecture Reform and Teaching Content Optimization of Electromagnetic Field and Wave Course

Shilie Zheng, **Xianmin Zhang**, **Yang Du**, **and Kangsheng Chen**
Department of Information Science & Electronic Engineering
Zhejiang University, Hangzhou, 310027, China

Abstract— With the development of electronic information technology, new research areas such as broadband wireless communication, high-speed digital circuit, microwave photonics and electromagnetic compatibility emerge endlessly, which bring new challenges to the course systems of Electromagnetic Field and Wave. Since the electromagnetic field and wave courses are among the most important and fundamental undergraduate courses in Electronic Engineering, restructuring these courses is in urgent need.

In this paper, the scheme of restructuring including architecture reform, content optimization and practical innovation is described. First, since both microwave and optic wave are electromagnetic waves, the original courses "Electromagnetic Theory", "Microwave and Optical Guide-wave Technology" "Antenna" and part of "Microwave Networks" are combined into one single course, "Electromagnetic Field and Wave". As such, the scope and contents of this resultant new course is greatly expanded. Its corresponding experimental course, "Experiments for Electromagnetic Wave" is also extended to the measurement of network parameters and micro strip circuit. A new practical course, "Design of RF and Microwave Circuit" is set up to improve the students' handon capability and meet the new requirements. Secondly, we optimize the knowledge modules of each course with certain predetermined features as guidelines. These features for the main course "Electromagnetic Field and Wave" are 1) to place teaching of time varying field before static field; 2) to effectively combine transmission line theory with the electromagnetic field; and 3) to pay equal attention to microwave and optic wave. All these aspects of reform have been carried out at Zhejiang University for the past eight years, with manifested achievements in keeping pace with up-to-date research progress and cultivating innovation thoughts and capacity of the students.

Vivid Teaching Methods in Undergraduate Electromagnetics Education

Hongsheng Chen
The Electromagnetics Academy, Zhejiang University, Hangzhou 310027, China

Abstract— Since Scottish Scientist James Clerk Maxwell established the electromagnetic theory in 1864, Maxwell equations has been the governing law for all electromagnetic phenomena inside material media that are described by constitutive relations. For many undergraduate students, electromagnetic theory is too abstract to learn. In this paper, we summarize some vivid teaching methods that can be used to attract students' interest, such as including some experimental demos in the class, telling some stories of the scientist who have derived the related equations that will be presented in the class, as well as using the electromagnetic theory to explain some phenomena commonly exist in the students live, etc. We found that these teaching methods are very helpful for students to understand the complicated equations and further to grasp the main points of the electromagnetic theory.

ACKNOWLEDGMENT

The author is very grateful to the late Professor Jin Au Kong for the encouragements and valuable suggestions in his teaching experiences.

Session 1P7
Electromagnetic Wave Applications in Material Processing and Characterization

Magnetization Dynamics in Hexagonal Multiferroic $HoMnO_3$ Single Crystals Probed by Wavelength-tunable Time-resolved Femtosecond Spectroscopy

H. C. Shih[1], **T. H. Lin**[1], **C. W. Luo**[1], **K. H. Wu**[1], **J.-Y. Lin**[2], **T. M. Uen**[1], **T. Kobayashi**[1], **and Jenh-Yih Juang**[1]

[1]Department of Electrophysics, National Chiao Tung University, Hsinchu 300, Taiwan
[2]Institute of Physics, National Chiao Tung University, Hsinchu 300, Taiwan

Abstract— How the magnetization constituted of ordered interacting electronic spins can be modified by optical excitation, and how can the responding changes be measured? These are the questions of fundamental interests which, in turn, triggered the fast growing field of femtosecond spectroscopy. In this paper, we demonstrate examples by showing the results unveiling the strong coupling between electronic structure and magnetic antiferromagnetic (AFM) ordering in the hexagonal $HoMnO_3$ single crystals by wavelength-dependent femtosecond spectroscopy. The appearance of long-range magnetic ordering and short-range ordering in the multiferroic manganites are unambiguously revealed by the abnormal blue-shift of Mn^{3+} 3d level around Néel temperature (T_N) and the slope near the transition of temperature-dependent $\Delta R/R$, respectively.

Measurement of the Dielectric Constants of Zinc Metallic Nanoparticles at Various Frequencies

Yi-Chen Yeh and Juh Tzeng Lue
Department of Physics, National Tsing Hua University, Hsin Chu, Taiwan

Abstract— The vacuum evaporated metallic nanoparticles mixed with a low loss tangent alumina powder dissolved in paraffin constructed in a cylindrical rod were inserted in the center of a cylindrical microwave cavity. The resonant frequencies and the quality factors measured from a resistance-inductance-capacitance (RLC) meter and a microwave network analyzer were exploited to compute the real and imaginary dielectric constants of zinc metallic nanoparticles at various frequencies from low radio frequency to microwave frequencies. The paraffin molecules are exploited to prevent the space from adsorbing moisture and air, which makes the measurement much accurately and stable. The magnitudes of the real part of the dielectric constants of zinc metallic nanoparticles decrease as the particle size decrease, which is satisfactorily consistent with the prescription of classical free electron Drude model.

A Study on the Complex Permittivity of Sheet-like Carbon Nanotubes Buckypaper in X Band with Cavity Perturbation Method

H. Y. Miao[1], **T. Y. Hou**[1], **and R. B. Yang**[2]

[1]Department of Electrical Engineering, Tunghai University, Taichung, Taiwan
[2]Department of Aerospace and Systems Engineering, Feng Chia University, Taichung, Taiwan

Abstract— Although, composites with carbon nanotubes embedded into a polymer host have been studied for microwave applications, but the characterization of the flexible buckypaper (BP) at microwave frequencies has less been explored.

Carbon nanotubes (CNTs), approximately 50,000 times thinner than a human hair, have attracted much attention recently due to their extraordinary electrical conductivity, heat conductivity and mechanical properties. CNTs-reinforced nanocomposites have the potential to revolutionize structural materials for aerospace, electrical and thermal conductors for energy applications, body armor and next-generation electronics and displays. But, except be an additive role, owing to tiny scale, it's hard to handle or to utilize CNT solo.

One convenient way to fabricate and utilize CNTs as a bulk composites material is Buckypaper (BP), a macroscopic aggregate of carbon nanotubes. It is made of well-disperse suspension of CNTs and forming by an elaborately designed filtrating process, with sheet-like shape and porous structure. BP, as a bulk material, can provide thermal conductivity properties to dissipate heat, electromagnetic-interference shielding and lightning-strike protection in composite structures, enhance the strength of composite structures, and be used for embedding sensors in composite materials. Some applications require the characterization of BP at the environment of microwave.

In this study, a measurement method that could get the property of the complex permittivity ($\varepsilon' - j\varepsilon''$) of BP at X-band (8–12 GHz) was presented. Home made multi-wall carbon nanotubes was the main material. Effective medium theory (EMT), effective medium approximation (EMA) and a resonant cavity perturbation method were employed.

The results show that the CNTs buckyaper is a highly metallic material. It is observed that for frequency 7.92 GHz $\sim$ 12.44 GHz, the real part of permittivity (ε') is $-68.4 \sim -65.3$ and the imaginary part of permittivity (ε'') starts at around 0 in magnitudes as frequency increases satisfactorily in complying with the portray from the free electron Drude model.

Study on the Duality of Frequency Selective Surfaces with Rectangular Complementary Elements

Xin Ma, **Guobin Wan**, **and Ning Ren**
School of Electronic and Information, Northwestern Polytechnical University, Xi'an 710129, China

Abstract— From Babinet's principle, the free-standing aperture-type and patch-type frequency selective surfaces (FSSs) are completely complementary. Whereas in the application of FSS to practical ends such as the antenna dichroic subreflectors and radar radome, FSS are etched on a substrate to provide mechanical support, and therefore the research of the dielectric effect on the duality of FSS is useful. In this paper, new dual structures which are aperture-type FSS residing on a dual magnetic dielectric slab and patch-type FSS on an electric dielectric slab are proposed. The relative permittivity of electric dielectric is equal to the relative permeability of magnetic dielectric. The duality of aperture-type and patch-type FSS without any dielectric, with an electric dielectric and with a dual magnetic dielectric are analyzed. The spectral Green's function is derived through spectral domain immittance approach first. The affection of substrate on the reflection and transmission characteristics of rectangular FSS compared with the FSS in a free space is considered, and the effects are discussed through changing thickness and parameter of dielectric. It shows that the proposed structures are complementary around resonant frequency, but resonant frequency offset emerges, and the magnitude of resonant frequency offset has relations with the dielectric type, thickness and parameter.

Multiple Quantum Wires Photodetector

Shu-Fen Hu[1], **Chang Hsueh Li**[2], **and Tsug-Han Li**[1]

[1]Department of Physics, National Taiwan Normal University
88, Sec. 4, Ting-Chou Road, Taipei 116, Taiwan
[2]Institute of Electro-optical Science and Technology, National Taiwan Normal University
88, Sec. 4, Ting-Chou Road, Taipei 116, Taiwan

Abstract— Multiple quantum wires (MQWRs) array transistors were fabricated as efficient ultraviolet to visible light phototransistors for light detection. The MQWRs photodetector exhibit not only high responsivity in wide range of $380 \sim 628$ nm wavelength light, especially in ultraviolet range, but also have sharp threshold characteristics than that measured in darkness. The I-V characteristics explain that illumination intensity and the external bias can easily enhanced the photocurrent. The optimal responsivity of approximately $R = 2.57\,\mathrm{A/W}$ measured at $V = 0.2\,\mathrm{V}$ and the quantum efficiency of 144% at the illumination wavelength of 380 nm. The advantages of these devices are high sensitivity, high response speed, and low working power and efficiently absorb wide range of light.

Biosensing, Cytotoxicity and Cellular Uptake Studies of Surface Modified Gold Nanorods

Ru-Shi Liu[1], **Harshala J. Parab**[1], **Hao Ming Chen**[1], **Jing Hong Huang**[2], **Tsung-Ching Lai**[2], **Michael Hsiao**[2], **Chung-Hsuan Chen**[2], **Din-Ping Tsai**[3], **and Yeu-Kuang Hwu**[4]

[1]Department of Chemistry, National Taiwan University, Taipei 106, Taiwan
[2]The Genomics Research Center, Academia Sinica, Taipei 115, Taiwan
[3]Department of Physics, National Taiwan University, Taipei 106, Taiwan
[4]Institute of Physics, Academia Sinica, Taipei 115, Taiwan

Abstract— Herein we report, the biorecognition studies towards protein IgG using biocomapatible gold nanorods as molecular probes. Surface modification of cetyltrimethyl ammonium bromide (CTAB) stabilized gold nanorods was carried out by using polystyrene sulfonate (PSS), in order to reduce the toxicity of as synthesized gold nanorods caused due to free CTAB. Zeta potential analysis confirmed the charge reversal on the surface of gold nanorods caused due to PSS coating. Surface plasmon resonance (SPR) exhibited by gold nanorods (GNRs) has been employed as a tool for analyzing the binding events for biomolecules. TEM results, showing the aggregation of gold nanorods, in addition with the shift in surface plasmon resonance peak in UV-Vis absorption measurements, upon the interaction of biomolecules with gold nanorods, confirmed the molecular binding. Morphological changes caused due to the cellular uptake of gold nanorods before and after PSS modification have been observed. The cell viability studies using gold nanorods were performed in order to study the cytotoxic effects of these molecular probes.

The Optical Properties of an Annular Periodic Multilayer Structure with Two Different Single-negative Materials

Mei-Soong Chen[1], **Chien-Jang Wu**[2], **and Tzong-Jer Yang**[3]

[1]Department of Electrophysics, National Chiao Tung University, Hsinchu 300, Taiwan
[2]Institute of Electro-optical Science and Technology, National Taiwan Normal University Taipei 116, Taiwan
[3]Department of Electrical Engineering, Chung Hua University, Hsinchu 300, Taiwan

Abstract— The optical properties of an annular periodic multilayer structure with two different single-negative materials as an unit cell are studied by the transfer matrix method of the cylindrical waves. The field solutions of the cylindrical Bragg waves for both TE and TM waves are dependent on the azimuthal mode number m, and optical reflectance is studied for different m values. For $m >$ or $= 1$, it is found that there is an additional photonic band gap (PBG) called mu-negative gap and episilon-negative gap for TE and TM waves, respectively. We also find that there exist some reflection dips when the magnetic plasmon frequency and the electric plasmon frequency are taken in the PBG for TE and TM waves, respectively. Such special filtering responds make it possible to design the structure of a narrowband resonator without introducing any defect layer to break the periodicity. The PBGs are strongly affected by the starting radius in addition to positive m values. Further discussion will also be made in this talk.

ACKNOWLEDGMENT

This work is partially supported by National Science Council through project number NSC 98-2112-M-216-001(Yang) and NSC 97-2112-M-003-MY3(Wu).

Subwavelength Microwave Guiding by Periodically Corrugated Strip Line

Tzong-Jer Yang, **Jin Jei Wu**, **Dichi Tsai**, **and Hung Erh Lin**
Department of Electrical Engineering, Chung Hua University, HsinChu 30012, Taiwan, R.O.C.

Abstract— The guiding properties of a periodically corrugated metal strip line at microwave frequencies are studied theoretically and experimentally. The edge of the metallic strip line is fabricated into the corrugated grooves with sub-wavelength size. This type of microwave transmission line can easily be excited the spoof surface plasmon polaritons (SPPs) for the appropriate structure parameters. The SPPs can be strongly confined in the vicinity of grooves. In this report, the corrugated metal strip line will be studied by finite element method to calculate Q value which is also measured in the microwave regime. We find that there is low coupling or crosstalk between this type of transmission lines and another normal strip lines. In this type of structure may be extensively used in the electromagnetic compatibility area.

ACKNOWLEDGMENT

This work is partially supported by National Science Council of R.O.C. through the grant number NSC98-2221-E-216-001.

Session 2A1
Scattering and Guiding Characteristics in Periodic Structures

Observation of Geometric Resonance in a Corrugated Waveguide

X. Y. Cheng, **R. Chakraborty**, **S. Mishra**, **V. A. Pogrebnyak**, **and J. J. Whalen**
Department of Electrical Engineering, Faculty of Engineering
State University of New York at Buffalo, 332 Bonner Hall, NY 14260-1920, USA

Abstract— Analysis of electromagnetic wave propagation in periodic structures is of great interest due to the diverse applications of such structures including photonic crystals, Bragg reflector lasers, distributed feedback (DFB) lasers and fiber gratings. It is well known that Bragg reflection leads to the opening of a forbidden gap in the transmission spectrum of a periodic structure. In a periodic waveguide, wave propagation becomes more complex, because the folding of dispersion curve results in interaction between different transverse wave modes. In a periodically corrugated waveguide, under particular waveguide parameters, geometric resonance could arise, which significantly changes the waveguide transmission spectrum. The geometric resonance was predicted in the paper [1].

In the present communication, we are reporting on experimental observation of this phenomenon in a periodically corrugated waveguide. Geometric resonance caused by the interaction between TE_{01} and TE_{02} modes is investigated. The term "geometric" contributes to the specific relation between period and height of the waveguide at which such resonance arises. Geometric resonance results in splitting of the TE_{02} mode cutoff frequency and opening of a band gap in the transmission spectrum.

We fabricated a rectangular waveguide with two periodically corrugated walls, one of which is fixed while another can freely slide with respect to the fixed one; the other two walls are smooth. Period of the corrugation is 3.15 cm, waveguide width is 6 cm, to observe geometric resonance, average height of the waveguide is chosen to be 2.75 cm. The measurements are done on an HP8510C vector network analyzer over a frequency span between 2 GHz and 15 GHz. Meanwhile, a similar waveguide with all smooth walls was also investigated for comparison of the cutoff frequencies and their shifts.

When the average height of the waveguide is adjusted to 2.75 cm, and the groves of the corrugated walls are in phase, geometric resonance occurs. It results in significant cutoff frequency shift for both TE_{01} and TE_{02} modes and opening of a band gap around the cutoff frequency of the TE_{02} mode. In our experiment, cutoff frequency of TE_{01} mode shifts from 5.5 GHz to 6.14 GHz comparing with smooth waveguide; a band gap opens between 9.82 GHz and 12.18 GHz. When the corrugated walls are out of phase for the same waveguide height, the band gap vanishes.

In conclusion, we observed band gap in the transmission spectrum as well as cutoff frequency shift for TE_{01} and TE_{02} modes in a periodically corrugated waveguide under specific geometry configuration. The results can be applied to improve functional capability of microwave, optical, electronic and other devices operating on the basis of periodic structures.

REFERENCES

1. Pogrebnyak, V. A., "Geometric resonance in a periodic waveguide," *J. Appl. Phys.*, Vol. 94, 6979, 2003.

Modal Expansion of Periodically Loaded Waveguides Extended to the Evanescent Frequency Domain

Y. Weitsch and T. F. Eibert
Lehrstuhl für Hochfrequenztechnik, Technische Universität Müchen, Germany

Abstract— A modal series expansion is presented, in which the field solution of the periodically loaded waveguide is formulated with the modal solutions of the homogeneous waveguide. The speciality in this technique is the analysis of not only the propagating but also of the evanescent frequency regime of the homogeneous waveguide. Providing an appropriate loading, left-handed (LH) wave propagation can be established in the evanescent region of the homogeneous waveguide. Due to the periodic trait, Bloch theorem allows the mere calculation of just one periodic unit cell sufficient to give the field solution for the entire architechture [1]. Is the unit cell too complex for an analytical computation numerical methods are required, which are implemented in commercial software tools like CST MWS. They cater accurate computations for driven field problems by full-wave analysis. Essential is the relation of the propagation constant γ to the wave transfer matrix $\mathbf{T}$

$$\mathbf{T}\vec{v} = e^{\gamma p}\vec{v} \tag{1}$$

with p denoting the length of the unit cell and $\vec{v}$ the eigenvector. The $\mathbf{T}$-matrix in turn can be converted into the scattering matrix $\mathbf{S}$. The scattering parameters are the result of a two-port driven problem solution delivered by the numerical method. Thereby, the simulation cell model is excited by few modes, proven to be sufficient in the frequency domain above and below the cut-off frequency of the homogeneous waveguide. Precondition is that evanescent modes are able to transport energy, which is verified in [2]. The reason is the complex nature and the phase difference of the in forward and backward direction decaying evanescent waves enabling a superposition of them in order to represent propagating modes, i.e. LH modes of the loaded waveguide. The field solution in the homogeneous port plane $\vec{e_p}(x,y)$ and $\vec{h_p}(x,y)$ are the modes of the conventional homogeneous waveguide. They are orthogonal and serve as basis functions for the modal series expansion to build up the transverse electric and magnetic field solution of mode k of the actual perturbed waveguide. The coefficients are the components of the eigenvector $\vec{v}_k$ belonging to the eigenvalue k,

$$\vec{E}_{tk}(x,y) = \sum_{n=1}^{N} a_{kn}\vec{e_p}(x,y) + b_{kn}\vec{e_p}(x,y) \tag{2}$$

$$\vec{H}_{tk}(x,y) = \sum_{n=1}^{N} a_{kn}\vec{h_p}(x,y) - b_{kn}\vec{h_p}(x,y) \tag{3}$$

where a_{kn} are the wave amplitudes of the forward propagating waves and b_{kn} the amplitudes of the backward traveling waves. The field solution of the loaded waveguide offers the definition of equivalent voltages and currents to the field solutions giving the Bloch impedance, an important feature for periodic structures useful also in terms of matching considerations. The Bloch impedance together with the propagation constant sufficiently characterise an eigenmode for many applications.

The method provides an efficient determination of eigenvalues because it partly employs an exact numerical computation, which is converted into an eigenvalue problem of very few unknowns. Consequently, it opens a fast characterisation of LH media in particular and thus promoting a fast forward design of metamaterials. The proposed eigenvalue calculation method is applied to reference RH/LH structures yielding dispersion results and the Bloch impedance verifying the procedure. The performance and details will be presented at the conference.

REFERENCES

1. Collin, R. E., *Field Theory of Guided Waves*, 2nd Edition, IEEE Press, New York, 1991.
2. Weitsch, Y. and T. F. Eibert, "Periodically loaded waveguide analysis by propagating and evanescent mode superposition," *European Microwave Conference*, Rome, Sept. 2009.

A Dual-band Branch-line-type Pphase Shifter Using Composite Right/Left Handed Transmission Lines

C. Y. Chin[1] and J. D. Tseng[2]

[1]Department of Electrical Engineering, Chiao-Tung University
1001, University Road, Hsinchu, Taiwan
[2]Department of Electronic Engineering, Chin-Yi University of Technology
35, Lane 215, Sec. 1, Chung-Shan Road, Taiping City, Taichung County, Taiwan

Abstract— In this paper, we present a dual-band branch-line-type phase shifter consisting of composite right/left handed (CRLH) transmission lines. To achieve dual-band operation, quarter-wave CRLH transmission lines are used. A shunt capacitor is added at the transmission port while the other one with equal capacitance is added at the coupling port in order to transform the original four-port network into a two-port network, which is shown to possess phase-shifting property by changing the value of shunt capacitance. Additionally, two central frequencies are designed at 940 MHz and 1800 MHz applicable in the global system for mobile communication (GSM). In our current design, capacitance ranging from 0.2 pF to 4 pF are chosen, although larger range of capacitance is feasible, the exact values are not discussed in this paper. The insertion loss is larger than −1.07 dB for each capacitance at 940 MHz and −1.36 dB at 1800 MHz. The maximum phase difference is 82° at 940 MHz and 134° at 1800 MHz.

Recently, electronically controllable phase shifters have gained significant attention in microwave and millimeter wave communities. Modern mobile communications suffer from the effect of multipath fading, and the need for electronically controllable phase shifters that are inexpensive and easy to fabricate arise. In radar application [1], multiple radiating elements incorporating phase shifters constitute a phased array antenna. Beams are formed by shifting the phase of signal emitted from each radiating element, to provide constructive or destructive interference so as to steer the beam in desired direction. Hayashi and Muraguchi used two quarter-wave length transmission lines to implement an analog phase shifter with compact size [2, 3]. A phase shifter without any additional phase delay line was presented by Wolff and Ahn utilizing an asymmetric ring hybrid and reflecting terminations [4]. Furthermore, a continuously adjustable phase shifter having phase-control range of 360° and frequency range of 5 to 6 GHz was fabricated [5].

REFERENCES

1. Didomenice, M. and R. H. Pantell, "An X-band ferroelectric phase shifter," *IEEE Trans. Microw. Theory Tech.*, Vol. 10, 179–185, May 1962.
2. Hayashi, H. and M. Muraguchi, "A miniaturized MMIC analog phase shifter using two quarter-wave-length transmission lines," *Gallium Arsenide Inteqrated Circuit (GaAs IC) Symposium*, 255–258, Oct. 1999.
3. Hayashi, H., T. Nakagawa, and K. Araki, "A miniaturized MMIC analog phase shifter using two quarter-wave length transmission lines," *IEEE Trans. Microw. Theory Tech.*, Vol. 50, 150–154, Jan. 2002.
4. Wolff, I. and H. R. Ahn, "Asymmetric ring-hybrid phase shifters and attenuators," *IEEE Trans. Microw. Theory Tech.*, Vol. 50, 1146–1155, Apr. 2002.
5. Ellinger, F., H. Jackel, and W. Bachtold, "Varactor-loaded transmission-line phase shifter at C-band using lumped elements," *IEEE Trans. Microw. Theory Tech.*, Vol. 51, 1135–1140, Apr. 2003.

Compact Coplanar-waveguide Band-rejection DGS Resonators

De-Liang Sun[1], **Chien-Jen Wang**[1], **Chia-Hsien Lin**[1], **and Yi-Che Tsai**[2]

[1]Depart. of Electrical Engineering, National University of Tainan, Tainan, Taiwan
[2]Depart. of Electrical Engineering, National Chiao-Tung University, Hsin-Chu, Taiwan

Abstract— In this paper, compact coplanar-waveguide (CPW) defected-ground-structure (DGS) resonators are demonstrated, by using two techniques, including placing floating patches and embedding shorting pins. Two T-shaped slots as a bandstop resonator are etched in two ground planes of a CPW 50 Ω transmission line. Two rectangular patches are symmetrically placed on the bottom layer of the substrate. The patches modeled as an additional capacitance increase the effective capacitance of the resonator. By tuning the geometrical dimension of the patches, the resonance frequency is lowered. Furthermore, frequency reduction and harmonic suppression are improved by embedding two shorting pins or adding two shorting walls inside the patches. The rejection bandwidth decreases and the quality factor (Q) increases due to enhancement of stored energy in the resonator.

Spatial Beam Splitter Design Using Fishnet-type Periodic Structure

N. C. Hsu, **C. Y. Chin**, **and R. B. Hwang**
Department of Electrical Engineering, National Chiao-Tung University
University Road 1001, Hsinchu, Taiwan 300, R.O.C.

Abstract— In this paper, we present a metamaterial-based beam splitter. Such a power splitter was made up of a metamaterial sandwiched by two metallic plates. The metamaterial consists of three-dimensional (3D) fishnet arranged in a two-dimensional square lattice. As is well known from Snell's law, the refracted wave tends to be normal to the interface when the wave is incident from a medium having effective refractive index much smaller than unity into the air region. We properly synthesize the metamaterial having effective refractive index smaller than unity. Furthermore, a line source made by a monopole was embedded in the metamaterial to excite four beams propagating toward four directions. In addition to the calculation of wave-propagating characteristics in the metamaterial, we also implemented a beam-splitting structure invoking the unique characteristic of the metamaterial. The electric-field radiating pattern was measured to prove its spatially beam-splitting characteristics.

Metamaterial is an artificially engineered structure which obtains its properties from its structure rather than directly from its composition. Generally, a metamaterial is synthesized by embedding specific inclusions, for example, periodic structures, in a host medium. The applications of metamaterial in waveguides and antennas designed were intensively developed [1, 2]. A metamaterial with zero-index was demonstrated to have the capability to narrow the far-field pattern associated with an antenna located within it. Besides, a matched zero-index slab could be used to transform curved wave fronts into planar ones [3]. The metamaterial made up of wire medium has been studied intensively, particularly on its effective refractive index, permittivity and permeability. Specifically, the structure composed of metallic mesh wires, which has very small electrical length in the period and wire thickness, can be characterized as a homogeneous medium with a low plasma frequency [4].

REFERENCES

1. Engheta, N. and R. W. Ziolkowski, "Introduction, history and fundamental theories of double-negative (DNG) metamaterials," *Metamaterials: Physics and Engineering Explorations*, Chap. 1, 5–41, IEEE Press, John Wiley & Sons, Inc., Jun. 2006.
2. Ziolkowski, R. W., "Propagation in and scattering from a matched metamaterial having a zero index of refraction," *Phys. Rev. E*, Vol. 70, No. 4, 046608, 2004.
3. Pendry, J. B., A. J. Holden, D. J. Robbins, and W. J. Stewart, "Low frequency plasmons in thin-wire structures," *J. Phys. Condens. Matter*, Vol. 10, No. 22, 4785–4809, 1998.
4. Garcia, N., E. V. Ponizovskaya, and J. Q. Xiao, "Zero permittivity materials: Band gaps at the visible," *Appl. Phys. Lett.*, Vol. 80, No. 7, 1120–1122, 2002.

Electromagnetic Scattering and Guidance by Layered Cylindrical Arrays of Circular Rods

Vakhtang Jandieri[1] and Kiyotoshi Yasumoto[2]

[1]Department of Electrical and Computer Engineering, Kumamoto University
Kumamoto 860-8555, Japan
[2]Kyushu University, Fukuoka, Japan

Abstract— Periodic dielectric or metallic structures are a subject of continuing interest because of their wide use for frequency selective or polarization selective devices in microwaves and optical waves. A periodic array of circular rods is typical of a discrete periodic structure. The electromagnetic response is characterized by the scattering properties of the individual rod and the multiple interactions among the rods periodically situated. Various analytical or numerical techniques have been developed over the years to formulate the electromagnetic guidance and scattering from the periodic arrays. However, the previous pertinent efforts have been mostly concerned with the planar arrays.

In this paper, we shall present a rigorous semi-analytical approach for analyzing electromagnetic scattering and guidance by layered cylindrical arrays as shown in Fig. 1. It consists of N-layered cylindrical arrays of circular rods situated in a homogeneous background medium. The M number of circular rods are symmetrically distributed on each of N-concentric circular rings with radii R_ν ($\nu = 1, 2, 3, \ldots, N$). The radii of the rings must satisfy the condition $R_{\nu+1} - R_\nu > r_{\nu+1} + r_\nu$ so that the circular rods on consecutive rings do not interpenetrate, where r_ν is the radius of the rods located on ν-th ring. The circular rods should be identical along one ring but those on different rings need not be necessarily identical in material properties and dimensions. The method is based on the three-dimensional vector wave formulation and uses the T-matrix of a circular rod in isolation, the reflection and transmission matrices of a cylindrical array based on the cylindrical harmonics expansion, and the generalized reflection and transmission matrices for a cylindrically layered structure. The detailed analytical procedure to calculate the guided mode fields and the scattered fields for specified initial excitations are presented.

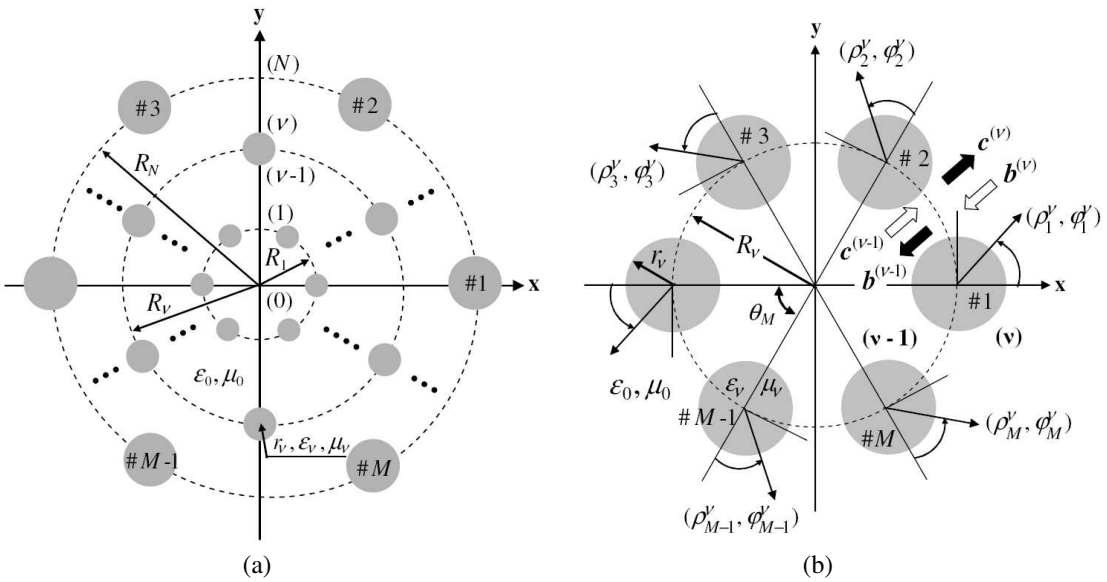

Figure 1: Cross sectional view of N-layered cylindrical arrays formed by M circular rods symmetrically distributed on each of concentric circular cylindrical surfaces with radii R_ν ($\nu = 1, 2, \ldots, N$); (a) a general view and (b) the details of the ν-th layer of the array with local coordinate systems $(\rho_j^\nu, \varphi_j^i)$ ($j = 1, 2, \ldots, M$).

Extraordinary Transmission of TE-polarized Waves through a Dielectric-coated Metallic Grating with Subwavelength Slits

Ruey-Bing Hwang
Department of Electrical Engineering, Chiao-Tung University, Hsinchu, Taiwan, R.O.C.

Abstract— Extraordinary transmission of electromagnetic waves through arrays of subwavelength slits has been intensively investigated [1–3]; particularly on the TM-polarized wave incident on a one-dimensional (1D) metal grating with plasma dielectric function. Due to the surface plasmon present at the interface between the air and metal region, such a guided wave can propagate through the narrow slit and contribute an extraordinary transmission [2, 3]. However, in microwave and millimeter wave regime, the behavior of metal is similar to perfect electric conductor (PEC) rather than plasma medium. Therefore, the surface plasmon is hard to be generated in the slit of a metal grating. Additionally, the transmission response has a cutoff frequency determined by that of the first parallel-plate waveguide mode, where the silts can be regarded as a parallel-plate structure. Transmissions in the frequency lower than the cutoff frequency seem to be impossible.

In this communication, we will present the scattering characteristics of TE-polarized wave through a 1D dielectric-coated metallic (PEC) grating. Interestingly to find that the dielectric-coated metal walls support a surface-plasmon-like wave responsible for the transmission in the frequencies lower than that of the cutoff frequency of the slit without dielectric coating. Additionally, the transmission property of the 1D grating slab exhibits frequency selectivity. Significantly, the transmission peaks can be successfully interpreted by the Fabry-Perot resonance of the surface-plasmon-like wave guided in the slit. We have calculated the scattering characteristics including the transmittance and reflectance for some incident and structural parameters. Besides, the electric and magnetic fields distribution were drawn to facilitate the understanding for physical process of wave guiding phenomenon in the slit. Numerous numerical results based on the rigorous mode-matching method will be presented in the oral presentation.

REFERENCES

1. Ebbesen, T. W., H. J. Lezec, H. F. Ghaemi, T. Thio, and P. A. Wolff, "Extraordinary optical transmission through sub-wavelength hole arrays, " *Nature*, Vol. 391, 667–669, London, 1998.
2. Xie, Y., A. R. Zakharian, J. V. Moloney, and M. Mansuripur, "Optical transmission at oblique incidence through a periodic array of sub-wavelength slits in a metallic host," *Opt. Express*, Vol. 14, 10220–10227, 2006.
3. Sturman, B. and E. Podivilov, "Theory of extraordinary light transmission through arrays of subwavelength slits," *Physical Review B*, Vol. 77, 075106, 2008.

Scattering of Electromagnetic Waves by Inhomogeneous Dielectric Gratings Loaded with Parallel Perfectly Conducting Strips

Tsuneki Yamasaki, **Ryosuke Ozaki**, **and Takashi Hinata**
Department of Electrical Engineering, College of Science and Technology
Nihon University, Japan

Abstract— The scattering of electromagnetic waves by dielectric gratings is of both theoretical and practical interest for integrated optics acousto-optics, optical filters, and holography. Because of recent advances, the refractive index can easily be controlled in the manufacture of periodic structures to serve as fiber gratings, frequency-selective or polarization-selective devices, and photonic crystals. Thus, many analytical and numerical methods have been proposed that are applicable to dielectric gratings having arbitrary structures. To deal with multilayered dielectric gratings such as photonic crystals, it is necessary to analyze the periodic circular arrays. We have also analyzed the scattering problem with multilayered columnar dielectric gratings loaded with rectangular dielectric constant for the case of permittivity variation in rectangular cylinders and elliptical cylinders, by utilizing an improved Fourier series expansion method, multilayer method, and Eigen value matrix method. However, most theoretical and numerical studies have considered the periodic structures in which the material forming grating was either metallic or dielectric in homogeneous media.

In this paper, we considered with inhomogeneous dielectric gratings loaded with parallel perfectly conducting Strips as shown in Fig. 1(a), using the combination of improved Fourier series expansion method and point matching method for TE and TM waves.

In the inhomogeneous dielectric region $S_2\,(0 < x < D)$, the permittivity profile $\varepsilon_2\,(x, z)$ is generally not separable with respect to the x and z variables. Main process of our methods are as follows: (1) The inhomogeneous layer is assembly of M stratified layers of modulated index profile $\varepsilon^{(1)}(z)$ with step size $d_\Delta (= D/M)$ as shown in Fig. 1(b). (2) Taking each layer as a modulated dielectric grating, the electromagnetic fields are expanded appropriately by a finite Fourier series. (3) In the perfectly conducting strip and gap regions at C_1 (or C_1) and C_2 (or C_2) boundary, the electromagnetic fields are matched using an orthogonality relation which makes the matrix relation on both sides using point matching method. (4) Finally, all stratified layers include the metallic regions are matched using appropriate boundary conditions to get the inhomogeneous dielectric gratings loaded with parallel perfectly conducting Strips.

Numerical results are given for the transmitted scattered characteristics for the case of incident angle and frequency with δ (α and β) for TE and TM waves.

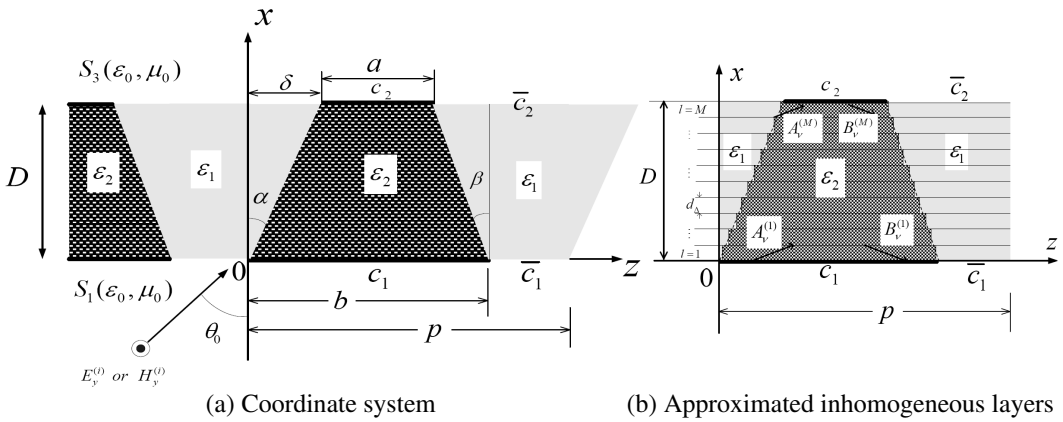

(a) Coordinate system (b) Approximated inhomogeneous layers

Figure 1: Structure of inhomogeneous dielectric gratings loaded with Parallel Perfectly Conducting Strips.

Session 2A2a
Electromagnetic Seismic Fluid Geophysical and Geological Exploration

A New Boundary Zone Absorption Condition for EM Wavefield Propagation

Jianhua Li[1], **Ganquan Xie**[1], **Mingxia Li**[2], **Tzon-Tzer Lu**[3], **and Xianwei Zhou**[4]

[1]GL Geophysical Laboratory, USA
[2]Computational Institute of Chinese Academy, China
[3]National Sun Yat-sen University, Taiwan, R.O.C.
[4]University of Science and Technology in Beijing, China

Abstract— In this paper, we propose a new boundary zone absorption condition for the electromagnetic wavefield propagation. A novel metamaterial has been proposed in Xie and Li's paper "GL double layer EM cloak". By using the cloak metamaterial to fill in the boundary zone, the boundary zone absorption condition is constructed. By GL EM modeling simulation, when the EM wavefield excited inside the domain, which is bounded by the boundary zone, is propagating into the boundary zone and becoming very slow and can not be reached to outer boundary of the zone at any long time. It means that the outgoing EM wave is full absorbed in the boundary zone. Our boundary zone absorption condition can be useful in finite difference method and finite element method simulation of wave in infinite domain.

Thermal Infrared Spectrum Property of Loaded Rock

Zhe Feng[1], **Shanjun Liu**[1], **Lixin Wu**[1, 2], **and Zhongyin Xu**[1]

[1]Institute for Geo-informatics and Digital Mine Research
Northeastern University, Shenyang 110004, China
[2]Academe of Disaster Reduction and Emergency Management
Beijing Normal University, Beijing 100875, China

Abstract— The phenomenon of satellite thermal Infrared anomaly before earthquake has been reported since the late 1980s. The reported abnormal rise of surface temperatures reaches 2–4°C, and occasionally higher than that. Usually, the anomaly appears from one month to several days before the earthquake.

To study the mechanisms of Infrared anomaly, some infrared radiation detection experiments for rock fracture were carried out. The experimental results showed that the TIR anomaly precursors appeared before the fracture of rock samples. There were two kinds of TIR anomaly as precursors of rock fracturing and failure: IR radiation image anomaly and IR radiation temperature curve anomaly, which are prospectively used as the monitoring index of remote sensing for rock fracturing phenomenon. The results of the simulation experiments indicated that TIR remote sensing will be prospectively applied to monitor the earthquake precursors. Further experiment showed that the increment of IR radiation temperature of wet rock was greater than the dry rock in rock compressed loading.

However which bands are suitable for detecting the stress and fracture of rock by the thermal infrared equipment is an open question by now. In this paper, we subjected several blocks of granite to uniaxial deviatory stress up to failure. We measured the IR spectrum variation from the rock samples over the 3–15 μm range by the TurboFT infrared spectroradiometer. The experimental result showed that the radiation strength variations were different in various bands, the radiation strength variations in band 3.6–3.7 μm and 8.5–10 μm were distinct along with the change of rock stress, but in other bands the radiation strength variations was not obvious or the relation between the infrared radiation and stress is not clear. It was possible to conclude that the bands 3.6–3.7 μm and 8.5–10 μm were the suitable bands for the detection of stress and fracture of rock.

New Global and Local Magnetotelluric Field Modeling

Ganquan Xie[1], **Jianhua Li**[1], **and Chow-Son Chen**[2]

[1]GL Geophysical Laboratory, USA
[2]National Centre University, Taiwan, R.O.C.

Abstract— A new Global and Local Magnetotelluric field modeling (GL MTM) is proposed in this paper. The half space or layered half space EM wave field is supposed as Global incident wave field excited by plan wave or by control multiple point sources. The target geophysical areas in Taiwan included the fractures and crack are divided as a set of the subdomains. The total MT wave field propagating the inhomogeneous geophysical area is decomposed as union of the several sub wave field and incident wavefield. Each sub wave field is scattering wave field by scattering interaction between the Global wavefield and local anomalous inhomogeneous geophysical EM material. The GLMTM MT modeling does not need to solve big matrix. Moreover, The GLMTM MT EM modeling does not need artificial boundary and needs not absorption boundary condition. The GL MTM MT modeling is fast and accurate and useful for MT inversion in Geophysical and Earthquake explorations.

Investigation of Ionospheric Anomalies Prior to 2008 Wenchuan Earthquake Based on Statistic Analysis and Signal Detection

Jianyong Li, **Guojie Meng**, **Xuhui Shen**, **and Min Wang**
Institute of Earthquake Science, China Earthquake Administration, Beijing 100036, China

Abstract— On 12 May 2008 at 14 : 28 LT a large earthquake Ms8.0 struck Wenchuan (31.0°N, 103.4°E) in southwest China. The global ionospheric map (GIM) of the total electron content and the greatest plasma frequency foF2 observed by ionosondes revealed clear precursors 3 days prior to the earthquake. In this paper, to have a better understanding of the ionospheric disturbance prior to the Wenchuan earthquake, data recorded by a network of 13 continuous GPS receiving stations in Sichuan are employed to derive TEC, then the GPS TEC are compared with and validated by the ionosondes. Defining anomaly bounds by quartile of TEC values for a sliding window, we analyze ionospheric TEC changes before and after the main shock. Observation reveals that anomalous enhancement of TEC appears in the afternoon of May 9th, 2008, and maximal abnormity reaches five TECU. Analysis of the ionospheric electron densities changes in an area of about 10° in latitude and 10° in longitude from the epicenter demonstrates that the electron density at the ionospheric F2 peak in the afternoon of May 9th, 2008 are significantly increased. In order to further quantify the statistics associated with the detection of a signal, the Neyman-Pearson signal detection method is employed to compute the probabilities of TEC abnormalities of the main shock. The probability of TEC abnormalities of 13 GPS receiving stations was calculated at each 15-min time. The result reveals that the Pd value on May 9th increase, with largest Pd value larger than 0.5, indicating that ionospheric abnormal enhancement on May 9th is most possibly a seismo-ionospheric signature. Based on the above results, possible mechanisms of ionospheric abnormity on May 9 prior to the Wenchuan earthquake are discussed.

Sumudu Magnetic Field Solutions of Maxwell Equations

Fethi Bin Muhammad Belgacem
Faculty of Information Technology, Arab Open University, Branch P. O. Box 830, Al-Ardhia 92400, Kuwait

Abstract— When Sumudu transformed Maxwell's Equations yield transient electric and magnetic field solutions. Previously, the Sumudu Reciprocity property was used to extract electric field solutions for Transversal Electromagnetic Planar, (TEMP), waves in a lossy medium. Here we present a parallel treatment for the magnetic field, using Sumudu newly established properties. Considered a Fourier transform derivate, with many unique properties including unit and scale preserving, in light of soaring applications in the literature, the Sumudu seems to be claiming more pragmatic fame.

Session 2A2b
Biomedical Electromagnetic Instruments and Electromagnetic Condense Materials and Imaging

Generalized Maximum Efficiency Theory on Multi-stage Inductive Coupling

S. Bai[1, 2], D. C. Ng[2], E. Skafidas[2], and I. M. Y. Mareels[1]

[1]Department of Electrical & Electronic Engineering, The University of Melbourne, Australia
[2]Victoria Research Laboratory, National Information & Communication Technology Australia
The University of Melbourne, Victoria 3010, Australia

Abstract— Inductive coupled coils have been implemented to transmit power wirelessly for many applications such as micro-systems, RFID, and many biomedical implants. All these applications benefit from the distinct advantage to power these devices without any physical connections comparing to conventional energy transmission method using wires and connectors. Despite their different modes, geometries, coupling distances and power consumption requirements, they share the same rules which govern the design of the coils in order to achieve better efficiency of power transfer. The efficiency is even more critical in biomedical implants since any power loss due to the inefficient power link will finally be transformed into heat accumulated in the body which leads to safety problem. A novel feature on maximizing the efficiency is derived in this paper and it is further generalized to multi-stages inductive links which may be of special interest to be used in a high-density 1024-electrode epi-retinal prosthesis. Although multi-stage coupling include more coils with power loss internally, it is still possible to attain higher overall efficiency by improving each coupling stage individually whenever wireless connection is required. This is especially in weakly-coupled case where the air gap between transmitter and receiver is too large. Such multi-stages coupling configuration is also suitable for surgery in epi-retinal prosthesis.

The Computation of Coupling onto the Wires Enclosed in Cavity with the Apertures

Jianshu Luo, **Jiyuan Shi**, **and Xufeng Zhang**
Science College, National University of Defense Technology, Changsha 410073, China

Abstract— The paper provides a new hybrid method based on MoM-GF (method of moments-Green's Function) and FWTLT (Full Wave Transmission line theory) method compute the coupling onto the wires enclosed in cavity with apertures under a plane electromagnetic wave. The MoM-GF method is sufficiently accurate to calculate the equivalent magnetic, and to get the electromagnetic field in cavity. Then, using the FWTLT to deal with the three-dimensional wire like structures enclosed in cavity. It is a fast and accurate moment method to analysis for wire bunds by employing the cavity Green's function. Last, numerical results of the wire coupling current is provided.

3D GL EMFH Modeling and Inversion for Leakless Auto EMS in Steel Metal Casting and Biomedical EM Instruments Design

Jianhua Li, **Ganquan Xie**, **Lee Xie**, **and Feng Xie**
GL Geophysical Laboratory, USA

Abstract— In this Paper, we propose a new 3D GL electromagnetic (EM) stirring method for steel and metal casting. The 2.5D GL stirring method has been published in PIERS 2007. The GL stirring method is researching up to 3D in advanced. The 3D GL EM stirring method is a coupled modeling and inversion. The 3D GL EM, fluid, heating, and crystal stress four processing models are consistently coupled in our 3D GL EM string method for the steel and metal casting. The method contains the macro and micro, periodic and non periodic steel and metal material structure and content analysis and simulation. It has wide application in steel and metal casting and biomedical EM instruments design.

Session 2A3
Plasmonic Nanophotonics 1

Imaging Mechanism of the Fractal Plasmonic Metamaterial Lens

Shiyi Xiao, **Xueqin Huang**, **and Lei Zhou**
Physics Department, Fudan University, Shanghai 200433, China

Abstract— Surface plasmon polaritons (SPPs) are electromagnetic (EM) eigenmodes bounded at metal/dielectric interfaces. Due to two important features — local field enhancement and subwavelength imaging capability, the SPP has attracted considerable attention recently and many SPP-based applications were proposed [1]. In 2005, Garcia-Vidal et al. [2] demonstrated that a metallic plate with periodic holes can mimic a plasmonic metamaterial in terms of SPP properties, with a well-defined effective ω_p. However, to make that idea work, one has to fill the holes with *high-index materials*.

In our recent work, we showed that a metallic plate with fractal-shaped slits supports transverse-electric (TE) and transverse-magnetic (TM) SPPs simultaneously, without using high-index insertions, and such a plasmonic metamaterial can work as a near-field lens for subwavelength imaging [3]. Microwave experiments demonstrated that the formed image exhibits a resolution of $\lambda/15$, and finite-difference-time-domain (FDTD) simulations showed that similar effects can be realized in infrared frequency regime with appropriate designs.

In this work, we explore the detailed working mechanism of such subwavelength near-field imaging effect. We found that the coupling between the evanescent waves and the SPP in the fractal lens leads to a unit-amplitude transfer of the high-momentum components of the source across the lens, resulting in an image formed without distortions. We further explored the imaging functionalities of the lens for various sources, and discussed the inherent limitations on the image resolutions.

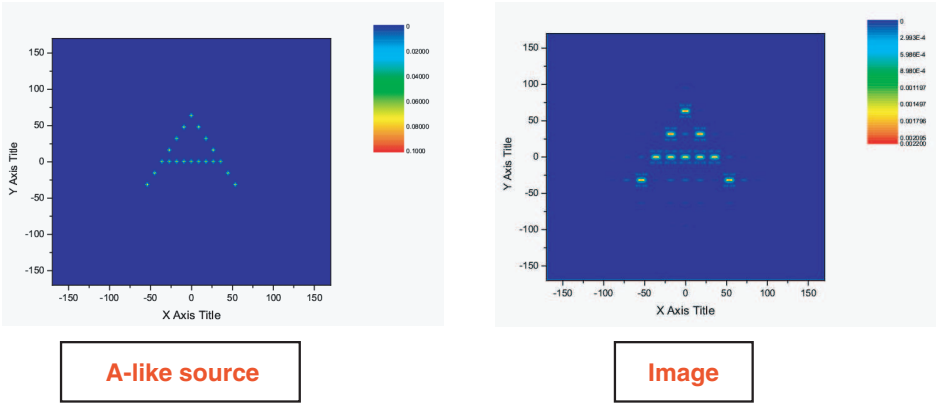

Figure 1.

REFERENCES

1. Ozbay, E., "Plasmonics: Merging photonics and electronics at nanoscale dimensions," *Science*, Vol. 311, 189, 2006.
2. Garcia-Vidal, F. J., et al., "Surface with holes in them: New plasmonic metamaterials," *J. Opt. A: Pure Appl. Opt.*, Vol. 7, S97, 2005.
3. Huang, X., et al., "Fractal plasmonic metamaterials for subwavelength imaging," *Appl. Phys. Lett.*, arXiv:0908.0201, 2009 (submitted).
4. Xiao, S., et al., unpublished.

Plasmonic Phase Transitions

Vasily V. Klimov and Mikhail Yu. Pikhota
Lebedev Physical Institute, Moscow, Russia

Abstract— Plasmonic properties of nanoparticles of complex shape are investigated both analytically and with computer simulations. Special attention is paid to morphology of ellipsoid, cuboid, octahedron, cubooctahedron and clusters of nanoparticles. It is shown for the first time that continuos transformation of nanoparticles shape or cluster geometry etc is accompanied with drastic changes in plasmon spectra [1]. Such transformation of shape occur, for example, during melting/crystalization of nanoparticles or operation of active plasmonic elements.

As an example the transformation of plasmonic resonant values of dielectric constant of nanoparticles of cubic morphology is shown on Fig. 1. During this transformation the nanoparticle shape changes from pure sphere to cube. Such transformation can be described by equation $x^n + y^n + z^n = 1$ with n from 2 (sphere) to infinity (cube). From this figure one can see that at $n \approx 3$ new high frequency plasmonic modes with with $0 > \varepsilon(\omega) > -1$ ($\omega_{pl} > \omega > \omega_{pl}/\sqrt{2}$) which are specific only to cubes appear. It means that starting from such point spectra of plasmon oscillation change radically. We call such effect as plasmonic phase transition.

Analogous phase transition occurs for tetrahedron, cubooctahedron and cluster of 2 nanoparticles [2] or even for infinite linear chain of nanoparticles when the distance between nanoparticles decreases. It is very important that plasmonic phase transitions occur only for nanoparticles of complex shape and do not occur for usually considered nanoparticles of trivial spheroidal or ellipsoidal shapes.

The results obtained are of great importance for spectroscopic characterization of nanoparticles transformation during their growth and melting. Besides such radical transformation of plasmonic spectra can be used for elaboration of active elements for nanoplasmonics. New high frequency plasmonic modes are also crucially important for description of van der Waals forces between plasmonic nanoparticles [3].

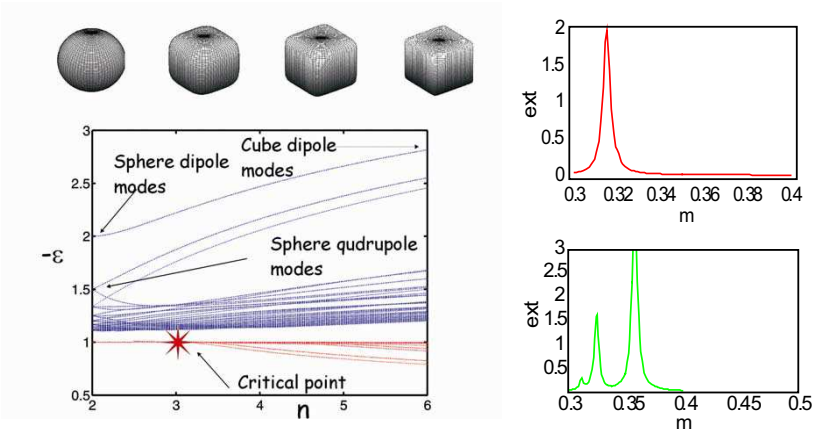

Figure 1: Plasmonic spectra of nanoparticle with surface described by $x^n + y^n + z^n = 1$ as function of shape (parameter n). At critical point ($n \approx 3$) new high frequency plasmonic modes with $0 > \varepsilon(\omega) > -1$ ($\omega_{pl} > \omega > \omega_{pl}/\sqrt{2}$) which are specific to cubes appear (top); extinction spectrum of silver sphere ($n = 2$) (middle);extinction spectrum of cube with additional lines (bottom).

ACKNOWLEDGMENT

Authors thank Russian Foundation of Basic Researches (grants No. 05-02-19647, No. 7-02-01328) for financial support.

REFERENCES

1. Klimov, V., *Physics — Uspekhi*, Vol. 51, 8, 839–845, 2008.
2. Klimov, V. and D. Guzatov, *Appl. Phys. A*, Vol. 89, 305, 2007.
3. Klimov, V. and A. Lambrecht, "Plasmonics," DOI 10.1007/s11468-008-9074-y, 2008.

Strong Hybridization of Localized Surface Plasmons and Anisotropic Molecular Layers in Different Orientation: Quasi-static and Full-wave Analysis

Yuwen King, **Yaxian Ni**, **and Lei Gao**
Jiangsu Key Laboratory of Thin Films, Department of Physics, Soochow University, Suzhou 215006, China

Abstract— The optical properties of a spherical plasmonic particle coated by anisotropic molecular layer are investigated by both quasi-static approximation and full-wave theory. We discuss two cases that molecules oriented parallel and perpendicular to the coating normal separately. Strong hybridization between the localized plasmonic resonances and so-called molecular resonances occurs in small-particle limit and thin-coating approximation, and the coupled-resonance condition is achieved analytically. For large particles, surface resonances of the coated particles are significantly influenced by the anisotropy of differently oriented molecular layer and the coupling effect, which is also affected by the thickness of the layer.

REFERENCES

1. Ambjörnsson, T., G. Mukhopadhyay, S. P. Apell, and M. Käll, "Resonant coupling between localized plasmons and anisotropic molecular coatings in ellipsoidal metal nanoparticles," *Phys. Rev. B*, Vol. 73, 085412, 2006.
2. Gao, L. and X. P. Yu, "Second- and third-harmonic generations for a nondilute suspension of coated particles with radial dielectric anisotropy," *Eur. Phys. J. B*, Vol. 55, 403–409, 2007.
3. Gao, L., T. H. Fung, K. W. Yu, and C. W. Qiu, "Electromagnetic transparency by coated spheres with radial anisotropy," *Phys. Rev. E*, Vol. 78, 046609, 2008.
4. Kociak, M., O. Stéphan, L. Henrard, V. Charbois, A. Rothschild, R. Tenne, and C. Colliex, "Experimental evidence of surface-plasmon coupling in anisotropic hollow nanoparticles," *Phys. Rev. Lett.*, Vol. 87, 075501, 2001.

Couplings of Localized Surface Plasmons in Nanoparticle Chains

Bin Xi, **Hao Xu**, **and Lei Zhou**
Physics Department, Fudan University, Shanghai 200433, China

Abstract— Metal nanoparticle chains are good candidates of subwavelength waveguides to transport optical signals. The coupling effect of localized surface plasmons in nanoparticle chains plays a key role in wave transportation along the chains [1, 2]. Previous studies on this issue, employing finite-difference-time-domain (FDTD) simulations or multiple scattering methods, were not able to establish a general and complete picture to understand the coupling effects between localized surface plasmons.

We found that such coupling effects are well understood with a framework of a tight-binding method (TBM) [3, 4], where an optical mode of the whole system is a linear combination of each individual localized surface plasmon in single nanoparticle. Here, we combine the FDTD simulations on realistic structures and the TBM to study the coupling effect of localized surface plasmons in nanoparticle chains. We found that the coupling strength between two nonoparticles strongly depend on the shape of the nanoparticle as well as the distance between them. The TBM combined with the full-wave simulation not only allows us to predict accurately the resonance frequencies in various nanoparticle chains, but also allows us to quantitatively determine the coupling strength between two adjacent localized surface plasmons. We finally discuss how a "dark mode" is formed when the shape of nanoparticle changes.

REFERENCES

1. Fung, K. H. and C. T. Chan, *Opt. Lett.*, Vol. 32, 973–975, 2007.
2. Maier, S. A., P. G. Kik, and H. A. Atwater, *Appl. Phys. Lett.*, Vol. 81, 1714, 2002.
3. Xu, Y., et al., *Phys. Rev. E*, Vol. 62, 7389, 2000.
4. Xu, H., et. al., unpublished.
5. Xu, H., et. al., unpublished.

Long-range Surface Magnetoplasmon on Thin Plasmon Film with Voigt Configuration

Yung-Chiang Lan
Institute of Electro-Optical Science and Engineering, National Cheng Kung University, Taiwan, R.O.C.

Abstract— Long-range surface plasmon (LRSP) is the high-frequency branch of the SP wave on a thin plasmon film. Due to the electric fields vanishing in the plasmon center, the LRSP is a low loss mode with a longer propagation distance on the film. The LRSP in an external static magnetic field is called the long-range surface magnetoplasmon (LRSMP) and has been investigated in the literature. However, the transition from LRSP to LRSMP under a dynamic external magnetic field and the transmission of a surface wave from a LRSP region to a LRSMP region have never been discussed. Moreover, the possibility of a new LRSMP mode existing in the second gap of the bulk magnetoplasmon have never been studied yet.

In this work, the properties of the LRSMP with Voigt configuration are investigated via computer simulation and theoretical analyses. The simulated geometry is a lossy thin plasmon film with a thickness of $0.14\lambda_p$ (λ_p is the plasma wavelength) and the damping constant $\Gamma = 0.076\omega_p$. The LRSP and LRSMP are excited by ATR method with the Otto configuration. The particle-in-cell finite-difference time-domain (PIC-FDTD) model is utilized to simulate the dynamics of the plasma and its response to incident radiation. In this model, the plasma oscillation and cyclotron motion of electrons are considered automatically. The dispersion relations of LRSP and LRSMP on the plasmon film are also derived and analyzed.

The simulated results indicate that, LRSP is transformed to LRSMP instantly as the external magnetic field is applied along with a distinct change of the reflected power. But the electric and magnetic fields become asymmetric and strongly depend on the direction of the external magnetic field. The simulated field patterns and dispersion relations agree with those of the theoretical prediction very well. When a surface wave propagates on a plasmon film with the LRSP-LRSMP-LRSP structure, a small part of the power will be transferred to the radiation mode at the interfaces. However, the field patterns in the third region recover ones of the original LRSP. Finally, the new SMP mode located above the fisrt magnetoplasmon branch with $\omega_{SMP} > \omega_p$ is verified by the PIC-FDTD simulation.

In conclusion, the properties of the LRSMP are illustrated. The new LRSMP mode with the frequency larger than the plasma frequency is verified.

Standing-wave-like Surface Plasmon Polariton between Two Silver Nanorings

Sheng Chung Chen[1] and Jr. Chau Shiu[2]

[1]Department of Optoelectronic Engineering, Far East University, Taiwan, R.O.C.
[2]Institute of Electrical Engineering, Far East University, Taiwan, R.O.C.

Abstract— Metal nanostructures exhibit a wide variety of extraordinary optical properties. All of these characteristics are ultimately related to the charge oscillations inside the metal nanostructures. It is a challenge to figure out the way of charge oscillation in nanosized metal particles experimentally, however, the corresponding evidences might be derived from the near-field distribution which is very sensitive to size and shape of a nanostructure, polarization of incident wave. In this research, we use numerical simulation to obtain the near-field distribution around the nanorings, and many exquisite prospects are unveiled.

Three dimensional finite-difference time-domain method, one of powerful time-dependent Maxwell's equations solvers, was applied to this study. In order to have a larger calculating space, parallel computation was implemented with MPICH (portable implementation of Message Passing Interface) library. The Yee cell is a cube with 1 nm in edge and perfectly matched layer absorbing boundary condition is used.

We study the doughnut-like nanoring, the radius of the nanoring hole is 10 nm, and the cross-section of the nano-doughnut has a radius of 5 nm. When a plane wave is passing through a single silver nanoring, a significant resonant effect is observed, such resonance is not found if the nanoring is replaced by a sizable spherical particle. And the order of the polar mode, which plays a critical role in extinction spectra, can be checked by depicting the electric components on the silver nanoring. If two identical silver nanorings are placed closely, besides an enhanced coupling resonance appears at the center of the nanorings, the interesting is a quasi-standing electromagnetic wave with ultra-short wavelength oscillates between two nanorings .

The detail of near-field distribution around silver nanorings is unveiled. The results are useful in explaining some extraordinary optical properties and helpful to raise the sensitivity in application to bio-sensors.

ACKNOWLEDGMENT

This research is supported by the National Science Council of Taiwan, R.O.C. through the grant number NSC 98-2120-M-002-004-.

Beyond-limit Light Focusing in the Intermediate Zone

K. R. Chen
Department of Physics, Institute of Electro-optical Science and Engineering
National Cheng Kung University, 1 University Road, Tainan 70101, Taiwan, R.O.C.

Abstract— Diffraction limits the light behaviour in optical systems and sets the smallest achievable line width at half the wavelength. With FDTD simulations and experiment measurements, we demonstrate that a new nanolens of designed plasmonic subwavelength aperture, which generates sub-limit wave functions and reduces the diffraction via an asymmetry, can focus light to a single-line with its width smaller than the diffraction limit of half the wavelength in the intermediate zone. The results indicate that the near-field effect on the light focused is negligible in the region $2 < kr < 4$ where the line-width is smaller than the limit. The fields focus outside of the near zone and hence are capable to propagate, as consistent with our prediction. The light focusing process, besides being of academic interest, is expected to open up a wide range of application possibilities.

Plasmonic Effect of Nanoshell Dimer for Molecular Fluorescence

Mao-Kuen Kuo[1], **Chi-San Chen**[1], **Cheng-Yu Lee**[1], **and Jiunn-Woei Liaw**[2]

[1]Institute of Applied Mechanics, National Taiwan University
1, Sec. 4, Roosevelt Rd., Taipei 106, Taiwan, R.O.C.
[2]Department of Mechanical Engineering, Chang Gung University
259 Wen-Hwa 1st Rd., Kwei-Shan, Tao-Yuan 333, Taiwan, R.O.C.

Abstract— The enhancement of a single molecule's fluorescence by a nanoshell dimer (a pair of Ag or Au nanoshells) is studied by the use of the multiple multi-pole (MMP) method. A two-stage model is used to analyze the fluorescence process: The excitation and the following emission stages. The molecule is assumed located within the dimer's gap. For the first stage, the amplification of local-field intensity is calculated by a model of an incident plane wave illuminating the dimer. Further, for the emission stage, the normalized nonradiative and radiative decay rates of an electric dipole (the excited molecule) in the presence of the dimer are also studied, and then the quantum yield of the system in terms of both decay rates is obtained. The results indicate that the overall effect of nanoshell dimer depends on the orientation as well as the absorption and emission spectra of the specific molecule. Moreover, the enhancement factor of a nanoshell dimer on the fluorescence is much higher than that of a solid-nanoparticle dimer in the longer-wavelength regime. In addition, the life time is significantly reduced by the nanoshell dimer, due to the energy transfer between the dipole and the dimer.

Transmission through Metallic Array Slits with Perpendicular Cuts

Yan Zhang, **Yanhua Wang**, **and Yingqi Wang**
Department of Physics, Capital Normal University
Xisanhuan Beilu 105, Beijing 100048, China

Abstract— Enhanced transmission through metallic subwavelength openings has inspired a great of interest since the work of extraordinary optical transmission (EOT) through a subwavelength holes array has been reported. Besides of subwavelength holes arrays, array of slits are another topic of considerable fascination to achieve extraordinary high transmission in several applications, including superlenses and optical filters. The initial work owes the EOT to surface plasmons, which can be modulated by adjusting both surfaces of slits or apertures in optical, microwave, and terahertz regions. Slits support a propagating transverse electromagnetic wave without cutoff, and the high transmission of slits was due to the Fabry-Perot (F-P) interferences for thick plate. The F-P cavity theory emphasizes the depth of slits. Up to now, most researchers put their emphasis on the surface configuration of metal plate, periodicity or depth of slit arrays or holes. However, the dependence of transmission on conformation inside apertures is not investigated systematically.

Lockyear et al. have investigated the transmission of a normally incident plane wave through a singly stepped subwavelength slit in a metal plate. The existence of the step, which locates in the middle of slits, increases the resonant wavelength substantially. The fields at resonant frequencies show all of the transmission maxima correspond to the fundamental F-P mode. In this presentation, the transmission spectra of periodic slits modified by perpendicular cuts in a metal plate are studied in the near infrared region. There exist three higher order F-P modes in the considered wavelength range. The existence of cuts in the middle of slits decreases the resonant wavelength of even order F-P mode, which is quite different from the case of odd order mode (The fundamental mode with mode number 1 also belongs to odd order mode). Remarkably, the resonant wavelength does not change monotonically, which depends on the location of perpendicular cuts. Widening the cuts at the center of slits, the resonant wavelength keeps nearly fixed for even order modes, while increases for odd order modes. These findings can not be interpreted by the established theories and raise new questions about the higher order resonances. To the best of our knowledge, this is the first work to investigate the influence of cuts on higher modes of slit, which is quite different from that on the fundamental mode studied in previous papers. Shifting the cuts along the vertical slits, we can get two kinds of resonances, which can be excited when the cuts locate at the center of electric or magnetic antinodes. In addition, we propose a new explanation model, in which we ascribe the resonance to three reasons: the F-P cavity theory, the surface current flow, and the surface charges. When the cut width is increased, the resonant wavelength for odd modes increases monotonically, while the resonant wavelength for even modes keeps nearly fixed. All calculated results are well explained by our proposed model.

Session 2A4
Transformation Optics and Metamaterials

Illusion and Cloaking Effects Created by Using Transformation Optics and Metamaterials

Y. Lai, **J. Ng**, **H. Y. Chen**, **D. Z. Han**, **J. J. Xiao**, **Z. Q. Zhang**, **and C. T. Chan**
Department of Physics, The Hong Kong University of Science and Technology
Clear Water Bay, Kowloon, Hong Kong, China

Abstract— We propose to use transformation optics to generate a general illusion such that an arbitrary object appears like some other object of our choice. This is achieved by an illusion device constructed with metamaterials such that it can transform the scattered light outside a virtual boundary into that as if scattered from the second object chosen for the illusion, regardless of the direction and profile of the incident wave. Cloaking effect is also achieved by creating a special form of illusion: the illusion of free space.

Negative Effective Parameters for Periodic Arrays of Dielectric Circular Cylinders

R. L. Chern[1] and Y. T. Chen[2]

[1]Institute of Applied Mechanics, National Taiwan University, Taipei 106, Taiwan, R.O.C.
[2]Institute of Photonics and Optoelectronics, National Taiwan University, Taipei 106, Taiwan, R.O.C.

Abstract— The effective permittivity and permeability are two of the most basic quantities of a composite medium. They are especially important in the study of metamaterials [1], which possess properties not available in naturally occurring materials such as negative permeability [2] or negative index of refraction [3]. These counterintuitive properties come from the interaction of electromagnetic waves with the structure rather than directly from the material composition. In particular, the dielectric photonic structure may exhibit a strong magnetic activity [4, 5] and gives rise to optical properties far from the volume average of the constituent material parameters. This feature is attributed to resonances inside the structure, and the fields outweigh the material in characterizing the effective parameters. To treat in effect a composite structure as a homogeneous medium, the microstructures that compose the medium have to be much smaller than the wavelength λ. The effective parameters are therefore *quasistatic* in nature. For a periodic microstructure with the lattice period a, the ratio a/λ has to be small for the effective parameters to be valid. A suitable effective medium theory for metamaterials should also be able to characterize the effective parameters up to a certain frequency range where the retardation effect and resonance feature are taken into account.

In this study, we investigate the effective parameters for periodic arrays of dielectric circular cylinders. The effective medium model based on the field averaging over an equivalent unit cell is used to characterize the effective permittivity ε_{eff} and permeability μ_{eff}. In the quasistatic regime, the effective parameters exhibit the Lorentz-like *anomalous* dispersion and give rise to negative values near the resonances. For TM polarization, the electric resonance is the leading-order response and the region of negative ε_{eff} spreads over a wide range of frequency. The magnetic resonance, on the other hand, is a high-order response with a smaller resonance width. In particular, there exists a frequency interval where ε_{eff} and μ_{eff} are simultaneously negative. For TE polarization, the role of electric and magnetic resonances are mutually exchanged and the resonance widths become smaller. The frequency interval of both negative ε_{eff} and μ_{eff} is not present. These features parallel with the results obtained by an alternative homogenization approach [**?**]. The mechanisms of anomalous dispersion for effective parameters are illustrated with the localized field patterns at the resonant frequencies. Validity of the effective parameters are further examined by the band structure calculation of the periodic structure. The regions where either ε_{eff} or μ_{eff} is negative coincide with the photonic band gaps. In the interval where both ε_{eff} and μ_{eff} are negative, there exist two propagating branches with special features. In the static regime, the effective parameters are simplified to the well-known Maxwell-Garnett mixing rule and the resonance feature becomes insignificant.

REFERENCES

1. Smith, D. R., J. B. Pendry, and M. C. K. Wiltshire, "Metamaterials and negative refractive index," *Science*, Vol. 305, 788–792, 2004.
2. Pendry, J. B., A. J. Holden, D. J. Robbins, and W. J. Stewart, "Magnetism from conductors and enhanced nonlinear phenomena," *IEEE Trans. Microwave Theory Tech.*, Vol. 47, 2075–2084, 1999.
3. Shelby, R. A., D. R. Smith, and S. Schultz, "Experimental verification of a negative index of refraction," *Science*, Vol. 292, 77–79, 2001.
4. O'Brien, S. and J. B. Pendry, "Photonic band-gap effects and magnetic activity in dielectric composites," *J. Phys.: Condens. Matter*, Vol. 14, 4035–4044, 2002.
5. Felbacq, D. and G. Bouchitté, "Theory of mesoscopic magnetism in photonic crystals," *Phys. Rev. Lett.*, Vol. 94, 183902, 2005.
6. Vynck, K., D. Felbacq, E. Centeno, A. I. Căbuz, D. Cassagne, and B. Guizal, "All-dielectric rod-type metamaterials at optical frequencies," *Phys. Rev. Lett.*, Vol. 102, 133901, 2009.

Full-parameter Realization of the Invisibility Cloak Based on Transmission-line Metamaterials

Xiao Liu, **Chao Li**, **Kan Yao**, **Xiankun Meng**, **and Fang Li**
Institute of Electronics, Chinese Academy of Sciences, Beijing, China

Abstract— The verifications of the invisibility cloak had been mainly numerical or simulated until the first two-dimensional realization was reported using resonant metamaterials. The required material parameters of the cloak are both inhomogeneous and anisotropic, so that reduced parameters have to be used in such realization to alleviate the design difficulties. In this article, we demonstrate that the two-dimensional full-parameter invisibility cloak in a cylindrical basis under the concept of transformation optics can be realized by employing specific transmission-line metamaterials. For a TM illumination, such metamaterial is anisotropic with three branches of its unit cells representing three nonzero elements of the constitutive parameter tensors. A relation has been set up between the required material properties of the cloak and the parameters of the branches, so that it is easy to design the transmission-line metamaterial by following the equation. Based on this independent control, the whole cloak shell can be approximated by a discrete metamaterial network with each cell representing the required properties at any position of the cloak medium. Hence full-parameter cloak can be achieved. According to the analysis, inductors and capacitors are suitable to implement the branches, so the cloak becomes an inductor-capacitor (L-C) network. Here we fabricate a cloak device using microstrip lines to realize the host interconnecting lines and lumped elements to implement the branches. The experimental demonstration shows that: for our L-C based cloak, the cloaking effect is evident that the electromagnetic wave interacts with the cloak causing little scattering. Due to the non-resonant property of the structure, broadband property can also be expected.

Homogenization of Metallic Metamaterials and Electrostatic Resonances

B. Guizal[1], **D. Felbacq**[1], **and F. Zolla**[2]

[1]University of Montpellier 2, Groupe d'Etude des Semiconducteurs UMR-CNRS 5650
Montpellier Cedex 05 34095, France
[2]Institut Fresnel, Marseille Cedex 20 13397, France

Abstract— It has been noted that the usual approaches for homogenization (e.g., Bruggeman) could lead to singularities when considering composites comprising materials with positive and negative permittivities. This situation is specifically encountered in the field of metamaterials, in particular in the visible range. The question then arises to unerstand if these resonances are just artifacts or possess, on the contrary, a clear physical meaning.

In this work, we study the homogeneous properties of a bidimensional structure that is made of a periodic set of metallic wires embedded in a dielectric host medium. The structure is considered in a region of wavelengths that are much larger than the period of the structure. The work comprises a theoretical part where we develop a two-scale approach to the homogenization of the structure. As it is the case for the common physical approach, it leads to an effective permittivity with strong (electrostatic) resonances as well. The theoretical results, and the presence of resonances, are confirmed by numerical computations based on a rigorous modal approach. In the numerical results we consider specifically the case of silver and gold nanowires, described by a dispersive negative permittivity. We show that the main parameters for the onset of resonances is the optical filling ratio of the structure. Keeping in mind the possibility of performing experiments, it is far easier to keep the geometrical filling ratio constant and to consider strongly dispersive materials in the range of wavelengths considered. Here, besides the crucial fact that they are widely used in nanotechnology, silver and gold nanowires comply with our needs in the visible region of the spectrum.

ACKNOWLEDGMENT

This work was done under the financial support of the Agence Nationale de la Recherche (grants POEM ANR-06-PNANO-001-08 and SCOP ANR-07-PNANO-053-01).

Subwavelength Imaging: Where Do Evanescent Waves Come from?

C. Ciraci, D. Felbacq, and B. Guizal
University of Montpellier 2, Groupe d'Etude des Semiconducteurs, UMR-CNRS 5650
34095 Montpellier Cedex 05, France

Abstract— Since the article by Pendry on the slab superlens, a great deal of articles have addressed the possibility of beating the diffraction limit by using negative index media. The main point at issue is the so-called "amplification of evanescent waves" which is shown to increase the resolution of the image.

It is interesting to note that the structures under study are considered to be homogeneous, e.g., a direct slab of negative index is considered. However, in practice, a negative index can only be obtained as an effective behavior of an otherwise strongly heterogeneous medium. In that case, when the (heterogeneous) structure is illuminated by a purely propagating wave (e.g., a plane wave), it gives rise to evanescent waves near the interfaces, despite the fact that there were none in the incident field. This shows that the simple statement that "evanescent waves" are amplified is in fact meaningless if the evanescent waves produced by the heterogeneity of the structure are not negligible. This simple fact shows that a more sublte theoretical approach is needed in order to understand how a metamaterial can help improving the resolution, if it can.

In this work, we develop several theoretical tools that allow to understand and quantify the way an incident field propagates inside a nanostructure. The mathematical approach is based on the transfer operator that possess a complete family of eigenvectors. One of the main results of the work is that it is possible that the field propagates mainly on evanescent waves rather than on propagating modes. A similar phenomenon called "canalization regime" has been identified by P. A. Belov.

ACKNOWLEDGMENT

This work was done under the financial support of the Agence Nationale de la Recherche (Grants POEM ANR-06-PNANO-001-08 and SCOP ANR-07-PNANO-053-01).

Superlenses and Optical Remote Scattering

A. Nicolet and F. Zolla
Institut Fresnel UMR CNRS 6133, Aix-Marseille Université
Ecole Centrale de Marseille, Campus de Saint-Jérôme, Marseille F-13013, France

Abstract— In recent years, transformation optics has become a very active new field. It has been popularized through the idea of J. B. Pendry that an invisibility cloak can be designed by transforming space and considering the corresponding equivalent material properties [1, 2]. Indeed, it is a deep property of the Maxwell's equations that they are purely topological (when written in the proper formalism [3]) and that all the metric aspects can be encapsulated in the electromagnetic material properties. A direct consequence is that any continuous transformation of space can be encoded in an equivalent permittivitty and permeability. Extending this principle beyond continuous transformations allows to design exotic optical devices such as the invisibility cloak. Another example of transformation optics devices are the superlenses [4]: even if these devices were proposed a few years before the rise of transformation optics, they are nicely interpreted as corresponding to a folding of the space on itself. It has been suggested that such devices allow a kind of "remote action" of the scatterers making possible things such as immaterial waveguides called "invisible tunnels" [5]. In this paper, we investigate numerically (using finite element modelling) the behaviour of cylindrical superlenses to show some of their amazing possibilities but also to define some of their limitations.

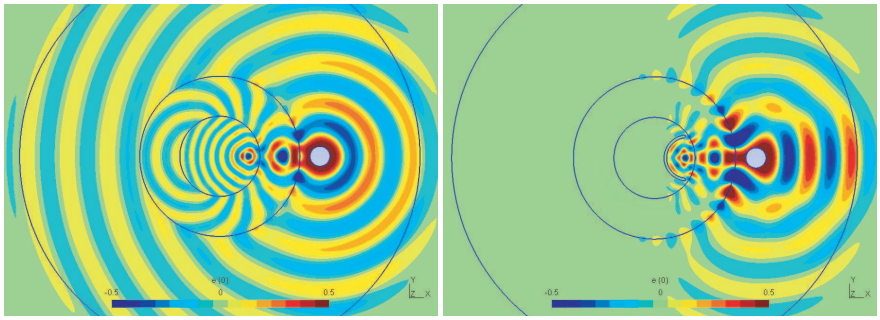

Figure 1: On the left, a superlens designed by folding the empty space on itself do not perturbate the cylindrical waves emitted by a wire antenna but for the attenuation due to the dissipation introduced in the superlens permittivity in order to avoid the anomalous resonances [6]. The antenna has an image inside the superlens and inside the central part of the device. On the left, a small perfectly conducting deflector acts on the image of the antenna in the central part of the device and forces the waves to propagate only to the right. This can also be interpreted as if the deflector has a four time larger image acting on the original antenna.

REFERENCES

1. Pendry, J. B., D. Shurig, and D. R. Smith, "Controlling electromagnetic fields," *Science*, Vol. 312, 1780, 2006.
2. Zolla, F., S. Guenneau, A. Nicolet, and J. B. Pendry, "Electromagnetic analysis of cylindrical invisibility cloaks and the mirage effect," *Opt. Lett.*, Vol. 32, 1069, 2007.
3. Nicolet, A., J. F. Remacle, B. Meys, A. Genon, and W. Legros, "Transformation methods in computational electromagnetism," *J. Appl. Phys.*, Vol. 75, 6036, 1994.
4. Pendry, J. B., "Negative refraction makes a perfect lens," *Phys. Rev. Lett.*, Vol. 85, 3966, 2000.
5. Zhang, J. J., Y. Luo, H. S. Chen, et al., "Guiding waves through an invisible tunnel," *Opt. Exp.*, Vol. 17, 6203, 2009.
6. Milton, G. W. and N.-A. P. Nicorovici, "On the cloaking effects associated with anomalous localized resonance," *Proc. R. Soc. Lond. A*, Vol. 462, 3027, 2006.

Homogenization of 3D-dielectric Photonic Crystals and Artificial Magnetism

G. Bouchitté[1], **C. Bourel**[1], **and Didier Felbacq**[2]

[1]Departement of Mathematics, Université de Toulon, BP 20132, 83957 La Garde Cedex, France
[2]GES UMR 5650, Place Bataillon, 34095 Montpellier Cedex 05, France

Abstract— In [1–4], a theory for artificial magnetism in two-dimensional photonic crystals has been developed for large wavelength (homogenization). The main idea was that a periodic crystal with high permittivity inclusions shows up micro-resonance effects from which an effective permeability law with anomalous dirpersion could be evidenced in a explicit way. The main drawback was however that in this model we assumed magnetic parallel polarization so that merely infinite photonic crystals (invariants in one direction) could be considered.

In this work, we propose a full 3D generalization of previous results: the diffraction of a finite 3D-dielectric crystal is considered at a fixed wavelength and a limit analysis as the period tends to zero is performed. We evidence a new microscopic vector spectral problem which turns out to rule the macroscopic behavior of the crystal. We obtain then an extension to the 3D-case of the results in [1, 3] by proving rigorously that permeability tensor laws can be reached where the effective tensor exhibits negative eigenvalues in appropriate range of frequencies. This suggests that periodic bulk dielectric inclusions could be an efficient alternative to the very popular metallic split-ring structure proposed by Pendry [5].

REFERENCES

1. Bouchitté, G. and D. Felbacq, "Homogenization near resonances and artificial magnetism from dielectrics," *CR Math. Acad. Sci. Paris*, Vol. 339, No. 5, 377–382, 2004.
2. Felbacq, D. and G. Bouchitté, "Left handed media and homogenization of photonic crystals," *Optics Letters*, Vol. 30, 10, 2005.
3. Felbacq, D. and G. Bouchitté, "Homogenization of wire mesh photonic crystals embdedded in a medium with a negative permeability," *Phys. Rev. Lett.*, Vol. 94, 183902, 2005.
4. Felbacq, D. and G. Bouchitté, "Negative refraction in periodic and random photonic crystals," *New J. Phys.*, Vol. 7, 159, 10.1088, 2005.
5. OBrien, S. and J. B. Pendry, "Magnetic activity at infrared frequencies in structured metallic photonic crystals," *J. Phys. Condens. Mat.*, Vol. 14, 6383–6394, 2002.

How to Modify the Optical Properties of Fibres in Twisting Them

F. Zolla[1], **A. Nicolet**[1], **Ould Agha**[1], **and D. Felbacq**[2]

[1]Institut Fresnel, UMR 6133, Faculté des Sciences de Saint Jérôme, Aix-Marseille Université
F-13013 Marseille, France
[2]GES, UMR-CNRS 5650, CC 074, Université Montpellier II
Place Eugène Bataillon, 34 095 Montpellier Cedex 05, France

Abstract— Optical fibres became, in the last three decades, a basic device in classical optics. One way to obtain more efficient fibres is to design exotic fibres with more complex geometries such as in the so called microstructured optical fibres [1]. Another way exploited in this paper is to bent and more explicitly to twist them in order to reveal artificial anisotropy [2,, 3]. The purpose of this paper is to investigate the effect of a twist on the optical properties (propagative or/and leaky modes) of simple fibres and microstructured optical fibers (MOF) as well. A helicoidal system of coordinates is introduced to define the structure and to set up the problem.

$$\begin{cases} x = \xi_1 \cos(\alpha\xi_3) + \xi_2 \sin(\alpha\xi_3), \\ y = -\xi_1 \sin(\alpha\xi_3) + \xi_2 \cos(\alpha\xi_3), \\ z = \xi_3, \end{cases} \tag{1}$$

These coordinates, albeit non-orthogonal, preserve the translational invariance in a way that allows a two-dimensional finite element model similar to that of classical straight waveguides. The Perfectly Matched Layer (PML) [4] technique is used to compute the leaky modes in the fibers. We stress on the electric and magnetic anisotropy induced by the twist.

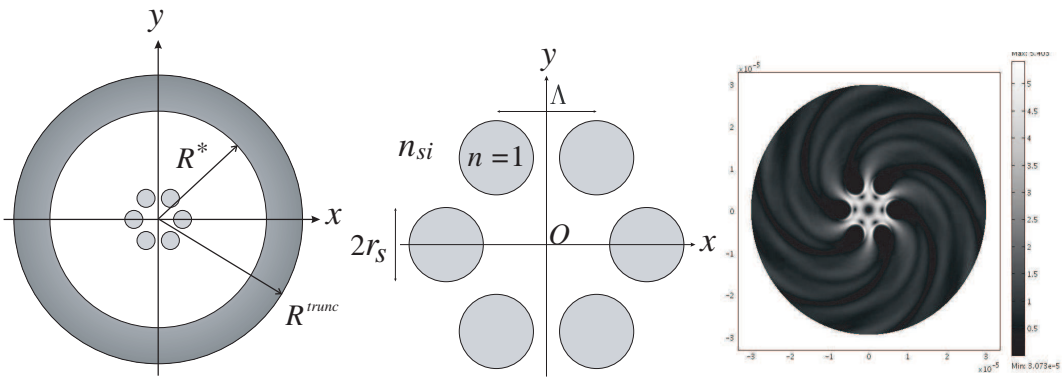

Figure 1: On the left, cross section of a twisted six hole MOF structure together with the surrounding annulus used to set up the PML ($R^* = 30\,\mu\text{m}$, $R^{trunc} = 40\,\mu\text{m}$). On the middle, a magnification of the hole structure with $\Lambda = 6.75\,\mu\text{m}$, $r_s = 2.5\,\mu\text{m}$, and $n_{Si} = 1.444024$. On the right, map of the norm of the longitudinal component of the electric field $E_z = \alpha\xi_2 E_{\xi_1} - \alpha\xi_1 E_{\xi_2} + E_{\xi_3}$ for the fibre described nearby and for a strongly twist ($\alpha = 50,000\,\text{m}^{-1}$) with very large losses . The map is truncated at the inner boundary of the PML, the field unit on the gray scale is arbitrary, and dimensions on the axes are in m.

REFERENCES

1. Zolla, F., G. Renversez, A. Nicolet, B. Khulmey, S. Guenneau, and D. Felbacq, *Foundations of Photonic Crystal Fibres*, Imperial College Press, London, 2005.
2. Ould Agha, Y., F. Zolla, A. Nicolet, and S. Guenneau, "On the use of PML for the computation of leaky modes: An application to gradient index MOF," *COMPEL*, Vol. 27, No. 1, Jan. 2008.
3. Igarashi, H. and T. Honma, "A finite element analysis of TE modes in twisted waveguides," *IEEE Transactions on Magnetics*, Vol. 27, No. 5, 4052-4055, Sep. 1991.
4. Bérenger, J.-P., "A perfectly matched layer for the absorption of electromagnetic waves," *Journal of Computational Physics*, Vol. 114, 185–200, 1994.

Chaos and Stability in a Photonic Billiard

D. Felbacq[1], **J. Bellessa**[2], **and B. Gil**[1]

[1]Groupe d'Etude des Semiconducteurs UMR-CNRS 5650, University of Montpellier 2
34095 Montpellier Cedex 05, France
[2]Laboratoire de Physique de la Matière Condensée et Nanostructures UMR 5586
Université Claude Bernard, 43 Bd du 11 Novembre 1918, 69662 Villeurbanne cedex, France

Abstract— Photonic crystals, i.e., artificial periodic structures exhibiting a photonic band gaps, have been studied at very different angles since the pioneering works of S. John and E. Yablonovitch. From the sole effect of acting like mirrors, the engineering of band structures and the more recent recognition that they are metamaterials they have shown a wide range of physical phenomena. However, they have not yet been considered, except a pioneering work, in the high frequency domain. In this letter, we aim at initiating a new direction of research by considering the propagation of light in periodic dielectric structure when the wavelength is very small with respect to the scatterers. Because it is a rather a new and wide field, we shall restrict ourselves to consider the limit case of ray optics in a periodic set of dielectric scatterers. The "Photonic Billiard" under study is a biperiodic set of dielectric cylinders, in which we want to study the trajectories of a ray by applying Snell-Descartes relations at the boundary of the cylinder and periodic conditions at the boundary of the cell. By using Poincaré sections, we will show the existence of stable trajectories embedded in a sea of chaos. As a consequence we find that there are still forbidden bands even in the ray optics approximation as soon as the dispersion of the materials constituting the scatterers is introduced. Comparisons with a rigorous multiple scattering code solving Maxwell equations rigorously will be given, showing clearly the relevance of the ray optics approximation.

ACKNOWLEDGMENT

This work was done under the financial support of the Agence Nationale de la Recherche (grants POEM ANR-06-PNANO-001-08 and SCOP ANR-07-PNANO-053-01).

Session 2A5
Advances in Numerical Techniques 1

Iterative Method for Differential Phase Shift Computation in the Azimuthally Magnetized Circular Ferrite Waveguide

Georgi Nikolov Georgiev[1] and Mariana Nikolova Georgieva-Grosse[2]

[1]Faculty of Mathematics and Informatics, University of Veliko Tirnovo "St. St. Cyril and Methodius"
Veliko Tirnovo BG-5000, Bulgaria
[2]Meterstrasse 4, Gerlingen D-70839, Germany

Abstract— The characteristics of the circular waveguides with azimuthally magnetized ferrite have been an object of extensive study in view of their possible application in the design of various microwave control components [1–6]. Such are, e.g., the nonreciprocal digital phase shifters, operating in the normal TE_{01} mode [2–6]. The development of the devices mentioned requires calculation of the differential phase shift which the configurations might produce. This however is a grave task [5].

Here an iterative method is elaborated and applied to reckon the differential phase shift provided by the circular waveguide, entirely filled with ferrite, magnetized in azimuthal direction by an infinitely thin central switching wire that supports normal TE_{0n} modes. The approach uses the characteristic equation of the structure $\Phi(a, c; x_0) = 0$ [2], derived in terms of complex Kummer confluent hypergeometric function [7] in that $a = c/2 - jk$, $c = 3$, $x_0 = jz_0$, $k = \alpha\bar{\beta}/\left(2\bar{\beta}_2\right)$, $\bar{\beta}_2 = \sqrt{1-\alpha^2-\bar{\beta}^2}$, $z_0 = 2\bar{\beta}_2\bar{r}_0$ (α — off-diagonal ferrite permeability tensor element, $\bar{\beta} = \beta/\left(\beta_0\sqrt{\varepsilon_r}\right)$, $\bar{\beta}_2 = \beta_2/\left(\beta_0\sqrt{\varepsilon_r}\right)$, $\bar{r}_0 = \beta_0 r_0\sqrt{\varepsilon_r}$, β — phase constant, β_2 — radial wavenumber, r_0 — guide radius, $\beta_0 = \omega\sqrt{\varepsilon_0\mu_0}$, ω — angular frequency of the wave, ε_r — ferrite relative permittivity). For fixed values of α ($|\alpha| < 1$) and $\bar{r}_0$ an arbitrary value of parameter k ($-\infty < k < +\infty$) is chosen and the relevant roots $\zeta_{k,n}^{(c)}$ of characteristic equation (the eigenvalue spectrum of geometry $\bar{\beta}_2 = \zeta_{k,n}^{(c)}/(2\bar{r}_0)$) are (is) found ($n = 1, 2, 3, \ldots$). The numerical equivalents of quantities α, k and $\zeta_{k,n}^{(c)}$ are put in the expressions $\bar{r}_0 = \left(k\zeta_{k,n}^{(c)}/\alpha\right)\left\{\left[1 + (\alpha/(2k))^2\right]/(1-\alpha^2)\right\}^{1/2}$ and $\bar{\beta} = \left\{(1-\alpha^2)/\left[1 + (\alpha/(2k))^2\right]\right\}^{1/2}$, ($n = 1$ for TE_{01} mode) [2]. The parameter k is varied, until the computed value of $\bar{r}_0$ coincides with the chosen one with the prescribed accuracy. The procedure is repeated twice for both signs of k, yielding the normalized phase constants $\bar{\beta}_+$ and $\bar{\beta}_-$ ($\bar{\beta}_- > \bar{\beta}_+$) for positive ($\alpha > 0$) and negative ($\alpha < 0$) magnetization, resp. the differential phase shift $\Delta\bar{\beta} = \bar{\beta}_- - \bar{\beta}_+$ ($\Delta\bar{\beta} > 0$). The dependence of $\Delta\bar{\beta}$ on $\bar{r}_0$ and $|\alpha|$ is presented numerically in tabular form.

REFERENCES

1. Che, W., E. K. Yung, and J. Wen, "Cutoff characteristics of modes in a circular waveguide filled with microwave ferrite," *J. Electromagn. Waves Applicat.*, Vol. 16, No. 8, 1103–1118, August 2002.
2. Georgiev, G. N. and M. N. Georgieva-Grosse, "A new property of the complex Kummer function and its application to waveguide propagation," *IEEE Antennas Wireless Propagat. Lett.*, Vol. 2, 306–309, December 2003.
3. Georgiev, G. N. and M. N. Georgieva-Grosse, "A property of the $L(c, \rho, n)$ numbers and its application to waveguide propagation," *Proc. XXIX URSI General Assembly*, in CDROM, BK.6(120), Chicago, IL, USA, August 7–16, 2008.
4. Georgiev, G. N. and M. N. Georgieva-Grosse, "Phase behaviour of a two-layered circular ferrite-dielectric waveguide with azimuthal magnetization," *PIERS Proc.*, 1473–1477, Moscow, Russia, August 18–21, 2009.
5. Georgiev, G. N. and M. N. Georgieva-Grosse, "An application of the complex Tricomi function," *Proc. Eleventh Int. Conf. Electromagn. Adv. Applicat., ICEAA'09*, 819–822, in CDROM, Turin, Italy, September 14–18, 2009.
6. Georgiev, G. N. and M. N. Georgieva-Grosse, "Effect of the dielectric filling on the phase behaviour of the circular waveguide with azimuthally magnetized ferrite toroid and dielectric cylinder," *Proc. Asia-Pacic Microwave Conf., APMC-2009*, in CDROM, WE4B-4(1680), Singapore, December 7–10, 2009.
7. Tricomi, F. G., *Funzioni Ipergeometriche Confluenti*, Edizioni Cremonese, Rome, Italy, 1954.

Light Propagation in a Disordered Waveguide System: Average Power

Akira Komiyama
Osaka Electro-Communication University, Hatsu-cho Neyagawa-shi 572-8530, Japan

Abstract— In a disordered waveguide system composed of randomly different cores in size mode waves are localized and are concentrated into a narrow region of several cores [1]. The modal density of states can be accurately calculated by the coherent potential approximation [2]. When one of cores is illuminated at the input end of the waveguide system several localized modes are excited and their modes propagate through the system. Outlines of the propagation properties of light can be easily known by solving numerically the coupled mode equation [3]. The amplitude of light can be divided into the coherent part (the average amplitude) and the incoherent part with zero average. The coherent part is transformed into the incoherent part and decreases exponentially with increasing distance. At sufficiently large distance the power distribution of the incoherent part in the cross section of the waveguide system becomes stationary. That is, the incoherent part is localized. However, from the numerical results it is difficult to understand a physical mechanism of the localization. The average amplitude of light has been analytically derived by the perturbation method [4]. In the derivation only successive scatterings from different cores are taken into account. The results obtained analytically are in good agreement with the numerical results.

In this paper the average power of the incoherent part is analytically derived by the perturbation method and it is shown that the power distribution becomes stationary at the infinite distance.

REFERENCES

1. Komiyama, A., "Localization of mode waves in a disordered multi-waveguide system," *Opt. Comm.*, Vol. 151, 25–30, 1998.
2. Komiyama, A., "Application of the coherent potential approximation to disordered waveguide system composed of randomly different cores in size," *IEICE Trans. Electron.*, Vol. J83-C, 900–903, 2000.
3. Komiyama, A., "Propagation and localization of light in a disordered waveguide system," *The Papers of Technical Meeting on Electromagnetic Theory, IEE Japan*, Vol. 06-46, 55–60, 2006.
4. Komiyama, A., *The Papers of Technical Meeting on Electromagnetic Theory, IEE Japan*, Vol. 08-120, 2008.

Comparison of Classical Precondition Techniques for Iterative Solution of Edge-based Finite Element Equations

Xuewei Ping, Wenming Yu, and Tiejun Cui
Institute of Target Characteristics and Identification, State Key Laboratory of Millimeter Waves
School of Information Science and Engineering, Southeast University, Nanjing 210096, China

Abstract— When three-dimensional scattering problems are investigated using the finite element method (FEM), the number of unknowns is usually up to tens of thousands even when a very small problem is considered, and systems with several millions of unknowns are routinely encountered for electrically large objects, which precludes the application of direct solvers. However, the ill-conditioning of the FEM linear system makes classical iterative methods hard to converge. Thus, the solution of FEM linear system is a bottleneck in raising the efficiency of FEM simulations.

In this paper, the classical preconditioning techniques, including the Jacobi (i.e., diagonal) preconditioning, symmetric successive over-relaxation (SSOR) preconditioning, incomplete Cholesky decomposition (IC) preconditioning, approximate inverse (AINV) preconditioning, are investigated for conjugate gradient (CG) iterative solution of FEM linear systems. The property and efficiency of each preconditioner is depicted briefly based on a great deal of numerical simulations.

Jacobi preconditioning takes the diagonal of the FEM matrix as the preconditioner and needs no computation time and extra memory. However, Jacobi preconditioning can only save about 30–50% iterations for most problems. The SSOR preconditioner utilizes all the information of the matrix and can converge much faster than Jacobi preconditioner. Compared with Jacobi preconditioning, about 2–4 times of iterations can be saved. Further more, the SSOR preconditioner permits efficient matrix-vector multiplications, which makes the computational counts comparable with unpreconditioned CG. The IC preconditioner is the most popular and promising preconditioner. However, standard IC usually breaks down when applied in solving FEM equations. A suitable perturbation to the diagonal may stabilize IC decomposition and make the IC preconditioner greatly outperform other classical preconditioners in convergence. However, the best perturbation parameter is very hard to determine. This circumvents IC to be applied in real applications as a black-box solver. The AINV preconditioner is very suit for parallel computation. As we have tested, the efficiency of AINV is usually better than SSOR. Compared with IC, it is very stable, though break down may also be encountered in theory. If a suitable non-zero pattern is determined, the efficiency of AINV can be further improved.

In our opinion, the AINV preconditioner is preferred in FEM. For larger problems, the SSOR preconditioner can be used to save memory at the expense of some efficiency. However, for very large problems, the utility of parallel computation is unavoidable.

Fully Probe-Corrected Inverse Equivalent Current Methods with Multilevel Fast Multipole Acceleration and Higher-order Current Expansion

T. F. Eibert, E. Kaliyaperumal, C. H. Schmidt, and Ismatullah
Technische Universität München, Germany

Abstract— Inverse equivalent current methods determine electric and/or magnetic current sources in such a way that the radiated fields of these sources agree as well as possible with some electric or magnetic fields prescribed in certain sample locations. Therefore, the inverse equivalent current problems can be posted in the form of integral equations, which are closely related to the integral equations used for the solution of electromagnetic radiation and scattering problems.

These integral equation methods are particularly successful in the form of surface integral equations derived from Huygens' principle, where the scattering or radiation objects are enclosed by a closed surface and where surface current densities on this surface are introduced as the unknown quantities. For the solution of radiation or scattering problems, the integral equations are derived by enforcing the required boundary conditions on the Huygens surface, whereas in the inverse equivalent current formulation the integral equation is derived by enforcing the agreement of the radiated/scattered fields with the field measured in the observation locations.

Due to the close relationship of both formulations, it is quite obvious that each method can benefit from the developments of the other method.

In this contribution, we discuss an inverse equivalent current method, which works with triangular surface discretization elements and divergence conforming hierarchical vector basis functions on the mesh, as known from the integral equation solution of radiation and scattering problems. Basis functions up to second order were implemented, which can be used for electric and magnetic surface current densities. The meshes can be derived by directly using the surface descriptions of the considered antennas or scattering objects or a virtual Huygens surface enclosing the actual source region.

Also adapted from the integral equation solution of radiation and scattering problems is the multilevel fast multipole method (with so-called near-field and far-field translations), which is utilized to efficiently evaluate the forward operator as well as the adjoint forward operator within the inverse problem formulation.

An important aspect for inverse equivalent current methods is, that the fields to be reproduced by the equivalent currents are typically derived from measurements. Therefore, only the measured signals at the output of the utilized measurement probes are known and it is often desirable to compensate for the influence of the probes on the measured fields. In this contribution, we will show how the influence of arbitrary measurement probes, which are only characterized by their far-field antenna patterns (amplitude and phase), can be compensated within the multilevel fast multipole accelerated evaluation of the forward operat

A variety of application results from the fields of near-field far-field transformation for antennas as well as from antenna diagnostics will be shown. Robustness and accuracy issues will also be addressed.

Fast Evaluation to Electromagnetic Scattering of Conducting Surfaces Using an Efficient Stationary Phase Method

Jun Zhang, **Wenming Yu**, **and Tiejun Cui**
State Key Laboratory of Millimeter Waves, Department of Radio Engineering
Southeast University, Nanjing 210096, China

Abstract— The stationary phase method is an efficient way to evaluate the electromagnetic scattering of conducting surfaces, in which the physical optics (PO) approximation has been applied for the induced currents. The integral comes from the contribution of certain critical points on the surface (e.g., specular, boundary and vertices). The difficulty one faces is how to identify if the critical points are coalesced with each other or not and we try to derive the heuristic discrimination conditions.

In this work, the scattering problem is described directly over the parametric surface, and hence it will be a challenging task to find all critical points on the surface one time. The conjugate-gradient method cannot meet our demand because it can only find no more than one extremum of a function. Thus an artificial immune network algorithm which is very suitable for multi-peak function optimization (opt-aiNet) is chosen for this purpose. Several simulation results on the radar cross sections (RCS) of conducting surfaces are provided using the efficient stationary phase method. Such results have been compared with those using the numerical method, which have good agreements, to verify the accuracy and efficiency of the proposed approach.

Further Comparison between Macro Basis Functions and Krylov Subspace Iterative Methods

Christophe Craeye
Université Catholique de Louvain, Belgium

Abstract— The direct solution of large problems with the Method of Moments rapidly becomes impractical. Hence, methods based on Krylov subspace iterations [1] and on the Macro Basis Functions [2–4] approach have been devised to overcome this limitation. In order to better exploit the advantages of both, it is useful to describe both of them, as far as possible, under the same formalism. This paper provides an extension of the work recently carried out in this direction. It consists of four steps, the first two have been already described in recent papers [5, 6]; the other two are new.

Step 1 [5]: Macro Basis Functions can be computed in a multiple-scattering fashion. It is possible prove that, if all MBFs are taken up to an order k, the subspace they subtend contains the space subtended by the order-k Krylov subspace.

Step 2 [6]: if Galerkin testing is considered, then the orthogonality conditions imposed by the Full Orthogonalization Method (FOM, [1]) are also fulfilled by the MBF approach, assuming the same order for both methods and same block-diagonal preconditioning. The imposed conditions by the MBF approach are stronger and the accuracy is much higher, at the cost of a larger system of equations.

Step 3: in the multiple-scattering MBF approach, when computing a new MBF over a certain subdomain i, it is beneficial to first compute the solution over a larger domain i^1 containing subdomain i. The comparisons made in Steps 1 and 2 still exactly hold in that case, provided that the initial system of equations is transformed with the help of a generalized shield-block preconditioner [7]. This step enables the accurate treatment of connected subdomains with arbitrary shapes and unequal sizes.

Step 4: Krylov subspace iterative methods like FOM and GMRES can be "restarted" to circumvent limitations in terms of memory and computation time, i.e., the approximation obtained at a certain step is considered as a new initial guess and the process is started anew. A similar process can be considered for the improvement of solutions obtained with multiple-scattering MBFs, through the incorporation of a plane-wave spectrum which represents the interactions with distant subdomains.

Examples of the strong improvement of the solution of the traditional MBF approach will be given for the cases of metallic plates and of electrically interconnected antenna arrays.

ACKNOWLEDGMENT

The author is grateful to Prof. Paul Van Dooren (UCL, Belgium) for helping him to distinguish between different types of Krylov subspace methods.

REFERENCES

1. Saad, Y., *Iterative Methods of Sparse Linear Systems*, PWS/ITP Publishing, Boston, 1995.
2. Suter, E. and J. R. Mosig, "A subdomain multilevel approach for the efficient MoM analysis of large planar antennas," *Microwave Optical Technol. Lett.*, Vol. 26, 270–277, Aug. 2000.
3. Ooms, S. and D. De Zutter, "A new iterative diakoptics-based multilevel moments method for planar circuits," *IEEE Trans. Microwave Theory Techn.*, Vol. 46, Mar. 1998.
4. Yeo, J., V. Prakash, and R. Mittra, "Efficient analysis of a class of microstrip antennas using the Characteristic Basis Function Method (CBFM)," *Microwave Optical Technol. Lett.*, Vol. 39, 456–464, Dec. 2003.
5. Craeye, C., T. Gilles, and X. Dardenne, "Efficient full-wave characterisation of arrays of antennas embedded in finite dielectric volumes," *Radio Science*, Feb. 2009.
6. Craeye, C., "On the connection between multiple-scattering based Macro basis functions and Krylov subspace iterative methods," *Proc. of ICEAA2009 Conference*, Torino, Sep. 2009.
7. Pissoort, D., E. Michielssen, D. Vande Ginste, and F. Olyslager, "A rank-revealing preconditioner for the fast integral-equation based characterization of electromagnetic crystal devices," *Microw. Opt. Techn. Letters*, Vol. 48, No. 4, 783–789 Apr. 2006.

Applications of Periodic FMM for Maxwell's Equations in Optics

Y. Kurami[1], **T. Hatano**[2], **T. Ishihara**[2], **and N. Nishimura**[1]

[1]Dept. Applied Analysis and Complex Dynamical Systems, Kyoto University, Japan
[2]Dept. Physics, Tohoku University, Japan

Abstract— The group of the last author have proposed a periodic FMM for Maxwell's equations which was shown to be effective in optical applications such as photonic crystals. The proposed paper presents further applications of the periodic FMM in optics. Specifically, we consider a metallic photonic crystal slab which consists of a thin layer of gold (thickness = 40 nm) on a quartz substrate. This slab is with periodic holes (radius = 120 nm) located two dimensionally (period = 500 nm). Hatano et al. (PRL, 2009) have found experimentally that an obliquely incident circularly polarised light induces an electrical voltage in the direction perpendicular to the incident plane. They also proposed a theory to explain this photo-induced voltage (PIV), but little comparison has been made between the prediction of the theory and experiments. In the proposed presentation, we show that the periodic FMM is effective in evaluating quantities, such as the one proposed by Hatano et al., which are in terms of volume integrals, since one can integrate local expansions. In the present application, we can further enhance the efficiency of the computation because the major contributions to these volume integrals are converted into surface integrals which are evaluated easily with the solutions of the boundary integral equations. It is found that the behaviour of the quantity proposed by Hatano et al. resembles the experimental results of the PIV very much. In the proposed presentation, we also plan to include other applications of the periodic FMM in optics.

A New Idea for the Synthesis of Non-uniform Linear Arrays with Shaped Power Patterns

Yanhui Liu[2], **Zaiping Nie**[2], **and Qing Huo Liu**[1]

[1]Department of Electrical and Computer Engineering
Duke University, NC 27708, USA
[2]Department of Microwave Engineering
University of Electronic Science and Technology of China
Sichuan 610054, China

Abstract— The synthesis of shaped power patterns has many applications in communications and radar. Many synthesis techniques for shaped patterns have been developed in the past years, and most of them deal with only uniformly spaced linear arrays. As we know, the synthesis of uniformly spaced arrays sometimes requires a large number of elements to radiate a desired pattern shape. Naturally, utilizing nonuniform element spacings is potentially very useful for reducing the total number of elements. However, this is a highly nonlinear inverse problem which involves finding the solution of many unknowns (element positions, excitation amplitudes and phases). Many iterative synthesis techniques cannot guarantee a global optimum for all the variables. Some stochastic optimization algorithms capable of finding the global optimal solutions may be appropriate, but they can be time-consuming. In addition, to our knowledge, most of existing nonuniform array geometry synthesis techniques are proposed for the case of pencil beam patterns, and it is not clear whether they can be directly applicable to the synthesis of shaped-beam patterns.

Here, we present a new idea for the synthesis of nonuniform linear antenna arrays with shaped power patterns. The idea is to factorize the whole synthesis process into three steps. First, we find a satisfactory power pattern for the required radiation characteristics by solving a constrained linear least-squares problem which is obtained with the help of non-redundant representation of squared amplitude of a linear array factor. Then, we factorize the polynomial associated with the power pattern by using polynomial root-finding, and consequently obtain the corresponding field patterns. Finally, the weighted forward-backward matrix pencil method is used to obtain a nonuniform linear array with optimal excitation amplitudes, phases and locations for any choice of field patterns. The new array has a smaller number of elements than the one with uniformly spaced elements for the same pattern characteristics. Note that we can choose the 'best' one by scanning all the synthesis results for different field patterns. Several synthesis experiments have been conducted, and the results have shown the effectiveness of the proposed method and the robustness for different radiation pattern characteristic requirements.

Fast Multipole Acceleration for Nyström Discretization of Surface Integral Equations

M. S. Tong and W. C. Chew
Department of Electrical and Computer Engineering, University of Illinois at Urbana-Champaign, USA

Abstract— Fast multipole algorithm (FMA) is a robust accelerator for solving matrix equations and has been recognized as one of top ten algorithms in the 20th century [1]. The FMA has been deeply studied in electromagnetics (EM) and was enhanced to a more advanced multilevel scheme or MLFMA [2]. Through its acceleration, the extremely large problems with over 200 millions of unknowns have been solved on parallel workstations recently [3, 4]. The distinctive feature of the MLFMA is the rapid evaluation of the matrix-vector multiply in the iterative solution of matrix equations. Also, the matrix elements are not explicitly stored except for those near-interaction entries, leading to a matrix-free scheme and dramatic reduction on memory requirement. The MLFMA performs the matrix-vector multiply through radiation pattern, translator and receiving pattern based on the addition theorem for the Green's function. With the use of the multilevel tree structure, the diagonalization of the translation operator, and the interpolation or anterpolation for wave expansions at different levels, the MLFMA can reduce the original $O\ (N^2)$ complexity, both in CPU time and in memory usage, to $O\ (N \log N)$ complexity. This is a significant reduction in computational costs when N is very large.

However, the MLFMA implementation is usually based on the method of moments (MoM) discretization of integral equations. With the robust Rao-Wilton-Glisson (RWG) basis function, the MoM is the most widely used tool in transforming integral equations into matrix equations. Nevertheless, the MoM could suffer from a basis function problem in representing the magnetic current if the structures include penetrable or composite materials since both electric and magnetic current exist [5]. In this work, we develop a different MLFMA based on the Nyström discretization for integral equations. The primary advantages of the Nyström discretization include the direct evaluation of integrands for far-interaction elements, no use of basis functions, and lower requirements on geometrical discretization. When combined with the MLFMA, these advantages could be more significant since the fast pattern storage, simple implementation, and no worry on expanding the magnetic current in composite objects are very desirable in the MLFMA. Numerical examples for EM scattering by large scatterers are presented to demonstrate the robustness of the proposed MLFMA.

REFERENCES

1. Board, J. and K. Schulten, "The fast multipole algorithm," *IEEE Comput. Sci. Eng.*, Vol. 2, No. 1, 76–79, 2000.
2. Song, J. M., C. C. Lu, and W. C. Chew, "Multilevel fast multipole algorithm for electromagnetic scattering by large complex objects," *IEEE Trans. Antennas Propagat.*, Vol. 45, No. 10, 1488–1493, 1997.
3. Ergül, Ö. and L. Gürel, "Efficient parallelization of the multilevel fast multipole algorithm for the solution of large-scale scattering problems," *IEEE Trans. Antennas Propagat.*, Vol. 56, No. 8, 2335–2345, 2008.
4. Ergül, Ö., Ph.D. Dissertation, Department of Electrical and Electronics Engineering, Bilkent University, Ankara, Turkey, 2009.
5. Sheng, X. Q., J. M. Jin, J. M. Song, W. C. Chew, and C. C. Lu, "Solution of combined-field integral equation using multilevel fast multipole algorithm for scattering by homogeneous bodies," *IEEE Trans. Antennas Propagat.*, Vol. 46, No. 11, 1718–1726, 1998.

Novel Hybrid Transfer Matrix FDTD Method for Modeling the Optical Properties of Periodic Structures

Alexei Deinega[1], **Sergey Belousov**[1], **and Ilya Valuev**[2]

[1]Russian Research Centre, Kurchatov Institute, Kurchatov Sq. 1, Moscow 123182, Russia
[2]Joint Institute for High Temeperatures of RAS, Izhorskaya 13, Bld. 2, Moscow 125412, Russia

Abstract— Frequency domain computational methods are widely used for calculation of the optical properties of layered periodic structures. One of the most popular among them is the plane wave expansion method [1]. This method is rather efficient and simple, but it faces a number of problems in case of structures containing dispersive materials. For the structures consisting of spherical scatterers, the alternative is multiple-scattering methods [2], but usage of these methods in case of arbitrarily shaped scatterers is problematic. The transfer-matrix method [3] is free from all these disadvantages. In this method, the calculated volume is split into sub-layers of sufficiently small thickness, and the transfer matrices are found for each of the sub-layers, which relate the electro-magnetic field values on the opposite sides of the sub-layer. The transfer matrices of each sub-layer are combined to obtain the transfer matrix for the whole structure, which ultimately relates the field values on the opposite sides of the whole structures and can be used to obtain the frequency dependent transmission and reflection coefficients for the structure.

We propose a method for transfer matrix calculation using the finite-difference time-domain method (FDTD) [4]. This approach inherits all advantages of the FDTD: relative simplicity of implementation, ease of complex geometry simulation and ability to handle dispersive and non-isotropic media. Within this method the structure is decomposed into the set of repeating layers. For each layer the series of numerical experiments are performed using generated incident plane wave impulse with fixed polarization and Bragg direction. To do this we use the technique taken from the spectral FDTD method [5]. Transfer matrix elements are obtained by Fourier-transforming of the field recorded during numerical experiment in time and space domains. Evaluation of transfer matrix elements corresponding to the evanescent waves requires some special developed procedure.

Compared with the direct FDTD simulation of the whole multilayered layered structure, our approach has an advantage when there is a need to vary the number of layers and their positions, because the transfer matrix for each layer only needs to be calculated once and then can be used for repeated calculations.

Our method may also be utilized for photonic crystals band structure computation. Compared to the direct eigenmode calculation by the FDTD [6], our method requires much less computation to resolve the whole band structure.

REFERENCES

1. Ho, K.-M., C. T. Chan, and C. M. Soukoulis, "Existence of a photonic gap in periodic dielectric structures," *Phys. Rev. Lett.*, Vol. 65, 3152, 1990.
2. Stefanou, N., N. Yannopapas, and A. Modinos, "Heterostructures of photonic crystals: Frequency bands and transmission coefficients," *Comput. Phys. Commun.*, Vol. 113, 49, 1998.
3. Pendry, J. B., "Photonic band structures," *J. Mod. Opt.*, Vol. 41, 209, 1994.
4. Taflove, A. and S. H. Hagness, *Computational Electrodynamics: The Finite Difference Time-domain Method*, Artech House, Boston, 2005.
5. Aminian, A. and Y. Rahmat-Samii, "Spectral FDTD: A novel technique for the analysis of oblique incident plane wave on periodic structures," *IEEE Trans. Antennas and Propagation*, Vol. 54, 1818, 2006.
6. Fan, S., P. Villeneuve, and J. Joannopoulos, "Large omnidirectional band gaps in metallodielectric photonic crystals," *Phys. Rev. B*, Vol. 54, 11245, 1996.

Session 2A6
Microstrip and Printed Antennas, Phase Array Antennas 1

Planar Antenna with a Grounded Inverted L-shaped Strip for WUSB Application

Wen-Shan Chen, **Bau-Yi Lee**, **and Ching-Hung Chen**
Southern Taiwan University, Taiwan

Abstract— To increase the transmitted speed of Pen Driver, Wireless-USB (WUSB) uses the first group spectrum (3.1–4.85 GHz) of 802.15.3a standard to process huge amount of data. This paper presents a printed antenna fabricated on a printed circuit board (PCB) with a small size of $10 \times 29 \times 0.8\,\text{mm}^3$. The proposed antenna consists of a rectangular radiation patch ($L_1 \times W_1$) and ground plane that has a rectangle ($L_3 \times W$) plate and an inverted L-shaped strip. Without adding the inverted L-shaped strip, the proposed antenna has only one resonated mode at 5 GHz that operates frequency band from 4.2 to 5.41 GHz. This frequency band can not cover the wireless-USB (WUSB) operation band. After the inverted L-shape strip was added, three resonated modes located at 3.23, 4.06 and 5.22 GHz were produced. The low operated band is resonated by the inverted L-shape strip; the intermediate operated band is resonated by the rectangular radiation patch and the inverted L-shape strip; the high operated band is resonated by the rectangular radiation patch. The combination of these operated bands provides an impedance bandwidth of 3.07 to 5.86 GHz, which covers the WUSB operation band. The effects of the antenna with different ground length are also investigated. The antenna covers wide bandwidth and keeps the impedance bandwidth for different ground length. In addition, the proposed antenna has advantages of simple structure, wide bandwidth, low cost, low profile, and good radiation characteristics. Simulated and measured results of the proposed antenna design are described, and experimental results of a constructed prototype are presented and discussed.

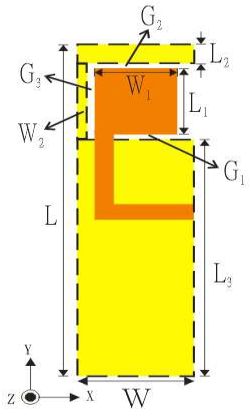

A Novel Printed Antenna for PDA Phone

Wen-Shan Chen and Bau-Yi Lee
Southern Taiwan University, Taiwan, R.O.C.

Abstract— Multi-band antenna has become the mainstream for modern wireless communication system because the wireless products carry two or more functions. PIFA and multi-layers antennas have been used in multi-band applications for more than a decade; however, these antennas need extra height to place in the circuit board. Planar monopole antenna having the advantages of low profile, low cost and ease to fabricate becomes a promising candidate in multi-frequency operation. Owning to the portable and compact of wireless products, the physical size of antenna has to fit into the system architecture. Folded or meandered monopole, which can easily reduce the antenna size, plays an important role in compact antennas. Insufficient bandwidth is always come with these folded types of antennas, especially at lower frequency bands. Using parasitic element, which can couple or excite extra path, is a useful method to increase the required bandwidth. This paper presents a dual mode method to fulfill the bandwidth requirement.

The proposed novel planar antenna has a simple inverted-U shaped in driven part and two low frequency paths with a tunable slot in ground plane. The inverted-U element and ground plane are printed on the same side of the substrate. The total length of inverted-U operates a quarter wavelength of 1200 MHz and the mode is not used in this design. The other two resonant modes at 1800 and 2400 MHz are also produced by using the inverted-U element. The 1800 MHz and 2400 MHz modes operate frequency bands of DCS (1710–1880 MHz), PCS (1850–1990 MHz), UMTS (1920–2170 MHz) and WLAN (2400–2484 MHz). The two low frequency paths operate two low frequency modes. By adjusting a slot located between the two low frequency paths, the two low frequency modes are close at 900 MHz to operate GSM (890–960 MHz) band. The overall dimension of proposed antenna is 100 mm (length) × 60 mm (width) × 0.8 mm (thickness), and it would be used in multi-network PDA phone.

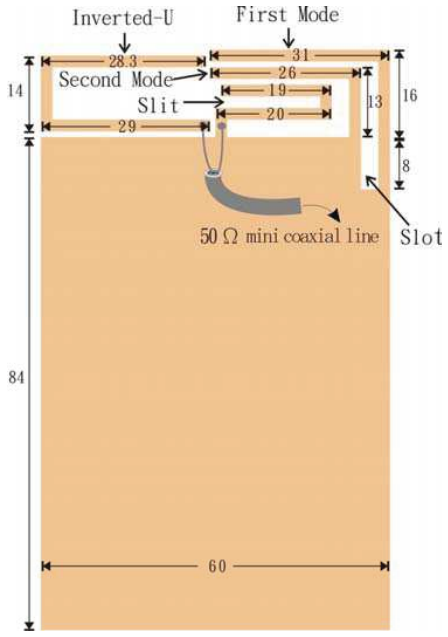

Figure 1.

The Ambiguity Problem of a LCMV-based Space-time Cascade 2D Array

Ho-Hsuan Chan, **Tsung-Cheng Wu**, **and Shih-Chiang Lin**
Department of Communication Engineering, I-Shou University, Taiwan

Abstract— For a wideband beamforming system, the propagating signals are processed and combined temporally as well as spatially, which thus is a space-time two dimension (2D) array, to extract the desired information such as the directions of propagation and their frequency contents. We discussed and compared the performance of three different space-time 2D arrays which are the space-time joint (STJ), the time-space cascade (TSC) and the space-time cascade (STC) processing configuration, respectively. The linear constraint minimum variance (LCMV) algorithm is applied to calculate the dynamic weighting functions for these 2D adaptive arrays. The STJ processor can achieve better resolution, signal separation and interference suppression capacities than the other two types do, but the joint of space and time processing is subject to heavy computing load on the evaluation and updating the array weighting functions. On the other hand, both the STC and TSC processors have the implementation advantage than STJ due to simplicity and lower computing load. However these two processors will encounter detection ambiguity problem which the bearing measurements made give ambiguous DOA and frequency contents under the multibeam constraint conditions. We explained and derived theoretically the existence of ambiguity problem and provided simulation results to demonstrate our arguments.

There is no much novelty the topics of space-time 2D array and beamforming techniques, but it seems that there were no much references can be traced regarding the ambiguity problem presented in this article. We still wonder whether or not the ambiguity problem is not worthy to mention or there may be other view points on this problem. We sincerely hope that we can attract more attention or may stimulate possible discussions on this subject.

A Franklin Array Antenna for Wireless Charging Applications

Shih-Hsiung Chang, **Wen-Jiao Liao**, **Kuo-Wei Peng**, **and Chih-Yao Hsieh**
Department of Electrical Engineering, National Taiwan University of Science and Technology
43, Sec. 4, Keelung Rd., Taipei 106, Taiwan

Abstract— A Frankin array antenna is proposed in this work to be used the receiving antenna for wireless charging applications. It is a fascinating idea to use radio wave as the power source. However, due to the relative long wavelength, the power density of microwave radiation dilutes as it propagates. According to power budget analysis, at a distance of one meter, if transmitting and receiving antennas of moderate gains are used, only a few mW is available with one watt power transmission. In order to enhance the available power level and increase the separation distance, larger antennas, which intercept more radiated power, can be employed.

The proposed planar Franklin array antenna contains 8 antennas as shown in Fig. 1(a). Each Franklin array antenna comprises 4 patches connected in series. Antennas are grouped into two sets and placed perpendicularly on top a metal ground plane. The overall antenna panel size is 52 cm by 52 cm, and the thickness is 6.5 mm. Fig. 1(b) provides the translated farfield radiation pattern measured in a spherical nearfield chamber. The maximum gain is approximately 12 dBi. Note there are a couple of side-lobes, which are due to the extended patch element spacing.

Wireless charging performance was evaluated by connecting the Franklin array antenna with loads and the RF rectification circuitry, which is made of RF diodes. Experiment results indicate that by employing a large antenna aperture, the charging distance can be elongated to a few meters. A one mF super capacitor can be charged up within tens of seconds. Different rectification circuit connecting fashions were also attempted. By combing the received RF power first with a power divider, then performing rectification with a single RF rectification circuit, the charging distance can be optimally extended. On the other hand, if the RF power from each Franklin array is rectified first, then combined as DC sources, the charging distance is limited since certain power level ($\sim$0 dBm) is required to turn on RF diodes. However, at a short distance, the latter connecting fashion provides more power to the load.

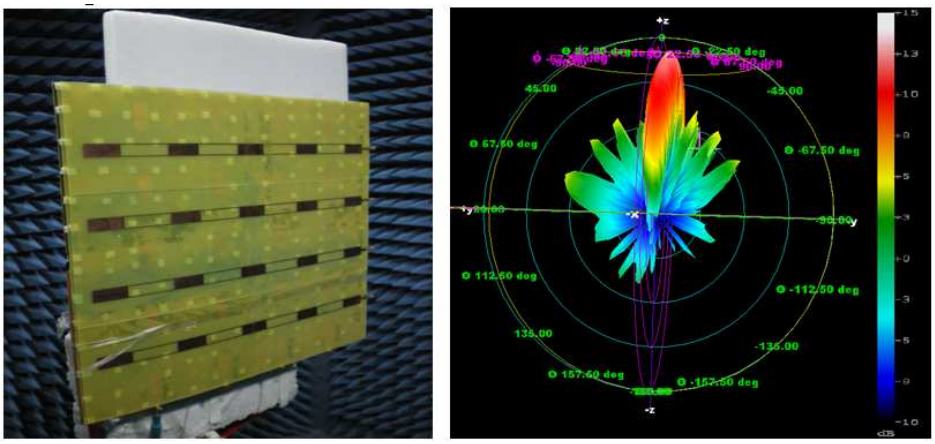

Figure 1: (a) Fabricated Franklin array antenna. (b) Measured radiation pattern.

A Miniatured WLAN/Wi-MAX Chip Antenna for Mobile Phone Applications

Long-Kun Li, **Wen-Jiao Liao**, **and Shao-En Hsu**
Department of Electrical Engineering, National Taiwan University of Technology, Taiwan, R.O.C.

Abstract— The wireless communication market has been growing rapidly since the last two decades. Now, people not make phone calls, but also demand to transmit and receive data from mobile devices. Therefore, connection capability to wireless local area network (WLAN) or worldwide interoperability micro-wave access (Wi-MAX) is a must. In recent years, due to the popularity of mobile devices and the demand of multiple system integration, antenna miniaturization becomes an important research topic. Conventional antenna miniaturization techniques include using meandered metal strip structure and employing dielectric loading. Meander line structures maintain the electric length required for resonance while minimize the antenna physical size. The dielectric loading method uses high dielectric constant materials to slow down the wave velocity, which in turns reduces the resonance length. The so-called "chip antenna" combines above two techniques to further minimize the antenna size.

In this work, compact WLAN/Wi-MAX dual band chip antennas for mobile phones are presented. Due to different band allocations in different regions, two chip antenna designs are proposed. One works for WLAN(2.4 ∼ 2.48, 5.15 ∼ 5.35, 5.725 ∼ 5.85 GHz) and Wi-MAX(3.4 ∼ 3.7 GHz) bands. The antenna dimensions, as shown in Fig. 1, are 3 mm × 9 mm × 1.6 mm. The other covers the WLAN and Wi-MAX band at 2.5 ∼ 2.7 GHz. Its dimensions are 3 mm × 11 mm × 1.6 mm. Both chip antenna designs comprise two resonant branches and take advantage of branches' second order resonance to create two near resonant frequencies. Such technique helps to achieve a triple-band response. One attractive feature of the proposed chip antenna is that no empty space is needed, which is suitable for mobile devices. An FR4 substrate of 45 mm by 100 mm serves as the platform to mount the chip antenna.

Simulations and measurements on return loss spectra as well as radiation patterns were performed and are largely agree. The radiation patterns are omni-directional in general as shown in Fig. 2. Simulated results indicate the resonance is largely invariant to the changes in test board size, so the proposed miniatured chip antenna is particularly attractive for mobile devices such as the PDA, smart phone or notebook.

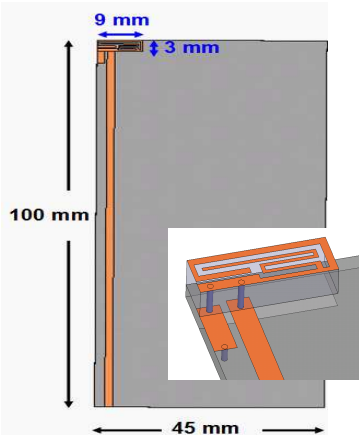

Figure 1: Proposed WLAN/Wi-MAX (3.4 ∼ 3.7 GHz) chip antenna.

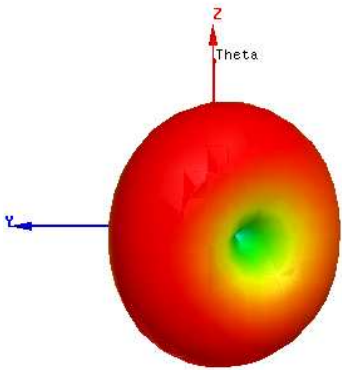

Figure 2: 3-D radiation pattern (2.4 GHz) of the proposed chip antenna.

A Beam Switching Planar Yagi-patch Array for Automotive Applications

Shao-En Hsu, **Wen-Jiao Liao**, **Wei-Han Lee**, **and Shih-Hsiung Chang**
Department of Electrical Engineering, National Taiwan University of Science and Technology, Taiwan

Abstract— Interference and multi-path fading in urban and indoor environment are important issues for wireless communications. In this work, a Yagi patch antenna of four directive beams is proposed to counteract multi-path interference. The beam switching antenna, as shown in Figure 1, comes with the Yagi patch antenna, a one-to-four RF switch and the control circuit. The Yagi patch antenna comprises four driven patch elements, which are connected via a one-to-four RF switch and five parasitically-coupled director patch elements. By selecting a specific through path of the RF switch, RF power is fed to one of the driven patch elements. Since directive radiating elements are used, the beam switching antenna can utilize spatial diversity to extend connection distance and prevent interference.

Figure 2 shows the configuration of the beam switching planar Yagi-patch array. The antenna is designed to operate around GSM 1800/1900 MHz for cellular phone uses. The size and the height of the fabricated prototype antenna are 293 mm × 293 mm × 3 mm, respectively. Measurement results indicate the antenna's gain is approximately 9.478 dBi with a 3 dB beamwidth of 68 degrees. Detailed design parameters as well as performance features such as operational frequency, gain, isolation, 3 dB beamwidth, front-to-back ratio and squint angle are reported in this paper.

Because of the planar structure, this antenna can be employed for automotive environment. For instance, the planar antenna configuration can be mounted on top of a vehicle for with a low profile. The switching directive beam enables the moving vehicle to track a specific base station and extends the communication distance. Such a planar beam switching antenna can be used for mobile devices to ensure connection quality via spatial diversity.

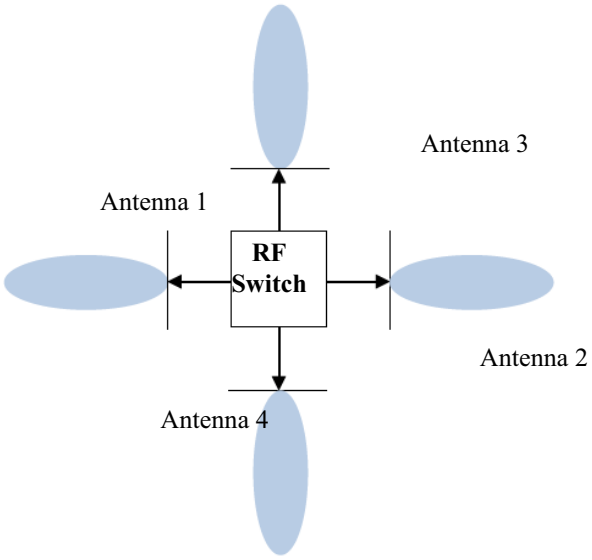

Figure 1: One-to-four beam switching antenna system.

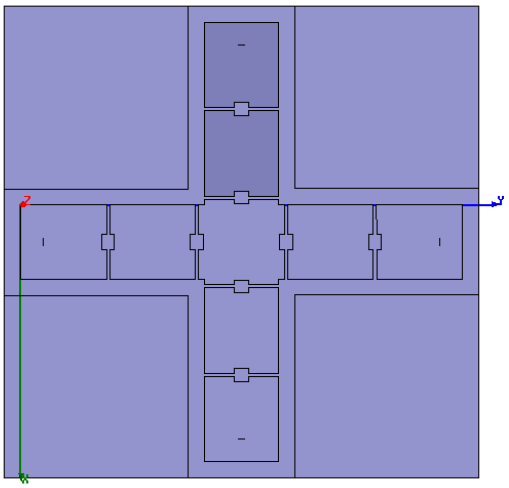

Figure 2: A beam switching planar Yagi-patch array.

Dual-band Dual-polarized Hybrid Antenna Array

L. N. Zhang[1], **S. S. Zhong**[1], **and X. L. Liang**[2]

[1]School of Communication and Information Engineering, Shanghai University, China
[2]Department of Electronic Engineering, Shanghai Jiao Tong University, China

Abstract— Recently, the dual-band and dual polarized antenna array have been studied for satellite and wireless communication applications, particularly for the synthetic aperture radar (SAR) application [1, 2]. The microstrip antenna (MA) and the dielectric resonator antenna (DRA) as two classes of array elements have been investigated and extensively used in the last decades. The microstrip antenna has good performance in lower frequency, but in higher frequency, its radiation efficiency deteriorates apparently, for example, it decreases by 15% as the frequency rises from C band to X band. Compared to the MA, the radiation efficiency of the DRA is as high as 95% even for frequencies up to 10 GHz, due to the absence of inherent conductor losses [3].

In this paper, we propose a novel hybrid antenna array with the combination of MA and DRA elements for the dual-band dual-polarized SAR application. Owing to higher efficiency of the DRA, the DRA is used as the higher frequency radiation element in X band. In order to obtain the dual polarization and to reduce the cross-polarization level, horizontal polarization of the DRA elements is fed in the center of the DR and the vertical polarization fed by means of the 180° out of phase feed technique. For lower frequency of S band, the traditional microstrip dipole antenna is adopted as the element, where two separate orthogonal microstrip dipoles are used to provide the horizontal and vertical polarization, respectively. The spacing of the elements is about $0.7\,\lambda_0$ at 9.6 GHz and about $0.7\,\lambda_0$ at 3.2 GHz. As a test model, the 2×1 elements and 2×6 elements are simulated and analyzed.

Array simulation results shows that the impedance bandwidths of return loss less than -10 dB are 6.6% (3.08–3.29 GHz) for S band and 11.5% (8.92–10.01 GHz) for X band, respectively. The cross-polarization levels of the antenna array are -40 dB for X band and -27 dB for S band in both planes respectively. The antenna array has advantages such as small size, simples structures, low cost, high efficiency, perfect polarization purity and easy to expand into a large array. Thus it is promising candidate for the SAR application.

REFERENCES

1. Pozar, D. M. and S. D. Targonski, A shared-aperture dual-band dual-polarized microstrip array," *IEEE Trans. Antennas and Propagation*, Vol. 49, No. 2, 150–157, 2001.
2. Zhong, S. S., Z. Sun, and X. R. Tang, "Progress in dual-band dual-polarization shared-apertures SAR antennas," *Frontiers of Electrical and Electronic Engineering in China*, Vol. 4, No. 3, 323–329, 2009.
3. Lai, Q., G. Almpanis, C. Funmeaux, H. Benedickter, and R. Vahldieck, "Comparison of the radiation efficiency for the dielectric resonator antenna and the microstrip antenna at Ka band," *IEEE Trans. Antennas and Propagation*, Vol. 56, No. 11, 3589–3592, 2008.

An Outdoor Bistatic Scattering Assessment Using Array Antennas

Chih-Yao Hsieh, **Wen-Jiao Liao**, **and Long-Kun Li**
Department of Electrical Engineering, National Taiwan University of Science and Technology
43, Sec. 4, Keelung Rd., Taipei 106, Taiwan

Abstract— Passive coherent detection (PCL), which is also known as passive radar, is of increasing interest lately. In a passive radar system, the transmitting and receiving antennas are not located at the same position. Therefore, it detects targets' bistatic scattering instead of monostatic scattering in conventional radars. In this work, we designed an experiment which evaluates the bistatic radar cross section from targets in the UHF band. The preliminary measurement configuration is shown in Fig. 1, which includes two directive antennas connected to a network analyzer. One is a four dipole array of approximately 10 dBi gain, while the other is a Yagi antenna of 7 dBi gain. Both antennas are aimed toward the target. Since the output power from the NA is relatively weak and the bistatic RCS from the target may be small in certain angles, the transmitted power is cranked up to 50 dBm using RF components including power amplifiers, attenuators, circulators and terminations. In order to evaluate targets' bistatic scattering correctly, interference from nearby clutters need to be minimized. Hence, the testing range is set up on a building's roof top to avoid reflections from other buildings.

The bistatic RCS of a scattering target is not only determined by the target geometry, but also a complicated function of incident angle, reflection angle, frequency, and the target's surface property. As a result, several sets of experiments were proposed to assess the target's RCS characteristics and the measurement validness as well. Parameters studied include target's shape, orientation, distance to antenna, and antenna polarization. For example, Fig. 2 is the scattering spectra of co-pol and cross-pol antenna setups. The target is a cardboard box wrapped in aluminum foil and is located 8 meters away from the transmitting and receiving antennas. The difference is around 20 dB indicating the planar surfaces of the target provides little cross-pol reflection. Note because the size of the target is close to the wavelength, the scattering spectra exhibit some interference patterns. The bistatic RCS are calculated according to the radar equation. Although the RCS value varies under different testing scenarios, the targets' electrical sizes, in general, are three to ten times larger than their physical sizes. Also, the RCS of a box target is much larger than the one of a spherical target.

According to the measurement results, the variation in bistatic RCS complies with physical expectation. As to the future work, the target should be elevated to reduce interference from background clutters.

Figure 1: Testing range setup.

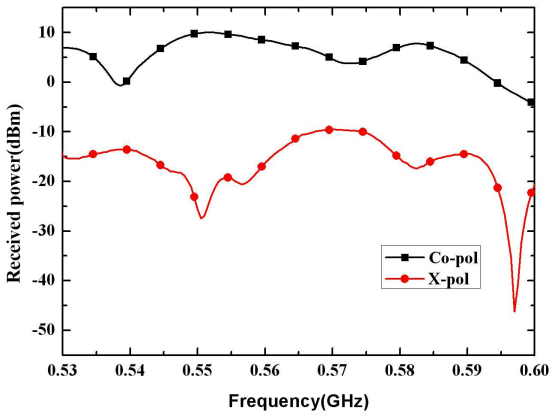

Figure 2: Scattering spectra of co-pol and cross-pol antennas.

Microstrip Antenna Subarray for Circularly-polarized Synthetic Aperture Radar

Merna Baharuddin, Josaphat Tetuko Sri Sumantyo, and Hiroaki Kuze
Center for Environmental Remote Sensing, Chiba University
1-33, Yayoi, Inage, Chiba 263-8522, Japan

Abstract— The design of a circularly-polarized microstrip antenna subarray intended for use in circularly-polarized synthetic aperture radar (CP-SAR) systems operated in L-Band (1.27 GHz) is presented. The CP-SAR sensor is a new sensor for Earth observation applications, with the advantage of sensitive measurements on Earth object characteristics, providing greater amount of information than conventional linear-polarization systems. Microstrip antenna has the advantages of lightweight, low profile, and low volume, as well as the relatively low fabrication cost. In spite of its narrow bandwidth and low gain, microstrip antenna is a suitable choice for airborne SARs. The subarray is the essential component that will compose the full array CP-SAR antenna. The full antenna, in turn, will be implemented on an Unmanned Aerial Vehicle (UAV) CP-SAR, currently under development in the Microwave Remote Sensing Laboratory, Chiba University. The array antenna requirements are (i) broad-band input impedance, (ii) sufficient Axial Ratio bandwidth, (iii) a cosecant-squared beam pattern in the elevation plane (E-plane), (iv) a pencil beam in the azimuth plane (H-plane), (v) relatively good gain and (vi) low cross polarization levels. There are a number of technical challenges in achieving such specifications required for the CP-SAR sensor. The subarray is comprised of CP microstrip elements, and every element is a dual-polarized, Right Handed Circular Polarization (RHCP) and Left Handed Circular Polarization (LHCP), microstrip antenna. The microstrip element is an elliptical patch antenna which is radiating circularly-polarized wave. A single proximity-coupling method is applied for feeding the antenna element. The subarray design will involve the right spacing between elements in order to minimize the mutual coupling and to achieve the required pattern. A well-matched feeding system is also indispensable for the implementation of the dual-polarized circularly-polarized subarray system.

Design of a Printed Antenna Array for Cost-effective ATE to Reduce the Radiated EMI Yield Loss

Cheng-Nan Hu[1], **Hsuang-Chung Ko**[2], **and Deng-Yao Chang**[2]

[1]CRC, Oriental Institute of Technology
No. 58, Sec. 2, Sihchuan Rd, Ban-Ciao City, Taipei County, Taiwan, R.O.C.
[2]King Yuan Electronics Co. Ltd.
No. 58, Sec. 2, Sihchuan Rd, Ban-Ciao City, Taipei County, Taiwan, R.O.C.

Abstract— RF semiconductor devices are changing to match the needs of increasingly innovative wireless standards. In turn, device functionality and integration drive core parametric, configuration, and usage trends for RF ATE (Auto-Test-Equipment) and signal bandwidths and carrier frequencies supporting greater data throughput rates are increasing steadily [1–3]. Usually, RFIC manufacturers conduct the Go No-Go test procedure (Fig. 1(a)) to perform the qualification test. However, this approach has to suffer the yields loss caused by radiated EMI noises existing in the testing environment.

To improve the radiated EMI yield loss, design of a multi-band, dual-polarized printed antenna array is proposed to be implemented onto the load board of the ATE (Auto-Test-Equipment) as the EMI sensor (Fig. 1(c)) to monitor the existing interference signals such that the correlation between the test data and background noise can be analyzed in order to identify the root causes of yield loss. When the radiated EMI is detected at production line, a re-testing procedure is trigged by ATE test program (Fig. 1(b)) to reduce the radiated EMI yield loss.

In this study, theoretical analysis of a specified PHS transceiver IC based on the Monte-Carlo procedure validates the proposed cost-effective ATE design approach. Experimental results of a printed antenna array design confirm the performance of EMI sensor. System validation of the specified device that occurred with a suspected EMI low yield in the production line indicates that the proposed approach can reduce yield loss from 34% to 13%, or by 21% which is very consistence with the numerical results of 21.3% using Monte-Carlo approach.

Wang-shaped Patch Antenna with a Simple Feed Network

Chi H. Wong and Kwok L. Chung
Department of Electronic and Information Engineering, The Hong Kong Polytechnic University
Hung Hom, Hong Kong, China

Abstract— Microstrip patch antennas have attracted much attention of antenna researchers because of its low cost, low profile and easy fabrication, but narrow bandwidth is a major disadvantage that limits the applications of microstrip antennas. Methods to enhance impedance (or return-loss) bandwidth including the addition of U-slot [1], the *E*-shaped patch [2, 3], and the meandering-probe with stacked patch [4]. The U-slot patch and *E*-shaped patch designs are capable of $> 30\%$ return-loss (10-dB) bandwidth but suffer from high cross-polarization (*x-pol*) of greater than -15 dB in one plane [13]. The Meandering probe fed stacked patch enhances the impedance bandwidth up to 37% (SWR < 1.5) and the *x-pol* down to -20 dB. However, it requires an additional patch and a complex probe fabrication [4]. Recently, a *Wang*-shaped patch fed by a dual *L*-probe with an enhanced return loss bandwidth of 42% has been reported [5]. Two mirrored *E*-shaped patches are combined to form a single patch. This combination makes the topological shape of the patch to resemble a Chinese character, 王 (pronounced *Wang*), hence this novel patch is denoted as *Wang*-shaped patch antenna. *Wang*-shaped patch has a symmetric geometry in both the principal planes whereas the *E*-shaped patch has current flows in opposite directions of *E*-field. The latter causes the asymmetric radiation patterns and the high *x-pol* level in *H*-plane. *Wang*-shaped patch comes to solve such problems by balancing current flows in opposite directions. An external phase shifter was used in the *proof-of-concept* version [5]. By exciting two identical *L*-probes with anti-phase currents in equal magnitudes, the cancellation of leakage radiation from the vertical probes and hence the suppression of cross-polarization have been achieved.

In this paper, a simple feed network is designed to replace the external phase shifter for a Wang-shaped patch. This antenna is aimed to be operated in a frequency range of 1.66 GHz to 2.43 GHz for covering the major standards in mobile communications. A dual *L*-probe feed is proposed in the current design. The feed network is applied to excite the probes with equal magnitude currents in 180 deg out of phase, as the similar function of an external phase shifter. A 1.52-mm thick Rogers RO3003 dielectric substrate ($\varepsilon_r = 3.0$, $\tan\delta = 0.0013$) is used to facilitate the feed network. The dual *L*-probe fed Wang-shaped patch antenna features a 10-dB return-loss bandwidth of 37.7%, whilst the cross-polarization levels are suppressed below -20 dB within the bandwidth range of 1.78 GHz and 2.31 GHz. The broadside gain is simulated as high as 6.5 dBi at the mid-band frequency. The detailed antenna geometry and the measurement results will be presented and discussed in the conference.

REFERENCES

1. Luk, K. M., Y. X. Guo, K. F. Lee, and Y. L. Chow, "*L*-probe proximity fed U-slot patch antenna," *Electronic Letters*, Vol. 34, 1806–1807, Sep. 1998.
2. Yang, F., X. X. Zhang, X. Ye, and Y. Rahmat-Samii, "Wide-band *E*-shaped patch antennas for wireless communications," *IEEE Trans. Antennas Propagat.*, Vol. 49, 1094–1100, Jul. 2001.
3. Wong, K. L. and W. H. Hsu, "A board-band rectangular patch antenna with a pair of wide slits," *IEEE Trans. Antennas Propagat.*, Vol. 49, 1345–1347, Sep. 2001.
4. Lai, H. W. and K. M. Luk, "Wideband stacked patches antenna fed by a meandering probe," *Electronic Letters*, Vol. 41, Mar. 2005.
5. Fung, H. Y. and K. L. Chung, "A Wang-shape suspended patch antenna," *Proceedings of the 11th Australian Symposium on Antennas*, 18, Sydney, Australia, Feb. 18–19, 2009.

Session 2A7
RF Safety Issues

Biological Model in Electromagnetic Exposure Safety

Sergey Perov[1], **Quirino Balzano**[2], **and Niels Kuster**[3]

[1]RAMS Research Institute of Occupational Health, Moscow, Russia
[2]Department of Electrical and Computer Engineering, University of Maryland, Maryland, USA
[3]Foundation for Research on Information Technologies in Society, Zurich, Switzerland

Abstract— At present time, there are two very different criteria for setting electromagnetic field (EMF) exposure safety (hygienic) standards. These regulations are based on different science-based approaches using different metrics, such as specific absorption rate (SAR-ICNIRP) and power exposure (PE-Russia).

The exposure metrics of the International Commission on Non-Ionizing Radiation Protection (ICNIRP) require the measurement of electric, magnetic field strength and power density (PD). In the frequency band 100 kHz–10 GHz, the ICNIRP basic restrictions hinge on the concept of specific absorption rate (SAR) which is defined as

$$\mathrm{SAR} = \frac{\sigma E^2}{\rho} = c_i \frac{dT}{dt} \tag{1}$$

where E is the RMS value of the electric field in tissue, σ and ρ are the tissue conductivity and mass density. In (1) also, c_i and $\frac{dT}{dt}$ are the specific heat of tissue and the time derivative of the temperature at the onset of the RF exposure. SAR measures the rate of EMF energy absorption in the unit of weight of an exposed object. SAR is used to quantify tissue exposure from EMF in the far and the near field of RF sources, where PD might not be defined or even definable. The SAR basic restrictions of ICNIRP are time independent because the rate of energy absorption is limited, not its total amount.

The Russian approach to exposure assessment and dosimetry has two main differences from those of ICNIRP. First, the concept of SAR was never adopted, because near field measurements were not required until recently. The near field evaluation is performed by computations extrapolating the far field measurement values using theoretical equations. Second, the dosimetry is based on the parameter "power exposition" (PE) which is a dynamic estimate of the EMF biological effects from the exposure. This parameter differentiates the exposure dose during a given time interval. In other words, the Russian exposure limitations consider cumulative the biological effects of RF EMF. PE values depend on time, field level and frequency range.

The Russian exposure limitation approach and its dosimetry define a dose-dependent biological action of RF EMF and, so, a dependence of time and intensity of the safe RF exposure.

Unfortunately, both approaches have not fully developed a common consistent assessment of EMF exposure and biological effects. That's why there is a need to fix accurate criteria for the definition of biological effects that are of import for the safety of humans exposed to EMF.

The simplest and most direct approach to finding correlation between SAR and PE is based on common and clear biological models. Using this approach we can establish adequate and reliable assessments of EMF exposure levels and the related biological effects. This is a necessary foundation step to find the safe EMF levels for safety standard harmonization.

Considerations on the Limitations of RF Bioresearch

Quirino Balzano[1], **Asher Sheppard**[2], **and Mays Swicord**[3]

[1]University of Maryland, Kim Building, Rm 2135, College Park, MD 20742, USA
[2]Asher Sheppard Consulting, 108 Orange Street, Ste. 8, Redlands, CA 92373 USA
[3]Motorola Inc., 1033 NE 17th Way, Unit 1101, Ft. Lauderdale, FL 33301, USA

Abstract— For more than half a century there has been a substantial effort to investigate the biological effects of RF energy. These studies remain inconclusive for exposures in the athermal regime. Experimental support for the hypothesis that subtle and potentially deleterious effects are caused by long-term exposures common in today's environment mainly comes from exposed cell preparations. The effects have been attributed to nonlinear interactions between amplitude-modulated RF and living tissue or cells. Recent experimental evidence with an ultra-sensitive cavity detector showed that the physical responses of cells and tissues do not exhibit the nonlinear behavior necessary for detecting the modulation that could trigger a biological response, as previously hypothesized [1]. The lack of a tissue-generated second harmonic of the incident signal, which is the hallmark of nonlinear behavior, should not be a surprise. Although there might be nonlinear molecular complexes in living cells, these cannot be excited exclusively within a tissue volume or in a thin tissue slice at microwave frequencies. Given the wavelength of RF signals in air and water at, for example, 10 GHz, (3 cm and 0.5 cm respectively), it is impossible to selectively excite cellular components, e g., a few oscillators within DNA, RNA, or protein pools, without eliciting a response in similar ultrastructures that would either cancel or mask one another. Assuming localized nonlinear responses occur in living cells exposed to environmental RF signals, they might be impossible to measure because the extremely low levels of radiated second harmonic are below practical and theoretical detection limits. Thus any non-linear RF demodulation response of a cell preparation to environmental signal levels would be inconsequential for biological systems at all levels of organization.

REFERENCES

1. Kowalczuk, C., et al., "Experimental outcomes of a test to detect nonlinear responses in biological preparations exposed to RF energy," *Bioelectromagnetic Society Meeting BIOEM 2009*, 10-2, Davos, Switzerland, June 14–19, 2009.

Novel Technologies and Functions of Mobile Phones: A Challenge to Current SAR Measurement Protocols?

Tongning Wu, **Xiaojun Lin**, **Jun Yang**, **Chen Zhao**,
Chen Zhang, **and Qing Shao**
Telecommunication Metrology Center of Ministry of Industry and Information Technology
No. 52, Huayuan Bei Road, Beijing 100191, China

Abstract— Novel technologies and functions have drastically changed mobile phones. Bar-style handsets with dipole antennas and plastic shells have been substituted by more diversified products. They could be of flip shell, clam shell, sliding shell, metallic package and internal antenna. They operate on various GSM/WCDMA/CDMA2000/TD-SCDMA platforms. The dimensions are also minimized. Besides the compacted design, new functions are integrated into the mobile phones. Bluetooth, touch screen with stylus, dual-SIM card slots, high resolution cameras, projectors and etc.

To evaluate the compliance of the Specific Absorption Rate (SAR) of the mobile phones with the standards, measurement protocols have been well established. Test houses have streamlined their measurement tasks as "check position", "tilt 15°" and low-middle-high frequency measurements. However, trials should be made to check whether current measurement protocols/configurations would also be modified to cater for the novel designs and functions.

Two examples are presented:

1. TD-SCDMA mobile phone w/o OTA hand phantom. Recent measurement programs have demonstrated that the existence of hand phantom may unpredictably change the SAR of some GSM mobile phones. Similar measurements have been launched but with TD-SCDMA mobile phones. Some cases have been observed that the SAR is slightly higher with the existence of the hand model.
2. Compact mobile phone with dual-SIM card slots and touch stylus. Compact mobile phones often pose the problem as very complicated micro-electronic circuit layout and thus irregular radiation pattern. SIM cards and touch stylus are made of metal. They are supposed to unintentionally couple with the radiation pattern of the compact mobile phones. The SAR might be influenced at different extent. Measurements have been made with 2 SIM cards in slots + metallic touch stylus vs. only 1 SIM card in slot without stylus. Results show difference in terms of SAR.

In conclusion, novel aspects of the mobile phones should be considered for SAR measurement of the "worst case". Individual measurement plans should be drafted for some special design/new technology mobile phones. Large scale international projects are proposed to settle these problems. Discussion is needed to help clarify whether the discrepancy of these results are from system uncertainty or the various configurations.

Human Exposure Assessment for Wireless Power Transmission System

J. H. Oh[1], **T. H. Kim**[1], **J. H. Yoo**[1], **J. K. Pack**[1], **Y. M. Yoon**[2], **M. Y. Choi**[2], **and S. Y. Lee**[2]

[1]Chungnam National University, South Korea
[2]Korea Radio Promotion Agency, South Korea

Abstract— In this paper, we investigated the possible health effects of the human exposure due to WPT (Wireless Power Transmission) for MICS (Medical Implanted Communication Service) devices, by numerical simulation for two phantom models (Korean model and VHP model). The analyzed the typical WPT systems and three important MICS devices.

Introduction: WPT technique can be used to supply the power of a MICS device, in which the use of a battery is not possible or inappropriate. Our previous study of channel modeling for WBAN (Wireless Body Area Network) system shows that the electromagnetic wave at 403.5 MHz attenuates about 70 dB when it propagates 20 cm through a human body. So, a WPT system can cause some hazardous health effect due to the excessive EMF absorption exceeding a given human protection guideline. In this paper, we investigated the possible health effects by analyzing SAR distribution in a human body for exposure from WPT system.

Phantom Models and Simulation Results: We used two phantom models for numerical simulation: VHP (Visible Human Project) model and Korean phantom model. The Korean phantom model was developed by ETRI (Electronics and Telecommunications Research Institute) in South Korea and consists of 26 tissues with 3 mm voxel size. VHP model used is well known one. The simulation was performed by the FDTD method. The MICS devices for analysis include pacemaker, insulin pump and capsule endoscope. Two typical WPT systems, magnetic resonance type and RF transmission type, were investigated. The simulation results for SAR distribution as well as the field distribution will be discussed.

Conclusions: Our analysis shows that WPT system of current technology could cause health effects and thus such effects must be analyzed in prior to apply a WPT system for MICS.

ACKNOWLEDGMENT

"This research was supported by the MKE (Ministry of Knowledge Economy), Korea, under the ITRC (Information Technology Research Center) support program supervised by the NIPA (National IT Promotion Agency)" (NIPA-2009-(C1090-0902-0034)).

REFERENCES

1. Tesla, N., "The transmission of electrical energy without wires as a means for furthering peace," *Electrical Worlds and Engineer*, No. 7, 21, Jan. 1905.
2. Brown, W. C., "The history of power transmission by radio waves," *IEEE Trans. on MTT*, Vol. 32, No. 9, 1230–1242, 1984.

A Comparison of Ansoft HFSS and CST Microwave Studio Simulation Software for Multi-channel Coil Design and SAR Estimation at 7 T MRI

M. Kozlov and R. Turner
Max Planck Institute for Human Cognitive and Brain Sciences
Stephanstrasse 1A, D-04103, Leipzig, Germany

Abstract—

Purpose: At magnetic fields of 7T and higher, coil performance and electromagnetic field behavior become complex. Our goal was to compare simulation results obtained for a commercially available Rapid BioMed 7T multi-channel coil by Ansoft HFSS frequency domain and CST Microwave studio time domain solvers, and to investigate the conditions that influence the precision of results and the simulation time.

Method: In our 3-D EM model we included all construction details for the resonance elements, simulated with realistic dimensions and material electrical properties. We employed co-simulation of the RF circuit and 3-D EM fields [1]. SAR was evaluated by loading the coil by the Ansoft human body model with different scaling factors: 1, 0.9, 0.8. For CST simulations, mesh definition has a significant influence on representation of areas that include ports and lumped elements. In the simulated coil, ports and lumped elements are not aligned parallel to a coordinate axis. In these areas the mesh step was decreased until the relevant mesh vertexes were accurately positioned as start and end points for integration across ports or lumped elements (Fig. 1). If too coarse a mesh is used, integration defining a significant dependence of port impedance and lumped element properties may erroneously include conductor material. This may result in overestimation or underestimation of SAR by up to 30%. In this report, the CST results were obtained with correct port and lumped element mesh definition (mesh step size as small as 0.25 mm). In additional the coil element mesh size was step by step decreased until the difference between experimental and simulated trim capacitor values vanished (Table 1). Correct trim capacitor estimation was obtained in an HFSS simulation, which used S parameter coverage criteria as better as 0.05 and reached 2 million tetrahedra after 5 mesh adaptation steps.

Results and Discussion: For CST simulation, increasing the number of mesh cells resulted in nearly the same B1+ profile within a phantom (Fig. 2), but approximately a 25% variation of peak SAR value for some head models (Table 1). SAR was found to be coupled to two different electrical field sources (conservative and non-conservative). The first is the penetration of the E field from the distributed capacitors commonly used in high field coils, the second is the E field that accompanies the propagating magnetic field. When the conservative E field has significant influence, care must be taken to ensure that the mesh definition is smaller than 1.25 mm, whenever a part of the human body model is close to a capacitor (Fig. 3). For the mainly non-conservative E field within the body, the SAR value for the coil investigated does not change once the mesh cell size is less than 2 mm isotropic for coil elements. For the reliable simulation of distributed capacitance, the CST mesh has to be smaller than the thin dielectric elements of the coil — more important for coil tuning (e.g., trim capacitor) estimation than for SAR. There is no observable difference between field and SAR data for HFSS and CST simulations, when the simulated trim capacitor values are equal to actual values. Such simulations required four weeks and about 8 GB RAM memory for CST, and two days and 62 GB RAM memory for HFSS projects running on the same computer, without simulation parallelization and hardware acceleration. The memory size disadvantage for HFSS is not severely problematic today, with commercially available 64 GB memory workstations. The computational time disadvantage for CST is a consequence of the inverse proportionality of the simulation time to the length of the smallest mesh cell, which for reliable simulation of a complex MRI coil has to be rather small. In addition, if the computation is performed in CST, each port is simulated independently. This means that the simulation time for the entire project is linearly proportional to the number of ports, and simulation of a multi-channel coil, with for example 16 ports, could take a week, despite using several computers for port simulation parallelization.

HFSS offers a reliable mesh adaptation algorithm and several simulation coverage criteria, that are enough to obtain reliable simulation data in one run. CST includes S-parameter-based coverage criteria and simple mesh adaptation procedures, based on increasing the mesh per wavelength ratio. This refinement of the entire model volume is a less robust approach, compared with HFSS

Table 1: Influence of the CST mesh resolution on simulation data obtained for 8 Watt transmitted power.

Coil element mesh [mm]	2.25× 2.25×5	2.25× 2.25×2.5	2×2×2	1.5×1.5×1.5	1.25×1.25×1.25	1×1×1
Number of mesh cells [M]	6.9	12.03	15.8	26.0	35.7	57.2
tune capacitor [pF]	62.2	29.74	24.86	17.10	16.06	12.8
SAR for Head model	2.0842	1.9929	1.8655	1.4274	1.3774	1.2968
SAR for Head 0.8 scaled model	1.6881	1.7305	1.6379	1.6839	1.7093	1.7393
SAR for Hugo model	1.35	1.34	1.34	1.4311	1.45	1.4874
SAR for Hugo 0.8 scaled model	1.7159	1.8188	2.1242	2.1982	2.2473	2.17

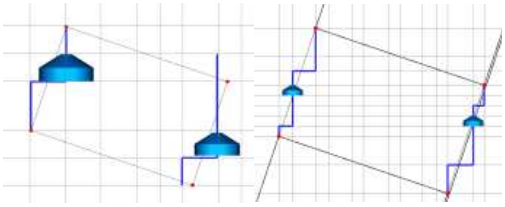

Figure 1: Lumped element mesh.

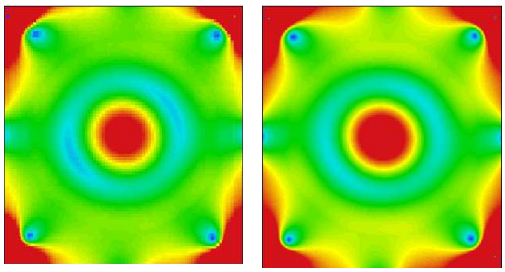

Figure 2: B1+ transverse profile of the phantom. left for 6.9 M, right for 57.2 M mesh cell projects.

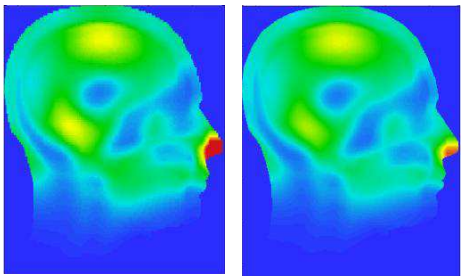

Figure 3: 10 gram SAR profile for Head model. left $2.25 \times 2.25 \times 2.5$ mm mesh, right $1 \times 1 \times 1$ mm mesh projects

mesh refinement, which is performed mostly in the volumes containing maximum field values. For complex MRI coil CST simulations, coverage criteria are used rather seldom, due to the extremely long computational times. In addition, mesh refinement for a given wavelength makes it impossible to keep the same mesh for phantom and human model simulations. The latter is important if the vendor has tuned the coil using the same phantom. In this case, changing the simulation object from the phantom to a head model corresponds to experimental substitution of the phantom by an in-vivo subject inside the tuned and matched MRI coil.

Conclusion: The reliability of SAR estimation, based on CST simulation without coverage check and agreement with experimental RF measurement data, is rather poor. It is inadequate merely to show a similarity of simulated and measured B1 profile shape. HFSS based co-simulation of the RF circuit and 3-D EM fields can significantly speed up MRI coil design, because the simulation time no longer depends strongly on simulated port numbers and the length of the smallest mesh cell.

We present comparison of RF simulations with Ansoft HFSS and CST Microwave studio software, for a commercially available 7T multi-channel coil. We investigated the conditions influencing precision and simulation time. If CST simulation is performed with an inconsistent mesh the SAR estimates are poor, when compared with those predicted from experimental RF measurements. Once simulation parameters are correctly chosen, so that simulated trim capacitor values are equal to actual values, the two simulation methods reach numerical agreement. HFSS can significantly speed up MRI coil design, because the simulation time is not strongly dependent on simulated port numbers and the size of the smallest mesh cell.

REFERENCES

1. Kozlov, M. and R. Turner, *Journal of Magnetic Resonance*, Vol. 200, 147–152, 2009.

Test Methods and Standards for Magnetic Resonance (MR) Safety and Compatibility of Medical Devices

Gregor Schaefers
MR Safety Testing Laboratory, MR:comp GmbH, Germany

Abstract—

Introduction: MR safety and image compatibility are internationally recognized as important issues for medical devices. ASTM International F2503-05 [1] provides comprehensive marking requirements. FDA guidelines, first European EN and international IEC [2, 3] and ISO standards contain MR safety and imaging compatibility requirements. Medical devices and items that can be exposed to an MR environment must be tested on magnetically induced forces, torques, RF heating, induction of voltages and safe functioning as well as MR image artifacts.

Subjects & Methods: Magnetically induced displacement force and magnetically induced torque are safety issues relevant for medical devices. ASTM F2052 [4] and F2213 [5] provide testing methods of force and torque.

Besides these interactions, radio frequency (RF) induced heating is a complex and multi-parameter dependent MR safety issue. RF pulses are in the area of MHz and apply the main amount of heating energy. Not only device properties like electric conductivity, dimension, etc. have to be considered, but also the geometric arrangement relative to the specific MR environment. ASTM F2182 [6] provides a basic test method. In this area computer simulation of electro magnetic fields, SAR and temperature distribution is currently developed to assist in heating testing. Gradient magnetic fields contribute negligibly to heating effects due to the lower frequencies in kHz range. However, as well as RF pulses, switched gradients can induce voltages in conductive structures and can increase the risk of unintended tissue stimulation or can lead to burns. A parallel interaction can be gradient-induced vibration due to interaction with the static magnetic field. So far, no appropriate standardized test methods for induced voltages and vibration are available, but under development.

Further safety concerns for active and non-active devices are the safe function of the MR system and the device respectively. A device must undergo an individual testing procedure.

MR imaging artifacts do not affect the patient safety primarily. As an appropriate standard test method ASTM F2119 [7] can be used.

Discussion & Conclusion: Comprehensive investigation of all interactions and worst-case scenarios is deemed to be necessary. ASTM International has developed useful standardized MR test methods for magnetic force, torque, RF heating and MR artifacts. Continuous redefining and adaptation of international standard test methods is required. Safety issues on induced voltages have to be examined for appropriate test methods standardization. Multi-parameter dependent MR testing issues need implementation of appropriate computer based simulation. Currently ISO/IEC Joint Working Group is defining RF and gradient test methods as well as methods for MR electromagnetic compatibility.

Standardized MR testing of medical devices and items used in the MR environment is compulsory for providing the MR user with a comprehensive and reliable MR safety marking for the daily clinical routine. Standardized tests minimize patient risk and are guiding device manufacturers in development of MR safe devices as well as the MR user by support of meaningful experimental results.

REFERENCES

1. ASTM F2503-05, "Standard practice for marking medical devices and other items for safety in the MR environment," 2005, www.astm.org.
2. IEC 60601-2-33, "Medical electrical equipment — Part 2–33: Particular requirements for the safety of magnetic resonance equipment for medical diagnosis," 2006, www.iec.org.
3. IEC 62464-1, "Magnetic resonance equipment for medical imaging — Part 1: Determination of essential image quality parameters," 1st Edition, 2007, www.iec.org.
4. ASTM F2052-06e1, "Standard test method for measurement of magnetically induced displacement force on medical devices in the magnetic resonance environment," 2006, www.astm.org.
5. ASTM F2213-06, "Standard test method for measurement of magnetically induced torque on passive implants in the magnetic resonance environment," 2006, www.astm.org.

6. ASTM F2182-02a, "Standard test method for measurement of radio frequency induced heating near passive implants during magnetic resonance imaging," 2002, www.astm.org.
7. ASTM F2119-01, "Standard test method for evaluation of MR image artifacts from passive implants," 2001, www.astm.org.

Meta-analysis: Genotoxicity in Mammalian Cells Exposed to Radiofrequency Radiation

Vijayalaxmi
Department of Radiology, University of Texas Health Science Center
San Antonio, Texas 78229, USA

Abstract—

Background: During the years 1990–2005, several investigators have examined the extent of genotoxicity in mammalian somatic cells exposed to radiofrequency radiation (RFR). A meta-analysis of all reported data was conducted to determine whether exposure of cells to RFR, indeed, induced significantly increased genetic damage as compared with those in un-exposed/sham-exposed cells.

Method: The methods employed were based on the recommendations made in several standard textbooks [1–4].

Results and Conclusions: Among the several variables in the experimental protocols employed in individual investigations, the influence of three specific variables related to RFR exposure characteristics was examined in the meta-analysis: (i) Frequency, (ii) specific absorption rate, and (iii) exposure as continuous wave, pulsed wave and occupationally-exposed/mobile phone users. The overall data indicated that (1) the difference between RF radiation-exposed and sham-/unexposed controls as well as the 'effect size' (or standardized mean difference) due to RF radiation exposure was small with very few exceptions, (2) at certain RF radiation exposure conditions there was a statistically significant increase in genotoxicity assessed from some end-points, and (3) the mean frequencies for chromosomal aberrations and micronuclei in RF radiation-exposed and sham-/unexposed control cells were within the spontaneous levels reported in historical data-base. Considerable evidence for publication bias was found in the meta-analysis.

REFERENCES

1. Hedges, L. V. and I. Olkin, *Statistical Methods for Meta-analysis*, Academic Press Inc., New York, 1985.
2. Lipsey, M. W. and D. B. Wilson, *Practical Meta-analysis*, SAGE Publications, London, 2001.
3. Hunter, J. E. and F. L. Schmid, *Methods of Meta-analysis: Correcting Error and Bias in Research Findings*, 2nd Edition, SAGE Publications, London, 2004.
4. Lang, T. A. and M. Secic, *Synthesizing the Results of Related Studies: Reporting Systematic Reviews and Meta-analyses. How to Report Statistics in Medicine: Annotated Guidelines for Authors, Editors, and Reviewers*, 2nd Edition, Chapter 17, 255–279, American College of Physicians, Philadelphia, 2006.

Established Adverse Health Effects versus Possible Biological Effects of RF Exposure

C-K. Chou
Enterprise Mobility Solutions, Motorola Inc., Fort Lauderdale, FL, USA

Abstract— Research has been conducted since the 1950s to address RF safety concerns with exposure to radar, and then expanded to radio and TV broadcasting in the 1960s, microwave ovens in 1970s, police radar in 1980s and mobile phones and other wireless communication devices in the last 15 years. Other RF-emitting devices addressed by this research include video display terminals and medical devices such as for diathermy and magnetic resonance imaging. According to the WHO, scientific knowledge in this area is now more extensive than for most chemicals. The collection of scientific literature in the WHO database has more than 2000 peer-reviewed articles relating to RF bioeffects that includes more than 700 papers on mobile telephony exposure. WHO has estimated that at least $250M have been spent on mobile telephone RF safety research and another $250M committed for more research in various national programs. The already extensive RF database has been utilized by both the International Commission on Non-Ionizing Radiation Protection (ICNIRP) and the International Committee on Electromagnetic Safety (ICES) of IEEE to develop exposure limits to protect against established adverse health effects. For public exposure, safety margins up to 50X have been included in both exposure limits.

In the database, there are low-level or so called "non-thermal" effects reported. A group of scientists, some of whom have reported low-level effects, have posted on the internet a BioInitiative Report. This BioInitiative Group along with other activist groups is promoting much lower exposure limits to avoid "possible biological effects" as a precautionary measure. They acknowledged that these "possible biological effects" are not proven. As a precaution, the BioInitiative Report recommends that the current exposure limits as developed by ICNIRP and ICES should be lowered by 10,000 to 100,000 times in power density. Unlike the ICNIRP and IEEE exposure limits, the BioInitiative recommendation is not supported by any scientific rationale. For this reason and other limitations, the BioInitiative Report is not considered an objective scientific report by several national health agencies.

It is important to distinguish between "possible biological effects" and "established adverse effects". The IEEE C95.1-2005 standard defines an established adverse effect as "*A biological effect characterized by a harmful change in health that is supported by consistent findings of that effect in studies published in the peer-reviewed scientific literature, with evidence of the effect being demonstrated by independent laboratories, and where there is consensus in the scientific community that the effect occurs for the specified exposure conditions*". Biological effects, on the other hand, are "*alterations of the structure, metabolism, or functions of a whole organism, its organs, tissues, and cells. Biological effects can occur without harming health and can be beneficial. Biological effects also can include sensation phenomena and adaptive responses*". A safety standard by definition should prevent adverse health effects. Concerning reported low-level effects, the IEEE standard states: "*Despite more than 50 years of RF research, low-level biological effects have not been established. No theoretical mechanism has been established that supports the existence of any effect characterized by trivial heating other than microwave hearing. Moreover, the relevance of reported low-level effects to health remains speculative and such effects are not useful for standard setting*".

Both ICNIRP guidelines and IEEE standards are based on reviews of the RF literature, including human and animal studies, short-term and long-term exposure studies, and studies describing both thermal and non-thermal effects. During the last ten years, more than 50 statements from independent expert groups and government health authorities have acknowledged the protective nature of the internationally accepted exposure limits recommended by ICNIRP and IEEE.

Session 2AP
Poster Session 1

Development of Wave Absorbing Coating Optimization Software

Jianzhou Li, **Changying Wu**, **Gao Wei**, **and Jiadong Xu**
School of Electronics and Information, Northwestern Polytechnical University
Xi'an 710072, China

Abstract— Design and optimization of wave absorbing coating are of great interest in engineering practice to decrease the scattering intensity of typical targets, such as missiles and aircrafts. Aimed to automatically select particular materials from the material database and design the thickness of each layer to form the optimized multi-layer wave absorbing coating, a universal software based on the genetic algorithm is developed using C++. Many important features and functions, such as optimization in multiple bands with multiple incident angle and different incident wave polarization, partially assign and partially optimization of wave absorbing layer parameters, build-in radar absorbing material database management, reflection coefficient calculation and display of arbitrary wave absorbing coating are achieved in the developed software. The software development flow chart and basic modules are discussed. The functions and corresponding friendly user interface are given. Sufficient numerical examples are shown at last, which demonstrate reasonable optimization results, high efficiency and stability of the developed software.

Rotational Vector Addition Theorem and Its Effect on T-matrix

M. S. Khajeahsani and F. Mohajeri
Shiraz University, Iran

Abstract— In this paper, we prove the vector addition theorem for rotation of vector spherical wave with zero divergence by the use of vector rotation operator. In this theorem, a rotated vector spherical wave function is extended by fixed vector spherical wave functions. Then by the use of this theorem the relation between T-matrices for one object in two different concentric coordinate systems is formulated. Also, the relation between two coordinate systems is considered by Euler angles.

Why Cannot We Put a Metal in a Microwave Oven?

Leila Mashhadi[1] and Gholamreza Shayeganrad[2]

[1]Physics Department, Amirkabir University of Technology, Tehran, Iran
[2]Islamic Azad University, Karaj Branch, Karaj, Iran

Abstract— In this paper, the physical basis of sparking metal objects within the microwave oven cavity has been theoretically and experimentally investigated. Using cavity Q-factor, the characteristics of both TE and TM electromagnetic resonant modes in the oven cavity are determined. Assuming electrostatic field approximation and solving Laplace equation in both cylindrical and elliptical coordinate systems, electric field components around the metal disks and sharp points are theoretically determined.

It implies that the field strength around the sharp points and edges becomes approximately equal to the dielectric strength of air and charge deposits near the edges. Moreover, the induced current on the metal surface resonates with the microwave frequency and produce high voltage at the tips. Induced current heats metal and increases temperature of several points of metal up to the melting or vaporizing point of the metal and some tracks on the surface at these points are appeared. Field within the tracks is increased dependently to the track width; smaller track width greater track field. This effect varies with the object's shape and the composition. If metal is not thin, or if there are sinke within the metal, discharge will not occur. This effect can be seen clearly on aluminum foil, CD-ROM or DVD. Experimental results show a good agreement with the theoretical predictions.

Optical Analogue of Borrmann Effect in Photonic Crystals

M. Bogdanova[1], **S. Eiderman**[1], **and Yu. Lozovik**[2]

[1]Kintech Lab, Moscow 123182, Russia
[2]Institute of Spectroscopy, Russian Academy of Sciences, Troitsk 142190, Russia

Abstract— We propose a new optical effect in three-dimensional metal-dielectric photonic crystals — the direct analogue of the Borrmann effect observed in X-ray spectroscopy of usual crystals. We considered faced cubic cell opal-like photonic crystal consisting of two-layered metal-dielectric spheres. The absorption coefficient dependence on wavelength and angle of incidence is obtained using computer simulation by the layered Korringa-Kohn-Rostoker method. In our calculations we taken into account the losses in metal (tungsten) with the dispersion relation in Drude-Lorentz form. The wavelength region at which the absorption changes sharply with minor variations in the incidence angles is found out. This region is concerned with the interference of optical wave on the family of crystal planes (-111). The spatial energy distributions of electromagnetic wave inside each layer of the photonic crystals for two angles of incidence 23° and 30° corresponding to minimum and maximum of the absorption at wavelength 455 nm are analyzed using the Finite-Difference Time-Domain method. It is shown that in a peak of absorption, sharp maxima of the electromagnetic field energy are localized near the surface of absorbing metal cores of spheres. Furthermore in a minimum of absorption maxima of the energy distribution of the electromagnetic field are localized mainly between nodes of photonic crystals lattice. This means the drastic realignment of Bloch modes inside single unit cell of photonic crystals with minor variation of light incidence angle for fixed value of wavelength. This effect could be used in optical high-speed switchers based on the fluorescence within the metal-dielectric photonic crystals.

REFERENCES

1. Borrmann, G., *Zs. Phys.*, Vol. 42, 157, 1941.
2. Borrmann, G., *Zs. Phys.*, Vol. 127, 297, 1950.
3. Von Laue, M., *Acta Crystallographica*, Vol. 2, 106, 1949.
4. Bogdanova, M. V., S. L. Eiderman, Y. E. Lozovik, and M. Willander, *Laser Physics*, Vol. 18, 417, 2008.
5. Belousov, S., M. Bogdanova, A. Deinega, Y. Lozovik, I. Valuev, and S. Eiderman, *Matematicheskoe Modelirovanie*, Vol. 21, No. 5, 21–40, 2009.

The Nonlinear Absorption of a Strong Electromagnetic Wave by Confined Electrons in Rectangular Quantum Wires

N. Q. Bau and H. D. Trien
Faculty of Physics, Hanoi University of Science, Vietnam National University, Vietnam

Abstract— Analytic expressions for the nonlinear absorption coefficient of a strong electromagnetic wave by confined electrons in rectangular quantum wires with infinite potential are calculated by using the quantum kinetic equation for electrons in two cases: electron-optical phonon scattering and electron-acoustic phonon scattering. The dependence of the nonlinear absorption coefficient on the intensity E_0 and frequency Ω of the external strong electromagnetic wave, the temperature T of the system and size L of wires are obtained. The analytic expressions are numerically calculated and discussed for GaAs/GaAsAl rectangular quantum wires. The results are compared with those for the normal bulk semiconductors and quantum well to show the difference.

Lattice Spectroscopy in Near Field

Pin Han
Institute of Precision Engineering, National Chung Hsing University
250, Kuo Kuang Road, Taichung 402, Taiwan, R.O.C.

Abstract— It has been shown that the structure information for a lattice or periodic pattern can be obtained by measuring the diffracted spectrum of a broad-band light source at one spatial position in the far field. It is achieved by using the Fresnel-Kirchhoffer integral and Fourier transform with the far field approximation. However, for realistic applications, it is necessary to fulfill this technique in the near field. In this work, we demonstrate that this target can be accomplished by means of a focusing mirror without introducing the chromatic aberration. The quadratic phase term can be cancelled by the curvature of the mirror to obtain the lattice information in the near field. With a two dimensional lattice as an example, the analytic form the diffracted near field spectral intensity is given and the followed numerical results shows that the near field lattice information can be gained successfully by measuring the spectrum in near field. This approach can make improvements in the new lattice spectroscopy method.

Theory of the Acoustomagnetoelectric Effect in a Superlattice

N. Q. Bau and N. V. Hieu
Faculty of Physics, Hanoi University of Science, Vietnam National University, Hanoi, Vietnam

Abstract— The acoustomagnetoelectric (AME) effect in a superlattice (SL) induced by the interaction of acoustic phonons with the conducting electrons is calculated for an acoustic wave whose wavelength $\lambda = 2\pi/q$ is smaller than the mean free path l of the electrons and hypersound in the region $ql \gg 1$ (where q is the acoustic wave number). The analytical expression for the AME current j^{AME} is obtained by using the classical Bonltzmann kinetic equation in the case of relaxation time of momentum τ constant approximation. The result indicates that the existence of j^{AME} in a SL is attributed to the finite gap band, and the periodicity of the electron spectrum along the SL axis. Numerical calculations have been done and the result is analysed for the GaAs/AlAs SL. In the limit case at $\omega_q = 10^{13}\,\mathrm{s}^{-1}$, $H = 2 \cdot 10^3\,\mathrm{Am}^{-1}$, we have $j^{AME} \approx 10^{-4}\,\mathrm{mAcm}^{-2}$, which agrees with the experimental result, and this result is also compared with the result of the experiment in normal bulk semiconductors in the weak magnetic field region to show the difference.

Influence of the Output Electrical Parameters on Multistage Depressed Collector Characteristics in a Coupled Cavity TWT

Yinghui Zhang, **Jirun Luo**, **Wei Guo**, **and Min Zhu**
Institute of Electronics, Chinese Academy of Sciences, Beijing 100190, China

Abstract— Using a depressed collector to collect the residual energy of the electron beam is an important way to improve the total efficiency of traveling wave tube (TWT). Because the operating frequency band of the TWT is very wide, the electron beam in the collector disperses with the different state after it interacts with the microwave at different frequency. In this article, based on a coupled cavity TWT design software, Orprogr code, the simulation design of a X band coupled cavity TWT has been performed, in which the output power of over 120 kW has been reached at the maximum electronic efficiency of 20.5% and 1 dB bandwidth of greater than 17%. Under the condition of the above-mentioned design results, a depressed collector has been designed with the maximum collector efficiency of 76.7% and the total efficiency of the TWT of 39.5%, and the electron beam evenly spreads on the surface of each sub-area of the depressed collector by choosing appropriate electrode shape and voltage drop. The simulation results show that when the electron efficiency increases with electrical parameter variation, the longitudinal velocity of the electron beam decreases, its laminar flow may become worse and the trajectories of the electron beam are disordered in the collector. The landing point of electron beam on the collector surface moves backward and distribute unevenly. And the cutting angle of the moving direction of the electron beam with the collector surface increases, which may effectively suppress the production of secondary electrons. When the electron efficiency decreases, the longitudinal velocity of the electron beam increases and its laminar flow may become better. However, the electron beam landing on the collector surface becomes dense, the electron energy intercepted by the depressed collector increases and the heat dissipation may become more difficult, and the cutting angle of the moving direction of the electron beam with the collector surface decreases, which may promote the production of secondary electrons. A three-stage depressed collector has been designed through rationally selecting the electrical parameters, which shows the collector efficiency of more than 70% may be reached with a relatively homogeneous distribution of the electron beam on the collector surface in the whole operating frequency range.

Numerical Study on Readout Characteristics of Near-field Optical Disk

S. Iwata and T. Kitamura
Faculty of Engineering Science, Kansai University, Osaka, Japan

Abstract— The capacity of optical storage system has been improved by shortening wavelength, or increasing the numerical aperture of an objective lens. However, the recording density has a limitation due to optical diffraction limit. Recording methods based on near-field optical principles are one of the candidates that can overcome the limitation. Many researchers have been interested nano-apertures for the method to obtain near-field light and many types of apertures have been proposed so far. In order to obtain high emission intensity and small spot size simultaneously, they have discussed various aperture shapes such as triangular, H, I or C shaped, figure-eight or bow-tie shaped, ridge waveguide type, rectangular holes with a metallic slit, and so on.

In this paper, we focus on readout characteristics of recorded marks on a phase change disk illuminated by near-field optical light through an acute-edged metallic nano-aperture. We deal with a two-dimensional structure in order to simplify the discussion. Here, we assume silver as a metallic material. The incident light is a p-polarized Gaussian beam with the wavelength of 650 nm and the numerical aperture of an object lens is assumed to be 0.6. In the analysis, we use FDTD method into which motion equations of free electrons are installed to analyze a metallic material. We show that the field intensity of near-field light can be increased by adjusting edge angles of the aperture. We also investigate the influence of the edge angles on output through the recorded marks.

Getting Excitation Characteristic Curves of PTs with Linear Interpolation Method

Zheng-Wang Du[1], **Heng-Xu Ha**[2], **Lei Zhai**[3], **Hai-Quan Zhou**[2], **Song-Bo Gou**[1], **and Chong-Shan Zhong**[1]

[1]ShengLi Oil Field Power Company, Dong Ying, China
[2]Dept. of Electric & Electronics Engineering, Shandong University of Technology, Zibo 255049, China
[3]School of Electrical Engineering Automation, Hebei University of Technology, Tianjin, China

Abstract— Ferro-resonance over-voltage is a common internal over-voltage, which occur frequently in the neutral grounded distribution network and occasionally in the neutral ungrounded. Ferro-resonance leads to over-voltage and over-current which seriously affect the safe operation of the system.

The excitation characteristics of the non-linear component in power system is the important factor resulting in ferro-resonance. In order to protect transmission and distribution equipment in the power system and to ensure the network security, operation reliability and stability, at the same time, to recognize abundantly the mechanism of the ferro-resonance over-voltage, the flux-current characteristic of the voltage transformer plays an important role for non-linear Ferro-magnetic analysis.

In tradition, the disadvantage of the excitation curve fitting method using the model of polynomial terms lies in that the linear part fitting is not perfect, while, the non-linear part has the good fitting results, which is not accord with the PT excitation characteristic. With fitting order number increasing, insufficient samples will also lead to unfavorable fitting results.

In this paper, line interpolation will be first carried out for the linear part of the measuring volt-ampere characteristics, then sample points will be increased by utilizing least squares fit, which will greatly improves the fitting precision of the linear part and the overall fitting accuracy of the non-linear part. The simulation results show that the error of the linear part does not exceed 0.3% and the error of the non-linear part drops from 2.5% to 1.5% when the linear part is given 11 order line interpolations.

A New Approach to Periodical Structure Analysis

R. Kadlec, **P. Drexler**, **and P. Fiala**
Department of Theoretical and Experimental Electrical Engineering, Brno University of Technology
Kolejni 2906/4, Brno 612 00, Czech Republic

Abstract— Paper presents usage numerical modeling of propagation electromagnetic waves. For this method a numerical model was prepared. The numerical model was created in the MatLab program environment. For layered heterogeneous medium is deduced algorithm for reflection on several layers. Several layers are in form of periodical structures which are composite of homogenous material. The reflection and refraction are analyzing accordance with Snell's law for electromagnetic waves. Deduced algorithm was project for the visible spectrum. Reflection and refraction on heterogonous material is solving by numerical method. This method is suitable for design application of the metamaterial. This method is suitable for specific purposes of detail analysis for design nanomaterial. Analysis propagation of wide THz band signal for $\lambda \in \langle 400; 700\,\mathrm{nm}\rangle$ as propagation of electromagnetic waves is very time demanding.

REFERENCES

1. Dědek, L. and J. Dědková, *Elektromagnetismus 2*, ISBN 80-214-1548-7, Vitium, Brno, 2000.
2. Moss, C., "Numerical metods for electromagnetic wave propagation and scattering in comlex media," 2004, available from www: <http://portal.acm.org/citation.cfm?id=1023429>.
3. Stratton, J. A., *Teorie Elektromagnetického Pole*, STNL, Praha, 1961.
4. Zhang, J., J. A. Kong, et al., "Cloak changing with background," *PIERS Online*, Vol. 4, No. 5, 596–600, 2008.
5. Fiala, P., "Finite element method analysis of a magnetic field inside a microwave pulsed generator," *2nd European Symposium on Non-lethal Weapons*, Ettlingen, SRN, May 13–15, 2003.

A Numerical Simulation Study of the Effect of Array Shape on the Performance of Antennas

Danoosh Davoodi and Shahin Sharifzad
Sadjad Instate of Higher Education, Mashhad, Iran

Abstract— A single-element antenna is usually not enough to achieve technical needs. That happens because its performance is limited. A set of discrete elements, which constitute an antenna array, offers the solution to the transmission and/or reception of electromagnetic energy. The geometry and the type of elements characterize an antenna array. This paper presents a comprehensive study on the performance of a half-wave length dipole antenna standalone and in various types of arrays. The dipole antenna length is 150 mm. All the simulations are done for three deferent distance between the antennas ($\lambda/2$, $\lambda/4$, $\lambda/10$). All antennas are excited with a 50 Ω microstrip feed line. Number of antenna elements in each array is 10. Radiation patterns and VSWR of this antenna are computed for standalone antenna as well as each array. In addition, radiation efficiencies, gain, directivity of the antennas are discussed. All numerical simulations are performed using the Ansoft HFSS software.

Analysis of Electromagnetic Field Affected by Liquid in Water Area Magnetotelluric Exploration

Ling-Hua Xu[1], **Jian-Xin Liu**[1], **Jian-Rong Xu**[2], **Zhen-Wei Guo**[1], **Ya Sun**[1], **and Xiao-Zhong Tong**[1]

[1]School of Info-physics Geomatics Engineering, Central South University, Changsha 410083, China
[2]Team 814, East China Bureau of Noneferometal Geological Exploration, Zhenjiang 212005, China

Abstract— By studying the relation of electromagnetic fields and impedance of sill like medium between water surface and water floor, we have gained the attenuated coefficient and the attenuation law of electromagnetic fields in water area. It is obvious that the signals are attenuated worse when the frequency increases, but the liquid attenuation characters upon electric field and magnetic field are different. First, the attenuation amplitude of magnetic field is far greater than electric field in same condition, and the frequency range is wider. Second, the attenuation of electric field not only lies on mostly the character of liquid self (the depth and resistivity of liquid), but also on the media property below the water, that is, the higher the resistivity is the more severe the attenuation of the magnetic field, the attenuation of magnetic field relates to the characters of liquid medium. The condition in which the water effect can be neglected in water magnetotelluric sounding (MT) exploration of electromagnetic signal sampling is as follows: the water depth is less than 3 m in MT and 2 m in CSAMT.

The Study of Field Source Static Shift in Frequency Domain Controlled-source Electromagnetic Sounding with Long Wire Source

Ya Sun[1], **Zhan-Xiang He**[2], **and Jian-Xin Liu**[1]

[1]The Institute of Info-physics and Geometrics Engineering, Central South University
Changsha, Hunan 410083, China
[2]Graduate Workstation of Geophysical and Geochemical, BGP, Zhuozhou 0727511, China

Abstract— In frequency domain controlled-source electromagnetic sounding with long wire sourcethe static shift is generated by shallow inhomogeneous body which is placed in the measurement points has been extensively studied and taken good correction. According to reciprocal principle, when the inhomogeneous body is placed in the long wire source, static shift will also be existedand this is called field source static shift. So the law of field source static shift is studied, in this paper, through the three-dimensional model, which includes the model size, burial depth and the all time apparent resistivity of horizontal electric field component have been simulated. At last, we have obtained that the static effects are changes as the inhomogeneous body burial depth, and the field source static shift reaches the maximum, when the length of inhomogeneous body is five times than the source.

The Physical Modeling Experiments Analysis of the Exploration Depth of Conventional Electric Survey

Jie Li, **Jian-Xin Liu**, **Xiao-Zhong Tong**, **and Zhen-Wei Guo**
School of Info-physics and Geometrics Engineering, Central South University, Changsha, China

Abstract— Conventional electric survey is one of the most important geophysical methods. The chief issue which affects the level and the foreground of application area of the conventional electric survey is the depth of exploration and its resolving power.

Direct current electrical method and dual frequency induced polarization method was used in this text. At first we analyze their exploration ability of these two methods in the theory, and then we analyze the depth of exploration and the resolving power of the conventional electric survey by the experiment which takes place in a tank laboratory with a graphite nodule act as a unconventional object. The experiment is carried on in the tank with 5.0 m in length, 4.0 m in breadth and 2.0 m in depth. The model we used a graphite nodule whose semidiameter is 10 cm and a graphite columniation whose diameter is 10 cm. The equipment we adopted is symmetry quadrupole setting of the electrical sounding method. In the direct current electrical method, we use the DDC-5 to find out the infection to the depth of exploration by changing the AB's polar distance. In the induced polarization method, we use the SQ-3C to find out the infection to the depth of exploration by changing the AB's polar distance, supply current and frequency.

The experimental results indicate that the exploration depth and the resolving power of the direct current electrical method and dual frequency induced polarization method are related with the distance between AB-polar and its shape. In the dual frequency induced polarization method, the supply current and frequency do not influence the exploration ability very much.

Cole-Cole Model Based on the Frequency-domain IP Method of Forward Modeling

Wei Zhang[1, 2], **Jian-Xin Liu**[1, 2], **Zhen-Wei Guo**[1, 2], **and Xiao-Zhong Tong**[1, 2]

[1]The Institute of Info-physics and Geometrics Engineering, Central South University
Changsha, Hunan 410083, China
[2]Key Laboratory of Non-ferrous Resources and Geological Hazard Detection
Changsha, Hunan 410083, China

Abstract— Induced polarization method (IP) is an electrical prospecting method which is based on rock, ore, metal induced polarization effects to find and solve hydro-geological, engineering geological issues. It can be divided into two groups: DC-induced polarization method (time domain method) and the exchange of AC-induced polarization method (frequency domain method). At present, because of itself advantages, Frequency-domain induced polarization method (frequency domain method) has be widely applied in production. However, because the induced polarization effect of rock or ore are very complex and subjected to many kind of factors, so it is very difficult to describe the induced polarization effects very accurately at present. Therefore, the induced polarization method has many problems in data interpretation and data analysis what has limited the practical application of induced polarization method.

The Cole-Cole model is a formula for Describing dielectric polarization, it has the same forms with the formula of induced electrical Frequency characteristic of Complex resistivity. The description of induced polarization phenomenon of rock and ore can be more imaginal, as the basis of the frequency-domain IP for effective forward modeling, can accurately describe the Characteristics of induced polarization effects for rock and ore and develop a adaptive Software of forward modeling for induced polarization method.

The results of this paper have great significance in Studying on induced polarization effect of rock and ore and the real production of induced polarization method and provide a platform for understanding the phenomenon of induced polarization, Help to enhance people's understanding of the phenomenon of induced polarization and the Accuracy of data resolving of induced polarization method in real production, which can greatly promote the practical application of induced polarization method in frequency domain and the actual national production.

Electric Field around a Metal Disk within a Microwave Resonator: Electrostatic Approximation

Gholamreza Shayeganrad[1] **and Leila Mashhadi**[2]

[1]Islamic Azad University, Karaj Branch, Karaj, Iran
[2]Physics Department, Amirkabir University of Technology, Tehran, Iran

Abstract— In this work a rectangular resonator cavity with non-ionization electromagnetic radiation at frequency of 2.45 GHz or wavelength of 12.24 cm involving a metal disk has been considered. We have shown electrostatic field is a suitable approximation to study a metal disk within a cavity with alternative field at frequency of 2.45 GHz and it leads to solve Laplace's equation. We have solved this equation in elliptical coordinate in detail considering boundary conditions and determined electric field around the disk. Solving Laplace's equation in elliptical coordinates is the appropriate method for determining electric and magnetic fields in the vicinity of the metals with striped or circular types.

Study on Compact UWB Filter Composed of Defected Parallel Plates and Meander Line

H. Takeuchi[1], **T. Kitamura**[1], **and Y. Horii**[2]

[1]Faculty of Engineering Science, Kansai University, Osaka, Japan
[2]Faculty of Informatics, Kansai University, Osaka, Japan

Abstract— Since the unlicensed use of ultra-wideband (UWB) frequency spectrum (3.1–10.6 GHz) for indoor and hand-held wireless communications is released in 2002, great attention has been paid to applications of UWB technology on wireless communication system. According to this, various kinds of bandpass filters with specified ultra-wide passbands have been proposed.

In this study, we propose a compact ultra-wideband bandpass filter. The proposed filter is composed of a pair of parallel plates (size 2.0 mm × 2.0 mm, distance between the plates 0.31 mm), a meander line (line width 0.1 mm, slit width 0.1 mm, total length 6.1 mm), and a thin conductor column (diameter 0.2 mm, length 0.31 mm). The column is located between the parallel plates and links them in the center of each one. One side of the meander line is connected to the center of the column and the other is terminated to the ground. They construct a kind of quarter-wavelength resonator. The center of each parallel plate is defected in a square shape (0.6 mm × 0.6 mm) and thin lines (width 0.1 mm, length 0.3 mm) are added between the column and the parallel plates. I/O strip lines are located on either side of the parallel plates, on at the top of it and the other bottom of it. The whole structure is fabricated in a ground enclosure filled with a dielectric material with a relative permittivity of 2.59.

We analyze the filtering characteristics by using a full-wave EM-simulator Ansoft HFSS Ver.11 based on the finite element method. The results show that the wide passband from 2.0 GHz to 9.0 GHz is obtained and attenuation poles are created at both sides of the passband. The attenuation-pole frequency around 9.0 GHz can be adjusted by changing the defected structure of the parallel plane. We also investigate the characteristics by using the equivalent circuit.

FDTD Analysis of Light-beam Scattering from DWDD Disk with Control Layer

Yuya Matsunami and Toshiaki Kitamura
Faculty of Engineering Science, Kansai University, Osaka, Japan

Abstract— The magneto-optical (MO) disks are used as rewritable media of information. Recently, various technologies of higher density version that exceed optical resolution have been proposed for MO disk, and put to practical use. In those technologies, the domain wall displacement detection (DWDD) is one of the excellent readout methods, which utilizes the characteristic of magnetic film called wall-displacement phenomenon by temperature gradient. This method has no limit of resolution in principle. However, it has a problem that ghost signals are caused by so-called rear process (RP) due to continuously recorded marks.

In this study, we deal with a DWDD disk model that has a control layer to suppress ghost signals. We use FDTD method for the analysis. So far, we have applied FDTD method to the analysis of light-beam scattering and detected signal characteristics from various types of optical disks such as digital versatile disks (DVD) and MO disks and demonstrated that it can be a powerful tool for the numerical simulation of light-beam diffraction from conventional DVD and MO disk structures.

We analyze light-beam scattering from the disk model. We also investigate main-polarized and cross-polarized components of scattered far field and phase differences between them. We show that by adding the control layer the ghost signal can be suppressed.

Study on Stepped Impedance Comb-line Filter with Defected Ground Structure

N. Tatsumi[1], **T. Kitamura**[1], **and Y. Horii**[2]

[1]Faculty of Engineering Science, Kansai University, Osaka, Japan
[2]Faculty of Informatics, Kansai University, Osaka, Japan

Abstract— Miniaturization of microwave filters is highly demanded. Especially for handy mobile telephones specially, ceramic laminated filters have been widely used, and in particular, the stratifying technology of ceramic using low-temperature co-fired ceramics (LTCC) technology is one of the key technologies for reducing the device dimensions. This technology makes it enables the unification of various kinds of devices in a multilayered structure.

In this study, we consider comb-line filters in which both sides of the substrate are utilized. Comb-line filters consist of two quarter-wavelength resonators, and attenuation poles can be created in the frequency characteristics of the transmission parameter by changing the coupling locally along the resonators. The stopband characteristics can be improved by arranging the attenuation poles around the passband. In this paper, we discuss the method of installing a coupling capacitor by inserting slots into the ground plane. The proposed filter is composed of two microstrip step impedance resonators that are arranged on the substrate. Each resonator is terminated through the ground plane at one end using a through hole. As an I/O port, a microstrip line is directly connected to each resonator. A square-shaped coupling capacitor is fabricated by inserting slots into the ground plane. It is thought to be a kind of defected ground structure (DGS). It produces a strong coupling locally along the resonators. We investigate the filtering characteristics through numerical simulations by means of FDTD method.

Generalized Coherent States for Quantized Electromagnetic Fields in Time-varying Linear Media

Jeong Ryeol Choi[1] **and Mustapha Maamache**[2]

[1]School of Electrical Engineering and Computer Science, Kyungpook National University
Daegu 702-701, Republic of Korea
[2]Laboratoire de Physique Quantique et Systèmes Dynamiques, Faculté des Sciences
Université Ferhat Abbas de Sétif, Sdtif 19000, Algeria

Abstract— To investigate the precise nonclassical behavior of radiation fields, it is crucial to quantize the electromagnetic fields. The quantization of light in vacuum cavities or in infinite free space, that is treated in most text books of quantum optics, gives the same results as the case of standard harmonic oscillator. Such traditional quantization procedure may also be extended to that of light described by time-dependent Hamiltonians by means of LR (Lewis-Riesenfeld) invariant operator method introduced by Lewis and Riesenfeld. The LR invariant operator method is very useful in investigating the quantum properties of various types of time-dependent Hamiltonian systems. If the parameters of the materials, such as electric permittivity, magnetic permeability, and conductivity, vary explicitly with time, the corresponding Hamiltonian is a time-dependent form and one can classify such materials as the time-varying media of light. We present the quantization problem of light fields in time-varying linear media using invariant operator theory of LR. The choice of Coulomb gauge in charge free space allows us to evaluate quantized electric and magnetic fields by expanding only the vector potential, since the scalar potential in this case is zero. The generalized coherent states, i.e., Gaussian Klauder coherent states, of electromagnetic fields confined inside a cavity filled with a nontrivial conductive media is investigated. The quantum and classical correspondence can be shown using Gaussian Klauder coherent states which provide a general means of construction for Husimi-Wigner distributions. We confirmed that the uncertainty product in Gaussian Klauder coherent state is the same as the minimum uncertainty product in number state. This is well agree with the theory for the standard harmonic oscillator developed by Fox and Choi [1]. The uncertainty product in this state fluctuates more or less as time goes by.

REFERENCES

1. Fox, R. F. and M. H. Choi, *Phys. Rev. A*, Vol. 61, 032107, 2000.

An Alternative Explanation for the Fraunhofer Sun Lines

S. L. Vesely[1] and A. A. Vesely[2]

[1]I.T.B., C.N.R., via Fratelli Cervi 93, Segrate (MI) I-20090, Italy
[2]via L. Anelli 13, Milano 20122, Italy

Abstract— It is well known that the Sun light dispersed through an accurately grinded prism of a quite homogeneous glass features a lot of dark lines, called the Fraunhofer lines. They superimpose onto the broad Sun emission spectrum if a narrow perpendicular slit is interposed in between the source and the prism. W. Wollaston, the first researcher to observe those dark lines in 1802, supposed that the prism would form an image of the slit for each different color in the rainbow. Therefore he claimed that the Sun lines were separating distinct colors. Nearly ten years later J. Fraunhofer, who was aiming at calibrate prismatic spectra of different glasses for the purpose of compensating the lenses' chromatic aberrations [1], showed that the luminous background changed too smoothly to justify the appearance of such strong marks. As the spectra of the lamps in use at that time did not exhibit analogous patterns, he further assumed them to depend on a characteristic feature of the light of solar origin. Today those patterns are believed to be chemical in origin, and to stem from gas absorption. However, the features amenable to terrestrial elements are blended with others, which could arise from ionization of already strongly excited atoms [2], and are therefore assigned to chemicals in the cooler solar photosphere. Much effort has been devoted to explain the latter lines [3], as it appears to be the only way to discover the composition of farther stars. Nevertheless the proposal of explaining the whole of the Fraunhofer lines in such a way remains quite elusive. We shall rather try and connect the phenomenon with the observation of schlieren effects. It is a simple alternative explanation more inline with the older ones. At the outset we consider that spatial coherence was the characteristic feature missed by the lamps at Fraunhofers disposal. Then a glass, which is very homogeneous in every other respect, behaves also as a phase filter if it is prism-shaped, i.e., it dephases light differently between the apex and the base. Finally, if the slit is sufficiently narrow, many different images of it do indeed form because of the prism, as Wollaston claimed. The coherent beams of the images interfere and let the phase modulations, to whom the human eye is insensitive, become light intensity modulations.

REFERENCES

1. Fraunhofer, J., *Bestimmung des Brechungsund Farbenzerstreuungsvermögens verschiedener Glasarten in bezug auf die Vervollkommnung achromatischer Fernröhre*, Verlag von Wilhelm Engelmann, Leipzig, 1905.
2. Ladenburg, R., "Dispersion in electrically excited gases," *Rev. Mod. Phys.*, Vol. 5, No. 4, 243–256, 1933.
3. Bruggencate, P., R. Lüst-Kulka, and H. H. Voigt, "Methodisches zur berechnung von fraunhoferlinien im sonnenspektrum," *NachGöttingen Mathematisch-Physikalische Klasse*, 257–283, Göttingen, Germany, February 1955.

Finite-element Analysis of Complex Axisymmetric Invisibility Cloaks

Yong-Bo Zhai, **Xue-Wei Ping**, **Wei-Xiang Jiang**, **and Tie-Jun Cui**
State Key Laboratory of Millimeter Waves, Southeast University, China

Abstract— Invisibility cloaking based on metamaterials has aroused great interest recently. Several methods have been used to simulate invisibility cloaks. Ray-tracing simulations were reported in the geometric optics limit. Analytical solutions were available for circularly cylindrical cloak and spherical cloak. The discrete dipole approximation method has been applied to simulate the 3D spherical cloaks and irregular 3D cloaks approximately. However, the full-wave analysis and simulation of three-dimensional (3D) cloaks are still limited due to the large amount of computational burden. For example, the Comsol software cannot be used to simulate a large 3D cloak since the huge memory requirement and computational time.

When scattering from body of revolution (BOR) is involved, the problem can be efficiently solved using a two-dimensional (2D) computational method by taking advantage of the rotational symmetry property of the problem. The method of moments (MOM), the finite difference method (FDM), and the finite element method (FEM) can be applied to this problem. Of these methods, FEM is very flexible, and has significant computational advantages for simulations of arbitrary inhomogeneous and anisotropic dielectric BORs.

In this work, we present a finite-element analysis of axisymmetric invisibility cloaks. The method is based on the electric field formulation with the transverse field expanded in terms of first-order edge-based vector basis functions and the azimuth component expanded using two-order nodal-based scalar basis functions. The FEM mesh is truncated using cylindrical perfectly matched layer (PML). Because of the singular behavior of the material properties on the inner boundary of the cloak and the strong inhomogeneity and anisotropy, we find that the method is more accurate and stable than the first-order formulations. Several invisibility cloaks with different shapes are analyzed to show the accuracy and capabilities of the method.

Simulations of an Electromagnetic Microsystem Used in Biomedical Applications

T. Creutzburg and H. H. Gatzen
Institute for Microtechnology, Leibniz Universität Hannover, Garbsen, Germany

Abstract— Electromagnetic systems are used in a wide range of macro and micro applications. A proven approach for the design of microsystems is to create a Finite Element (FE) model for these systems and simulate their behavior when excited [1]. This paper reports on simulations of a electromagnetic microsystem intended to be used in a microactuator which serves as an inner ear implant to overcome amblyacousia.

The electromagnetic device consists of a microcoil system and soft-magnetic flux guides. In principle, the structure corresponds to a pot magnet. The circular-shaped soft-magnetic lower core and inner pole, the flux closure as well as the ring-shaped outer pole consist of NiFe45/55. The coil system lies above the lower core between inner and outer pole underneath the flux closure and is made of Cu. The system is embedded in the photosensitive epoxy SU-8^{TM}.

Using the ANSYS^{TM} simulation software, the design and optimization of the electromagnetic microsystem were accomplished by Finite Element Method (FEM) analyses at the Institute for Microtechnology (imt). The design process contained 2D and 3D simulations. The 2D-simulations served as parametric studies of the system. 3D simulations were done afterwards to verify the results of the 2D simulation. Design limitations were given by the aspects of microtechnological fabrication and the geometry of the inner ear implant the electromagnetic system should drive and had to be considered in the simulations. To do so, different designs were modelled, changing the geometry of the flux guides and the number of the coils. These systems were modelled using the ANSYS^{TM}. Parametric Design Language (APDL). By combing ANSYS^{TM} rectangle primitives, the structures of the systems, i.e., the flux guides and the coil system, were set up by using the rotational symmetry of the systems. Overlapping the created structures with a half circle forming the surrounding air resulted in the final axisymmetric model. The SU-8^{TM} embedding was neglected because SU-8^{TM} behaves like air in an electromagnetic simulation. Using the elements Infin110 and Plane53, the models were meshed applying the appropriate material properties. Infin110 elements were used to mesh the outer element layer of the surrounding air, modelling the effect of far-field decay. Additionally, the outer nodes were selected and flagged as infinite surface. The Plane53 elements were used to mesh the rest of the model. In the following, a component was created containing the elements of the flux closure. Using the macro FMAGBC, MAXWELL and virtual work force boundary conditions were applied to this component. The excitation was carried out by supplying current density loads to the areas of the coil system. By changing the air gap and simulating the systems, the respective force-air gap curve for each system was analyzed.

In the following, the requirement-matching system was modelled in 3D. The modelling procedure was carried out like in the 2D-simulation. The geometry model was generated using ANSYS^{TM} primitives in full symmetry. The coil system was modelled as a stranded coil, defining the properties with a real constant. The meshing of the model was carried out using Solid97, Infin111, and Circu124 elements, respectively Infin111 elements were again used for the outer layer of the modelled air acting like Infin110 elements in a 2D-simulation. The excitation of the stranded coil was done by using Circu124 elements. Changing the air gap again, the force-air gap curve was analyzed. Comparing the 3D with the 2D-simulation, the curves showed nearly the same characteristics. In respect to the simulations, the designed electromagnetic system fulfils the requirements to drive the microactuator.

REFERENCES

1. Dinulovic, D. and H. H. Gatzen, "An approach for simulating magnetic microactuators," *International Conference on Thermal, Mechanical and Multi-Physics Simulation and Experiments in Microelectronics and Micro-Systems, EuroSimE 2008*, 1–4, 2008.

Characterization of Eddy-current Probe with Tilted Coil Using Multiphysics Finite Element Method

Cheng-Chi Tai and Yen-Lin Pan
Department of Electrical Engineering, National Cheng Kung University, Tainan, Taiwan

Abstract— Characterizing eddy current probes has been a critical issue in nondestructive testing (NDT) over past decades. However, probe tilt has been recognized as the one reason of producing deviation in eddy current testing (ECT), such as the flaw manual scanning or the manufacture of probes with irregular orientation coils. The inability to calibrate and characterize the structure of eddy current probes with tilted coils makes it impossible to accurately inspect the surface cracks. The photoinductive imaging (PI) method is a novel inspection technique for detecting or sizing cracks. Furthermore, it dramatically overcomes disadvantages of previous eddy current probe field-mapping techniques, such as large probe size, poor signal to noise ratio, or insensitivity to the tangential component of the magnetic field.

The PI method is very similar to the photothermal imaging method. By scanning a focused laser beam across the surface, an image of the dynamic responses of the sample can be obtained, which produces localized variation on the subsurface features. The coil probe is placed close to the specimen surface and excited with sufficient voltage and at the desired frequency. When laser beam is focused on the specimen surface from below, the absorption of heating energy by the metal film causes variations in electrical conductivity, which, in turn, induces a change in the impedance of the coil probe.

In this paper, the numerical modeling of the PI method with electromagnetic and heat transfer analysis was performed and simulated with two-dimension finite-element method (2-D FEM) to analyze the influence of tilted coils. The proposed model calculates the probe's impedance above a thin metal film for mapping the electric field of EC probe and the distribution of EC on the foil surface. The FEM simulation results for varied tilted angles of coil, thicknesses of metal foil, materials of metal foil, and lift-off distances of EC probe are shown and discussed. The results show that the PI method is appropriate for mapping the structure of EC probes and that the clear characterization of the coil probe can also be obtained given an appropriate quantity of factors.

Using Fictitious Currents for Calculating Electric Fields Produced by Capacitor Dielectrics

R. Ravaud and G. Lemarquand
Universite du Maine, France

Abstract— MRI Yokeless Devices are composed of tile permanent magnets uniformly magnetized with various magnetizations [1]. Such structures, also called Halbach structures, are used for creating a polarizing magnetic field whose uniformity is the most important criterion.

Different analytical approaches can be used for studying the magnetic field created by cylindrical Halbach structures. Authors generally use three-dimensional linearized models based on the magnetic field produced by parallelepiped magnets for calculating the three magnetic field components outside of the permanent magnets [2]. By using this linearized analytical approach, the cylindrical structure is replaced by a bar-shaped permanent magnet and the magnetic field is determined only in the near field, that is, close to the magnets. Such an approach is useful because it is fully analytical. However, as mentioned in [1], it does not forecast some typical three-dimensional effects that occur in the near field.

Other analytical methods have been proposed for calculating the magnetic field in the centre of the structure. Such methods are based on the equivalent dipole representation and are typically adapted for the design of MRI structures in which the region of interest is mainly concentrated in the centre of the structure, that is, far from the magnets. In addition, they are useful because they have a very low computational cost but they are not appropriate for studying the magnetic field in the near field. Consequently, some general analytical methods are required for calculating the magnetic field for all points in space, whatever the tile dimensions.

We present in this paper a three-dimensional analytical model for calculating analytically the exact magnetic field created by cylindrical Halbach structures. For this purpose, the three magnetic field components are determined by using the coulombian model of a magnet. Each tile permanent magnet has a magnetization that can be radial, tangential or directed along any direction in the (R, θ) plane. The magnetic field is expressed in semi-analytical forms and we show that for some observation directions, it is possible to express the three magnetic field components in terms of classical elliptic integrals.

The algorithms used for calculating such elliptic integrals are robust and very fast. Consequently, the expressions obtained can be used for optimization purposes. The general expression of the magnetic field produced by a Halbach structure is composed of a fully analytical part and a semi-analytical part based on one numerical integration. It is noted that the semi-analytical part cannot be expressed in terms of classical elliptic integrals with the coulombian approach because the magnetizations we consider are uniform, as it is generally the case in practice.

By applying the principle of superposition to each tile permanent magnet, the total magnetic field can be determined quickly as the problem considered is purely linear. In addition, as we use analytical expressions, the change in shape of the magnetic field can be studied easily when the observation point varies along the three directions in space.

By using these three-dimensional analytical exact expressions, we propose some optimized structures that can be used for the design of electrical machines. As the computational cost of such expressions is very low, such optimizations are carried out easily. We discuss the interest of using tile permanent magnets with different angular widths and we show that some structures can be optimized by using tile permanent magnets with only radial and tangential magnetizations.

REFERENCES

1. Ravaud, R. and G. Lemarquand, "Magnetic field in MRI yokeless devices: Analytical approach," *Progress In Electromagnetics Research*, PIER 94, 327–341, 2009.
2. Ravaud, R., G. Lemarquand, V. Lemarquand, and C. Depollier, "Discussion about the magnetic field created by permanent magnets," *Progress In Electromagnetics Research B*, Vol. 11, 281–297, 2009.

Numerical Modeling of Light Sources with R-FEM Method in CFX Environment

J. Mikulka, **T. Kříž**, **E. Kroutilova**, **and P. Fiala**
Department of Theoretical and Experimental Electrical Engineering, Brno University of Technology
Kolejní 2906/4, Brno 612 00, Czech Republic

Abstract— Paper presents usage of the R-FEM method in the CFX environment. The R-FEM method was used for modeling of special light sources and to compute lighting of surfaces from these sources with very good results. Basic description of the R-FEM method is described below. For modeling of the light sources in the CFX environment was used combination of the Finite Volume Method and the radiation method which are included with the CFX (The Discrete Transfer Model and The Monte Carlo Model). Numerical results are presented by models with basic optical geometry (parabolic surface with light source placed in focus point and reflecting surfaces with different angular displacement). There are presented numerical results for mirrored reflecting surfaces and diffusion reflecting surfaces with different degrees of diffusion.

The R-FEM method is a new way in the modeling of lighting systems. It utilizes the similarity between physical models. This paragraph demonstrates the usage of analogy between different physical models for the modeling of light problems. The R-FEM method is able to solve tasks that fulfill the condition $\lambda_S \ll \max(D) \wedge \lambda_S < 10.\ \max(D)$, where λ_S is the source of light wavelength and D is one of the geometrical dimensions of the modeling task. It can be used for models with more complicated physical structures than the methods mentioned up to now. An example of a more complicated physical problem, which we can solve by the R-FEM method, is the modeling of light intensity distribution in interior or exterior spaces with non-homogeneous environment, where the light has passed through some impure air (e.g., filled with smoke, fog, mist, vapour, dust, etc.).

REFERENCES

1. Fiala, P., E. Kroutilova, and T. Kriz, "Numerical modelling of the special light source with novel R-FEM method," *PIERS Proceeding*, 822–826, Cambridge, USA, 2008.
2. Kroutilova, E., *Způsob návrhu odrazných ploch reflexních zařízení pomocí analogie teplotního pole-radiace a vlnové rovnice a zařízení v podobě světelné soustavy určené pro numerickou optimalizaci požadovaných světelných parametrů odrazných ploch*, Patent No. PV 2008-65, Czech Republic, Leden 2008.
3. Kadlecova, E., "Automated system of calculation of reflecting surface of light sources," Ph.D. thesis VUT v Brně, FEKT, Brno srpen 2004.

Two-dimensional Magnetotelluric Regularization Inversion Jointed with TE- and TM-mode Data

Jian-Xin Liu, **Ling-Hua Xu**, **Xiao-Zhong Tong**, **Ya Sun**, **and Zhen-Wei Guo**
School of Info-physics Geomatics Engineering, Central South University
Changsha 410083, China

Abstract— The magnetotelluric inverse problem is ill-posed and the inverse results are unstable and non-unique. It means that different geo-electrical model could fit the observed data with the same accuracy. A stable solution of the ill-posed inverse problem can be obtained by utilizing the regularization methods in the objective function. Solving large scale linear equation of inverse problem, the damped Gauss-Newton algorithm was adopted, which can improve local convergence of Gauss-Newton method. In order to better inversion results, TE- and TM-mode magnetotelluric data are jointed. Through the synthetic model simulation, the inversion results truly reflected the geo-electrical parameters of the model and accurately showed the depth and size of the abnormal body.

Three-dimensional Magnetotelluric Forward Modeling for Static-shifted Model

Xiao-Zhong Tong, **Jian-Xin Liu**, **Ya Sun**, **and Zhen-Wei Guo**
School of Info-physics Geomatics Engineering, Central South University
Changsha 410083, China

Abstract— Magnetotelluric (MT) static shift is a non-inductive change of the MT apparent resistivity response that severely impairs the interpretation of data. In two-dimensional (2-D) models, static shift is manifested in the data as vertical, parallel shifts of log-log apparent resistivity sounding curves, the impedance phase being unaffected. In order to get the static shift features of three-dimensional model, we use the finite element method for three-dimensional MT forward modeling. The finite element algorithm is very efficient, ant it has a lot of advantages: the high precision, the canonical process of solving problem, meeting the internal boundary condition automatically and adapting to all kinds of distribution of multi-substances. Through the simulation of the three-dimensional MT static-shifted model, the results show that the apparent resistivity at every site is affected and the impedance phase is normal.

A Practical Scheme for 3D Geoelectrical Forward Modeling with Finite-infinite Element Coupling Method

Jing-Tian Tang and Jin-Zhe Gong
School of Info-physics and Geomatics Engineering, Central South University, Changsha 410083, China

Abstract— In this study, fast and visualized pre and post processing for finite element method was achieved by customized development based on the universal 3D modeling software named GiD, while infinite elements were introduced to form the finite-infinite element coupling method, which could substitute the conventional mixed boundary conditions and solve the problems cased by artificial boundary conditions. For the customized development on GiD, we only need to program the so-called problem types with simple script language, then models could be build in the graphic interface and output in the format fitting our calculation program. As to our finite-infinite element method, Astley mapped wave envelope infinite elements were employed to continue the electrical potential to infinity. Then, a new type of shape functions was created and it was proved to be the optimal one in both accuracy and time consumption by comparing with several other shape functions. Finally, the availability and superiority of this coupling algorithm were confirmed by several numerical tests with various electrode arrays.

MPI-based Parallel FDTD for EM Scattering from Coated Complex Targets

Xiao-Fei Qi, **Li-Xin Guo**, **and Hao Tsang**
School of Science, Xidian University, Xi'an 710071, China

Abstract— The study of EM scattering by targets has been playing an important role in areas such as radar detection, target identification and so on. Many high-frequency algorithm and numerical algorithm have been proposed to solve this problem. Among these methods the FDTD algorithm attracts more and more attention since its first proposed by Yee in 1966. FDTD has the unique advantages in dealing with the rough surface scattering: it could be either dielectric or conductor. In addition, the results calculated by this method are in the time domain, and can indicate both the transient behavior and the steady state. However, it needs more storage capacity and more computing time to solve the problems of scattering from complex targets with electrically large size, which restricts the realization of FDTD resulting from PC's capacity and computing power. Until recently, the computing power of a stand-alone PC still cannot meet the agreement with the electrically large size problems, although it has been rising that the local PC performance in the rapid development of computing speed and storage capacity. The parallel FDTD method is an effective way to solve such problems. The FDTD algorithm has the natural ability for parallel computing, because of its special feature of involving only the neighbor interactions when the electric (magnetic) filed components are updated at each time step.

This paper studies the EM scattering from coated complex targets with MPI-based parallel FDTD. It begins with the MPI-based parallel COW system, and further information on the parallel FDTD algorithm has been also introduced, such as domain decomposition, data exchange and the synchronization technology. The modeling of the coated complex targets is described in the following, and the uniaxial anisotropic perfectly matched layer (UPML) absorbing boundary, the connecting boundary (total field/scattering field, TF/SF) as well as the Near-to-Far field transformation method have been mentioned. Some numerical examples have been given to show its priority to solve the scattering from coated complex target with electrically large size.

Galerkin's Method Using the Annular Patch Segments to Solve a Round Disk Capacitor

Kyung-Soo Kim and Che-Young Kim
School of Electrical Engineering and Computer Science, Kyungpook National University
Sankyuk-dong Puk-gu, Daegu 702-701, South Korea

Abstract— In this paper, a numerical method is presented to calculate the charge density distribution and capacitance of a round disk capacitor by using the annular patch segments to gain more benefits over the conventional triangular patches. The proposed annular patches successfully eliminate the discretizing errors often encountered in the triangular patches, thereby it leads us to get more accurate solutions. Furthermore, the Galerkin's method is utilized to accelerate the solution convergence and also to obtain more accuracy at the matrix formulation stage. By specializing the method of moments to an integral equation, the charge distribution and capacitance can be obtained. To examine the accuracy of the proposed method, numerically computed charge density and capacitance are compared to the corresponding exact solutions for a single circular disk. Based on these error comparisons, the Galerkin's method equipped with annular patches ensures the superiority to the triangular patches and to the point matching method. The proposed Galerkin's method is applied to the round disk capacitor to calculate both the charge density distribution and the capacitance. Finally, equipotential lines are drawn around the round disk and some discussions are given to the fringing fields associated with these equipotential lines.

Determination of Eigenvalues of Closed Lossless Waveguides Using the Least Squares Optimization Technique

O. Demiryurek[1] and N. Yener[2]

[1]Gungoren Endustri Meslek Lisesi, Tozkoparan Mah., Esitler Sok. No. 3, Gungoren, Istanbul, Turkey
[2]Technical Education Faculty, Kocaeli University, Umuttepe Campus, Izmit 41380, Kocaeli, Turkey

Abstract— It is known that in lossless and closed guides filled with gyroelectric or gyromagnetic media, Maxwell's equations are transformed into an infinite linear algebraic equation system by application of the Galerkin version of Moment method. Propagation constant of the problem whose exact solution is not known is found as the square root of the eigenvalue of the coefficient matrix of this infinite linear algebraic equation system. However, the quantities determined from the Moment method do not have much physical meaning by themselves. This is why it is desired to express the propagation constant as a function of frequency. Therefore with the help of algebraic function theory we attempt to express eigenvalues of the coefficient matrix, i.e., the squares of the propagation constants, as a series expansion. By this technique Laurent and Puiseux series expansions in the neighborhood of singular points are obtained for these functions. The series expansions which are obtained by the algebraic function approximation in the eigenvalue problems of closed, lossless, uniform waveguides, bring about a function theoretic insight in order to investigate the properties of the propagation constant functions. In previous work reported in the literature there exists a derivation of these expansions accomplished by using differentiation of the characteristic equation of above coefficient matrix, considering it as an implicit function of the propagation constant function and the frequency. In this work computation of the necessary expansion coefficients of the Laurent and Puiseux series, is achieved by the least squares technique (LST) which is a curve fitting method. In this way we attempt to find a simple solution to the problem of computation of these coefficients, which dates back to Sir Isaac Newton and in general which is rather tedious.

The Study of Numerical Simulation on Dual-frequency IP Method with FEM

Jiayong Lin[1, 2], **Maobin Ding**[1], **Jing-Tian Tang**[1], **and Hong Yan**[1, 3]

[1]School of Info-physics and Geomatics Engineering, Central South University
Changsha 410083, China
[2]Geophysical and Geochemical Exploration Team
Yunnan Geology and Mineral Resources Bureau, Yunnan 652100, China
[3]The Third Institute of Geology and Mineral Exploration of Qinghai Province
Qinghai 810008, China

Abstract— Based on the finite element method and Cole-Cole model, the paper studied the numerical simulation on dual-frequency IP method. First of all, the paper introduced the primary theory of the dual-frequency IP method and gave the boundary value problem and variational equations, then replaced the complex resistivity of the model with the Cole-Cole model's parameters under ignoring the EM effect. Through solving the last linear equations, electric potentials of all the model's points were obtained. With changing model's parameters, we got different curves of the and phases. Finally, according to the results of the simulations, the algorithm was proved to be correct and adaptable.

An Improved Algorithm of Orthogonal Vector Spectral Estimation Method

Dengshan Huang, **Xingzhao Liu**, **and Jie Ren**
School of Electronics and Information, Northwestern Polytechnical University
Xi'an, Shaanxi 710072, China

Abstract— Orthogonal Vector Spectral Estimation method — OVSS method, with high statistical stability, high resolution, is much better than other existing spectral estimation methods (such as the MUSIC method). But while the method is used for dealing with superposition of multiple sinusoidal signals, the pseudo-peaks will often appear. In this paper, the principle of the OVSS is investigated in detailed. A new matrix is formed by using the elements of the primary eigenvectors and the right singular vector corresponding to the zero singular value of the matrix is orthogonal with signal space.Actually, the signal information can be extracted by extending the processing of autocorrelation matrix. However, when there are several signals, pseudo-peaks will appear inevitably because of spurious zeros. From this view, a new method for eliminating the pseudo-peaks should be finded.Based on the matrix above, a modified matrix is formed through reusing the specific elements on specific positions, and then following the steps of OVSS method, a modified OVSS method can be gained. A large number of simulation experiments show that, the pseudo-peaks can be eliminated by using the modified OVSS method, with a little loss of resolution in low SNR cases, and without significant loss of statistical stability in high SNR cases.

Parallel GPU Implementation of K-way Tree Classification Based on Semi-Greedy Structure Applied to Multisource Remote Sensing Images

Yang-Lang Chang
Department of Electrical Engineering, National Taipei University of Technology, Taiwan

Abstract— Most of the optimization problems associated with more complicated structures are not easy to be solved by many efficient optimization algorithms resolved in polynomial time. In Ref. [1], the *matroid* defines a *subset system*. All the instances of optimization problem in the *subset system* can be solved by *greedy* algorithm. Many efficient optimization algorithms (e.g., sorting, weighted matching, and minimum spanning tree methods) associated with these *matroid subset systems* have been successfully applied to different research communities for years. In our previous works a *semi-greedy* structure, also known as an extension of *matroid* method, was proposed by applying the concept of *matroid subset systems* to *minimum classification error* (MCE) [2]. By using this *semi-greedy* structure, the optimal stack filter and *generalized positive Boolean function* (GPBF) classifiers [3] can be applied to remove noises and discriminate the classes respectively. The optimal *positive Boolean function* (PBF) can be found by *stacking truth graph* (STG) criterion. There is an isomorphism between PBF and STG. An optimal PBF can therefore be determined by joining each node of Boolean function according to MCE of STG criterion. The *greedy* method considers only one node while the proposed *semi-matroid* method examines more than one node (with various combinations of neighbor nodes) iteratively to find the optimal PBF.

In order to break through the limited classification performances caused by classifying a large number of classes, and the problem of unbalanced numbers of positive and negative samples when MCE is applied to GPBF, a novel *parallel semi-matroid k-way tree* (PSMK) classifier is proposed in this paper. It modifies the *cost (objective) function* of MCE criterion to adapt *positive* and *negative* samples as the training parameters, and the search algorithm of STG criterion to accommodate the label and unlabeled samples as the *region based semi-greedy* structure, instead the *pattern-node based semi-greedy* structure implemented in GPBF. Furthermore, because some regions of the feature subspaces include different classes, they need to be divided into smaller regions if the discriminatory qualities of the features of the specific class are strong enough, so as to decide the samples of these regions as the specific class.

The proposed PSMK is organized by a *parallel k-way tree* in which every node (*semi-independence part in semi-greedy* structure) is composed of a set of *k-dimensional positive* and *negative* labeled samples as represented as a percentage, i.e., the corresponding ratio between a specific class and other classes. PSMK iteratively divides the *d-dimensional* hyperplane into 2^d subspaces according to the centroids of labeled (training) samples of all classes. The statistical ratios among different classes are then compared as a basis for stopping the new subspace separation and identifying which subspace belongs to which class. By delivering both *positive* and *negative* samples of different classes to PSMK learning modules, PSMK outperforms GPBF and traditional classifiers in terms of classification accuracy. Different PSMK are operated for different classes to speed up the training and classification performances. The computational speed of PSMK is improved by parallel techniques which include GPU (graphics processing unit) based *compute unified device architecture* (CUDA), *message passing interface* (MPI), and *open multi-processing* (OpenMP) applications. The effectiveness of the proposed PSMK is evaluated by fusing *MODIS/ASTER airborne simulator* (MASTER) images and *airborne synthetic aperture radar* (AIRSAR) images for land cover classification during the Pacrim II campaign.

REFERENCES

1. Steiglitz, K., *Combinatorial Optimization: Algorithms and Complexity*, Prentice-Hall, 1982.
2. Juang, B. H., W. Chou, and C. H. Lee, "Minimum classification error rate methods for speech recognition," *IEEE Trans. Speech Audio Process.*, Vol. 5, No. 3, 257–265, 1997.
3. Chang, Y.-L., L.-S. Liang, C.-C. Han, J.-P. Fang, W.-Y. Liang, and K. S. Chen, "Multisource data fusion for landslide classification using generalized positive boolean functions," *IEEE Trans. Geosci. Remote Sensing*, Vol. 45, No. 6, Part 1, 1697–1708, 2007.

Rigorous Computation of Large Radiation Problems by Means of an Iterative Approach

Carlos Delgado, **Felipe Cátedra**, **Iván González**, **Josefa Gómez**, **and Abdelhamid Tayebi**
Computer Science Department, Universidad de Alcalá, Spain

Abstract—

Introduction: It is well known that, despite the fact that the Moment Method (MM) is usually taken as a reference for the analysis of scattering or radiation problems, its practical implementation suffers from a heavy burden posed by the size and the density of the impedance matrix. Different approaches have been developed in the past years in order to reduce the computational requirements of the conventional MM, among which we can mention the Fast Multipole Method or its multilevel implementation, which allows a fast matrix vector product calculation in the iterative solution process, as well as a noticeable reduction in the memory requirements due to the fact that only the near field coupling terms are to be stored. However, it is important to remark that some realistic problems can still suffer from convergence issues or slow iteration time because of the size of the problem under analysis or the geometrical features of the problem. Moreover, in many realistic problems most of the parts of the geometry are weakly coupled, which allows to make use of high-frequency approaches instead of using rigorous solvers. The aim of the approach we present in this work is to obtain similar results to those given by the MM, highly reducing the computational effort by taking advantage of the MM-MLFMA method combined with an iterative technique used to compute interactions between different parts of the geometry in a totally adaptive fashion.

Analysis Procedure: The volume that contains the mesh to be analyzed is divided in a preprocessing step into a set of cubic volumes called *windows*. It can be done following an automatic process, or a user-defined window partitioning scheme. Next, we follow the steps highlighted below:

Full-wave analysis of each window. All the unknowns contained inside a given window are considered fully coupled, and the induced currents due to the external sources are computed for each window, considering that it is isolated from the rest of the geometry. By following this procedure we solve several smaller problems instead of a very large one. In order to avoid artificial edge behavior of the calculated induced currents at the limits of the windows, it is convenient to define an extended version of each window, calculate the induced currents for the extended version and only retain those unknowns that are confined inside the original window. The currents calculated in this step will be called *primary currents*. After this step, the iterative process of the approach is performed to take into account the interactions between different windows.

Iterative search for contributions and update of the existing currents. After computing the primary currents, these are updated by considering different interactions between different parts of the geometry. However a "brute force" approach where every single window interacts with the rest is not desirable. Given a primary current on a window, we can estimate where the radiated field will be stronger by aggregating the primary current to one or several points and determining the radiation pattern from the resulting multipole expansion. It is straightforward to detect the main peaks in this radiation pattern and determine that the windows which will interact with the given one are those will intersect the rays shot in those directions indicated by the radiation pattern of the active primary currents. This procedure can obviously be performed repeatedly to compute an arbitrary number of interactions between different windows. The stop condition of this procedure can be given by a maximum number of interactions, as well as the computed error for each step, which can be very easily calculated, since we know the tangential fields on the geometry due to external sources and also the updated values of the induced currents for each iteration.

Application Cases and Examples: The method outlined above can be applied to the analysis of scattering or radiation problems involving realistic structures like large antennas, arrays, RCS, on-board antennas etc. Also, multiscale problems can take advantage of this methodology, since only the resulting fields radiated by an active window are required to feed the passive window. We have observed good convergence properties in a wide variety of problems analyzed, and the approach can be parallelized very easily because little communication between processing nodes is required. Different nodes can be solving independent problems and exchange the resulting far fields if an interaction between two different windows is required to be computed.

Advantages of DOF's Continuous Matching in EIT Inverse Problem

J. Dědková, R. Kubásek, and K. Ostanina
FEEC BUT, UTEE, Kolejní 2906/4, Brno 612 00, Czech Republic

Abstract— This paper proposes new possibilities to solve the electrical impedance tomography (EIT) inverse problem. Usually, a set of voltage measurements is acquired from the boundaries of an investigated volume, whilst this is subjected to a sequence of low-frequency current patterns. To find the unknown conductivity distribution inside investigated object we can use the deterministic approach based on the Least Squares method. Due to the ill-posed nature of this nonlinear problem, regularization has to be used. For example the standard Tikhonov Regularization method (TRM) with a Newton-Raphson method can be applied to solve the inverse EIT problem. This procedure is commonly used in the EIT inverse problem for its fast convergence and good reconstruction quality. However, it is likely to be trapped in local minima and so additional regularization must be taken into account to obtain the demanded solution. The stability of the TRM algorithm is a bit sensitive to the setting of a starting value of conductivity; to number of unknown values (DOFs) and to an optimal choice of the regularization parameter provides balance between the accuracy and the stability of the solution.

In recent years is very often used the Level Set method (LSM) to identify regions with different image or material properties. The distribution of unknown conductivity σ can be described in terms of level set function F depending on the position of the point r with respect to the boundary Γ between regions with different values of σ

$$\sigma(r) = \begin{cases} \sigma_{\text{int}}\{r : F(r) < 0\} \\ \sigma_{\text{ext}}\{r : F(r) > 0\} \end{cases} \qquad \Gamma = \{r : F(r) = 0\}.$$

To improve the stability and the accuracy of EIT image reconstructions new algorithm was created. This algorithm uses both of mentioned methods TRM and LSM. During iteration process based on minimizing objective function $\Psi(\sigma)$ the boundary Γ is searched in accordance with request that the $\sigma(r)$ minimizes the $\Psi(\sigma)$, too. New algorithm was applied to the several image reconstructions, with different type of constrains. Further are presented results of conductivity reconstruction for those examples.

REFERENCES

1. Cheney, M., D. Isaacson, and J. C. Newell, "Electrical impedance tomography," *SIAM Rev.*, Vol. 41, No. 1, 85–101, 1999.
2. Burger, M., "A level set method for inverse problems," *Inverse Problems*, Vol. 17, 1327–1356, 2001.
3. Sethiah, J., *A Level Set Methods and Fast Marching Methods*, Cambridge University Press, Cambridge, 1999.
4. Chan, T. and L. Vese, "Active contour without edges," *IEEE Trans. Imag. Proc.*, Vol. 10, 266–277, 2001.
5. Osher, S. and R. Fedkiw, *Level Set Methods and Dynamic Implicit Surfaces*, Springer-Verlag, New York, 2002.

A Calculation Method for Frequency Dependent Characteristic Impedance and Slow-wave Factor of Microwave Transmission Lines with a Perturbation

Jongsik Lim[1], **Jun Lee**[1], **Jaehoon Lee**[1], **Yongchae Jeong**[2], **Sang-Min Han**[1], **and Dal Ahn**[1]

[1]Soonchunhyang University, Republic of Korea
[2]Chonbuk National University, Republic of Korea

Abstract— A frequency-dependent slow-wave factor (SWF) and equivalent circuit model of transmission lines with a perturbation such as photonic band-gaps (PBGs), defected ground structures (DGSs), and so on, is proposed in this work. DGS is adopted as an example of the perturbation structure imposed on the ground plane of transmission lines (Fig. 1). Once S-parameters of the transmission line with DGS are given, the conventional equivalent circuit elements are extracted using 3 dB cutoff and resonant frequencies ($F_{c.3\,\mathrm{dB}}$ and F_o) as the first step. Using these initial equivalent circuit elements and simple transmission line theories, a frequency-dependent equivalent transmission line model is established through an analytical method. In the proposed method, the equivalent characteristic impedance (Z) of the transmission line with a perturbation depends on frequency (Fig. 2), while it has been known to be a fixed value. Finally the frequency-dependent SWF is calculated (Fig. 3). The proposed equivalent circuit of the transmission line with a perturbation element is composed of frequency dependent series resistance (R_s) and characteristic impedance (Z). The obtained equivalent circuit and SWF are frequency-dependent and more reliable than the conventional result because even small insertion loss within the available pass band is considered in calculating characteristic impedance (Z) and SWF, while they have been ignored in the conventional way. The S-parameters calculated using the obtained frequency-dependent equivalent circuit elements and frequency-dependent characteristic impedance (Z) are in an excellent agreement with the original S-parameters of the transmission line with the perturbation. The proposed method is well applicable to find the more reliable equivalent characteristic impedance and SWF of all transmission lines having PBGs, DGSs, and other periodical perturbation patterns on the ground plane.

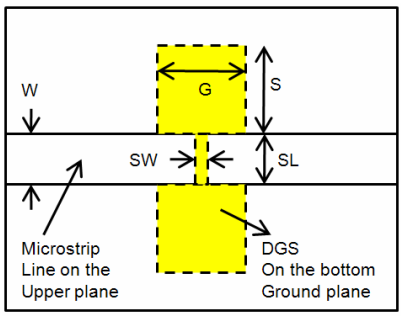

Figure 1.

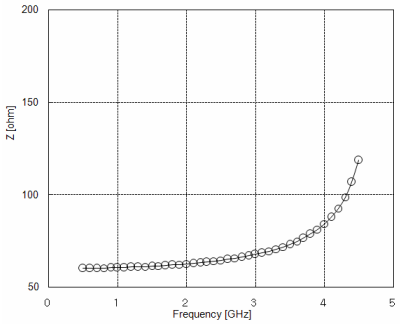

Figure 2.

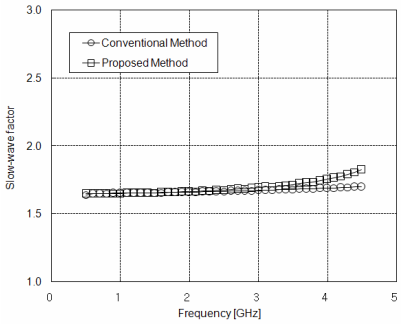

Figure 3.

The Measurements of RF Dielectric Constant, Dielectric Loss Coefficient, and Conductor Loss Coefficient in PCB

Yun-Hsih Chou[1], **Ming-Jer Jeng**[2], **Yang-Han Lee**[3], **and Yih-Guang Jan**[3]

[1]Department of Electronic Engineering, St. John's University
499, Sec. 4, Tam King Road, Tamsui, Taipei 251, Taiwan, R.O.C.
[2]Department of Electronic Engineering, Chang Gung University
259 Wen-Hwa 1st Road, Kweishan, Taoyuan 333, Taiwan, R.O.C.
[3]Department of Electrical Engineering, Tamkang University
151 Ying-chuan Road, Tamsui, Taipei 25137, Taiwan, R.O.C.

Abstract— In this paper, we fabricate a 10 cm transmission line with characteristic impedance 50 ohm of a PCB with a 0.72 mm thick substrate and a 0.04 mm thick copper foil and use the HP8735D vector network analyzer to measure the S-parameter of this fabricated transmission line and in cooperating with the ADS software of Agilent's EDA product it can measure and analyze all characteristic coefficients of loss transmission lines. Its process and measurements are by inputting the S-parameter obtained from HP8735D vector network analyzer into the ADS and then utilizing the optimized functionalities provided by ADS. From the generated optimized results, the transmission line has characteristic impedance $Z = 48.3$ ohms, effective dielectric constant $K = 3.19$, attenuation coefficient $A = 0.996696$ dB/m, dielectric loss tangent $\tan D = 0.0195152$. Then from using the transmission line formula we can calculate the transmission line's conductor loss, dielectric loss and effective dielectric constant for frequency in the range of 100 MHz to 3 GHz. From the measured data of impedance loss and dielectric loss, it shows that when the PCB's operating frequency is higher than 100 MHz the main attenuation coefficient is generating from the dielectric attenuation coefficient. We also utilized the ADS's Momentum program and through try-and-error method to measure the conductivity of the fabricated PCB. Finally, we used microstrip transmission line to fabricate a 600 MHZ quarter wavelength open stub resonator and inserted the relevant parameter values obtained in this paper into the resonator to simulate its resulting conductivity value through ADS's Momentum program and it is found that both the measured and the simulated data have comparable results.

Highly Miniaturized On-chip Impedance Transformer Employing Coplanar Waveguide with Periodic Ground Structure on GaAs MMIC

Young-Bae Park, Bo-Ra Jung, Suk-Youb Kang, Jang-Hyeon Jeong, Jeong-Gab Ju, and Young Yun
Department of Radio Communication Engineering, Korea Maritime University, Republic of Korea

Abstract— In this work, a highly miniaturized on-chip impedance transformer employing periodic ground structure (PGS) was developed for application to broadband on GaAs MMIC. Its fabricated size was 0.64% compared with conventional impedance transformer on GaAs MMIC. The proposed impedance transformer showed a good performance from 0.5 to 50 GHz.

Figure 1 shows a structure of coplanar waveguide employing PGS on GaAs substrate. As shown in this figure, PGS exists at the interface between SiN film and GaAs substrate, and it was electrically connected to top-side ground planes (GND planes) through the contacts. Figure 2 shows a photograph of the impedance transformer employing coplanar waveguide with PGS fabricated on GaAs substrate. The line width and length of the $\lambda/4$ transformer with a center frequency of 9.25 GHz are 20 and 500 µm, respectively. If the $\lambda/4$ transformer is fabricated by conventional microstrip line on GaAs substrate, the line width and length are 560 and 2780 µm, respectively. Therefore, the size of impedance transformer employing coplanar waveguide with PGS is 0.64% of the one fabricated by conventional microstrip lines. Figure 3 shows the measured return loss S_{11} and insertion loss S_{21} of impedance transformer employing coplanar waveguide with PGS. As shown in Figure 3, we can also observe a good return and insertion loss in the vicinity of 26 GHz as well as 9.25 GHz. Actually, the second center frequency is accurately 27.75 GHz, however, the second center frequency as shown in Figure 3 is 26 GHz, because the wavelength of PGS is not linearly proportional to a frequency due to its parasitic elements. If impedance transformer with a center frequency of 26 GHz is fabricated by conventional microstrip line on GaAs substrate with a thickness of 100 µm, the line width and length are 560 and 962 µm,

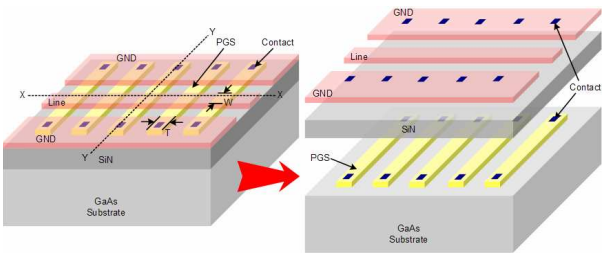

Figure 1: The structure of coplanar waveguide employing PGS.

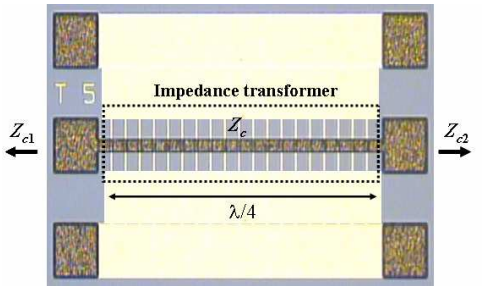

Figure 2: The photograph of impedance transformer employing coplanar waveguide with PGS on GaAs MMIC.

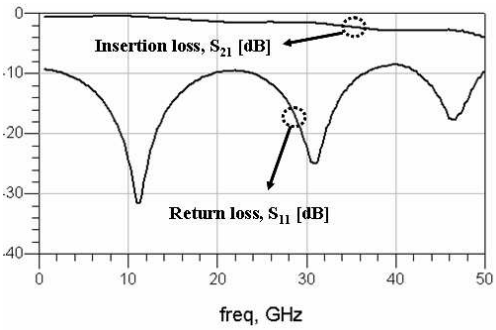

Figure 3: Measured return loss S_{11} and insertion loss S_{21} of impedance transformer employing coplanar waveguide with PGS.

respectively. Therefore, compared with the conventional impedance transformer operating at 26 GHz, the size of impedance transformer employing PGS is only 1.86% of conventional one. Table 1 describes the measured RF performance, bandwidth and size of impedance transformer employing the coplanar waveguide with PGS.

Table 1: Measured RF performance, bandwidth and size of impedance transformer employing coplanar waveguide with PGS.

T [μm]	Transformation impedance (Z_{c1}/Z_{c2})	S_{11} / S_{21} at first center frequency	First and second center freq. and bandwidth	Size comparison at first and second center freq.
5	24 Ω / 12 Ω	-31.6 dB / -0.52 dB at 11 GHz	11 ± 8.5 GHz, 32 ± 9.1 GHz	1% and 2.91% of conventional transformer
10	20 Ω / 10 Ω	-33.5 dB / -0.64 dB at 9 GHz	9.25 ± 7.2 GHz, 26 ± 5.3 GHz	0.64% and 1.86% of conventional transformer
20	16 Ω / 9 Ω	-44.1 dB / -0.78 dB at 8 GHz	8 ± 7.2 GHz, 23 ± 4.3 GHz	0.47% and 1.35% of conventional transformer

Analysis of Characteristics of Coplanar Waveguide with Finite Ground-planes by the Method of Lines

Min Wang, **Bo Gao**, **Yu Tian**, **and Ling Tong**
College of Automation Engineering, University of Electronic Science and Technology of China
Chengdu 610054, China

Abstract— The method of lines (MoL) has been used to analyze the characteristics of various structures of coplanar waveguide widely. And the MoL provides accurate results with the high computational efficiency in a large range of frequency. However, a large number of literatures do not study the effects of the ground-planes width on the propagation characteristics, especially characteristic impedance.

In this paper, the method of lines with nonequadistance discretization to analyze the characteristics of coplanar waveguide with finite ground-planes is presented. In the part of analysis procedure, as an example of the symmetrical shielded coplanar waveguide configuration, the process of calculation of the propagation constant is described in detail. It is worth mentioning that the process to calculate the characteristic impedance of the symmetrical coplanar waveguide by MoL is introduced to which most of literatures do not refer.

In the next Section, numerical results are presented to verify the validity of this method and analyze the effects of the ground-planes on the propagation characteristics. Specifically, to verify the validity of this method, the comparison results of the effective dielectric constant obtained by MoL, HFSS and the literature and the comparison results of characteristic impedance computed by MoL and simulated by HFSS are separately shown. In this part, it also shows the results of the effective dielectric constant and characteristic impedance with some different finite ground-planes widths and its frequency is up to 120 GHz. To discuss the effects of finite ground-planes width, both the effective dielectric constant and characteristic impedance versus the finite ground-planes width are shown.

A Study on Equivalent Circuit of Highly Isolated Coupled Microstrip Line Employing PGS on GaAs MMIC

Jang-Hyeon Jung, **Bo-Ra Jung**, **Young-Bae Park**, **Jeong-Gab Ju**, **Suk-Youb Kang**, **and Young Yun**
Department of Radio Sciences and Engineering, Korea Maritime University, Korea

Abstract— In this work, we propose highly isolated coupled microstrip line employing PGS (Periodic Ground Structure), and its equivalent circuit was thoroughly studied for application to circuit design.

Figure 1 shows a coupled microstrip line employing PGS. The PGS was inserted at the interface between SiN film and GaAs substrate, and the PGS serves as ground plane because it was electrically connected to backside ground metal through the via-holes. Fig. 2 shows the equivalent circuit of adjacent two lines, which corresponds to the equivalent circuit of the Nth unit section of the periodic structure surrounded by rectangular box in Fig. 1. C_b corresponds to the capacitance between top line and PGS, which is shown in Fig. 1, and it is proportional to the cross area W·T of line and PGS. The coupled microstrip line showed much better isolation characteristic than conventional one, because parasitic inductance and capacitance comprise RC resonance structure as shown in Fig. 2. Table 1 shows measured isolation characteristic of coupled microstrip line and conventional one.

Table 1: Measured isolation for the coupled microstrip line employing PGS and conventional one at 60 GHz.

Microstrip line employing PGS	−45 dB
Conventional microstrip line	−8 dB

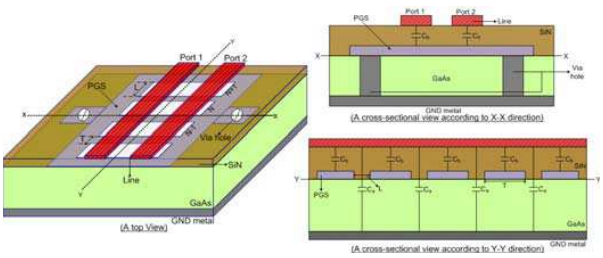

Figure 1: Coupled microstrip line structure employing PGS.

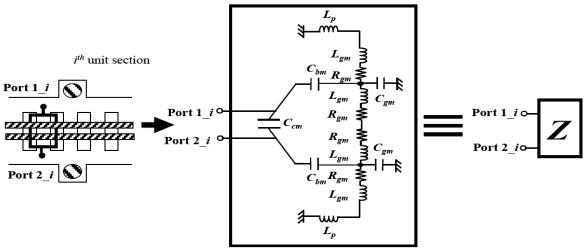

Figure 2: An equivalent circuit for a unit cell of the micriostrip line employing PGS.

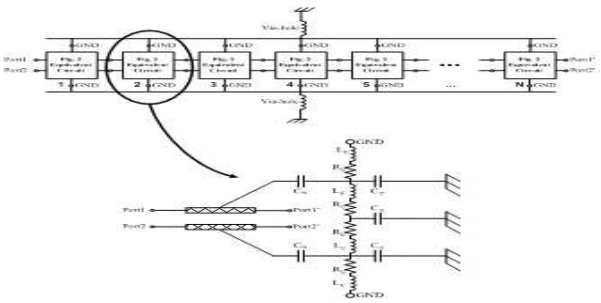

Figure 3: The equivalent circuit for microstrip line structure employing PGS.

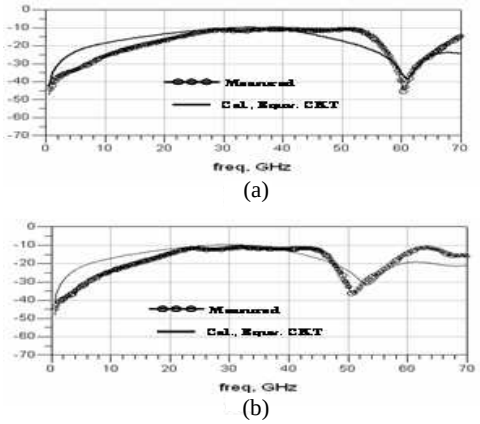

Figure 4: Measured and calculated insertion loss S_{21} for microstrip line employing PGS.

Equivalent circuit for single cell of the microstrip line employing PGS is shown in Fig. 2. The lumped parameters were expressed by following equations,

$$C_b = \left[0.019 + \left(\frac{T}{d_i}\right) \times 7 \times 10^{-5} - \left(\frac{T}{d_i}\right) \times 2 \times 10^{-7}\right] (\text{pF}) \quad C_g = \frac{T}{d_s} \times 10^{-3} (\text{pF})$$
$$L_g = \frac{l_s}{T} \times 1.875 \times 10^{-3} (\text{nH}) \quad R_g = \frac{l_s}{T} \times 3.125 \times 10^{-2} (\Omega)$$

where, d_i is thickness of SiN (See Fig. 1). The whole equivalent circuit is shown in Fig. 3. As shown in this figure, a number of the equivalent circuits of unit section are connected to each other, and via-hole was expressed as lumped inductor. Fig. 4 shows measured and calculated insertion loss S_{21} for microstrip line employing PGS. For the calculation result, equivalent circuit of Fig. 3 and above closed form equations were used. As shown in this figure, we can observe a fairly good agreement between calculated and measured results.

Design of Suppressing Crosstalk by Vias of Serpentine Guard Trace

W.-T. Huang[1], **C.-H. Lu**[2], **and D.-B. Lin**[2]

[1]Department of Computer Science and Information Engineering
Minghsin University of Science and Technology, Taiwan, R.O.C.
[2]Graduate Institute of Computer and Communication Engineering
National Taipei University of Technology, Taiwan, R.O.C.

Abstract— The structure design of the serpentine guard trace [2] is to add two terminally matching resistances, called the "serpentine guard trace [SGT]" approach, for getting the advantages of the use area and suppress far-end crosstalk. This method neglects the interference of near-end crosstalk. Therefore, in this study, we propose an approach, namely, "vias of serpentine guard trace [VSGT]", which the grounded-vias are added on the guard trace by a proper location and the scale between horizontal and vertical length of the guard trace can be adjusted in a better state such that the near-end crosstalk [NEXT] and far-end crosstalk [FEXT] coefficient will be minimum and get the optimal performance. Hence, our proposed design can simultaneously suppress NEXT and FEXT and extent the first resonance to the non-working frequency area. Verified in the frequency-domain simulation results as shown in Fig. 1(a), our proposed approach, VSGT, can improve not only NEXT by 3.7 and 0.83 dB but also FEXT by 5.11 and 0.1 dB compared to the three-width rule [1] and the SGT design [2], respectively. Moreover, verified in the time-domain simulation results as shown in Fig. 1(b), our method can reduce not only NEXT by 34.67 and 27.5% but also FEXT by 46.78 and 6.91% than that of the three-width rule [1] and the SGT design [2], respectively. Note that $\mathrm{NEXT}_{\mathrm{method}}$ ($\mathrm{FEXT}_{\mathrm{method}}$) is to denote NEXT (FEXT) of the design approach and the suffix "method" is one of the VSGT, 3-W ruler, and SGT methods.

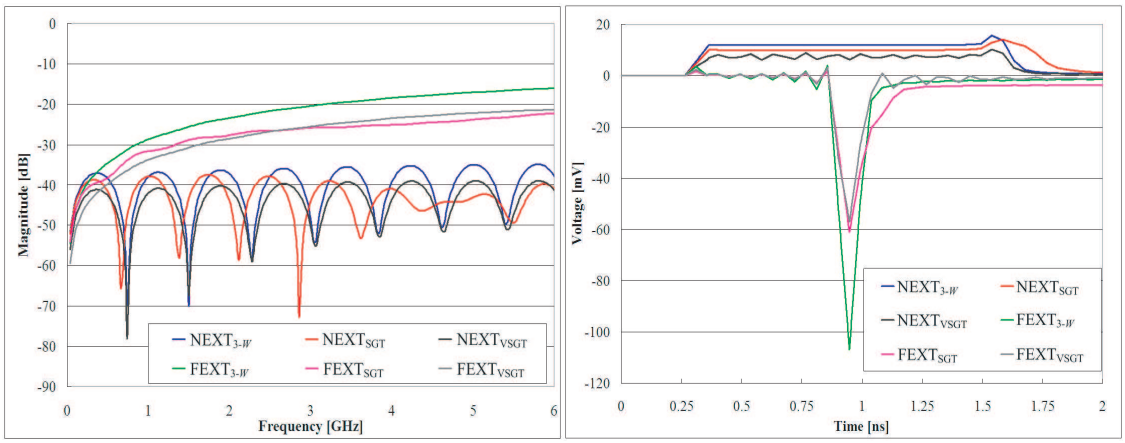

(a) (b)

Figure 1: Comparison of simulation results among NEXT and FEXT of VSGT, 3-W ruler [1] and SGT. (a) Example of over frequency-domain. (b) Example of over time-domain.

REFERENCES

1. Montrose, M. I., *EMC and the Printed Circuit Board: Design, Theory, and Layout Made Simple*, *IEEE Press*, 1998.
2. Lee, K., H. B. Lee, H. K. Jung, J. Y. Sim, and H. J. Park, "A serpentine guard trace to reduce the far-end crosstalk voltage and the crosstalk induced timing jitter of parallel microstrip," *IEEE Transactions on Advanced Packaging*, Vol. 31, 809–817, Nov. 2008.

Model and Performance Analysis of Coplanar Waveguide Based on Different Oxide Structure HR-Si Substrate

Xi Li, **Yanling Shi**, **and Yanfang Ding**
Department of E. E., East China Normal University, Shanghai 200241, China

Abstract— Coplanar waveguide (CPW) has gained wide interest in MMICs as interconnects and matching networks because the grounds in CPW structure are on the same surface as the signal line, which eliminates the need for via holes and substrate thinning, and simplifies the fabrication process. However, the performance of integrated circuits on conventional Si wafers is very poor at microwave frequency due to the high loss coming from the low resistivity of the substrate. The loss is primarily caused by penetration of the electric field of the device into the conductive Si, inducing parasitic substrats currents. Using high-resistivity Si substrate is one of the approaches to reduce transmission loss, which extends the application of HR-Si in RF circuits.

Usually, CPWs are fabricated on oxided Si because transmission lines and microwave devices are always on wiring layers. Different SiO_2 structures will make different influence on transmission characteristics which changes the substrate model of transmission lines. In this paper, through conventional CMOS processing, three kinds of 50 Ω CPWs on HR-Si, HR-Si with continuous SiO_2 layer and HR-Si with discontinuous SiO_2 layer where the SiO_2 between signal and ground line is etched are designed and fabricated. The measurement shows that CPW on HR-Si owes the least transmission loss while the one on HR-Si with continuous SiO_2 the most. The insert losses at 20 GHz are −0.88 dB, −2.50 dB and −1.06 dB respectively.

Different from traditional charge analysis in the oxide layer, theoretical study based on the two-port network analysis of the equivalent model of the coplanar waveguide based on different oxide structure HR-Si substrate has been discussed. Characteristic difference of CPWs on different SiO_2 structures has been validated with the theory derivation and the model discussion. It has been proved that the major factors influencing the transmission loss are resistivity of substrate, oxide capacitance and coupling capacitance. With this conclusion, the theoretical analysis is consistent with the measured results.

A Band-notched Ultrawideband Filter Design with Genetic Algorithms

Ming-Huei Chen, **Cheng-Yu Tasi**, **and Hao-Hui Chen**
Department of Electronic Engineering, National Kaohsiung First University of Science & Technology
Kaohsiung, Taiwan, R.O.C.

Abstract— Since Federal Communication Commission (FCC) released the 3.1–10.6 GHz band for commercial applications in 2002, ultrawideband (UWB) technology has received great attention in various high-data-rate mobile systems. Hence, the development of UWB components such as antennas, filters, and amplifiers has become an attractive research in modern communication. Although the UWB technology covers the frequency band ranging from 3.1 to 10.6 GHz, to prevent the possible interference with other wireless communication networks, especially the 5.2/5.8 GHz WLAN and 5.5 GHz WiMAX systems, the band-notched feature is usually a critical consideration in the design of an UWB component. In this work, an UWB filter with a notch band located at 5–6 GHz, which can reject the 5.2/5.8 GHz WLAN and 5.5 GHz WiMAX signals and suppress the coexistent interference in the UWB spectrum, is presented. Fig. 1 shows the prototype of the proposed filter design, where the filter is basically implemented using a co-planar waveguide (CPW) structure on a single substrate. In this filter design, a bandpass filter with the passband being 3.1–10.6 GHz is first designed by a CPW with four short-circuited stubs using the standard filter design formulas. Then the split-ring resonators (SRRs) deposited on the backside of the substrate or the complementary split-ring resonator (CSRRs) etched on the center strip of the CPW are employed in the filter to create the desired band-notched characteristics. The SRR and CSRR, which has been fully studied in [1], can excite resonant modes and thus the band-stop features at a desired frequency band with suitable designs. Also, they can be simply modeled by an equivalent parallel LC resonant tank. With the equivalent LC circuit, the proposed band-notched UWB filter design can be easily synthesized and analyzed. However, due to the mismatch between the SRR/CSRR and the CPW line, the SRR/CSRR structures can also deteriorate the filter performance. The genetic-algorithm (GA) optimization is therefore applied in this work to fine tune the CPW line and the SRR/CSRR of the obtained initial design. From which the overall performance of the band-notched UWB filter can be optimized to meet the required response. With the proposed design, an UWB filter with a notch band located at 5–6 GHz is designed and fabricated on a 0.8-mm thick FR4 substrate. The filter performances, the details of the design considerations, as well as the manipulation of GA optimization for the filter design will be presented and discussed in the symposium.

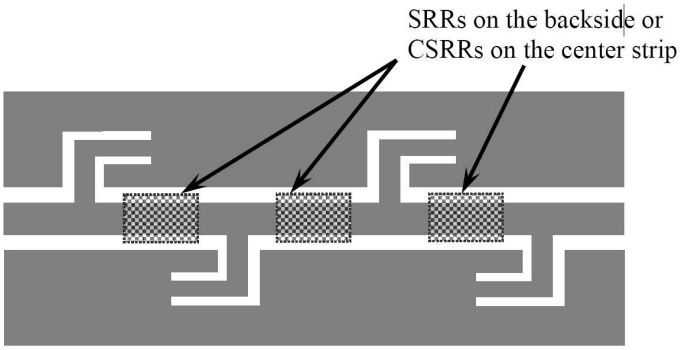

Figure 1: A band-notched UWB filter using SRRs/CSRRs.

REFERENCES

1. Baena, J. D., et al., "Equivalent-circuit model for split-ring resonators and complementary split-ring resonators coupled to planar transmission lines," *IEEE Trans. Microw. Theory Tech.*, Vol. 53, 1451–1461, Apr. 2005.

Novel Rectangular Coupled Line Bandpass Filter

Souren Shamsinejad[1], **Shila Shamsadini**[2], **and Mohamad Soleimani**[1]

[1]Electrical Engineering Department, Iran University of Science and Technology (IUST), Tehran, Iran
[2]Electrical Engineering Department, South Tehran Branch, Azad University, Tehran, Iran

Abstract— This paper reports a novel band pass filter without any periodic response. The novel filter has been named Rectangular Parallel Coupled Line filter (RPCL) and derived from reforming the conventional parallel coupled line filters. The novel BANDPASS filter HAS extra narrowband response. RPCL filter with center frequency of 475 MHz, 1 dB passband of 10 MHz and 20 dB stopband of 40 MHz has been reported here. The area which has been occupied by this RPCL filter is approximately about 52 cm^2. The RPCL can be TUNED for various applications at desired center frequency and passband. The occupied area by the filter reduced related to the center frequency of RPCL. High power transmission capability is another distinguished feature of the RPCL filter. Furthermore, at high frequencies applications the filter can be designed due to use in high power MMIC packages. The periodic frequency responses related to approximately all types of Microstrip passive filters has been suppressed in the novel RPCL filter. The novel RPCL filter can be designed for dual band applications such as 3G/GSM in a 3 cm^2 MMIC package.

Optimization of Broadband Withdrawal Weighted SAW Filters

Ying Liu, **Yali Qin**, **and Changming Xie**
Zhejiang Key Research Lab of Fiber-optic Communication Technology
Colleage of Information Engineering, Zhejiang University of Technology, HangZhou, China

Abstract— The surface acoustic wave (SAW) interdigital transducers (IDT) with uniform electrodes is one of the most commonly used structures in SAW devices. It is usually used together with an overlap weighted (apodized) transducer. Apodization is a very flexible and convenient technique for the realization of a specified IDT frequency response (FR). However sometimes extremely compact filter layouts need such a small aperture that any overlap weighting is undesirable because of diffraction effects.

Withdrawal weighting (WW, deleting some electrodes from regular structures) of IDT has been shown to be a very useful technique for device design. It is not as flexible as overlap weighting but it does have the advantages that it allows both transducers to be weighted using this technique and it minimizes problems due to diffraction.

The object of this paper will discuss the WW technique and designing of highly selective broadband SAW IDT with uniform electrodes. Unlike the familiar methods of WW transducer optimization, these algorithms choose the best IDT structure on the basis of how well it meets the specifications in frequency domain. The optimization algorithm considered here is intended for the design of broadband SAW filters. The key feature that distinguishes this algorithm from the widespread methods of WW transducer optimization is the analysis of various transducer structures on the basis of how well it meets the specifications. As any optimization process includes a great deal of computation, founding a simple, "quick" model is very important for the simulation of an IDT FR. The algorithm analyzes all possible combinations of removed electrodes within some limited "window" 10 to 15 electrode positions, as a rule. The "window" scans step by step through the IDT many times. The process continues until an improvement of the FR takes place.

The proposed method can be used to meet specifications not only for amplitude FR but also for phase characteristics as well. The effectiveness of the proposed technique was illustrated by a number of designed and fabricated SAW devices with bandwidths of 0.5 to 15%, shape factors of 1.07 to 1.8 and stopband rejection of better than 40 dB.

Design of Miniaturized Shorted End Coupled Line Section Using Parallel PI Capacitor Network

Young-Huang Chou[1], **Yung-Chin Hung**[1], **and Hao-Hui Chen**[2]

[1]Department of Electronic Engineering, Huafan University
Taipei, Taiwan, R.O.C.
[2]Department of Electronic Engineering
National Kaohsiung First University of Science and Technology
Kaohsiung, Taiwan, R.O.C.

Abstract— Coupled line sections are usually adapted in the design of modern filter circuits. Because of the requirement of miniaturization in RF component, development of the coupled line miniaturized structure in advance will be a very important work for overall filter design. Recently, ground capacitors parallel to the ports of the shorted end coupled line section were implemented to reduce the length of coupled line lower than $\lambda_g/4$ which used in the conventional design. These two capacitors could compensate the resonant length of coupled line effectively. However, this miniaturized method suffered the disadvantage of signal transition bandwidth reduction which would cause the insufficient bandwidth of the final filter design.

In this work, a miniaturized shorted end coupled line section using parallel PI capacitor network will be present to possess wider bandwidth operation (Fig. 1). The line length reduced by ground capacitors causes the characteristic of weaker coupling which could be intensified by the series capacitor connected in parallel PI network. The compensated coupling performance will keep or increase further the bandwidth of shorted end coupled line section and still possess the characteristic of miniaturization. By using the multilayer substrate design environment, such as LTCC, the integration between PI capacitor network and shorted end coupled line can be achieved easily to realize the miniaturization.

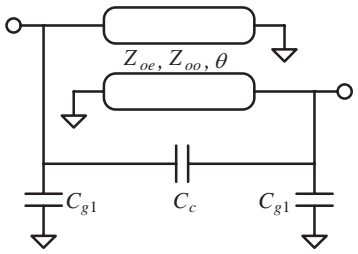

Figure 1: Shorted end coupled line section having parallel PI network between ports.

Analysis of the Magnetic Coupling Effect between Lump T-type Resonator Circuits

Young-Huang Chou, **Ming-Sian Lin**, **Wen-Jhao Sie**, **and Sin-Ning Chen**
Department of Electronic Engineering, HuaFan University
No. 1 Huafan Rd., Shihtin Hsiang, Taipei Hsien, Taiwan, R.O.C.

Abstract— In the development of miniaturized RF filter, the resonator composed of lump elements, that is L and C was usually adapted in the circuit design. The parallel and serial resonant frequency occurred in the designed resonator always decides the location of the pass band and the transmission zero respectively. Because of the requirement of physical size reduction in circuit design, limiting area constructed in the LTCC multilayer environment is a very popular technology to realize the resonator circuits. However, these integrated resonators suffer coupling effect each other in such small layout regions.

In this work, the magnetic coupling effect will be analyzed between two equivalent designed T-type resonator circuits (Fig. 1). Coupling mechanism coming from the inductors embedded in the resonators will cause the variation of the frequency response when integrated. By using simple circuit network analysis, the characteristic of zero frequency splitting will be discussed, and the changing of matching bandwidth will also be investigated within this work.

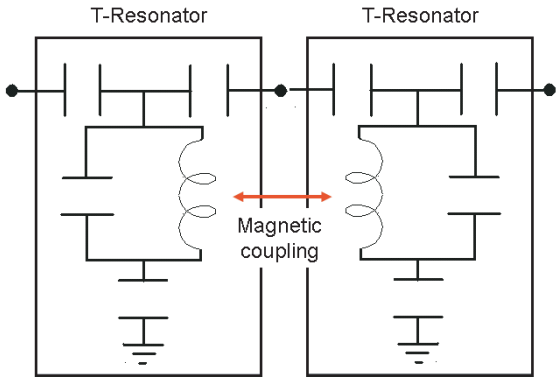

Figure 1: Circuit possesses two coupling T-type resonators.

Microstrip Cross-coupled Interdigital Hairpin Diplexer

Hsin-Han Tung, **Chen-Kang Hsu**, **and Cheng-Hsing Hsu**
Department of Electrical Engineering, National United University
1 Lien-Da, Kung-Ching Li, Miao-Li 36003, Taiwan

Abstract— A planar microwave diplexer with using cross-coupled compact hairpin filter is proposed. Miniaturization hairpin resonator is realized by using an interdigital structure having parallel coupled lines. The full-wave simulator IE3D is used to design the interdigital hairpin resonator, and to calculate the coupling coefficient of the basic coupling strictures. The response of the fabricated diplexer using FR4 substrate is designed at a GSM/DSC system. The performance of this class of diplexer has been demonstrated.

The Application of the Equal Area Law in Ferroresonance for Distribution Power System

Zheng-Wang Du[1], **Heng-Xu Ha**[2], **Lei Zhai**[3], **Hai-Quan Zhou**[2], **Song-Bo Gou**[1], **and Chong-Shan Zhong**[1]

[1]Shenli Oil Field Power Company, Dong Ying, China
[2]Dept. of Electric & Electronics Engineering, Shandong University of Technology, Zibo, China
[3]School of Electrical Engineering & Automation, Hebei University of Technology, Tianjin, China

Abstract— There are many capacitive and inductive components in the power system, such as transformers, generators, arc-suppression coil, reactor, circuit wire inductor, line wires and alternate with of capacitance, compensation electrical appliances, the stray capacitance of the high-voltage equipment, etc. When operating the system or failure occur, the capacitors and the inductors formed oscillation circuit components which may have resonance phenomenon. Resonance will lead to the system or component over-voltage and thus endanger the equipment or insulation, and to produce over-current caused equipment overheating and even burning.

Ferro-resonance over-voltage is a common internal over-voltage, which occur frequently in the neutral grounded distribution network and occasionally in the neutral ungrounded. Ferro-resonance leads to over-voltage and over-current which seriously affect the safe operation of the system. Therefore, the quantitative analysis of ferro-resonance, and to give the criteria, which has far-reaching significance for the safe operation of the system to avoid its occurrence.

In order to effectively suppress the complex phenomena of the system, this paper introduces the time-varying phasor, while, establishes the time-varying phasor mathematical model corresponded it. Based on this, the Equal Area Rule is applied to the ferro-resonance circuit analysis as a innovative way, that makes the analysis of ferro-resonance increased from qualitative analysis to quantitative analysis, while, defines the energy function which gives the calculation method of the system stability margin. This paper verify the actual of the time-varying Equal Area Rule applied in the ferro-resonance analysis through simulating the simple resonant circuit with ATP, that provide the theoretical basis to effectively prevent the ferro-resonance.

Design and Analysis of Ultrawideband Dielectric Resonator Antenna

Zibin Weng[1], **Tayeb A. Denidni**[2], **Yue Song**[1], **and Yongchang Jiao**[1]

[1]Xidian University, Xi'an, China
[2]Université Laval, Canada

Abstract— Dielectric resonator antennas (DRAs) have receivedlots of attention in the last two decades due to severalattractive characteristics, such as high radiation efficiency, light weight, and low profile. Besides, DR antennas can be designed with various shapes and excited by different feeding mechanisms. Recently, one major aspect of the research with DRAs has been focused on the bandwidth, and several techniques have been proposed to broaden their operation bandwidth. One type of these effective methods uses some special composite DR structures. For example, stacked DRs with different materials have been studied by Shum, and Kishk et al. have proposed a wideband DRA by using stacked DRs with different materials to obtain multi-resonance operation. After that, Walsh et al. have investigated an embedded stacked DRA and achieved a bandwidth from 2.5 GHz to 4.5 GHz. Other configurations of DR can also be used to broad the bandwidth, such as tetrahedron and triangular, L-shaped or T-shaped and so on. In this work, the properties of a wideband strip-fed rectangular dielectric resonator antenna (DRA) is presented. The dielectric resonator is lifted from the ground plane and a space is obtained to form an isolated DR. It is found that the bandwidth of the resonant modes can be greatly enhanced by using an isolate DR instead of the conventional DRA. As a result, a smooth transition from one resonant mode to another can be achieved by using the isolated DR structure and a wide operating bandwidth can be obtained. Parametric studies have been carried out to investigate the performances of the proposed DRA. By combining the fist three modes of the isolated DR, a strip-fed DRA working from 2.76 GHz to 7.1 GHz with return loss less than -10 dB is achieved. In addition, this operational concept can also be extended to higher order modes, so that an ultrawideband operation bandwidth can be obtained by introducing a modified inverted-L bevel feeding patch. A modified DRA prototype has been fabricated and measured, showing a bandwidth from 2.8 GHz to 23.4 GHz.

High Input Impedance Electronically Tunable Voltage-mode Multifunction Filter

Hua-Pin Chen[1], **Wei Chien**[2], **Chi-Hsien Sun**[3], **Chien-Ching Chiu**[3], **and Yi Sun**[4]

[1]Department of Electronic Engineering, Ming Chi University of Technology, Taiwan
[2]Department of Electronic Engineering, De Lin Institute of Technology, Tu-Cheng, Taipei, Taiwan
[3]Department of Electronic Engineering, Tamkang University, Tamsui, Taiwan
[4]School of Electrical Engineering, Beijing Jiaotong University, Beijing, China

Abstract— A new high input impedance electronically tunable voltage-mode multifunction filter with single input and three outputs employing two single-output current-controlled current conveyors, one differential difference current conveyor and two grounded capacitors is proposed. The proposed filter can be realized the second-order highpass, bandpass and lowpass filter functions simultaneously without component matching conditions. The input of the filter exhibits high input impedance so that the synthesized filter can be cascaded without additional buffers. The proposed circuit employing two grounded capacitors which is very suitable to further develop into an integrated circuit implementation. The parameter sensitivities are very low and the structure does not employ external resistors thus is an active-C filter. HSPICE simulation results based on using TSMC 0.35 μm CMOS model are included to verify the theoretical analysis.

The Loop Ring BSF Design and Its Application in BPF Stopband Enhancement

Min-Hua Ho and Yi-Chao Lin
Graduate Institute of Communications Engineering, National Changhua University of Education, Taiwan

Abstract— The microstrip loop ring structure is investigated for the bandstop filter (BSF) design. This structure alone or together with the traditional quarter-wavelength open stub creates a band rejection response. The ring is in rectangular shape with its circumference dimension being one wavelength or one and half wavelengths. The rectangular ring's each side might be in different width. Shown in Fig. 1 is the proposed loop-ring BSF's transmission line structure and the equivalent circuit block. The frequency response is calculated from transforming the obtained circuit block model in Fig. 1(b) to an S-parameter function.

The quarter-wavelength open stub may tap to one of the corners to further increase the rejection response. Frequency responses of several different impedances, Z_{01} and Z_{02}, with or without the open stub attached are computed for bandstop performance comparison. Shown in Fig. 2 are the sample frequency responses of the loop-ring BSF with the open stub. Finally, the BSF is applied to a parallel-coupled bandpass filter (BPF) to suppress the second harmonic for increasing the stopband bandwidth (BW). Experiment will be conducted to verify the circuit designs.

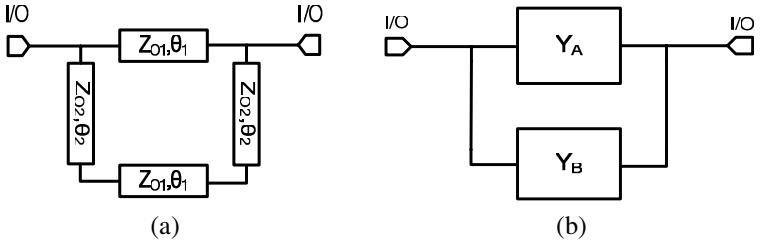

Figure 1: (a) The transmission line model of the proposed BSF and (b) its equivalent circuit block.

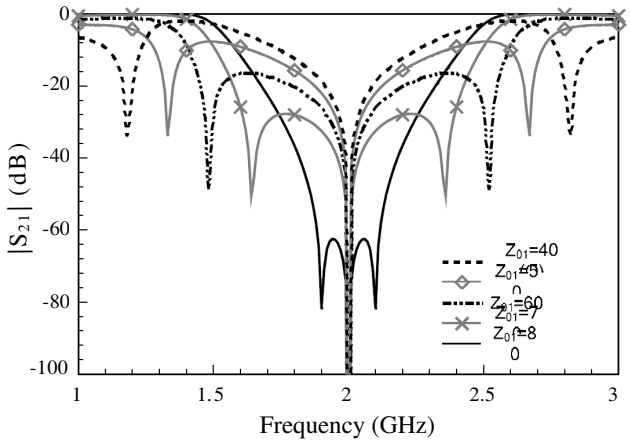

Figure 2: The calculated frequency responses for the loop ring BSF of different impedances.

Voltage-mode Highpass, Bandpass and Lowpass Filters Using a Single DVCC

Hua-Pin Chen and Tsang-Yen Hsieh
Department of Electronic Engineering, Ming Chi University of Technology, Taishan, Taiwan

Abstract— Despite the extensive literature on current conveyor-based voltage-mode multifunction biquads with single input and three outputs, no filter circuits have been reported to date which simultaneously achieve all of the advantageous features: (i) the employment of only one differential voltage current conveyor (DVCC), (ii) the employment of only two grounded capacitors, (iii) the employment of only three resistors, (iv) simultaneous realization of voltage-mode highpass, bandpass and lowpass filter signals from the three output terminals, respectively, (v) no need to employ inverting type input signals, (vi) no need to impose component choice, (vii) low passive sensitivity performance and (viii) simpler configuration due to the use of single DVCC only. This paper describes a novel voltage-mode multifunction biquadratic filter with single input and three outputs. The proposed configuration employs a single DVCC, two grounded capacitors and three resistors. The use of grounded capacitors makes the circuit suitable for integration because grounded capacitor circuit can compensate for the stay capacitances at their nodes. The proposed circuit has all the above features simultaneously, and without trade-offs. HSPICE simulation results based on using TSMC 0.35 μm CMOS model are included to verify the theoretical analysis.

Modified Approximation Types for Lossy Building Blocks

Martin Friedl, **Lubomír Fröhlich**, **and Jiří Sedláček**
Brno, FEEC BUT, UTEE, Kolejní 2906/4, Brno 612 00, Czech Republic

Abstract— Active RC filters designed using non-cascade filter synthesis realized on the base of passive RLC filter prototypes exhibit some advantages — namely low sensitivities. Usage of new modern active elements (operational amplifiers with high GBW) and possibilities of goal — directed lossy RLC ladder prototypes enable to design optimized ARC filter realizations with simple and economic active building blocks to higher frequency range. These simple grounded active selective blocks working only with one active element enable in present time to design active filters of low pass (LP), high pass (HP), as well as band pass (BP) filter types with optimized parameters.

In paper here are discussed some possibilities of filter optimization by using of active buildings blocks (simulated inductors and frequency dependent negative resistances — FDNRs) with modern active elements at higher frequencies. In some practical examples there are briefly prescribed new possibilities and resulting parameters of designed and realized ARC low pass, high pass and band pass filter types with different modified approximation functions. The presented optimization process was requested for pre-processing analogue signals before digitalization in the NMR signal processing area. The process of filter optimization is very important in most higher order filters namely in case of special or stringent filter requirements.

REFERENCES

1. Hájek, K. and J. Sedláček, *J. Kmitočové Filtry*, Vydavatelství BEN Praha, 2002.
2. Bruton, L. T., *RC — Active Circuits, Theory and Design*, 07632, Prentice Hall, Inc., Engelwood Cliffs, N. J., USA, 1980.
3. Daryanani, G., *Principles of Active Network Systems and Design*, Bell Lab. Inc., USA, 1976.
4. Hájek, K. and J. Sedláček, "Lossy LC ladder prototypes and their use for ARC filter optimization," *Wseas Transactions on Electronics*, Vol. 2, No. 3, 94–99, July 2005.

Optimization of ARC Component Filter Sensitivity

Martin Friedl and Jiří Sedláček
FEEC BUT, UTEE, Kolejní 2906/4, Brno 61200, Czech Republic

Abstract— Non-cascade method of filter design, where active filter realizations are growing from passive RLC ladder prototypes, exhibit much lower pass band sensitivity then the equivalent cascaded method filter realizations. The filter sensitivity of such designated active filters is not so quite as low as for the equivalent passive RLC ladder filters because the active circuits require many more components. The active elements (operational amplifiers), which must be in circuits used also are not ideal and their influence on resulting filter parameters can be also very significant.

In the presented contribution are discussed some optimization methods leading to improving of resulting parameters of active filters designated using above mentioned non-cascade method. Here are discussed and compared real parameters of active filters with modern active elements derived from singly or doubly terminated RLC passive prototype networks. In some examples of designated ARC filters there are prescribed some possibilities and optimization methods which enable in nowadays to design and optimization of active filters with modern active elements. The process of filter optimization is very important in most higher order filters namely in case of special or stringent filter requirements.

REFERENCES

1. Hájek, K. and J. Sedláček, *Kmitočové Filtry*, Vydavatelství BEN, Praha, 2002.
2. Daryanani, G., "Principles of active network systems and design," *Bell Lab. Inc.*, USA, 1976.
3. Hájek, K. and J. Sedláček, "Lossy LC ladder prototypes and their use for ARC filter optimization," *Wseas Transactions on Electronics*, Vol. 2, No. 3, 94–99, ISSN 1109–9445, July 2005,
4. Hájek, K. and J. Sedláček, "Modern operational amplifiers and their degeneracy effects on active filter performance," *IC — SPETO 2006*, 505–507, Gliwice-Ustroň, 2006.

A Compact Microstrip Power Divider Using Periodic DGS and HIOS

S. A. Mohassieb[1], **I. M. Barseem**[1], **E. A.-F. Abdallah**[2], **and H. M. El-Hennawy**[3]

[1]Akhbar Elyom Academy, 6th October City, Egypt
[2]Electronics Research Institute, Dokki, Giza, Egypt
[3]Faculty of Engineering, Ain Shams University, Cairo, Egypt

Abstract— Recent development in wireless communication systems has presented new challenges to design and produce high-quality miniature components with a dual-band operation. For example, global systems for GSM operate at both 900 and 1800 MHz. IEEE 802.11b and IEEE 802.11a wireless local area network (LAN) products operate in the unlicensed industrial-scientific-medical (ISM) 2.4 and 5 GHz bands, respectively. Therefore, to reduce the size and weight of communication circuits and equipments, many dual-band components, including couplers, antennas and filters have recently received much attention and been developed. A -3 dB and -10 dB branch-line couplers (BLCs) can be used as passive circuit components for wireless receivers or transmitters in microwave and millimeter wave region. The conventional BLC consists of four quarter-wavelength transmission lines of loop structure. However, the BLCs tend to occupy huge area when it is fabricated on a thin substrate, or under the MIC or MMIC technology. Therefore, a variety of size-reduction techniques such as defected ground structure (DGS) and high-impedance open stub (HIOS) have been proposed. So that BLCs with DGS and HIOS may be a good choice for the applications, in which we need wide bandwidth, high power handling capability and suppression of the higher order modes. Furthermore, it helps in decreasing the fabrication costs and increasing the yields because it does not contain any element that needs a multilayer.

In this paper miniaturized BLCs is designed, simulated and fabricated using FR4 substrate with dielectric constant 4.3, dielectric height 1.6 mm and loss tangent of 0.02. These BLCs operate at 2.4 GHz. First of all high impedance open stubs are used to miniaturize the conventional BLC using the T, π and combinational models. The proposed design is reduced by more than 69% compared to the conventional design. The second step was to use DGS underneath the BLC. The proposed design is capable to achieve any dividing ratio without reducing the width of the line, which means that the power handling capability is not reduced. In addition, suppression of higher order modes is achieved more than 18% reduction in size as compared to the conventional shape is achieved. As a final step, the two techniques are combined together and a third BLC is proposed. Good agreement is found between experimental and simulated results.

Mode Conversion at Via Discontinuities in Microwave Circuits

Wenxue Zhu, **Yu Tian**, **and Tong Ling**
University of Electronic Science and Technology of China, Chengdu, China

Abstract— Mode conversion of vias in multilayer interconnect structures is investigated. Electromagnetic waves travelling in such transmission channels generally excite higher order evanescent modes as well as other propagating modes when encountering discontinuities. The phenomenon of new mode excitation at discontinuities is called mode conversion.

Current distributions along the signal transmission channel is governed by Pocklinton Integral Equation and can be determined by the method of moments (MoM) and the Galerkin weighting procedure if piecewise sinusoidal (PWS) basis function is used to approximate the current density.

The current distribution can be further decomposed into the superposition of the fundamental and higher order modes. This procedure is done by the matrix pencil technique. The current distribution along the transmission channel is then split into forward and backward multiple mode traveling-wave amplitudes, these two categories of modes are both consisted of one fundamental mode and several higher order modes separately. The fundamental mode which is characterized by a small attenuation coefficient can travel through the entire transmission channel, while the higher order modes decay rapidly in regions far enough from the impressed source port and the discontinuities.

Radiation is the crucial issue in full-wave modeling, and we assume that the structures under study are open. We postulate from the very beginning that the surface currents existing on the conducting parts will radiate. The fundamental mode is used here for further analysis about radiation mechanism.

The mode conversion presented in this paper give a detailed explanation of the mechanism of the effect via discontinuities have done to Electromagnetic waves travelling in signal transmission channels.

The Feasibility of Numerical Calculations of Vias Using the Matrix-Penciled Moment Method

Hailiang Li, **Yu Tian**, **and Ling Tong**
College of Automation Engineering, UESTC, Chengdu, China

Abstract— With the increasing density of multi-chip module, the discontinuity of microwave interconnect was the choke point which restrains its integral performance. A good amount of researches have been done to analyze its behavior. In the past, Show-Gwo Hsu and Ruey-Beei Wu proposed the Matrix-Penciled Moment Method (MP-MM) to investigate the full wave characterization of a through hole. In MP-MM, via discontinuity has been analyzed by using equivalent magnetic frill-array models. And the effects of the via-hole structure are examined by thin-wire approximation and the matrix pencil method.

The advantage of MP-MM is its accuracy and computational speed by using the piecewise sinusoidal basis functions and degrading the three-dimensional problem to one-dimensional by equivalent thin-wire approximationbut all previous literatures including Show-Gwo Hsu's didn't pay enough attention to the following two equivalence or approximation in the method:

1) The shapes of the microstrip/strip lines in horizontal segment is ignored and treated as circular cylinder. This equivalence is accurate when the length of transmission lines is infinite, but in actual microwave circuits, due to the restriction of trace and the measure of microwave circuit boards, the microstrip/strip line can't extend to infinity.

2) MP-MM is based on Pocklinton Equation obtained by considering the antenna as thin wire. That means the method can only be used when the transmission lines can be seen as thin-wire.

At present, most literatures about this method merely introduce its principles and/or some particular calculation examples, neglecting the investigation about the application spectrum in which the method can be used, that is the key point of this paper.

From the equivalence theory and simulation results, the MP-MM's requirement to the via structures (e.g., the via height, wire width, and the permittivity of the dielectric) is presented. It's shown that the MP-MM can't be used when the via nears the source port, and a formula is given to calculate the upper bounded operating frequency beyond which MP-MM is not applicable. The tool used for simulation is HFSS.

ACKNOWLEDGMENT

This work was sponsored by basic research item of National Key lab of Electronic Measurement Technology, P.R.C..

Microstrip Bandstop Filter Using E-shaped Dual Mode Resonator

X. D. Huang and C. H. Cheng
College of Electronic Science and Engineering, Nanjing University of Posts and Telecommunications
Mailbox 280#, 66 Xinmofan Road, Nanjing 210003, China

Abstract— After a short survey of the history of the bandstop or band rejection filter, bandstop filters using dual mode resonators are emphasized since their compact size. The dual mode resonators could be classified simply into two types. One is degenerate mode type, which has been applied to the bandstop filter applications in the reported literatures. The main drawback of the bandstop filters using the degenerate dual mode resonator is their weak passband matching ($|S_{11}| > -20.0\,\mathrm{dB}$). The other is the non-degenerate type, which has not been reported for the bandstop filter use. With the purpose of both miniaturization and good passband matching, an E-shaped transmission line structure is used as the distributed non-degenerate dual mode resonator of a bandstop filter in this research. This resonator has been applied to some bandpass filter designs by former researchers.

The proposed bandstop filter consists of the mentioned E-shaped resonator and a microstrip feed line, the gap between them is used as the coupling structure. The filter is investigated by numerical and experimental approaches. The mode splitting and bandwidth control could be realized by adjusting the dimensions of the central strip of the E-shaped resonator. The simulated results show that two balanced refection zeroes could be obtained beside the stopband to improve the passband performance, after adjusting the bend ratio of the resonator's arms carefully whereas keeping good in-band rejection. Filter samples are designed, fabricated and measured. As a result, a rejection level of $-16.7\,\mathrm{dB}$ (Bandwidth $= 3.5\%$) is realized at the central frequency 6.01 GHz. Two reflection zeros ($< -45.0\,\mathrm{dB}$) at 5.64 GHz and 6.24 GHz are observed as predicted. In addition, the wideband matching in the passband is better than $-30.0\,\mathrm{dB}$, which shows good out-band matching is achieved.

Arbitrary Microwave Filters Using Waveguides Filled by Dielectric and Magnetic Layers

M. Khalaj-Amirhosseini and H. Ghorbaninejad-Foumani
College of Electrical Engineering, Iran University of Science and Technology, Iran

Abstract— Microwave filters are an inevitable requirement of microwave circuits and communication circuits. Some various structures have been used for microwave filters such as microstrip filters [1–4], substrate integrated waveguides (SIWs) [5], dielectric resonator (DR) filters [6, 7] and waveguide filters [1–4, 8, 9]. Usually, waveguide filters utilize inductive elements such as irises, rods, diaphragms and posts as impedance inverters between two hollow or dielectric-filled regions of a waveguide [1–4], [8]. Fabrication of these filters has some difficulties because of implementing inductive elements into a waveguide. In this paper, a new structure is proposed to design waveguide filters with arbitrary frequency response and easy fabrication. This structure utilizes a waveguide filled by several dielectric and magnetic layers in a manner that each dielectric layer is followed by a magnetic layer and there is no requirement to any inductive elements such as diaphragms. In fact, the proposed structure is a multi-layer Longitudinally Inhomogeneous Waveguide (LIW) [10–12]. The relative electric permittivity, the relative magnetic permeability and the thickness of the layers are optimally obtained using least mean square approach. Therefore, the proposed structure has the capability to design filters with arbitrary frequency response in addition to the conventional ones such as bandpass and bandstop filters. The usefulness of the proposed structure and its performance is verified by an example.

Figure 1 shows the proposed waveguide filter which is a waveguide with dimensions a, b and d, filled by K dielectric layers and K magnetic layers, alternately. The relative electric permittivity and the thickness of dielectric layers are $\varepsilon_{r,k}$ and d_{dk}, respectively, and also the relative magnetic permeability and the thickness of magnetics are $\mu_{r,k}$ and d_{fk}, respectively, for $k = 1, 2, \ldots, K$.

In this paper, a general method is proposed to design optimally the Multi-Layer dielectric and magnetic LIW microwave filters. The method is based on the minimization of a suitable error function along with some constrained conditions to determine optimum values of the permittivity and thickness of dielectrics as well as the permeability and thickness of magnetic layers. One may define the following error function for M frequencies f_1, f_2, ..., f_M which are greater than f_c.

$$\text{Error} = \sqrt{\frac{1}{M}\sum_{m=1}^{M}\left|\frac{|S_{21}(f_m)| - |H(f_m)|}{|H(f_m)|}\right|^2} \tag{1}$$

where $H(f)$ is the arbitrary desired transfer function of the filter. Moreover, defined error function has to be restricted by some constraints.

In this paper, an arbitrary filter is optimally designed using a multi-layer dielectric and magnetic waveguide structure. Consider a WR-90 waveguide ($a = 0.9\,\text{in}$ and $b = 0.4\,\text{in}$) filled by $K = 10$ dielectric and magnetic layers. We would like to design a 3-order chebyshev bandpass filter with the center frequency of 10 GHz, the relative bandwidth of 10% and equal ripples of 1.0 dB. Using the proposed optimization method and considering $d_{d,\min} = d_{f,\min} = 0.4\,\text{mm}$, $\varepsilon_{r,\max} = \mu_{r,\max} = 8$, $f_1 = 8\,\text{GHz}$ and $f_M = 12\,\text{GHz}$ ($M = 200$), the optimum values of the filter parameters were obtained. It is seen that the frequency response of designed filter is very closer to the desired transfer function than the frequency response of the conventional waveguide filters consisting of inductive elements, as is seen in [8].

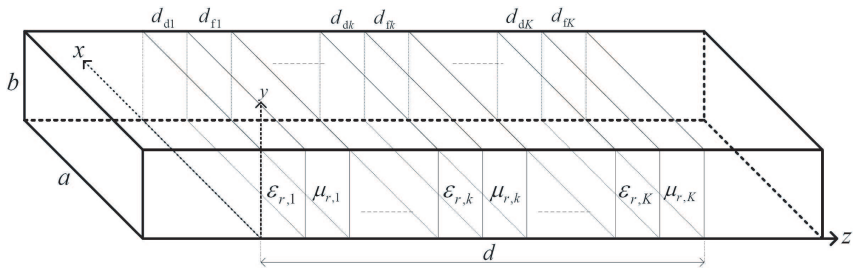

Figure 1: A waveguide filled by several dielectric and magnetic layers.

Waveguide Bandpass Filters Utilizing Only Dielectric Pieces

Mohammad Khalaj-Amirhosseini and Habib Ghorbaninejad-Foumani
College of Electrical Engineering, Iran University of Science and Technology, Tehran, Iran

Abstract— Bandpass filters have a large variety of applications in microwaves and communication circuits. Some various structures have been used for microwave bandpass filters such as microstrip filters [1–4], substrate integrated waveguides (SIWs) [5], dielectric resonator (DR) filters [6, 7] and waveguide filters [1–4, 8, 9]. Usually, waveguide bandpass filters utilize inductive elements such as irises, rods, diaphragms and posts as impedance inverters between two hollow or two dielectric filled regions of a waveguide [1–4, 8]. Fabrication of these filters has some difficulties because of implementing inductive elements into a waveguide. In this paper, a new method is introduced to design of waveguide bandpass filters, whose fabrication is easy. In this method, a waveguide is filled only by several dielectric pieces and there is no needing to inductive elements such as irises, rods, diaphragms and posts. Moreover, the length of introduced filters may be less than that of filters consisting of hollow waveguides with inductive elements. Also, because there is no discontinuity in the introduced filters, their analysis is easy and accurate and so we do not need to optimization process to design them. The usefulness of the proposed structure and its performance is verified by an example and simulation using a full-wave simulator.

Figure 1 shows the proposed dielectric filled waveguide bandpass filter consisting of $2N + 1$ dielectric filled regions in a rectangular waveguide. The cross section of the waveguide has dimensions of a and b and the lengths of dielectric filled regions are a quarter- or a half-wavelength alternately. In Fig. 1, λ_{gn} is the waveguide wavelength in the n-th region. The n-th region ($n = 1, 2, \ldots, 2N + 1$) has been fully filled by a dielectric with relative electric permittivity $\varepsilon_{r\,n}$, where $\varepsilon_{r\,0} = \varepsilon_{r,\,2N+2} = 1$. In fact, each quarter wavelength dielectric filled waveguide act as an impedance invertor and each half wavelength dielectric filled waveguide acts as a resonator. We have to choose appropriate values of relative electric permittivity for each section, whose values are determined in the following.

Now we desire to model the proposed waveguide filter shown in Fig. 1 as a bandpass filter consisting of N series resonators and $N + 1$ impedance invertors, at center frequency f_0. For this purpose, two modelings are presented. Then two bandpass filter are designed (fully and partly dielectric filled) utilizing a WR-90 waveguide ($a = 0.9$ inches and $b = 0.4$ inches). We design two 3-order chebyshev type bandpass filter with center frequency 10 GHz, the relative bandwidth 9% and equal ripples 0.5 dB. Two designed filters are simulated using full-wave software HFSS, which is based on the finite element method FEM. It is seen that the performance of the fully dielectric filled filter is identical to that of the partly dielectric filled filter while the length of former one is 41.43 mm and that of the latter one is 71.14 mm. Therefore the fully dielectric filled filter has about 41.7% compactness compared to the partly dielectric filled filter. Of course, the fully dielectric filled filter requires to higher permittivity dielectrics with respect to the partly filled filter. It is seen that the length of fully dielectric filled filter (41.43 mm) is less than that of waveguide filter consisting of hollow waveguides with inductive diaphragm (50.79 mm) [8]. From the above example one may satisfy regarding to the good performance of the proposed waveguide bandpass filters. Moreover, it is obvious that the advantages of the proposed filters could be mentioned as the followings:

1. The fabrication is easy because there is no needing to the elements such as diaphragms, iris, rods and posts and the dielectrics could glue easily to the walls of the waveguide and consequently the waveguide could be made monolithic instead of multi-sectional.

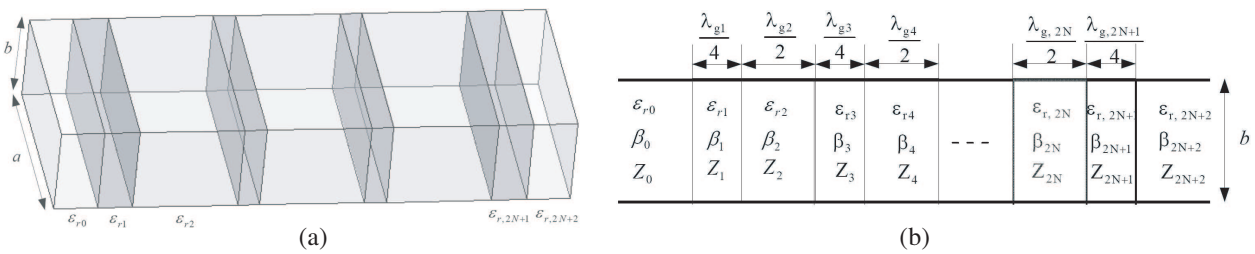

Figure 1: The proposed dielectric filled waveguide bandpass filter. (a) Three dimensional view, (b) top view.

2. The mechanical stability is good because there is a monolithic waveguide filled by dielectrics glued to the walls and each other.
3. It is suitable for high power microwave circuits because the breakdown voltage of dielectrics is higher than that of the air.
4. The required length may be less than that of filters consisting of hollow waveguides with inductive elements.
5. Their analysis is easy and accurate because there is no discontinuity and so only dominant mode is existed in the waveguide. Therefore, there is no needing to optimization process in design step.

PIFA Antenna with Coupling Effect for Bandwidth Enhanced Design and Measurement

Kekun Chang[1], **Guan-Yu Chen**[1], **Jwo-Shiun Sun**[1], **and Y. D. Chen**[2]

[1]Department of Electronic Engineering, National Taipei University of Technology, Taiwan
[2]Antenna and EMC Laboratory, HTC Corporation, Taiwan

Abstract— The planar inverted-F antenna (PIFA) is popular for mobile handset (Fig. 1) because of its low profile and compact size. The PIFA is designed to reference a ground plane. The paper (Fig. 2) presents results from a comprehensive investigation on the performance of a conventional PIFA with a parasitical patch radiator to enhance antenna bandwidth. The proposed PIFA with coupling effect antenna is analyzed and the influence of structure on bandwidth, gain, and radiation efficiency are presented. These results are very useful in the design of a PIFA for applications requiring a parasitical radiator. Enhanced gain of PIFA antenna loaded with a parasitical patch has been demonstrated. Measurements show that the bandwidth of the antenna can be improved without sacrificing the antenna radiation efficiency. The gain enhancement mechanism, bandwidth, and antenna radiation gain and patterns are presented and discussed. The new radiators are developed by adding parasitic elements or tuning devices to a familiar PIFA. Simulation based upon the method of moments (Microwave Office) is used to model the performance of the antennas. Comparisons with measured results on fabricated antenna structures are provided for simulations validation.

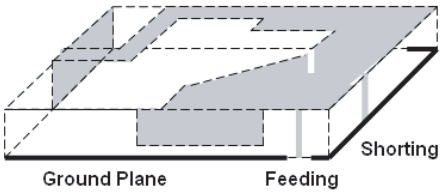

Figure 1: Traditional PIFA.

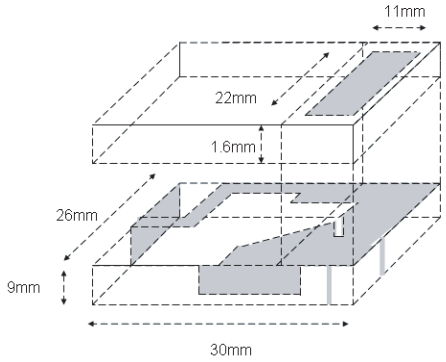

Figure 2: The proposed PIFA.

Meander Line Antenna for GPS Phone Operation

Kuo-Liang Wu[1], **Guan-Yu Chen**[1], **Jwo-Shiun Sun**[1], **and Y. D. Chen**[2]

[1]Department of Electronic Engineering, National Taipei University of Technology, Taiwan
[2]Antenna and EMC Laboratory, HTC Corporation, Taiwan

Abstract— The general GPS functions of PDA support the assisted functionality in 2.5/3G wireless networks. Traditional antennas such as monopoles, dipoles and patches are not suitable to meet the requirements of modern wireless communication and highly demanding mobile GPS systems. As a result, there is the need for alternative approaches to small antenna and high performance design. This paper describes a miniaturized meander shorting monopole for integration in modern GPS wireless systems. The resonance mode of a shorting meander wire antenna (Fig. 1 and Fig. 2) covers the GPS communication bandwidth of 1571.42–1579.42 MHz. The simple wire tuning expansion are introduced to confine the resonance mode region and to facilitate the frequency modes and impedance match expansion easily for antenna and wireless system integration design. The design requirements for GPS antenna is combined into multiple objective goals, such as simplicity of the antenna geometry, radiation pattern, return loss, antenna impedance and polarizations. This design in general to a mobile communication apparatus and global positioning system antenna, and more particularly to a mobile communication system, which utilizes a small-scale metal for the GPS antenna design.

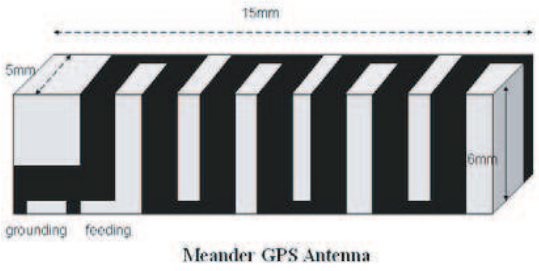

Figure 1: The proposed antenna.

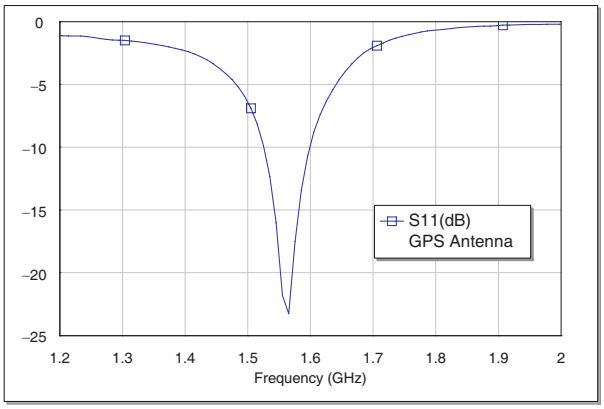

Figure 2: The measured data.

Antenna Measurement System for CTIA OTA Operation

Guan-Yu Chen[1], **Kuo-Liang Wu**[1], **Jwo-Shiun Sun**[1], **and Y. D. Chen**[2]

[1]Department of Electronic Engineering, National Taipei University of Technology, Taiwan
[2]Antenna and EMC Laboratory, HTC Corporation, Taiwan

Abstract— Wireless systems, especially require antennas and wireless system integration and requirements. They include operation near the human body effect, operation in a multi path and fading environment, extremely small antenna size, receiver diversity, multi frequency operation, radiation pattern performance and adaptive antenna techniques. Unique quality factors, in contrast to the classical ones, are also introduced such as parameters of total radiation efficiency, mean effective gain and correlation coefficience. The mobile phone under test of far-field range testing has been the plan at the Cellular Telecommunications & Internet Association (CTIA) certification program test requirements for performing radiated power and receiver performance measurement. In this paper, facilities of antenna pattern measurement have recently commissioned a spherical far-field measurement system. The low profile far-field spherical scan system provides significant advantages over the older far-field testing including elimination of problem of simple theta (θ) and phi (ϕ) rotary axis with indoor far-field range testing, complete measurement characterization of the antenna, and improved accuracy. This paper will discuss the antenna and wireless system integration tested, spherical antenna measurement for far-field system, and the results being achieved.

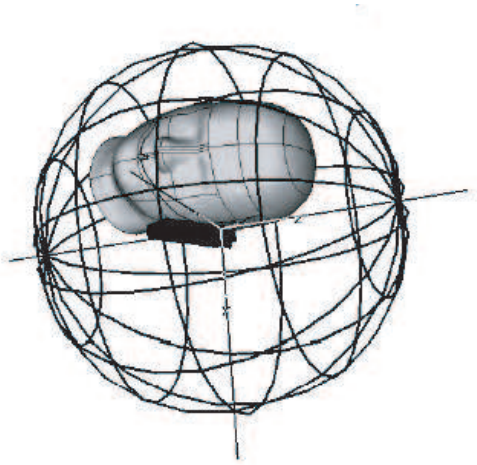

Figure 1: 3D antenna measurement.

New Antenna Modelling Using Wavelets for Heavy Oil Thermal Recovering Methods

M. D. Santos[1], **A. D. Neto**[2], **J. P. Silva**[3], **and W. Mata**[4]

[1]Departamento de Ciências Exatas e Naturais
Universidade Federal Rural do Semi-Árido — UFERSA, Brazil
[2]Departamento de Engenharia de Computação e Automação
Universidade Federal do Rio Grande do Norte — UFRN, Brazil
[3]Departamento de Ciências Ambientais e Tecnológicas
Universidade Federal Rural do Semi-Árido — UFERSA, Brazil
[4]Departamento de Ciências e Engenharia de Petróleo
Universidade Federal do Rio Grande do Norte Campus Universitário — UFRN, Brazil

Abstract— This paper presents a new computational mathematical model to investigate the use of a cylindrical antenna, dipole type, adapted for local heating in dissipative medium of heavy petroleum reservoirs. The thermal methods occupy an important position among the advanced recovery methods due to their applicability in heavy oil reservoirs. These methods consist of furnishing heat, normally using hot fluids as steam or hot air, to the heavy oil reducing its viscosity. Alternatively, this can be also done by electromagnetic heating effects directly in the formation fluids. The electromagnetic heating is based on the transformation of electric energy in thermal through the direct interaction between the electromagnetic excitement field and the electrically sensitive particles of the medium. The antenna is implemented using an asymmetrically center-driven dipole with concentric insulated layers geometric well adapted for heavy oil extraction. This antenna exhibits a simple geometry, and has been analyzed through a mathematical model based on Maxwell equations. Here, the conventional moment method in conjunction with wavelets bases functions are used to obtain the antenna current distribution. The results show that the wavelets can be used to show important aspects in different resolution levels to improve the energy transfer to the dissipative medium. The mathematical models and the numeric techniques approached in this study were implemented in computational algorithms. Detailed expressions for electric field and power distribution are also developed and calculated. The results obtained for the viscous oil reservoirs were stable, presenting a good agreement with the models and results found in the literature.

Double-ridged Horn for 3D Antenna Measurement

Jui-Yi Yang[1], **Guan-Yu Chen**[2], **Yung-Sheng Chen**[1], **Jwo-Shiun Sun**[2], **and Y. D. Chen**[3]

[1]Department of Electrical Engineering, Yuan Ze University, Taiwan
[2]Department of Electronic Engineering, National Taipei University of Technology, Taiwan
[3]Antenna and EMC Laboratory, HTC Corporation, Taiwan

Abstract— A 1–18-GHz broadband double ridged horn antenna by 3D far field pattern measurement is studied. The measurements are in good agreement with the theories over the 1–18-GHz operational bandwidth and indicate that the use of double ridged horn in antenna chamber application. This paper will discuss the high gain antenna measured by spherical far-field system. Antenna measurement technique refers to the testing of antenna to ensure that the antenna meets specifications or simply to characterize it. Typical parameters of antennas are gain, radiation pattern, beamwidth, polarization, and impedance. Based on 3D antenna measurement is the ratio of power actually radiated to the power put into the antenna terminals. This paper presents a 3D antenna measurement system which allows, in addition to standard far field measurements, a full 3D measurement of the radiation pattern of a double ridged horn antenna. To prove measurement results, a simple antenna system has been created, which allows comparison with simulation and theory results.

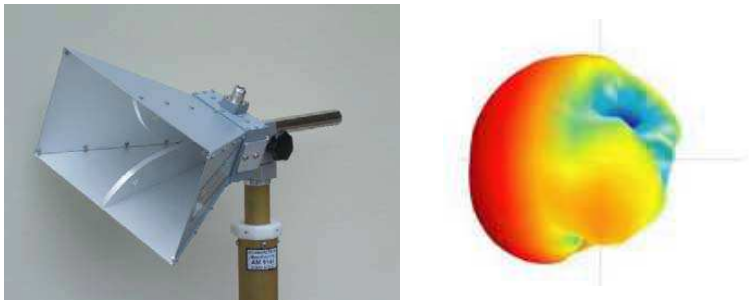

Figure 1: Double ridged horn antenna by 3D antenna measurement.

Research on the Radiation Characteristics of Cage Antenna of EMP Radiating-wave Simulator Based on Parallel Computing

Xiang-Qin Zhu[1] **and Jian-Guo Wang**[1, 2]

[1]Northwest Institute of Nuclear Technology, Xi'an, Shaanxi 710024, China
[2]School of Electronic and Information Engineering, Xi'an Jiaotong University
Xi'an, Shaanxi 710049, China

Abstract— Considering the target is electrically large, a parallelized finite difference time domain (FDTD) algorithm based on MPI platform, combined with antenna theory, is presented for analysis of the radiation characteristics of the biconical-cylindrical cage antenna fed through the coaxial transmission line and excited by a double-exponential pulse, which can not be done on a personal computer due to over long time and prohibitive computation resources. The number of total cells for parallelized FDTD computing is about 2 billion. Numerical results show that cage antenna radius do not have a significant effect on the rise time, the peak value and pulse width of the radiated electric field when the cage antenna radius is more than 3.5 m. The results of analysis also show that the wider half-width of the excited pulse, the wider half-width of the radiation field, but the rise time and the peak value are not very sensitive to the half-width of excited pulse. In addition, the reflection and the loss from the ground have a great effect on the rise time, the peak value and pulse width of the radiated E-field in the horizontal plan above the ground up to 0.5 m and have little effect on the rise time and the peak value of the radiated E-field in the horizontal plan above the ground up to 6m except the pulse width of the radiated E-field at the same point. Father the wave propagation distance in the horizontal plan above the ground up to 0.5 m, more the effect of the reflection and the loss from the ground on the rise time, the peak value and pulse width of the radiated E-field. It is found that nearer to the ground, faster the decrease of the peak value.

A Compact Microstrip Coupled-fed Planar Antenna for WLAN and WiMAX Applications

Hao-Hui Chen[1], **Wen-Jen Tseng**[2], **Wen-Kai Wu**[3], **and Ming-Huei Chen**[1]

[1]Department of Electronic Engineering, National Kaohsiung First University of Science & Technology Kaohsiung, Taiwan, R.O.C.
[2]Wha Yu Industrial Co., Ltd., Hsinchu, Taiwan, R.O.C.
[3]Department of Electronic Engineering, Huafan University, Taipei, Taiwan, R.O.C.

Abstract— With the rapid growth of the demand for low-power, low-cost, and high-integration wireless communication products, integrating various communication systems (such as GSM, WLAN, and WiMAX) in a single platform has received great attention recently. Hence, the development of an antenna with multi-frequency operation capabilities has emerged as a critical issue for both the industry and the academia. Several promising antennas for multi-band operation, such as the dual-slot antennas, the coupled-fed and direct-fed planar invert-F antennas, and the dual-band planar monopole antennas, have been reported in the published literature. However, due to the bandwidth limitation, very few of them can fully cover all the operating bands of WLAN and WiMAX systems. In this work, a compact planar antenna covering all the WLAN and WiMAX operating bands, including 2.4/5.2/5.8 GHz WLAN and 2.5/3.5/5.5 GHz WiMAX bands, is presented. Fig. 1 shows the prototype of the proposed design, where the antenna is simply implemented on a substrate. In this antenna design, the radiation mechanism is controlled by the shorted F-shaped metal strip. By appropriately designing the length and width of the two arms of the F-shaped radiator, three resonances can be excited under 8 GHz. Further, a coupled feeding structure formed by a microstrip line with the signal trace being terminated by a rectangular patch is deposited on the other side of the substrate. Such a coupling feed can broaden the resonant bandwidth considerably. The F-shaped radiator together with the microstrip coupling feed can therefore provide three wide operating bands and is suitable for multi-band operation. With the proposed design, an antenna having three wide operating bands located at about 2.5, 3.5, and 5.2 GHz (i.e., 2.3–2.7, 3.3–3.7, and 4.9–5.9 GHz), which covers the 2.4/5.2/5.8 GHz WLAN and 2.5/3.5/5.5 GHz WiMAX applications, is designed and fabricated on a 0.8-mm thick FR4 substrate. The size of the designed antenna is $8.5 \times 15\,\text{mm}^2$ only (not including the ground plane). Due to the compact size and simple structure, the proposed antenna is very attractive for WLAN and WiMAX mobile applications. Details of the design guidelines and considerations as well as the antenna performances will be presented and discussed in the symposium.

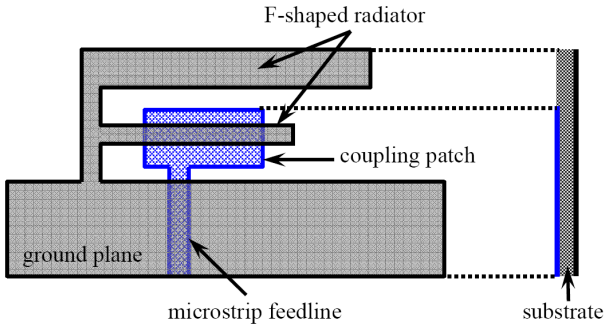

Figure 1: A microstrip coupled-fed multi-band antenna.

Support Vector Modeling of Manufacturing Tolerance Influencing Electrical Performance for Cavity Filters

Jinzhu Zhou[1], **Baoyan Duan**[1], **Hongbo Ma**[1], **Liang Li**[2], **Jin Huang**[1], **and Daiwen Yang**[1]

[1]Key Laboratory of Electronic Equipment Structure Design of Ministry of Education, Xidian University Xi'an 710071, China

[2]National Key Laboratory of Antenna and Microwave Technique, Xidian University, Xi'an 710071, China

Abstract— Cavity filter is used widely in the modern communication system. However, the manufacturing tolerance of cavity filter has a great effect on the electrical performance, and it often requires great efforts to adjust a detuned filter once they have been assembled. In order to select a proper manufacturing precision for guiding the manufacturing and reducing the tuning efforts, this paper presents a modeling method of the coupling model between the manufacturing tolerance and the electrical performance of cavity filters. In the approach, a novel machine learning model is firstly developed by using a modified linear program support vector regression (LPSVR) which is an effective small sample machine learning algorithm, according to some actual datasets from the manufacturing process of filters. The machine learning model shows the influencing relationship of manufacturing tolerance on the changing amount of coupling matrix relative to the ideal coupling matrix, which can be obtained at the designing stage of filters by using synthesis theory of coupling matrix. Then, by using the developed machine learning model, the ideal coupling matrix is modified, and an actual coupling matrix which reveals the effect results caused by the manufacturing tolerance of filters is obtained. Finally, according to the existing relationship of coupling matrix and the electrical performance of filters, the support vector coupling model is obtained to show the influence of actual manufacturing tolerance on the electrical performance of cavity filters. The model is validated by experiments of an actual cavity filter with central frequency 960 MHz. The results confirm the effectiveness of the method proposed in this paper. Moreover, the result also shows the coupling model established by the modified LPSVR proposed in the paper is more accurate than the one by neural network. The accurate coupling model will be used to obtain the optimal manufacturing tolerance of filter and help the manufacturing of filter in the future. The proposed modeling method is also suitable to develop a computer-aided tuning system of volume-producing filters.

A Planar Antenna Array with Separated Feed (PAASF) with Air Gap Technique

M. T. Ali[1], **T. A. Rahman**[1], **M. R. Kamarudin**[1], **R. Sauleau**[2], **M. N. Md Tan**[1], **and M. F. Jamlos**[1]

[1]Wireless Communication Center (WCC), Universiti Teknologi Malaysia
81310 UTM Skudai, Johor, Malaysia
[2]Institut d'Electronique et de Télécommunications de Rennes (IETR)
UMR CNRS 6164, University of Rennes 1, France

Abstract— A novel antenna of Planar Antenna Array with Separated Feed (PAASF) with lower side lobe pattern and higher antenna gain was designed. The unique property of this antenna design is that instead of fabricating all together in the same plane, the antenna's feeding network is separated from the antenna radiating elements (the patches) by an air gap distance. In this paper, the characteristics radiation pattern of two different radiating structures have been studied and compared. The first antenna configuration ("Structure 1") is a 16-element planar antenna array whose feed line is printed on the same plane as the radiating elements (Fig. 1(a)). The second one ("Structure 2") is a 16-element planar antenna array whose feed network is separated from the radiating elements by an air gap (Fig. 1(b)). Both antennas are designed at 5.8 GHz. The PAASF technique is enables to reduce the unwanted spurious effects from the feed line. From the comparison results, it obviously shown that the "Structure 2" is given better sidelobe to mainlobe ration of −11.9 dB while "Structure 1" only −5.35 dB. In this structure, not only improvement is achieved in the sidelobe reduction pattern, but also better performance in term of the antenna gain. The antenna gain generated by "Structure 2" of 11.78 dB is higher compared to 8.539 dB generated by "Structure 1". Since some of the transmission line is placed to another board in PAASF, the size of that antenna become smaller compare to "Structure 1". Finally, in order to proof the validity of the antenna design, the simulated results (CST 2008 software) have been compared with measurements, and good agreement has been found as shown in Fig. 2.

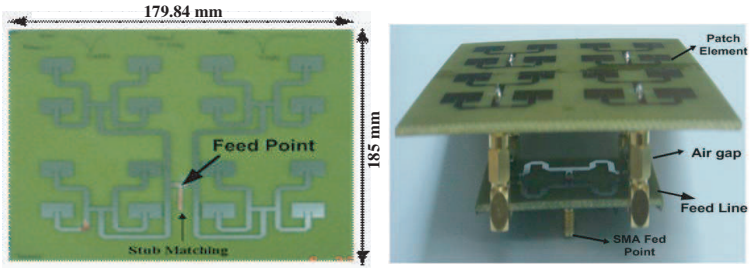

(a) (b)

Figure 1: Fabricated antenna. (a) Structure 1 antenna, (b) structure 2 antenna, (PAASF).

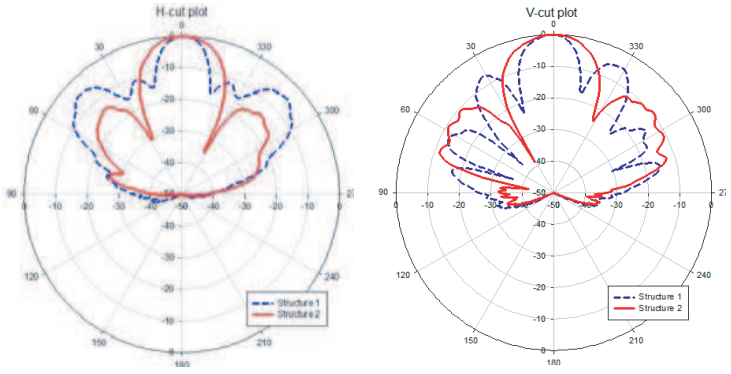

(a) (b)

Figure 2: Measured result of normalized radiation pattern for both structures. (a) Hcut-plane, (b) vcut-plane.

Elements Reduction Using Unequal Spacing Technique for Linear Array Antenna

M. N. Md Tan[1], **T. A. Rahman**[2], **S. K. A. Rahim**[2], **M. T. Ali**[1], **and M. F. Jamlos**[2]

[1]Faculty of Electrical Engineering, University Technology Mara (UiTM), Shah Alam, Selangor, Malaysia
[2]Wireless Communication Center (WCC), University Technology Malaysia (UTM), Skudai, Johor, Malaysia

Abstract— The basic idea of this paper is to use unequal spacing technique not only to reduce the side-lobe level but also to reduce the number of element of linear array antenna. The arrangements of the elements followed the arrangement given by R. F. Harrington and Y. T. Lo. Most of the simulation done by previous researches focused on the algorithm, where the mutual coupling effect contributed by the elements was not included. The simulation started with 16 elements rectangular micro-strip patch of linear array antenna with one half wavelength spacing between the elements at an operating frequency of 5.8 GHz, using FR4 substrate with dielectric constant of 4.6, and thickness of 1.6 mm using CST2008 software. The result obtained will be put as a reference and will be compared to the unequal spacing simulation. It will be followed by the simulation of unequal spacing antenna for both symmetrical and asymmetrical arrangement where the amplitude of the excitation is assumed to be constant. Under symmetrical arrangement, another two different arrangements that are space tapered and non-tapered were investigated. The simulation started with 10 elements and was increased until its performance equal or was comparable with the 16 elements equal spacing antenna. The simulations result shows that by using the unequal spacing technique, the linear array antenna has better potential to have fewer numbers of elements but the performance was comparable. In this paper, the number of element reduced from 16 elements to 13 elements with better side-lobe level, same half power beam-width (HPBW) value and produced comparable antenna gain.

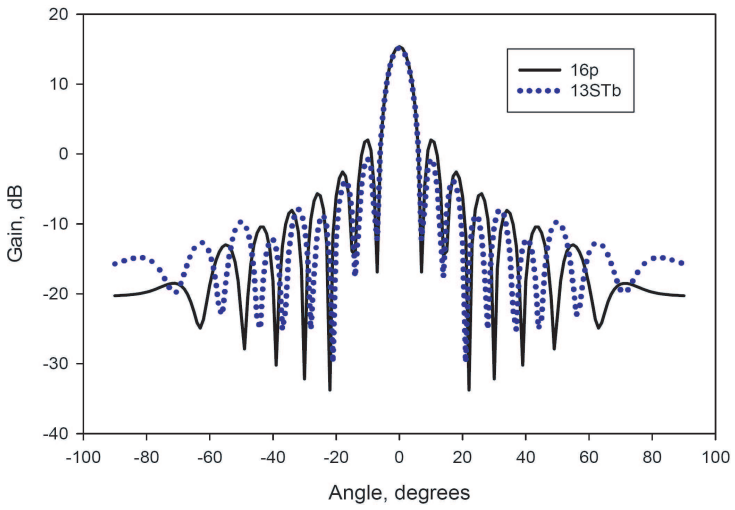

Figure 1: Rectangular pattern for 16 elements equal spacing and 13 elements space tapered arrangement.

Reconfigurable Aperture Coupled Planar Antenna Array at 2.3 GHz

M. F. Jamlos[1], **T. A. Rahman**[2], **M. R. Kamarudin**[2], **M. T. Ali**[2], **M. N. Md Tan**[2], **and P. Saad**[3]

[1]Faculty of Computer and Communication Engineering, University of Malaysia Perlis (Unimap), Malaysia
[2]Wireless Communication Center (WCC), University of Technology Malaysia (UTM), Malaysia
[3]Faculty of Computer Science and Information System (FSKSM)
University of Technology Malaysia (UTM), Malaysia

Abstract— Reconfigurability in an antenna system is a desired characteristic that has been the focus of much interest in recent years. This paper describes the concept of reconfigurable antenna and how advances in switch technology have made these designs realizable. Complete design of the radiating patches, diode switches and biasing circuitry are also discussed. The structure of modified corporate-feed network is used to realize the array antenna consisting of 16 elements of rectangular patches at 2.3 GHz. The antenna patches through deployment of 4 PIN diodes switches at the feeding lines enabled the radiation pattern to be altered with respect to the beam shaping characteristics. While the planar arrays design making it more feasible for other antenna performances to be enhanced. The resistance for OFF and ON states of PIN diodes could strongly affect the performance of antenna. Hence, in order to improve the performance of the antenna, aperture coupled configuration is used to boost the antenna gain and directivity. The slot's geometry of aperture coupled antenna is stressed out as it determines the amount of coupling to the patches from feeding lines of the antenna. It is shown through simulations and measurements that 4 types of radiation pattern of the antenna can be well reconfigured by turning the diode switches on and off. The gain, directivity, beamwidth and return loss are also changed. The radiation pattern and beamwidth becomes narrower and higher in magnitude as numbers of activated switches are increased. Indirectly, the directivity and gain are increased. Good agreement between the simulations and measurements were obtained. These results extend the validity of the analysis and will be useful for applications involving this type of reconfigurable antenna.

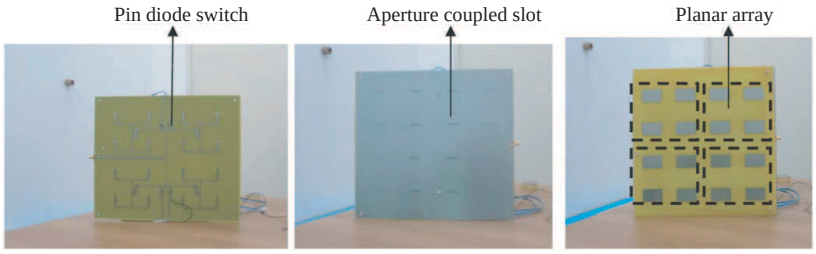

Figure 1: Reconfigurable aperture coupled microstrip antenna.

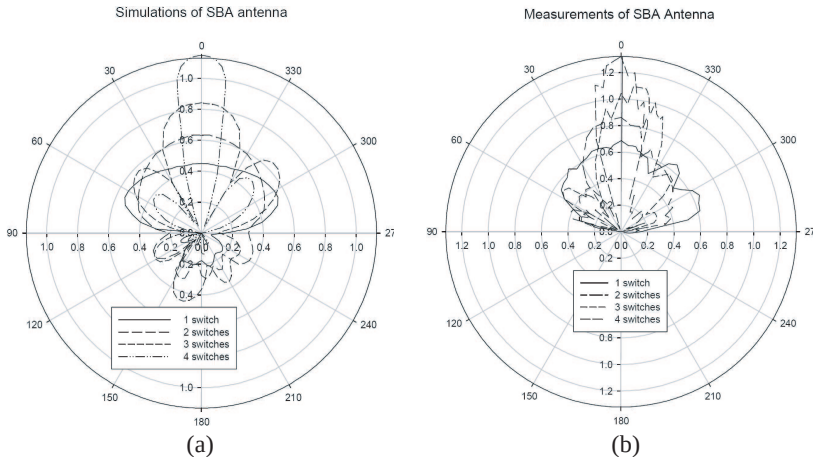

Figure 2: Simulations and measurements results of radiation pattern.

Tunable All-dielectric Isotropic Near-zero-index Lens

Qian Zhao[1], **Fuli Zhang**[2], **Lei Kang**[3], **Ji Zhou**[3], **and Yonggang Meng**[1]

[1]State Key Lab of Tribology, Department of Precision Instruments and Mechanology
Tsinghua University, Beijing 100084, China
[2]Department of Applied Physics, School of Science
Northwestern Polytechnical University, Xi'an 710129, China
[3]State Key Lab of New Ceramics and Fine Processing, Department of Materials Science and Engineering
Tsinghua University, Beijing 100084, China

Abstract— All-dielectric isotropic near-zero-index lens were demonstrated experimentally and numerically in an array of dielectric particles using the electric or magnetic resonances of Mie resonances. It shows that a strong sub-wavelength magnetic or electric resonance can be excited in dielectric particles corresponding to the respective first or second Mie resonance mode, where the zero- permeability or zero-permittivity can occur. And thus isotropic near-zero-index occurs at such resonant regions, different from that of the metal wire or split ring resonance arrays. The directivity of an embedded source (monopole antenna) in such planar lens is largely improved and the out rays at the interface are near along the normal direction in the surrounding media, which significantly narrows the far-field pattern associated with an antenna located within it as a consequence. Using frequency dependent dielectric property of ferroelectric particle, the adaptive isotropic near-zero-index lens is also demonstrated at multiple frequency regions by changing the temperature. These tunable near-zero-index metamaterials can be widely used to develop a new class of adaptive antenna or source.

Comparison of Microwave Waveguide Applicators for Thermotherapy

Jaroslav Vorliček, **Jan Borovka**, **and Jan Vrba**
Dept. of Electromagnetic Field, Czech Technical University, Czech Republic

Abstract— Microwave thermotherapy or hyperthermia is a method commonly used for cancer treatment in oncology. Together with radiotherapy or chemotherapy it is applied to improve the treatment results. It is based on the principle that cancer cells are more sensitive to higher temperatures. Healthy cells survive temperatures up to 45°C, whereas cancer cells only up to 42°C. Heating biological tissue in temperature interval (42–45°C) results in only cancer cells are being destroyed. In a healthy tissue the blood flow increases together with increasing temperature causing further temperature increase to stop. In tumor tissue, however, this mechanism does not happen because of lack of a sophisticated vascular system.

The paper deals with the survey of prospective types of microwave applicators for thermotherapy. The discussed applicators are strip TEM wave applicator, lucid horn applicator and TE_{10} applicator. In this article is widely discussed their design, construction as well as their advantages and suitability of use in the clinical applications. All the applicators have the same size of the aperture 120×80 mm to make them easy to compare. Numeric verification of SAR distribution in homogenous plane phantom is accomplished by electromagnetic field simulator SEMCAD 13.4.

Our main aim was to compare the microwave applicators, their effective field size (EFS) and the depth of effective penetration (DEP). From the results based on the simulations in simulator of electromagnetic field SEMCAD 13.4, we can say that the most suitable applicator for the superficial thermotherapy covering the largest area of tissue among those three is the strip waveguide applicator with TEM mode wave. Its EFS is 57% and the depth of effective penetration is 18 mm. On the other hand the waveguide applicator with TE_{10} mode wave has the smallest effective field size ($EFS = 31\%$) but the radiated field is more focused and the depth of effective penetration is the highest among those three applicators ($DEP = 25$ mm) which makes this applicator perfect for heating small superficial tumours which are located not more than 30 mm under the skin.

ACKNOWLEDGMENT

This research is supported by Grant Agency of the Czech Republic, project: "Non-standard application of physical fields — analogy, modeling, verification and simulation" (102/08/H081).

Compact Blue/Green Laser Sources for Projection Display

Kang Li[1], **N. J. Copner**[1], **C. B. E. Gawith**[2], **Ian G. Knight**[3], **Hans-Ulrich Pfeiffer**[4], **and Bob Musk**[5]

[1]Faculty of Advanced Technology, University of Glamorgan, Pontypridd, CF37 1DL, UK
[2]Covesion Ltd., Romsey, SO50 9AQ, UK
[3]Bookham Technology Plc, Caswell, NN12 8EQ, UK
[4]Bookham (Switzerland) AG, CH-8045, Zürich, Switzerland
[5]Gooch & Housego, Torquay, TQ2 7QL, UK

Abstract— High power laser sources in the blue/green frequency range have been attracting increasing interest in the various application fields such as displays, optical recording and storage, bio-medical instrumentation, digital imaging and reprographics, space based satellite laser and underwater strategic communication etc [1–3]. In particular, high-brightness, high-efficiency, low-cost red-green-blue laser sources constitute a large and potentially high margin market opportunity in laser projection display systems that allow scalable screen size, high contrast, and high brightness. In this paper, we review a design and fabricate an engineering prototype laser based on a universal module design platform applicable for blue/green and power levels as needed for projection display applications. The "state of the art" manufacturable lasers operate with a wavelength of 465 nm and 532 nm exploiting intra-cavity frequency doubling of an edge emitting laser bar with approximately 50 emitters.

Our new cavity design uses an external dichroic mirror coated for high reflectivity in the near-infrared range and transparent for blue/green light emission is used as output coupling mirror. Ultra-low reflectivity coating on the output facet of a Bookham near infrared laser diode gives less than 0.1% in the wavelength range of ±15 nm, which eliminates the original diode laser cavity allowing the extended longer laser cavity to dominate. A Doric sylindrical lenses is used to collimate the fast axis of the diode. The slow axis micro-lens array consisting of 50 lens is aligned with the individual emitters so as to create 50 beams with 24 µm beam radius focused to the midpoint of a 10 mm-long 5.0 µm period PPLN crystal supplied by Covesion. 1 dimensional micro-lens array which transforms the output from each individual emitter creates a series of parallel output beams (50 beams) with a symmetrical beam waist (radius) of 24 microns at a distance of between 7–10 mm from the micro-lens output surface. The retro-reflection of the IR light is achieved at the output coupler, providing superior stability and allows the complete laser bar (all 50 separate emitters) to lase. A thin film narrow bandwidth IR filter is inserted in the cavity before the PPLN to restrict the spectral laser bandwidth to < 0.1 nm so that optimal frequency conversion can be obtained.

Watts-level of blue light at wavelength of 465 nm and green light at 532 nm was achieved based on our compact novel intra-cavity frequency doubling module design platform. Quasi-phase-matching technique was used by the optimal phase-matching Mg:PPLN bulk with precise temperature control. We will discuss how more stable and efficient ICFD of multi-emitter diode laser could be achieved by enhancing the properties of anamorphic lens, focusing lens, IR filter and polarisation control. Further improvements are now possible through careful design of the lens used on the fast and slow axis beam waists and use of lower-temperature MgO-doped PPLN waveguide. With this blue/green light being generated from 50 emitters creates enormous speckle reduction and will allow this technology to provide disruptive lighting opportunities in laser-based projection displays.

REFERENCES

1. Shchegrov, A. V., et al., "532-nm laser sources based on intracavity frequency doubling of extended-cavity surface emitting diode lasers," *Proc. SPIE*, Vol. 5332, 151, 2004.
2. Watson, J. P., et al., "Laser sources at 460 nm based on intracavity doubling of extended-cavity surface-emitting lasers," *Proc. SPIE*, Vol. 5364, 116, 2004.
3. Hartke, R., et al., "MgO-doped PPLN with cascaded structure for intracavity frequency doubling of optically pumped semiconductor disk lasers," *CLEO/Europe and IQEC 2007 Conference Digest*, paper CD8_2, 2007.

Influence of the Ground Truth Parameters on Forest Polarimetric Scattering Versus Age

Pierre Borderies and Ludovic Villard
ONERA-DEMR, 2-Avue E. Belin, 31055 Toulouse-Cédex, France

Abstract— A forest may be described as a collection of discrete scattering elements. At low frequencies such as P band, most scattered power is originated by trunks and branches. Branches have typical values of a few cm radii and a few m length then at P band their scattering regimes are between the Rayleigh region and the resonance region, so that that the electromagnetic field scattered grows as long as their dimensions grow for each individual element. This paper analyses this effect for the single element as well as a collection of them as a function of the descriptive parameters: radius, moisture content, volume fraction and concentration. Afterwards, a global forest is considered at various stages of growth is considered and the influence of the various descriptive parameters on the polarimetric scattering is analyzed as a function of age.

Nanostructures of Water Revealed in Recent Biophysical Experiments Are They Coherent Domains of Water Predicted by the Quantum Electromagnetic Field Theory (QEMFT)?

Livio Giuliani and Enrico D'Emilia
Laboratorio Inquinamento da Radiazioni e Ultrasuoni, ISPESL, Monte Porzio Catone, Rome, Italy

Abstract— Recent experiments revealed the electromagnetic activity of water around sequences of DNA [1] as well as electron transfer from and to DNA, due to interaction with electromagnetic signals [2, 3] while interactions between microwaves and DNA inducing apoptosis and survival signals has been evidenced some years ago [4].

On the other hand the Ion Cyclotronic Resonance (ICR) effects on aminoacids in aqueous solution has been investigated since 90s years [5–7] and the updated interpretation of these effects involves the QEFMT [8–10].

According to this theory [11–13] water outcomes to be a two-phases liquid, at room temperature, where a coherent phase, made of nanostructures with a size in the order of 100 nm, named Coherent Domains (CDs), is mixed with an incoherent phase, made of single molecules. Furthermore CDs are flickering open structures and single molecules enter and leave them continuously.

Meanwhile very impressive progresses in investigating the structure of water [14–16] and its relationship with life have been done [17–21]. The ICR has been found to be a powerful tool acting interactions with living matter, peculiarly with biomolecules, able to induce maturation and differentiation in stem cells [19, 22].

Advanced experiments investigated the inner structure of water revealing the ordinary presence in liquid water of nanostructures constituted by hundreds or thousand water molecules [23]. The role of these *nanostructures* or *molecular clusters* has been investigated by several authors both in the frame of classical or quantum physics [24, 25]. According with the last two authors the QEMFT appears to provide the best fitting model for the existing two phases of liquid water.

Recent investigations about the floating water bridge, arising between two glasses of water under an electric field in the order 100–1000 kV/m have shown that nanostructures or microstructures of water are circulating along the bridge while it is up [26].

Even if there is not yet fully concordance between the size of clusters experimentally detected and the size of pure water CDs concordance seems to be found with reference to the size of mixed CDs (CD including solute in aqueous solutions), the structure of liquid water predicted by QEMFT has been more and more invocated to explain both the inner structure of liquid water and the interaction of ICR magnetic fields ICR with living matter.

Authors suggest that also the recently discovered electromagnetic signals of DNA are mediated by the CD of water around the DNA segments involved in the electromagnetic activity i.e., in the EZ water in contact with the DNA structure.

REFERENCES

1. Montagnier, L., et al., *Interdiscip. Sci. Comput. Life Sci.*, 2009.
2. Blank, M. and R. Goodman, *J. Cell. Bioch.*, 1999.
3. Blank, M. and R. Goodman, *Pathophys.*, 2009.
4. Marinelli, F., et al., *J. Cell. Physiol.*, 2004.
5. Zhadin, M. N., et al., *Bioelectrom.*, 1998.
6. Giuliani, L., et al., *Biomagn. Res. Tech.*, 2008.
7. Giuliani, L., et al., *J. Biom. Sc.*, 2009.
8. Del Giudice, E., et al., *Bioelectrom.,* 2002.
9. Zhadin, M. N. and L. Giuliani, *Electrom. Biol. Med.*, 2006.
10. Del Giudice, E. and L. Giuliani, *ICEMS Monographs*, 2009.
11. Arani, R., et al., *Int. J. Mod. Phys. B*, 1995.
12. Preparata, G., *Scientific World*, 1995.
13. Del Giudice, E., G. Preparata, and M. Fleischmann, *J. Elec. Chem.*, 2000.
14. Zheng, J. and Pollack, *Phys Rew. E*, 2003.
15. Chai, B., et al., *J. Phys. Chem. B*, 2009.

16. Zheng, J., et al., *J. Coll. Interf. Sc.*, 2009.
17. Zheng and Pollack, *Springer Neth. Books,* 2006.
18. Pollack, G. H. and J. Clegg, *Springer Neth. Books*, 2008.
19. Lisi, A., et al., *Electrom. Biol. Med.*, 2006 and 2008.
20. Voeikov, V. and E. Del Giudice, *Water J.*, 2009.
21. Brizhik, L., et al., *Electrom. Biol. Med.*, 2009.
22. Gaetani, R., et al., *Cardiovasc. Res.*, 2009.
23. Huang, C., et al., *PNAS*, 2009.
24. Tigrek S. and F. Barnes, *ICEMS Monographs*, 2009.
25. Yinnon, C. A. and T. A. Yinnon, *Mod. Phys. Let. B*, 2009.
26. Fuchs, E., et al., *Physics D: Ap. Phys.*, 2007 and 2009.

Session 2P1
Scattering, Diffraction, and Inverse Scattering

Off-axis Scattering Particle Holography: A Numerical Study

Xuecheng Wu[1], **Gérard Gréhan**[2], **Siegfried Meunier-Guttin-Cluzel**[2], **Ruiyang Qu**[1], **Minglun Gu**[1], **Jiaping Xu**[1], **Linghong Chen**[1], **Kunzan Qiu**[1], **and Kefa Cen**[1]

[1]State Key Laboratory of Clean Energy Utilization, Institute for Thermal Power Engineering
Zhejiang University, 38#, Zheda road, Hangzhou 310027, China
[2]LESP, UMR 6614 / CORIA, CNRS, Université et INSA de Rouen, Site du Madrillet
Avenue de l'Université, BP12 76801 Saint Etienne du Rouvray, France

Abstract— In recent years, the digital holographic imaging technique has been developed and demonstrated to be a powerful three-dimensional (3D) diagnostic in a variety of applications. Due to the poor recording resolution of CCD, forward scattering in-line hologram recording is normally adopted, which causes severe speckle noise and large depth of focus in the hologram reconstruction. In this paper, particle holograms at off-axis scattering in-line recording are investigated. A code based on the near field Lorenz-Mie framework capable of calculating particle hologram with arbitrary size, location and refractive index at arbitrary off-axis scattering angle has been developed. Characteristics of off-axis particle holograms at full scattering angle from 0° to 180° will be analyzed. The advantages, limitations and potential of particle characterization (refractive index, location, size, etc.) using off-axis scattering in-line recording will be discussed.

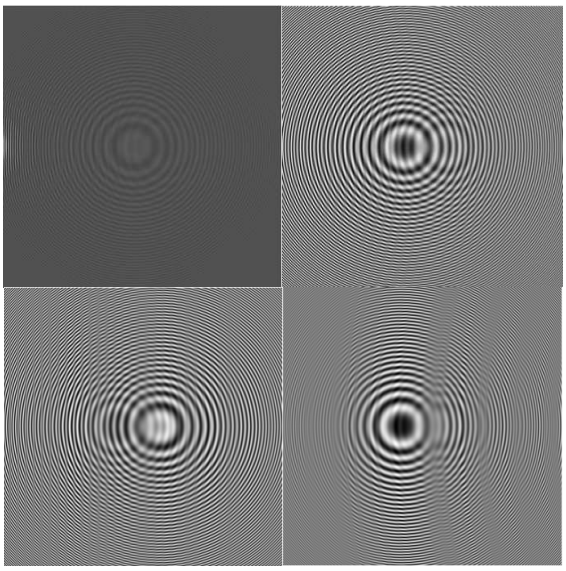

Figure 1: Calculated holograms for a 60 μm water droplet with a 1 mm recording distance at 10.5°, 30°, 90° and 140° scattering angle, respectively.

Electromagnetic Imaging of Water Content in a Column of Soil Using LSM Method

X. Zhang[1], **H. Tortel**[1], **S. Ruy**[2], **and A. Litman**[1]

[1]Aix-Marseille Universite, Ecole Central Marseille, CNRS, Institut Fresnel
Domaine universitaire de St Jerome, Marseille 13013, France
[2]EMMAH, UMR INRA-UAPV 1114, Domaine Saint Paul, Site Agroparc, Avignon, France

Abstract— This paper deals with the inverse scattering problem from scattered field data measured inside a closed microwave scanner system. This system is presently being developed to demonstrate the potentiality of a non-invasive microwave imaging system for volumetric water content monitoring. The final goal is to retrieve soil moisture information as it is an important parameter for understanding fluid flow modeling as well as the water uptake by plant roots. The water content of soil is directly related with the soil permittivity, so retrieving soil moisture information can be accomplished by reconstructing the profile of permittivity. And reconstructing the profile of permittivity from the measured scattered field data is in the framework of inverse scattering problem. It is well known that the quality of the solution found by solving this kind of ill-posed problem strongly depends on the amount of a-priori information introduced in the algorithm. Among the different parameters the a-priori knowledge of the support of the scatterer and its evolution with respect to time is very important. In the present paper we address this problem with the help of a rapid and rather robust method: the Linear Sampling Method (LSM). The evolution of the water content in the soil is simulated thanks to the Richards equations and stored at different time steps. From the values of the water content and using the Dobson model we obtain the evolution of the permittivity with respect to time for a column of soil. The numerical scattered fields are finally generated thanks to a finite element software. In this paper we have tested the LSM for various parameters: one or two sources in the soil, diffusion in a homogeneous or heterogeneous background. The influence of noise in the scattered field data is also taken into account. The favorable imaging results attest that the needed a-priori information can be achieved through application of LSM.

A RCS Reduction Design of Object with Anisotropic Impedance Surface Using Genetic Algorithm

Jing-Jing Yao, **Si-Yuan He**, **Hai-Tao Chen**, **and Guo-Qiang Zhu**
School of Electronic Information, Wuhan University, Wuhan 430079, China

Abstract— In this paper, a universal radar cross section (RCS) reduction design method for the object with anisotropic impedance surface is proposed. It is effective to reduce RCS of the target with anisotropic impedance surface, because the anisotropic material can not only absorb the incident radar wave, but also redistribute the scattering energy in the whole space, by controlling the principal axis of the anisotropic material. The whole procedure of the proposed method is composed of three parts: Universal geometry modelling, high-frequency method and standard genetic algorithm. First, the universal geometry modelling based on triangular meshing can exactly describe the geometry features of the object. Then the high-frequency method Physical optics (PO) is adopted as the forward algorithm to calculate the RCS of the target in desired angle range. Finally, in the standard genetic algorithm, the surface impedances of the target and the direction of the principal axis are considered as the optimized parameters. A reduction example of a square plate which is first illustrated in the paper demonstrates that the method is effective for the RCS reduction. In the following, the study focuses on how to reduce the RCS of a figure-complicated target in desired angle range and the DF31 missile's is taken as the example. As a comparison, the optimization of RCS for the isotropic impedance object is also presented at the same time. The simulation results demonstrate that the RCS of the object with the anisotropic impedance surface can be reduced evidently. It is found that the RCS reduction of the target coated by anisotropic material is better than the object with isotropic material coating in our research.

Asymptotic Waveform Evaluation in Anisotropic Impedance Wedge's Scattering Problem Including the Diffraction of Surface Waves

Ji Li, **Jing-Jing Yao**, **Si-Yuan He**, **and Guo-Qiang Zhu**
School of Electronic Information, Wuhan University, Wuhan 430079, China

Abstract— In this paper, the asymptotic waveform evaluation (AWE) technique is introduced to solve the anisotropic impedance wedge's scattering problem. When a plane wave is obliquely incident on an anisotropic impedance wedge, the diffraction field of the wedge is difficult to obtain by using the classical uniform geometrical theory of diffraction (UTD), because the coupling of the electric field and the magnetic field is complicated. Due to the limitation of the perturbation approach, no satisfactory UTD solution is available for the case of large deviations from normal incidence or the grazing to the edge incidence. In this paper, we starts from the anisotropic impedance boundary conditions (IBC's) and then the AWE technique is proposed to extrapolate the angle of skew incidence based on the Sommerfeld-Maliuzhinets Method. With the AWE technique, the spectral function is expanded by a product of Maliuzhinets special function, meromorphic function and a rational function achieved from the series expression via Pade approximation. When dealing with impedance surfaces, the surface wave (SW) excitation phenomenon must be carefully considered as it may play an important role in the evaluation of the scattered field. Although the diffraction fields of the SW field don't contribute much in the total field, these contributions can't be ignored in some special area (near the wedge face). So the total field is divided into three parts, the geometrical optical (GO) field, the SW field and the diffraction fields of the GO and SW field. The general asymptotic expressions (in UTD forms) for the fields diffracted by anisotropic impedance wedge at skew incidence are illustrated. The numerical result proves that the method can effectively resolve the general scattering problem of anisotropic impedance wedge.

Electromagnetic Scattering from Anisotropic Inhomogeneous Impedance Cylinder of Arbitrary Shape with Generalized Impedance Boundary Condition

Ding-Feng Yu[1], **Ke Li**[2], **Jing-Jing Yao**[1], **and Guo-Qiang Zhu**[1]

[1]School of Electronic Information, Wuhan University, Wuhan 430079, China
[2]Shanghai Institute of Satellite Engineering, Shanghai 200240, China

Abstract— In this paper, the electromagnetic scattering from inhomogeneous anisotropic impedance cylinder of arbitrary shape, whose surface satisfies most general impedance boundary, is investigated by Method of Moments (MoM). Cylinder is illuminated by monochromatic plane wave polarized in the cylinder axis (z-axis). The scattered field is calculated using the electric field integral equation of Stratton-Chu, current continuity equation and two-dimensional Green's function. In consideration of the difficulty in solving the vector integral equation, transformation from cylindrical coordinates to Cartesian coordinates is adopted to simplify the electric field integral equation using impedance boundary condition. For simplicity and high efficiency, pulse basis expansion functions are chosen for MoM. It is noteworthy that not only the induced electric current, but also the induced magnetic current and electric charge make contribution to the scattered field, so the derivative of pulse function will appear in the equation. Differential is replaced by difference to cope with the derivative of pulse function as an approximation. When the integral terms appear in the expression of impedance matrix elements, QDAGS function in the IMSL Libraries is used to ensure the accuracy of the calculation. Once the radius of the cylinder is equal to a constant value, the proposed method in this paper is still valid. Obtained scattering width results are compared with those obtained by analytical method or physical optics (PO) method, and good agreements are observed.

Scintillations in Weak Turbulence of Annular Beams Whose Individual Components Are Incoherent

Y. Baykal[1], **H. T. Eyyuboğlu**[1], **and Y. Cai**[2]

[1]Electronic and Communication Engineering Department, Çankaya University
Öğretmenler Cad. No. 14, Yüzüncüyıl, Balgat 06530, Ankara, Turkey
[2]School of Physical Science and Technology, Soochow University, Suzhou 215006, China

Abstract— The scintillation index, arising from the intensity fluctuations in weak atmospheric turbulence of annular beams whose individual components are incoherent, is formulated. For such beams whose annularities are obtained by varying the source sizes of the individual beams, evaluations show that at very small sized beam structures, thinner beams possess smaller scintillations. As the sizes increase, the scintillation index values of thick and thin beams approach each other, eventually exhibiting the same scintillation behavior at large sized beam structures. Examination of the intensity fluctuations of the annular beams, whose individual incoherent components are at the same size but at different magnitudes, yield reverse behavior such that at very small sized beam structures, thicker beams possess smaller scintillations, however the scintillation values are very close to each other. Again, for large sized beams, the scintillation index values of thick and thin beams approach each other, eventually exhibiting the same scintillation behavior at large sized beam structures. Comparing the scintillation indices of annular beams whose individual components are incoherent to those of traditional annular beams of coherent components, it seems that for large sized beams, incoherently added beams are advantageous, however, the reverse is valid for very small sized beam structures.

An Application of a Fixed Point Iteration Method to Object Reconstruction

F. S. V. Bazán[1], **K. H. Leem**[2], **and G. Pelekanos**[2]

[1]Federal University of Santa Catarina, Brazil
[2]Southern Illinois University, Edwardsville, USA

Abstract— Kirsch's factorization method is a fast inversion technique for visualizing the profile of a scatterer from measurements of the far-field pattern. The mathematical basis of this method is given by the far-field equation, which is a Fredholm integral equation of the first kind in which the data function is a known analytic function and the integral kernel is the measured (and therefore noisy) far field pattern. We present a Tikhonov parameter choice approach based on a fast fixed point iteration method which constructs a regularization parameter associated with the corner of the L-curve in log-log scale. The performance of the method is evaluated by comparing our reconstructions with those obtained via the L-curve and we conclude that our method yields reliable reconstructions at a lower computational cost than the L-curve.

Frequency Dependence of Image Reconstruction of Linear Sampling Method in Electromagnetic Inverse Scattering

G. H. Li, **X. Zhao**, **and K. M. Huang**
College of Electronics and Information Engineering, Sichuan University, Chengdu 610064, China

Abstract— The inverse electromagnetic scattering problem, one of the classical inverse problems, is to determine the geometrical and/or physical properties (such as position, size, shape, permittivity, conductivity and permeability) of a scatterer from the knowledge of the scattered field or its far-field pattern. With increasing application demands in remote sensing, non-destructive testing, medical imaging and geographical exploration, the inverse EM scattering problems have attracted great research interest.

However, characteristics of severe ill-posedness and strong non-linearity in the EM inverse scattering problem lead to the difficulties in theoretical research and numerical implementation. To overcome the tough problems, the traditional approaches based on the weak scattering approximation methods or the non-linear optimization schemes combined with regularization techniques are adopted. But these classical methods have deficiency in computational speed and/or accuracy. Moreover, they also require a priori knowledge of the number of scatterers, the boundary conditions and so forth. Linear sampling method, however, has the advantages of independence on any a priori information, a notable computational speed and high accuracy of reconstruction. In addition, the parallelization of computation is very easy to perform due to its intrinsic parallel feature.

Application of the linear sampling method in two-dimensional and three-dimensional reconstruction is presented in this paper. Under the circumstance of a specified set of incident and observation angle, shape reconstruction is mainly discussed when the scatterer is irradiated at different frequency within a range. The procedure of numerical experiment is performed as follows: firstly, scattered fields and their far field pattern of perfectly conducting cylinder and media cylinder are attained from the direct scattering computation. Secondly, a discrete equation is established from a linear Fredholm integral equation of the first kind, which is an equivalence of the non-linear inverse scattering problem without any approximation. Thirdly, the discrete equation is solved at each sampling point, and the Euclidean norm of the resulted vector is computed. Finally, the shape can be reconstructed by plotting gray values transformed from the norms.

The numerical results indicate that no matter whether the cylinder is impenetrable or not, the reconstruction resolution varies remarkably with the changing of frequency of the incident wave. And a conclusion can be drawn that linear sampling method is highly dependent on frequency. In fact, for a given scatterer with particular dimension and of specified shape, an optimum frequency range exists in which the reconstruction resolution would be better than that of other frequencies.

A further understanding of the behavior of linear sampling method can be obtained according to this paper, meanwhile, a guide is provided as for how to choose a sensible frequency range in the application of linear sampling method.

Focusing Properties of a Twisted Gaussian Schell-model Beam in Turbulent Atmosphere

Shijun Zhu and Yangjian Cai
School of Physical Science and Technology, Soochow University
Suzhou 215006, China

Abstract— Propagation of a twisted Gaussian Schell-model (GSM) beam through a thin lens in a turbulent atmosphere is formulated. Focusing properties including focal shift and spectral shift in turbulent atmosphere are investigated in detail. It is found that the focal shift and spectral shift of a focused twisted GSM beam are closely related to the twist phase, coherence width of initial beam and the structure constant of the turbulent atmosphere. The relative focal shift increases as the absolute value of the twist factor of initial beam and the structure constant of turbulent atmosphere increase or as the coherence width of initial beam decreases.

Diffraction Properties of Partially Coherent Elegant High-order Beam

Fei Wang[1], **Yangjian Cai**[1], **Halil T. Eyyuboğlu**[2], **and Yahya Baykal**[2]

[1]School of Physical Science and Technology, Soochow University, Suzhou 215006, China
[2]Department of Electronic and Communication Engineering, Çankaya University
Öğretmenler Cad. 14, Yüzüncüyıl Balgat Ankara 06530, Turkey

Abstract— Partially coherent elegant higher-order beam is introduced as a natural extension of coherent elegant higher-order beam. An explicit and analytical formula is derived for the cross-spectral density of a partially coherent higher-order beam propagating through paraxial ABCD optical systems. The intensity and diffraction properties of a partially coherent elegant higher-order beam in free space are studied as a numerical example. We find that the initial spatial coherence affects the intensity and diffraction properties of a partially coherent elegant higher-order beam upon propagation, and a partially coherent higher-order beam spreads more slowly than a partially coherent standard higher-order beam, which has potential application in free-space optical communications.

Improvements Algorithms to Compute the Radar Cross Section of Electrically Large Complex Targets Considering n-bounces

Lorena Lozano, Ma Jesús Algar, Iván González, and Felipe Cátedra
Computer Sciences Department, Universidad de Alcalá, 28871 Alcalá de Henares, Madrid, Spain

Abstract— This abstract presents a new iterative algorithm to accelerate the ray-tracing for computing efficiently monostatic and/or bistatic radar cross section (RCS) of electrically large complex targets (metallic, dielectric and RAM (Radar Absorbing Material)) considering multiple bounces. The iterative algorithm is based on Physical Optics (PO), the Equivalent Currents Method (ECM), and Geometrical Optics (GO) and on a combination of the Angular Z-Buffer (AZB), the Space Volumetric Partitioning (SVP) and the Depth-Limited Search Method. Complex targets are defined by a 3D geometrical file that uses flat and/or parametric surfaces, in particular NURBS (Non- Uniform Rational B-Spline).

To achieve the goal, the process for computing the RCS of complex targets is divided into two steps: Pre-processing step where the AZB and SVP matrices are filled and the shadowing test is analyzed. Some improvements in hidden process have been developed to assure more reability in the results. Calculating step where the potential surfaces that can contribute to the final RCS value are analysed and their contributions are calculated.

The new algorithm, implemented in a new code called PROGCROS, is extremely efficient to compute the RCS of large and complex bodies modeled by a high number of flat surfaces taking into account ray paths with multiple bounces. POGCROS includes also an useful user interface, that permits to input and editing the geometry files of targets generated by many CAD tools, or generating these files from scratch.

In order to verify the new iterative algorithm several results will be presented. In this abstract, a complex target has been studied. The geometrical model has been defined with 4225 flat surfaces. The results are presented with different reflection levels, horizontal polarization and frequency 2 GHz at $\theta = 80°$, sweeping for $\phi = 0°$ to 360° and for 1000 directions. The case has been run in a SUN V40Z server using only 224 MB of RAM. The CPU time used to compute the monostatic RCS is 22, 67, 87 and 110 minutes, considering 2, 6, 10 and 20 reflections, respectively.

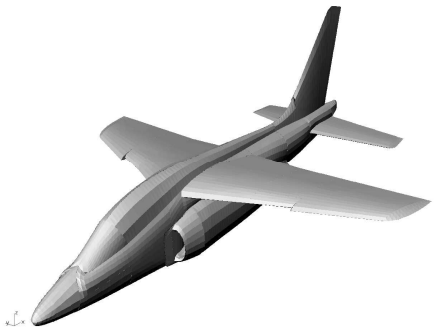

Figure 1: Airplane defined with 4225 surfaces.

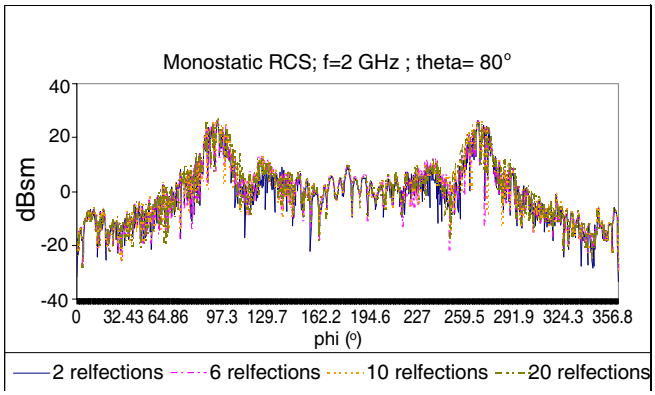

Figure 2: Monostatic RCS with different levels of reflections.

Diffraction of Apertured Gaussian Beams

Xiaoling Ji
Department of Physics, Sichuan Normal University, Chengdu 610068, China

Abstract— The diffraction of apertured Gaussian beams propagating in free space and in atmospheric turbulence is studied. The analytical expression for the average intensity of apertured Gaussian beams is derived, and average intensity distributions are examined by using numerical calculation examples. It is shown that in free space there exist lobes due to the aperture diffraction. However, the average intensity distribution becomes a Gaussian-like profile in turbulence. On the other hand, the analytical expression for the mean squared beam width of apertured Gaussian beams is also derived. It is found that the beam spreading depends on the aperture diffraction in free space and the strength of turbulence. The beam spreading due to aperture diffraction will reduce the effect of turbulence, but the turbulence will dominate the beam spreading when the propagation distance is long enough.

Radar Cross Section of a Cavity in a Finite Elliptic Cylinder

N. Altın[1] and E. Yazgan[2]

[1]Turkish Aerospace Industries, Inc., Ankara, Turkey
[2]Electrical & Electronics Engineering Department, Hacettepe University, Turkey

Abstract— In this study, the part of the cockpit of the air vehicle in the far field due to the plane wave of warning, scattering fields from the cockpit part is assumed to be radiated in free space. Fuselage of the air vehicle is modeled as finite elliptical cylinder and a large cavity is mounted in the sidewall of a finite elliptical cylinder. The shape of the cockpit of the air vehicle is modeled close to the real model. A Radar Cross Section (RCS) analysis of cockpit part is calculated by using together Shooting and Bouncing Ray (SBR) and Geometrical Optics (GO) methods. RCS analysis of elliptical cylinder is calculated by using a Uniform Geometrical Theory of Diffraction (UTD) and Physical Optics (PO) methods. Shooting and Bouncing Ray (SBR) using for analyses does not limit the form of model. By using of proposed method, outputs for cockpit part and fuselage RKA analyses were provided.

Session 2P2
Electromagnetic Wave in the Materials and Dispersion Simulation for Cloak Metamaterials and Photonic Crystals

A Novel GL Double Layer Electromagnetic Cloaks in Broad Frequency Band and Reciprocal Law

Ganquan Xie, **Jianhua Li**, **Feng Xie**, **and Lee Xie**
GL Geophysical Laboratory, USA

Abstract— In this paper, we propose the following physical statements. (1) In the domain consist of free space, single layer cloak and its cloaked concealment with normal material, the two sources reciprocal law is damaged. (2) In the domain consist of free space, single layer cloak and its cloaked concealment with some special double negative refractive index metamaterial, the two sources reciprocal law is recovered, but the cloak invisibility function is lose. (3) In the domain consist of free space, GL double layer cloak and its cloaked concealment with any material, the two sources reciprocal law is satisfied, and the cloak invisibility function is complete, robust and sufficient. The paper is for answering the question on the reciprocal and cloak in PIERS 2009, Moscow.

High Transmission Y-shaped Waveguides in 2D Photonic Crystals with Square Lattice

Wu Yang[1, 2], **Xiaoshuang Chen**[1], **Xiaoyan Shi**[2], **and Wei Lu**[1]

[1]National Laboratory for Infrared Physics
Shanghai Institute of Technical Physics, Chinese Academy of Sciences
500 Yutian Road, Shanghai 200083, China
[2]College of Science, Henan University of Technology, Zhengzhou 450001, China
[3]College of Science, Information Engineering University of PLA, Zhengzhou 450001, China

Abstract— Photonic crystal waveguides, line defects formed in photonic crystal, are expected to provide low loss transmission and well-confined branches when being operated at wavelengths within the photonic band gap. They can play an important role in future optical circuits. Waveguide branches split the input power into the output waveguides without significant reflection or radiation losses. T-shaped and Y-shaped photonic crystal waveguides of highly efficient transmission have already been proposed in past years.

Ordinary, T-shaped photonic crystal waveguide is based on square lattice and Y-shaped photonic crystal waveguide is based on triangular lattice. In this paper, we design a high transmission Y-shaped photonic crystal waveguide based on square lattice. We create an input waveguide by removing a single row of rods and an 135° output waveguide by removing two row of rods. We add additional rods in 135° output waveguide edge for increasing transmission coefficient. The coupled mode theory is used to analyze the transmission properties. Based on the coupled mode theory, two additional rods are placed between the input waveguide and the 135° output waveguide to improve transmission coefficient. A dipole located at the entrance of the input waveguide creates a pulse with a Gaussian envelope in time. The field amplitude is monitored inside the guide at two points, one before the Y-junctions and one after Y-junctions. Although most of the light reaching the edge of the computational cell is absorbed by the boundaries, some light is reflected back from the ends of the waveguide. By using a sizable computational cell of 120×20 lattice constants and positioning each monitor point appropriately, we can distinguish and separate all the different pulses propagating in the cell. Four pulses are sent down the waveguide, and each covers different ranges of frequencies. By the Fourier transforms, the transmission coefficients are obtained for each frequency of the pulses. The combined transmission and the reflection coefficients add up to unity to within an accuracy of 0.1%. It indicates that our calculation gives an accurate description to the response function of the waveguide branch. The numerical simulation results by the finite-difference time-domain method shows that total transmission up to 99% is obtained.

Exploration of Electromagnetic Interferences on GPS Reception in PDA Phone

Yao Huang Kao[1] and Hui Chun Yang[2]

[1]Department of Communication Engineering, Chung Hua University
Hsin-chu, Taiwan 30050, China
[2]Department of Communication Engineering, National Chiao Tung University
Hsin-chu, Taiwan 30050, China

Abstract— Recently, personal digital assistant (PDA) as a wireless platform is requested to install multi functions, such as GPS, Bluetooth, and camera. In the meantime, the platform is requested to be small size, light weight, and low power consumption. The sensitivity is by no means affected by the digital and analog functions. The deteriorations are from conductive and coupling noises. In this study, the sensitivities in GPS and 2G/3G are investigated. The sources are identified step by step by turning on each application function. It is found that in GPS the key factors are from digital functions of camera and SD card. Both are allocated near the GPS antenna, but the solutions are different. The SD card, which is outside the metal closure, generates the conductive noises. As for the camera, it resides in the metal closure. Many steps are utilized to enhance the grounding and bypassing. The leakage from slit during molding is also avoided. After the solutions, the results are improved as shown in Table 1. Same phenomena are also found in the reception of 2G/3G operation. It will be discussed in the conference.

Table 1: Deterioration factors on GPS C/N ratio.

GPS C/N test report			
	Test Item	Original Degrade	Add Solution
1	GPS_Only (initial C/N=41 dB)	0dB	0
2	2G/3G network on	-0.5dB	-0.5dB
3	WiFi_on	-0.5dB	0
4	Camera_on	-1.5~3 dB	0
5	SD_card (read/write)	-4 dB	-0.5
6	2G/3G +WiFi (on)	-0.5 dB	0
7	Camera +2G/3G +WiFi (on)	-2 dB	-1
8	SD_card +2G/3G +WiFi (on)	-4.5~5 dB	-1
9	SD_card +2G/3G +WiFi+ Camera (on)	-5~6 dB	-1

Surface Plasmon Resonance Electro-optic Light Modulator Based on Polymer Grating Coupler

Wen-Kai Kuo and Meng-Ting Chen
Department of Electro-Optics Engineering, National Formosa University
64 Wenhua Rd., Huwei, Yunlin 63208, Taiwan, R.O.C.

Abstract— In this study, an electro-optic light modulator based on grating-coupled surface plasmon resonance (SPR) is numerically investigated using finite-difference time-domain (FDTD) simulation. A new grating coupler structure is proposed and compared with the conventional one. The numerical simulation results show that the new structure has higher modulation efficiency. Since the SPR is highly sensitive to changes in the refractive index on the metal surface, this technique has been extensively applied to bio-chemical sensing [1]; moreover, it has also played an important role in optical modulators. Further, the SPR technique can be combined with an electro-optic (EO) polymer in order to implement a simple and high-speed optical modulator. The principle of the modulator is based on electrically varying the refractive index of the EO polymer and hence controlling the efficiency of coupling the incident TM light beam onto the surface plasmons. This type of device has been theoretically described first [2] and experimentally demonstrated later with different advancements [3]. Here, we propose an EO polymer modulator based on a new SPR grating coupler structure as shown in Fig. 1. The new structure can be divided into two parts: The top glass substrate with an indium-tin-oxide (ITO) layer and the grating structure on the downside, and the bottom glass substrate coated with dielectric, gold, and silver films on the upside. The refractive indexes of all materials in this structure for simulation are as follow: (from bottom to top): $n_0 = 1.515$ (glass), $n_1 = 0.14 + 4.15i$ (silver), $n_2 = 0.166 + 3.15i$ (gold), $n_3 = 1.457$ (dielectric passivation, SiO_2), $n_4 = 1.489$ (polymer), and $n_5 = 1.72$ (ITO). The thicknesses of silver, gold, SiO_2, polymer, and ITO are 100 nm, 5 nm, 125 nm, 1 m and 100 nm, respectively. Its FDTD simulation result is as shown in Fig. 2. The result shows that the resonance angle shifts significantly for a small index increment of 0.001 in the EO polymer grating structure.

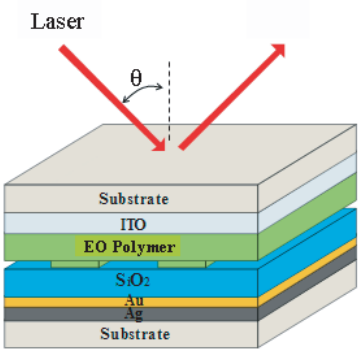

Figure 1.

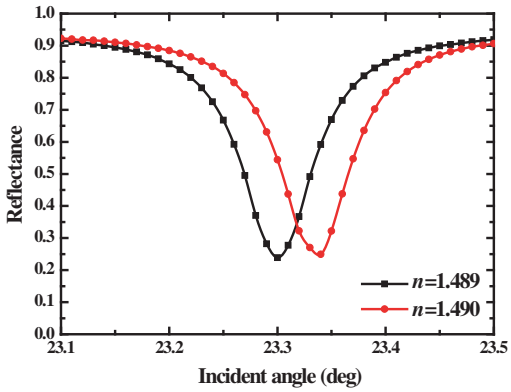

Figure 2.

REFERENCES

1. Homola, J., S. S. Yee, and G. Gauglitz, "Surface plasmon resonance sensors: Review," *Sensor and Actuators B*, Vol. 56, 3, 1999.
2. Schildkraut, J. S., "Long-range surface plasmon electrooptic modulator," *Appl. Opt.*, Vol. 27, 4587, 1988.
3. Solgaard, O., F. Ho, J. I. Thackara, and D. M. Bloom, "High frequency attenuated total internal reflection light modulator," *Appl. Phys. Lett.*, Vol. 61, 2500, 1992.

Theoritical Analysis of Some Homogenized Metamaterials and Application of PML to Perform Cloaking and Back-scattering Invisibility

P. H. Cocquet, V. Mouysset, and P. A. Mazet
Department of Information Treatment and Modelization (DTIM), ONERA Toulouse, France

Abstract— Electromagnetic phenomenons in homogenized chiral photonic crystals can be modelized [1] by the following Drude-Born-Fedorov (1) system (1)–(2):

$$\begin{cases} \text{Find } (e,h) \in H(\text{curl},\Omega)^2 \text{ such that :} \\ (K_0(p,x)+K_1(p,x)\mathbb{M})\begin{pmatrix} e \\ h \end{pmatrix} = f,\ x\in\Omega \\ \mathbf{n}(x)\times(e+\Lambda(x)\mathbf{n}(x)\times h)=0,\ x\in\partial\Omega\ , \end{cases} \tag{1}$$

$$\mathbb{M} = \begin{pmatrix} 0 & -\nabla\times \\ \nabla\times & 0 \end{pmatrix},$$

$$K_0(p,x) = \begin{pmatrix} p[\varepsilon] & 0 \\ 0 & p[\mu] \end{pmatrix}, \tag{2}$$

$$K_1(p,x) = \begin{pmatrix} \mathbb{I}_3 & p[\beta][\varepsilon] \\ -p[\beta][\mu] & \mathbb{I}_3 \end{pmatrix}.$$

where e and h are the electric and the magnetic fields, the permitivity $[\varepsilon]$, the permeability $[\mu]$ and the chirality $[\beta]$ are the homogenized parameters, e.g., [1], of the media which are depending smoothly both of $p = iw$, w is the pulsation, and x, $f \in L^2(\Omega)^6$, Ω is a bounded domain in $\mathbb{R}^3$ with C^1 boundary whose outward unitary normal is denoted $\mathbf{n}$ and $\Lambda \in \text{Lip}(\Omega, \mathcal{L}(\mathbb{C}^6))$ such that $\text{Re}(\Lambda(x)+\Lambda^*(x))$ is nonnegative.

However, the well-posedness of this kind of system often remains a steady point. Futhermore, lots of systems modelling electromagnetic phenomenons in chiral metamaterials can be formulated with the 1 system (1) or with the Maxwell's system in presence of homogenized metamaterials by setting $K_1 = \mathbb{I}_6$ in (1).

So, in this paper, we are going to study a generalized 1 problem (1) where $(K_j)_{j=0,1}$ depend both on $x \in \Omega$ and on $p \in D \subset \mathbb{C}$. Under some regularity assumption on x and behavior hypothesis on w which have been stated in [3] and are compatible with some models in the literature as [1], we will show that system (1) is L^2 well-posed for almost all p in D and, as a consequence, Maxwell's system in presence of homogenized metamaterials will be well-posed too. Corollary from this, we show theorically that Maxwell's equations with some general convex absorbing boundary conditions of PML type [2] is well-posed.

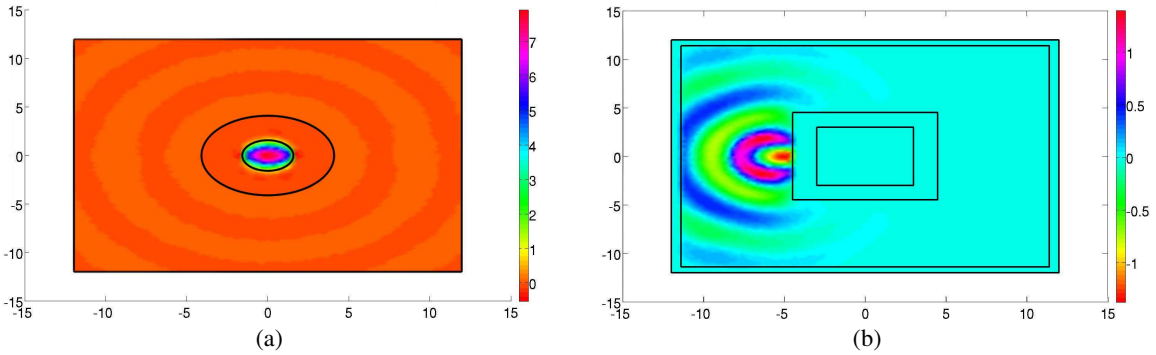

Figure 1: Cloaking and back-scattering invisibility.

This result lead us to investigate some properties of PML, like cloaking and back-scattering invisibility. At last, some numerical results, using finite volumes method for T.M-Maxwell's equations, will be presented to illustrate these cloaking and back-scattering invisibility effects (see Figure 1).

REFERENCES

1. Guenneau, S. and F. Zolla, "Homogenization of 3D finite chiral photonic crystals, science direct," *Physica B*, Vol. 394, 145–147, 2007.
2. Lassas, M., J. Liukkonen, and E. Somersalo, "Complex riemanninan metric and absorbing boundary conditions," *J. Math. Pures Appl.*, Vol. 80, No. 7, 739–768, 2001.
3. Veselago, V. G., "The electrodynamics of substance with simultaneously negative values of ε and μ," *Soviet Physics USPEKHI*, Vol. 10, No. 4, 1968.

Nonlinear Dynamics and Microwave Frequency Comb Generation in an Optical Pulse-injected Semiconductor Laser

Fan-Yi Lin and Yu-Shan Juan
National Tsing Hua University, Taiwan

Abstract— We study the nonlinear dynamical characteristics of an optical pulse-injected semiconductor laser both numerically and experimentally. A slave laser is injected by an optical pulse train generated from a master laser with optoelectronic feedback. By changing the delay time in the optoelectronic feedback loop, optical pulses with different repetition rates are obtained. By injecting the optical pulses generated into the slave laser, frequency locking states and chaos oscillation states are observed and ultra wideband microwave frequency combs are generated. Within a spectral flatness of ±5 dB, microwave frequency combs with bandwidths more than 20 GHz are obtained and a single sideband phase noise of −60 dBc/kHz (−90 dBc/Hz estimated) in the first harmonic is achieved. Compared with the microwave frequency comb generated by a negative optoelectronic feedback semiconductor laser making use of the harmonic frequency-locked states, the microwave wave frequency combs generated have much lower nonharmonic spurious noise and wider bandwidths. We also measure the corresponding pulses generated in the time domain, which have pulsewidths of 24 ps and timing jitter of 18.7 ps, which are comparably shorter and more stable than the pulses used for injection. Utilizing the microwave frequency combs generated, application of signal broadcasting is also explored. To understand the role of the DC optical component in the dynamics of pulse injection, the characteristics of the slave laser under different DC injection levels are therefore investigated. Under different DC injection levels, frequency multiplexing and frequency division are both observed. The experimental results match the simulation results very well.

Surface-wave Model of the Extraordinary Optical Transmission

Haitao Liu[1] and Philippe Lalanne[2]

[1]Key Laboratory of Opto-electronic Information Science and Technology, Ministry of Education
Institute of Modern Optics, Nankai University, Tianjin 300071, China
[2]Laboratoire Charles Fabry de l'Institut d'Optique, CNRS, Université de Paris-Sud
Campus Polytechnique, 91127 Palaiseau cedex, France

Abstract— Extraordinary optical transmission (EOT) [1] through a two-dimensional subwavelength hole array drilled in a noble-metal membrane has significant applications in subwavelength lithography, chemical sensing and optoelectronic detection. The explanation of the phenomenon is an interesting but difficult problem and is important for understanding and tailoring the optical properties of textured metallic surfaces that play a central role in the emerging field of plasmonics. On the basis of the classical modal expansion method, the EOT phenomenon is associated with the excitation of a surface Bloch mode on the two membrane surfaces [2], which reinforces the surface fields and thus enhances the tunneling of light through holes. However, such a surface Bloch mode arises from a collective effect of all the holes of the array and the physical origin of its formation needs clarifying. To overcome this deficiency, other explanations are involved with some kinds of surface waves like the surface plasmon polariton (SPP) and other waves, which are assumed to be first excited at individual apertures and then propagate on the metal surface before being further scattered by nearby apertures, but hot debate exists among different views [3–5]. Here we report an analytical model of EOT that relies on a multi-scattering of two surface waves, the SPP and a so-called quasi-cylindrical wave (CW) [6]. By treating the generation and the multi-scattering of the surface waves in a proper way, the model can predict the EOT phenomenon in a quantitative manner compared with the fully-vectorial data obtained by solving the Maxwell's equations. Our model gives insight into the EOT physics and thus helps in intuitively designing the relevant devices and in reconciling the previous different views.

REFERENCES

1. Ebbesen, T. W., et al., "Extraordinary optical transmission through sub-wavelength hole arrays," *Nature*, Vol. 391, 667–669, 1998.
2. Martin-Moreno, L., et al., "Theory of extraordinary optical transmission through subwavelength hole arrays," *Phys. Rev. Lett.*, Vol. 86, 1114–1117, 2001.
3. Gay, G., et al., "The optical response of nanostructured surfaces and the composite diffracted evanescent wave model," *Nature Phys.*, Vol. 2, 262–267, 2006.
4. García-Vidal, F. J., S. G. Rodrigo, and L. Martín-Moreno, "Foundations of the composite diffracted evanescent wave model," *Nature Phys.*, Vol. 2, 790, 2006.
5. Lalanne, P. and J. P. Hugonin, "Interaction between optical nano-objects at metallo-dielectric interfaces," *Nature Phys.*, Vol. 2, 551–556, 2006.
6. Liu, H. T. and P. Lalanne, "Microscopic theory of the extraordinary optical transmission," *Nature*, Vol. 452, 728–731, 2008.

An LCAO Description of Plasmonic Bands

Kazuaki Sakoda
Quantum Dot Research Center, National Institute for Materials Science
1-1 Namiki, Tsukuba 305-0044, Japan

Abstract— Metallic photonic crystals may have peculiar photonic bands created by structural and plasmonic electromagnetic resonances. A simple example is the extremely flat bands found in a square array of metallic cylinders with a dielectric constant of the Drude type [1], which are shown in Fig. 1. The flat bands originate from plasmonic resonant states that are strongly localized around the cylinder as shown in Fig. 2. Due to their localization, the LCAO (linear combination of atomic orbitals) description may be a good approximation for the electromagnetic eigenmodes. In this study, we examine the accuracy of the LCAO approximation with the resonant states calculated by the Mie theory as a basis set. We also discuss the extension of this method to the case of the structural resonance that is relevant to metamaterials and left-handed materials, and show that the idea of "effective negative permeability", which may have a fundamental difficulty in its rigorous definition, is not necessarily required for the description of the electromagnetic waves in these materials.

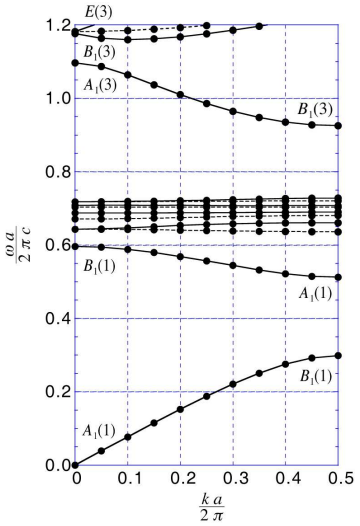

Figure 1: Photonic bands of a square lattice of metallic cylinders.

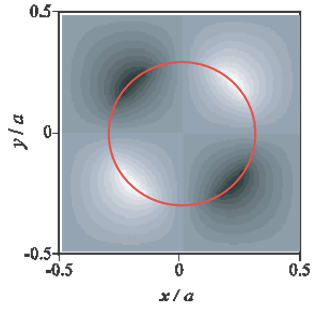

Figure 2: Magnetic field distribution of a B_2 mode on the Γ point. The red circle denotes the cylinder.

REFERENCES

1. Ito, T. and K. Sakoda, "Photonic bands of metallic systems. II. Features of surface plasmon polaritons," *Phys. Rev. B*, Vol. 64, 045117, 2001.

Localization of Electromagnetic Energy in a Finite Region with Complementary Media

Chao Li, **Xiao Liu**, **and Fang Li**
Institute of Electronics, Chinese Academy of Sciences, Beijing, China

Abstract— It is well known that two complementary media can produce an ideal optical annihilation to each other, and therefore cancel a certain volume of space in an optical system. This concept has aroused great interest in applied physics and optics society, and has motivated various applications, such as the "perfect lens" with super-resolution abilities, the "super-scatterers" to enhance the scattering of an object, the "anit-cloaks" to enlarge the scattering cross section of a cloaked object, and the "novel cloaks" to conceal objects at a distance outside the cloak shells. In this paper, we propose a new kind of devices to localize electromagnetic (EM) energies and fields in a finite region. The idea is based on combining the concepts of complementary media and transformation optics. With such devices, we can completely confine all the EM fields excited by a source in a finite region with no power radiating outwards the region. Hence, an open resonant cavity with finite volume can be formed. The complementary media is designed based on the form invariant transformation of Maxwell's equations in different spaces. The localized modes and the anomalous resonance inside such devices were studied through exact analysis. With lossless complementary media, the fields outside the confined region are verified to be exactly zero. Numerical simulations based on finite-element method (FEM) were also performed to support our theoretical predictions. The new energy-localization devices proposed in this paper can be readily realized by metamaterials (MTMs) and may have potential applications in high-quality optical devices.

Angle- and Thickness-dependent Photonic Band Structure for a One-dimensional Superconducting Photonic Crystal

Chien-Jang Wu[1] **and Tzong-Jer Yang**[2]

[1]Institute of Electro-optical Science and Technology, National Taiwan Normal University
Taipei 116, Taiwan
[2]Department of Electrical Engineering, Chung Hua University
Hsinchu 300, Taiwan

Abstract— The angle- and thickness-dependent photonic band structures in a one-dimensional superconducting photonic crystal are theoretically investigated based on the Bloch theorem and transfer matrix method. The band structure is studied near and below the threshold frequency at which the superconducting material has a zero permittivity. The gap structure is analyzed as a function of the thicknesses of the two constituent superconducting and dielectric materials. In the angular dependence of the band structure, it is found that, in the TM-polarization, there exists a strongly localized superpolariton band in the vicinity of the threshold frequency. Based on the calculated angle-dependent gap map, the existence of the omnidirectional photonic bandgap in such a photonic crystal is also found.

Dual Band Antenna for HSDPA USB Dongle

Yao Huang Kao, **Jhih Liang Lu**, **and Hui Chun Yang**
Department of Communication Engineering, Chung Hua University
Hsin-chu 30050, Taiwan, R.O.C.

Abstract— Recently, High Speed Downlink Packet Access (HSDPA), which is a part of 3GPP release 5 of W-CDMA, is proposed to enhance the broadband multimedia mobile communication. It enables the wireless downlink peak rate up to 14 Mbps. In this study, the small antenna shown in Fig. 1 in USB dongle with HSDPA capability is developed, which should involve the services from 2 G to 3.5 G. Two shunted meander lines are utilized to achieve the resonances at the respective bands. The high band is allocated on the top face. The low band antenna is wounded around three lateral faces to increase the path length. The current distribution is simulated by the 3D EM software. The bandwidth is broadened by shaping the regions with high current density. The size of the Antenna Carrier is 15 mm × 21 mm × 7 mm. Curve I and II in Fig. 2 are the return loss without and with notebook grounding effect, respectively. The return loss at high band 1700 MHz∼2200 MHz and low band 824∼960 MHz has −5 and −3 dB, respectively. The radiations are also measured to verify the simulations. The radiation efficiency is larger than 65% to cover the DCS1800, PCS1900, and UMTS2100. As for the lower band GSM850 and EGSM900 the radiation efficiency is at least larger than 54%. The return losses with and without note book effect are also studied and will be presented in the conference.

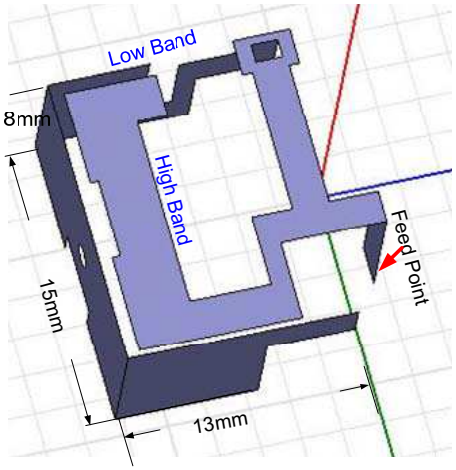

Figure 1: Antenna size and shape.

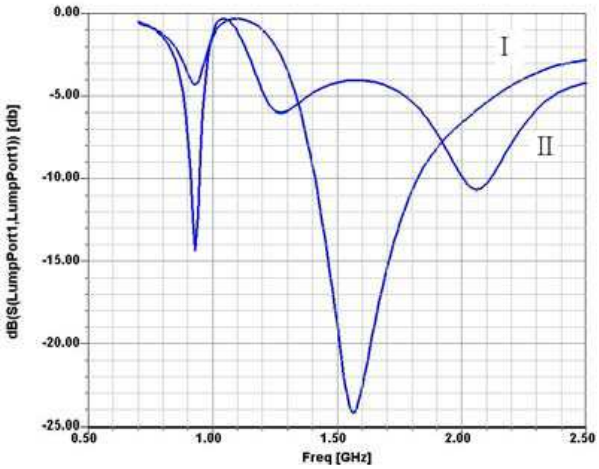

Figure 2: Return loss from 0.8 to 2.4 GHz.

Numerical Investigation on Graphene-like Two-dimensional Microwave Photonic Crystals

Yunhui Li[1,2], **Yun Jiang**[1,2], **Haitao Jiang**[1,2], **and Hong Chen**[1,2]

[1]Pohl Institute of Solid State Physics, Tongji University, Shanghai 200092, China
[2]Shanghai Key Laboratory of Special Artificial Microstructure Materials and Technology, China

Abstract— In this paper, numerical simulations are carried out to verify the transmission properties of Dirac point in Graphene-like two-dimensional (2D) microwave photonic crystals (PCs). Extremal transmission is found in this PCs, which is inversely proportional to the longitudinal dimension (L) of the PCs. Dirac point is a conical singularity where two bands of some special 2D PCs (like triangular or honeycomb lattices) touch as a pair of cones. At Dirac point, the band gap may become vanishingly small at the corners of Brillouin zone. It is also found that, these 2D PCs have some unusual properties, such as frequency dependent conductivity, collective excitations (plasmons), thermoplasma polaritons, and so on. They are also an excellent candidate for experimental demonstration of the quantum relativistic effect, such as Zitterbewegung effect and Klein paradox. In this work, 2D microwave PCs hiring triangular lattices is investigated by CST Microwave Studio. The 2D PC is consisting of air holes periodically drilled on dielectric substrate of microstrip lines (Fig. 1). The simulated transmissions (T) (Fig. 2) show clearly there does exist a very narrow gap with its transmission inversely proportional to the propagating distance of microwave inside the photonic crystal (L). The linear relationship between T and $1/L$ is also shown in Fig. 3, which demonstrates the property of Dirac Point clearly. Furthermore,

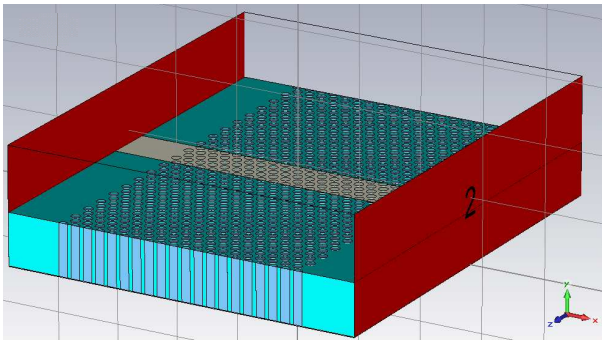

Figure 1.

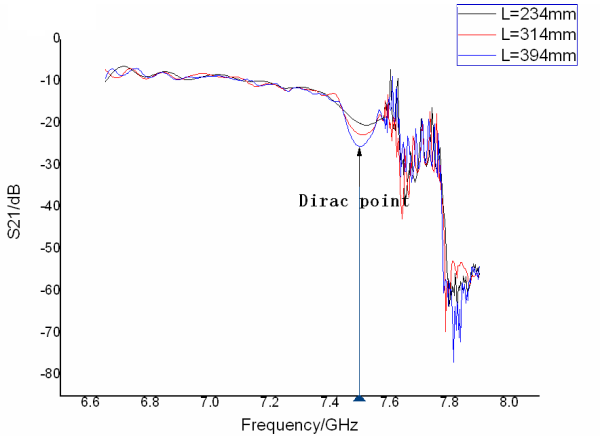

Figure 2.

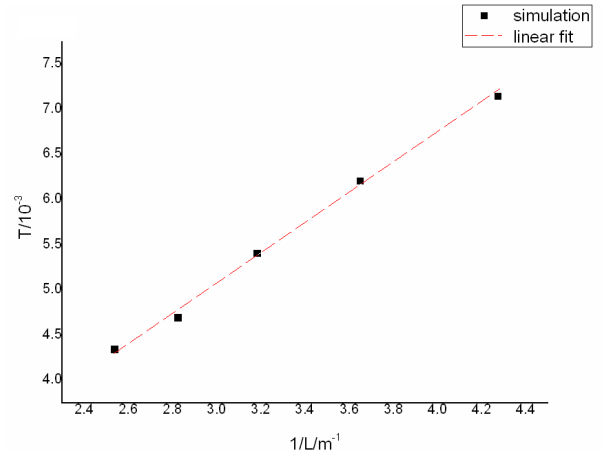

Figure 3.

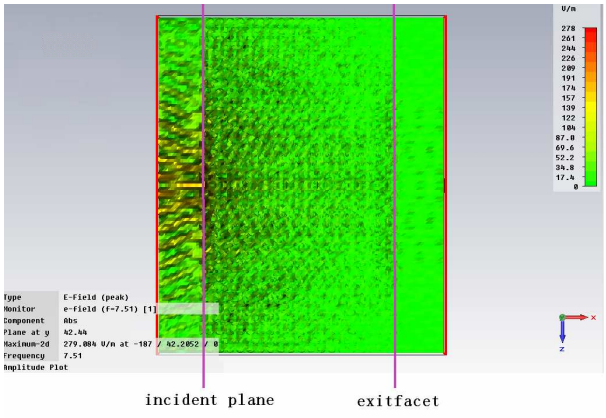

Figure 4.

the field distribution of the scattered field near the Dirac point is also simulated. (Fig. 4) The result shows the pseudodiffusive property of microwave near Dirac point, which is similar to the diffusion behavior of waves through a random medium. It is also worth pointing out that this structure is feasible to be realized in microwave region. Corresponding experiments are being optimized recently, and will be carried out soon. We also hope the Graphene-like 2D microwave PCs will be a convenient platform for demonstration of unique properties of Graphene.

Numerical Analysis of Optical Birefringence and Confinement Loss of Square Lattice Photonic Crystal Fibers with Rectangular, Elliptical, Rhomboidal and Circular Air Holes

Yuan-Fong Chau
Department of Electronic Engineering, Ching Yun University, Jung-Li 320, Taiwan, R.O.C.

Abstract— We numerically investigate the optical birefringence and confinement loss of square lattice photonic crystal fibers (PCFs) with rectangular, elliptical, rhomboidal and circular air holes using a full-vector finite element method. Numerical results shows that an extraordinarily high modal birefringence and low confinement loss of our proposed square lattice PCF with rectangular air holes at $\lambda = 1550\,\mathrm{nm}$ can be achieved at a magnitude of 8.1×10^{-2} (which is the highest value to our knowledge) and less than $5 \times 10^{-3}\,\mathrm{dB/km}$ (which is acceptable for practical applications), respectively.

Design of a Compact and Super Broadband Volumetric Folded Dipole Antenna for Mobile Applications

Ali Houssein Harmouch[1] **and Elias Nassar**[2]

[1]American University of Science and Technology, Lebanon
[2]Notre Dame University, Lebanon

Abstract— Miniaturization of antennas in mobile applications has become a major aspect of technology with the continuously emerging wireless standards. Minimizing the size of an antenna in terms of the wavelength causes the directional characteristics, the bandwidth, as well as the efficiency to become incompatible. The purpose of this study is to provide a miniaturized volumetric folded dipole antenna with ideal electrical and mechanical characteristics such as broadbandness, good impedance matching, compactness (light weight, cheap), and rigidness; compared to other competitors such as biconical antennas and others. It is formed out of two miniaturized folded monopoles placed at an angle of 90 degrees with respect to each other, joined at the centers of their top sides. Our study is based on the previous experimental results of a study showing that there is an improvement of impedance between a miniaturized triangular flat dipole and an ordinary flat dipole. In addition, initial results show that the volumetric triangular folded dipole antenna has better impedance than the flat triangular dipole antenna. Our proposed antenna is competent at low frequencies especially in the HF range where there is a need for small sized antennas. Antenna parameters such as impedance, quality factor and radiation patterns will be obtained using strict electrodynamics calculations.

Session 2P3a
Plasmonic Nanophotonics 2

Nonlinear and Switchable Plasmonic Metamaterials: Part 1

N. Zheludev[1], **A. Nikolaenko**[1], **K. F. Macdonald**[1], **V. Fedotov**[1], **D. Hewak**[1], **G. Adamo**[1], **Z. Samson**[1], **E. Plum**[1], **D. P. Tsai**[2], **E. Difabrizio**[3], **and F. De Angelis**[3]

[1]Optoelectronics Research Centre, University of Southampton, SO17 1BJ, UK
[2]National Taiwan University, Taipei 10617, Taiwan
[3]The University of Magna Graecia, Viale Europa 88100 Catanzaro, Italy

Abstract— We demonstrate a new class of "coherent" metamaterials, where narrow band responses are formed by collective and coherent excitations of strongly interacting meta-molecules while the transmission and reflection spectra depend on the size of the array.

Coherent meta-materials provide a promising platform for various applications including slow-light and polarization controlling devices and the "lasing spaser" which we illustrate in a number of microwave, THz and optical experiments.

We show experimentally that resonant properties and losses in photonic metamaterial may be controlled by gain while hybridization with nonlinear media leads to enhanced nonlinear response and strong switching performance.

Nonlinear and Switchable Plasmonic Metamaterials: Part 2

N. Zheludev[1], **A. Nikolaenko**[1], **K. F. Macdonald**[1], **V. Fedotov**[1], **D. Hewak**[1], **G. Adamo**[1], **Z. Samson**[1], **E. Plum**[1], **D. P. Tsai**[2], **E. Difabrizio**[3], **and F. De Angelis**[3]

[1]Optoelectronics Research Centre, University of Southampton, SO17 1BJ, UK
[2]National Taiwan University, Taipei 10617, Taiwan
[3]The University of Magna Graecia, Viale Europa 88100 Catanzaro, Italy

Abstract— We demonstrate a new class of "coherent" metamaterials, where narrow band responses are formed by collective and coherent excitations of strongly interacting meta-molecules while the transmission and reflection spectra depend on the size of the array.

Coherent meta-materials provide a promising platform for various applications including slow-light and polarization controlling devices and the "lasing spaser" which we illustrate in a number of microwave, THz and optical experiments.

We show experimentally that resonant properties and losses in photonic metamaterial may be controlled by gain while hybridization with nonlinear media leads to enhanced nonlinear response and strong switching performance.

The Role of Magnetic Polaritons in Grating Structures

L. P. Wang and Z. M. Zhang
George W. Woodruff School of Mechanical Engineering, Georgia Institute of Technology
Atlanta, Georgia 30332, USA

Abstract— The optical properties of subwavelength periodic structures have been extensive studied and the phenomena associated with surface plasmon polaritons (SPPs), Wood's anomaly, and cavity-like resonance have been well documented. Recently, magnetic polaritons (MPs) have been understood as a mechanism for magnetic response in the optical frequencies and can play a vital role in periodic structures. We use the rigorous coupled-wave analysis to study the effect of magnetic polaritons on the optical properties of gratings, including simple gratings, double-layered gratings, and complex gratings. In deep gratings, transmission and absorption peaks can be explained in terms of localized MPs between the strips. The electromagnetic field distribution indicates the presence of magnetic resonance, while the flat dispersion curves distinct them from SPP. An equivalent LC circuit model is developed to predict the dispersion of the fundamental MP mode. When two simple gratings are separated by a dielectric layer, strong absorption and enhanced transmission can be achieved at specific wavelengths due to MPs. In some cases, the MPs between the two grating layers and that between two strips can coexist and interact with each other. A complex grating may include several different slit and strip width within the same grating unlike a binary grating. The effect of MPs in complex gratings will also be addressed and a parametric study will be performed to further demonstrate the influence of MPs and explore their characteristics. The understanding and insight obtained from this study may facilitate the design of subwavelength periodic structures.

Localized Surface Plasmon Resonance (LSPR) Sensoric at the Single Particle Level

Andrea Csaki, **Thomas Schneider**, **Marie Löchner**,
Andrea Steinbrück, **and Wolfgang Fritzsche**
Institute of Photonic Technology (IPHT), P. O. Box 100239, Jena 07702, Germany

Abstract— In nanostructured noble metals, light induces localized surface plasmon resonance. This effect leads to absorption bands of particle solutions or peaks in the scattering spectra even of single particles. The dependence of this resonance on material, dimensions, geometry and immediate environment exhibits the potential for various applications. The environmental influence leads to sensoric applications because molecules binding to the particle surface induce changes in the spectral properties which can be detected.

A setup was established that is able to follow the optical properties of nanoparticles at a single molecule level in-situ during wet chemical reactions. On the other hand, correlative microscopy combining AFM measurements of a particle with its spectrum allow for the characterization of structure-property relations. These instruments were used to study the growth of metal layers on the nanoparticles, the influence of analyte in the surrounding as well as the highly specific binding of analyte at special receptors attached to particles even at the single particle level. Preliminary findings point to Au/Ag core/shell particles of certain dimensions as especially sensitive to spectral changes upon analyte binding as compared to pure metal particles with comparable dimensions.

Localized Plasmonic Devices Based on Highly Ordered Anodic Porous Alumina

Hideki Masuda[1, 2], **Kazuyuki Nishio**[1, 2], **and Toshiaki Kondo**[2]

[1]Department of Applied Chemistry, Tokyo Metropolitan University
1-1 Minamiosawa, Hachioji, Tokyo 192-0397, Japan
[2]Kanagawa Academy of Science and Technology
Nishjihashimoto, Sagamihara, Kanagawa 229-1131, Japan

Abstract— Fabrication of functional devices based on the localized surface plasmon (LSP) in small metal particles has attracted increasing attention due to its capability for various application fields such as chemical or biological sensing. Precise control of the sizes and shapes of the small particles is important because the properties of LSP are substantially dependent on the geometrical structure of the metal particles. Anodic porous alumina, which is formed by anodization of Al in acidic solution, is a typical self-ordered material and is promising candidate for the starting structure of nanofabrication [1]. Advantage of the use of anodic porous alumina for the preparation of is its controllability of the dimension of the structures besides its easiness of the preparation. The ordered structure prepared from highly ordered anodic porous alumina showed unique optical properties originated from the LSP, which was dependent on the size and shapes of the structures [2]. In the present report, fabrication of ordered structures of metal nanoparticles using highly ordered anodic porous alumina, and its application to surface enhanced Raman scattering (SERS) will be presented [3, 4].

REFERENCES

1. Masuda, H. and K. Fukuda, "Ordered metal nanohole arrays made by a two-step replication of honeycomb structures of anodic alumina," *Science*, Vol. 268, 1466, 1995.
2. Matsumoto, F., M. Ishikawa, K. Nishio, and H. Masuda, *Chem. Lett.*, Vol. 34, 432, 2005.
3. Kondo, T., F. Matsumoto, K. Nishio, and H. Masuda, *Chem. Lett.*, Vol. 37, 466, 2008.
4. Kondo, T., K. Nishio, and H. Masuda, "Surface-enhanced raman scattering in multilayered au nanoparticles in anodic porous alumina matrix," *Appl. Phys. Express*, Vol. 2, 032001, 2009.

Spectral, Amplitude and Phase Sensitivity of a Plasmonic Gas Sensor in a Metallic Photonic Crystal Slab Geometry. Comparison of the Near and Far Field Phase Detection Strategies

L. Shi, **A. Kabashin**, **and M. Skorobogatiy**
École Polytechnique de Montréal, C.P. 6079, Centre-Ville, Montreal, QC H3C 3A7, Canada

Abstract— Using finite-difference time-domain method, we investigate phase and amplitude reflective properties of a metallic photonic crystal slab comprising a two-dimensional array of gold disks placed on top of a thin gold film resting on a dielectric substrate. Photonic crystal slab overcladding is a gaseous analyte. Throughout the paper we discuss prospectives of application of such photonic crystal slabs to sensing of changes in the gas refractive index. We start by studying the field distributions and spectral positions of two types of surface plasmons supported by such PhCs as a function of the photonic crystal lattice period, the gold film thickness, and the gold disk size. First, we find that the spectral positions of plasmon peaks depend almost linearly on the photonic crystal lattice constant, which is a manifestation of the delocalized nature of a plasmon extending over the PhC lattice. This is possible due to connectivity between metallic disks via an underlying thin metallic film. Second, we find that the width of plasmonic peaks is highly sensitive to the relative size of the metallic disks compared to the lattice period. This can be well explained via interaction between the localized plasmons situated at the disc edges in the adjacent unit cells. We therefore find that plasmons in the metallic PhC slabs featuring metallic discs connected by a metallic film exhibit both strong local and non-local properties. Third, we find that, generally, there are two types of plasmons supported by such metallic PhCs. One type is a plasmon with a large fraction of its field located in the gas overcladding, which is most suitable for sensing. In contrast, another plasmon type has its field concentrated at the interface between a thin metal film and a substrate; such plasmons are only weakly sensitive to the refractive index of the sensor overcladding, and, therefore, can serve as convenient references for the sensor measurements. Finally, we report sensor sensitivities to changes in the real part of the gas refractive index when using amplitude and phase-based detection strategies. We start by demonstrating that when measured in the sensor far field, the phase sensitive detection provides much lower detection limit (1.8×10^{-6} RIU) compared to that of the amplitude-based detection (1.5×10^{-4} RIU). We then find that sensor phase and amplitude sensitivities can be considerably enhanced when performing measurements using point detectors placed in the near field of a sensor. Particularly, we have established that both phase and amplitude sensitivities are maximal when measured in the sensor near field along the normal to the sensor surface going through the point of the highest symmetry of a photonic crystal unit cell (Γ point). Sensor resolution as high as 2.2×10^{-7} RIU for the phase-based detection and 7.4×10^{-5} RIU) for the amplitude-based detection are found, with the most dramatic enhancement observed for the phase detection approach. We believe that experimental verification of the sensor sensitivity enhancement using phase detection in the sensor near field can be accomplished by using scanning near-field optical microscopy.

Session 2P3b
Optics, Photonics and Nano-photonics

Self-field Theory-new Photonic Insights

A. H. J. Fleming
Biophotonics Research Institute, Melbourne, Australia

Abstract— Self-field Theory (SFT) is a new description of electromagnetic interactions. At its heart are bispinorial motions for both the EM fields and the interacting particles. Among its recent successes it has solved the hydrogen atom, obtained an analytic estimate for the mass of the photon, and provided the first glimpses of structure within the photon that may yield a boson organizational structure reminiscent in some ways to the chemical table that was glimpsed by Mendeleev in 1860 via a two-dimensional array of elemental properties. As well SFT obtained an analytic expression for Planck's number providing a basis for its understanding as a variable of motion applying equally to the electron, the proton and the photon. While there are many differences, this report shows how the fields of SFT vary from classical electromagnetics and quantum field theory (QFT).

In classical EM the field covers all solid angles around a charge and is defined as a vector. QFT models the field as quanta shown as small wavy lines within Feynman diagrams; the mathematics does not specify an actual path, only the start and the finish points where a Dirac-delta function is used to insert a propagator kernel or Greens function. Basically QFT models the field as an impulse specified at space points; the field in QFT is undefined over solid angle even though the Feynman diagram indicates a wavy line motion. The uncertainty within QFT field is related to the lack of a complete EM bispinorial field form. The fields in SFT are discrete streams of photons, rather than the continuous fields of Maxwell's classical electromagnetics. The photon motions are specified via the bispinorial function as various motions including spiral-helices between the electron and proton of the hydrogen atom.

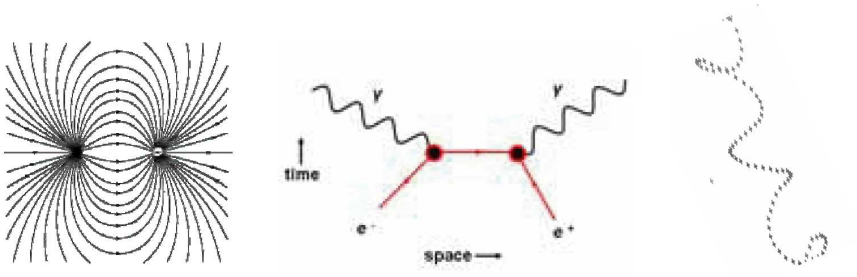

(a) (b) (c)

Figure 1: 2.3 Field forms. (a) Classical EM. (b) Quantum field theory. (c) Self-field theory.

REFERENCES

1. Fleming, A. H. J., "Electromagnetic self-field theory and its application to the hydrogen atom," *Physics Essays*, Vol. 18, No. 3, 265–285, 2005.
2. Fleming, A. H. J., "Analytic estimate for the mass of the photon," *Progress In Electromagnetics Research Symposium*, Moscow, Russia, August 18–21, 2009.
3. Fleming, A. H. J., "Self-field theory, analytic spectroscopy of the ordinary photon," *Proc. 2nd EHE Intl Conf.*, 18–23, Wroclaw, Poland, 2007.

Optical Characterization of Au-Ag Alloy Nanocylinder with Radial Dielectric Anisotropy Cylindrical Shell

Tao Pan[1], **Tao-Cheng Zang**[1], **Guo-Ding Xu**[1], **and Lei Gao**[2]

[1]Department of Physics, Suzhou University of Science and Technology, Suzhou 215009, China
[2]Jiangsu Key Laboratory of Thin Films, Department of Physics, Soochow University, Suzhou 215006, China

Abstract— The optical properties of Au-Ag alloy nanocylinder with radial dielectric anisotropy cylindrical shell have been investigated based on quasi-static theory. Numerical study results show that the surface plasmon resonant (SPR) peak is red-shifted with an increasing amount of Au, the extinction section at the SPR increase with increasing amount of Ag, which indicates that induced charges on the surface of Au-Ag alloy nanocylinder which has large proportion Ag are much more than that has large proportion Au. While with increasing the $\varepsilon_t/\varepsilon_r$-value ($\varepsilon_t$ and ε_r are the tangential and the radial dielectric function of the shell respectively), the SPR wavelength is also red-shifted, at the same time the extinction section is decreased. The electric field enhancements near the outer and inner surface of the shell have been studied, and the origin of the field enhancement between both interface of dielectric media have been analyzed using the Maxwell-Garnett approximation (MGA). Specially, near the inner surface of the shell the maximum enhancements can occur along the polarization direction or be perpendicular to the incident polarization according to the $\varepsilon_t/\varepsilon_r$-value, in other words, the orientation of the maximum field enhancements can be controlled by changing the $\varepsilon_t/\varepsilon_r$-value. We also give the whole near-field distribution contour figure regarding our model, the effect of the anisotropy parameters on the field distribution are analyzed. In addition we also study the case of off-resonance wavelength, analytical results show that the field distribution can be modulated by changing the wavelength, but the field will weaker than that at resonance.

GHz-Electrooptic Modulation in Silicon-organic Hybrid Nanophotonic Structures

Manfred Eich[1], **Stefan Prorok**[1], **Jan Hendrik Wülbern**[1], **Jan Hampe**[1], **Alexander Petrov**[1], **Martin Jenett**[1], **Arne Jacob**[1], **Jingdong Luo**[2], **Alex K.-Y. Jen**[2], **Andrea Di Falco**[3], **Thomas F. Krauss**[3], **and Jürgen Bruns**[4]

[1]Hamburg University of Technology, D-21073 Hamburg, Germany
[2]Department of Materials Science and Engineering, University of Washington Seattle, USA
[3]School of Physics and Astronomy, University of St. Andrews, Scotland, UK
[4]Fachgebiet Hochfrequenztechnik, Technische Universität Berlin, Germany

Abstract— Two dimensional photonic crystal waveguides in high index materials enable integrated optical devices with an extremely small geometrical footprint on the scale of micrometers [1–3]. Slotted waveguides are based on the guiding of light in low refractive index materials and a field enhancement in this particular region of the device. Here, we experimentally demonstrate electro-optic modulation at multi GHz frequencies in slotted photonic crystal waveguides based on silicon-on-insulator substrates covered and infiltrated with highly nonlinear guest host optical polymers [4]. A photonic crystal heterostructure is used to create a cavity, while simultaneously serving as an electrical connection from the slot to the metal electrodes that carry the modulation signal.

REFERENCES

1. Wülbern, J. H., J. Hampe, A. Petrov, M. Eich, J. Luo, A. K.-Y. Jen, A. Di Falco, T. F. Krauss, and J. Bruns, *Appl. Phys. Lett.*, Vol. 94, 241107, 2009.
2. Wülbern, J. H., A. Petrov, and M. Eich, *Opt. Express*, Vol. 17, 304, 2009.
3. Baehr-Jones, T., B. Penkov, J. Huang, P. Sullivan, J. Davies, J. Takayesu, J. Luo, T.-D. Kim, L. R. Dalton, A. K.-Y. Jen, M. Hochberg, and A. Scherer, *Appl. Phys. Lett.*, Vol. 92, 163303-3, 2008.
4. Kim, T.-D., J. Luo, Y.-J. Cheng, Z. Shi, S. Hau, S.-H. Jang, X.-H. Zhou, Y. Tian, B. Polishak, S. Huang, H. Ma, L. R. Dalton, and A. K.-Y. Jen, *J. Phys. Chem. C*, Vol. 112, 8091, 2008.

Non-markovian Dynamics of Excitonic Polar-trion in Quantum Dots

Kuan-Ming Hung and Wei-Jun Hong
Department of Electronics Engineering, National Kaohsiung University of Applied Sciences
Kaohsiung, Taiwan

Abstract— The coupling of an open system to its environment results in the non-Markovian dynamics [1, 2]. In this work, the excitonic polar-trion, a new composite quasi-particle of exciton, photon and longitudinal-optical (LO) phonon, in quantum dots (QD) is observed. The coupling of the quasi-particle to its environments via the photon and LO-phonon results in a non-Markovian quantum dissipation. The observed phenomenon provides another possible way on the controlled manipulation of localized excitonic states in the QD using Rabi oscillations (RO) for quantum-information applications [3, 4].

Three-level independent-Boson model is used to demonstrate the system of an exciton interacting to photons, in the rotating wave approximation, and LO-phonons in QD. An effective decay rate of $\sim 0.1\,\mathrm{ps}^{-1}$ is used to describe the dissipation of the system according to the radiative and anharmonic decay. The dynamics of the system is studied by the Wigner-Weisskopf coupled-mode-equation method. In this formalism, an analytical solution is available.

The Rabi oscillations (RO) of the system with an exciton initially presented at the vacuum state are shown in Figure 1 for the exciting photon strengths of 1.2, 2.0 and $2.8\,\mathrm{ps}^{-1}$, and the temperature of 70 K. A non-monotonic field dependence of RO appears in the figure, a non-Markovian behavior. The anti-crossings in the RO dispersions, shown in Figure 2, are observed according to the excitonic polar-trion resonance.

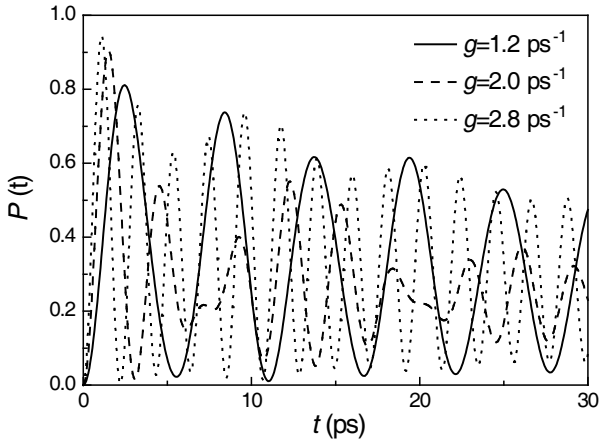

Figure 1.

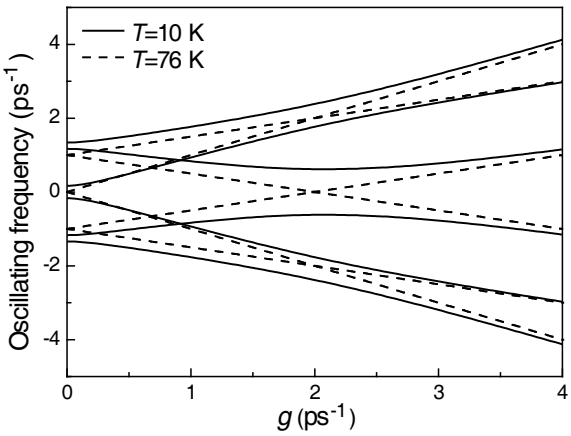

Figure 2.

REFERENCES

1. Vagov, A., et al., "Nonmonotonic field dependence of damping and reappearance of Rabi oscillations in quantum dots," *Phys. Rev. Lett.*, Vol. 98, 227403, 2007.
2. Vagov, A., et al., "Nonmonotonous temperature dependence of the initial decoherence in quantum dots," *Phys. Rev. B*, Vol. 70, 201305, 2004.
3. Biolatti, E., et al., "Quantum information processing with semiconductor macroatoms," *Phys. Rev. Lett.*, Vol. 85, 5647, 2000.
4. Troiani, F., et al., "Exploiting exciton-exciton interactions in semiconductor quantum dots for quantum-information processing," *Phys. Rev. B*, Vol. 62, 2263, 2000.

Microstructured and Photonic Bandgap Fibers for Applications in the Resonant Bio- and Chemical Sensors

M. Skorobogatiy
École Polytechnique de Montréal, C.P. 6079, Centre-Ville Montreal, QC H3C 3A7, Canada

Abstract— We review application of microstructured and photonic bandgap fibers for designing resonant optical sensors of changes in the value of analyte refractive index. This research subject has recently invoked much attention due to development of novel fiber types, as well as due to development of techniques for the activation of fiber microstructure with functional materials. Particularly, we consider two sensors types. The first sensor type employs hollow core photonic bandgap fibers where core guided mode is confined in the analyte filed core through resonant effect in the surrounding periodic reflector. The second sensor type employs metalized microstructured or photonic bandgap waveguides and fibers, where core guided mode is phase matched with a plasmon propagating at the fiber/analyte interface. In resonant sensors one typically employs fibers with strongly non-uniform spectral transmission characteristics that are sensitive to changes in the real part of the analyte refractive index. Moreover, if narrow absorption lines are present in the analyte transmission spectrum, due to Kramers-Kronig relation this will also result in strong variation in the real part of the refractive index in the vicinity of an absorption line. We finally demonstrate that resonant sensors based on Photonic Crystal Fibers allow detection of minute changes both in the real part of the analyte refractive index ($10^{-7} - 10^{-4}$ RIU), as well as in the imaginary part of the analyte refractive index in the vicinity of absorption lines.

REFERENCES

1. Skorobogatiy, M., "Resonant bio-chemical sensors based on photonic bandgap waveguides and fibers. Case of hollow core fibers and plasmonic waveguides," *Optical Guided-wave Chemical and Biosensors*, Springer Series on Chemical Sensors and Biosensors, Editors: M. Zourob, A. Lakhtakia, 2009.
2. Gauvreau, B., A. Hassani, M. Fassi Fehri, A. Kabashin, and M. A. Skorobogatiy, "Photonic bandgap fiber-based Surface Plasmon Resonance sensors," *Opt. Express*, Vol. 15, 11413–11426, 2007.

Surface Plasmon Resonance-like Integrated Sensor at Terahertz Frequencies for Gaseous Analytes Using Porous Fibers Covered with a Thin Layer of Ferroelectric Plastic

A. Hassani and Maksim Skorobogatiy
École Polytechnique de Montréal
C.P. 6079, Centre-Ville, Montreal, Quebec, H3C 3A7, Canada

Abstract— In the visible and ultraviolet range, the collective oscillation of free charge carriers at a metal-dielectric interface yields a surface plasmon wave propagating along the surface of the metal. The sensitivity of plasmon excitation to changes in the refractive index of the dielectric medium has been widely exploited for sensing applications. At frequencies significantly below the plasma frequency (like the THz range), large negative permittivity strongly prohibits electromagnetic fields from penetration inside a metal, and plasmon excitation on the metal/dielectric interface becomes challenging. Therefore, efficient plasmonic excitation at lower frequencies requires materials with lower plasma frequencies. Recently, Pendry et al. have suggested an artificial material in the form of a 2D subwavelength metallic wire lattice for which the effective plasma frequency is designable. Alternatively, some materials can naturally support plasmon-like excitations in the THz regime due to resonances in their dielectric constant. Particularly, polyvinylidene fluoride (PVDF) is a ferroelectric semi-crystalline polymer with a small absolute value of permittivity in the visible and near-IR regions, while having a resonance in its dielectric constant in the THz range.

In our work, plasmon-like excitation at the interface between fully polymeric fiber sensor and gaseous analyte is demonstrated theoretically in terahertz regime. Such plasmonic excitation occurs on top of a $\sim 30\,\mu$m ferroelectric PVDF plastic layer wrapped around a subwavelength porous polymer fiber. In a view of designing a fiber-based sensor of analyte refractive index, phase matching of a plasmon-like mode with the fundamental core guided mode of a low loss porous fiber is then demonstrated for the most challenging case of a gaseous analyte. We then demonstrate the possibility of designing high sensitivity sensors with amplitude resolution of 3.4×10^{-4} RIU, and spectral resolution of 1.3×10^{-4} RIU in THz regime. Finally, novel sensing methodology based on detection of changes in the core mode dispersion is proposed.

Session 2P4a
Electromagnetic Nondestructive Evaluation and Modeling

Impact of Network Topology on the Matched-pulse-based Fault Detection

L. Abboud[1], **A. Cozza**[1], **and L. Pichon**[2]

[1]Département de Recherche en Électromagnétisme, SUPELEC
3 rue Joliot-Curie, Gif-sur-Yvette 91192, France
[2]Laboratoire de Génie Électrique de Paris (LGEP) — CNRS/SUPELEC
11 rue Joliot-Curie, Gif-sur-Yvette 91192, France

Abstract— Location of faults on wires has become an area of international concern [1]. Today, wire networks are found everywhere: in transportation systems, industrial machinery, buildings, nuclear facilities, power distribution systems, etc., so that faulty electrical wiring has been considered among the most significant potential cause of failure and maintenance cost in these structures [2].

Reflectometry methods are widely used today to help detecting and locating wire faults [1, 3]. These methods use a testing signal that is injected into the wire network; the signal reflected from an eventual fault is then analyzed in order to locate its position and impedance value. Generally, hard faults (open and short circuits) are observable through reflectometry, whereas soft faults are more critical to be detected. Additional complexity arises when using wire networks, because faults can be masked by the presence of several reflection sources (such as junctions, branches, mismatched loads, etc.); this produces multiple echoes, making it difficult to identify the one corresponding to the actual fault, especially in complex network configurations.

In [4], we presented a new concept to fault detection in wire networks, based on the idea of adapting the testing signal to the system, unlike reflectometry methods which use a predefined testing signal. The proposed approach was called the Matched Pulse approach (MP). We showed the benefits of this technique compared to standard Time Domain Reflectometry (TDR).

In this paper, we propose to study the impact of the network's topology on the performance of the MP approach. That is, a sensitivity analysis of this method that will allow us to evaluate its advantages, together with its limitations. We will analyze different network configurations, and different types of faults, in order to observe the factors influencing the efficiency of the MP, and in which cases the advantage of this method over the TDR becomes more important. The study will also include a physical interpretation of the obtained results, showing the echoes propagation in the studied systems, and explaining the reasons why the MP might be more beneficial in some cases than in the others. The whole study will eventually lead to a better understanding and characterization of the MP approach.

REFERENCES

1. Furse, C. and R. Haupt, "Down to the wire," *IEEE Spectrum*, Vol. 38, No. 2, 34–39, Feb. 2001.
2. "Review of federal programs for wire system safety," Final Report, National Science and Technology Council, White House, Nov. 2000.
3. Furse, C., Y. C. Chung, C. Lo, and P. Pendayala, "A critical comparison of reflectometry methods for location of wiring faults," *Smart Structures and Systems*, Vol. 2, No. 1, 25–46, 2006.
4. Abboud, L., A. Cozza, and L. Pichon, "Utilisation of matched pulses to improve fault detection in wire networks," *International Conference on ITS Telecommunications*, Oct. 2009.

Efficient Finite Element Model for Simulating Eddy Current Testing of Aircraft Skin Structures

Zhiwei Zeng
Department of Aeronautics, Xiamen University, Xiamen, Fujian 361005, China

Abstract— Three-dimensional finite element (FE) modeling of eddy current testing (ECT) of aircraft skin structure is a challenging task because of the exhaustive consumption of computation resources, especially when considering the scanning of ferrite-core probe over aluminum plates with ferrite fasteners. Therefore the development of efficient model is very desirable. Conventional FE models use one mesh to discretize the whole solution domain. Re-meshing is necessary when the probe is moved to another position, which is cumbersome and labor intensive. More importantly, it results in very inefficient solution process and noisy signal due to different computation error for different meshes at different probe positions. The author has proposed an efficient FE model to overcome the above problem. The model uses different meshes to discretize the ferrite core and the test sample separately and does not mesh the coil. A few fast iterations are performed to update the total magnetic field until the preset convergence criterion is reached. By this way, re-meshing for changing probe position is avoided and the preconditioning of stiffness matrices is performed only once regardless of the number of probe positions. The model has proved to be very efficient.

In this work, the above model is generalized to consider multiple ferrite objects in the simulation. When modeling ECT of multilayer aircraft skin structure with steel fasteners, separating steel fastener from the aluminum plates can further improve the efficiency of simulation. Investigation of FE formulations reveals that nodal FE formulation with Coulomb gauge is the most efficient formulation for modeling problems without ferrite materials. When ferrite materials are involved, however, Coulomb gauge cannot be applied. Without applying Coulomb gauge, both nodal FE and edge FE formulations are very inefficient. Separating steel fastener from the aluminum plates allows utilizing nodal FE method with Coulomb gauge to model the aluminum plates. Both ferrite core and steel fastener have simple geometries and small dimensions. Therefore, either nodal FE or edge FE formulation can be used to model ferrite core and steel fastener without apparent reduction of efficiency for the whole solution process. Another advantage of the proposed method is that the difficulty in mesh generation due to the small air gap between fastener and aluminum plates is removed.

Modelling and Validating Ferrite-core Probes for GMR-eddy Current Testing in Metallic Plates

M. Cacciola, **G. Megali**, **D. Pellicanò**, **S. Calcagno**, **M. Versaci**, **and F. C. Morabito**
DIMET Department, University "Mediterranea" of Reggio Calabria
Via Graziella Feo di Vito, I-89100 Reggio Calabria, Italy

Abstract— Non Destructive Testing techniques are more and more exploited in order to quickly and cheaply recognize flaws into the inspected materials. Within this framework, modelling is a powerful tool for inspection improvements. It helps probe-coil designers to optimize sensors for each examination requirement, providing better understanding of the involved physics, supporting operator training and increasing defect analysis reliability. The effect of the ferrite core is analyzed in order to optimize the design of probe-coils and study various configurations of inspection. Particularly, Finite Element based analyzes will be carried out into this path. Direct problem will be assessed, and direct model will be formulated, dependent by different parameters, e.g., coil shape, working frequencies and so forth. The model will be subsequently validated by in-lab experimentations.

Introduction: In order to improve manufacturing quality and ensure public safety, components and structures are commonly inspected for early detection of defects or faults which may reduce their structural integrity. Non Destructive Testing and Evaluation (NDT/E) techniques present the advantage of leaving the specimens undamaged after inspection. Typical testing configurations [1] may consist of ferrite core coil probes, placed above a planar conductive specimen and operating in the time-harmonic domain, at frequency depending on the problem [2]. This work proposes an integrated approach starting from the design and implementation of a novel probe in order to optimize the sensor effect and the drop-in suppression, the operating parameters of the frequency and field strength. For our purposes, a Finite Element Analysis (FEA) code has been exploited. Subsequently, inspecting performances have been tested by experimentations carried out at our NDT Lab. Exploited sensing will be based on a Giant MagnetoRestistance (GMR) device [3] and a board able to transmit the electromagnetic response to a general purpose Personal Computer. Subsequently, in-lab experimentations exploiting GMR sensors have been carried out in order to validate the model.

REFERENCES

1. Yamada, S., M. Katou, M. Iwahara, F. P. Dawson, and S. M. Yamada, "Eddy-current testing," *IEEE Trans. Magn.*, Vol. 31, No. 6, 3185–3187, 1995.
2. Theodoulidis, T. P., "Model of ferrite-cored probes for eddy-current nondestructive evaluation," *J. Appl. Phys.*, Vol. 93, 3071–3078, 2003.
3. Megali, G., M. Cacciola, D. Pellicanò, and F. C. Morabito, "Recent patents on integrated software/hardware GMR-based systems and applications for PCB inspection," *Recent Patent on Electrical Engineering*, Vol. 2, 82–91, 2009.

A New Method for Performance Specification and Verification Using Gamma Distribution

Ameet V. Joshi
Microline Technology Corporation, Traverse City, Michigan, USA

Abstract— Typically a statistical analysis approach used for performance specification/validation of a NDT system deals with prediction of three quantities based on signed errors in prediction: Tolerance or allowable percent error, Certainty and Confidence level. In order to have desired statistical certainty and confidence for the results presented for a particular NDT tool, it is assumed that the data used for the experiment, follows a certain known distribution. Due to various theoretical and practical reasons, Gaussian or Normal distribution is a common choice [1]. However it is observed that in many cases, the distributions do not follow the Gaussian distribution, as can be tested using various "goodness of fit" tests, e.g., Chi-square test, Kolmogorov-Smirnov test. In some cases, when the Gaussian distribution is not suitable, Binomial distribution has also been used [2] with following rule: when the error in prediction falls inside the tolerance level it is called as success and failure otherwise. The drawback of binomial assumption is that it cannot distinguish between two distributions as long as the number of successes is same.

A new approach is presented here that uses absolute errors instead of signed errors. Tolerance being an unsigned quantity, the sign of error does not play any role in its prediction. Using standard distribution fitting techniques, the distribution of absolute errors is fitted to Gamma distribution $f(x; k, \vartheta)$ with desired confidence level (100(1-β)%). It can be proved that any error distribution would fit to a Gamma distribution with a unique set of parameters ($\{k, \vartheta\}$) unlike the case of Gaussian distribution. In other words, the results computed with this approach are always valid and reliable. This approach proves to solve all the problems associated with Gaussian and Binomial assumptions. It also provides a unified approach for computing all the three quantities for performance specifications/validation.

REFERENCES

1. NcCann, R., R. McNealy, and M. Gao, "In-line inspection performance verification," *NACE Corrosion Conference and Expo*, Paper No. 07132, 2007.
2. Worthingham, R., T. Morrison, N. S. Mangat, and G. Desjardines, "Bayesian estimates of measurement error for in-line inspection and field tools," *International Pipeline Conference*, 2002.

Rotating Electromagnetic Field for Crack Detection in Railway Tracks

M. Cacciola, **G. Megali**, **D. Pellicanò**, **S. Calcagno**, **M. Versaci**, **and F. C. Morabito**
DIMET Department, University "Mediterranea" of Reggio Calabria
Via Graziella Feo di Vito, Reggio Calabria I-89100, Italy

Abstract— The main problem about a railway analysis is detection of cracks in the structure. If these deficiencies are not controlled at early stages they might cause huge economical problems affecting the rail network. Within this framework, the early and continuous use of Non Destructive Tests can be useful. In recent years, scientists measure the component of magnetic field normal to the inspected surface. In this paper we exploit the measure of normal component, with respect to the scanned surface, of magnetic field. Whilst the scientific literature proposes a lot of solutions for detecting sub-superficial defects, an open problem is related to the geometrical complexity of the structure and the relevant difficulty of crack detection. In this paper, we propose a Finite Element based approach for modelling a fast and accurate evaluation of the defect in railways cracks. In particular, we propose a solution exploiting a rotating electromagnetic field with very encouraging results.

Introduction: In order to improve manufacturing quality and ensure public safety, components and structures are commonly inspected for early detection of defects or faults which may reduce their structural integrity. Non Destructive Testing and Evaluation (NDT/E) techniques present the advantage of leaving the specimens undamaged after inspection. NDT/E in the field of defects identification in metallic elements plays a remarkable role with special regard to those sectors where the material integrity is strictly required. As a consequence, the detection of defects in metallic materials provides the operator with useful information on the actual mechanical integrity of the specimen. It is presently possible to very precisely and rapidly perform forward numerical simulations [1–3] and concerning different applications of the NDT/E. Cracks or other in-service expected discontinuities occurring in railway may lead to fracture and thus to operational danger. Where necessary, operational safety is guaranteed by the periodic non-destructive inspection of these components. Irregularities may not exceed a specified and limited extension. Moreover, irregularities are closely related to operating speed, covering distance, quality of the track, acceleration, profile wear, rail wear, stiffness bogey, and so on. For this reason, the initial inspection shall be exploited in order to observe all discontinuities or damages. Procedures have to follow international standards (EN, European standard; ISO, International Standard) and UIC (Unit Identification Code) code. For tires inspection, Eddy Current Testing are generally exploited. Therefore, an insensitive way of inspection could be very useful in order to improve the quality of the analysis. It can be represented by a magnetic rotating field, generated by a multi-transmitter exciting coil, inducing variation of the eddy current density without a mechanical movement. For our purposes, a Finite Element code has been exploited for physical modelling. We verified the variation of magnetic field density [4] caused by the presence of defect. As our experimentations demonstrate, Rotating Magnetic Field provides a good overall accuracy in discriminating defect presence.

REFERENCES

1. Bowler, J. R., "Eddy current interaction with an ideal crack: I. The forward problem," *J. Appl. Phys.*, Vol. 75, 8128–8137, 1994.
2. Tagaki, T., M. Hashimoto, H. Fukutomi, M. Kurokawa, K. Miya, and H. Tsuboi, "Benchmark models of eddy current testing for steam generator tube: experiment and numerical analysis," *Int. J. Appl. Electrom.*, Vol. 4, 149–162, 1994.
3. Tagaki, T., H. Huang, H. Fukutomi, and J. Tani, "Numerical evaluation of correlation between crack size and eddy current testing signals by a very fast simulator," *IEEE Trans. Magn.*, Vol. 34, 2582–2584, 1998.
4. Dod, C. V. and W. E. Deeds, "Analytical solutions to eddy-current probe-coil problems," *J. Appl. Phys.*, Vol. 39, 2829–2838, 1968.

Numerical Simulation of Electromagnetic Acoustic Testing Signals with Consideration of Electromagneto-mechanical Coupling Effect

Wenjing Wu, **Cuixiang Pei**, **and Zhenmao Chen**
MOE Key Laboratory for Strength and Vibration, School of Aerospace, Xi'an Jiaotong University
Xi'an, Shaanxi 710049, China

Abstract— Up to now, the numerical simulation of Electromagnetic Acoustic Transducer (EMAT) is performed without considering the effect of the additional electric field induced due to the velocity effect. To clarify the influence of such an electro-magneto-mechanical coupling effect on the simulated EMAT signals, a numerical code with consideration of the coupling effect is developed in this paper by introducing the $v \times B$ term in the governing equation of eddy current problem. In practice, the reduced vector potential (Ar) method is applied for the eddy current simulation with the coupling term treated as an additional current source. For ultrasonic wave simulation, based on the elasticity mechanics theory, a strategy of finite element method is adopted in addition with a step by step time integration algorithm, according to which the corresponding code is developed. The feature of the simulated EMAT signals and the propagation pattern of the simulated ultrasonic wave demonstrate that the algorithm and the corresponding numerical code are efficient. To investigate the influence of the coupling effect, EMAT signals of different conditions are simulated by using both the codes with and without the coupling effect considered. By comparing the numerical results of different frequency, current density, liftoff etc., it is demonstrated that the coupling term does not give significant influence on the EMAT signals. In practical application, with the coupling term ignored is reasonable. Another application case is also extended to the numerical simulation of EMAT for thermal barrier coatings (TBC), with a comparison of the traditional result and the coupling effect considered result.

Session 2P4b
Advances in Microwave Imaging

High Resolution, Wide Coverage Termite Imager

N. W. D. Le Marshall[1], **G. A. Rankin**[2], **and A. Z. Tirkel**[3]

[1]School of ITEE, University of NSW@ADFA, Canberra, ACT 2600, Australia
[2]EWA Australia, Innovation House, Mawson Lakes Boulevard, Mawson Lakes, SA 5095, Australia
[3]Scientific Technology, 8 Cecil Street, East Brighton, VIC 3187, Australia

Abstract— This paper describes a 24 GHz radar sensor array, designed to detect and image termite activity, behind a wall, floor or ceiling. Here, we introduce an enhanced transmit MIMO beamforming algorithm, to steer a null, computed by a convex optimization algorithm to an arbitrary direction, and present simulation results. Beam patterns demonstrating a single elevation null and a complex azimuth null are shown in Fig. 1 below.

The sensor array is composed of three sub-arrays. A transmit sub-array, a DOA sub-array, for wide area detection of targets at long ranges (1000–1500 mm), and a 3D imaging sub-array, for high resolution imaging of individual target activity at short ranges (100–150 mm). The sensor array employs transmit Multiple Input Multiple Output (MIMO) beamforming, a Matrix Enhanced Matrix Pencil (MEMP) algorithm for Direction of Arrival (DOA) estimation, enhanced to resolve arbitrary numbers of targets, and receive focusing for 3D high resolution imaging. The MEMP DOA estimation accuracy depends critically on the SNR, the presence of far field targets, and targets with vastly different bearings. Far field targets can be rejected by using a chirp, and low-pass filtering in the receiver (FMCW range gating). A method of dealing with targets with bearings outside the sector of interest has been presented in [1]. In some circumstances, aliased targets outside the beamformed pattern may be resolved. An enhancement, which improves the SNR and rejection of out of sector targets, is transmit beamforming, which concentrates more power on the target of interest, and less power on spurious targets, thus improving the SNR. Traditionally, this has been accomplished by controlling the magnitude and phase of the transmit signal fed to a transmit array. A major drawback of this approach is that only one beam can be formed at a time, and therefore sequential beamforming is required to complete a scan of a wide field of interest. Also, controlling the magnitude and phase of the radiated signals from individual transmit elements is difficult and inaccurate. In contrast, processing the digitized signals from the receive elements is precise, and can be performed in parallel in a FPGA. Therefore, MIMO processing, which allows transmitter beamforming after digitization at the receiver, is an attractive solution. In our implementation, the transmit elements are fed signals which are modulated by a set of orthogonal codes. At each receive element, the signals from each transmit element are able to be processed separately, allowing transmitter beamforming to be implemented before DOA processing. MIMO methods enable us to utilize a beamformed transmitter with the actual beamforming process performed after the data is received. Receiver beamforming cannot be used with the MEMP, and hence transmitter beamforming is a valuable method for spatially pre-filtering a sector of interest before the array transformation is applied to compensate an imperfect real array.

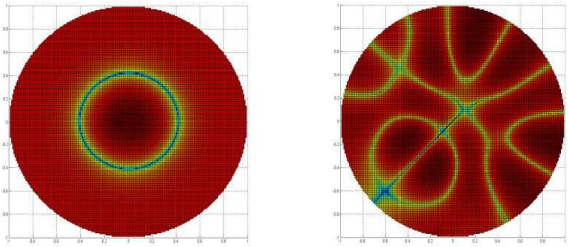

Figure 1: Elevation/Azimuth nulls produced by MIMO beamforming of the transmitter pattern at the receiver.

REFERENCES

1. Le Marshall, N. W. D. and A. Z. Tirkel, "The application of the MEMP and beamforming to determine the presence of termites in situ," *IEEE EUROCON 2009 Proceedings*, 1568–1572, 2009.

A Study of Multifractal Dimensions for Classification of Multi-band Multi-polarized SAR Image

Hse Tzia Teng[1], **Hong Tat Ewe**[2], **and Sin Leng Tan**[3]

[1]Faculty of Engineering, Multimedia University, Malaysia
[2]Faculty of Information and Communication Technology
Universiti Tunku Abdul Rahman, Malaysia
[3]Department of Mathematical and Actuarial Sciences
Faculty of Information and Communication Technology
Universiti Tunku Abdul Rahman, Malaysia

Abstract— The study and application of fractal dimension in the SAR image classification has been explored and implemented in the remote sensing community. However, despite previous initial studies on the use of multifractal dimensions in this, more thorough and systematic investigation of utilizing multifractal dimensions in this area is to be explored further and shall be reported in this paper.

Multifractal dimensions D_q for real q are a more general parameter than the fractal dimension in describing geometrical properties. D_q can be written as

$$D_q = \frac{1}{q-1} \lim_{\varepsilon \to 0} \frac{\log \sum_{i=1}^{N} \mu_i^q}{\log \varepsilon} \tag{1}$$

for $q \neq 1$. For $q = 1$, D_1 is defined by taking the limit when q approaches 1 and by using L'Hopital's Rule:

$$D_1 = \lim_{\varepsilon \to 0} \frac{\sum_{i=1}^{N} \mu_i \log \mu_i}{\log \varepsilon}. \tag{2}$$

It has been shown that the four multifractal dimensions D_{-1}, D_0, D_1 and D_2 are able to extract different surface information of SAR images. In this paper, we showed that surface information as described by D_q for $q > 2$ can be reduced to D_2 and thus it is sufficient to use correlation dimension D_2 to extract surface information since it is more computation expensive to calculate D_q for $q > 2$. Further more, we have also shown that fractal properties as described by D_q for $q \leq -1$ are reducible to the case D_{-1}. Hence, the four multifractal dimensions, D_{-1}, D_0, D_1 and D_2 are used to extract different surface information and by combining these information, we are able to characterize the pixel based on more textural information and thus would help describe the texture image more accurately.

These multifractal dimensions were applied to classify a multi-band multi-polarized AIRSAR image with *C*-, *L*- and *P*- bands of *HH*, *HV* and *VV* polarizations with four land use classes. Each band and each polarization gives different spatial information and this information can be further enhanced by calculating their multifractal dimensions D_{-1}, D_0, D_1 and D_2. We compared the effectiveness of multifractal dimensions by applying individual multifractal dimension to classify different land use classes of multi-band multi-polarized image. It is shown that there is no single dimension value that is suitable for all bands and all polarization. For image of a particular band and polarization, certain multifractal dimension gives better land use classification result as compared to others. We have also shown that except for classification of "water body" using L-band associated with any one of the multifractal dimensions, other classes are better classified using the combination of all four multifractal dimensions in a vector-form. The combination of multifractal dimensions portray consistency in classification for all land use classes, while the single multifractal dimension would give different accuracies on these land use classes when applied on images of different bands and polarizations.

In general, a relation among land use classes, image polarization and multifractal dimensions is studied in this paper and the results are analyzed. A hybrid approach combining multifractal dimension and other suitable classifier can be a suitable direction to focus at.

A GPU-based Fast Algorithm for Spaceborne SAR Image Simulation

Cheng-Yen Chiang[1], **Kun-Shan Chen**[1, 2, 3], **Chih-Tien Wang**[3], **and Tim Lee**[2]

[1]Department of Computer Science and Information Engineering, National Central University Chung-Li 32001, Taiwan
[2]Communication System Research Center, National Central University, Chung-Li 32001, Taiwan
[3]Center for Space and Remote Sensing Research, National Central University, Chung-Li 32001, Taiwan

Abstract— SAR image simulation is an effective means for understanding image characteristic, testing and evaluating focusing algorithms, among others. For example, in target detection, recognition, and identification, building numerous image database is more efficiently by generation of simulated image taking into account the sensor and target geo-locations relative to the Earth, movement of the platform, radar system parameters, and radiometric and geometric characteristics of the target; namely, in two main steps: echo signal generation and SAR processing. However, one of the problematic issues is the computation time. In particular, the most time consuming is in calculating radar echo for each slant range elements. The complexity is $O(n^3)$ where n is number of polygons times number of azimuth and range samples in target's RCS modeling and SAR image pixel size, respectively. Generally, n is very large making the simulation extremely inefficiently. This means it takes years to complete a single target simulation by nowadays PC with Quad CPUs (2.33 GHz, 8 GB memory). To overcome this drawback, in this paper, we develop an acceleration method to take full advantage of GPU and maintain same high accuracy. Testing on a MD80 airplane over the airfield mapped by TerraSAR-X satellite SAR system, the speed can be accelerated about 50 times with 240 GPUs running on Linux system. In general, the complexity becomes $O(n)$, a significant reduction. Details of the algorithms and more testing results with 480 GPUs will be reported.

Compressive Inverse Synthetic Aperture Radar Imaging

Suman K. Gunnala and Saibun Tjuatja
Wave Scattering Research Center, Department of Electrical Engineering
The University of Texas at Arlington, UTA Box 19016, Arlington, TX 76019-0016, USA

Abstract— Classical ISAR images are limited in resolution. Both down range resolution and cross range resolutions of the ISAR images are limited in practice due to finite bandwidth and unavailability of larger angular sector over which target is observed. To date there are several super-resolution algorithms [1] which are computationally intensive and require extrapolation of information outside the measurement aperture. In this paper, a method based on compressive sampling [2–5] to achieve super-resolution in ISAR imaging is presented.

The proposed super-resolution ISAR imaging estimates the target's signal subspace from the measured signal space by exploiting the sparsity of the targets' scattering centers in the image domain. The sparsity of target's signal satisfies the restricted isometric property (RIP) condition as required by compressive sampling for accurate recovery of signal from its compressed samples. The super-resolution ISAR imaging algorithm is implemented by enforcing the sparsity constraints via random compressive sampling of the measured data. Sparsity constraint ratio (SCR) is used as a design parameter. Mutual coherence is used as quantitative measure to determine the optimal SCR. ISAR data from controlled laboratory measurements for full angular sector as well as different partial angular sectors are utilized in this study to validate the proposed approach. Results show that significant resolution enhancement is achieved at SCR in the 20% range. More details about the super-resolution ISAR imaging and results of different measured data sets will be presented in the full paper.

REFERENCES

1. Xu, X. and R. M. Narayanan, "Enhanced resolution in SAR/ISAR imaging using iterative sidelobe apodization," *IEEE Transactions on Image Processing*, Vol. 14, No. 4, 537–547, Apr. 2005.
2. Candes, E., J. Romberg, and T. Tao, "Robust uncertainity principles: Exact signal reconstruction from highly incomplete frequency information," *IEEE Transaction on Information Theory*, Vol. 52, No. 2, 489–509, Feb. 2006.
3. Baraniuk, R. and P. Steeghs, "Compressive radar imaging," *IEEE Radar Conference*, 128–133, Boston, Apr. 2007.
4. Herman, M. and T. Strohmer, "High-resolution radar via compresses sensing," *IEEE Transactions on Signal Processing*, Jul. 2008.
5. Gunnala, S. K., J. Hall, and S. Tjuatja, "Localization of scattering centers in radar imaging based on sparsity constraints," *Proceedings of SPIE*, Vol. 7337, 73370J–73370J8, Apr. 2009.

Impact of Scatterers Description as Components for Forest Electromagnetic Scattering Models

Pierre Borderies and Ludovic Villard
ONERA-DEMR, 2-Avue E. Belin, 31055 Toulouse-Cédex, France

Abstract— In usual models for forests electromagnetic scattering, branches are often represented by straight homogeneous cylinders of finite length. According to the category of tree under consideration, this assumption may be reasonable or unduly exaggerated according to the way branches are curved or exhibit a section evolution, as they follow a thinning from the trunk to the extremities. Actually, there is the possibility of representing a long, curved branch into smaller straight ones, but the electromagnetic computation may be affected by this way of representation. The present paper treats these points numerically using Finite Differences in Time Domain for these shape effects, including curvature and thinning effects.

Implementation of Polarimetric Scattering Matrix Power Decomposition with Coherency Matrix Rotation Applied to ALOS-PAL-SAR Image Data Sets

Wolfgang-M. Boerner[1], **Yoshio Yamaguchi**[2], **Akinobu Sato**[2], **Ryoichi Sato**[2], **Hiroyoshi Yamada**[2], **and Kun-Shan Chen**[3]

[1]University of Illinois, USA
[2]Niigata University, Japan
[3]CSRSR, NCU, Taiwan

Abstract— This paper extends our earlier work and presents the four-component scattering power decomposition using a rotation of coherency matrix to distinguish vegetation and oriented urban area scattering characteristics. For arbitrarily oriented incidence urban area and vegetation signatures are decomposed into the same volume scattering mechanism. A new decomposition scheme of first using a rotation of coherency matrix to the polarimetric scattering matrix decomposition is presented and is applied successfully to decompose respective POLSAR data sets. It is shown that oriented urban areas are clearly distinguishable from volume scattering for flat, hilly and mountainous terrain.

Introduction: Since the launch of ALOS-POLSAR in 2006, a large number of fully polarimetric (Quad-Pol.) data sets have been acquired from space. Although the fully polarimetric mode is hitherto an experimental one, it has provided us with precious data sets of various places spread over the planet earth. The total number of scenes exceeds more than 190,000 as of June 2009. There are various image analysis methods for quad-pol. data sets as reviewed in [1, 2]. The representative and fundamental methods are based on ensemble averaging of several pixels bearing the second order statistics of polarimetric information: i) The HV basis imaging, ii) The Pauli basis imaging, iii) HAlpha-Anisotropy imaging, and iv) Power decomposition imaging.

The three-component or four-component decomposition schemes decompose polarimetric data of imaging pixel area into surface scattering, double bounce scattering, volume scattering, and helix scattering components. They have been successfully applied to POLSAR image analysis; however, there appear the following problems: Man-made structures orthogonal to radar illumination are clearly distinguishable, whereas for general urban areas with road and building structures aligned at arbitrary directions this is not so.

In order to resolve this arbitrarily oriented urban structures problem, we present in this paper a new decomposition scheme using an idea of desying, first conceived by Huynen [2]. If quad-pol data are acquired by actual POLSAR system, the image may be rotated around the radar line of sight. By rotation of the image (or equivalently data sets), we can obtain rectified images with vertical orientation. We then perform the four-component decomposition using this rotated data.

As the second example, the decomposed image corresponding to Fig. 1 is shown in Fig. 2, where the green areas in oriented urban areas as well as man-made structures are correctly turned into "red".

Figure 1: Example of four-component decomposition of Niigata area.

Figure 2: New decomposition of Niigata area corresponding to Fig. 1.

Conclusion: This paper presented a new decomposition scheme implementing a rotation of the coherency matrix before carrying out the four-component decomposition. By minimizing the cross-polarized component, the rotation angle is retrieved. Using the angle the coherency matrix is rotated. The decomposition algorithm is provided using coherency matrix elements only. This method is quite simple and effective. It is successfully carried out to quad. pol. SAR (Pi-SAR and ALOS-PALSAR) data and discriminated oriented urban blocks and vegetation as different scattering objects which previously were difficult to be discriminated. Arbitrarily oriented urban areas are classified into double bounce man-made structures. In addition, the image quality increased compared with the original decomposition within the fixed specification frame of radar resolution.

REFERENCES

1. Yajima, Y., Y. Yamaguchi, R. Sato, H. Yamada, and W.-M. Boerner, "POLSAR image analysis of wetlands using a modified four-component scattering power decomposition," *IEEE Trans. Geosci. Remote Sens.*, Vol. 46, No. 6, 1667–1773, 2008.
2. Yamaguchi, Y., A. Sato, R. Sato, H. Yamada, and W.-M. Boerner, "Four-component scattering power decomposition with rotation of the coherency matrix," Submitted to *IEEE Trans. Geosci. Remote Sens.*, Fall, 2009.

Session 2P5
Advances in Numerical Techniques 2

Semi-Analytical Mode Match Approach for Scattering Computation of Randomly Densely-distributed Conductive Targets

Hongxia Ye and Ya-Qiu Jin
Key Laboratory of Wave Scattering and Remote Sensing Information (MoE), Fudan University
Shanghai 200433, China

Abstract— A Numerical Mode Match method (NMM) for cylindrical wave function expansion is developed to fast compute electromagnetic scattering from a combined model of 2D conductive target with random position, size and shape. Firstly, the scattering field of each target is expanded as series summation of Hankel functions in its own local coordinate. The total scattering field in outside position is the summation of all targets, and the field inside each target is zero. Finite sample points on each target's surface are chosen to numerically match boundary conduction equation, and it yields a matrix equation about the expansion coefficients. In order to well restrict the boundary conduction on all targets surface, the sample point number should be more than the unknown expansion coefficients, and the matrix equation is over-determined. The singular value decomposition (SVD) or least squares method is used to obtain the optimal solution. Then the scattering field in outside region can be computed as series summation of cylindrical wave functions. This paper also analyzes the problem of series truncation, and obtains the relation of series number and target size for different shapes. Finally, numerical simulation is made for scattering analysis of multiple random shapes 2D conductive targets, and comparison is made with MoM computation to validate the new method.

The Decomposition of the Angular Spectrum Domain in the Parallel Multilevel Fast Multipole Algorithm

Xingang Wang[1, 2], **Bin Cheng**[1], **Hongxia Zhang**[3], **and Weiqin Tong**[1]

[1]School of Computer Engineering and Science, Shanghai University, Shanghai 200072, China
[2]College of Information Engineering, Zhejiang University of Technology, Hangzhou 310014, China
[3]Aviation Industry Development Research Center of China, Beijing 100012, China

Abstract— This paper discusses the decomposition of the angular spectrum domain in the parallel Multilevel Fast Multipole Algorithm (MLFMA), including the equational scheme, the strip scheme and the block scheme. The characteristics and the applicable principles of three methods are analyzed theoretically and numerically. The experiment results show that the block scheme is very efficient for enlarging the parallel scale, and can significantly improve the parallel efficiency.

Lanczos Biconjugate A-Orthonormalization Methods for Surface Integral Equations in Electromagnetism

B. Carpentieri[1], **Y.-F. Jing**[2], **and T.-Z. Huang**[2]

[1]CRS4 Bioinformatics Laboratory, Italy
[2]University of Electronic Science and Technology of China, China

Abstract— Integral equations methods are receiving a growing interest for solving Maxwell-type problems eciently on modern parallel computers. They solve for the induced electric and magnetic currents on the surface of the object and require a simple description of the geometry by means of triangular facets. Therefore, a 3D volume problem is reduced to solving a 2D surface problem simplifying considerably the mesh generation especially in the case of moving objects. In an integral equation context, the standard EM scattering problem can be formulated in variational form as follows:

Find the surface current $\vec{j}$ such that for all tangential test functions $\vec{j}^t$, we have

$$\int_\Gamma \int_\Gamma G(|y-x|) \left(\vec{j}(x) \cdot \vec{j}^t(y) - \frac{1}{k^2} \mathrm{div}_\Gamma \vec{j}(x) \cdot \mathrm{div}_\Gamma \vec{j}^t(y) \right) dxdy = \frac{i}{kZ_0} \int_\Gamma \vec{E}_{inc}(x) \cdot \vec{j}^t(x) dx. \quad (1)$$

We denote by $G(|y-x|) = \frac{e^{ik|y-x|}}{4\pi|y-x|}$ the Green's function of Helmholtz equations, Γ the boundary of the object, k the wave number and $Z_0 = \sqrt{\mu_0/\varepsilon_0}$ the characteristic impedance of vacuum (ϵ is the electric permittivity and μ the magnetic permeability). Eq. (1) is called Electric Field Integral Equation (EFIE) and can be applied to arbitrary geometries. The Galerkin discretization of Eq. (1) leads to dense complex non-Hermitian linear systems $Ax = b$ that are ill-conditioned especially at high frequency, and are characterized by many complex eigenvalues with large negative real part. In this talk we present a novel family of iterative Krylov methods for the solution of dense complex non-Hermitian systems [1]. The class of algorithms is derived by means of a Biconjugate A-Orthonormalizaion procedure imposing the residual r_0 be orthogonal at each iteration to the constraints subspace $W = A^H K_m(A^H, r_0^*)$, where we denote by K_m the Krylov subspace of size m and r_0^* is chosen to be equal to $P(A)r_0$, with $P(t)$ an arbitrary polynomial with respect to the variable t. Accordingly, the first method is named Biconjugate A-Orthogonal Residual (BiCOR) method and the two variants are called the Conjugate A-Orthogonal Residual Squared (CORS) method and the Biconjugate A-Orthogonal Residual Stabilized (BiCORSTAB) method. We illustrate an application to solving realistic electromagnetic scattering problems arising from radar-cross section calculations in industry. We report on experiments to show the competiteveness of the proposed class of algorithms with other popular standard approaches based on Arnoldi orthonormalization or Lanczos Biorthonormalization procedures such as GMRES, BiCGSTAB, QMR. Finally, we address the issue of the construction of robust parallel preconditioners which is another critical component of the iterative solution in this context.

REFERENCES

1. Jing, Y.-F., T.-Z. Huang, Y. Zhang, L. Li, G.-H. Cheng, Z.-G. Ren, Y. Duan, T. Sogabe, and B. Carpentieri, "Lanczos-type variants of the COCR method for complex nonsymmetric linear systems," *Journal of Computational Physics*, Vol. 228, No. 17, 6376–6394, 2009.

Analysis of Polynomial and Geometric Conductivity Profiles in PML Layers: A Comparison

M. Benavides-Cruz[1,3], **M. Álvarez-Cabanillas**[2], **M. Enciso-Aguilar**[1], **and J. Sosa-Pedroza**[1]

[1]ESIME-SEPI, Posgrado en Telecomunicaciones, Instituto Politécnico Nacional
UPALM Edif. Z-4, 3er. piso, Zacatenco 07738, México, D.F., México
[2]Centro de Investigación y Desarrollo de Tecnología Digital, Instituto Politécnico Nacional
Av. Del Parque 1310, Mesa de Otay, Tijuana, Baja California, México
[3]Facultad de Ingeniería Electrónica y Comunicaciones, Universidad Veracruzana
Prolong. Av Venustiano Carranza s/n, Poza Rica, Veracruz, México

Abstract— A basic consideration for the Finite Difference Time Domain (FDTD) method is to limit the computational space domain, to this end, the Absorbing Boundary Conditions (ABC) should be defined to simulate an infinite domain. Special attention has devoted to this issue since the beginning of the method, from the theory of scattered-wave annihilating differential operators of Bayliss and Turkel to the current Perfect Matched Layer (PML). In this paper we report on the reflexion coefficients computed for several incidence angles to the PML by using two main conductivity distributions: Polynomial and Geometrical. The study was carried out by implementing the FDTD method over a free divergences region employing a propagating TM mode Gaussian pulse as a source.

Time-domain Analysis of Electromagnetic Scattering Problems by Numerical Inversion of the Laplace Transform

S. Ohnuki, **Y. Kitaoka**, **and S. Kishimoto**
Department of Electrical Engineering, College of Science and Technology, Nihon University, Japan

Abstract— A novel computational technique is proposed to investigate time-domain analysis of electromagnetic scattering problems. In our technique, the scattered waves in the complex frequency domain are obtained by using such as the method of moments and the waves in the complex frequency domain are transformed into the time domain by using the numerical inversion of the Laplace transform. The method of the inversion is based on the approximation of the exponential function in the Bromwich integral and expressed by the infinite series in the algorithm. We will discuss that our proposed technique is error controllable and reliable simulation in time domain can be preformed for arbitrary shapes of targets.

Figure 1 shows the backscattered response when a sine wave impinges on a conducting sphere. The solid line indicates the computational result obtained by our method. We can confirm that the result is in complete agreement with the exact solution indicated by dots.

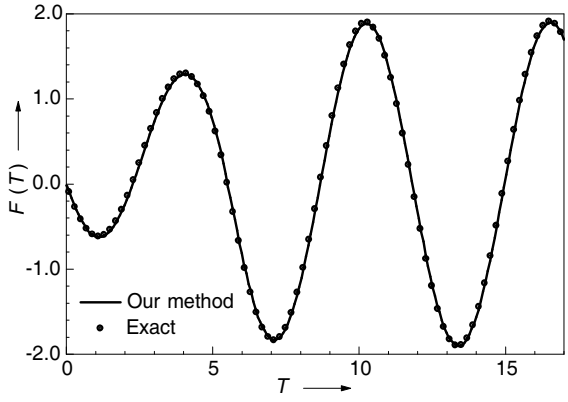

Figure 1: Backscattered response from a conducting shpere.

Interconnect and Packaging Analysis Based on the Dual Basis Expansion of Magnetic Current in the Method of Moments

M. S. Tong[1], **W. C. Chew**[1], **A. Deutsch**[2], **B. J. Rubin**[2], **J. D. Morsey**[2], **and L. Jiang**[2]

[1]Department of Electrical and Computer Engineering
University of Illinois at Urbana-Champaign
Urbana, IL 61801, USA
[2]IBM T. J. Watson Research Center, Yorktown Heights, NY 10598, USA

Abstract— Electromagnetic (EM) simulation and analysis for interconnect and packaging structures in high-speed digital microelectronic devices rely on the accurate solutions of relevant EM equations. In the integral equation approach, surface integral equations (SIEs) are usually preferred when the inhomogeneity of involved materials can be neglected because one only discretizes the object surfaces or boundaries with a less number of unknowns. When the SIEs are solved with the method of moments (MoM), however, one has to use two appropriate basis functions to represent the unknowns because both equivalent electric current and magnetic current exist on the boundaries. The robust Rao-Wilton-Glisson (RWG) basis function is a natural choice for expanding the electric current, but how one represents the magnetic current will affect the solving of the electric field integral equation (EFIE) and magnetic field integral equation (MFIE). One could choose the RWG basis function again or $\hat{n} \times$ RWG basis function, where $\hat{n}$ is a unit normal vector on the object boundaries, to represent the magnetic current, but the former choice will result in a very ill-conditioned system matrix and the later choice will create line charges on the boundaries [1].

Although the $\hat{n} \times$ RWG choice could be used in some situations, it might not be tolerated in interconnect and packaging analysis because of the severe requirements of application. The interconnect structures are usually in multiscale, i.e., the conducting parts are much smaller compared with the dielectric parts and the geometrical discretization usually includes many meshes with very high aspects [2]. Also, there is a low-frequency effect in the solutions since the structures are very small compared to the wavelength. Both challenges require a more accurate representation for the magnetic current in solving the EFIE or MFIE.

Chen and Wilton proposed the dual basis function to represent the magnetic current in 1990 [3]. The advantages of the basis function include the approximate orthogonality to the RWG basis function, the constant charge density within each polygon and the vanishing total charge within a polygon pair, and no fictitious line charge along polygon boundaries. This basis function is very similar to the RWG basis function in property although it is much more complicated in implementation. In this work, we applied this basis function to expand the magnetic current in the MoM solutions for interconnect and packaging structures. Numerical examples show that the basis function can work well even for such challenging structures. It is found that the multiscale problem and low-frequency effect can be greatly alleviated due to the accurate representation of dual basis function for the magnetic current in the simulations.

REFERENCES

1. Sheng, X. Q., J. M. Jin, J. M. Song, W. C. Chew, and C. C. Lu, "Solution of combined-field integral equation using multilevel fast multipole algorithm for scattering by homogeneous bodies," *IEEE Trans. Antennas Propagat.*, Vol. 46, No. 11, 1718–1726, 1998.
2. Liao, E. B., A. A. O. Tay, S. S. Ang, H. H. Feng, R. Nagarajan, and V. Kripesh, "Numerical analysis on compliance and electrical behavior multi-copper-column flip-chip interconnects for wafer-level packaging," *IEEE Trans. Adv. Packag.*, Vol. 29, No. 2, 2006.
3. Chen, Q. L., "Electromagnetic modeling of three-dimensional piecewise homogeneous material bodies of arbitrary composition and geometry," Ph.D. Dissertation, Department of Electrical Engineering, University of Houston, 1990.

Fast and Broadband Simulation of Large-scale Microstrip Structures

Yongpin Chen[1], **Jie L. Xiong**[2], **and Weng Cho Chew**[1, 2]

[1]Department of Electrical and Electronic Engineering, University of Hong Kong
Pokfulam, Hong Kong, China
[2]Department of Electrical and Computer Engineering, University of Illinois at Urbana-Champaign
Urbana, IL 61801, USA

Abstract— Simulation of microstrip structures has attracted intensive studies for many years. The integral equation method (IEM) based on layered medium Green's function (LMGF) is one of the most popular methods, since the number of unknowns can be drastically reduced compared to other methods, such as the volume-surface integral equation method (VSIE). The difficulty mainly lies in the evaluation of the LMGF, which is usually time consuming. This makes the standard moment method implementation very inefficient.

Recently, a generalized thin-stratified medium fast-multipole algorithm (TSM-FMA) was successfully developed by our group. Compared to its original form, this new TSM-FMA can handle microstrip antennas or arrays with vertical structures that may straddle different layers, making it more applicable in microwave engineering. However, when the operating frequency decreases, the interaction partially falls into the low frequency regime, this fast algorithm breaks down. In this paper, a mixed-form thin-stratified medium fast multipole algorithm (MF-TSM-FMA) is proposed to solve this problem.

For well-separated interactions, the LMGF can be accelerated by deforming the Sommerfeld integral path into the vertical branch cut, where the integrand becomes much smoother and decays more rapidly. Gauss-Lengendre quadrature is then applied to discretize the integral. Since the LMGF can be expressed as a summation of several Hankel functions weighted by some z-dependent parameters, the calculation can be accelerated by two-dimensional multilevel fast multipole algorithm (2D MLFMA).

In this paper, we combine the multipole expansion and plane wave expansion of the 2D addition theorem into a single multilevel tree, to account for the circuit physics as well as wave physics simultaneously. A transition between the two expressions is derived. At leafy levels, where the size of the box is much smaller than the wavelength, the outgoing wave is calculated by multipole expansion. When the size of box becomes large enough, the transition is applied to transfer the multipole information into the plane wave one. By doing this, different physics can be captured separately by utilizing the multilevel nature of the MLFMA. Several numerical results are demonstrated to validate this algorithm.

The Voronoi-delaunay Dual Diagram and a Co-volume Integration Scheme for Computational Electromagnetics in the Time Domain

Z. Q. Xie, **Oubay Hassan**, **and Kenneth Morgan**
Civil and Computational Engineering Centre, School of Engineering
Swansea University, Swansea, Wales, UK

Abstract— Computational methods are widely employed for the solution of Maxwell's equations in a variety of different application areas that fall within the general field of electromagnetics. For practical applications, the requirement of modeling complex geometries means that unstructured mesh methods are particularly attractive, as fully automatic unstructured mesh generation procedures are now widely available. Following this philosophy requires the identification of a suitable unstructured mesh based solution algorithm and several low order 3D time domain procedures have been proposed.

Co-volume methods, which are staggered in both time and space, exhibit a high degree of computationally efficiency, in terms of both CPU and memory requirements compared to, for example, a finite element time domain method. Despite the fact that real progress has been achieved in unstructured mesh generation methods since late 1980s, co-volume schemes have not generally proved to be effective for electromagnetic simulations involving general domains of complex shape. This is due to the difficulties encountered when attempting to generate the high quality meshes that are needed to satisfy the mesh requirements necessary for co-volume methods.

In this work, we concentrate on electromagnetic wave scattering simulations and describe a Voronoi-Delaunay dual diagram co-volume scheme on unstructured meshes. The necessary properties that the mesh must satisfy are identified. A structured hexahedral mesh is employed in the far field, with a PML used to satisfy the outer boundary condition. The hexahedral mesh is connected to an unstructured inner mesh by the use of wedge shape elements. A new technique has been developed to improve the overall quality of the resulting Voronoi-Delaunay dual diagram and we implement an approach for generating appropriate three-dimensional meshes. The co-volume solution algorithm for electromagnetic waves has the advantage of preserving the energy and, hence, maintaining the amplitude of plane waves. It also provides a better approximation of the field near sharp edges, vertices and wire structures, without the need to reduce the element size. This extension of Yee's scheme to unstructured meshes for general geometries should prove to be particularly attractive for the simulation of complex industrial problems.

A Multi-region Domain Decomposition Method for Analysis of Multiple Antennas Mounted on Complex Platform

X. Wang and J.-F. Lee
Department of Electrical and Computer Engineering, The Ohio State University, USA

Abstract— Modern aircraft are usually equipped with multiple antennas for a variety of purpose, e.g., communication, target tracking, etc. The existence of platform usually introduces the mutual coupling among the antennas, which may compromise the antenna performance or even prevent them from operating simultaneously. A Multi-Region Domain Decomposition Method (MR-DDM) is proposed to analyse this problem. It first decomposes the computational domain into a large PEC platform region and several antenna regions which have a lot of local fine features as well as complex materials. Then MoM and FEM-DDM are applied to solve these regions respectively. The communication among regions are implemented by near field coupling, which is accelerated by ACA algorithm. The MR-DDM provides a framework to integrate the existing Maxwell equation solver without significant modification, as long as the solver can solve the problems with incident wave. To enhance the robustness, which is usually challenged when the multiple objects have strong coupling, Krylov solver is implemented in the outer loop. In this implementation, the coupling between the touching surfaces of neighbouring regions are implemented with union-mesh technique, which means that the regions no longer need to be disjointed. This significantly enhances the flexibility of this method in the scenarios where some dielectric objects are just touching the surface of large PEC platform. We apply this method on the analysis of mutual coupling between two antennas mounted on realistic aircraft. Numerical result will be presented in conference. This method provide a practical way to analyse the antenna performance with presence of large complex platform.

Reflection Coefficient of the Isotropic-Dispersion Finite-Difference Time-Domain (ID-FDTD) Method at Planar Dielectric Interfaces

Pingping Deng and Il-Suek Koh
Graduate School of Information Technology & Telecommunications
Inha Unvierstiy, South Korea

Abstract— The standard finite difference time-domain (FDTD) method has been popular to simulate complex electromagnrtic problems. However, the standard FDTD method inherently has a critical disadvantage of "numerical dispersion", and thus has mainly been used for electrically small and phase insensitive problems. To rectify the dispersion error, several methods have been proposed including Fang's higher-order scheme, non-standard FDTD (NSFDTD) scheme, ID-FDTD scheme and so on [1]. Among the low-dispersion FDTD schemes, the ID-FDTD scheme shows the lowest dispersion error [2]. However, the behavior of the ID-FDTD scheme is not clearly understood, which is the motivation of the paper. First, this paper presents analytical formulations of the numerical reflection coefficients of the ID-FDTD algorithm at a planar dielectric boundary for a TM and TE wave incidences. The formulations are obtained based on two different methods such as "difference method [3]" and "matrix eigen-value method [3]". The matrix eigen-value method can provide exact result for the reflection coefficient, but the final equation of the reflection coefficient is a cubic equation. Hence, it is very difficult to obtain a closed-form solution for the coefficient based on the matrix eigen-value method. Exact reflection coefficients for the Yee scheme can be formulated based on the difference method, but the method can be directly applied to the ID-FDTD scheme. Based on the difference method, however, approximate coefficients can be derived, whose accuracy is numerically verified by comparing the results of the approximate formulation, matrix eigen-value method, and ID-FDTD scheme. Based on the approximate solution and numerical simulations, effective permittivity and permeability for the grid on the dielectric interface are obtained, which are the same as those for the Yee scheme.

REFERENCES

1. Shlager, K., J. Schneider, and S. Lockheed-Martin, "Comparison of the dispersion properties of several low-dispersion finite-difference time-domain algorithms," *IEEE Transactions on Antennas and Propagation*, Vol. 51, No. 3, 642–653, 2003.
2. Koh, I., H. Kim, J. Lee, J. Yook, and S. Chang, "Novel 2-D FDTD scheme with isotropic dispersion and enhanced stability," *IEEE Transactions on Antennas and Propagation*, Vol. 54, No. 11, 3505–3510, Nov. 2006.
3. Christ, A., S. Benkler, J. Fröhlich, and N. Kuster, "Analysis of the accuracy of the numerical reflection coefficient of the finite-difference time-domain method at planar material interfaces," *IEEE Transactions on Electromagnetic Compatibility*, Vol. 48, No. 2, May 2006.

Analyzed of Yagi Antenna by the Theory of Maxwellian Circuits

Wenhui Shen[1], **Yanzhong Ma**[1], **Mingliang Wu**[1], **and K. K. Mei**[2]

[1]School of Communication and Information Engineering, Shanghai University, Shanghai 200072, China
[2]Department of Electrical Engineering and Computer Science, University of California, Berkely, USA

Abstract— In this paper, the theory of Maxwellian Circuits (MC) is applied to Yagi antenna, the geometry of the Yagi antenna is formulated in detail. Combining with Hallen's Equation and Lorenz Gauge, the voltage cancellation technique is used which transforms the voltage into analytic form, which avoids differential-integral computation in solving voltage as well as simplifies the calculation. Yagi antenna with three elements is calculated as examples. Currents distribution and the radiation pattern are presented. In order to check the procedure, currents and radiation pattern by Method of Moment (MoM) are used as standard. The good agreement of the two results show that MC is an efficient numerical method, its accuracy is as high as MoM.

Modelling of Coil-loaded Wire Antenna Using Composite Multiple Domain Basis Functions

A. A. Lysko
Meraka Institute, Council for Scientific and Industrial Research (CSIR), South Africa

Abstract— The work discusses aspects of and applies a novel impedance matrix compressing technique [1] to model a coil-loaded monopole. The technique reduces the number of variables required for modeling of structures with curvatures and structures with electrically small features. The presented realization of the technique assumes usage of piece-wise linear geometrical approximation. This approximation is seen as the core to the inefficiency in modeling of the above-mentioned types of geometrical structures with a traditional method of moments (MoM). The reduction in the number of variables is accomplished by a logical aggregation/grouping of the individual wire segments into equivalent continuous wires. This permits to apply a single basis function over several wire segments, and to decouple the number of unknowns from the number of geometrical segments. Aggregation of small features aims a reduction in the impedance matrix condition number [2]. The method used in this paper borrows the matrix form of expressions from [3] and develops it further, as to use a Galerkin approach [1, 5].

The modeled antenna includes two straight wire segments and a helical coil placed between them [4]. The coil is modeled using up to 128 piecewise linear wire segments per turn. A delta gap generator used as the feed is attached to a wire with zero radius at that end. The monopole was tested using an equivalent loaded dipole.

The model was first verified using a traditional MoM with low and higher-order polynomial basis functions [5], where the low order functions are the same as those used in [1]. This stage included a comparison of the frequency dependence and current distribution profiles against the experimental data [4], and has confirmed validity and quality of the numerical meshes and resultant models.

Next, a set of simulations with various values of the meshing parameters and meshing algorithms were performed in order to generate the convergence curves (of error versus number of variables). The results at the finest mesh were used as the reference.

The convergence plots show that the proposed novel algorithm converges quicker than the traditional MoM based on the piecewise linear (PWL) basis functions, especially if only few unknowns are available or permitted for modeling. When the number of unknowns is few, an order of magnitude improvement in the accuracy of the solution was observed. In addition, it was observed that the condition number of the compressed solution for a dipole is much lower than that of the traditional solution for the same and closely matching one for a monopole model.

REFERENCES

1. Lysko, A. A., "Using piecewise sinusoidal basis functions to blanket multiple wire segments," *IEEE Int'l Symp. on Ant. & Propag. and USNC/URSI Nat. Radio Science Meeting*, North Charleston, USA, Jun. 2009.
2. Chew, W. C., J. Jin, E. Michielssen, and J. Song, *Fast and Efficient Algorithms in Computational Electromagnetics*, Artech House, 2001.
3. Rogers, S. D. and C. M. Butler, "An efficient curved-wire integral equation solution technique," *IEEE Trans. Ant. and Propag.*, Vol. 49, 70–79, Jan. 2001.
4. Taguchi, M., K. Yamashita, K. Tanaka, and T. Tanaka, "Analysis of coil-loaded thin-wire antenna," *IEEE AP-S Intl. Symp. 3*, 273–276, 1990.
5. Kolundzija, B. M. and A. R. Djordjević, *WIPL-D: Electromagnetic Modeling of Composite Metallic and Dielectric Structures — Software and User's Manual*, Artech House, Boston, 2000.

A Method of Applying Single Higher Order Polynomial Basis Function over Multiple Domains

A. A. Lysko
Meraka Institute, Council for Scientific and Industrial Research (CSIR), South Africa

Abstract— A technique has been devised where one set of higher order polynomial-based basis functions [1] can be applied over several wire segments, thus permitting to decouple the number of unknowns from the number of segments, and thus also from the geometrical approximation accuracy. The technique extends the prior art based on the piecewise uniform [2], linear [3] and sinusoidal [4] basis and testing functions onto polynomials. The technique has been derived and applied to a surface form of the electrical field integral equation within the framework of a method of moments (MoM). The main advantage of the proposed method is in permitting to reduce the required number of unknowns for curved structures and structures including electrically small features.

The technique is based on an approximating equation $\mathbf{I}_1 = \mathbf{M} \cdot \mathbf{I}_2$ relating the unknowns in a traditional (original) formulation of the MoM to the unknowns in the new formulation [2–4]. In this equation, $\mathbf{I}_1$ is the column vector with N_1 original unknowns, which are the unknowns used in the direct solution with the traditional method of moments. The column vector $\mathbf{I}_2$ is the vector with N_2 new unknowns. The compression of the impedance matrix is based on N_2 being smaller than N_1. The matrix $\mathbf{M}$ of size N_1 by N_2, relates the two sets of unknowns, and is herein referred to as a *compression matrix*.

The method discussed in this work focuses on establishing the matrix $\mathbf{M}$, when both the original (sub-domain) and new (composite) sets of basis functions are hierarchical polynomials. For simplicity, the derivations are done for a single continuous wire represented by a multiplicity of shorter wire segments. The derivations can be readily expanded onto an arbitrary combination of the wires. It is assumed that each original basis function is written as $a_k \cdot (x - x_{c1})^k$, where x_c and x_{c1} are in a coordinate system common for all the wire segments composing the wire. A composite basis function is supposed to cover several wire segments. It is also assumed that each geometrical element uses K unknowns. A similar form of $A_k \cdot (x - x_c)^k$ is assumed for the new compressed set of basis functions over the wire. The new co-ordinate system can be related to the original local co-ordinate systems by a simple shift in the coordinate.

The work shows that the matrix $\mathbf{M}$ can be written in the form $\mathbf{M} \equiv \mathbf{X} \cdot \mathbf{G} \cdot \mathbf{X}^{-1}$. Here, the matrix $\mathbf{X}$ relates the set of original basis functions, $\mathbf{BF}_{\text{old}}$, and their decomposition into terms of a polynomial, $\mathbf{P}_{\text{old}}$ as $\mathbf{BF}_{\text{old}} = \mathbf{X} \cdot \mathbf{P}_{\text{old}}$, while the matrix $\mathbf{G}$ defines a conversion from the hierarchical polynomials defined in the original local coordinate system, $\mathbf{P}_{\text{old}}$, into the new local co-ordinate system, $\mathbf{P}_{\text{new}} : \mathbf{P}_{\text{old}} = \mathbf{G} \cdot \mathbf{P}_{\text{new}}$. The elements of the matrices are derived. The computational cost of the process has been estimated in terms of K etc.

REFERENCES

1. Kolundzija, B. M. and A. R. Djordjević, *Electromagnetic Modeling of Composite Metallic and Dielectric Structures*, Artech House, 2002.
2. Rogers, S. D. and C. M. Butler, "An efficient curved-wire integral equation solution technique," *IEEE Trans. Ant. and Propag.*, Vol. 49, 70–79, Jan. 2001.
3. Lysko, A. A., "Grouping individual wire segments into equivalent wires or chains, and introduction of multiple domain basis functions," *IEEE Int'l Symp. on Ant. & Propag. and USNC/URSI Nat. Radio Science Meeting*, North Charleston, USA, Jun. 2009.
4. Lysko, A. A., "Using piecewise sinusoidal basis functions to blanket multiple wire segments," *IEEE Int'l Symp. on Ant. & Propag. and USNC/URSI Nat. Radio Science Meeting*, North Charleston, USA, Jun. 2009.

Modelling a Wire Mesh Reflector by Grouping into Sub-meshes

Albert A. Lysko[1, 2]

[1]Meraka Institute, CSIR, South Africa
[2]Norwegian University of Science and Technology, Norway

Abstract— This paper extends a recently developed method for aggregating multiple wire segments into composite equivalent wires [1] to modeling of wire meshes. The multiple domain basis function (MDBF) technique for the method of moments (MoM) [1] permits to cover multiple individual wires (chains) with a single common basis function. This can reduce the number of unknowns required for modeling curved structures and structures with electrically small features with little or no loss in the accuracy. The present work expands the original technique [1] onto wire meshes.

The considered wire mesh is composed of a multiplicity of individual wire quadrilaterals, each having four wires (although the technique can also be applied to wire meshes of any shapes, including triangles and hexagons). In a wire mesh, most of the quadrilaterals, except for the peripheral ones, are attached to each other with all four sides. The current in each wire composing a quadrilateral requires at least one unknown. This is inefficient when the wire mesh is used to model a curved solid surface or when the size of a mesh cell is made electrically small to model a specific geometrical feature. One approach to reduce the number of unknowns is to use a rougher mesh with larger cells. This approach cannot handle fine geometrical details accurately and has higher transparency, i.e., lets the electromagnetic waves penetrate through the rough mesh more than the fine mesh, which introduces errors.

The proposed method considers grouping the small quadrilateral cells into larger quadrilaterals (including several the small ones). There, only the current on the sides of the larger quadrilaterals contributes to the count of the required unknowns. However, unlike roughening the mesh, the current on the inner wires of the larger cells (the ones composing the original fine cells) is not neglected but is instead interpolated from the current on the sides of the larger cells. In terms of the approximation error [2], this is interpreted as current interpolation and integration errors with respect to the finer mesh.

The introduced method has been applied to a wire mesh reflector. A comparison of the rough and original fine mesh when using traditional MoM [3, 4] showed that the rough mesh permits more energy through and also introduces errors in the magnitude of the radiation pattern. Next, the proposed interpolation technique was applied. The obtained results were found to be closer to the results produced by the original fine mesh, yet fewer unknowns were required to solve the problem.

Summarizing, a novel technique for electromagnetic modeling of fine wire meshes has been devised, which can be easily applied to existing MoM codes. An example of a wire reflector antenna confirmed that the proposed technique can produce results of better accuracy than the usual roughening of a mesh, yet uses fewer unknowns.

REFERENCES

1. Lysko, A. A., "Using piecewise sinusoidal basis functions to blanket multiple wire segments," *IEEE Int'l Symp. on Ant. & Propag. and USNC/URSI Nat. Radio Science Meeting*, North Charleston, USA, Jun. 2009.
2. Chew, W. C., J. Jin, E. Michielssen, and J. Song, *Fast and Efficient Algorithms in Computational Electromagnetics*, Artech House, 2001.
3. Kolundzija, B. M. and A. R. Djordjević, *Electromagnetic Modeling of Composite Metallic and Dielectric Structures*, Artech House, 2002.
4. Kolundzija, B. M. and A. R. Djordjević, *WIPL-D: Electromagnetic Modeling of Composite Metallic and Dielectric Structures — Software and User's Manual*, Artech House, Boston, 2000.

Session 2P6a
Microstrip and Printed Antennas, Phase Array Antennas 2

The Study on the Antenna Optimization

Junping Geng, **Ronghong Jin**, **Xianling Liang**, **Hao Wu**, **Ye Sheng**, **and Bangda Zhou**
E. E. Dept., Shanghai Jiao Tong University, Shanghai 200240, China

Abstract— What is the optimal antenna? No one give a precise answer. In fact, some one optimize the antenna's parameters to get some best performance in some limited range based on experience model. In the further, some others divides a 2-D rectangular area into some grids, then the initial 2-D chromosome population is produced randomly. The size of population is the number of grids, "1" represent the metallized areas and "0" represent the areas without metal. But the fatal problem is that two diagonally metal grid connected at one point in simulation, and it maybe unclear in manufacturing, joint or not?

Here a continuing method is presented to optimize microstrip antenna to try to overcome the shortcoming of those two method — Experience model and random grids. Firstly, the procedure is divide into 2 steps: 1) Crude model is constructed based on the continuing rule — The second metal grid always connects the former one with one edge, so that the whole metal area is continuous. 2) Precise model optimization: The crude model is regularized by the surface currency, then it is described by some parameters, and optimize these main parameters to get the best performance of antenna in some range. A multi-band antenna is optimized by this method, and the measured results is good.

High Performance Antenna Array with Patch Antenna Elements

Dau-Chyrh Chang[1, 2], **Bing-Hao Zeng**[2], **and Ji-Chyun Liu**[3]

[1]Department of Communication Engineering, Oriental Institute of Technology
Banciao, Taipei 220, Taiwan
[2]Department of Communication Engineering, Yuan Ze University
Chung-li, Tao-yuan 32003, Taiwan
[3]Department of Electronics Engineering, Ching Yun University
Chung-li, Tao-yuan 32097, Taiwan

Abstract— In general, the overall efficiency of patch array is low. In this paper, array antenna with four patch antenna elements for the application is developed. By adjusting the thickness of patch antenna element and geometry of antenna array, the maximum gain of array can be achieved. Although the required frequency is within 2.4 ∼ 2.5 GHz, the simulated and measured frequency range is 2.30 ∼ 2.65 GHz. The gain of simulation and measurement antenna array is about 13 dBi. The overall efficiency is over 65% over the operating band. The test results of power gain and return loss are quite agreed with that of simulation.

Antenna Design and Simulation with 4-element Array Antenna: Base on the requirements of compact size, high gain, narrower beamwidth is designed as shown in Fig. 1. The antenna array is composed of four patch antenna elements. The physical dimension of the radiating array is 203 mm by 220 mm. The radiating patch antenna elements distribute on the FR substrate. The substrate is FR4 with dielectric constant of 4.4, and the thickness of the substrate is 1.5 mm. The size of each patch is 54 mm by 43 mm with air dielectric height h 5 mm.

The simulated tool is using GEMS. The simulation return loss with various heights with air substrate of patch antenna element is compared as shown in Fig. 2. For best return loss is with air substrate height 5 mm. The result of return loss is smaller than 10 dB at the 2.4 GHz band. The detail performance and design will be discussed during presentation.

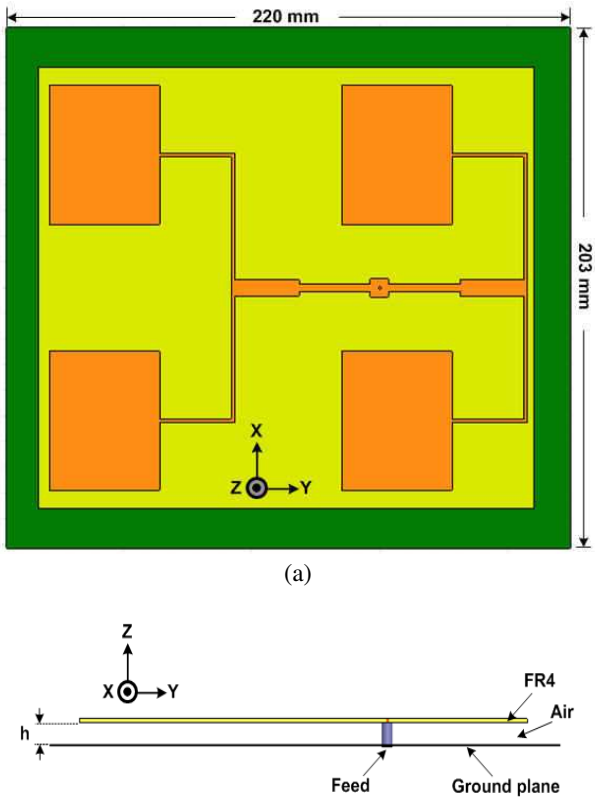

Figure 1: Simulated structure of array antenna: (a) top view, (b) side view.

A Multiple Antenna System for RFID Access Control Management

Yinlong Huang, **Wei He**, **Weihua Sun**, **and Jiang Xu**
Anti-counterfeit Information Department, The Third Research Institute of MPS, China

Abstract— In this paper, a multiple antenna system for RFID access control management is presented. This multiple antenna system is at UHF (ultra high frequency) band operation and consists of two circular polarization antenna arrays. Two antenna arrays with UHF reader, exploiting antenna diversity selection by radio frequency (RF) chain switches, are used for compensating deficiencies in reading ability of single antenna. In application, a human being with RFID card must be read by both antenna arrays can be permitted to enter the control guard. Designing this system make it a suitable candidate for RFID application in access control for some importance meetings and sporting contests etc.

Session 2P6b
Mobile Antennas and Antenna with Metamaterials

60 GHz Meta-material Wideband Antenna for FPGA Giga Bit Data Transmission

Ying Peng and Zhirun Hu
School of Electrical and Electronic Engineering, The University of Manchester
Manchester, UK

Abstract— With the recent progress and rapid increase in digital high definition technology, wideband wireless systems are being taken into actual use, such as HD media transmission, demanding compact wideband antennas. A dipole antenna with folded elements at both ends gives an enhancement of over 55% bandwidth [1]. Although it is easily assembled for its planar structure, a folded dipole antenna usually operate at low frequency spectrum. In 2001, the Federal Communications Commission (FCC) allocated 7 GHz in the 57–64 GHz band for unlicensed use. Within those past few years, substantial knowledge on 60-GHz millimeter-wave (MMW) channel has been accumulated for commercial applications. Most of recent 60 GHz antenna study based on dielectric substrate like GaAs, SiGe and InP because of its fast speed and low noise implements. However, compared with CMOS technology, they are quite poor integration and high cost.

In this paper, a 60 GHz half wavelength folded dipole antenna in meta-material cavity based on standard CMOS technology is proposed. The full wave simulation results reveal a wide operating bandwidth of 7 GHz (VSWR < -2) from 59 GHz to 66 GHz, which is shown in Fig. 1. The simulated radiation patterns are shown in Fig. 2. It can be seen that 5 dB enhancement on the gain has be achieved. A 100 Ω CPS is used to feed the 1.5 mm folded dipole antenna and the cavity size is 4 mm × 2.8 mm. The superstrate thickness is of 500 µm. As the meta-material

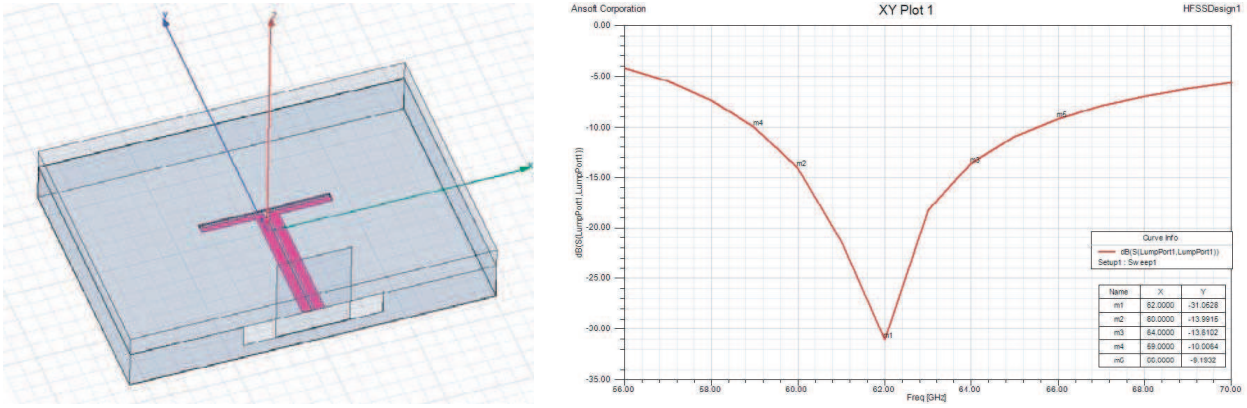

Figure 1: Antenna structure and S_{11} simulation result.

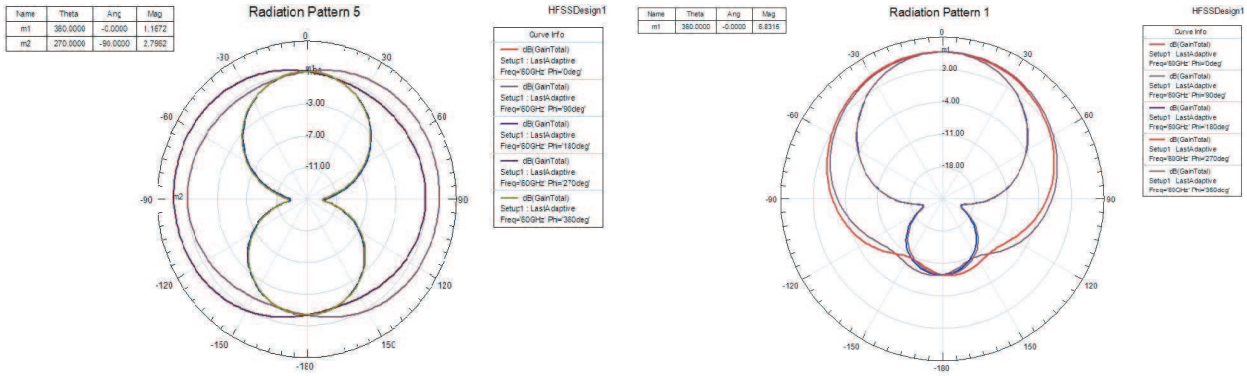

(a) (b)

Figure 2: (a) Antenna gain without cavity, (b) antenna gain with cavity.

cavity can shield objects on the other side, the antenna's performance will be insensitive to its surrounding packages and other metal structures.

REFERENCES

1. Kim, Y., H. Morishita, and S. Horiuchi, "Wideband planar folded dipole antenna with self-balanced impedance property," *IEEE Transactions on Antennas and Propagation*, Vol. 56, No. 5, 1223–1228, May 2008.

A Miniature Coupled Loop Antenna to be Embedded in a Mobile Phone for Penta-band Applications

Sheng-Yu Lin, **Hsien-Wen Liu**, **Chung-Hsun Weng**, **and Chang-Fa Yang**
Department of Electrical Engineering, National Taiwan University of Science and Technology
Taipei, Taiwan

Abstract— A compact coupled loop antenna of the mobile phone for GSM850/GSM900/ DCS/PCS/UMTS penta-band applications is presented. This antenna comprises folded loop strips and a coupled gap to be embedded inside the mobile phone. By adding a gap between two loop elements for coupling, a resonant mode in the GSM850/900 band can be excited. Simulated and measured results are compared, which show good agreements. Also, good radiation efficiency and return loss are obtained. This antenna can be fabricated with a low cost and can be built in the mobile phone for penta-band applications.

ACKNOWLEDGMENT

This work was supported in parts by Chant Sincere Company, Ltd. (COXOC) and National Science Council of ROC under Grant NSC 97-2221-E-011-024.

A Novel Design of Planar Spiral Antenna with Metamaterial

Nakun Jing, **Huiling Zhao**, **and Lihao Huang**
Northwestern Polytechnical University, Xi'an, Shaanxi 710072, China

Abstract— This paper presents the design of the spiral antennas with metamaterial. It is a new way of producing a low-profile and wide-band antenna. According to the relationship of spiral antenna's active region and frequency, a circumferential multilayer substrate is designed with a reduced antenna total height. Based on effective media theory, circumferential multilayer substrate is implemented with aligned disk lattice. Simulation results demonstrated that the novel spiral antenna has relatively high gain, while S_{11} of the spiral antenna with metamaterial is not as good as expected.

Compact Multi-band Antenna for Global Navigation Satellite Systems

Steven Gao and Li Zheng
Surrey Space Centre, University of Surrey, Guildford GU2 7XH, UK

Abstract— In this paper, a compact multi-band antenna suitable for Global Navigation Satellite Systems (GNSS) will be presented. GNSS is the generic term for satellite navigation systems that provide autonomous geo-spatial positioning with global coverage. Nowadays, GNSS includes Global Positioning Systems (GPS, USA), Beidou (P. R. China), GLObal NAvigation Satellite System (GLONASS, Russia), and Galileo (Europe), etc. It has been widely used in the precise positioning of spacecrafts, air plane, boats, ships and mobile vehicles on the ground. Space-borne GNSS receiver is also useful for other applications such as remote sensing, occulation measurement and ocean reflectometry. Antenna is a critical component in GNSS receivers. A highperformance GNSS antenna is required for precise positioning.

Many types of antennas have been proposed for GNSS applications, including Quadrifilar helix antenna (QHA), microstrip antennas, dielectric antennas, etc. QHA is one of the most popular types of antennas used for GNSS, due to its excellent circular polarization property, broad beamwidth, flexibility in its design and relatively compact size.

Several frequency bands have been used in GNSS, which requires the design of multi-band antennas or multiple single-band antennas covering each band individually. For space-borne GNSS receivers, the use of multi-band antenna instead of multiple antennas can minimize the number of antennas used onboard, leading to smaller size and lower cost of spacecrafts. It is important to design an antenna which can satisfy the multi-band performance while occupying a very small size.

This paper will present the design, simulation, implementation and measurement results of a novel multi-band antenna for GNSS receivers which can be put onboard a small satellite. The antenna operates at two frequency bands which are L1 (1.575 GHz) and L2 band (1.227 GHz). It has achieved good circular polarization performance within a broad 3-dB beamwidth, which will enable the small satellite to receive signals from several GNSS satellites. Both the antenna and its feed network are designed. The antenna has very small size, light weight and low cost. Both simulation and measurement results will be presented. The antenna is also useful for GNSS receivers onboard aircrafts and ground terminal.

A Numerical Study of the Interaction between Handset Antennas and Human Head/Hand in GSM 900, DCS, PCS and UMTS Frequency Bands

Danoosh Davoodi and Shahin Sharifzad
Sadjad Institute of Higher Education, Mashhad, Iran

Abstract— The interaction between human head/hand tissues and handset antennas is a crucial concept in mobile communications. Mobile handsets are used in proximity to user's body and this affect the transmitted or received power of the handset and some other characteristics e.g., VSWR, radiation pattern. This paper presents a comprehensive study on the performance of various types of handset antennas (two internal, two external) next to human head and hand. The investigated frequency range covers GSM 900, DCS, PCS and UMTS frequency bands. Simulations are performed on antennas next to a simplified two layer cubical hand model and a six layer spherical head model. Radiation patterns and VSWR of these antennas are computed in free space as well as in the presence of head and hand. In addition, radiation efficiencies of these handset antennas are computed in the presence of head and hand. All numerical simulations are performed using the Ansoft HFSS software.

Session 2P7
Materials, Devices, Processes and Characterizations for Organic Electronics

Chiral Nematic Liquid Crystal/Fe_3O_4 Nanoparticles Composites with Magnetically Controllable Characteristics of Selective Reflection

Wang Hu[1], **Li Song**[1], **Haiyan Zhao**[1], **Hui Cao**[1], **Zhou Yang**[1], **Zihui Cheng**[1], **Huai Yang**[1], **and Lin Guo**[2]

[1]Department of Materials Physics and Chemistry, School of Materials Science and Engineering
University of Science and Technology Beijing, Beijing 100083, China
[2]School of Chemistry and Environment, Beijing University of Aeronautics and Astronautics
Beijing 100083, China

Abstract— A Fe_3O_4 nanoparticles/chiral nematic liquid crystal (N*-LC) composite was prepared and filled into a planar treated cell. Fe_3O_4 nanoparticles have been modified by oleic acid to achieve a homogeneous disperation. If a magnetic field was scanned on the outer surface of the cell locally, Fe_3O_4 nanoparticles would move towards the inner surface of the cell correspondingly, and the black expected information could be displayed. After some polymer network walls were prepared in the composite, the resolution of information displayed increased. Then, by the formation of hydrogen bonds (H-bonds) between nanoparticles and chiral pyridine compound (CPC) doped in the composite, the pitch length of the N*-LC could be adjusted by adjusting the intensity of the applied magnetic field and the composite doped with the CPC could be used as the material of a kind of reflective color paper.

High Performance Organic TFT and Nonvolatile Memory Using High-κ Dielectric Layers

Albert Chin[1], **M. F. Chang**[2], **P. T. Lee**[2], **and C. H. Wu**[3]

[1]Department of Electronics Engineering, Chiao-Tung University, Hsinchu, Taiwan
[2]Department of Photonics & Institute of Electro-Optical Engineering, Chiao-Tung University Hsinchu, Taiwan
[3]Department of MicroElectronics Engineering, Chung Hua University, Hsinchu, Taiwan

Abstract— Organic thin-film transistors (O-TFTs) are attractive because of the important merits of low-cost, light weight, and novel application to flexible displays and ICs. Besides, the fabrication of O-TFTs needs only a very low thermal budget that is in sharp contrast to Poly-Si TFTs requiring prolonged high-temperature annealing to activate the ion-implanted dopants at source-drain. This low temperature and fast process is vital for environment energy conservation. One difficult challenge for O-TFT is the low hole mobility and poor sub-threshold swing (SS) that limit the needed drive current when operated at low voltage. The O-TFT-based ICs also require nonvolatile memory (NVM) functions for System-on-Chip (SoC) designs, but unfortunately the previous organic NVM (O-NVM) suffers from the fast charge loss and undesired high voltage operation. To address these fundamental challenges, we first demonstrated a high performance O-TFT that uses a high-κ gate dielectric. The O-TFTs on SiO_2 show excellent device integrity of a low threshold voltage (V_{th}) of -1.3 V with a record small sub-threshold swing (SS) of only 78 mV/decade. These device performances are even comparable with the best reported Si TFTs. We further integrated the high-κ/pentacene O-TFT onto low-cost flexible polyimide substrates. The pentacene O-TFTs still exhibited good performance of a low SS of 0.13 V/decade, a low V_{th} of -1.25 V and a low operating voltage of only 2.5 V. Based on the good O-TFT device, we have fabricated the pentacene O-NVM on flexible polyimide substrate. Very low program/erase (P/E) voltage was ± 12 V, at a speed of 1 ms/100 ms. The initial memory window was 2.4 V, and a 0.78 V memory window after 48 hours. This good device performance results from the high gate capacitance with relatively thin high-κ tunnel layer (for high P/E speed), while the small band-gap high-κ trapping layer with deep trapping energy yields good data retention.

Fabrication of Electrodes for Organic Field-effect Transistors through Spin-coating Technique with Incorporation of Surface Wettability Treatment

Yan-Han Chen[1], **Jeng-Rong Ho**[1, 2], **and J.-W. John Cheng**[2]

[1]Graduate Institute of Opto-Mechatronics, National Chung Cheng University, Chia-Yi 621, Taiwan, R.O.C.
[2]Department of Mechanical Engineering, National Chung Cheng University, Chia-Yi 621, Taiwan, R.O.C.

Abstract— Spin coating is a low-cost and powerful thin-film coating technique for many solution-based polymers. Lack of the ability in local patterning is, however, its demerit. With selective modification of local surface wettability of a SiO_2 substrate, this study presents a method that can pattern the electrodes for organic thin film transistors through the spin-coating or dip-coating technique. The three electrode materials studied are silver, graphene and polyethylene dioxythiophene-polystyrenesulfonate (PEDOT : PSS). The silver is reduced from silver nitride solution while the solutions for graphene and PEDOT : PSS are prepared by dissolving them in water. The steps for fabricating patterned electrodes are as follows. First, the designated hydrophobic patterns on the SiO_2 substrate were formed by the use of octadecyltrichlorosiane (OTS) treatment. Both the hydrophilic and hydrophobic regions could be further shaped by the subsequent O_2 plasma treatment. The electrode solution was then coated over the substrate by the spin-coating method. The electrode can only be deposited on the hydrophilic region. Finally, the patterned electrodes had been fabricated after the solution was dried. The feasibility of the present approach is demonstrated through the following preliminary results. Fig. 1(a) shows the CCD images for the SiO_2 surface after the wettability treatments where the hydrophobic and hydrophilic regions can be clearly identified. The line width is about 50 μm, Figs. 1(b)–1(e) are the CCD images for resulting patterned electrodes of silver, graphene and PEDT : PSS, respectively. Characteristics of an OTFT using graphene as source/drain electrodes are demonstrated in Fig. 2. Here the conjugated polymer poly (3-hexylthiophene-2,5-diyl) (P3HT, MW 50000) was for the semi-conducting material.

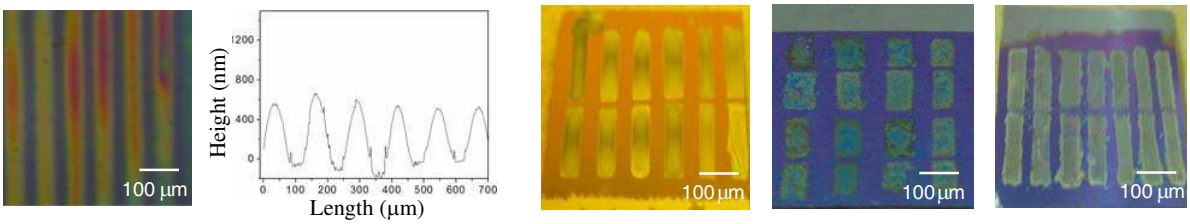

(a) (b) (c) (d) (e)

Figure 1.

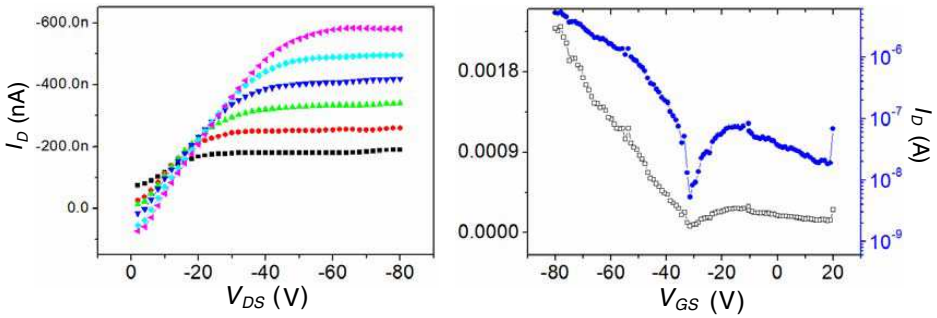

(a) (b)

Figure 2.

Toward High Efficiency Polymer-nanoparticle Hybrid Solar Cell

Wei-Fang Su
Department of Materials Science and Engineering, National Taiwan University
1, Roosevelt Road, Sec. 4, Taipei, Taiwan

Abstract— Hybrid materials made from conducting polymer-nanoparticle are attractive for solar cell because of the prospect of light weight, low cost, high throughput, high energy density using reel-to-reel or spray deposition on flexible substrate.

In this research, we are investigating thermal stable polymer-metal oxide hybrid material for solar cell. We are able to greatly improve the efficiency of the hybrid solar cell by fabricating highly ordered nano structure hybrids, studying the morphology and interlayer characteristics of hybrid, and modifying the surface of metal oxide. The device usually has the construction of ITO/PEDOT/hybrid/Al four layers. The inclusion of TiO_2 nanorods into MEHPPV conducting polymer that increases the ordering of polymer and its absorption spectrum was red shifted; the exciton life has been decreased to less than half of the neat polymer [1]. The efficiency of MEHPPV-TiO_2 solar cell can be increased by 2.5 times by inserting a TiO_2 nanorod layer between the hybrid active layer and Al electrode due to the enlargement of the interconnecting network between the hybrid and electrode [2]. The carrier mobility can be increased by 9 times using column structured ZnO electron transport layer infiltrated with the P3HT-TiO_2 hybrid due to efficient charge transport [3]. The effect of polymer molecular weight on the nanoscale morphology that related to the performance of P3HT-TiO_2 hybrid solar cell was studied by scanning near field optical microscopy (SNOM), atomic force microscopy (AFM) and confocal Raman microscopy. The results are correlated well with the carrier transport behavior of different molecular weight polymer investigated by the time-of-flight technique [4] The solar cell fabricated from surface modified TiO_2 nanoparticles with bandgap tuned linker and P3HT hybrid has achieved the relatively high power conversion efficiency of 2.2% under simulated AM 1.5 illumination ($100\,mW/cm^2$) [5, 6].

The efficiency of the device is expected to be further improved by using newly developed self assembled highly ordered nano structure copolymers of P3HT-P2VP [7] and low bandgap conducting copolymers [8, 9].

ACKNOWLEDGMENT

This project is supported by the National Science Council of Taiwan (95-3114-P-002-003-MY3) and the AOARD of US Air Force (AOARD-07-4014).

REFERENCES

1. Lin, Y.-T., et al., *Nanotechnology*, Vol. 17, 5781–5785, 2006.
2. Zeng, T.-W., et al., *Nanotechnology*, Vol. 17, 5387–5392, 2006.
3. Lin, Y.-Y., et al., *J. Mater. Chem.*, Vol. 17, 4571–4576, 2007.
4. Wu, M.-C., et al., *J. Mater. Chem.*, Vol. 18, 4097–4102, 2008.
5. Lin, Y.-Y., et al., *Appl. Phys. Lett.*, Vol. 92, 053312, 2008.
6. Lin, Y.-Y., et al., *J. Am. Chem. Soc.*, Vol. 131, 3644, 2009.
7. Dai, C.-A., et al., *J. Am. Chem. Soc.*, Vol. 129, No. 36, 11036–11038, 2007.
8. Pal, B., et al., *Macromolecules*, Vol. 40, 8189–8194, 2007.
9. Pal, B., et al., *Macromolecules*, Vol. 41, 6664–6671, 2008.

Side Chain Crystallization Effect on the Performance of Bulk Heterojunction Solar Cells

Wen Y. Huang and S. G. Wang
Department of Photonics and Semiconductor Technology Research and Development Center
National Sun Yat-Sen University, Kaohsiung, Taiwan

Abstract— Poly(3-alkylthiophene)(P3AT) formed regular, layered arrays and showed liquid crystalline structures in the solid state. To elucidate the nanophase segregation in poly(3-alkylthiophene)/fullerene blends, XRD, AFM, SEM and POM are conducted. The effect of side chain influence on the photovoltaic properties of solution-processed poly(3-alkylthiophene)/fullerene blends have been studied in this paper. Side chains investigated here include butyl, hexyl and dodecyl groups. It shows that the photovoltaic performance is strongly affected by the length of side groups, which alters the morphology of the photoactive layer due to changes in solvent solubility, miscibility and fullerene diffusion rate in the blends.

Morphology Manipulation for Polymer Solar Cells

Fang-Chung Chen
Department of Photonics and Display Institute, National Chiao Tung University, Hsinchu 300, Taiwan

Abstract— Polymer solar cells have received widely attention due to their low-fabrication cost. The key to highly efficient devices is to well-control the polymer morphology. In this presentation, we report several methods for controlling the morphology of the materials in polymer photovoltaic devices with high power conversion efficiency. First, we report submicro-scale manipulation of phase separation in the devices. The morphology of the polymer blends can be controlled by using microcontact printing of self-assembled monolayers on the device buffer layer to modify the surface energies, thereby achieving spontaneous surface-directed phase separation. We find that the efficiency increases with decreasing pattern features. Secondly, solvent mixtures with a high boiling point additive have been used to fabricate the devices. Device improvement has been demonstrated. Finally, we recently discovered that one nanoscale cathode buffer layer, poly (ethylene glycol) (PEG), could be formed through spontaneous vertical phase separation. The interlayer enhances the efficiency and stability of polymer solar cells. PEG molecules was blended into the photoactive layer and they spontaneously migrated to the surface of the polymer blend to form the interfacial buffer, thereby reducing the contact resistance after undergoing chemical reactions with the Al atoms of the cathode. Finally, detailed experiment results and discussion will be given in this presentation.

Modeling of Moisture Diffusion in Heterogeneous Epoxy Resin Containing Multiple Randomly Distributed Particles Using Hybrid Moisture Element Method

De-Shin Liu[1], **Zhen-Wei Zhuang**[1], **Ching-Yang Chen**[2], **and Cho-Liang Chung**[3]

[1]Department of Mechanical Engineering, National Chung Cheng University
168, University Rd., Min-Hsiung, Chia-Yi, 621, Taiwan, R.O.C.
[2]RiTdisplay Corporation, No. 12, Kuanfu N. Road, Hsin Chu Industrial Park, 303, Taiwan, R.O.C.
[3]Department of Materials Science and Engineering, I-Shou University
No. 1, section 1, Shiuecheng Road, Dashu Shiang, Kaohsiung Country 840, Taiwan, R.O.C.

Abstract— This paper employs a novel numerical technique, designated as the hybrid moisture element method (HMEM), to model and analyze moisture diffusion in a heterogeneous epoxy resin containing multiple randomly distributed particles. The HMEM scheme is based on a hybrid moisture element (HME), whose properties are determined by equivalent moisture capacitance and conductance matrixes calculated using the conventional finite element formulation. A coupled HME-FE scheme is developed and implemented using the commercial FEM software *ABAQUS*. The HME-FE scheme is then employed to analyze the moisture diffusion characteristics of a heterogeneous epoxy resin layer containing particle inclusions. The analysis commences by comparing the performance of the proposed scheme with that of the conventional FEM method in modeling the moisture diffusion process. Having validated its performance, the scheme is then employed to investigate the relationship between the volume fraction of the particles in the resin composite and the rate of moisture diffusion. It is found that moisture diffusion is retarded significantly as the volume fraction of particles increases.

The HMEM approach proposed in this study provides a straightforward and efficient means of modeling moisture diffusion in a heterogeneous epoxy resin containing multiple randomly distributed particles since only one HME moisture characteristic matrixes needs to be calculated for all HMEs sharing the same characteristics. Furthermore, different volume fractions can be modeled without modifying the original model simply by controlling the size of the inclusion region within the HME domain.

Micro-contact Printing of Semiconductive, Dielectric and Conductive Polymers

J.-W. John Cheng[1], **Jeng-Rong Ho**[1, 2], **Jia-De Jhu**[1], **Chun-Yi Lee**[1], **Chang-Pen Chen**[3], **and Yeh-Min Lin**[3]

[1]Department of Mechanical Engineering, National Chung Cheng University
Chia-Yi 621, Taiwan, R.O.C.
[2]Institute of Opto-Mechatronics, National Chung Cheng University
Chia-Yi 621, Taiwan, R.O.C.
[3]Metal Industries Research & Development Centre
Kao-Hsiung 811, Taiwan, R.O.C.

Abstract— Because of its flexibility, suitability for large-area applications and low-cost fabrication, and bio-compatibility, flexible electronics has attracted an enormous interest from the industry since 1987 when the first practical organic light emitting diode was announced. This presentation addresses the low-cost fabrication of the flexible electronics by proposing a new effective micro-contact printing process. In particular, printing of the electroluminescent poly (2-methoxy 5- (2'-ethyl hexyloxy) phenylene vinylene) (MEH-PPV), dielectric poly (4-vinylphenol) (PVP) and conductive poly (3,4-ethylenedioxy thiophene) : poly (styrene sulfonate) (PEDOT : PSS) will be investigated. Furthermore, to evaluate the applicability and effectiveness of the new micro-contact printing, polymeric light emitting diodes based on the MEH-PPV will be demonstrated.

Nanoscale Imaging and Analysis of Organic Electronic Devices Using Cluster Ion Beam

Jing-Jong Shyue[1], **Jwo-Huei Jou**[2], **Bang-Ying Yu**[1], **Wei-Chun Lin**[1], **and Wei-Ben Wang**[2]

[1]Research Center for Applied Sciences, Academia Sinica, Taiwan
[2]Department of Materials Science and Engineering, National Tsing Hua University, Taiwan

Abstract— Understanding the relationship between the fabrication process, nano-scale structure, and physical properties is crucial to prepare highly-efficient, long-life organic electronic device. However, it has been difficult to analyze the microstructure of organic materials. By using a high-energy buckminsterfullerene (C_{60}^{+}) and a low-energy single-atomic (Ar^{+}) ion source to sputter the surface layer away concurrently, organic thin-films can be profiled with insignificant alteration to the remaining surface. Combining with surface analysis techniques like x-ray photoelectron spectrometry (XPS) and time-of-flight secondary ion mass spectrometry (ToF-SIMS), elemental and molecular distribution at nm scale in depth can be probed. Using these cluster-ion-based profiling techniques, effect of fabrication process on the microstructure of light emitting layer in organic light emitting diode (OLED) is reported and related to the difference in device efficiency. In addition, the electron migration of small molecule as one of the intrinsic degradation mechanism of OLED is observed. Furthermore, by using scanning techniques like scanning ToF-SIMS and scanning probe microscopy (SPM) that yields nm scale lateral resolution, 3D nanostructure in the bulk of the device can be observed. For polymeric solar cells (bulk heterojunctions), the phase-separated bi-continuous phase provides a path for charge carrier hence enhance the efficiency of charge separation. As the result, the controlled phase separation dramatically enhances the performance of polymeric solar cell. On the other hand, the phase separation in polymeric LED traps the charge carrier less effectively and the prepared device is less efficient than that without phase separation.

Organic Light-emitting Devices with Micro- and Nano-structures

Mao-Kuo Wei[1], **Chii-Wann Lin**[2], **Jiun-Haw Lee**[3], **and Hoang-Yan Lin**[3]

[1]Institute of Opto-Electronic Engineering and Department of Materials Science and Engineering
National Dong Hwa University, Hualien, Taiwan, R.O.C.
[2]Department of Electrical Engineering and Institute of Biomedical Engineering
National Taiwan University, Taipei, Taiwan, R.O.C.
[3]Graduate Institute of Photonics and Optoelectronics and Department of Electrical Engineering
National Taiwan University, Taipei, Taiwan, R.O.C.

Abstract— Extraction efficiency of a conventional organic light-emitting device (OLED) was limited by total internal reflection due to the planar structure. To improve the external quantum efficiency, micro- and nano-structure were employed to couple out the waveguiding light inside the device. By using microstructure on an OLED, it was possible to redirect the light rays from the substrate mode to the air mode. Such kind of microstructure can be brightness enhancement film and diffuser, which are commonly used for backlight unit of the liquid crystal display. Besides, it was also possible to use microlens array for this purpose. Typically, 50% enhancement can be achieved with suitable design of the microstructure and OLED. However, at the same time, it resulted in a serious blur. That means it may be only suitable for lighting, but not for display applications. On the other hand, by using nanostructure near the organic layer, it was possible to extract the organic, ITO and plasmonic modes, which yielded a dramatic increase in extraction efficiency. 6x increases in optical intensity was observed in a certain viewing angles with certain wavelengths, due to efficient coupling of the waveguiding modes. However, because the dimension of the nanostructure was close to the emission wavelength, it resulted in serious scattering and viewing-angle dependent emission. That is, emission wavelength and intensity is strongly dependent on the viewing angle, which may be not suitable either for display or lighting. On the other hand, it shows a possible application for sensing small refractive index difference with suitable device design.

Artificial Sunlight by Using Organic Light-emitting Diode

Jwo-Huei Jou
Department of Materials Science and Engineering, National Tsing-Hua University
Hsin-Chu 30013, Taiwan

Abstract— Incandescent bulbs and fluorescent tubes provide fundamental lighting needs but barely satisfy our desire for natural lighting, as from the sun, with time-varying color temperature. To have sunlight-style illumination, emission with daylight chromaticity and a wide color-temperature span is essential. However, no single lighting device, including previously published white organic light-emitting diodes (OLED) as well as the latest white light emitting diode, exhibits daylightlike emission with a color-temperature range covering that of sunlight. We will demonstrate herein an OLED lighting device that yields sunlight-style illumination with tunable color-temperature ranging between 2300 and 8200 K, matching that of the entire daylight at different times, weathers and regions. The OLED employs a device-architecture capable of simultaneously generating all the emissions required to form a series of daylight chromaticities. The wide color-temperature span may be attributed to that the recombination core therein can easily be shifted along the different emissive zones simply by varying the applied voltage via the use of a thin carrier-modulating layer.

Microlens Array Diffuser Films Fabricated by Combination of Breath Figures and Replica Molding Methods

Chia Chen Hsu[1, 2, 3], **Cheng Yi Wu**[1], **and Ting Hsuan Chiang**[2]

[1]Department of Physics, National Chung Cheng University, Chia-Yi 621, Taiwan, R.O.C.
[2]Graduate Institute of Opto-Mechatronics, National Chung Cheng University, Chia-Yi 621, Taiwan, R.O.C.
[3]Department of Photonics, National Sun Yat-sen University, Kaohsiung, 804, Taiwan, R.O.C.

Abstract— This work demonstrates the fabrication of a simple, low-cost microlens array (MLA) diffuser film by a combination of "breath figures" (BFs) and micro-replica molding methods. Polystyrene (PS) molds obtained by BFs method contain concave, hexagonal packed air holes formed by the condensation of water vapor on cooling surfaces in a chamber in which relevant influence factors can be controlled. The sizes of the air holes in the BFs PS molds can be controlled by varying such factors as chamber temperature, chamber relative humidity, substrate temperature and others. The temperature distribution on the substrate affects the distribution of diameters of the air holes formed in a BFs PS mold. Convex PDMS (poly-dimethylsiloxane) MLAs were obtained by molding from the BFs PS molds. The focal lengths of MLAs were measured and compared with theoretical values. The diffusion effect of the diffuser films with MLAs of diameters 6 μm and 3 μm were compared. The results indicate that an MLA with a smaller diameter has a larger diffusion effect.

Session 3A1
Microwave Innovative Techniques and Systems in Exploring Planetary Bodies

Interpreting the Geology of Titan Using SAR Data from Cassini

R. M. Lopes[1], **E. R. Stofan**[2], **C. A. Wood**[3], **S. Wall**[1], **J. Radebaugh**[4], **K. L. Mitchell**[1], **T. G. Farr**[1], **F. Paganelli**[1], **and the Cassini RADAR Team**[1]

[1]Jet Propulsion Laboratory, California Institute of Technology, USA
[2]Proxemy Research, Maryland, USA
[3]Wheeling Jesuit University, Virginia, USA
[4]Brigham Young University, Utah, USA

Abstract— Interpreting geology from SAR data presents some unique challenges. Geologic units will only be apparent if their backscatter characteristics are sufficiently different from those of surrounding terrains. Structures are more easily recognized when oriented perpendicular to the radar's look direction. At Titan, the SAR mode of the RADAR instrument is used at altitudes under ∼4,000 km, resulting in resolution cell size ranging from ∼350 m to > 1 km, which is in some places insufficient to identify different geologic units on the surface. On Titan, the candidate surface materials (water ice, water-ammonia ice and other ice mixtures, hydrocarbons, tholins) are different from the rocky surfaces more usually imaged with radars; in particular, volume scattering at Titan is thought to be significant. We have, however, been able to identify a wide variety of geologic features on Titan's surface using SAR swaths, which now cover ∼40% of the surface. These data reveal that Titan's surface is geologically complex and has been modified by all the major geologic processes seen on Earth — volcanism, tectonism, impact cratering, and erosion and deposition by fluvial, mass wasting, and aeolian activity. Although some of these processes are very different from those on Earth (such as cryovolcanism vs silicate volcanism), the morphology of the landscape is remarkably Earth-like. We will discuss how we use SAR data to interpret geologic features and to examine temporal relationships between units wherever possible. We conclude that aeolian and fluvial/pluvial/lacustrine processes are the most recent on Titan's surface, while tectonic processes that led to the formation of mountains and Xanadu are likely the most ancient.

A Radar Eye on the Moon: Potentials and Limitations for Earth Imaging

M. Calamia[1], **G. Fornaro**[2], **G. Franceschetti**[3], **F. Lombardini**[4], **and A. Mori**[1]

[1]Dipartimento di Ingegneria Elettronica e Telecomunicazioni (DET), Università di Firenze, Italy
[2]Istituto per il Rilevamento Elettromagnetico dell'Ambiente (IREA), Italy
[3]Dipartimento di Ingegneria Biomedica Elettronica e delle Telecomunicazioni
Università di Napoli Federico II, Italy
[4]Dipartimento di Ingegneria della Informazione, Università di Pisa, Italy

Abstract— Among the next space missions goals the exploitation of the Moon, the natural Earth satellite, is gaining an increasing interest. Colonization of the Moon is along the usual track of human civilization and economic expansion; it is also related to a large number of scientific issues, including Earth Observation (EO).

EO is traditionally carried out by means of sensors mounted on artificial satellites mainly orbiting on sun-synchronous Low Earth Orbits (LEO). With respect to standard LEO satellite commonly used in remote sensing, Moon has specific features, such as: A longer distance between the sensor and the imaged area, non sun-synchronous orbits, a large surface for the installation of sensors and equipments, etc.

In this work we analyze the potentials as well as the limitations related to active microwave remote sensing with Synthetic Aperture Radar (SAR), giving particular emphasis to its distinguished characteristic from LEO satellites in terms of imaging characteristics and potential applications. One of the major expected problems of Lunar EO with respect to standard LEO satellites is associated with the considerable increase of the distance between the scene and the sensor. This fact plays an important role for both passive systems and active SAR remote sensing equipments. In the case of passive systems the distance increase leads to an unavoidable resolution loss. On the contrary, for SAR systems the increase of the distance could, in principle, drastically impact the power budget leading to a transmitted power level demand that could be hardly provided with standard technology. Nonetheless, there are many expected advantages related to the use of a lunar SAR system that make worth further investigations: Among them is the possibility to overcome, without the need of any antenna steering, the limit of half antenna length azimuth resolution.

Modeling Radar-bright Regions on Titan Using FDTD Code

Ph. Paillou[1], **M. Janssen**[2], **A. Le Gall**[2], **T. Farr**[2], **S. Wall**[2], **H. Zebker**[3], **and L. Wye**[3]

[1]University of Bordeaux, 2 rue de l'Observatoire, Floirac 33270, France
[2]Jet Propulsion Laboratory, Pasadena, CA, USA
[3]Stanford University, Stanford, CA, USA

Abstract— The Ku-band Radar instrument, on-board the Cassini spacecraft, is imaging Saturn's moon Titan through a thick atmosphere. Recent discovery of dunes, rivers, lakes and seas have shown that the surface of Titan is a geologically-rich place, with an active methane cycle. While the dielectric constant of Titan's surface is low (between 2 and 3 for its real part), unusual high radar scattering regions were observed by the Radar instrument, with a normalized backscattered power that can reach 5 dB at high incidence angles around 20°. Radar-bright regions are in particular located over Xanadu, a large province of possible cryo-volcanic origin, surrounded by dune fields. Interpretation of Radar observations over Xanadu, in both passive (radiometer) and active (scatterometer, SAR) modes, suggests that some very specific scattering phenomena occur there, such as coherent, multiple and volume scattering. They should be related to the nature and the geometry of the near sub-surface on Xanadu, since Ku-band can penetrate up to 2 meters in Titan's surface. We present here FDTD-based simulations, reproducing the observed high-backscattered radar power, for several surface and sub-surface geometries (bubbles, pebbles, cracks, rocks) in the 0–60° incidence angle range, at both H and V polarizations. Implications for the geological nature and history of the Xanadu province are discussed.

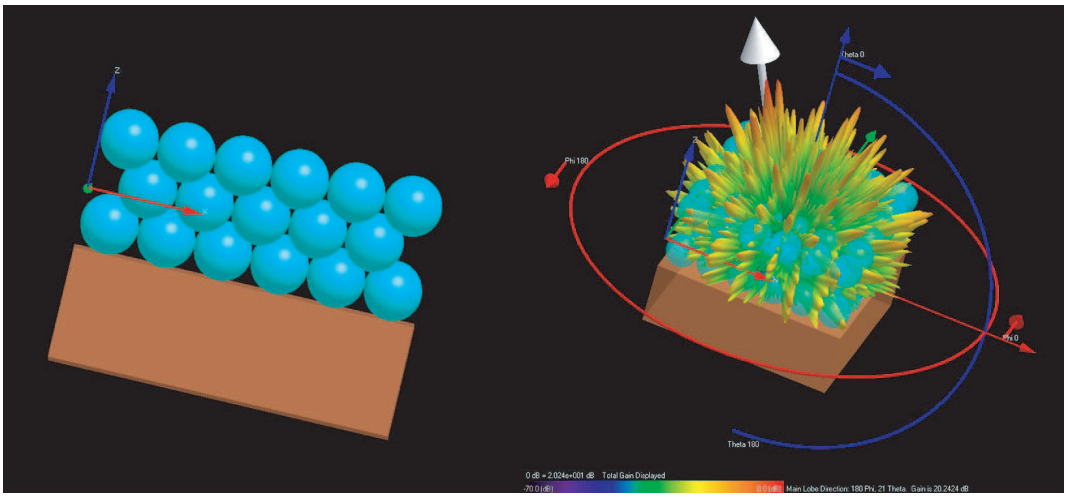

Figure 1: FDTD-computed far-field (Ku-band, H polarization, 20° incidence angle) for regular layers of water-ammonia ice spheres lying on a flat tholin surface.

REFERENCES

1. Le Gall, A., M. A. Janssen, P. Paillou, and R. D. Lorenz, "Radar-bright channels on Titan," *Icarus*, submitted, 2009.
2. Paillou, P., J. I. Lunine, G. Ruffié, P. Encrenaz, S. D. Wall, R. D. Lorenz, and M. A. Janssen, "Microwave dielectric constant of Titan-relevant materials," *Geophysical Research Letters*, Vol. 35, L18202, 2008.
3. Paillou, P., K. L. Mitchell, S. D. Wall, G. Ruffié, C. A. Wood, R. D. Lorenz, E. R. Stofan, J. I. Lunine, R. M. Lopes, and P. Encrenaz, "Microwave dielectric constant of liquid hydrocarbons: Application to the depth estimation of Titan's lakes," *Geophysical Research Letters*, Vol. 35, L05202, 2008.
4. Paillou, P., M. Crapeau, C. Elachi, S. Wall, and P. Encrenaz, "Models of SAR backscattering for bright flows and dark spots on Titan," *Journal of Geophysical Research*, Vol. 111, E11011, 2006.

Remote Sensing of Titan's Surface from the Huygens Probe and Cassini Orbiter

Ralph D. Lorenz
Johns Hopkins University Applied Physics Laboratory
11100 Johns Hopkins Road, Laurel, MD 20723, USA

Abstract— The surface of Titan has been studied since 2004 by instruments on the Cassini orbiter, in particular by a Ku-band RADAR instrument, the Imaging Science Subsystem (ISS) and the Visual and Infrared Mapping Spectrometer (VIMS), but also by bistatic sensing using the Radio Science Subsystem (RSS) and temperature sensing by the Composite Infrared Spectrometer (CIRS). Additionally, while the Huygens probe which descended by parachute in 2005 is noted as an in-situ platform, it performed several measurements that can be considered remote sensing. These local measurements will be reviewed, and discussed in comparison with the orbiter measurements that provide a global context.

The principal, and best-known, remote measurements from the Huygens Probe are the visible and near-IR imagery and spectroscopy from the Descent Imager and Spectral Radiometer (DISR). However, the surface was also probed acoustically by a sonar in the Surface Science Package (SSP), which detected surface echoes from about 100 m above the ground down to impact 20 seconds later. Further, two engineering systems on the probe yielded other surface information. First, a pair of Ku-band radar altimeters gave a height profile along the probe's descent track, giving an estimate of nadir surface backscatter and terrain height variation. Second, a bistatic scattering experiment was inadvertently performed after impact — the S-band transmission to the Cassini orbiter showed a distinctive fading pattern as the orbiter set on the horizon as seen from the probe. This multipath fading, recorded in the was due to constructive and destructive interference of the direct beam with RF radiation reflected from the surface, and yielded constraints on surface roughness and dielectric constant (as well as a usefully-precise estimate of the height of the probe above the surface.) While not a remote measurement, a mutual impedance experiment on the Huygens Atmospheric Structure Instrument (HASI) also measured the dielectric constant of the surface in a small volume around the spacecraft.

These results underscore the importance of documenting the calibration of engineering systems such as AGC, since they can contain valuable scientific information. Together, the Huygens data indicate an organic-rich surface, perhaps with some small amount of water ice. The immediate vicinity of the probe is flat, although hills ~ 100 m high to the west are indicated by the altimeter and stereo imagery — it is from these hills that methane rivers presumably flowed in the past to provide the rounded cobbles seen in post-landing imagery around the probe.

The Huygens landing site is just one small locality in what emerges to be a very diverse landscape. Since the descent, the landing site has been imaged by Radar and in the near-IR. These observations provide a regional context for the probe results, while the latter provide important ground truth for interpreting the orbiter data globally. It is interesting as a thought experiment to speculate what Huygens' measurements might have looked like had the probe landed elsewhere, such as among the equatorial dunefields or in the polar lakes, the environment for which in many ways the probe had been designed.

A Fractal Approach for Understanding Altimeter Data

Gabriella Bernardi, **Giorgio Franceschetti**, **Antonio Iodice**, **and Daniele Riccio**
Department of Electronic Biomedical and Telecommunication Engineering
University of Naples "Federico II", Via Claudio 21, Napoli 80125, Italy

Abstract— In this paper, a novel approach to model the altimeter received waveforms is presented; a new simulation procedure for the altimeter return is also discussed, particularly appropriate for the exploration of planets and their natural satellites. The electromagnetic model and the associated procedure provide a complete solution of the direct problem consisting of evaluating the received altimeter echo provided that the sensed surface is modeled. This complete solution to the direct problem is a candidate to address the inverse problem, too, the latter consisting in extracting from the altimeter echo-shapes not only the height of the surface on the ground, but also some surface value-added information.

Up to now the altimeter signal return has been computed in a meaningful form only in the case of ocean surface. As a matter of fact, this is a somehow standard scenario, that allows to get, under appropriate hypotheses, an analytical closed form for the altimeter echoes [1]: in this case, the echoes model includes some relevant sea state parameters [1], and an easy inversion of this model can be conceived to achieve these information [2, 3]. Such a model does not apply to natural solid surfaces, because some crucial hypotheses that are only valid for ocean surfaces are missing. These hypotheses are mainly related to the representation of the surface under survey and the electromagnetic model adopted to sum up the returns form different areas on the surface (see [1] for more details). In particular, the main assumptions in [1] concern the surface which is considered flat with a superimposed Gaussian roughness, and the scattering mechanisms which is supposed mostly incoherent. Clearly this model is not appropriate for most of solid surfaces. Then, in this presentation the natural sensed surface is modeled by means of the fractal geometry, which was proved to be very powerful and correct to represent natural surfaces [4, 5], and the employed scattering mechanism is related to a coherent fractal one [6]. It is noted that the appropriate model for natural surfaces of planets and their natural satellites is just the fractal one. The fractal model adopted in this paper is the *fractional Brownian motion* (*fBm*) stochastic process, whose realizations are obtained by means of the *Weierstrass Mandelbrot* (*WM*) function [6]; this choice turns out to be appropriate to represent many classes of natural surfaces [7], solid or not. Hence, the newness of the proposed computation procedure lies in showing the correct link between the electromagnetic return shape and most relevant (fractal) surface topographic features, including height, slope, possible stratifications, and different scales of roughness.

REFERENCES

1. Brown, G. S., "The average impulse response of a rough surface and its applications," *IEEE Trans. Antennas Propagat.*, Vol. 25, No. 1, 67–74, 1977.
2. Berry, P. A. M., J. A. Freeman, C. Rogers, and J. Benveniste, "Global analysis of envisat RA-2 burst mode echo sequences," *IEEE Trans. Geosci. Remote Sens.*, Vol. 45, No. 9, 2869–2874, 2007.
3. Montefredini, E., F. Morelli, G. Picardi, and R. Eu, "A non-coherent surface backscattering model for radar observation of planetary bodies and its application to Cassini radar altimeter," *Planet. Space Sci.*, Vol. 43, No. 12, 1567–1577, 1955.
4. Mandelbrot, B. B., *The Fractal Geometry of Nature*, Freeman, New York, 1983.
5. Falconer, K., *Fractal Geometry*, John Wiley, Chichester, England, 1990.
6. Franceschetti, G. and D. Riccio, *Scattering, Natural Surfaces and Fractals*, Elsevier, Academic Press, Burlington, MA, USA, 2007.
7. Franceschetti, G., P. S. Callahan, A. Iodice, D. Riccio, and S. D. Wall, "Titan, fractals, and filtering of cassini altimeter data," *IEEE Trans. Geosci. Remote Sens.*, Vol. 44, No. 8, 2055–2062, 2006.

A Review of the Use of Electromagnetic Radiation for Remote Sensing of Natural Surfaces

Stephen D. Wall
Jet Propulsion Laboratory, California Institute of Technology
Pasadena, CA 91109, USA

Abstract— The inability to physically study natural surfaces at close range is mitigated in many ways under the general heading of "remote sensing". In planetary exploration, where most surfaces under study will not be visited by humans, the longest-lived and most often used remote sensing involves measurements of either the natural electromagnetic emission of the surface ("passive") or the reflection of electromagnetic radiation from other sources "active"). Methods including photographic interpretation, directional analysis (e.g., stereography), spectral analysis, and application of radiative transfer theory are used to analyze these measurements so that characteristics and context of the surface can be addressed and perhaps even understood. Most commonly used portions of the electromagnetic spectrum are from $\lambda = 0.1$ micron ($f = 10\text{E}15$ Hz) to $\lambda = 10$ cm ($f = 10\text{E}9$ Hz), but extensions in both directions are made. Both incoherent and coherent techniques are used at most of these wavelengths.

Any analysis of remote-sensed data should consider the nature of the interaction of the radiation and the surface. Too frequently, data are converted to image formats and interpreted as representations of the visually-perceived surface; in fact, many distinct kinds of surface properties are detected (or can be inferred from) by these sensors, but analysis of the returned data must always be done with a proper understanding of both the radiation interaction and the characteristics of the sensor. With sufficient modeling, quantitative measures of the surface properties (dielectric constant, loss tangent, emissivity, surface roughness, etc.) can be derived.

In this paper we will review the surface characteristics that are actually sensed by various common remote-sensing techniques, we will show some examples of both correct and incorrect interpretations, and we will describe some innovations in the use of electromagnetic radiation to make new discoveries in planetary sciences.

The research described in this paper was carried out at the Jet Propulsion Laboratory, California Institute of Technology, under a contract with the National Aeronautics and Space Administration.

Titan Surface Topography from Cassini SAR Data: An Amplitude Monopulse Comparison Method

Bryan W. Stiles[1], **Scott Hensley**[1], **Yonggyu Gim**[1], **David M. Bates**[1], **Randolph L. Kirk**[2], **Alex Hayes**[7], **Jani Radebaugh**[5], **Ralph D. Lorenz**[4], **Karl L. Mitchell**[1], **Philip S. Callahan**[1], **Howard Zebker**[3], **William T. K. Johnson**[1], **Stephen D. Wall**[1], **Jonathan I. Lunine**[8], **Charles A. Wood**[6], **Michael Janssen**[1], **Frederic Pelletier**[1], **Richard D. West**[1], **Flora Paganelli**[9, 1], **Chandini Veeramacheneni**[1], **and the Cassini RADAR Team**[1]

[1]Jet Propulsion Laboratory, California Institute of Technology, USA
[2]United States Geological Survey, USA
[3]Stanford University, USA
[4]Applied Physics Laboratory, Johns Hopkins University, USA
[5]Department of Geological Sciences, Brigham Young University, Provo, Utah 84602, USA
[6]Wheeling Jesuit University, USA
[7]California Institute of Technology, USA
[8]Lunar and Planetary Laboratory, University of Arizona, USA
[9]Department of Earth and Space Sciences, University of California, Los Angeles, USA

Abstract— An amplitude monopulse comparison technique, SARTopo, has been developed [1] for obtaining surface height estimates with 10 km horizontal resolution and 75 m vertical resolution of the surface of Titan along each Cassini Synthetic Aperture Radar (SAR) swath. We describe the technique and present maps of the co-located data sets including regions recently observed by Cassini and not presented in [1]. A global map and various regional maps including the northern hemisphere and southern hemisphere hydrocarbon lakes districts are included in the results. A strength of the technique is that it provides topographic information co-located with SAR imagery. Having a topographic context vastly improves the interpretability of the SAR imagery and is essential for understanding Titan.

One of the more vexing dilemmas for the Cassini RADAR team was the necessity to choose between altimetry and SAR imaging of a surface. Radar altimetry is optimally obtained from nadir observations, whereas SAR requires off-nadir observation in order to construct an image. Co-located nadir altimetry and SAR only occur when observations taken at different times happen to overlap. Stereo techniques can also be used to estimate topography in SAR images, but they also require multiple overlapping observations. Interferometric techniques typically used to obtain heights from SAR are not possible for Cassini RADAR. SARTopo determines surface heights for most of the SAR-imaged surface of Titan. Currently nearly 40% of the surface is within 100 km of a SARTopo height profile. Other competing techniques provide orders of magnitude less coverage.

Like other amplitude monopulse comparison implementations [2], SARTopo determines the height of the surface by observing the same region on the ground with two different antenna beams and comparing the gains of the returned echoes. The technique requires: 1) accurate spacecraft pointing, 2) accurate spacecraft ephemeris, 3) precise knowledge of the antenna pattern of the RADAR, and 4) downlinked echo data covering the entire antenna footprint. The fourth requirement is met through synergy with Cassini SAR coverage requirements. Cassini SAR commanding and pointing is designed to utilize as much of the antenna footprint as possible in order to maximize cross-track coverage. Of the four constraints the one that impacts height accuracy most severely in our case is spacecraft attitude knowledge. We correct the height estimates for attitude knowledge errors using an overlapping network of SARTopo and nadir altimetry height profiles.[1]

REFERENCES

1. Stiles, B. W., S. Hensley, et al., "Determining Titan surface topography from Cassini SAR data," *Icarus*, Vol. 202, No. 2, 584–598, 2009.
2. Chen, C. W. and S. Hensley, "Amplitude-based height-reconstruction techniques for synthetic aperture ladar systems," *J. Opt. Soc. Am. A*, Vol. 22, No. 3, 529–538, 2005.

[1]The research described here was carried out at the Jet Propulsion Laboratory, California Institute of Technology, under a contract with the National Aeronautics and Space Administration.

Pushing the Envelope with the Cassini RADAR

R. West[1], **B. Stiles**[1], **L. Wye**[2], **H. Zebker**[2], **Y. Anderson**[1], **P. Callahan**[1], **A. Le Gall**[1], **Y. Gim**[1], **G. Hamilton**[1], **M. Janssen**[1], **W. T. K. Johnson**[1], **K. Kelleher**[1], **R. Kirk**[3], **R. Lorenz**[5], **J. Lunine**[4], **C. Veeramachaneni**[1], **S. Wall**[1], **and the Cassini RADAR Team**[1]

[1]Jet Propulsion Laboratory, California Institute of Technology
4800 Oak Grove Dr., Pasadena, CA 91109, USA
[2]Stanford University, Stanford, CA, USA
[3]USGS, USA
[4]University of Arizona, USA
[5]JHU-APL, USA

Abstract— During the four year Cassini Prime Mission and the two year Equinox Mission which ends in July 2010, the radar instrument has been used to acquire a wide variety of data going beyond the original proposal plan. By the end of the Equinox Mission, the radar will have acquired data during 33 close Titan flyby's and 77 observations of other icy satellites along with several radiometer scans of Saturn and its rings. In addition to the planned SAR imaging coverage and scatterometry and radiometry scans, the radar was pushed to acquire other kinds of data. High altitude ($\sim 20,000$ km) imaging is performed to improve coverage of Titan and to acquire disk resolved data on Iapetus and Enceladus. Tone-only transmissions are used to acquire disk integrated radar albedos of the icy satellites at very high ranges ($\sim 200,000$ km) and to probe the atmosphere of Titan for methane rain. The data have also been processed in unusual ways to extract more information about the surface. SAR data is processed at beam boundaries for topographic information that greatly aids the interpretation of surface imaging. Topographic data from SAR and Altimeter data are linked with Stereo overlaps to provide more detailed topographic data in selected areas. Altimeter data obtained over methane lakes shows a specular echo which is processed to constrain the surface smoothness. This presentation will show the design trade-offs made to acquire a diverse radar data set, and summarize some of the findings made so far.

ACKNOWLEDGMENT

This work is supported by the NASA Cassini Program at JPL — CalTech.

Session 3A2a
Rough Surface Scattering and Volume Scattering

Study on Backscattering from Rough Sea Surface

Jia Zheng[1], **Zhen-Sen Wu**[1], **and Yu-Shi Zhang**[2]

[1]School of Science, Xidian University, Xi'an 710071, China
[2]China Research Institute of Radiowave Propagation, China

Abstract— With the radar applying in science and technology widely, the study on electromagnetic scattering from rough sea surface is becoming more and more important. The backscattering coefficient of the rough sea surface can response the sea surface clutter distribution to reduce the negative effect. In this paper, the dependence of backscattering coefficient for L-band of the rough sea surface on incident angle is obtained by doing the sea surface clutter experiment in Qingdao, specially analyzed the condition of the backscattering coefficient at Low-Grazing-Angles (0°–10°). In theory, the backscattering coefficient of the rough sea surface is numerically calculated by small slope approximation (SSA), Kirchhoff Approximation (KA), hybrid method combining the moment of method with the kirchhoff approximation (KA-MOM), and modified the methods by shadowing factor. The results of experiment and theory are compared and the difference between them is analyzed. The results of the theoretical methods agree with the experiment result at Low-Grazing-Angles is not as good as other angles, although the application of shadowing modify factor correcting the result a certain extent this problem will be the mainly work next research.

Temporal Intensity Correlation Function of Speckle from Rough, Rotating Spheres

Geng Zhang, Zhensen Wu, and Mingjun Wang
Science School, Xidian University, Xi'an 710071, China

Abstract— The correlation properties of time-varying laser speckle from rotating, rough objects contain information about the motion of the object. The effect of movement of a rough coherently illuminated body on speckle characteristics has been investigated theoretically. The investigation in this paper is based on the temporal correlation function of the intensity which is derived from a geometrical model for the correlation function of the optical field scattered from large rough spheres. The geometrical model is developed using the method of Kirchhoff Approximation and it is assumed that the rough surface is randomly distributed Gaussian rough surface which is greatly simplified the difficult of the derivation of the correlation function. The expression for the correlation function is obtained finally after detailed mathematical derivation. When the time difference goes to zero, the correlation will be simplified as the backscattered intensity of the rough object which has been discussed both experimentally and theoretically before. The correlation time is defined as the time difference when the value of the temporal intensity correlation function decreases to $\exp(-1)$. Then the power spectral density of the frequency which is the Fourier transformation of the correlation function against the time difference is got. From the analysis, the spectral broadening and Doppler Effect due to the object rotation are shown clearly. This paper gives the dependence of statistical properties of the dynamic speckles of rough spheres on the rotating rate and the roughness of the spheres which provides theoretical basis for the following research on the target recognition and its motion detection.

Nonlinear Optics Controlled by Quantum Coherence

Yuri Rostovtsev
University of North Texas, Denton, Texas 76203, USA

Abstract— Using quantum coherent effects provides means to control nonlinear optical processes in various media. We predict several new effects: For example, forward Brillouin scattering and enhancement and control of coherent generation in the backward direction by applying only forward propagating fields. The applications range from development of hyper-dispersive materials, improvement of spatial resolution beyond diffraction limit to generation of squeezed and entangled light.

Research on Characteristics for Optical Pulse Propagation in Fog Channel

Rong-Rong Wang[1, 2] **and Zhen-Sen Wu**[1]

[1]School of Science, Xidian University, Xi'an 710071, China
[2]School of Science, Xi'an Shiyou University, Xi'an 710065, China

Abstract— In this paper, the characteristics of optical pulse propagating in fog channels are investigated based on optics pulse propagation theory in discrete random media, and the attenuation and the two-frequency mutual coherence function for optics pulse propagation in the fog are also studied. By means of Mie theory, the characteristic of 1.06 μm pulsed laser propagating in fogs with various densities are obtained. According to the size distribution of the fog particles, the optical pulse attenuations is researched by the two-frequency mutual coherence function differential equation which is solved using Fourier transform technique. The two-frequency mutual coherence function solution is numerically analyzed. The dependence of the amplitude and phase of the two-frequency mutual coherence function on coherence bandwidth, pulse width extension in time domain is obtained. The pulse shape is substantially unchanged when the optical distance is less, while a long tail and the considerable pulse spread and delay occur when the optical distance is getting larger. Therefore, when the density of fog is large, the effects of the attenuation on the optical pulse characteristics should be taken into account.

Numerical Calculation of Scattering Matrix about Wafers and Impurity Particles above

Lei Gong and Zhen-Sen Wu
School of Science, Xidian University, Xi'an 710071, China

Abstract— The scattering matrix about wafers and impurity particles above is focused on in this paper. The scattering matrix is one of the most important physical parameters which is used to describe scattering character and polarization character. It is believed that the value of scattering matrix elements can carry valuable information on the perspective of dust-particle characterization and sizing. Firstly, taking the advantage of the BV theorem, the scattering model about wafers and impurity particles above is established. The scattering process is described and the expressions of scattering matrix elements are derived through expansion Vector spherical harmonic function. Secondly, the results are compared with DSM method, both of which are identical very well. In the end, the angle distribution about the scattering matrix elements of impurity particles among different incident angles is derived. An efficient theoretical method is given for the detection of defects on silicon wafers. From the results, it is can be seen that a small sphere remains very sensitive to the size although its size is much smaller than the wavelength. Thus the state of polarization can be seen through calculating the scattering matrix elements and polarization can be a valuable tool in the field of surface-scanning devices. However, this paper is just considered the dust on the wafer. There are some cases are not considered such as subsurface defects and small defects in wafers.

Vector Electromagnetic Scattering from Multilayer 2D Arbitrary Random Rough Surfaces for Remote Sensing of Soil Moisture

Xueyang Duan and Mahta Moghaddam
University of Michigan, USA

Abstract— The problem of electromagnetic scattering from arbitrarily random rough surfaces has been a subject of numerous studies over the past several decades for its important applications in microwave remote sensing. Being representative of many naturally occurring surfaces and subsurface structures, such as soil, snow, and ice, the model of electromagnetic scattering from single or multiple-layered random rough surfaces gives indispensable knowledge of the interaction between electromagnetic waves and these remote sensing targets. Currently, one of the major applications of radar technology is to map the distributions of soil moisture whose temporal and spatial variations are inuential parameters in both climatic and hydrologic models. With the recent development of low frequency radar systems, e.g., at UHF and VHF bands, the capability of probing deep and root-zone soil moisture is significantly enhanced due to the large penetration depth. Studying the interaction of low-frequency radar signals with subsurface soils requires an accurate and ecient scattering model of realistic soil, which often involves multilayer rough surfaces and inhomogeneous dielectric profiles.

Due to the extremely large computational load for solving the electromagnetic scattering from two-dimensional rough surfaces using numerical techniques, current applicable solutions are mainly analytical and based on approximation techniques, e.g., small perturbation method (SPM), Kirchhoff approximation (KA), and small-slope approximation (SSA), which limit the surfaces to either small or large roughness regimes. To be able to accurately analyze the scattering from surfaces of arbitrarily roughness with comparably high computational efficiency, our work is concentrated on solutions using the extended boundary condition method (EBCM). Previously, we have solved and presented the bistatic scattering solution from a single-layered surface, which plays a basic and important role in the solution to the scattering problem from multilayer surfaces using EBCM. This solution shows good agreement in comparison with the solutions given by available analytical (SPM, KA and SSA) and numerical methods (Method of Moments (MoM)) within their respective validity regimes. Currently, the extension of this model to double-layered and multilayer scenarios is under investigation. By expressing the propagating waves in Floquet modes and matching the extended boundary conditions on the test surfaces in each region separated by the actual surfaces, a matrix system can be constructed to solve the unknown field at each actual surface and further to derive the scattered fields. The limit of this model due to the ill-conditioning of the matrix, which is caused by the poor sampling of the evanescent wave spectrum using EBCM, will be treated with matrix regularization. Validation of this multilayer rough surface scattering solution can be done by comparing with the results from SPM and MoM for 2D surfaces.

Development of this model will provide a chance for quantitative comparison between theoretical analysis and actual radar measurements of soil moisture. It will also serve as a forward solver in the inverse model for soil moisture which will be investigated in future work.

Session 3A2b
Scattering and Rough Surface Scattering

Plane Wave Scattering by a Coated Thin Wire

A. Ike Mowete[1] and A. Ogunsola[1, 2]

[1]Department of Electrical and Electronics Engineering
Faculty of Engineering, University of Lagos, Lagos, Nigeria
[2]Parsons Group International, Rail Transit Division, London, United Kingdom

Abstract— This paper addresses the problem of scattering by an insulated perfectly conducting thin-wire, illuminated by a uniform, plane electromagnetic wave. The conductor is modeled by the usual 'thin-wire approximation', and the dielectric insulation, by a volume polarization current [1, 2], defined in terms of a quasi-static electric field [3], which derives from the distribution of current along the axis of the bare-wire scatterer through the equation of continuity. The model for the composite structure then emerges as the sum of two axially directed currents radiating in free-space. In the moment-method technique subsequently utilized for the solution of the problem, testing functions, which are critical to specification of the voltage excitation matrix, are taken as having the two component parts indicated by the choice of model for the coated scatterer. Computational results obtained for the selected example of a cross-wire [4] suggest that this analytical approach is valid, as the results reveal that the influence of the coating on the wire's bi-static radar cross-section is consistent with those generally reported in the open literature [5].

REFERENCES

1. Li, X., K. E. K. Drissi, and F. Paladian, "A galerkin moment-method for the analysis of insulated wires above a lossy half-space," *Annales des Telecommunications*, Vol. 58, No. 7/8, 1157–1177, 2003.
2. Richmond, J. H. and E. H. Newman, "Dielectric coated wire antennas," *Radio Science*, Vol. 11, No. 1, 13–20, 1976.
3. Adekola, S. A., A. I. Mowete, and A. Ogunsola, "On the problem of dielectric coated wire antennas," *Progress In Electromagnetics Research Symposium*, Moscow, August 2009.
4. Taylor, C. D., S. M. Lin, and H. V. McAdams, "Scattering from crossed wires," *IEEE Trans. Antennas and Propagation*, Vol. 20, No. 6, 133–136, 1970.
5. More, J. and M. A. West, "Simplified analysis of coated wire antennas and scatterers," *Proceedings of IEE Microwaves, Antennas and Propagation*, Vol. 142, No. 1, 14–18, 1995.

Fast Bistatic ISAR Imaging Simulations for 3D Scattering Center Analysis of Vehicles

H. Buddendick[1] **and T. F. Eibert**[2]

[1]Institut für Hochfrequenztechnik, Universität Stuttgart, Pfaffenwaldring 47, Stuttgart 70569, Germany
[2]Technische Univerität München, Germany

Abstract— One possibility to handle very large and complex environments in deterministic radio channel simulation approaches is the use of pre-computed and compressed scattering center models [2]. These models are based on the observation that the EM scattering phenomena at very high frequencies are typically well focused local effects. A well known technique to describe these scattering mechanisms is ISAR, Inverse Synthetic Aperture Radar, which can be used to localize dominating scattering centers.

In our case a 3D bistatic scattering center model is required and consequently also the ISAR imaging should provide this information. Typically, ISAR imaging is based on multi-dimensional Fourier processing, which requires costly data acquisition in multiple dimensions as well (e.g., frequency and aspect). In this paper a fast simulation approach is presented which requires only a single aspect simulation run to produce comparable images. The simulation is based on a high frequency Shooting and Bouncing Rays algorithm, incorporating Geometrical Optics and Physical Optics field calculations. Similar to [1], the single aspect imaging algorithm exploits the ray path interactions, inherently known by the ray tracer. Considering a narrowband system with small aspect variation the contribution of individual rays can be determined analytically. The approach presented in this paper is adapted to the use in the hybrid GO/PO simulation and operates on the basis of surface currents. In this way a flexible bistatic evaluation of the ISAR images is possible.

Figure 1 depicts a 2D example, which shows the good quality of the presented approach. The final paper will contain a detailed formulation of the ray image contribution for both, horizontal and vertical polarized imaging.

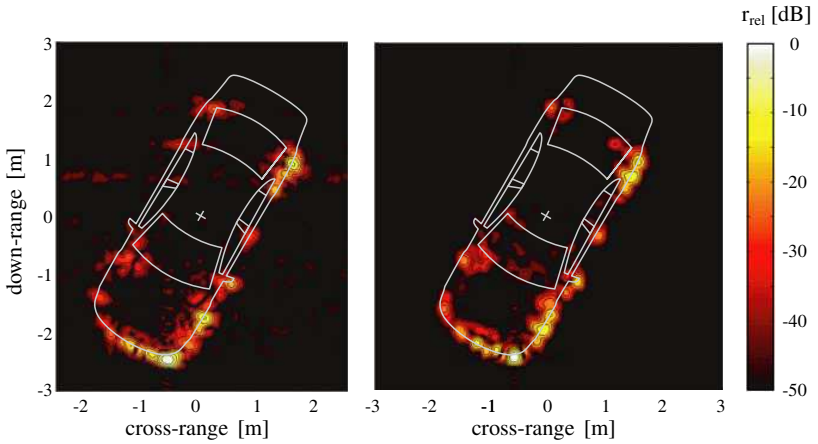

Figure 1: Monostatic ISAR image simulation of a passenger car. Classical 2D Fourier processing (left) and in comparison the result with the fast single shot simulation.

REFERENCES

1. Bhalla, R. and H. Ling, "A fast algorithm for signature prediction and image formation using the shooting and bouncing ray technique," *IEEE Trans. Antennas Propag.*, Vol. 43, 727–731, Jul. 1995.
2. Buddendick, H. and T. F. Eibert, "Radio channel simulations using multiple scattering center models," *Proc. IEEE AP-S'09*, Charleston, SC, Jun. 2009.

Transmission Characteristic of Sea Surface Scattered GPS Signal Trapped in Atmospheric Duct

Jin-Peng Zhang, Zhen-Sen Wu, and Rong-Xu Hu
Xidian University, China

Abstract— The atmospheric duct phenomenon forming in anomalous atmosphere environment can result in the occurring of radar hole and beyond-the-horizon propagation of radar wave. The real-time inversion technique of atmospheric duct height and intensity makes the real-time modification of radar wave propagation trace come true, and the performance of radar system can be improved.

Owing to the advantages of GPS signal, such as all areas and all time, the monitor and inversion of atmospheric duct using GPS signal receiver are not restricted by time and place, and having robust feasibility. The inversion of atmospheric duct based on sea surface scattering GPS signal differs from that based on radar sea clutter, for it does not need the special transmitter and belongs to passive inversion technique. It is worthy of noting that the atmospheric duct inversion process using GPS is based on the forward simulation of GPS signal traveling in atmospheric duct, and the veracity of forward simulation determines the validity of inversion process directly. The forward propagation model of GPS signal is studied in this paper.

The parabolic wave equation (PWE) is solved in this paper using discrete mixed Fourier transform (DMFT) with the initial filed which is the sea surface scattering field of GPS signal in a certain height range. The spatial distribution of path loss of GPS signal scattering from sea surface is calculated and presented in a 2-D map. The duct trapping effect is obvious in the map, which validates the scattered GPS signal is trapped and propagates in atmospheric duct for a certainty. In next step, the power of sea surface scattered GPS signal with respect to the range can be calculated using the path loss, and it is the very input for the atmospheric duct inversion algorithm.

Composite Scattering between Plate and Sea Surface: The Theory and Verified Experiment

Jing-Jian Zhang[1], **Zhen-Sen Wu**[1], **and Xiao-Bing Wang**[2]

[1]Xidian University, China
[2]The 802nd Research Institute of Shanghai Academy of Spaceflight Technology, China

Abstract— The study on composite electromagnetic scattering between a target and rough surface is always of extensive application in the field of EM. In classical research on composite scattering, the rough surface and target is studied separately. In fact, rough surface and target must be taken as a whole. Not only should the scattering of target and rough surface be investigated respectively, but also the coupling scattering between them.

In this paper, the dependence of composite scattering on the incident angle is analyzed and the results of Ref. [1] are verified by an experiment done in Shanghai. The experiment is about composite scattering between plate targets and smooth sea surface. The results of Ref. [1] get good agreement with the experiment, which proves the validity of the theory in Ref. [1].

The study on electromagnetic scattering from target in actual background of sea surface provides important theoretic foundation for oceanic surveillance and target detection. So that the investigation of composite scattering with the diffraction of target fringe taken into account has important signification of application.

REFERENCES

1. Wu, Z.-S., J.-J. Zhang, and L. Zhao, "Composite electromagnetic scattering from the plate target above a one-dimensional sea surface: Taking the diffraction into account," *Progress In Electromagnetics Research*, PIER 92, 317–331, 2009.

Session 3A3
Microwave/Terahertz Photonics Technologies and Their Applications

Experimental Investigation on a Radio-on-free-space Optical System Suitable for Provision of Ubiquitous Wireless Services

Mitsuji Matsumoto[1], **Kamugisha Kazaura**[2], **Kazuhiko Wakamori**[3], **Takeshi Higashino**[4], **Kastutoshi Tsukamoto**[4], **and Shozo Komaki**[4]

[1]Graduate School of Global Information and Telecommunication Studies (GITS), Waseda University, Japan
[2]Research Institute for Science and Engineering (RISE), Waseda University, Japan
[3]Global Information and Telecommunication Institute (GITI), Waseda University, Japan
[4]Department of Electrical, Electronic and Information Engineering
Graduate School of Engineering, Osaka University, Japan

Abstract— Recent advancements in microwave and terahertz photonics technologies has led to development of innovative advanced wireless communications systems. One of the emerging promising technologies is Radio-on-Free-Space Optical (RoFSO) system described in this paper. RoFSO is achieved by combining Radio-over-Fiber (RoF) technique and free-space optical (FSO) communication technology using the seamless connection of free-space and optical fiber. With this system it is possible to transmit simultaneously multiple RF signals representing different wireless services through free-space using WDM technique. In this paper we describe the design concept of the RoFSO system and highlight the performance evaluation based on the transmission of the various wireless services signals transmitted over it. The results obtained show satisfactory performance and demonstrate potential of the RoFSO system as a suitable platform for provision of ubiquitous wireless services. Moreover the link design of the RoFSO system and application scenario as an ubiquitous network are considered based on the experimental result.

Stimulated Terahertz Emission from Optically Pumped Epitaxial Graphene-on-Si Heterostructures

T. Otsuji[1,3], **H. Karasawa**[1], **T. Komori**[1], **T. Watanabe**[1], **M. Suemitsu**[1,3], **A. Satou**[2,3], **and V. Ryzhii**[2,3]

[1]Research Institute of Electrical Communication, Tohoku University, Sendai 9808577, Japan
[2]Computational Nano-Electronics Laboratory, University of Aizu, Japan
[3]JST-CREST, Tokyo 1020075, Japan

Abstract— Linear dispersion relations for the electron and hole energy spectra with zero energy band gap in graphene [1] provide nontrivial features like negative-dynamic conductivity in far infrared and terahertz (THz) spectral ranges [2]. Due to a very short time of the optical phonon emission $\tau_0 \approx 10^{-12}$ s, the photogeneration of electrons and holes leads to the emission of a cascade of optical phonons, so that the photoelectrons and photoholes occupy the states with the energies close to $\varepsilon_N \approx \hbar(\Omega/2 - N\omega_0) < \hbar\omega_0$, where $\hbar\Omega$ the pumping photon energy, $\hbar\omega_0$ the optical phonon energy, and N the number of emitted optical phonons. As a consequence, photoelectrons/holes recombine to radiate THz photons with the energy $\hbar\omega \approx 2\varepsilon_N$ (inset in Fig. 1(a)) [1]. The incident photon spectra will reflect on the THz photoemission spectra as a proof of occurrence of such a process.

We experimentally observed the fast relaxation and relatively slow recombination dynamics of photogenerated electrons/holes in an epitaxial graphene-on-Si heterostructure under pumping with a femtosecond pulsed fibre laser. Time-resolved electric-field intensity originated from coherent terahertz photon emission was electrooptically sampled in total-reflection geometry. Its Fourier spectrum ranging from 1.8 to 5.2 THz fairly traces the pumping photon spectrum. The result well supports the occurrence of negative dynamic conductivity in the terahertz spectral ranges.

An ultra-thin graphene layer was grown by the thermal decomposition of an 80-nm-thick 3C-SiC film heteroepitaxially grown on a B-doped Si(110) substrate [3]. Its 2D-band Raman spectra proven the existence of mono- and bilayer of graphene, and the G-band spectra at 1595 cm^{-1} corresponds to the optical phonon energy of 198 meV [3]. A 1550-nm, 20-MHz, 80-fs pulsed fibre laser beam (Fig. 1(a)) was impinged to the sample (normal to the surface). Its frequency spectra exhibit non-exponentially bumped big side-lobes apart from the main-lobe (Fig. 1(a)). Time-resolved electric-field intensity originated from the THz photon emission was electrooptically sampled by a CdTe crystal placed on the sample in total-reflection geometry [4]. Measured temporal profile (inset in Fig. 1(b)) exhibited frequency-up/down chirped relaxation oscillation, and was damped in an exponential decay on the order of ∼10 ps corresponding to the relaxation of radiative electron-hole recombination. Its Fourier spectra roughly trace the pumping photon spectra (Fig. 1(b)). The spectral drop below 2 THz in the lower side-lobe might be caused by the band-gap opening due to existing bilayer graphene with the built-in vertical potential slope arisen at the heterointerface.

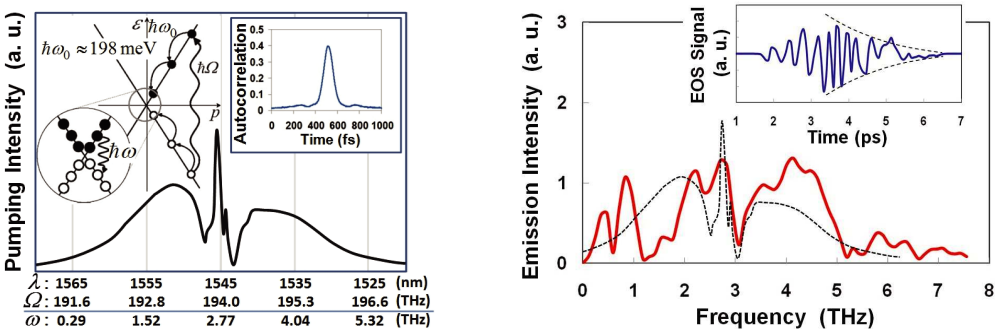

Figure 1: Experimental results of THz emission spectroscopy for an epitaxial graphene heterostructure on 3C-SiC-Si(110). (a) Autocorrelation (inset) and spectral profiles for the pump & probe laser pulse, (b) measured temporal profile (inset) and its Fourier spectrum (red line). The pumping photon energy spectrum is also shown with a dashed line.

In conclusion, we successfully observed coherent, stimulated terahertz emission owing to the fast relaxation and relatively slow recombination dynamics of photogenerated electrons/holes in an epitaxial graphene heterostructure. The result well supports the occurrence of negative dynamic conductivity leading to a new type of terahertz lasers.

REFERENCES

1. Geim, A. K. and K. S. Novoselov, "The rise of graphene," *Nat. Mater.*, Vol. 6, 183–191, 2007.
2. Ryzhii, V., M. Ryzhii, and T. Otsuji, "Negative dynamic conductivity of graphene with optical pumping," *J. Appl. Phys.*, Vol. 101, 083114, 2007.
3. Suemitsu, M., Y. Miyamoto, H. Handa, and A. Konno, "Graphene formation on a 3C-SiC(111) thin film grown on Si(110) substrate," *e-J. Surface Sci. and Nanotech.*, Vol. 7, 311–313, 2009.
4. Otsuji, T., Y. M. Meziani, M. Hanabe, T. Nishimura, and E. Sano, "Emission of terahertz radiation from InGaP/InGaAs/GaAs grating-bicoupled plasmon-resonant emitter," *Solid State Electron.*, Vol. 51, 1319–1327, 2007.

Terahertz Quantum Cascade Lasers and Their Possible Applications

Iwao Hosako, **Norihiko Sekine**, **and Kaori Fukunaga**
National Institute of Information and Communications Technology (NICT)
4-2-1, Nukuikita, Koganei, Tokyo 184-8795, Japan

Abstract— In recent years, there has been a rapid progress in the development of semiconductor device working in the terahertz frequency range, especially in the terahertz quantum cascade laser (THz-QCL) technology. The THz-QCL is a newly developed semiconductor laser that operates in the frequency range from 1 to 5 THz with milliwatt-class output power, and is expected to apply to various applications that will make the best use of the feature of the terahertz electromagnetic radiation. The potential application of terahertz technology is a nondestructive and contact-less inspection, and ultra-fast wireless communications [1]. The methods of such inspection are terahertz imaging and terahertz precision spectroscopy. In the terahertz imaging and terahertz precision spectroscopy, and terahertz wireless communications, the THz-QCL will play important roles as an illumination lamp, local oscillator (LO) of a heterodyne receiver, and the LO of receiver and signal transmitter respectively.

For the terahertz imaging, we have constructed a portable system which consists of a liquid nitrogen cooled THz-QCL illumination (3.1 THz) and un-cooled micro-bolometer camera [2]. The portable THz imaging system can obtain real-time images of 60 fps. The imaging system can be applied to many fields such as art conservation [3].

In this paper, we discuss on our THz-QCL research and their possible applications such as a real-time THz imaging and a possibility of ultra-fast wireless communication systems using the THz-QCL.

ACKNOWLEDGMENT

I would like to thank members of our research; Prof. Kaz. Hirakawa of University of Tokyo, Dr. Naoki Oda of NEC Corporation, Dr. Hiroaki Yasuda of NICT, and Dr. Yuichi Ogawa of Kyoto University for their cooperation, fruitful discussions, and efforts.

REFERENCES

1. Hosako, I., N. Sekine, M. Patrashin, S. Saito, K. Fukunaga, Y. Kasai, P. Baron, T. Seta, J. Mendrok, S. Ochiai, and H. Yasuda, "At the dawn of a new era in terahertz technology," *Proceedings of the IEEE*, Vol. 95, No. 8, 1611–1623, 2007.
2. Fukunaga, K., Y. Ogawa, S. Hayashi, and I. Hosako, "Terahertz spectroscopy for art conservation," *IEICE Electronics Express*, Vol. 4, No. 8, 258–263, 2007.
3. Oda, N., H. Yoneyama, T. Sasaki, M. Sano, S. Kurashina, I. Hosako, N. Sekine, T. Sudoh, and T. Irie, "Detection of terahertz radiation from quantum cascade laser using vanadium oxide microbolometer focal plane arrays," *Proc. SPIE*, Vol. 6940, 69402Y-1–69402Y-12, 2008.

Analysis of Optical Coupling for SOI Waveguides

Hirohito Yamada
Department of Electrical and Communication Engineering
Graduate School of Engineering, Tohoku University, Japan

Abstract— Photonic integrated circuits based on SOI waveguides are attractive for applying future ultra-high speed optical networks. Thus far, various optical device functions have been demonstrated on the SOI waveguides. However, there are few reports for integrating light sources on the SOI waveguides. In this paper, we propose a method for integrating LD chips on the waveguides and analyze optical coupling loss between the waveguides and LDs. We also describe optical input/output (I/O) interface between external optical circuits with single mode optical fibers (SMFs).

Our proposed method that is mounting LDs with flip-chip bonding on the SOI substrate and light output from LDs is directly coupled to the waveguides with spot-size converters. We calculated optical coupling loss between LDs and the waveguides with BPM method, and we found that about 2 dB of minimum coupling loss can be attained. Enough tolerance for the positioning offset of LD chip when mounting on the waveguides was also confirmed. We measured the coupling loss and confirmed the validity of the calculation.

Optical I/O interface for external optical circuits will be also proposed. The interface consisting of a grating coupler can introduce light signal from vertical direction to the substrate although grating couplers reported so far must be used for tilting SMFs from the vertical direction in order to obtain high coupling efficiency. We analyzed coupling loss for SMFs with 3D FDTD method. And we found that less than 3 dB of coupling loss can be attained with the interface and enough tolerance for the positioning offset of SMF was also confirmed.

High-speed and Precise Lightwave Modulation for High-speed Transmission Systems

Tetsuya Kawanishi[1], **Takahide Sakamoto**[1], **Akito Chiba**[1], **and Hiroyuki Toda**[2]

[1]National Institute of Information and Communications Technology
4-2-1 Nukui-Kita, Koganei, Tokyo 184-9795, Japan
[2]Faculty of Science and Engineering, Doshisha University
1-3 Tatara-Miyakodani, Kyotanabe, Kyoto 610-0321, Japan

Abstract— Recently, huge-capacity transmission over 20 Tb/s was achieved by using differential quadra-ture-phase-shift-keying (DQPSK) which can provide enhanced tolerance to chromatic dispersion and polarization mode dispersion, together with high spectral efficiency [1, 2], where integrated lithium-niobate (LN) modulators consisting of sub Mach-Zehnder interferometers (MZIs) embedded in main MZIs were used for high-speed DQPSK signal generation over 40 Gbaud [3]. The integrated modulator is called a dual parallel Mach-Zehnder modulator (MZM), which can also used for various modulation formats, such as amplitude- and phase-shift-keying (APSK), quadrature-amplitude-modulation (QAM) [4], etc. MZMs can be also used for optical comb generation, where an input continuous-wave lightwave is modulated to generate higher-order sideband frequency components. These components can be used as a frequency comb because the signal has a spectrum with a constant frequency spacing [5]. A balanced MZM can provide pure amplitude modulation without parasitic phase modulation. Basically, MZMs cannot arbitrarily control optical phase, however, the polarity of the output lightwave amplitude can be flipped by using the minimum transmission bias point of the modulator. Thus, the MZMs can provide 180-degree optical phase shift and generate binary phase-shift-keying (BPSK) signals with 180-degree phase deviation. We can also control the amplitudes of in-phase (I) and quadrature (Q) components individually, by using a dual parallel MZM. However, fabricated modulators have residual chirp or parasitic phase modulation due to manufacturing error. Imbalance in an MZM, which is typically less than 10% in optical or electric amplitudes, would degrade the performance of the transmission using multi-level modulation formats or small signal operation [6, 7]. In this paper, we describe impact of imbalance in MZMs on optical phase in modulated signals. Optical phase error in the modulator output was investigated by using a mathematical model. By using active trimming technique, on-off extinction ratio (ER) of the modulated lightwave can be larger than 70 dB.

REFERENCES

1. Gnauck, A. H., et al., "25.6-Tb/s C+L-Band transmission of polarization-multiplexed RZ-DQPSK signals," *Optical Fiber Communication Conference 2007*, PDP19, 2007.
2. Masuda, H., et al, "20.4-Tb/s transmission over 240 km using bandwidth maximized hybrid raman/EDFAs," *Optical Fiber Communication Conference 2007*, PDP20, 2007.
3. Kawanishi, T., et al., "40 Gbit/s versatile $LiNbO_3$ lightwave modulator," *European Conference on Optical Communication 2005*, Th2.2.6.
4. Sakamoto, T., et al., *European Conference on Optical Communication 2007*, PDP 2.8.
5. Sakamoto, T., et al., "Optical frequency comb generation using asymmetrically dual-driven mach-zehnder Modulator," *European Conference on Optical Communication 2005*, We4.P.121.
6. Kawanishi, T., et al., "Study of precise optical modulation using Mach-Zehnder interferometers for advanced modulation formats," *European Conference on Optical Communication 2007*, 6.2.3.
7. Kawanishi, T., et al., "Duobinary signal generation using high-extinction ratio modulation," *Optical Fiber Communication Conference 2008*, OWL2.

Continuous-wave Terahertz Spectroscopy System Based on Photodiodes

Tadao Nagatsuma[1, 2], Akira Kaino[1], Shintaro Hisatake[1], Katsuhiro Ajito[2], Ho-Jin Song[2], Atsushi Wakatsuki[3], Yoshifumi Muramoto[3], Naoya Kukutsu[2], and Yuichi Kado[2]

[1]Graduate School of Engineering Science, Osaka University
1-3 Machikaneyama, Toyonaka, Osaka 560-8531, Japan
[2]NTT Microsystem Integration Laboratories, NTT Corporation
3-1 Morinosato Wakamiya, Atsugi, Kanagawa 243-0198, Japan
[3]NTT Photonics Laboratories, NTT Corporation
3-1 Morinosato Wakamiya, Atsugi, Kanagawa 243-0198, Japan

Abstract— Terahertz (THz) waves, which cover the frequency range from 100 GHz to 10 THz, have been actively applied to sensing, radars, spectroscopy, measurement and communications. THz pulses based on femto-second pulse lasers have proven to be useful for imaging of objects, and spectroscopy of gas, liquid and solid materials [1, 2]. In particular, the time-domain spectroscopy (TDS) system based on THz pulses has been established as a laboratory standard for the THz spectroscopy, and is commercially available. In the THz-TDS system, frequency characteristics are obtained by Fourier transforming the time-domain data.

Recently, spectroscopy systems based on continuous wave (CW) technology, which uses monochromatic sources, have attracted great interest [3]. The CW source-based system provides a higher signal-to-noise ratio (SNR) and spectral resolution. When the frequency band of interest is targeted for the specific absorption line of the objects being tested, the CW system with the selected frequency-scan length and resolution is more practical in terms of data acquisition time as well as system cost.

1.55-μm telecom-wavelength technology is essential in universal instrumentation of CW systems, since low-loss/low-dispersion optical fiber cables can be employed similar to the use of coaxial cables in the conventional RF systems, and optical components are highly reliable and matured. At 1.55 μm, high-power THz photodiodes such as uni-traveling-carrier-photodiodes (UTC-PDs) [4] are superior to photoconductors based on, for example, low-temperature grown InGaAs in terms of output power as THz signal generators or emitters, while only photoconductors have been used as THz detectors in the CW spectroscopy system [5, 6].

In this paper, we propose and demonstrate the use of photodiodes for "both" generation and detection in the CW spectroscopy system. First, we experimentally show two kinds of operation modes in photodiodes at 260–420 GHz; one is a square-law detector under forward bias, and the other is a down converter under reverse bias. Then, we compare them with respect to sensitivity and dynamic range. Finally, we demonstrate the spectroscopic measurement using all-photodiode-based CW systems.

REFERENCES

1. Cooke, M., "Filling the THz gap with new applications," *Semiconductor Today*, Vol. 2, No. 1, 39–43, 2007.
2. Zhang, X.-C. and J. Xu, *Introduction to THz Wave Photonics*, Springer, 2009.
3. Deninger, A., A. Roggenbuck, S. Schindler, I. C. Mayorga, H. Schmitz, J. Hemberger, R. Güsten, and M. Grüninge, "CW THz spectrometer with 90 dB SNR and MHz frequency resolution," *Proc. IRMMW-THz 2009*, T4A03.0193, 2009.
4. Nagatsuma, T., "Generating millimeter and terahertz waves," *IEEE Microwave Magazine*, Vol. 10, No. 4, 64–74, 2009.
5. Ducournau, G., A. Beck, K. Blary, E. Peytavit, M. Zaknoune, T. Akalin, J.-F. Lampin, M. Martin, and J. Mangeney, "All-fiber continuous wave coherent homodyne terahertz spectrometer operating at 1.55 μm wavelengths," *Proc. IRMMW-THz 2009*, T4A02.0362, 2009.
6. Stanze, D., H.-G. Bach, R. Kunkel, D. Schmidt, H. Roehle, M. Schlak, M. Schell, and B. Sartorius, "Coherent CW terahertz systems employing photodiode emitters," *Proc. IRMMW-THz 2009*, T4A01.0176, 2009.

Image Observations and Analyses of RF Wave Propagations on the Basis of LEI Camera

T. Shiozawa[1, 2], **A. Kanno**[2], **K. Sasagawa**[3], **and M. Tsuchiya**[2]

[1]Kagawa National College of Technology, Japan
[2]National Institute of Information and Communications Technology, Japan
[3]Nara Institute of Science and Technology, Japan

Abstract— In this paper, we overview recent progress of the novel experimental scheme to intuitively analyze RF signal wave propagations.

The scheme is based on a live-electrooptic-imaging camera (LEI camera; http://lei-camera.nict.go.jp/), which has been invented and originally prototyped by NICT, and involves real-time visualization of phase evolution in RF wave electric fields. The scheme was demonstrated to be effective at grasping the immediate essence of RF wave propagations.

Pursuing an experimental scheme to visualize propagating electrical waves in an instantaneous manner is a considerably interesting topic of research; such a scheme can potentially facilitate the development of an advanced and fairly attractive tool for the immediate and intuitive grasp of the essential wave properties of microwave components and circuits. Such a tool can enable effective and efficient analysis and/or diagnosis of RF circuitry. While numerical simulation methods are powerful tools that can be used for this purpose, a quick experimental approach is highly desirable, especially for research and development on novel circuits having a higher degree of complexity.

The LEI scheme offers an attractive solution to the demand. An LEI camera can take images instantaneously with resolutions of 100×100 pixels to visualize microwave electrical field distributions over a circuit. Moreover, real-time movie monitoring is possible as LEI cameras have a frame rate of greater than 30 frames per second (fps); the highest rate achieved thus far is 1000 fps. The bandwidth of the "measurement" at each pixel has been demonstrated to be > 100 GHz and the system can be applied to W-band waves. In addition, intuitive image analyses on wave properties have been demonstrated.

In this paper, we provide the configuration and principle of the LEI camera first. Second, application examples are shown for three kinds of microstrip line circuit patterns; a T-shaped branch, a 90 degrees hybrid, and a meander line. Finally, the real-time visualization of 100 GHz waves, which travel in a semiconductor (ZnTe) slab waveguide is demonstrated.

Radio on LCX as Universal Radio Platform and Its Application

T. Higashino, **K. Tsukamoto**, **and S. Komaki**
Division of Electric, Electronic and Information Engineering, Graduate School of Engineering
Osaka University, Japan

Abstract— In the next generation wireless system, different kind of radio services coexist. To provide a common entrance network of those radio wireless services, broadband transparent network is required.

In addition to radio frequency/radio service independent entrance networking such as Radio on Fiber (RoF)/Radio on Free Space Optics (RoFSO), broadband common remote antenna elements are required. One of the candidates of common antenna element, the Radio on leaky coaxial cable (RoLCX) system and its applications are introduced. Main aiming of remote LCX fed by radio on fiber is to make arbitrary coverage area compared to omni-antenna element.

In this paper, WiFi service performance fed by LCX are experimentally evaluated. In the experiment, received RF power in the coverage and the voice quality in voice over WiFi are provided. In addition to the experimental results, new applications of wireless positioning, signal multiplexing method based on array antenna (AA) are proposed.

Close Proximity Wireless Communication Technologies Using Shortwaves, Microwaves, and Sub-terahertz Waves

Yuichi Kado[1], **Mitsuru Shinagawa**[1], **Ho-Jin Song**[1], **and Tadao Nagatsuma**[1, 2]

[1]Smart Device Laboratory, NTT Microsystem Integration Laboratories
3-1 Morinosato Wakamiya, Atsugi, Kanagawa 243-0198, Japan
[2]Graduate School of Engineering Science, Osaka University
1-3 Machikaneyama, Toyonaka, Osaka 560-8531, Japan

Abstract— As the digital terrestrial broadcasting service becomes a main stream with a nationwide coverage in Japan, TV broadcasting is fully shifting to HDTV capability. An innovation of video technology is not closed at this level. Higher picture quality and image resolution are principal elements, and so called ultra realistic functionalities such as a 3D image, a 4K cinema, and Super Hi-Vision video are also found among ongoing research activities.

But there is a problem. Data files of Super Hi-Vision video will become large in capacity up to hundreds of gigabytes. So, it becomes harder to transfer the data in real time than to record. This limits the potential for playback and sharing and creates a kind of bottleneck between content production and content consumption.

Recently, there has been an increasing interest in the use of electromagnetic waves at frequencies above 275 GHz for wireless communications. We can possibly make full use of ultrawide bandwidth for high-speed communications [1, 2]. This powerful short range wireless communication using sub-THz waves in homes enables high speed transfer of large video data files between two electronic products such as mobile phones, digital cameras, camcorders, computers, TVs, and game products.

This paper describes a trend of close rang wireless communication technologies. First, an AC electric-field communication technology with a frequency (5–30 MHz) below the resonant frequency of the human body is introduced as a universal interface for transmitting data in various application areas [3]. Then, a near field microwave point-to-point technology applicable for a high speed data transfer is described. Finally, it focuses on photonic generation of ultrabroadband terahertz-wave signals at frequencies from 300 GHz to 400 GHz, and their application to giga-bit wireless communication systems.

REFERENCES

1. Piesiewicz, R., M. Jacob, M. Koch, J. Schoebel, and T. Krner, "Performance analysis of future multigigabit wireless communication systems at THz frequencies with highly directive antennas in realistic indoor environments," *IEEE Journal Selecterd Topics in Quantum Electronics*, Vol. 14, No. 2, 421–430, March/April 2008.
2. Jastrow, C., K. Münter, R. Piesiewicz, T. Kürner, M. Koch, and T. Kleine-Ostmann, "300 GHz channel measurement and transmission system," *Tech. Dig. 2008 Infrared, Millimeter and Terahertz Waves (IRMMW-THz 2008)*, M3A3.1342, September 2008.
3. Kado, Y., "A human-area networking technology as a universal interface," *2009 Symposium on VLSI Circuits*, 102–105, Plenary Session, Keynote Speech, Digest of Technical Papers, June 2009.

Convergence of WDM Access and Ubiquitous Antenna Architecture for Broadband Wireless Services

Katsutoshi Tsukamoto[1], **Tatsuya Nishiumi**[1], **Takuya Yamagami**[1], **Takeshi Higashino**[1], **Shozo Komaki**[1], **Ryogo Kubo**[2], **Tomohiro Taniguchi**[2], **Jun-Ichi Kani**[2], **Naoto Yoshimoto**[2], **Hideaki Kimura**[2], **and Katsumi Iwatsuki**[3]

[1]Graduate School of Engineering, Osaka University, Japan
[2]NTT Access Network Service Systems Laboratories, Japan
[3]NTT Service Integration Laboratories, Japan

Abstract— To provide various types of wireless internet services including real time high definition video at any places and any time, an object of next generation wireless access is to realize higher bit-rate equivalent to that in current fiber access. A strict limitation in radio frequency spectrum accelerates the reduction of cell size and the use of higher frequency band including microwave, millimeter-wave and terahertz band. Consequently a huge number of radio access point (AP) will be required. Femto cell architecture where broadband fiber access network is used as entrance between core IP network and small APs, is expected as a strong method to realize such a ubiquitous broadband wireless access.

This paper proposes a novel architecture for broadband wireless services over WDM access as a convergence of WDM access and ubiquitous antenna architecture (Figure 1). In the system, fiber entrance networks employ RoF technologies to realize the universality into entrance fiber network and APs for various types of air interfaces and to increase the flexibility for non-uniform traffic distribution and users' mobility. In addition, the scalabilities of WDM technologies are expected to improve the throughput up to 1 Gbps in wireless service area provided by RoF-MIMO antenna. This paper discusses about topology of WDM access network, construction method of center station and remote base stations, and achievable throughput in wireless service areas in the proposed network.

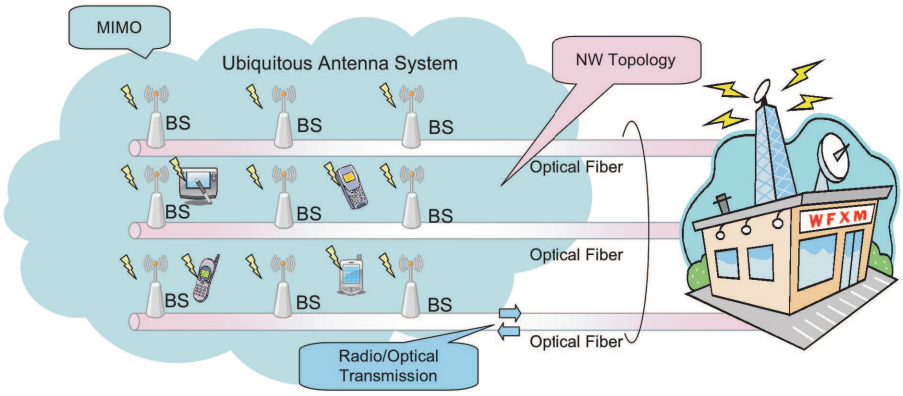

Figure 1: Broadband wireless services over WDM access network.

Session 3A4
Wave Propagation and Wave Interaction with Media

On the Statistical Approach to Characterize a Ionospheric Radio-channel

R. Talhi[1], **A. Lebrere**[1], **C. Blanchard**[2], **and M. R. Tripathy**[3]

[1]University of Tours and C.N.R.S — UMR 6115, Orleans 45071, France
[2]Department of Applied Physics, University of Granada, Granada 18071, Spain
[3]Dept. of Electronics & Communication, Institute of Engineering & Technology, Jind 126102, India

Abstract— The investigations of High-frequency wave processes through the ionosphere, which is considered as a very complex random multiple scattering medium, represent an important topic in many areas, as is well-known for example, in long-distance radio-communications and in ionospheric probing. Ionospheric propagation (negative) effects that influence radio-systems are numerous and various. One can mention delay and Doppler shifts and spread undergone by HF-waves reflected from mid or high-latitude ionosphere, and due to the large variability in propagation conditions of this random medium; moreover, another effect related to the non-perfectly horizontal character of the ionosphere is that HF-waves may have different modes of propagation and then different angles of arrival at a given receiver location in both azimuth and elevation, and the consequences can be significant to some radio-systems [1]. Hence, in order to reach a better quantitative understanding of the mechanisms of such effects, it is crucial to know how to characterize ionosphere variability, that is to have a more detailed knowledge of the characteristics of the ionospheric radio-channel. Despite the large number of publications devoted to this topic, many practical problems and theoretical open questions with different levels of complexity still exist [2–5]. One of the key questions is how to build up a technique (theory), as general as possible, to solve the problem of the ionospheric HF-waves propagation for realistic models of this complex random medium? Asymptotic methods and numerical methods, which involve some limitations of the validity of the approximation, are employed to model the HF propagation effects in the real ionosphere. In this paper, we focus on the statistical characteristics of scattered polarized radiation for the most general case of a three-dimensional (3-D) inhomogeneous ionosphere with electron density fluctuations (ionospheric turbulence). Numerical simulations have been made by means of Monte Carlo method. Influence of the turbulence strength and the electron density, among other factors, on the scattered polarized radiation are considered. If we look to the features of the angular power spectrum of scattered radiation, It is found that the maximum electron density controls the position (in the angular domain) of the maximum of the power spectrum, while the turbulence strength controls the broadening at mid-height of the power spectrum. This problem and some related questions are currently under intensive investigation.

REFERENCES

1. Goodman, J., "Space weather topics at ionospheric effects symposium," *Space Weather Int. Journal*, Vol. 6, S08004, doi: 10.1029/2008SW000424, 2008.
2. Galkin, I., et al., "Uncertainty and confidence of ionospheric specifications with the digisonde ARTIST-5 ionogram autoscaler," *12th International I.E.S.*, City of Alexandria, USA, May 13–15, 2008.
3. Warrington, E. M., et al., "Propagation modelling and prediction for trans-polar airlines routes," *12th International Ionospheric Effects Symposium*, City of Alexandria, USA, May 13–15, 2008.
4. Gardiner-Garden, R., et al., "Modelling uncertainty in a real-time model (nowcast) of the ionosphere," *12th International Ionospheric Effects Symposium*, City of Alexandria, USA, May 13–15, 2008.
5. Stocker, A. J., et al., "A comparison of observed and modelled deviations from the great circle direction for a 4490 km HF propagation path along the mid-latitude ionospheric trough," *Radio Science*, Vol. 38, No. 3, 1045, 2003.

Seasonal/Longitudinal Variations of Radiowave Scintillations Derived from the Topside Ionospheric Density Irregularities Observed by ROCSAT from 1999 to 2004

Y. H. Liu[1], **S.-Y. Su**[2], **and C. H. Liu**[3]

[1]Department of Electrical Engineering, National Central University, Chung-Li, Taiwan
[2]Institute of Space Science, Center for Space and Remote Sensing Research
National Central University, Chung-Li, Taiwan
[3]Academia Sinica, Taipei, Taiwan

Abstract— Seasonal and longitudinal (s/l) variations of radiowave scintillations derived from the topside ionospheric density irregularities observed by ROCSAT during the moderate to high solar activity years of 1999 to 2004 have been obtained. Using the thin phase-screen model of Rino (1979), the observed s/l distributions of density irregularities together with the density profiles from the International Reference Ionosphere (IRI) model are converted into the global seasonal scintillation index S_4 variations. The resultant s/l distributions of scintillation index S_4 show a better latitudinal variation of the peak S_4 occurrences away from the magnetic equator that is more realistic than any other scintillation model. In addition, this latitudinal variation of the s/l distributions of S_4 index is different from that of the s/l distributions of density irregularities which indicate a clear peak occurrence at the magnetic equator. Detail derivation and the significance of the newly derived S_4 map will be presented.

Comparison of Microwave Links Prediction Methods: Barnett-Vigants vs. ITU Models

Basile L. Agba[1], **Robert Morin**[2], **and Germain Bergeron**[2]

[1]Institut de Recherche d'Hydro-Québec, 1800 Lionel-Boulet, Varennes, Québec, Canada
[2]Hydro-Québec, 1500 University, Montreal, Québec, Canada

Abstract— The microwave links deployment, like any other wireless network, requires accurate prediction methods in order to minimise the discrepancies between simulation results and real system performance. Although numerous microwave links are deployed around the world, most of them can be considered as short-range or mean-range links for which the path length is less than 20 km.

Hydro-Québec operates one of the widest electricity networks in the world. The microwave network infrastructure is essential to manage the power grid in Québec and therefore, it is important to meet the reliability criteria that are generally above those accepted by traditional communication operators. In addition, over one third of the existing links have lengths between 70 km and 90 km and operate in extreme weather conditions and all year long. To address these constraints, the microwave links design needs to be as much accurate as possible. The aim of the research presented in this paper is to make a comparative study between two commonly used prediction models for microwave links: Barnett-Vigants and ITU-R P. 530.

The first part of this work considers each of the following aspects:

- unavailability due to multipath,
- unavailability due to rain,
- methods for diversity gain (space and frequency diversity),
- worst month values to annual values conversion methods.

We analyse each aspect as a function of various parameters such as frequency, fading margin and link length. The two models led to significantly different results for the unavailability due to multipath as a function of the link length, and also for the space diversity as a function of the gain difference between the main antenna and the diversity antenna. Remarkable differences between the two models were also observed when studying the unavailability due to rain as a function of the frequency.

The second part of this work compares the overall performance of both models in terms of the total outage probability over ten links with different lengths and different locations. The differences observed for some links are significant.

Several conclusions were drawn based on the theoretical analysis. Further experimental measurements are currently carried out over five targeted links as part of the validation process.

Tuneable Absorber Loading in the Reverberation Chamber by Using Active Frequency Selective Surfaces

Jung-Hwan Choi and Seong-Ook Park
Korea Advanced Institute of Science and Technology, Daejeon, Republic of Korea

Abstract— A reverberation chamber has been introduced for electromagnetic compatibility testing because of its advantages, such as cost-effectiveness, shorter measurement time, generation of high field strength with low input power, statistically uniform field distribution, and isotropic polarization characteristic. In recent years, the performance evaluations in the reverberation chamber have been widely researched for characterization of multiple-input-multiple-output (MIMO) handset antenna applications. Statistical properties of excited fields in a reverberation chamber were similar to those of real communication environments that experience multipath fading phenomena.

Resonance frequency and quality factor represent the characteristics of microwave cavity structures like a reverberation chamber. Normally, the value of quality factor is very high so that the time constant is very long. In viewpoint of communications, a reverberation chamber has very long delay spreads because many reflections are occurred with the low absorption. The value of quality factor can be controlled using microwave absorbers for making different propagation environments. That is, a power delay profile in a reverberation chamber is changed due to the energy absorption of microwave absorbers. Also, it can be thought that microwave absorbers change properties of metallic walls. As a result, direction-of-arrival of the received signal at RX antenna can be controlled.

The characteristics of excited fields in a reverberation chamber are dramatically changed according to the position and the number of microwave absorbers installed in a reverberation chamber. It is hard to reproduce exactly same environments by placing a microwave absorber on the same position at every measurement. In addition, this method is inconvenient and time-consuming because a user should install or move absorbers every time. In this paper, we propose the tuneable absorber loading technique that uses active FSSs which have absorber layer and different operating bands. According to the status of the pin-diode attached on FSS, absorber layers behind FSSs are visible or not because an active FSS can be operated spatial band rejection filter or spatial band pass filter.

Pecularities of the Total Electron Content and Their Reflections in the Ionospheric Model

O. A. Maltseva and T. Trinh Quang
Southern Federal University, Rostov-on-Don, Russia

Abstract— The total electron content TEC is a key ionospheric parameter in many applications from positioning and propagation methods, navigation, modern radio astronomy systems to investigation of space weather influence on environment. An empirical model of TEC can be desirable to solve many problems in these applications but such a model does not exist yet (Mendillo, 2006). To use the International Reference Ionosphere (IRI) model (Bilitza, 2001) is seemed to be very attractive but it is not empirical for TEC unlike its main parameters foF2, NmF2, hmF2, M3000F2, Nh-profile. Values of TEC are calculated as TEC = $\int$ Nhdh hence it is necessary to compare model and experimental values. For this purpose the other determination can be used: TEC = $\mathrm{NmF}_2^* \tau$ where τ is the effective ionospheric slab. Comparison was done by analysis of experimental factors K(TEC) = TEC(obs)/ TEC(IRI2001) = $K(\mathrm{NmF}_2) * K(\tau)$ and by analysis of correction factors K(corr) = TEC2007(corr)/TEC2001, K(NeQ) = TEC2007(NeQ)/TEC2001 of the IRI2007 model to appreciate which factor gives the biggest contribution into discrepancies ΔTEC = TEC(obs)-TEC(model) between experimental and model TEC. Data of Chinese chain of VS stations and TEC maps (JPL, CODE, UPS, ESA) are used to compare diurnal, seasonal, latitude and geomagnetic dependence of median and instantaneous (real-time) peculiarities. The main results are: 1) correction factors K(corr) and K(NeQ) of the IRI2007 model are always lower than 1 increasing correspondence to real $N(h)$-profiles but sometimes decreasing coincidence with experimental TEC values, 2) the IRI model provides sometimes TEC values differed strongly from experimental ones, specifically, because of large deviations |ΔfoF2| even for median foF2 but real time TEC values can give reliable coincidence with experiment, in particular using the empirical model of the slab, 3) factors K(NmF2) and $K(\tau)$ can give compatible contributions in median conditions and can lie in ranges 0.8–1.5 but during disturbances the biggest contribution gives $K(\tau)$ increasing to value of 3–4, 4) experimental $K(\tau)$ obtained by one VS station can be used to reconstruct foF2 distribution from TEC of neighbouring area.

Research of the Effect of Electromagnetic Interference on Magnetic Sensors due to the Data Transmitting System of the Seismic Electromagnetic Satellite

Ye An[1], **Ping-Lian Wang**[1], **Ping Liu**[2], **Yu-Rong Liu**[1], **and Rui Yan**[3]

[1]Academy of Opto-Electronics, Chinese Academy of Sciences, Beijing 100190, China
[2]Dalian University of Technology, Dalian 116024, China
[3]Institute of Engineering Mechanics, China Earthquake Administration, Ha Erbin 150080, China

Abstract— This paper explores the effects of Electromagnetic Interference (EMI) on Magnetic Sensors due to the Data Transmitting System (DTS) in order to aid the system design of the Chinese first Seismic Electromagnetic Satellite. The research was focused by two ways including the EMC prediction between the DTS and the Magnetic sensors and the DTS's EMC test. The result of the research indicates that: the distance between the induction magnetometer and the power line of the DTS should be 1.2 m at least; and also the frequency flow and permanent magnetic materials should be designed properly in order to make the DTS and the sensors compatible.

Dynamic Motions of Small Diamagnetic Particles Induced by Static Field in Microgravity Condition; Examination of Mass Dependence

Chiaki Uyeda, **Keiji Hisayoshi**, **and Shun Kanou**
Graduate School of Science, Osaka University, Toyonaka, Osaka 560-0043, Japan

Abstract— Rotational [1] and translational [2] motion caused by static magnetic field $\boldsymbol{B}$ were recently observed for various diamagnetic samples released in microgravity μG. The two types of motions are well known for conventional magnetic materials that bear spontaneous moments, however possibility of such motions has been ignored for weak magnetic materials. Acceleration a of the translational motion caused by field gradient force is described as $a = -(1/2)\mathrm{grad}(\chi_{DIA}B^2)$ [see Fig. 1(a)]; here χ_{DIA} denote diamagnetic susceptibility per unit mass, while m is the mass of the sample. The rotational motion derives from anisotropy of diamagnetic susceptibility $\Delta\chi_{DIA}$. A rotational oscillation follow an equation $I(d^2\theta/dt^2) = -m\Delta\chi_{DIA}B^2\theta$ [see Fig. 1(b)]; here I is the moment of inertia of the particle, while θ denote direction of magnetically stable axis with respect to field direction. Period of oscillation is described as $\tau = 2\pi(Im^{-1}\Delta\chi_{DIA})^{1/2}B^{-1}$. It is seen that a and τ are both independent to m. In a given distribution of field gradient, value of a uniquely depends on intrinsic χ_{DIA} value of the material [1]. As for rotational oscillation, τ is determined by Im^{-1} and intrinsic $\Delta\chi_{DIA}$ value of the material [2], in a given homogeneous field B. In the present report, the motions are measured for α-quartz single crystals that posses various m values. The mass independencies of the two motions discussed above are examined based on the observed results as shown in Fig. 2. Value of χ_{DIA} and $\Delta\chi_{DIA}$ are two basic parameters in investigating magnetic property of a material. The need of clarifying the properties for a single small particle is increasing rapidly with the growing interest on nano-sized materials. At present, these values are difficult to obtain for most of the diamagnetic materials using a conventional method. By observing the above-mentioned motions in μG, detection of χ_{DIA} and $\Delta\chi_{DIA}$ becomes possible on micron-sized sample [1]. This is because reduction of sample size is possible as long as motion of the sample is observable.

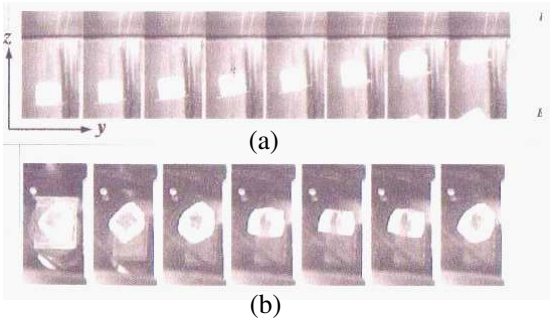

Figure 1: (a) Translational motion of Rochelle salt induced by field gradient [1]. (b) Rotational oscillation of calcite that derive from dimagnetic anisotropty [2].

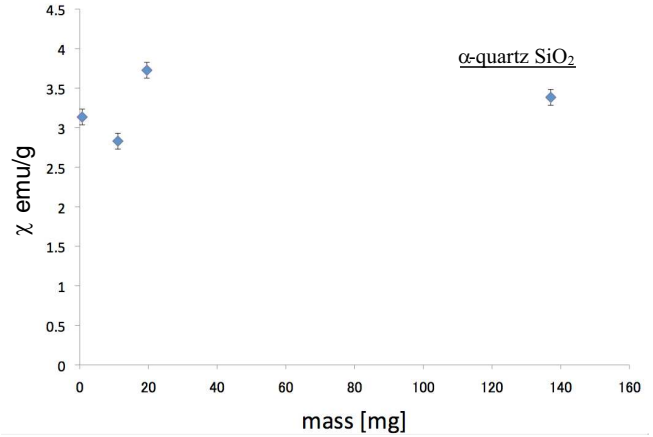

Figure 2: Relationship between measured χ [emu/g] and mass observed for α-quartz.

REFERENCES

1. Hisayoshi, K., S. Kanou, and C. Uyeda, *J. Phys.: Conf. Ser.*, in press.
2. Uyeda, C., M. Mamiya, R. Takashima, T. Abe, H. Nagai, and T. Okutani, *Jpn. J. Appl. Phys.*, Vol. 45, L124, 2006.

Charge Continuity Equation in the Gravitational Field

Ying Weng[1] and Zi-Hua Weng[2]

[1]College of Chemistry & Chemical Engineering, Xiamen University, Xiamen 361005, China
[2]School of Physics and Mechanical & Electrical Engineering, Xiamen University, Xiamen 361005, China

Abstract— The quaternion was first used by J. C. Maxwell in 1861 to describe the properties of electromagnetic field. Similarly, the algebra of octonions can be used to rephrase the features of gravitational field and electromagnetic field simultaneously, although these two kinds of fields are quite different. By means of the scalar invariant of octonions, we find that both electromagnetic strength and gravitational strength have an influence on the charge continuity equation.

In the electromagnetic field, the charge continuity equation is similar to the mass continuity equation. The conservation law is quite significant in the physics, with the numerous applications in the quantum mechanics, the electromagnetic theory, and the optics theory, etc. Rephrasing with the algebra of octonions, we obtain the charge continuity equation in the case for coexistence of electromagnetic field and gravitational field.

The charge continuity equation was limited to the case of weak electromagnetic strength. In the octonion space, the definition of charge continuity equation can be extended to the case for coexistence of electromagnetic field and gravitational field. With the features of the octonion, we study a few impact factors of the charge continuity equation in the electromagnetic field and gravitational field, including the velocity and field strengths.

The results state that either gravitational strength or electromagnetic strength has an influence on the charge continuity equation, although these impacts are usually tiny when the field strengths are weak. And then, the charge continuity equation is conserved in most cases. However, when the electromagnetic field and gravitational field are strong enough, the field strengths will affect the charge continuity equation obviously in the electrolytes.

ACKNOWLEDGMENT

The author is grateful for the financial support from the National Natural Science Foundation of China under grant number 60677039.

Pyroelectric Properties of the Sr-doped Ferroelectric Barium Iron Niobate

S. B. Bajaj[1], **R. L. Raibagkar**[2], **and G. N. Shinde**[3]

[1]PG Department and Research Center in Physics and Electronics, JES College
Jalna 431203, India
[2]Department of Post Graduate Studies and Research in Materials Science, Gulbarga University
Gulbarga 585106, India
[3]Indira Gandhi College, CIDCO, Nanded 431603, India

Abstract— Ceramic materials showing ferroelectric behaviour are being used in many optics and electro-optics application. A large number of applications of ferroelectric ceramics also exploit properties that are an indirect consequence of ferroelectricity, such as dielectric, piezoelectric and electro-optic properties. Ferroelectric relxors with high Curie temperature have been prepared by usual ceramic technique. All the samples of $(Ba_{1-x}Sr_x)(Fe_{0.5}Nb_{0.5})O_3$ [BSFN] were characterized at room temperature by X-Ray diffraction using Cu-Ka radiation and found to have single phase and cubic structure. Pyroelectric measurements were carried out in the temperature range 25°C to 400°C. The pyroelectric properties of Sr-doped ferroelectric BSFN and their solid solutions were investigated in the temperature range covering their transition points. In these ceramics, a peak in pyroelectric currents and coefficients were observed at Curie temperatures. These Curie temperatures are consistent with that investigated in dielectric and hysteresis property. It is observed that the peak value of current and coefficient changes with Sr-concentration.

Session 3A5
Advanced CEM Methods for Electrically Large Problems

Study of EM Scattering from Electrically Large Objects in Planarly Multilayered Media with a Fast Algorithm

Lei Zhuang, **Si-Yuan He**, **Jing-Jing Yao**, **Ding-Feng Yu**, **and Guo-Qiang Zhu**
School of Electronic Information, Wuhan University, Wuhan 430079, China

Abstract— This paper studies electromagnetic (EM) scattering from electrically large objects buried in planarly multilayered media with a fast algorithm, which combines the stabilized biconjugate gradient fast Fourier transform (BCGS-FFT) method with an improved discrete complex image method (DCIM). Filling the table of Green's function and solving the matrix equation constitute two barriers for fast evaluation of EM scattering by buried objects. An improved DCIM is introduced to get a closed-form dyadic Green's function (DGF) in multilayered media for the volume electric field integral equation (EFIE), which is accurate both in the near- and far-field regions in layered media without any quasi-static and surface-wave extraction. In the simulation, a split scheme is adopted to avoid applying the improved DCIM repeatedly. By splitting spectral DGF before utilizing the improved DCIM, we need to apply the improved DCIM for only several times. In this way, the time requirement of evaluation of the Green's function is further reduced. Consequently, the error between the simulation results by the improved DCIM and the results obtained via numerical integration of sommerfeld integrals (SIs) is further reduced. Meanwhile, the closed-form DGF enables the "spherical-mean" Green's function, which eliminates the singularity of Green's function. Then, the iterative solver the BCGS-FFT method is combined with the improved DCIM for solving the matrix equation. Numerical results show that the improved DCIM can save tremendous CPU time in scattering problems involving buried objects. The fast algorithm proves effective for EM scattering from electrically large objects in both lossless and lossy multilayered media.

Shooting and Bouncing Ray Tracing Method Based on Uniform Stationary Phase Approach

Wen Ming Yu, **Jun Zhang**, **Xiao Yang Zhou**, **and Tie Jun Cui**
State Key Laboratory of Millimeter Waves, Department of Radio Engineering
Institute of Target Characteristics and Identification
Southeast University, Nanjing 210096, China

Abstract— The shooting and bouncing ray (SBR) tracing method is the most efficient approach to obtain the electromagnetic characteristics of electrically large objects. Parametric-model based uniform stationary phase method can improve the accuracy and efficiency of the physical optics method significantly. However, an optimization procedure such as Newton iteration method should be applied to find the stationary phase points. It is very time consuming especially when the number of reflection points along the ray path is larger than one and the initial points to start searching are arbitrarily selected. Previous works on parametric-model based uniform stationary phase method consider only one or at least two reflections, several important coupling effects may not be taken into account especially for cavity problems, so these methods are not belong to SBR method actually. The ray tracing method using Kd-Tree constructor is very efficient to construct the ray paths when lights traveling among components of a scene. The reflection points determined by ray tracing are equivalent to the stationary phase points found through an optimization procedure. Because the ray tracing is an explicit procedure, rays should be sampled at the source points or in the incident plane, observation directions will be determined at the termination of the tracing procedure. On other hand, the procedure to find stationary phase points is implicit since source and observation points or directions are predetermined. Hence the exact stationary-phase points may be missed in the ray tracing procedure. In this paper, we introduce a novel shooting and bouncing ray tracing method based on uniform stationary phase approach which can efficiently find the stationary phase points with any number of reflections using the ray tracing procedure as a preconditioning. Several examples are presented to verify the validity of the method.

Efficient Analysis of Electromagnetic Scattering Problem Using Proper Orthogonal Decomposition

Chao-Fu Wang
Temasek Laboratories, National University of Singapore, Singapore

Abstract— This paper describes a novel approach for efficiently solving electromagnetic (EM) scattering problems using proper orthogonal decomposition (POD). As a proof of concept and demonstration of how to use the POD to solve EM scattering problems, two ways of implementation of the POD procedure have been proposed and realized for calculating EM scattering from 2D PEC targets using electric field integral equation (EFIE) for TE polarization and magnetic field integral equation (MFIE) for TM polarization. Preliminary results obtained show that the POD is quite accurate for reconstructing backscatter patterns over wide range of frequencies and angles of interest based on the given snapshots.

Electromagnetic Modeling of Finite Metallic Grid FSS Structures Using Scale Changing Technique

Euloge B. Tchikaya[1], **Aamir Rashid**[1], **Hervé Aubert**[1], **Hervé Legay**[2], **and Nelson Fonseca**[3]

[1]LAAS, France
[2]Thales Alenia Space, France
[3]CNES, France

Abstract— Nowadays global electromagnetic simulators are indispensable for accurate prediction of the overall electromagnetic performances of radiofrequency systems. The electromagnetic simulation of large and complex planar structures with fine-scale patterns by conventional numerical methods based on a spatial meshing (finite element method, finite difference method, method of moments) leads often to poorly conditioned matrices, numerical convergence problems or/and excessive computation time. To overcome these problems, an original technique called the *Scale Changing Technique* (SCT) has been proposed for whole-scale modeling of large planar structures with complex metallic patterns. In applications like FSS, reflectarrays and fractal antennas the dimensions of such patterns can vary over a wide range of scale, from many orders of magnitude lower to many orders higher with respect to the wavelength. These multi-scaled patterns can be defined as lying at different scale-levels at the surface of discontinuity plane. Therefore in SCT this multi-scale structure is seen as the cascade of *Scale-Changing Networks*, each network modeling the electromagnetic coupling between two successive scale levels. The electromagnetic coupling between the scales is modeled by the ports of the network and the modes defining these ports are called *active modes*. The fine-scale field variations with negligible coupling with adjacent scales are defined by higher-order modes named as *passive modes* (see [1]). The scalechanging networks are calculated independent of each other and are cascaded only at the final step to obtain the complete solution. Therefore SCT effectively computes a complex problem by scaling it in many simpler problems than can be solved independently. This leads to smaller sized matrices with much better condition numbers which translates to a significant reduction in terms of computational time and memory space as compared to conventional numerical methods that use linear meshing over the complete discontinuity plane.

In this communication, Scale Changing Technique has been applied for the electromagnetic modeling of nonuniform FSS arrays formed by a metallic grid of finite size and finite thickness (Fig. 1(i)). Modeling of these structures is performed using SCT and Ansoft HFSS®. SCT is found to be extremely efficient in the case of large sized arrays. The evolution of simulation times with respect to the increasing array-size for the case of a uniform array is plotted in Fig. 1(ii) for the two simulation tools. We can notice the linear increase in SCT computation time

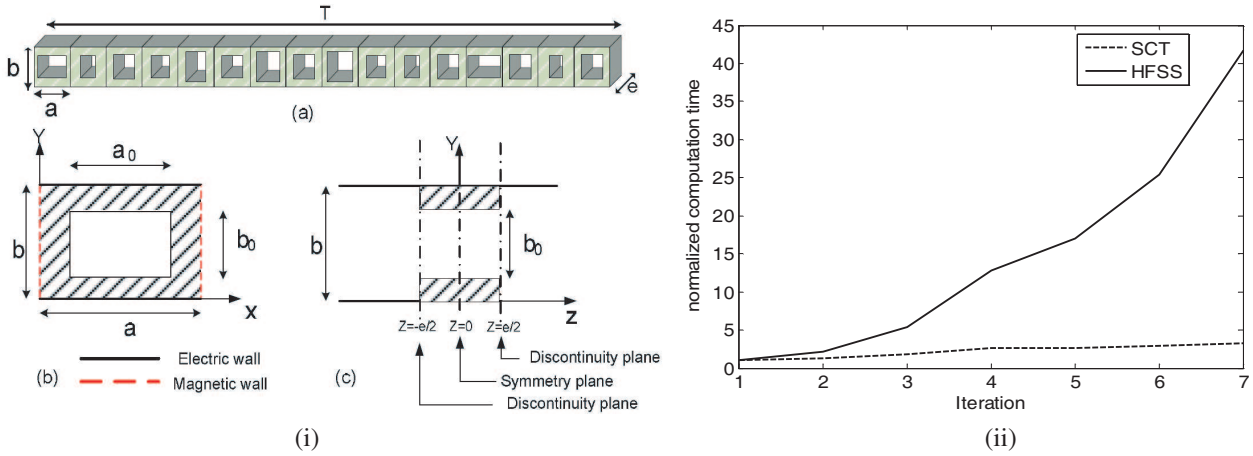

Figure 1: (i). (a) Finite-size 1-D metallic grid of non-identical cells, the width of the network is $T = 160\,\text{mm}$, (b) cross-section of an elementary cell in XY plane. (c) View in YZ plane (all the cells have same thickness e). (ii) Evolution of normalized simulation times of SCT and HFSS with respect to the simulated array size (Array size $= 2^{\text{Iteration}}$ unit-cells).

as compared to exponential increase in case of HFSS. A similar time relation can be observed in the case of non-uniform arrays if the SCT simulation is performed using parallel processing.

REFERENCES

1. Aubert, H., "The concept of scale-changing network in the global electromagnetic simulation of complex structures," *Progress In Electromagnetics Research Letters B*, Vol. 16, 127–154, 2009.

The Probability Distribution of the EM Fields in Single-cavity System and the Application of PWB Method

J. Liu, X. Zhao, and K. M. Huang
College of Electronics and Information Engineering, Sichuan University, Chengdu 610064, China

Abstract— It is difficult to successfully resolve the response, especially, the high frequency response of large complex electronic system to the external electromagnetic environment by using the traditional electromagnetic simulation methods. The main difficulties are the enormous computational cost of the traditional full-wave analysis and the uncertainty caused by the high sensitivity of the high-frequency response. Therefore, it is necessary to introduce some relatively simple estimation methods combined with the "statistic language" to analyze the coupling and the transmission processes of the external EM energy in the electronic system. It has very important theoretical and application perspectives for electromagnetic compatibility and electromagnetic effects evaluation. PWB (Power Balance) method is a kind of estimation method, used to estimate the magnitude of electromagnetic energy in complex system under the high-frequency interference. PWB method is based on statistical concepts. The main assumption is that when the considered system is large compared to wavelength of electromagnetic interference, EM fields at any point inside the cavity are uniformly distributed random variables of the position. As a result, the mean EM environment can be viewed as pseudo-homogeneous.

In this paper, the probability distributions of the EM fields in a single-cavity system with and without a mode stirrer are studied. The probability distribution curves of EM fields inside the cavity were obtained by using full-wave analysis method. By curve fitting, it was found that they obey the distribution function: $y = y_0 + A * e^{-e^{-z}-z+1}$, where $z = (x - x_c)/w$, y_0, x_c, w, A are the undetermined coefficients. This kind of probability density function is unimodal function, and the more intense the peak is, the more homogeneous the EM Environment is. Although this unimdal function are not very satisfied with the assumption of PWB, the power losses of cavity wall at different frequencies evaluated by PWB and the one calculated by full-wave analysis are comparable. The change trends of the two curves with frequency are almost coinciding with each other, and the difference is no more than an order of magnitude. However, it is remarkable that PWB method costs less than one minute while the full-wave analysis method costs about two hours, and PWB method saves almost 70% memory space. It means that PWB method can indeed give computed data which meet certain accuracy requirement with much smaller computational cost than the full-wave analysis method.

Finally, the inhomogeneous degree V is defined as $V = \sqrt{D}\Big/E$ to measure the inhomogeneity of EM field distribution inside the cavity, where D is the variance and E is the mean of the EM field magnitude. The numerical results show that the stirrer can make the EM fields inside the cavity more homogeneous, which accompanied by decreased V. This definition is a preparation for further study about inhomogeneous degree effects on calculation accuracy of the PWB method.

Although only single-cavity system is considered in this paper, the above conclusions can be easily extended to the case of multi-cavity system through PWB network formula.

Solving Low Frequency Scattering from Dielectric Objects by Improved IE-FFT

Jiliang Yin, **Jun Hu**, **and Zaiping Nie**
School of Electronic Engineering, University of Electronic Science and Technology of China
Chengdu, Sichuan 611731, China

Abstract— In this paper, the integral equation fast Fourier transform (IE-FFT) algorithm is presented to show the ability for overcoming the low-frequency breakdown problem. For electrically small dielectric objects, the volume integral equation (VIE) is chosen to characterize the problem for the equation has no low-frequency breakdown problem. The method of moment (MoM) is used discretize the integral equation and the IE-FFT is used to accelerate the matrix-vector multiplication in the iterative solver. When the object is discretized by very fine tetrahedrons (relative to wavelength), to solve the problem efficiently, the grid size is set to be very small, also the near-interaction threshold can be set to be very small while maintains the interpolation accuracy for the Green's function oscillate slowly for low frequency problem. We can achieve a very low complexity and memory requirement for this problem, which is competitive for the multilevel fast multipole algorithm (MLFMA). However, the traditional MLFMA can't get the correct result for it has sub-wavelength breakdown problem. To further reduce the memory requirement and CPU time for the IE-FFT algorithm, we use the floating stencil topology which reduces the near-interaction numbers. And some other recent advances made to the algorithm are discussed. It shows that the IE-FFT algorithm can straightforwardly apply to solve both low and high frequency problem efficiently.

An Efficient Domain Decomposition Method for Solving Extremely Large Cavity Scattering Problems

Z. Peng and Jin-Fa Lee
ElectroScience Lab., The Ohio State University, USA

Abstract— A variety of techniques have been developed to analyze the scattering by an arbitrarily shaped cavity. However, it is still thought to be a grand challenge for accurate and efficient numerical analysis when the cavities are electrically big and deep. In this work, a highly efficient domain decomposition method with second order transmission condition is developed to solve the challenge problem of scattering by an extremely large cavity, which is depicted in Fig. 1. Numerical results will be presented to illustrate the effectiveness of the proposed method.

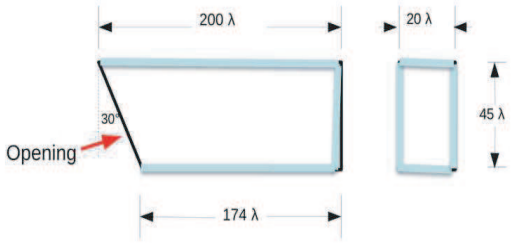

Figure 1: A extremely large and deep cavity.

A Hybrid Lattice-adaptable ADI-FDTD/PSTD Algorithm

Hong-Xing Zheng and Chong Peng
Tianjin University of Technology and Education, China

Abstract— Modern electromagnetic anechoic absorbers comprise the basic reflection-free means for measurement without disruption from ambient signals and outdoor interference. For a general bi-isotropic medium with the Tellegen and chirality parameter, the potential of efficient electromagnetic anechoic absorbers was presented [1]. On the basis of bi-isotropic medias structural coupling which produces both polarizations, they can offer an alternative perspective [2]. To keep pace with the rising standards, the absorber must be reconfigured; it is rather expensive designing task that can be effectively relieved by time-domain numerical methods. However, the dispersive profile of bi-isotropic media complicates their modeling since it may lead to serious instabilities and grid errors. In this paper, a 3-D hybrid time-domain technique with mesh-adaptable capabilities is developed. The proposed method divides the domain in distinct regions of fast field fluctuation and smooth periodical attributes. Being rather broadband, the algorithm assigns higher order frequency dependent finite-difference time-domain (FDTD) forms to the former regions and a Fourier Chebyshev pseudospectral time-domain (PSTD) interpolation to the latter. A key purpose of the hybrid methodology lies on the construction of advanced spatial-temporal operators capable of efficiently handling the large size of a test facility as well as the structural particularities. Then, the dispersive properties of bi-isotropic media as extra layers at the base of pyramids or wedges are described by Drude waveforms, while their chirality parameter is represented by a Condon model. For the analysis of discontinuities in the facility and the acceptable isolation of its quiet zone, a multimodal decomposition is present, which projects Maxwell's laws on preselected planes. The alternating- direction-implicit (ADI) technique is used to increase the computational efficiency. The hybrid methodology for the proficient design of optimized absorber in anechoic facilities is also introduced. Incorporating higher-order spatial operators and a family of consistent boundary conditions, the proposed ADI-FDTD/PSTD method provides very accurate outcomes with large system and time overall savings for test facilities. Therefore, issues like dispersion-error reduction, arbitrarily aligned interface treatment or artificial spurious mode suppression are very significant. Such benefits are verified via the characterization of different microwave and millimeter wave circuits supported with the proposed media, while diverse bi-isotropic setups of very low reflectivity are thoroughly investigated.

ACKNOWLEDGMENT

This work was supported by the National Natural Science Foundation of China under Grant 60871026.

REFERENCES

1. Holloway, C., P. McKenna, R. Dalke, R. Perala, and C. Devor, "Time-domain modeling, characterization, and measurements of anechoic and semianechoic electromagnetic test chambers," *IEEE Trans. Electromagn. Compat.*, Vol. 44, No. 1, 102–118, Feb. 2002.
2. Ngu, X., A. Nothofer, D. Thomas, and C. Christopoulos, "A complete model for simulating magnitude and phase of emmissions from a DUT placed inside a GTEM cell," *IEEE Trans. Electromagn. Compat.*, Vol. 49, No. 2, 285–293, May 2007.

A Soft Source Technique Introduced to the ADI-PSTD Method

Hong-Xing Zheng
Tianjin University of Technology and Education, China

Abstract— In popular 2-D or 3-D finite-difference-time-domain (FDTD) total field/scattered field formulation [1], the 1-D source propagation equation is solved first by using FDTD with the same grid size and time step. Then, the values of the incident plane wave are interpolated from the 1-D solution. Typically, the FDTD uses more than 16 grid points per wavelength so that the interpolation can be done quite accurately. But computer resource occupied leads to very lower computational efficiency for the large body with tiny structures. Recently, a pseudospectral timedomain (PSTD) method was proposed as an efficient algorithm for solving Maxwell's equations [2]. There is a significant computational advantage has been found, whereas only two grid points per minimum wavelength are required in the PSTD method compared to 10–20 typically found in FDTD. Thus, PSTD requires far less memory and time, and much more efficient than FDTD. However, there are several issues such as difficulty in introducing external soft sources, and in modeling of fine structures with the PSTD algorithm regarding to its application. In the FDTD, there is a well-developed total field/scattered field formulation, which only requires the incident field components to be calculated along a boundary connecting the field/scattered field regions. Thus, in this paper, a novel approach to introducing continuous soft sources in the PSTD algorithm is proposed for analyzing the wave scattering in an inhomogeneous medium, while maintaining its computational advantages. The alternating-direction-implicit (ADI) technique is used to increase the computational efficiency [3]. Prior PSTD algorithms have employed a scattered field formulation to deal with continuous soft sources. In a scattered field formulation, the incident terms are needed for the region where the scatters have different material properties to the background. 1-D and 2-D PML examples to support our findings are provided. These numerical experiments have confirmed the validity of such a method, and further show the feasibility of this method. To find the optimum curve with minimal Gibbs' phenomenon, several window functions have to be constructed. The B-H window function is found, which is well known in the digital signal processing community. Moreover, a scalar weighting term is introduced to the total field/scattered field. A 2-D scattering study of a dielectric cylinder is given.

ACKNOWLEDGMENT

This work was supported by the National Natural Science Foundation of China under Grant 60871026.

REFERENCES

1. Taflove, A. and S. C. Hagness, *Computational Electrodynamics: The Finite-difference Time-domain Method*, 2nd Edition, Artech House, Norwood, MA, 2002.
2. Liu, Q. H., "The PSTD algorithm: A time-domain method requiring only two cells per wavelength," *Microw. Opt. Technol. Lett.*, Vol. 15, No. 3, 158–165, June 1997.
3. Zheng, F. and Z. Chen, "Numerical dispersion analysis of the unconditionally stable 3-D ADI-FDTD method," *IEEE Trans. Microwave Theory Tech.*, Vol. 49, 1006–1009, May 2001.

Session 3A6
Antenna Theory, Radiation, Microstrip and Printed Antennas 1

Improved Team Progress Algorithm for Wide Sector Pattern Synthesis of Antenna Arrays

M. Zhang and Y. M. Bo
College of Electronic Science and Engineering
Nanjing University of Posts and Telecommunications, China

Abstract— Normally, narrow, scanned and low-sidelobe beams of antenna arrays can be obtained by using uniform or non-uniform amplitude excitations, while sector patterns can be obtained by complex excitation distributions. In a specific array application, both narrow beam scanning and wide sector beam coverage up to 90-degree are desired. In addition, the transmit/receive modules of the array must be in a state of full output power to satisfy the specification of equivalent isotropic radiated power within the coverage range in the sector mode. Thus, the wide sector pattern should be achieved in the condition of uniform amplitude distribution, which is much more difficult than the cases of non-uniform distributions for sector beams.

A minimization problem of a multivariate function without constraints can be interpreted as the task to find an optimal member with the best evaluation. Because both successful global optimization and fast convergence are required, these two sub-tasks will be accomplished using two search groups. For the tasks, a team with some members are established, and divided into the elite and the plain groups according to their evaluations. The elite and plain epitomes are simply defined as the arithmetic averages of the members in respective groups. Then, the evolution can be started up by using either the learning actions or the exploration actions and the member replacement rules, it is similar to the team progress algorithm (TPA) [1].

In the evolution process, a new individual of the group member is generated by randomly inheriting the properties of members in the stochastically selected group. The new individual must experience one of the learning and exploration actions to become a member candidate. The learning means that the new individual generated in the plain group moves towards the elite epitome and the one born in the elite group moves away from the plain epitome. In this paper, based on the analysis of the distribution function of the random number, the random number for learning is changed into Beta distribution, and that for exploration follows a Gaussian distribution. By means of the new distributions, the optimization performance of this improved evolutionary algorithm is obviously increased.

The improved TPA is tested using some well-known benchmark functions for a given accuracy. It can be found from the results that the average function evaluations of the improved TPA are greatly decreased by the new probability distributions, while the success rate of global searches are almost the same as the original TPA.

Then, the improved TPA is employed to synthesis of a wide sector pattern of an equidistant linear array with a sinusoidal element pattern and a uniform amplitude excitation, which is more difficult than arrays with complex or tapered amplitude excitations. A satisfactory result for a 26-element linear array with the spacing of a half wavelength is given. The ripple within the sector and the maximal side-lobe are less than 2 dB and -10 dB, respectively. The tolerance for the excitation is also verified for the application in a system.

It can be concluded that the improved TPA is more efficient for multimodal optimizations and has successfully been used for wide sector pattern synthesis of antenna arrays.

REFERENCES

1. Bo, Y. M., and B. Liu, "An epitome-based evolutionary algorithm with behavior division for multimodal optimizations," *Proceedings of IEEE Int. Conf. on Neural Networks & Signal Processing*, 406–411, Zhenjiang, China, June 8–10, 2008.

Design and Simulation of Planar Archimedean Spiral Antenna

Changjie Sun, **Guobin Wan**, **Zhang Hu**, **and Xin Ma**
School of Electronic and Information, Northwestern Polytechnical University, Xi'an 710129, China

Abstract— Planar Archimedean spiral antenna is widely used with its low profile, light weight, high efficiency, circular polarization and broad bandwidth. In this paper, the effects on the elctromagnetic characteristics of the planar Archimedean spiral antenna, which are owing to the changes of the diameter and the heights of the transmutative cavity and the width of the spiral, are investigated respectively. Results show that the changes of the diameter and the heights of the transmutative cavity have much influence on the input impedance and the gain of the Archimedean spiral antenna, while the changes of the width of the spiral have much influence on the input impedance of the Archimedean spiral antenna.

Dual-frequency Dual-polarization V-Band Reconfigurable Antenna

Xiaoyan Yuan, **Yasin Damgaci**, **and Bedri A. Cetiner**
Department of Electrical and Computer Engineering, Utah State University, USA

Abstract— The Wireless Personal Area Network (WPAN) system, IEEE 802.15.3c [1], provide short-range, very high speed multi-media data services to computer terminals and consumer applications located in rooms, office space and kiosks. IEEE 802.15.3c standard relates to broadband antennas of compact size which are capable of receiving or transmitting multi-polarized electromagnetic radiation. However, traditional antennas were often required to receive and transmit electromagnetic radiation over wide band while maintaining uniform radiation pattern and impedance characteristics within the operating band. Now, the problem of responding to transmitted signals over a broad band for multi sense of polarizations could be solved by multi-functional reconfigurable antennas (MRAs).

In this paper, we present the modeling, design and nanofabrication of a NEMS integrated dual-frequency dual-polarization patch antenna for IEEE 802.15.3c WPAN applications. This MRA is designed on benzocyclobutene (BCB) polymer with a relative permittivity of 2.6 and the thickness of 0.1 mm. BCB is chosen due to its high performance RF characteristics and compatibility with micro fabrication processes. The square patch is fed by a coaxial probe and consists of four inserted slits and a pair of truncated corners shown as below. This MRA is capable of providing dual frequency (57 GHz and 64 GHz) and dual polarization operation (linear and circular polarizations) with such a simple structure, which is achieved through nano-electromechanical systems (NEMS) switches strategically located in each slit gap [2]. The radiation characteristics (gain, shape of the pattern) remain the same for these four modes of operation. The main building blocks of the MRA are the new type of DC-contact double cantilever type NEMS switches. The design, nanofabrication and measured RF performance of these switches will be presented.

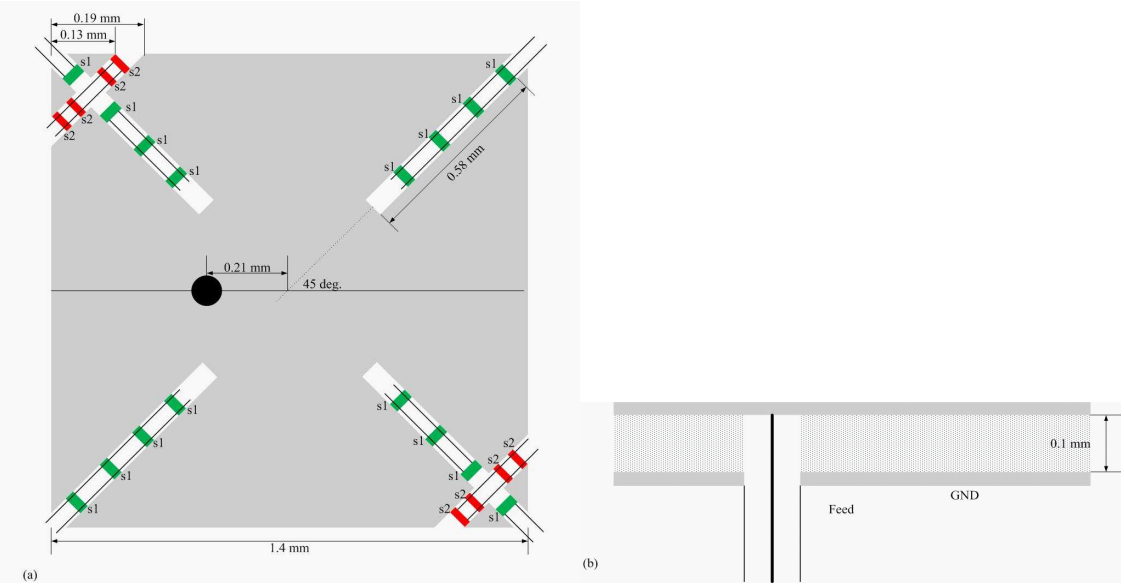

REFERENCES

1. Fisher, R., "60 GHz WPAN standardization with IEEE 802.15.3c," *Signals, Systems and Electronics International Symposium*, 103–105, Aug. 2007.
2. Biyikli, N., Y. Damgaci, and B. A. Cetiner, "A low-voltage small-size double-arm MEMS actuator," *IEEE Electronics Letters*, Vol. 45, No. 7, 149–152, 2009.

Capacitively Fed Wide-band PIFA with Modified Ground Plane

Hema Swaroop Mopidevi, **Ali Khoshniat**, **and Bedri A. Cetiner**
Department of Electrical and Computer Engineering, Utah State University, USA

Abstract— In the ever competitive world of mobile communications, miniaturization is a challenge faced by next generation antenna engineers. To overcome this, the size of the antenna must also be small without much degradation in the performance characteristics. PIFA serves this purpose well as it already reduces the size of microstrip patch by half. Our goal is to overcome the inherent disadvantage of narrow bandwidth in PIFA by combining three well known techniques — tapered type PIFA, T-shaped ground PIFA and capacitive feeding. This PIFA suits the public safety (PS) personnel communication needs by operating on a wide band, 700 MHz to 900 MHz which also helps in interoperable communication between the PS bands in times of emergency.

The legacy PIFA [1] in this band provides just 6% bandwidth. Individually, tapered patch provides 9% and T-shaped ground results in 19%. Using T-shaped ground [2] technique requires increasing the size of the ground plane, however helps in improving gain. PIFA with capacitive feeding alone results in a bandwidth of 8%. This feeding can compensate the inductance effect of probe in addition to simplifying fabrication process without the need to connect directly to the patch. The combination of all three techniques provides a bandwidth of around 30%. In addition to this, the gain is also improved from < 2 dB in simple PIFA to > 4 dB in final combination due mainly to the modifications in the ground plane. The antenna is fabricated and tested. The experimental results for both radiation patterns and impedance agree well with the simulations in HFSS, providing a strong foundation to the design concept presented herein.

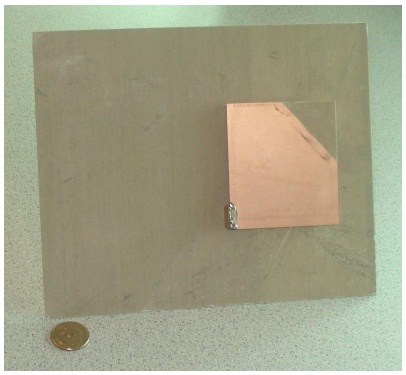

Figure 1: Top view.

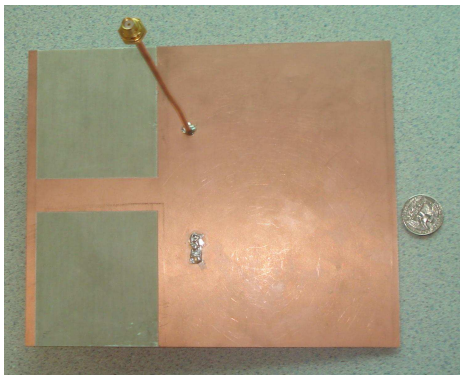

Figure 2: Bottom view.

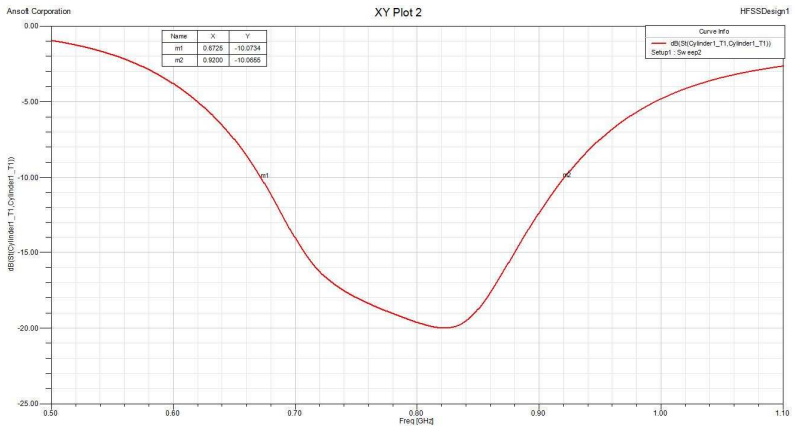

Figure 3: HFSS result.

Figure 4: Measured result.

REFERENCES

1. Hirasawa, K. and M. Haneishi, *Analysis, Design, and Measurement of Small Low Profile Antennas*, Artech House, Norwood, MA, 1992.
2. Wang, F., Z. Du, Q. Wang, and K. Gong, "Enhanced-bandwidth PIFA with T-shaped ground plane," *Electronics Letters*, Vol. 40, No. 23, 1504–1505, 2004.

Study on Optimize Efficiency of Particle Swarm Optimization for the Synthesis of Subarrayed Arrays

Ning Ren, **Guobin Wan**, **and Xin Ma**
School of Electronic and Information, Northwestern Polytechnical University, Xi'an 710129, China

Abstract— Antenna arrays have received significant attention of the researchers, since they find a wide-range of application in microwave technology such as communication and radar. In the past years, there has been a great interest in the design of antenna arrays using optimization algorithms, particularly derivative-free, evolutionary algorithms such as ant colony algorithm, particle swarm optimization (PSO), and genetic algorithms. However, the optimization efficiency of large antenna arrays and two-dimension antenna arrays is low. In this paper, subarrayed array antennas with the definition of the elements clustering into spatially contiguous subarrays and the corresponding weights to obtain the same sidelobe level pattern with the unsubarrayed antenna array are optimized via the modern heuristic particle swarm optimization technique. The problem is discussed through comparing the efficiency of PSO in the subarrayed array antennas with that in unsubarrayed antenna array. A set of representative results concerned with difference subarray element numbers and amplitude distributions are shown to compare the performance of PSO. Also, the PSO method for subarrayed array can be extended to two-dimension antenna arrays.

Directive Surface Wave Excitation Using Yagi-Uda Slots

Jinsheng Dong, **Liping Yan**, **and Kama Huang**
School of Electronics and Information Engineering, Sichuan University, Chengdu 610064, China

Abstract— The surface-wave is usually suppressed in microstrip antenna arrays. However, it needs to be excited properly for specific applications in recent years, such as quasi-optical slab beam power combiners and some other uses. The excitation of the dominant mode should be maximized and directed in those applications. Consequently, the slot antennas are the favorite candidates for TM_0 mode excitation. The CPW-fed three-slot Yagi-Uda launcher has been investigated for directive surface wave excitation. In this paper we proposed a five-slot Yagi-Uda launcher operating at 20 GHz to enhance the directivity. The launcher, which is composed of a driven slot, a reflector slot and three director slots instead of one, fed by a spoon shaped microstrip line, and manufactured on a 0.6 mm thick substrate with $\varepsilon_r = 2.65$, is used to excite surface wave in a grounded teflon slab, whose thickness is optimized as 5 mm for maximum surface-wave power excitation. The Numerical results show that the relative bandwidth in terms of −10 dB return loss is increased from 11.4% to 13.8%, when compared to those of a three-slot launcher with only one director. The forward/backward directivity ratio (FBR) is also obtained by calculating the amount of power propagating in the forward direction compared to that in the backward direction. This can be implemented by putting one receiving antenna in the front of the proposed launcher, and another same antenna at the back of it. Results show that the Maximum FBR is increased to 24.7 dB, while that of the three-slot launcher is only 16.7 dB for the same application.

Wideband Slot Antenna by Controlling Resonances

Hyengcheul Choi, **Sinhyung Jeon**, **Oul Cho**, **Seungwoo Kim**, **and Hyeongdong Kim**
Department of Electrical and Computer Engineering, Hanyang University
Haengdang-dong, Seongdong-gu, Seoul, Korea

Abstract— A wideband antenna is needed to use various wireless communication services with one mobile handset. Because antenna bandwidth is limited for one resonance by its size, small antenna for a portable devices has to excite multi-resonance to widen bandwidth. A branch-structural antenna can easily excite multi-resonance, but this structure increases the volume of an antenna and each resonance is affected by each other. The proposed slot antenna shown in Fig. 1 has wide bandwidth that is a result by controlling higher resonance modes of the slot antenna. The rectangular metal loop and dielectric material ($\varepsilon_r = 30$) is used for decreasing the third and fourth resonances of the slot antenna. The proposed antenna has 900 MHz (1750–2650 MHz) bandwidth under VSWR = 3 : 1 as shown in Fig. 2 and it is suitable for DCS/PCS/WDCMA/Bluetooth band.

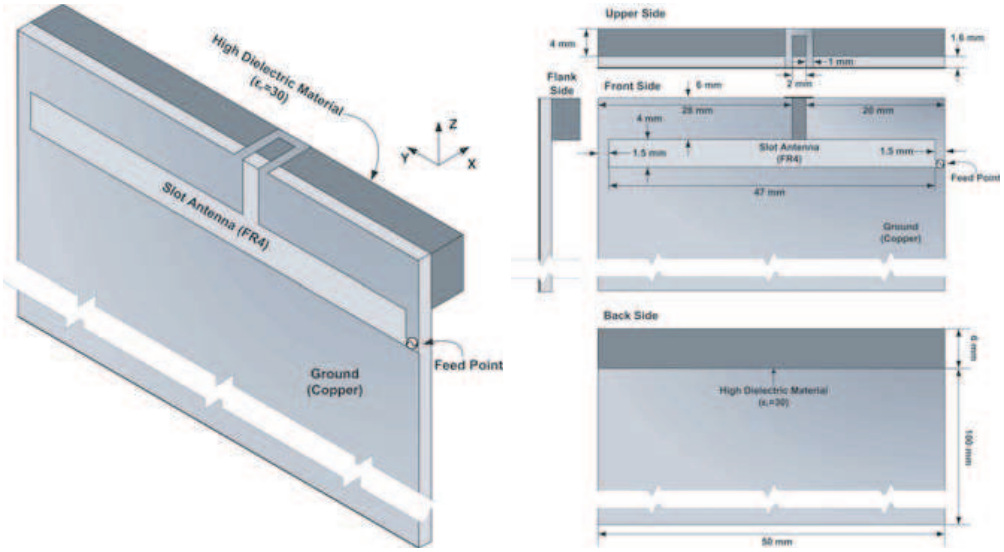

Figure 1: Geometry of the proposed antenna.

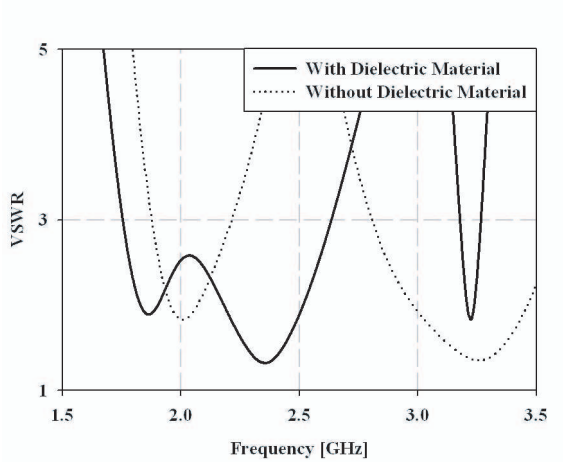

Figure 2: VSWR of slot antenna without/with dielectric material.

Design of a Gaussian Backscatter Antenna with Ring Focus Feed

W. Thaiwirot[1, 2], **R. Wongsan**[1, 2], **and M. Krairiksh**[3]

[1]School of Telecommunication Engineering, Institute of Engineering, Thailand
[2]Suranaree University of Technology, Nakhon Ratchasima, Thailand
[3]Faculty of Engineering, King Mongkut's Institute of Technology Ladkrabang, Bangkok, Thailand

Abstract— Low Earth Orbit Satellite (LEO Satellite) communication systems are one of the new and exciting developments in providing global communication services. The satellites contain sophisticated equipment for processing, transmitting through antennas that communicate from and to hand-held user terminals on the ground. Since satellites in low earth orbit change their positions relative to the ground positions quickly, therefore, time required for ground station-satellite communications is limited. Hence, wide beam antennas are needed. It was found that the axially displaced ellipse (ADE antenna) provides an excellent choice for compact high-gain spacecraft antenna applications. As a result, this paper presents the axially displaced ellipse antenna. The proposed antenna is a centrally fed displaced axis gaussian backscatter antenna with a ring focus feed as shown in Fig. 1. The antenna has axial symmetry. The curvature of main reflector is gaussian, and the subreflector is a portion of an ellipse. A backscattering technique is used with the main reflector to achieve wide beamwidth. A simple procedure for the design of gaussian backscatter antenna with a ring focus feed is given. Using five geometric input parameters, a set of equations is derived to find the remaining geometric parameters, fully defining the systems. Physical theory of diffraction (PTD) is utilized for analysis and design. The proposed antenna can produces high gain (maximum gain = 11.8 dB), wide beamwidth (coverage angle $\theta = \pm 65^{\circ}$) and small diffraction effects. We can conclude that gaussian reflector antenna with ring focus feed produces higher gain and smaller diffraction effects than a single gaussian reflector antenna. The propose antenna can be used for realizing earth coverage beam in LEO satellite or indoor wireless LAN applications.

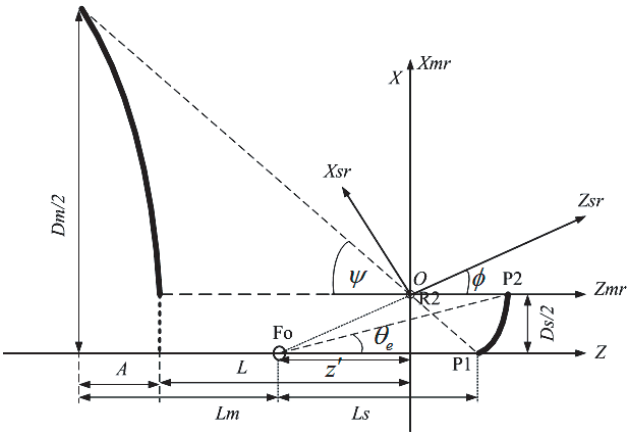

Figure 1: Cross-sectional view of the axially displaced ellipse antenna system.

High Directive Gain Antenna Using Shorted-end Curved Strip Dipole on Electromagnetic Band Gap

N. Fhafhiem, **P. Krachodnok**, **and R. Wongsan**
School of Telecommunication Engineering, Institute of Engineering
Suranaree University of Technology, Nakhon Ratchasima, Thailand

Abstract— A curved strip dipole is constructed of a metallic sheet that it is bended to a half annular. Because a simple dipole antenna's shape could be change easy, structure variety, and inexpensive, it is suitable to apply for wireless local area network (WLAN) system at 2.45 GHz. The concept of a simple dipole is omnidirectional beam, it's has low gain and the half power beamwidth (HPBW) on the E-plane is about 78 degree. This antenna will be usually placed at the wall of room or building. However, most kinds of this antenna has omnidirectional pattern, therefore, they are not suitable for field radiating in the large room because of power loss in unnecessary directions such as outside of service room. Also, this study is interested that qualification. This argues, if we can design an antenna to illuminate a predefined wide coverage area, it will have more efficiency for field radiating. We are bended a strip dipole to curved which length is πr for wider HPBW than a simple dipole and it is mounted over a dielectric for a durable of the antenna. However, the curved strip dipole antenna is not has sufficient gain therefore, the both end are shorted on EBG ground plane and feed point is located at center of curved strip dipole. The EBG surface is capable of providing a constructive image current within a certain frequency band, resulting in good radiation efficiency. For this reason, this antenna has achieved the maximum gain more than a simple dipole, in the same time, it could be cover bandwidth of IEEE standard (802.11 b/g).

The numerical results are given by CST Microwave Studio. Numerical results of this antenna, the frequency response of input impedance can be investigate, which is very useful to find the optimum matching condition by simply adjusting the length of curve strip dipole and structure of EBG. The results are gain about 8.2 dB which it is higher than a half-wave straight dipole. In addition, the antenna has wide beamwidth.

A Microstrip-fed Super-wideband Printed Elliptical Patch Antenna

Jianjun Liu[1, 2], **Karu Esselle**[1], **and Shunshi Zhong**[2]

[1]Centre for Microwave and Wireless Applications, Electronic Engineering
Macquarie University, NSW 2019, Australia
[2]School of Communication and Information Engineering, Shanghai University
Shanghai 200072, China

Abstract— With the development of high-speed integrated circuits and the requirement for miniaturization, the importance of the antenna, as a key component of communication system, has been growing rapidly. Due to the advantages of low profile and ease of fabrication and integration with circuits, printed antennas are considered as most promising antenna candidates for communication systems. However, standard printed antennas suffer from narrow impedance bandwidth. As a result, many techniques to expand the impedance bandwidth of printed antennas have been extensively studied, with great success. For example, in [1], a microstrip-fed printed triangular-ring antenna with a ratio bandwidth of 2 : 1 is presented. A printed circular disc monopole antenna, proposed in [2] for ultra-wideband (UWB) systems, is fed by a microstrip line and has a ratio bandwidth of about 3.5 : 1. A circular monopole antenna with trapezoid ground plane, presented in [3], has a 2 : 1 VSWR bandwidth of more than 10 : 1.

In this paper, a printed elliptical monopole antenna with a modified tapered microstrip-fed line is presented. It provides a theoretical impedance bandwidth from 0.8 GHz–25 GHz with a compact size. The optimized elliptical patch is used as the main radiating element. The ground plane is a part of impedance matching network, which can contribute to radiation as well.

Radiation characteristics of the proposed printed antenna were also analyzed and displayed. The antenna has almost omni-directional radiation at lower frequencies. The pattern is not omni-directional in the higher frequencies due to the presence of higher order modes. The gain, obtained from simulation, displays some fluctuation in the whole operating band and is about 5dB across the impedance-matched band.

ACKNOWLEDGMENT

This work has been supported by the Australian Research Council, Shanghai Leading Academic Discipline Project under Grant No. T0102, Macquarie University Research Excellence Scholarship (MQRES) scheme and the China Scholarship Council (CSC).

REFERENCES

1. Dissanayake, T., K. Esselle, and Y. Ge, "A printed triangular-ring antenna with a 2 : 1 bandwidth," *Microwave Opt. Tech. Lett.*, Vol. 44, No. 1, 51–53, 2005.
2. Liang, J., C. C. Chian, X. Chen, and C. G. Parini, "Study of a printed circular disc monopole antenna for UWB systems," *IEEE Trans. Antennas Propag.*, Vol. 53, No. 11, 3500–3504, 2005.
3. Liang, X.-L., S.-S. Zhong, and W. Wang, "Tapered CPW-fed printed monopole antenna," *Microw. Opt. Tech. Lett.*, Vol. 48, No. 7, 1242–1244, 2006.

Printed Temperature Sensors for Passive RFID Tags

Jinlan Gao[1], **Johan Sidén**[1, 2], **and Hans-Erik Nilsson**[1, 2]

[1]Mid Sweden University, Sweden
[2]Sensible Solutions AB, Sweden

Abstract— A concept is presented where a temperature sensitive printed nano structure is integrated into a UHF RFID tag antenna. The printed structure acts as a WORM memory (Write Once Read Many) allowing telling whether a tag has been exposed to excessive temperature since the last read. The 1-bit WORM used in experiments is defined through its resistance where a logical zero equals a high resistance over 2 kΩ and a logical one equals a lower resistance, typically less than 50 Ω. Setting the bit can be achieved through sintering, which is a process to enhance junctions among nano-particle silver and reduce resistivity by heating. The WORM is designed to modulate the impedance of a passive RFID tag antenna, aiming to change the tag from readable to unreadable or the other way around. The simplest way of modulation is to set the WORM to be parallel with the silicon chip. The tag then works well with the high WORM resistance apparent before sintering and poorly or preferably not working at all after sintered because the chip is short-circuited by the low WORM resistance. A variant of the half wavelength dipole has been used to demonstrate this concept and it should also work with other antenna patterns. Both the WORM memory and the tag antenna are printed on photo paper by an Inkjet printer and the silicon chip is connected to the antenna using the electrically conductive ink.

Compared to the sensor solutions that integrate the normal battery supported sensors into silicon chips with the aid of A/D converters, the sensor tag presented in this paper is much simpler and allowing easy fabrication. It has long lifetime, a smaller size as well as a lower cost. Since the WORM memory by definition stores the state and can be read out long time after it's been programmed this tag can tell about past events. Potential use include all applications where one wants to detect if a high temperature has occurred since the last time of read and where normal sensors either have too short lifetime or are too expensive.

Session 3AP
Poster Session 2

MIMO Channel Evaluation in Terms of Correlation and Capacity for LTE in Indoor Environment

Jinyoung Lee, **Jung-Hwan Choi**, **and Seong-Ook Park**
Korea Advanced Institute of Science and Technology, Daejeon, Korea

Abstract— It is well known that MIMO system performance heavily depends on the nature of multipath in the wireless communication channel. In our measurement campaign, we considered both the Line-of-sight (LOS) and non-line-of-sight (NLOS) scenarios. In the LOS case, RX and TX antennas were placed in a line without any obstruction in the propagation path. Distance between the TX and RX antennas was x m. Channel matrix, **H**, was measured for various distances between the TX and RX arrays.

Several dipole antennas were used as TX and RX antenna arrays, well matched at 750 MHz over bandwidth of 100 MHz. Transmission coefficient, S_{21}, was measured over the bandwidth at 101 frequency points. The transmitter was a virtual linear array with a separation of 0.5λ and 1.0λ. But two receiver antennas were connected to the network analyzer using RF switch changing the spacing between them in spatial steps of 0.1λ from 0 to 1λ.

Measured **H** matrix data was subsequently used to calculate the correlation and channel capacity. It has been observed that the channel capacity and correlation both are significantly affected by the antenna configurations and the propagation conditions. Through this analysis, we found out optimal configurations of the antenna arrays that offer good MIMO performances in the LTE frequency band.

Radiation Pattern Improvement of Wideband Bowtie Antenna Using High Impedance Surface

Xiankun Meng, **Chao Li**, **and Guangyou Fang**
Institute of Electronics, Chinese Academy of Sciences, Beijing, China

Abstract— Antennas with low profile and high gain features are required in many applications. In this paper, improvement of the radiation characteristics for Bowtie antennas with high impedance surface (HIS) was investigated. Bowtie antennas are broadband antennas which are widely used in the impulse ground penetrating radar (GPR), and usually play an important role in the performance of the radar system. The HIS is a type of Electromagnetic Bandgap (EBG) structure featured by frequency bandgaps and in-phase reflection.

In this paper, the electromagnetic characteristics of HIS were studied firstly. The Bloch analysis was applied to explain the mechanism of frequency bandgaps. The reflection phase of HIS was obtained by three-dimensional (3D) full wave simulations. Parametric study based on the unit cell analysis was carried out, providing reference for the optimization of HIS structure. With the properties of both frequency bandgap and in-phase reflection, HIS was adopted as a ground plane for a conventional bowtie antenna in order to improve its radiation characteristics. The HIS was designed to exhibit a large frequency bandgap to cover the relatively broad operational frequency bandwidth of the Bowtie antenna. As compared to the original antenna, the results suggest that a HIS can significantly improve the radiation pattern of the Bowtie antenna. The backside lobes are reduced, and the antenna gain is increased. Meanwhile, the profile of antenna was reduced due to the in-phase reflection of the HIS. It's also found that, the bandwidth narrowed due to the coupling between the Bowtie antenna and the HIS, can be effectively compensated by optimizing of the feeding networks of the antenna.

Outline of Noise Spectroscopy Potentialities

R. Kubásek[1], **P. Drexler**[1], **P. Fiala**[1], **and K. Bartušek**[2]

[1]Department of Theoretical and Experimental Electrical Engineering
Brno University of Technology, Kolejní 2906/4, Brno 612 00, Czech Republic
[2]Institute of Scientific Instruments, Academy of Sciences of the Czech Republic
Královopolská 147, Brno 612 64, Czech Republic

Abstract— In the complicated material structure for the micro-wave application (tensor and composite character) is its material properties study by classical single frequency methods connected with a difficulty [1]. In boundary changes with the size close to wave-length can occurs fake information about the examined objects [2]. One possible way to suppress the negative sources of signals is use of wide-band signals, as white noise, and study absorption in the examined material.

The article describe base study of wide-band noise signal use for material study [3]. The aim is find the metrology method for metamaterial study in the frequency range about 100 MHz to 10 GHz. That consist of antennas design, white noise generator and receiver assemble. Mathematical theory can be found in system identification theory and in general signal processing, nevertheless new approach should be done.

ACKNOWLEDGMENT

This work was supported within the project of the Grant Agency of the Czech Republic No. 102/09/0314.

REFERENCES

1. Maslovski, S., S. Tretyakov, and P. Alitalo, "Near-field enhancement and imaging in double planar polariton-resonant structures," *J. Appl. Phys.*, Vol. 96, 1293, 2004.
2. Freire, M. and R. Marques, "Near-field imaging in the megahertz range by strongly coupled magnetoinductive surfaces: Experiment and ab initio analysis," *J. Appl. Phys.*, Vol. 100, 063105, 2006.
3. Machac, J., P. Protiva, and J. Zehentner, "Isotropic epsilon-negative particles," *2007 IEEE MTT-S Int. Microwave Symp. Dig.*, Honolulu, USA TH4D-03, June 2007.

Analysis of the RCS and Radiation Pattern of a Planar Array Antenna Integrated with Dielectric and FSS

Wenming Tian and Xinyu Hou
State Key Laboratory of Electronic Thin Films and Integrated Devices
School of Microelectronics and Solid-State Electronics
University of Electronic Science and Technology of China, Chengdu, China

Abstract— This paper investigates the effect of a planar array antenna integrated with dielectric and FSS to it's backward RCS and radiation pattern. The results shows that dielectric layer can optimize radiation pattern of antenna when it is integrated on the surface of antenna, while it rarely influence radiation pattern when dielectric layer have some distance from antenna surface. And, dielectric layer influences the RCS of antenna very little. One-layer FSS makes radiation pattern of antenna significantly bad when it is integrated on the surface of antenna, while when it is put some distance above the surface of antenna, its influence to radiation pattern of antenna get very little. However one-layer FSS could dramatically optimize antenna's RCS at out of band.

Wide-Angle Transmision Wave Polarizers Using Dielectric Layers

Mohammad Khalaj-Amirhosseini
College of Electrical Engineering, Iran University of Science and Technology, Tehran, Iran

Abstract— Wave polarizers have found some applications in microwave and optical systems such as free-space optical switching networks, read-write magneto-optic data storage systems and polarization-based imaging systems [1–14]. In a wave polarizer only one of two possible modes (TE or TM) can be appeared in the transmission or reflection waves. One can classifies the into the following types [9, 14]: Dichroic polarizers, anisotropic crystal polarizers, Brewster angle polarizers, wire-grid polarizers and gyrotropic slab polarizers The most straightforward idea to design a wave polarizer is using the Brewster's angle to eliminate the TM mode in the reflection wave [8, 9]. The Brewster's polarizers firstly operate for the reflection wave and secondly work only at a narrow angle of incidence. In this manuscript, we use several dielectric layers as a wide-angle wave polarizer for the transmission waves to suppress the TE mode in the transmission wave. The introduced wave polarizer consists of several similar dielectric layers with high electric permittivity. Using a proposed method we analyze a polarizer for a wide range of parameters and then find out the optimum values of its parameters. The usefulness of the proposed structure is verified using a comprehensive example and the main principles for optimally design of polarizers is extracted.

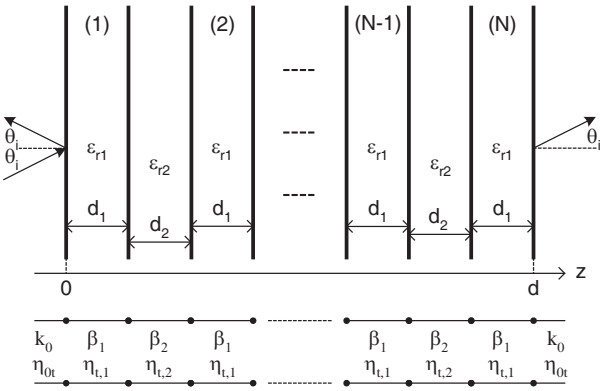

Figure 1: Several dielectric layers as a wave polarizer and its equivalent circuit.

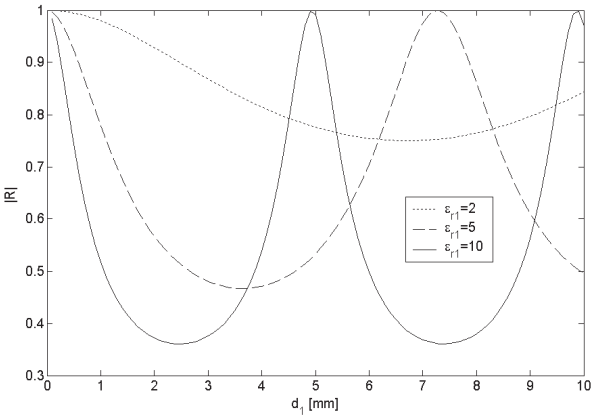

Figure 2: The absolute value of R for $N = 1$ dielectric layer.

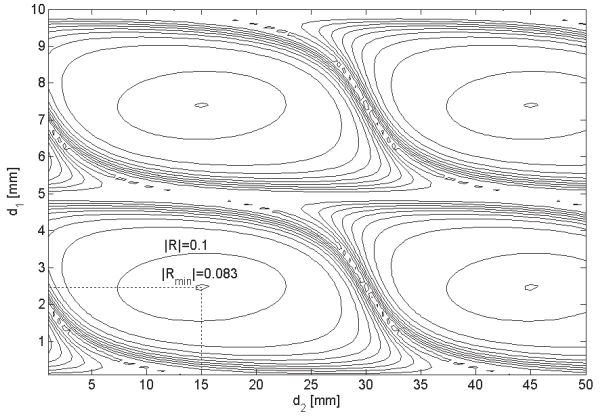

Figure 3: Contour of $|R|$ for $N = 2$ dielectric layers with $\varepsilon_{r1} = 10$ and $\varepsilon_{r2} = 1$.

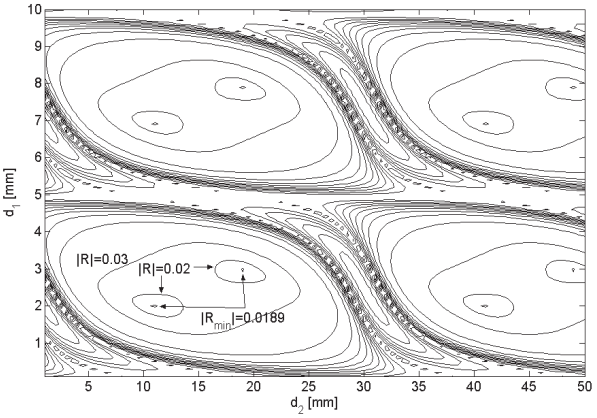

Figure 4: The contour of $|R|$ for $N = 3$ dielectric layers with $\varepsilon_{r1} = 10$ and $\varepsilon_{r2} = 1$.

Figure 1 shows the introduced wave polarizer consisting of N similar dielectric layers of thickness d_1 with electric permittivity ε_{r1}, while $N-1$ similar dielectric layers of thickness d_2 with electric permittivity ε_{r2} are being between them, alternately. The left and right mediums of the polarizer are assumed to be the free space. It is assumed that the incidence plane wave propagates obliquely towards positive x and z direction with an angle of incidence θ_i and electric filed strength E^i and with one of two possible polarizations TM or TE. We desire to design the introduced polarizer so that only TM mode is transmitted in the output medium, i.e., $z > d$, and TE mode can't be transmitted. To show the performance of a polarizer, we define the parameter R as the ratio of transmission coefficient of TE mode to that of TM mode, as $R = T_{\mathrm{TE}}/T_{\mathrm{TM}}$. It is evident that as R approaches to zero the performance of polarizer become better.

In this paper, we propose a general method to optimally design the introduced polarizer. In the proposed method, we analyze the polarizer and find the optimum values of its parameters. Without loss of generality, assume that we wish to design a polarizer at frequency $f = 10\,\mathrm{GHz}$ and at incidence angle $\theta_i = 60^\circ$. Figures 2–4 illustrate the absolute value of the ratio R versus d_1 and d_2 for $N = 1$, 2 and 3 dielectric layers, respectively. We see that R varies periodically with respect to d_1 and d_2 and has some minimums. According to the obtained results, one may conclude the following steps to optimally design the polarizer to work at frequency f and at incidence angle θ_i:

1. Select ε_{r1} as high as possible.
2. Select ε_{r2} as low as possible (the air).
3. Find $|R|$ versus d_1 and d_2 for some Ns to obtain minimum of $|R|$ for each N and then select N.
4. Select optimum values of d_1 and d_2 ($\lambda_1/4$ and $\lambda_2/4$ for $N = 1$ or 2).

Corrugated Tapered Slot Antenna Design and Measurement

Kekun Chang[1], **Guan-Yu Chen**[1], **Jwo-Shiun Sun**[1], **and Y. D. Chen**[2]

[1]Department of Electronic Engineering, National Taipei University of Technology, Taiwan
[2]Antenna and EMC Laboratory, HTC Corporation, Taiwan

Abstract— The Marchand balun for microwave band as a feeding network structure that effectively excited corrugated tapered slot antenna geometry is proposed (Fig. 1). The microstrip to slot line transition then to feed tapered slot antenna. The designed antenna has the merits such as wideband, simple feeding network, low profile compact size with fairly good antenna performances such as return loss, peak gain and radiation patterns. The radiation mechanism of a tapered slot antenna is based on traveling wave propagation along the tapered aperture slot, which results in an end-fire antenna. Tapered slot antenna exhibits some advantages such as wideband, wide scanning, high gain, low cross polarization and symmetrical E and H plane radiation patterns. In this paper, the Marchand balun with a balanced to unbalanced transition is shown good impedance matching and easy to integration and fabrication and the frame of the planar structure on corrugated tapered slot antenna was experimentally investigated. Measured results indicate that effects have significant impacts on the return loss, input impedance, radiation patterns and antenna gain of this antenna. The designed antenna fed by microstrip-slot transition is presented. It exhibits the merits of geometric simplicity, wide bandwidth, lightweight, low cross polarization, and high peak gain. This tapered slot antenna is suitable for UWB impulse radio operation and application.

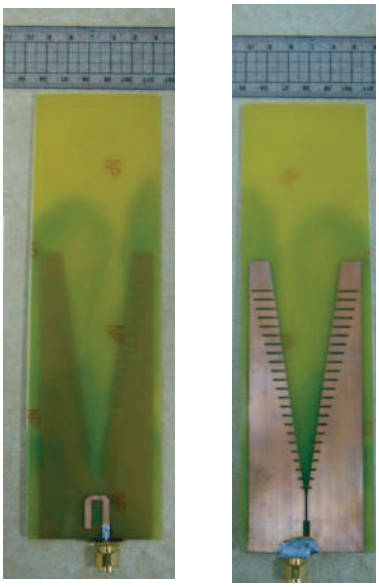

Figure 1: Corrugated tapered slot antenna.

Triple-band Antenna Design Using Enhanced Particle Swarm Optimization

W. T. Li, **C. L. Li**, **Z. Q. Lv**, **and X. W. Shi**
National Key Laboratory of Antenna and Microwave Technology, Xidian University
Xi'an 710071, China

Abstract— In this paper, a novel enhanced particle swarm optimization (EPSO) algorithm is proposed for triple-band antenna design. First, a new velocity updating process of PSO is defined with the purpose of improving the cooperation and competition ability of particles. Then, novel exceeding boundary control is adopted which can efficiently enhance the diversity of the particles. Furthermore, global best perturbation is introduced to intensify particles' speed in finding the optimum. Linked with the software HFSS, the antenna geometric parameters can be optimized by EPSO. A triple-band antenna is designed with three separate impedance bandwidths centered at 2.5, 3.5 and 5.6 GHz. Moreover, the proposed antenna is compact in size and shows insensitivity to size variations in its ground. The antenna is fabricated and measured. The measured results demonstrate that the proposed antenna is promising for WLAN/WiMAX uses. Good similar omnidirectional radiation patterns in the azimuth plane in the desired frequency bands can be obtained.

ACKNOWLEDGMENT

This work was supported by the National Science Foundation of China under Grant No. 60801039.

Design of a Highly-directive Patch Antenna with Honeycomb-like Metamaterial Cover

Hang Zhou[1], **Zhibin Pei**[1], **Shaobo Qu**[1], **Jieqiu Zhang**[1], **Chunhui Chen**[1], **Song Xia**[2], **and Zhuo Xu**[2]

[1]The College of Science, Air Force Engineering University, Xi'an, Shaanxi 710051, China
[2]Electronic Materials Research Laboratory, Key Laboratory of the Ministry of Education Xi'an Jiaotong University, Xi'an, Shaanxi 710049, China

Abstract— The design of a high-directivity patch antenna based on a honeycomb-like metamaterials is proposed. A comparison between conventional patch antennas and the new metamaterial patch antenna is given. Both the simulated and measured results show that the directivity of the metamaterial antenna is effectively enhanced compared with the conventional one.

Frequency Reconfigurable Top-loaded Monopole Based on Fractal Geometry

King Yin Cheung and Wing Shing Chan
Department of Electronic Engineering, City University of Hong Kong
Tat Chee Avenue, Kowloon, Hong Kong, China

Abstract— Nowadays, there are many wireless service in the market such as WiFi, WiMAX, GSM and WCDMA whose service needs to be available in a single wireless unit such as a hand set or a lap-top computer. All of these have different operating bands and follow different standards. Therefore, it is needed to develop a universal wireless receiver that can address both multi-band and multi-standard operation, commonly referred to as the Software Defined Radio. Frequency Reconfigurable antennas with excellent out-of-band rejection without the use of filters have found favor as a solution for the universal wireless receiver due the omission of the filter and superior antenna performance. This paper presents the design of a Top-loaded Monopole based on Hilbert geometry with electronic switching of the operating bands. By feeding the antenna at Different locations, the antenna can be excited via different resonant paths of the Hilbert Curve footprint.

Therefore, the Resonant Frequency of the antenna can be changed by switching the feed positions of the antenna. An antenna prototype with 2 operating states was fabricated. One of the states operates at 0.85 GHz while the other operates at 1.6 GHz. The footprint of the antenna was fabricated on a dielectric substrate with thickness of 1.57 mm and dielectric constant of 2.33. The size of the footprint is 30.4 mm by 30.4 mm, while the width of the metallic paths is 1.6 mm. Height of the footprint above the ground plane is 17.6 mm. The feed positions of the antenna are connected to a single pole double throw pin diode switch which is fabricated underneath the ground plane to realize the frequency reconfiguration. The Frequency Response and the radiation pattern for different states have been measured and shown below.

Design of Circularly Polarized Annular-ring Slot Antenna

Ching-Fang Tseng
Department of Electronic Engineering, National United University
No. 1, Lien Da, Kung-Ching Li, Miao-Li 36003, Taiwan

Abstract— A circularly polarized annular-ring slot antenna (ARSA) is developed and discussed. By introducing proper asymmetry in the annular ring slot structure, two pair of slits and feeding the ring slot using 50 Ω microstrip line, the bandwidth is increased and the circularly polarized is also formed for GPS application. An antenna prototype is fabricated to validate the design. It can be found that measured characteristics of the antenna are in good agreement with the simulated results. The measured results show that the return loss is lower than −10 dB from 1.36 to more than 2 GHz ($> 40\%$), the axial ratio is below 3 dB from 1.33 to more than 2 GHz and the radiation is right-hand circularly polarized.

Design of Slot Array Antenna at 24 GHz

Se-Hwan Choi, **Jin-Sup Kim**, **Kyu-Bok Lee**, **and Jae-Young Lee**
Korea Electronics Technology Institute, Republic of Korea

Abstract— Millimeter-wave antennas are important for the sensor system and low-cost communication. In recent years, Collision warning systems have been developing in the license-free 24 GHz industrial, scientific and medical (ISM) band. In this paper, we describe the 4 by 3 slot array antenna using an waveguide at 24 GHz. The antenna consists of a waveguide feed, waveguide power dividers and waveguide slots. There are two types of waveguide power dividers. One is π type that power is divided unequally and the other is T type that power is divided equally. The π type is used to reduce the sidelobe level. Feeding waveguide uses the WR-42 ($10.7 \times 4.3\,\mathrm{mm}^2$) standard waveguide. Waveguide slots are located by the offset from the center of waveguide. These offsets play a role of power divider and impedance matching.

The antenna is simulated by Ansoft HFSS V.11 and analyzed by a network analyzer HP8510c and a radiation pattern measurement system. This antenna has the gain of 18 dBi and the bandwidth of 0.55 MHz. The half power beamwidth and sidelobe level are 20 degree and 22 dB on the E-plane and 34 degree and -20 dB on the H-plane.

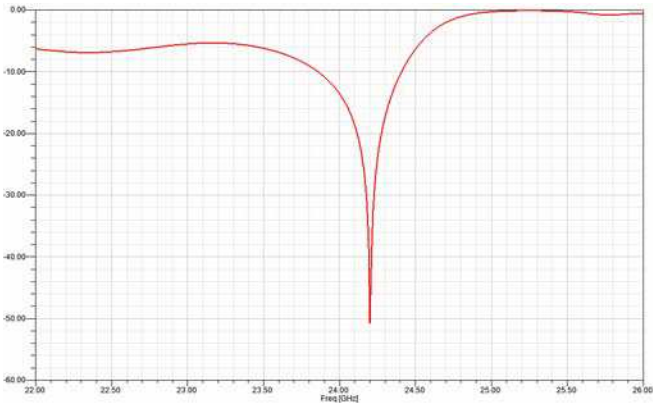

Figure 1: Return Loss.

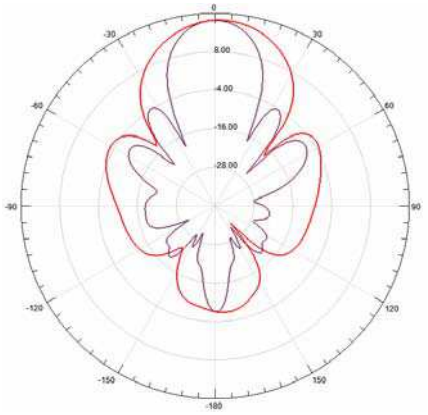

Figure 2: Radiation Patterns.

A Broadband Shorted-patch Antenna for DCS/PCS/UMTS Application

Dongya Shen[1, 2], **Jie Xu**[1], **Yanni Cui**[1], **Xiupu Zhang**[3], **and Ke Wu**[4]

[1]School of Information Science and Engineering, Yunnan University, Kunming, China
[2]State Key Lab of Millimeter Waves, Nanjing, China
[3]Department of Electrical Engineering, Concordia University, Canada
[4]Department of Electrical Engineering, Montreal University, Canada

Abstract— A broadband shorted-patch antenna suitable for DCS (1710–1880 MHz), PCS (1850–1990 MHz) and UMTS (1920–2170 MHz) application is presented. The antenna was fed by an aperture-coupled feed with an H-shaped coupling slot on the ground. The H-shaped aperture cut on the ground could result in a broader impedance bandwidth than aperture in other shapes. The substrate of the radiation patch is air and the height of the patch is 10 mm which is relatively thick. The radiation patch was shorted to the ground by a pair of shorting plates put at the two ends of the patch with proper width to achieve good impedance matching. The antenna has an impedance bandwidth (VSWR < 2) from 1700 MHz to 2200 MHz and the bandwidth is about 25.6% compared to the center frequency, which is greater than that of the microstrip line fed shorted-patch antenna. The width, length and height of the radiation patch is 40 mm, 23.5 mm and 10 mm respectively, and the volume is relatively small. Details of the antenna design are presented and the radiation patterns at 1800 MHz, 1900 MHz and 2050 MHz are given. Good broadside radiation characteristics of the proposed antenna at 1800 MHz, 1900 MHz and 2050 MHz have also been observed. The substrate of the microstrip feed line and the radiation patch are FR4 and air respectively, so the cost of the material is low. The impedance matching condition is greatly affected by the geometry of the antenna. The geometry of the antenna was optimized and the antenna could easily cover the DCS, PCS and UMTS frequency band.

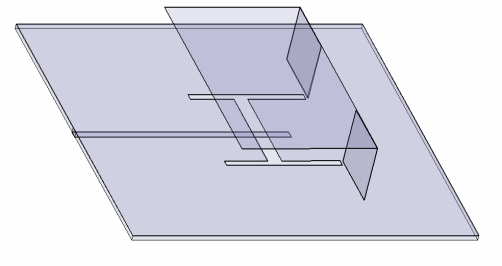

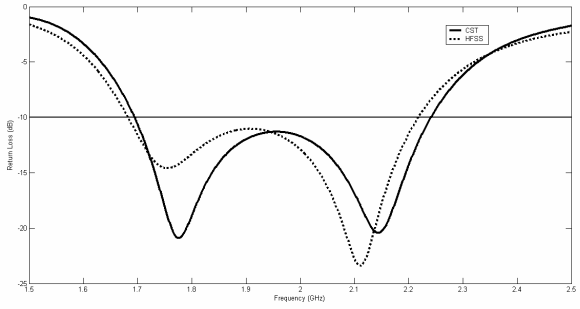

Design of Planar Monopole Antenna with Annulus Shape for Ultra-wideband Applications

Fangfang Yan and Jiadong Xu
School of Electronics and Information, Northwestern Polytechnical University
Xi'an 710129, China

Abstract— Since the allocation of 3.1–10.6 GHz frequency spectrum by the Federal Communications Commission (FCC) for the UWB radio applications, the UWB antennas have attracted a lot of interest in academic and industrial fields. Planar antennas are candidates due to their interesting properties such as small size, light weight and ease of fabrication.

A novel planar antenna with annulus shape for ultra-wideband (UWB) applications is presented in this paper. The element fed by microstrip line consists of an annulus patch and a truncated ground plane which is used to achieve good impedance match over a broad bandwidth. The performance of the antenna is analyzed and optimized to work at the band from 3.1 GHz to 10.6 GHz with the electromagnetic simulation software Ansoft HFSS. In the procedure, we have found that the distance between the center of inner circle and that of outer circle should be figured out carefully to reach good performance and positions of the two centers shouldn't be the same. The distance of the slot between the ground and the radiating element plays an important role in obtaining UWB behavior.

After the design procedure, the antenna has been fabricated by etching copper on the FR4 substrate whose dielectric constant is 4.4 and the measurement has been carried out by using E8363B Vector Network Analyzer of Agilent. The measurement has shown that the designed antenna covers the 3.1–10.6 GHz band allocated to UWB systems. It is found that the measured results agree very well with simulated results.

Wideband Reflectarray Using Sub-wavelength Ring Elements

Gang Zhao
National Key Laboratory of Antennas and Microwave Technology, Xidian University, Xi'an, China

Abstract— The conventional parabolic reflector antenna has been widely used in both terrestrial and satellite communication systems. This very efficient radiator is unwelcome in some applications due to its nonplanar reflector. Reflectarray antennas, combining some of the best features of microstrip arrays and conventional reflector antennas, have several advantages over conventional parabolic reflector antennas such as compactness, light weight, and low manufacturing cost. One of the primary disadvantages of microstrip reflectarrays is their relatively narrow bandwidth. In this paper, we present a wideband reflectarray antenna using sub-wavelength ring elements. The bandwidth of the conventional single-layer reflectarray antenna is inherently narrow, since the spacing of the phasing elements is about $\lambda/2$ and the reflection phase variation is highly nonlinear. In contrast, the approach described here employs a ring element with a reduced inter-element spacing to enhance the bandwidth of the reflectarray antenna. A sub-wavelength grid spacing ($\lambda/3$ at the center frequency) was selected, then the characteristics of the ring element were analyzed, and compared with ones of the conventional element with $\lambda/2$ grid spacing. The analysis was performed by full-wave simulations based on finite element method (Ansoft HFSS), and the infinite array approach was adopted to take into account the mutual coupling effects. According to the simulated results, a gentle slope of the phase variation is obtained by using the ring element with $\lambda/3$ grid spacing. Therefore, bandwidth improvements can be achieved. In order to examine the validation of the proposed phase elements, two prime-focus reflectarrays have been designed and simulated. One is designed with the $\lambda/2$ element spacing and the other one with $\lambda/3$ element spacing. The results demonstrate that the reflectarray antenna using the proposed elements achieves a larger gain bandwidth.

X-band Microstrip Antenna Array Using Stacked Structure and Aperture Coupling Feeding

Fan Zhang, **Fu-Shun Zhang**, **Gang Zhao**, **Chen Lin**, **and Yong-Chang Jiao**
National Key Laboratory of Antennas and Microwave Technology, Xidian University, Xi'an, China

Abstract— An X-band microstrip antenna array is proposed in this paper. For achieving broadband and high gain properties, the stacked microstrip antenna with aperture coupling feeding is employed as the radiators of the array. The utilized single antenna element is comprised by three dielectric layers with the same relative permittivity. The upper patch is fed through electromagnetically coupling by the lower driven patch etched on a lower substrate. Meanwhile, on the ground plane underneath the lower patch, a rectangular slot with triangle-shaped ends is etched and it is placed at the center of the lower patch. The patches are fed by aperture coupling method. By adjusting width of the rectangular slot, the flare angle of the triangular slot and the shape of the patches, a broad impedance bandwidth can be achieved. With optimized parameters, simulated results shows that the proposed antenna element exhibits a broad impedance bandwidth. Comprised by the proposed stacked antenna elements, a broad band 8×8 aperture coupled stacked microstrip antenna array is designed and simulated. For improving the efficiency of the antenna array, ingenious efforts have been made. For keeping the losses of the feeding network as low as possible a mirrored patch orientation has been accepted. This demands a slightly different feeding structure with a $\lambda_g/2$ offset between the original and mirrored element to provide the exact phase to the patches (180° phase shift), which reduces the number of transmission line discontinuities. Due to eliminated feed lines, an improved efficiency of the array is achieved. Measured results show the proposed antenna array exhibits a broad impedance bandwidth and remains a stable high gain performance across the frequency band.

Directive Circularly Polarized Antenna Using Low-profile Resonant Cavity Based on Metamaterial Superstrate

Gang Zhao, **Yong-Chang Jiao**, **and Fu-Shun Zhang**
National Key Laboratory of Antennas and Microwave Technology, Xidian University, Xi'an, China

Abstract— In the recent years, the science and engineering communities have witness an explosive growth of interest in metamaterials. Metamaterials, which exhibit unique properties not existing for natural materials, have found many applications in antennas and one such example is a metamaterial superstrate used as a cover of planar antennas for improving their directivity. The single-feed systems of these antennas allow the gain to be increased with low complexity, as compared to feeding networks used in conventional antenna arrays. In practice, however, if the operating frequency is low, this method significantly increases the height of the metamaterial superstrate. In this paper, we present a directive circularly polarized antenna with low-profile resonant cavity that utilizes a novel metamaterial surface as a superstrate. The primary radiation source is a dual-feed microstrip patch, which places underneath the superstrate and exhibits a circular polarization. Equal power with 90° phase difference to the feeds was obtained by using an external two-way Wilkinson power divider. By optimizing the dimensions of the metallic patterns on two surfaces of the metamaterial superstrate, proper reflection coefficient is obtained at the designed frequency. Due to the low reflection phase value of the metamaterial superstrate, the cavity height that is the distance between the superstrate and the ground plane, can be reduced to about $\lambda/8$. Several important parameters that characterize the metamaterial superstrate are investigated by considering suitable periodic boundary condition. Details of the antenna design are presented and the prototype is implemented and measured. The experimental results demonstrate that this low-profile resonant cavity antenna can provide high gain and good circular polarization performances at the operating frequency.

Universal UHF RFID Rose Reader Antenna

T. G. Abo-Elnaga[1], **E. A. F. Abdallah**[1], **and H. El-Hennawy**[2]

[1]Electronics Research Institute, Cairo, Egypt
[2]Faculty of Engineering, Ain Shams University, Cairo, Egypt

Abstract— RFID system has been developed for several years owing to its wide range of possible field applications. RFID system operating at UHF frequencies has received considerable interests for various commercial applications, such as supply chain management or inventory control. In this regard, a great demand of UHF RFID system is expected to replace the current position of barcode systems. Reader antenna is one of the important components in RFID systems, which is used to transmit or receive signal from a tag. Most RFID systems operate at ISM frequencies, such as 13.56 MHz, 2.45 GHz and 5.8 GHz, some work at UHF frequencies such as 840.5–844.5 and 920.5–924.5 MHz in China, 920–26 MHz in Australia, 866–869 and 920–925 MHz in Singapore, 952–955 MHz in Japan and 902–928 MHz in USA, Canada, Mexico, Puerto Rica, Costa Rica, Latin America, and so on. So, the UHF RFID frequency ranges from 840.5 to 955 MHz. Therefore, a universal reader antenna across the entire UHF RFID band with desired performance would be beneficial for RFID system implementation and configuration, as well as cost reduction. In order to communicate in the UHF frequency band the antenna size will be larger relative to the wavelength. In this paper, two meandered UHF RFID reader antennas are proposed in order to communicate with the tags working at UHF band where tag orientation is known and fixed and low power consumption is required in the reader system. Both antenna structures are composed of a single rose on the top of the substrate, which is meandered to obtain compact size, fed directly through microstrip line connecting the rose with the RF input, down the microstrip line and a finite ground line placed on the bottom of the substrate. The antenna input impedance can be controlled by adjusting the offset length of the ground line. Both antennas occupy areas of radius 25 mm and 21 mm, respectively compared to 72.5 mm for the conventional printed loop one. The measured bandwidths of the designed antennas cover the universal UHF frequency band, which agree well with the computed results. Other radiation properties are found to be acceptable for both proposed antennas.

Antenna Radome Using Split Ring Resonator

The-Nan Chang[1], **Jyun-Ming Lin**[1], **and Min-Chi Wu**[2]

[1]Tatung University, Taipei, Taiwan
[2]WHA YU Industrial Corporation, Hshin Chu, Taiwan

Abstract— In this paper, application of coupled square shaped split ring resonators (CSSSRR) is extended to enhance gain of a circularly polarized (CP) microstrip patch antenna. We etch coupled CSSSRR on both sides of a superstrate which is separated from the patch by an air layer. Open gaps of each CSSSRR on opposite side of the superstrate are orthogonally oriented to each other. This unique orientation allows the radome not only enhance gain but also maintain good CP performance for the patch antenna.

Design of the Novel Band Notched UWB Antenna with the Spiral Loop Resonators

Dang-Oh Kim, **Nam-I Jo**, **Dong-Muk Choi**, **and Che-Young Kim**
School of Electrical Engineering and Computer Science, Kyungpook National University
Sankyuk-dong, Puk-gu, Daegu 702-701, South Korea

Abstract— In this paper, a novel configuration of circular ultra-wideband (UWB) antenna with band rejection characteristic is presented. In order to obtain this characteristic, the spiral loop resonators resonating at the rejection frequency are located in both sides of the circular radiating patch. This novel structure provides the band-notched characteristic without the degradation of the UWB antenna performance itself. Furthermore, the notched band can be easily tuned by adjustment of resonator dimension because the size of the spiral loop resonators controls the corresponding resonance frequency. This prototype antenna has been fabricated on a substrate, Rogers 4003, with the thickness of 0.8 mm and relative permittivity of 3.55. The fabricated UWB antenna covers the frequency band from 3.1 to 11.23 GHz ($S_{11} \leq 10$ dB), and the band rejection characteristic appears near at 5.8 GHz band to which the wireless LAN service is assigned. And the far-field radiation patterns of the proposed antenna show omnidirectional and stable over the whole frequency band, which prospects the deployment in the UWB system. The measured results agree well with the simulation by the Microwave Studio of CST. This novel technique utilizing the spiral loop resonators might be useful to the planar antennas requiring the band rejection characteristics.

UWB Circular Polarization RFID Reader Antenna for 2.4 GHz Band

T. G. Abo-Elnaga[1], **E. A. F. Abdallah**[1], **and H. El-Hennawy**[2]

[1]Electronics Research Institute, Cairo, Egypt
[2]Faculty of Engineering, Ain Shams University, Cairo, Egypt

Abstract— Radio Frequency Identification (RFID), which was developed around World War II, is a technology that provides wireless identification and tracking capability. In recent years, RFID technology has been rapidly developed and applied to many service industries, distribution logistics, manufacturing companies, and goods flow systems. In RFID system, the role of antennas (for reader and tag) is very important. The reader antenna should have circular polarization (CP) characteristic since the tag antenna can be arbitrarily positioned on the target. When an RFID tag comprising an antenna and an application-specific integrated circuit (ASIC) is located in the reading zone of the reader antenna, the tag is activated and interrogated for its content information by the reader. Most RFID systems operate at ISM frequencies, such as 13.56 MHz, 2.45 GHz and 5.8 GHz, some work at UHF frequencies such as 840∼845 MHz, 920∼925 MHz (China), 952∼954 MHz (Japan), 868∼870 MHz (Europe) and 902∼928 MHz (USA), etc. In this paper an Ultra Wide Band (UWB) left hand, right hand circularly polarized antenna is proposed for the supper high frequency (SHF) 2.4∼2.483 GHz Radio Frequency Identification (RFID) applications. The antenna is composed of three layers, upper FR4 layer with four circular sector slots patch antenna on the top, middle foam layer, bottom FR4 layer with modified branch-line coupler on the top and ground plane on the bottom of this layer. The slotted circular patch is fed by two posts connecting the circular patch through the foam layer with the branch line coupler. By optimal design of both circular T-slotted patch antenna and modified branch line coupler, the proposed antenna bandwidth and the 3 dB axial ratio enhanced. The proposed antenna achieves −10 dB measured impedance bandwidth of 1.66 GHz from 2.34–4 GHz for both left hand and right hand circular polarization operation which agree well with the computed results. The proposed antenna has 3 dB axial ratio bandwidth of 488 MHz for the left hand circular polarization covering the range of 2.37299–2.86174 GHz and 591 MHz for the right hand circular polarization covering the range of 2.32154–2.91318 GHz. The proposed antenna offers an acceptable gain and other antenna parameters on its bandwidth.

A Compact UWB Antenna Design for Breast Cancer Detection

S. Adnan, **R. A. Abd-Alhameed**, **C. H. See**, **H. I. Hraga**, **I. T. E. Elfergani**, **and D. Zhou**
Mobile and Satellite Communications Research Centre, University of Bradford
Bradford, West Yorkshire, BD7 1DP, UK

Abstract— Breast cancer is the most common non-skin related malignancy and the second leading cause of cancer death among women in the world [1]. Every year thousand of women die from this disease. Early detection will be look upon as the best hope for reducing the serious toll of this disease until research uncovers a way to prevent breast cancer or to cure all women. The early detection of cancer by screening reduces mortality from cancer.

Fifty years ago there was not established method used for detection the breast cancer at its early stages, however, the new generation of the advanced technology and legal mandates have thoroughly changed the situation. The use of X-ray imaging for detection of breast was first suggested. Mammography was not an acceptable technology until the 1960s. Over the past decade the investment in breast cancer research including early detection has increased significantly. New or improved technologies are rapidly emerging and providing hope of early detection.

The X-ray mammography is proved to be the most effective tool and play an important role in the early breast cancer detection. Despite showing high percentage of successful detection compare to other screening tools, X-ray mammography also has its limitations. Both false positive and negative rate have been reported which subsequently introduce to alternative screening. Another issue that rises the concern by using X-ray mammography is the radiation level from ionizing X-ray.

All these imperfection factors have motivated and encouraged to search for the better solution. One of the alternative under investigation is microwave imaging which create the required quality images related to the electrical properties of the breast tissue [2].

This paper presents a compact UWB antenna for the tumor sensing. The application is similar to the GPR but operating at high frequency band. Figure 1 shows the geometry of the antenna. The antenna is placed on the ground plane of dimension $L = W = 40\,\text{mm}$ and thickness 0.5 mm. It fed by vertical plate of maximum height of 5.5 mm and width of 15 mm, in which it is connected to the feeding probe through a slot of 4 mm diameter in the ground plane. The antenna is modelled and optimised using high frequency structure simulator (HFSS) in which a parametric study is carried out. This study helps to optimise the antenna performance before the antenna is manufactured and tested experimentally. Different antenna parameters are considered for optimising the operated bandwidth subject to suitable radiated power gain values. To check the influence of these parameters on the impedance bandwidth one parameter is varied and the remaining parameters remain fixed. The antenna is also modelled using CST software package for comparison. Figure 2 shows the simulated return loss obtained from HFSS and CST softwares. The results present reasonable agreement and also encouraging for the practical implementation of this antenna as suitable candidate for the microwave imaging.

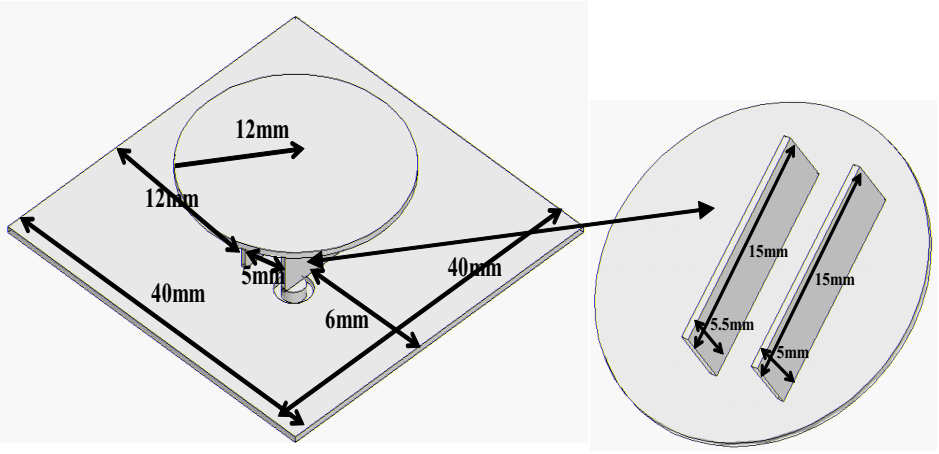

Figure 1: Geometry of the proposed antenna.

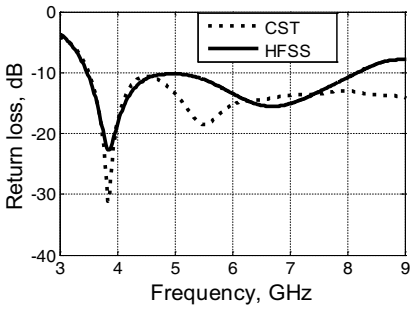

Figure 2: Simulated return losses.

REFERENCES

1. Blanks, R. G., S. M. Moss, C. E. McGahan, M. J. Quinn, and P. J. Babb, "Effect of NHS breast screening programme on mortality from breast cancer in England and Wales, 1990-8: comparison of observed with predicted mortality," 665–669, 2000.
2. Yun, X., E. C. Fear, and R. H. Johnston, "Compact antenna for radar-based breast cancer detection," *IEEE Trans. Antenna Propagat.*, Vol. 53, 2374–2380, Aug. 2005.

An 8-element Tapered Slot Antenna Array with a Bandwidth in Excess of 16.5:1

Yue Song, **Yong-Chang Jiao**, **Nai-Biao Wang**, **Tian-Ling Zhang**, **and Fu-Shun Zhang**
National Laboratory of Antennas and Microwave Technology, Xidian University
Xi'an, ShaanXi 710071, China

Abstract— A one-dimension single-polarized tapered slot antenna (TSA) array fed by microstrip line with a bandwidth in excess of 16.5:1 is built. The proposed TSA array, which contains 8 antenna elements connected each other fed by a modified microstrip-to-slotline Marchand transformer and a 8-way equal T-junction power divider with multiple section impedance transformers, is fabricated on a 0.6 mm thick substrate with the dielectric constant $\varepsilon_r = 2.65$.

An overall size of the prototype is $0.67\lambda_{\text{lower}} \times 0.61\lambda_{\text{lower}}$, where λ_{lower} is the wavelength of the lower frequency in the free space, corresponding to $250 \times 230 \times 0.6\,\text{mm}^3$. The element spacing is 20.2 mm, less than the wavelength of the highest operating frequency in the free space.

A broadband microstrip-to-slotline transformer, which obtains the impedance matching the operating band, is used to feed the proposed TSA array element. A modified microstrip stub contains a quarter of circle, a quarter of ellipse, and a polygon used to connect the stub to microstrip line. Simulated result of a pair of back-to-back Marchand baluns demonstrates a broadband characteristics (175% for VSWR < 2).

An 8-way wideband T-junction power divider is designed to feed this TSA array. This power divider contains 3 sections T-junction, which also include multiple-section quarter-wave transformers in order to satisfy the broadband operating requirement. The simulated result shows that the return loss of this power divider is lower than -13.7 dB from 1.0 to 12.8 GHz.

The proposed TSA array is also measured in a anechoic chamber. The measured results show that a VSWR ≤ 2 frequency range of the proposed wideband TSA is from 0.8 to 13.2 GHz, and good directive radiation patterns with the cross polarization in the operating band are both less than -17 dB.

New Antenna System Measurement Technology for GPS OTA Operation

Jui-Yi Yang[1], **Guan-Yu Chen**[2], **Yung-Sheng Chen**[1], **Jwo-Shiun Sun**[2], **and Y. D. Chen**[3]

[1]Department of Electrical Engineering, Yuan Ze University, Taiwan
[2]Department of Electronic Engineering, National Taipei University of Technology, Taiwan
[3]Antenna and EMC Laboratory, HTC Corporation, Taiwan

Abstract— In this study, new 3D antenna measurement system associated with GPS test systems, ensures 3D GPS antenna radiated pattern measurement, sensitivity measurement and GPS intermediate channel measurement. It will be fully compliant with the CTIA's test plan for mobile station over-the-air performance. In this paper, Bluetooth (BT) transmission (Fig. 1) to replace traditional USB data link by cable (Fig. 2) and reduce cable effect by 3D antenna OTA measurement. BT is an open wireless protocol for exchanging data over short distances from fixed and mobile devices, creating personal area networks originally conceived as a wireless alternative to RS232 data cables. It can connect PDA and Notebook (NB) devices, overcoming problems of synchronization. Based on this new measurement technology can improve GPS and A-GPS receiver sensitivity measurement by 3D antenna OTA system.

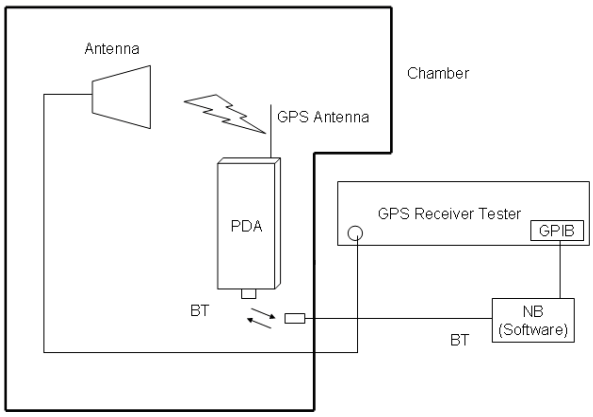

Figure 1: The proposed GPS OTA measurement.

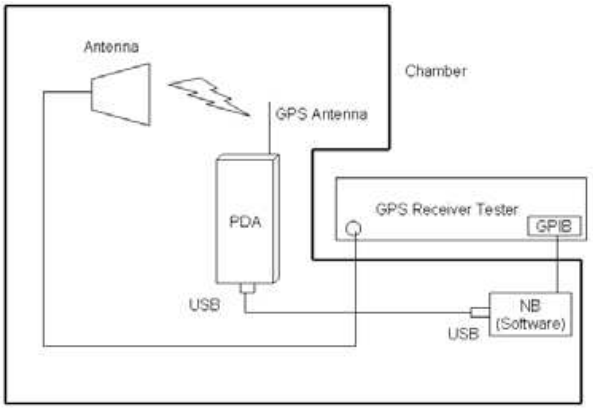

Figure 2: The traditional GPS OTA measurement.

Comparison between Empirical and Deterministic Models to Predict the Propagation Losses in Indoor Scenarios

Oscar Gutiérrez Blanco[1], **Antonio Juliá López-Barrantes**[2], **M. Francisco Sáez De Adana**[1], **and Rainer Kronberger**[3]

[1]Sciencie Computation Department, Alcalá University, Escuela Politécnica, Campus Universitario Alcalá de Henares 28871, España
[2]Communication Department, Universidad Politécnica de Valencia, Grao de Gandia 46730, España
[3]High Frequency Laboratorios, Cologne University of Applied Sciencies Betzdorfer Str. 2, Cologne D-50679, Alemania

Abstract— Nowadays the wireless communications is a broad field of research, mainly due to the increasing of the Wifi networks. The study of the propagation in indoor scenarios plays an important role in the design of these networks. For this reason it is important an accurate tool for propagation prediction.

The propagation prediction models can be classified in empirical and deterministic. The first ones are based on statistical analyses obtained from a great amount of measurements, and have close expressions. The deterministic models are applications of the electromagnetic techniques to a specific description of the model. The accuracy of the deterministic is greater than the deterministic, however deterministic are simpler and the computational cost is lower.

In this paper, two different models for indoor propagation prediction are compared. One empirical and another deterministic based on ray-tracing. The empirical model is based on the propagation losses in free space and incorporates the transmission losses due to the walls and floors [1]. The deterministic model is based on ray-tracing and on the Geometrical Theory of Diffraction [2]. This last has been widely validated with measurements proving its accuracy [3].

Results for two different scenarios have been obtained, one corridor and one office building. The results obtained with both methods are similar; the average difference is around 5 dB's in both cases, with an average deviation of 1.2 dB approximately. Given that the deterministic model has been validated, the results proof that the empirical model is valid to predict the propagation losses in indoors scenario, and it is a valid tool to design wireless networks; taking the advantage of simplicity of implementation and the low computational cost required. However in the case that high accuracy will be needed in a particular point, the empirical model is not valid. This is the case of the fingerprinting technique for mobile location, where the location is performed from the level power in a lot of points or fingers.

REFERENCES

1. Cheung, K.-W., H.-M. S. Jonathan, and R. D. Murch, "A new empirical model for indoor propagation prediction," *IEEE Trans. on Vehicular Technology*, Vol. 47, No. 3, 996–1001, Aug. 1998.
2. Saez De Adana, M. F., O. Gutierrez, I. Gonzalez, J. Perez, and M. F. Catedra, "Propagation model based on ray tracing for the design of personal communication systems in indoor environments," *IEEE Trans. on Vehicular Technology*, Vol. 40, No. 6, 2105–20112, Nov. 2000.
3. Pérez, J. and M. F. Cátedra, *Cell-planing Personal Communications*, Artech House, MA, 1999.

IMS-based Multimedia Applications with QoS Guarantee

Zhimin Feng and Yang Du
Department of Information Science and Electronics Engineering
Zhejiang University, Hangzhou 310027, China

Abstract— The IP Multimedia Subsystem (IMS) specified by the 3GPP is used to transmit multimedia over an IP based infrastructure. Multimedia applications, such as video conference, and IPTV, require an end-to-end QoS guarantee. In order to provide QoS guarantee for multimedia applications, an end-to-end QoS support should involve not only establishing a session, but also reacting to dynamical changes during sessions. This paper proposes an IMS-based QoS control model using service-based local policy for the support of multimedia application. The proposed model is access independent and service independent thanks to standard interfaces and standardized service capabilities of IMS. This model is validated using an IMS-based video conference over a WLAN, UMTS, and GPRS system.

A Novel Indoor UWB Antenna Array Design by PSO

Shu-Han Liao[1], **Min-Hui Ho**[1], **Chien-Ching Chiu**[1], **Chien-Hung Chen**[2], **and Chien-Hui Chung**[1]

[1]Department of Electrical Engineering, Tamkang University, Tamsui, Taipei, Taiwan, R.O.C.
[2]Department of Computer and Communication Engineering, Taipei College of Maritime Technology
Shilin, Taipei, Taiwan, R.O.C.

Abstract— In this paper, a new ultra wideband circular antenna array (UCAA) combining Particle Swarm Optimization to minimize the bit error rate (BER) is proposed. The ultra wideband (UWB) impulse responses of the indoor channel for any transmitter-receiver location are computed by SBR/Image techniques, inverse fast Fourier transform and Hermitian processing. By using the impulse response of multipath channel, the BER performance of the binary pulse amplitude modulation (B-PAM) impulse radio (IR) UWB system with circular antenna array can be calculated. Based on the topography of the antenna and the BER formula, the array pattern synthesis problem can be reformulated into an optimization problem and solved by the genetic algorithm. The novelties of our approach is not only choosing BER as the object function instead of sidelobe level of the antenna pattern, but also consider the antenna feed length effect of each array element. The strong point of the genetic algorithm is that it can find out the solution even if the performance index cannot be formulated by simple equations. Simulation results show that the synthesized antenna array pattern is effective to focus maximum gain to the user which scales as the number of array elements. In other words, the receiver can increase the received signal energy to noise ratio. The synthesized array pattern also can mitigate severe multipath fading in complex propagation environment. As a result, the BER can be reduced substantially in indoor UWB communication system.

Short Range Propagation Characteristics of UHF Frequency Band for Moving Vehicles RFID

Deock-Ho Ha[1] and Yeon-Wook Choe[2]

[1]Department of Telecommunication Engineering, Pukyong National University, Busan, Korea
[2]Department of Control and Measurement Engineering, Pukyong National University, Busan, Korea

Abstract— In this paper, we describe the short range propagation characteristic of UHF RFID frequency band used for moving vehicles. To analyze the propagation characteristic of UHF RFID radio signals, we transmitted 910 MHz and 2.45 GHz continuous wave carrier signals used several polarized antenna combinations. From the measurement analysis, it can be clearly seen that the UHF RFID signal can be encountered to multipath interference rays due to ground plane and the reader/antenna equipment booth. In addition, it was found that the multipath interference signals can be effectively removed by using a circularly polarized antenna. Especially, in case of NLOS environment, it was also found that circular polarization diversity method using the two branches of vertical and horizontal receiving antenna shows better fading reduction effect.

Introduction and Measurement Results: In this paper, we analyzed the propagation characteristic for the UHF RFID frequency band. With the aim of reducing the multipath fading in short range wireless environment, we proposed a multi-polarized antenna system. From the measured data analysis, it was found that the C-C (circular-circular antenna) combination shows better fading reduction result than the cases of V-V (vertical-vertical antenna) and H-H (horizontal-horizontal antenna) combination in LOS environment, respectively. On the other hand, in the case of NLOS environment, it was also found that the polarization diversity effect using the two branches of C-V (circular-vertical) and C-H (circular-horizontal) branches shows better fading reduction effect than the cases of C-C, C-X (right handed polarized circular-left handed polarized circular), V-V and H-H. Figures 1(a) and 1(b) shows the correlation diagram for the two diversity branches. From the correlation diagrams, it can be also seen that the circular polarization diversity scheme indicates more reverse correlation characteristic compared to the linear polarization diversity.

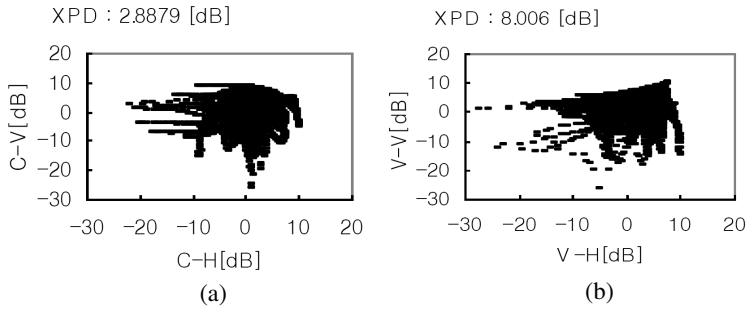

Figure 1: (a) C-VH diversity branches. (b) V-VH diversity branches.

A 1.2 V Low-power Receiver for Short Range Applications

Wei-Hsiang Hung, **Kuan-Ting Lin**, **and Shey-Shi Lu**
Graduate Institute of Electronics Engineering, National Taiwan University, Taiwan, R.O.C.

Abstract— Recently, the research of wireless sensor network for heart monitoring, biological detection or pollution sensing has gained a lot of attention. A wireless sensor node consists of many distributed system blocks that need to operate continuously over a long time with only a single battery. Therefore, the need of a highly integrated, low-cost and low-power single chip transceiver is indispensable. In this context, direct conversion transceiver architecture has the advantages of high level of integration with reasonable performance and low-cost. Nevertheless, design tradeoffs between power, dc offset, linearity and noise figure (NF) still need to be considered seriously.

In this paper, a 1.2-V 2.4 GHz low power receiver front-end system for short range communication is demonstrated. The system consists of a common source (CS) LNA, an active balun and a subharmonic passive mixer, leading to not only low power consumption but also solid performance. The CS LNA is chosen for achieving high gain and low noise performance simultaneously under properly designed. The following active balun not only provides a single-to-differential transformation but also keeps desired signals immune from noise. Moreover, subharmonic conversion is selected for two main considerations. First, it minimizes the effect of self-mixing dc-offset generated from the local oscillator. The LO signals fed-back to LNA will be amplified if they fall within the LNA passband. Consequently, a large dc offset is thus generated. Secondly, the LO buffers consume less power due to the fact that LO frequency is reduced to half of the targeted frequency. In other words, the receiver saves both dynamic and biasing power.

This receiver front-end operating at 2.4 GHz has been implemented in standard 0.18 μm CMOS technology. It draws 7.3 mA from a 1.2-V supply. The active area only occupies $0.71\,\mathrm{mm}^2 \times 0.37\,\mathrm{mm}^2$. This subharmonic RX also achieves 19 dB of conversion gain, 8-dB of noise figure and −15 dBm of IIP3. Measurement results indicate that this subharmonic receiver front-end is suitable for short range applications.

Design of a Novel Three-way Tri-band Power Divider

Xin Huai Wang, **Yan Fu Bai**, **Dong Zhou Chen**, **Xiao Wei Shi**, **and Xin Li**
National Key Laboratory of Science and Technology on Antennas and Microwaves
Xidian University, Xi'an 710071, China

Abstract— Power dividers are fundamental components of many RF and wireless communication circuits and subsystems. Conventional power dividers have been designed for two or even-number of outputs. However, when it comes to three or an odd-numbered output, 3-D resistors are required and are difficult to realize in a planar form in monolithic microwave integrated circuits (MMIC) or hybrid microwave integrated circuits (HMIC). Therefore, many new three-way power dividers have been proposed [1, 2]. These three-way power dividers operate only at one design frequency or dual-band frequencies. However, multi-standard operation of wireless transceivers is of increasing importance in practical applications and so components that work at three or more frequencies are of interest. Therefore, these are not suitable for some multi-band operations. In 2005, a three-section transmission-line transformer was introduced by M. Chongcheawchamnan [4], which can operate at any three arbitrary frequencies f_1, f_2, and f_3. A two-way tri-band Wilkinson power divider with this transformer section has been reported in [5].

This paper presents the technique to analyze and design a novel three-way tri-band power divider with 50 Ω impedance terminations based on a three-section transmission-line impedance transformer. The topology of the circuit is six sections of three transmission lines and planar isolation resistors, which provides high isolation and good amplitude balance simultaneously at three arbitrary frequencies of interest f_1, f_2, and f_3. The structure of the power divider and the formulas used to determine design parameters are presented. The technique is validated by experimental results on a 900/1800/2400 MHz power divider, which can be applied in the present global system for mobile communication (GSM), the personal communication system (PCS), and wireless local-area network (WLAN). Good performances of the proposed power divider at three frequencies are obtained.

REFERENCES

1. Nagai, N., E. Maekawa, and K. Ono, "New n-way hybrid power dividers," *IEEE Trans. Microw. Theory Tech.*, Vol. 25, 1008–1012, 1977.
2. Feng, C., "Planar three-way dual-frequency power divide," *Electron. Lett.*, Vol. 44, No. 2, 133–134, Jan. 2008.
3. Chongcheawchamnan, M. and S. Patisang, "Analysis and design of a three-section transmission-line transformer," *IEEE Trans. Microw. Theory Tech.*, Vol. 53, No. 7, 2458–2462, Jul. 2005.
4. Chongcheawchamnan, M. and S. Patisang, "Tri-band wilkinson power divider using a three-section transmission-line transformer," *IEEE Microw. Wirel. Compon. Lett.*, Vol. 16, No. 8, 452–454, Aug. 2006.

Bit Error Rate Reduction of Multi-user by UWB Antennas

Chien-Hung Chen[1], **Shu-Han Liao**[2], **Min-Hui Ho**[2], **and Chien-Ching Chiu**[2]

[1]Department of Computer and Communication Engineering, Taipei College of Maritime Technology
Shilin, Taipei, Taiwan, R.O.C.
[2]Department of Electrical Engineering, Tamkang University, Tamsui, Taipei, Taiwan, R.O.C.

Abstract— In this paper, a new ultra wideband circular antenna array (UCAA) combining genetic algorithm to minimize the bit error rate (BER) is proposed. Based on the topography of the antenna and the BER formula, the array pattern synthesis problem can be reformulated into an optimization problem and solved by the genetic algorithm. Simulation results show that the synthesized antenna array pattern is effective to focus maximum gain to the multi-user which scales as the number of array elements. In other words, the receiver can increase the received signal energy to noise ratio. The synthesized array pattern also can mitigate severe multipath fading in complex propagation environment. As a result, the BER can be reduced substantially in indoor UWB communication system.

UWB Communication Characteristics for Different Distribution of Pedestrian

Chien-Hung Chen[1], **Min-Hui Ho**[2], **Shu-Han Liao**[2], **and Chien-Ching Chiu**[2]

[1]Department of Computer and Communication Engineering, Taipei College of Maritime Technology Shilin, Taipei, Taiwan, R.O.C.

[2]Department of Electrical Engineering, Tamkang University, Tamsui, Taipei, Taiwan, R.O.C.

Abstract— A comparison of UWB communication characteristics for different distribution of pedestrian is investigated. The impulse responses of these cases are computed by applying shooting and bouncing ray/image (SBR/Image) techniques and inverse Fourier transform. The frequency dependence utilized in the structure on the indoor channel is accounted for in the channel calculation. The bit error rate (BER) performance for UWB indoor communication is calculated. The outage probability for binary antipodal-pulse amplitude modulation (B-PAM) system has been presented. Numerical results have shown that the multi-path effect by pedestrian is an important factor for BER performance. Finally, it is worth noting that in these cases the present work provides not only comparative information but also quantitative information on the performance reduction.

Ultra-wideband (UWB) Dipole Antenna Design and Measurement

Guan-Yu Chen[1], **Kekun Chang**[1], **Jwo-Shiun Sun**[1], **and Y. D. Chen**[2]

[1]Department of Electronic Engineering, National Taipei University of Technology, Taiwan
[2]Antenna and EMC Laboratory, HTC Corporation, Taiwan

Abstract— This paper proposes an omni-directional UWB dipole antenna (Fig. 1), low voltage standing wave ratio (VSWR), and easy to construct antenna for ultra wideband (UWB) systems. The designed antenna uses the balanced coaxial feed line to excite dipole antenna. The UWB dipole antenna suitable for IEEE 802.15.3a and IEEE 802.16 UWB communication applications at 3.1–10.6 GHz and 2–11 GHz bands is presented (Fig. 2). This paper discusses the phenomenon of dispersal in UWB antennas and presents a simple design to evaluate the radiated fields from antennas structures. Measured results exhibits extend return loss bandwidth and lower omni-directional pattern. The proposed UWB dipole antenna structure is capable of achieving broadband and omni-direction characteristics within 2–11 GHz for UWB wireless communication applications.

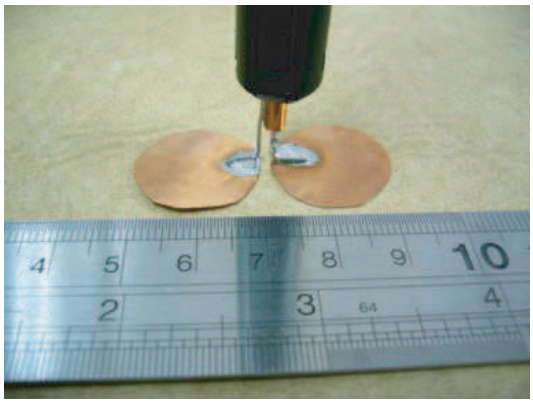

Figure 1: The proposed UWB antenna.

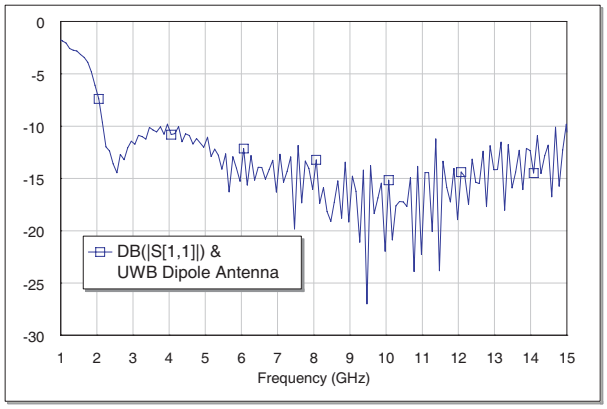

Figure 2: The measured data.

Wire Inverted-F Antenna Design for WLAN and Bluetooth Operation

Kuo-Liang Wu[1], **Guan-Yu Chen**[1], **Jwo-Shiun Sun**[1], **and Y. D. Chen**[2]

[1]Department of Electronic Engineering, National Taipei University of Technology, Taiwan
[2]Antenna and EMC Laboratory, HTC Corporation, Taiwan

Abstract— A high performance wire inverted-F antenna (Fig. 1) fabricated using a metal wire line as radiator is presented. A prototype of the proposed inverted-F antenna with a compact area size of 8.5 mm × 7 mm × 6 mm is implemented, and the multi-function WLAN/Bluetooth antenna shows a wide operating bandwidth (2400 MHz∼2500 MHz) for WLAN and Bluetooth bandwidth, making it easy to cover the IEEE 802.11b and IEEE 802.11g bands for wireless communication and high speed wireless communication operations. In this paper, the shorting monopole antenna has several advantages over conventional monopole-like antenna and planar antenna for mobile handsets. The co-design of folded metal wire antenna can overcome the problem of narrow band of the conventional antenna. By adding a low-Q resonator as a radiator, the coupling between the folded wire radiator can be improved. The design of monopole antenna with folded path of wire line radiator for WLAN applications is shown in Fig. 1. The proposed folded inverted-F wire antenna is designed of compact size of 8.5 mm × 7 mm × 6 mm. This long folded wire radiator has a total length of about 21.5 mm, which excited band operation. The total length of the effective radiator wire path of the designed antenna is close to one quarter wavelength at free space of the center frequency about 2450 MHz of operation band. By fine-tuning the length of the length of the folded radiator, the antenna resonant frequencies can be effectively controlled.

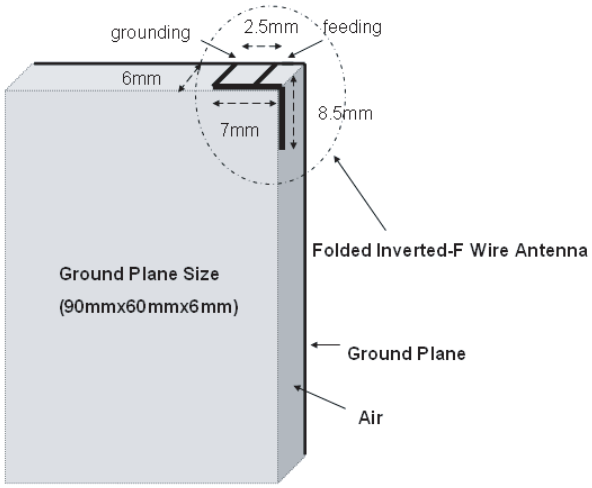

Figure 1: The proposed antenna.

Compact Ultra-wideband Antenna for Mobile Handsets

Ho-Jun Lee, Jong-Kyu Kim, and Se-Hwan Choi
Convergence Communication Components Research Center
Korea Electronics Technology Institute, R. O. Korea

Abstract— In this paper, we proposed a novel design of ulrtra-wideband (UWB) antenna for mobile handsets. The proposed antenna configuration is shown in Figure 1(a). This antenna has a coplanar waveguide (CPW) fed that is optimized the 50 Ω impedance matching by positioning via and substrate height and radiator size. Antennas in this paper are simulated by using the Ansoft simulation software high-frequency structure simulator (HFSS). The measurements of electrical characteristics such as radiation patterns, VSWR, and return loss of the implemented antenna were conducted in an anechoic chamber equipped with a HP 8510C network analyzer and far field measurement system. Figure 1(a) shows VSWR characteristics. The measured impedance bandwidth of the antenna is from 2.9 to 10.6 GHz for VSWR < 2. Figure 1(b) shows a photograph of the fabricated antenna. This antenna is made by using low temperature co-fired ceramic (LTCC) process and the size of this antenna is $10 \times 8 \times 1\,\text{mm}^3$. We manufactured the antenna based on the results of optimized simulation results and measured characteristics of the suggested antenna in the anechoic chamber. Details of the proposed antenna designs are described, and typical experimental results are presented and discussed.

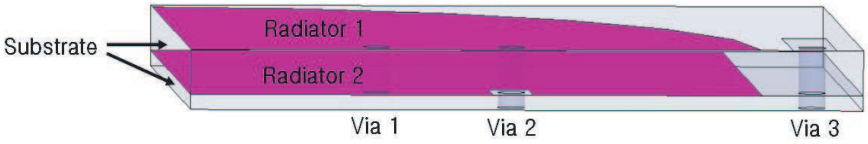

Figure 1: Proposed antenna.

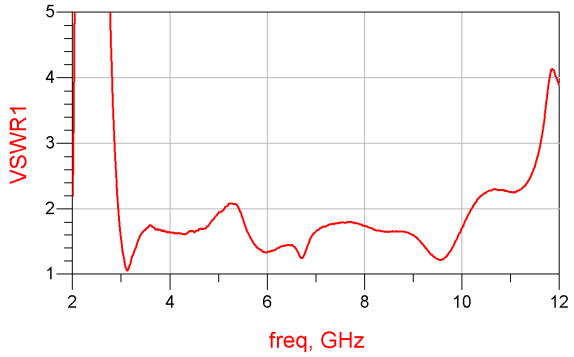

Figure 2: Measured VSWR.

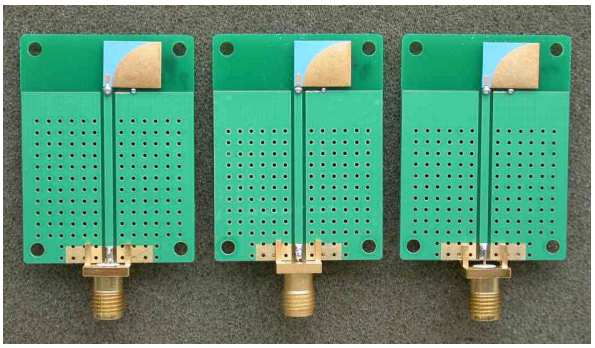

Figure 3: Photograph of the fabricated antenna.

REFERENCES

1. Anon, FCC First Report and Order on Ultra Wideband Technology, Feb. 2002.
2. Choi, S.-H., H.-J. Lee, and J.-K. Kim, "Design of miniaturized ultra-wideband antennas with band notch characteristic," *Microwave Opt. Tech. Lett.*, Vol. 51, No. 3, 720–725, 2009.

Design of a 1.575 GHz Helical LTCC Chip Antenna for GPS Application

Tao Huang and Yali Qin
Key Lab of Fiber Telecomunication, Colleage of Information Engineering
Zhejiang University of Technology, Hangzhou, China

Abstract— The exploding growth of wireless communications systems leads to an increasing demand for integrated compact low-cost antennas, to satisfy these needs, Low Temperature Cofired Ceramic (LTCC) technology has been extensively studied by many researchers. The most direct way of reducing the dimensions of the antenna is the use of very high dielectric constant of the LTCC material, however, in the view point of the antenna, the high dielectric constant causes serious problems to the design of antennas with high gain and good radiation pattern. Also, another concept to reduce the size of a antenna at a given resonant frequency is to increase its electrical surface-current length by changing the radiating element's shape, such as utilization of a meandering line structure, so blindly decrease in the physical size of antennas shouldn't be the sole aim for designing antennas, a variety of factors including suitable LTCC material and good structure must be integrated to seek for the best balance point between the physical size and the electric performance parameter when we design the antenna.

Based on the LTCC technology, this paper presents the design simulation, implementation and measurement of a miniaturized new-type helical LTCC chip antenna, the helical radiating patch is realized by using via holes to connect upper- and lower-layer radiating elements which are in staggered arrangement. By employing the Ansoft HFSS 3-D EM simulator to design and simulate, the antenna could be got with the central frequency 1.575 GHz, bandwith 60 MHz and size 10 mm × 3 mm × 0.77 mm, the maximum gains are −1.321 dBi and −1.316 dBi, respectively, in x-y plane and y-z plane measurement. Simulated return losses for different values of spacing between radiating element and via-hole height have been compared. Satisfactory agreement between the simulated and measured results for the antenna have been achieved, the results shown the antenna completely meet the needs of GPS and other wireless.

Pattern Synthesis for Cone Conformal Array with Optimized Polarization Properties

Fan Zhang
National Key Laboratory of Antennas and Microwave Technology
Xidian University, Xi'an, China

Abstract— Conformal array antennas will find their potential and promising applications in a variety of fields ranging from space-borne, air-borne, ship-borne, and missile-borne radar, space vehicles and wireless communications to sonar, etc. They present many new challenges to the antenna designer, including varying element normal due to curvature, serious cross-polarization effect and complex pattern synthesis. When an array is curved, linear or planar array methods often do not apply to curved arrays. In particular, since different elements along a curved surface generally radiate preferentially in different directions, the total far field cannot be written as the product of an array factor with an element pattern. Aiming at directing the main beam of the cone conformal array at the axial direction and improving the radiating characteristic of the conformal array, a new method based on array elements rotation is exploited and discussed. The conventional microstrip antennas are employed as the radiators of the conformal array. However, different from the linear or planar array, the polarization properties of the conformal arrays depend, not only on the elements, but also on the curvature of the platform. For improving the polarization properties of the array, each antenna element is rotated in its local coordinate, and the linear polarization direction of the microstrip antenna is rotated accordingly. A projection criterion is applied for determining the rotation angle of each element, which is in great favor of the achievement of directing the main beam along the direction of cone axis. The 3D polarization pattern of the cone conformal antenna array with specific linear polarization is analyzed and synthesized. By applying the Differential Evolution (DE) algorithm for the optimization of radiating characteristics (pattern and polarization) of the array, the sidelobe levels (SLL) of the co polarization was successfully reduced and the cross polarization was restrained.

A Compact Band Notched UWB Antenna for Mobile Applications

Nam-I Jo, **Dang-Oh Kim**, **and Che-Young Kim**
School of Electrical Engineering and Computer Science, Kyungpook National University
Sankyuk-dong Puk-gu, Daegu 702-701, South Korea

Abstract— A compact circular UWB(ultra-wideband) antenna with WLAN 802.11a/n band (5.15∼5.825 GHz) rejection characteristic is proposed for the mobile applications. The proposed UWB antenna was compact enough to be loaded into a mobile handset. The performance of the suggested antenna is mostly dependent on the gap between circular radiator and the ground plane. In order to have the band notched operation, the CSRR (complementary split ring resonator) is etched inside the circular patch of the UWB antenna.

MWS (Microwave Studio) of CST company was utilized in the design stage. The antenna was constructed on a substrate, Rogers 4003, with the thickness of 0.8 mm and relative permittivity of 3.38. A size of substrate is 24×37.5 mm and a radius of circular radiator is 5 mm. The proposed antenna covers the frequency band from 3.5 to 10.6 GHz ($S_{11} \leq 10$ dB), and the band rejection occurs about 5.7 GHz band. A simulation shows the maximum gain of 5.2 dBi, and radiation pattern is nearly omni-directional over the entire -10 dB return loss bandwidth. It also shows the group delay below 1 nsec over UWB communication band (3.5 GHz∼10.6 GHz) except WLAN band. Based on the experimental results, the proposed antenna could be a good candidate for the handheld mobile handsets.

Numerical Modeling a Microwave and Detection of Partial Discharge inside of HV Transformer

P. Fiala, **E. Gescheidtová**, **and T. Jirku**
Brno, FEEC BUT, UTEE, Kolejní 2906/4, Brno 612 00, Czech Republic

Abstract— The aim of this paper is to present the particulars of new research in the special measurement method modeling of starting process partial discharge inside of high voltage transformer. The numerical analysis of these effects can help to set up conditions to decrease it and get of information for preparing detection apparatuses and measurementmethods.

Different diagnostic techniques are currently known and available for on-line insulation condition assessment of high voltage transformers. The UHF technique has been recently presented in the field of transformer diagnostics in different texts. This paper describes numerical results from FEM analysis for experimental investigations conditions inside of transformer which have been carried out to study the partial discharge detection quality insulation method. The UHF technique has been applied and analysed on a model of 150 MVA 420/16.75 kV power transformer. There was analysed spectral distribution signal transmitted from differential part of transformer and detected on reference points. The analysis results were used for internal UHF sensor design through dielectric window. On older transformers that have a higher risk of failure these windows might be added by replacing manhole covers in its general tests time.

ACKNOWLEDGMENT

The research described in the paper was financially supported by FRVŠ (a fund of university development) by research plan No. MSM 0021630513 ELCOM, No. MSM 0021630516 and grant Czech ministry of industry and trade MPO No. FR-TI1/001.

REFERENCES

1. Kaneiwa, H., Y. Suzuoki, and T. Mizutan, "Characteristics of partial discharges, artificial simulated tree channels during in tree propagation," *IEEE Transactions on Dielectrics and Electrical Insulation*, Vol. 8, No. 1, February 2001.
2. Fiala, P., "Secondary winding model of current transformer-switchable variant," Research report, Laboratory of Modeling and Optimization Field in Electromagnetic Systems, FEI VUT and ABB EJF a.s. Brno No. 1/99, 21.1.1999, Brno, Czech Republic, 1999.
3. Fiala, P., "Transformer partial discharge modeling, minimal breakdown value set in a critical parts of transformer design," Research report, Laboratory of Modeling and Optimization Field in Electromagnetic Systems, FEI VUT and ABB EJF a.s. Brno No. 2/99, 18.3.1999, Brno, Czech Republic, 1999.
4. Fiala, P., "Optimization of two-pole voltage transoformer design $U_{max} = 25\,kV$, new variant 2000," Research report, Laboratory of Modeling and Optimization Field in Electromagnetic Systems, FEI VUT Brno No. 1/00, 20.2.2000, Brno, Czech Republic, 2000.
5. Sarathi, R., A. J. Reid, and M. D. Judd, "Partial discharge study in transformer oil due to particle movement under DC voltage using the UHF technique," *Electric Power Systems Research*, Vol. 78, 1819–1825, Elsevier, 2008.
6. Manuals ANSYS, v.8.1, USA.
7. Fiala, P., "Coupled electromagnetic model of smoothing choke," *AMTEE'01 5th International Conference*, ISBN 80-7082-756-4, str. C05, Plzeň, October 9–December 9, 2001.

Progress in Studies of Radio Frequency Radiation of the Wireless Communication Device

Chaoqun Jiao and Lei Gao
School of Electrical Engineering, Beijing Jiaotong University, China

Abstract— Through reading a lot of literature, the progress in Studies of Rradio frequency radiation of the wireless communication device is presented in this paper. Then, the disadvantage and advantage of these methods are pointed out. Finally, with different situation, it is suggested that which method is chosen to resolve the pratical problem.

Introduction: The wide application of wireless communication has attracted a lot of concern about safety of wireless devices [1–3]. Many investigations have been carried out to determine the effects of Radio Frequency (RF) radiation on human body using various exposure scenarios and models [1, 4–6]. Among these investigations, the Specific Absorption Rate (SAR) is considered as an index that quantifies the rate of energy absorption in biological tissues. Dimbylow et al. studied the SAR in human head exposed to a cell phone at 2 mm resolution with the frequency bandwidth ranging from 10 MHz to 3 GHz by using Finite-Difference Time-Domain (FDTD) method [5]. Martinez-Burdalo et al. further analyzed SAR depositions in different-aged human heads exposed to electromagnetic radiation resulted from a mobile phone [6]. Most of these studies have been focused on radiation effects from mobile phones and base stations. The work has been reported on the studies of radiation effects and radiation efficiency of wireless medical devices in interaction with human body [7]. Modern wireless technology is playing a more and more important role in telemedicine. Some wireless sensor platforms for pervasive healthcare monitoring have been designed in order to improve the quality of human life and minimize restrictions on daily activities [8–11]. Most of the related reports only analyzed the radiation efficiency and radiation effects of external sources such as wearable medical sensor devices. In fact, more and more implantable or ingestible devices are clinically employed, such as pacemakers, implantable defibrillators, capsule endoscope, implanted therapeutic devices and so on [12–14]. Recently, the research on biological effects of Ingestible Wireless Device (IWD) has been proposed particularly due to the persistence and high local energy deposition of antennas that are imbedded in human tissues [15–17]. Kim et al. found that the radiated power was the largest when a dipole antenna was located at the center of head model in comparison with other positions [18, 19]. The wireless multi-parameter monitoring of gastrointestinal (GI) tract [20–22], as well as wireless capsule endoscope [23], which allows high-resolution video being transmitted, has been widely applied. Among all the commercially available wireless capsule endoscopes, 434 MHz is the most often used frequency for video transmission [14, 23]. The frequencies of 315 MHz and 400–500 MHz are also used in some publications [24, 25]. At low transmission frequency, the antenna of the IWD is electrically small due to its compact size required for swallowing. Recently, 1.2 GHz and 2.4 GHz are also reported being used for ingestible capsule endoscopes in [26, 27]. Ito et al. evaluated the radiation characteristics of a helical antenna located in a cylindroid whole body phantom at 150 MHz and showed that the gain could be improved 5 dB or more by setting the target of local SAR and controlling the matching condition [28]. Chirwa et al. studied the radiation patterns and near fields of IWD in human body between 150 MHz and 1.2 GHz and suggested that the radiation characteristics of the sources in the GI tract should be optimized for a higher efficiency [29]. Chan et al. estimated the attenuation of a human body trunk at frequencies ranged between 100 MHz and 6 GHz from internal sources using a simplified experimental model [30]. However, the influence of frequency on biological effects and radiation efficiency were not studied. Chirwa et al. analyzed the ingestible sources in five positions at three orientations with the frequency ranging from 150 MHz to 1.2 GHz [29]. Lisheng Xu analyze the worst radiation intensity outside of human body model and, actually, the worst cases should be considered because the radiation characteristic of IWD is frequency, orientation and position dependent. The FDTD method is applied to analyze the electromagnetic interaction of IWD with human body and the bio-heat equation [31] is used to calculate the temperature rise resulting from the SAR deposition. Ally Y. Simba calculate the SAR of anatomically realistic human models exposed to RF electromagnetic fields from mobile phones used in elevators [32].

Comparation of These Studies and Suggestion: The disadvantage and advantage of these studies are pointed out and will be developed in the extended paper.

Conclusion: The progress in Studies of radio frequency radiation of the wireless communication device is presented in this paper. The disadvantage and advantage of these stuiess are pointed out. It is suggested that which studies is better with regard to the pratical problem.

Behavioral Models for Power Amplifier Using a Difference-frequency Dual-signal Injection Method

Hui Wang and Peiguo Liu
School of Electronic Science and Engineering, National University of Defense Technology, Changsha, China

Abstract— In this paper a difference-frequency dual-signal injection method is developed to modeling of RF power amplifiers (PAs) in nonlinear microwave circuits. In this method, the dual-signal is with different frequency spacing and power levels. By varying the frequency spacing of dual-signal, PAs model can be extracted without memory effects and with memory effects. For verification, the difference-frequency dual-signal is implemented with a 30 W class-AB PA and tested using a dual sinusoidal signal with 15 MHz frequency spacing from 1 GHz $\sim$ 2 GHz, and 1 dBm power spacing from -15 dBm $\sim$ 3 dBm. From the measured results, it is found that the model improves ACPR prediction accuracy by over 8 dB and 2 dB, compared to the conventional memory polynomial model and with conventional Volterra-based behavioral model respectively.

Analysis and Design for High-gain Antenna with Periodic Structures

Han-Nien Lin and Chun-Chi Tang
Department of Communications Engineering, Feng-Chia University
100 Wen-Hua Rd., Taichung 40724, Taiwan

Abstract— Unlike metal as conventional Perfect Electric Conductor (PEC) for unidirectional beam reflector, the periodic structures are now attracting more attention form academia and industrial as High Impedance Surface (HIS) or Artificial Magnetic Conductor (AMC) reflector. Because quarter wavelength ($\lambda/4$) separation between antenna and PEC reflector is needed for unidirectional beam applications, it inevitably increases the profile and stringently limits the operation bandwidth of the antenna system. However, the utilization of AMC of periodic structures as reflector not only significantly reduces the antenna profile with phase enhancement, but it will also enhance its gain and directivity performance. In this paper, we use monopole antenna with center frequency at 2.45 GHz and design periodic structure operated in frequency range between 2.4 GHz and 2.483 GHz to investigate the applications of EBG structure on antenna. We will finally compare the simulated result and measured result to further predict the optimization of the antenna-EBG system design parameters.

High Frequency Parameters of a Hermetic Motor and Their Effects on Conducted Emission

Ming Chen, **Xudong Sun**, **and Lipei Huang**
Country State Key Lab of Power Systems, Department of Electrical Engineering
Tsinghua University, Beijing 100084, China

Abstract— Three phase inverters are widely used in variable-frequency air conditioners to drive the hermetic motors assembled in the compressors. The rapid transition of voltage and current when the power semiconductor switches in the inverter turn on or off would cause electromagnetic emission to the distribution grid through the motor and the passive devices in the inverter. Therefore, the motor is an important part of the propagation path for conducted electromagnetic interference (EMI), and the high frequency parameters of the motor have a significant effect on the characteristics of the propagation path and the conducted EMI of the inverter.

In order to evaluate the effect of the hermetic motor on the conducted EMI to the distribution grid, the high frequency equivalent circuit model of the motor was established. The parameters of the model were extracted by measurement since it is very difficult to obtain them by calculation due to the hermetic and complex structure of the motor.

The impedance characteristics of the motor with respect to frequency were measured by an impedance analyzer, and then a least-squared data fitting procedure was applied to obtain the parameters from the impedance characteristics. The impedance characteristics should be measured for the motor operating normally, when the fluorocarbon in it is in gas state. However, because of the limitation of the instrument, they can be measured only after the motor stops while the fluorocarbon becomes liquid, resulting in a different value of the equivalent capacitance duo to the change of dielectric constant of the fluorocarbon. An alternate extraction method was adopted to solve such a problem. The impedance characteristics were measured after the fluorocarbon was entirely exhausted and air filled it, which can be considered as quite close to the situation when the fluorocarbon is in gas state. The parameters of the motor in both the two states were then obtained, and some difference between them existed.

A comprehensive model of the propagation path of the conducted emission was then constructed by connecting the model of the motor with the high frequency circuit models of the other parts of the inverter which have been proved accurate and effective before. Based on the model, the effect of the parameters of the motor on the conducted emission was investigated by simulation. The results indicate that the equivalent winding-to-ground parasitic capacitance is the essential parameters of the motor, and also the important parameter to affect the characteristics of the propagation path. The overall magnitude of the emission spectrum changes a little with the value of the capacitance, whereas the frequency of the peak point of the spectrum varies a lot, and becomes higher when the capacitance value gets smaller.

An experiment was conducted to measure the conducted emission spectrum when the motor operates normally to verify the above model and analysis. The spectrum obtained by simulation with the parameters when the motor stops and the fluorocarbon is exhausted matches in general with the measured one, which shows that the hermetic motor model is effective and the analysis results are credible.

Using Grey Decision Making Approach to Improve FPGA Performance

Jan-Ou Wu[1], **Yang-Hsin Fan**[2], **and San-Fu Wang**[3]

[1]Department of Electronic Engineering, De Lin Institute of Technology, Tu-cheng, Taipei, Taiwan, R.O.C.
[2]Department of Computer Science and Information Engineering, National Taitung University
Taitung, Taiwan, R.O.C.
[3]Graduate Institute of Computer and Communication Engineering
National Taipei University of Technology, Taipei, Taiwan, R.O.C.

Abstract— In this paper, we study LUT-based field programmable gate arrays (FPGAs) architectural parameters association with the LUT cluster size N and input number k for FPGA targeting at delay, area, and power to improve performance. This performance problem has been proved that the different pair of LUT cluster size N and input number k can lead to different trade-off the FPGA in delay, area, and power consumption previously. Hence, we present an efficient methodology based on the grey decision making technology to apply LUT-based FPGA physical design of the electronic design automation (EDA) tools. This methodology can cluster association with the LUT cluster size N and input number k to FPGA optimal performance architecture. Experimental results demonstrate that our proposed can get optimal performance architecture to minimum area, energy, and delay in association with the different pair of LUT cluster size N and input number k decision for MCNC benchmark circuits, respectively. Furthermore, our results show that the min-delay logic block architecture has cluster size 6 and input number k size 7, the min-area logic block architecture has cluster size 8 and input number k size 4, and the min-energy logic block architecture has cluster size 8 and input number k size 4.

Stability Study of Subwavelength Image in Photonic Crystal Slab

Chen-Yu Chiang and Pi-Gang Luan
Department of Optics and Photonics, National Central University, Jhongli 320, Taiwan

Abstract— Since John Pendry proposed the idea of left-handed material (LHM) superlens to overcome diffraction limit, large amount of literatures about subwavelength imaging have been published. In them researchers demonstrated that negative refraction and subwavelength imaging can be realized experimentally. Pentry argued that the evanescent wave can be amplified in a LHM slab and form a deep subwavelength point image in the image plane. Although the originally fabricated LHM is consisted of metallic constituents, researchers soon found that photonic crystals (PC) can also have such subwavelength imaging ability. Although evanescent wave is important in forming subwavelength image, there are other key factors affecting the image quality which we study in this paper. Past works had found that not-so-good-quality image were obtained when shifting the source position in the lateral direction. In this paper, we further study these factors and explore thoroughly how they influence the subwaelength image quality. After finding the worse image qualities in some cases, we found the main reasons. Evanesce wave is helpful for subwavelength imaging but it is sensitive to the positions of the cylinders that makes the photonic crystal slab. A more ideal slab is the triangular cylinder slab, which uses mainly the far field wave components to form a subwavelength image and the image quality is more stable, thus might be a better choice for a real application. We also found that the wider the slab in the lateral direction, the better the image periodicity and a little absorption can help to reduce the boundary effect. We believe a more clear understanding of these affecting factors can provide some references for designing new subwavelength imaging devices.

Effect of Heat Treatment on Property of Giant Magnetostrictive TbDyFe Films

Yirui Liang and Xiaojing Zheng
School of Civil Engineering and Mechanics, Lanzhou University, China

Abstract— As one kind of new intelligent material, giant magnetostrictive materials are usually used in MEMS (micro electromechanical system) due to their characteristics of high energy output, high frequency and contactless operation. In those MEMS, application of giant magnetostrictive films is most widespread. So, giant magnetostrictive films have drawn significant interest in recent years. Because giant magnetostrictive films is applied usually under low magnetic field environment, therefore enhances the low magnetic field performance of giant magnetostrictive films is very important. In this paper, the magnetostrictive characteristics and the magnetic properties of $Tb_{0.29}Dy_{0.71}Fe_{1.8}$ films vacuum-annealed for different time long at various temperatures are studied systematically. Through the experimental study, we found enhanced the low magnetic field performance of giant magnetostrictive films the best vacuum-annealed mode. The results show that the magnetostrictive characteristics of $Tb_{0.29}Dy_{0.71}Fe_{1.8}$ films vacuum-annealed at 475°C for 10 min at the low magnetic field is comparatively well in $Tb_{0.29}Dy_{0.71}Fe_{1.8}$ films vacuum-annealed at 475°C for different time long. The magnetostrictive characteristics of the $Tb_{0.29}Dy_{0.71}Fe_{1.8}$ films vacuum-annealed at 450°C at the low magnetic field are better than those of the films vacuum-annealed at 475°C under the same vacuum-annealing time long. The $Tb_{0.29}Dy_{0.71}Fe_{1.8}$ films vacuum-annealed at 450°C for 60 min possess bigger in-plane saturation magnetization, smaller coercivity and larger magnetostriction at the low field in all the samples. Using these optimized giant magnetostrictive films, the performance of MEMS (micropump, linear ultrasonic motor) may enhance large scale in the future.

Finite Element Analysis of Electromagnetic Valve Actuation for Engine

Shizuo Li
College of Electrical Engineering, Guangxi University, Nanning, Guangxi 530004, China

Abstract— Electromagnetic valve actuation (EVA) is a new type of valve actuation, it uses electromagnet to drive and control valve instead of camshaft. EVA can simplify the structure of engine, and can control every valve separately. A new structure of EVA is introduced and illustrated in Fig. 1, it is rotational symmetry. There are two symmetrical cores and windings on the two sides, the current in the two windings are equal in magnitude but opposite in direction. The central core and winding is fixed on axis, and can move to right or left side which can drive valve open or off. If the current of central winding has same direction with that of right winding, the axis move to right side, and vice versa, so we can control the current of central winding to drive valve.

Finite element method is used to calculate the magnetic field of EVA. Distribution of magnetic field is shown in Fig. 2.

Calculation shows that the electromagnetic force of this new structure can meet the dynamic requirements of EVA. Research result is beneficial to optimization of structure parameter and achievement of control method for EVA.

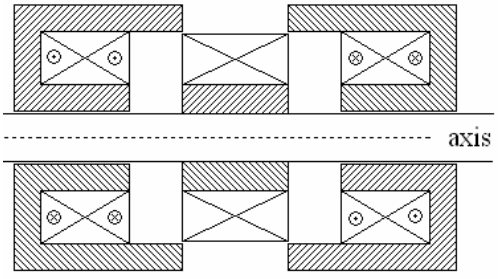

Figure 1: Structure of EVA.

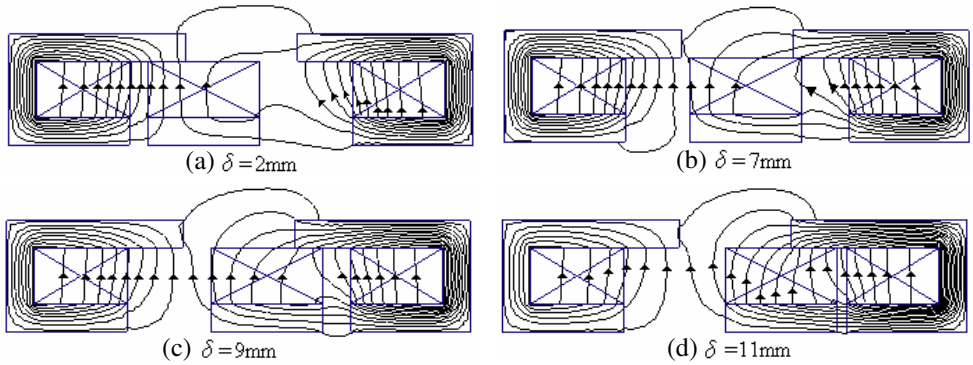

Figure 2: Distribution of magnetic field.

Seismic Traveling Macroscale Irregularities at Ionospheric F2-region on Data of Distance Sounding

U. K. Kalinin[1], **N. P. Sergeenko**[2], **and M. V. Rogova**[2]

[1]Fedorov Institute of Applied Geophysics, Moscow, Russia
[2]Pushkov Institute of Terrestrial Magnetism, Ionosphere and Radiowaves Propagation Troitsk, Moscow, Russia

Abstract— The properties of travelling ionospheric macroscale irregularities (their horizontal sizes are 1–4 thousand kms, excesses of a background are 15–30%), formed in F2 layer as a result of strong earthquake in time of heliogeophysical perturbations are explored. The irregularities arise 10–15 h before earthquakes and move horizontally with a transonic speed on distances of a few thousand kms up to round — the-world trajectories focused approximately along an arc of a major circle, transiting above epicenter region. Information of spent examination was caused by spatial-time differences of dynamics of F2-layer of an ionosphere in time of the heliogeophysical disturbances from dynamics of quasi-causative seismic macroscale ionospheric irregularities.

The complex analysis of the arrays of critical frequencies of F2-layer of an ionosphere (foF2) of a world network of automatic ground ionospheric stations of vertical sondage was carried out. Also the ionograms of board sondage of space station "Mir" were used for the analysis. Global TEC maps was used to detect the ionospheric irregularities associated with earthquake precursors. Analyses of all these data confirmed a hypothesis about occurrence of macroscale positive ionospheric irregularities in the vicinity of strong earthquakes ($M > 5$) epicenters also.

The analysis was carried out as on the basis of statistical methods with use of representations about Poison stream of events, and on the basis of the causal approach to separate irregularities.

As a result of these examinations, the geophysical patterns of ionospheric effects incipient at superimposition of macroscale irregularities and ionospheric disturbances of solar and magnetospheric origin were synthesized.

Based on the Coherent Point Tartget Monitoring Urban Subsidence in Beijing

Hong-Li Zhao[1, 2], **Jian-Ping Chen**[1, 2], **Jing-Hui Fan**[3], **Xiao-Fang Guo**[3], **and Huan-Huan Liu**[1, 2]

[1]School of the Geosciences and Resources, China University of Geosciences (Beijing), Beijing 100083, China
[2]Beijing Land Resources Information Development Research Laboratory, Beijing 100083, China
[3]China Aero Geophysical Survey & Remote Sensing Centre for Land & Resources, Beijing 100083, China

Abstract— Beijing has seriously suffered from land subsidence caused by ground water over-extraction. Although Beijing's in-situ subsidence monitoring system is necessary and reliable, its sparse data grid in the area is a limitation which makes it difficult for us to understand the whole deformation field. Compared with the traditional monitoring method, differential SAR interferometry (D-InSAR) is more cost-efficient and preciser. D-InSAR can monitor movements on the earth surface at centimeter or even millimeter levels. Therefore, many earth physical phenomena can be discovered and analyzed, such as earthquake, volcano, atmosphere meteorology, ice sheet movement, subsidence, landside, and so on. However, temporal decorrelation and atmosphere phase delay degrade the accuracy of D-InSAR for small deformation monitoring. As these factors cannot be eliminated by SAR data processing, some auxiliary data such as leveling data and DEM data have been introduced into D-InSAR data processing.

In this paper, we present a Coherent Point Targets interferometery approach to retrieval the phase history, extract the linear deformation information from interferometry phase and eliminate atmosphere phase delay. During the interferometric point target analysis, the interferograms are only interpreted for the coherent selected points. Considering efficiency and data storage, vector format data structures are used instead of the raster data format used in conventional interferometry. In addition, the phase regression model is used to estimate the linear deformation rate and delta height and residual phase over an area of the coherent point targets. It is a very step-wise improvement that the information retrieval from the objective of the iteration concept. The standard deviation from the regression function serves as a quality measure for the regression function and the derived parameters. Besides, the minimum cost flow (MCF) algorithm is used to minimize the total cost associated with phase discontinuities in the scene associated with noise and layover. It is worth mentioning that delaunay triangulation is used to generate an optimized irregular triangular network of the points to be unwrapped.

In this paper, the linear deformation rate and accumulation deformation for each point was achieved with a least square regression based on 20 ENVISAT ASAR images of the whole Beijing area covering the period from June 2003 to March 2007. At the same time, Beijing' subsidence result based on the multi-baseline was compared with that based on the single-baseline.

A Study of the High Resolution COSMO-SkyMed SAR Data for Ground Subsidence

Hong-Li Zhao[1, 2], **Jing-Hui Fan**[3], **Zhen-Chao Wang**[1], **Jian-Ping Chen**[1, 2], **Huan-Huan Liu**[1, 2], **and Xiao-Fang Guo**[3]

[1]School of the Geosciences and Resources, China University of Geosciences (Beijing), Beijing 100083, China
[2]Beijing Land Resources Information Development Research Laboratory, Beijing 100083, China
[3]China Aero Geophysical Survey & Remote Sensing Centre for Land & Resources
Beijing 100083, China

Abstract— The satellites of COSMO-SkyMed, which are an Earth observation satellite system funded by the Italian Ministry of Research and Ministry of Defense and conducted by the Italian Space Agency (ASI), have some significant advantages: an area of interest is unmatched revisit 4–6 hours with 4 satellites; observations of the area will be repeated several times a day in all-weather conditions; COSMO SkyMed is equipped with a polarimetric X-band SAR, and satellites can acquire high quality images with very high resolution (1 m for civil applications). So they are very suitable for natural disaster monitoring.

While DInSAR has proven its remarkable potentiality for mapping ground deformation phenomena over tens-of-kilometers-wide areas with centimeter-scale accuracy levels, it is used in this paper as a powerful tool to monitor ground subsidence. The basic idea of D-InSAR is that a reference interferogram is simulated based on the DEM. Based on the reference SAR geometry, the interferometric baseline model, and the height map in radar geometry, the unwrapped interferometric phase corresponding exclusively to topography is calculated. Because of the big spatial baseline, there are significant residual stripe phases. So in order to improve the result, there are three important steps as follows: refinement of the differential interferogram for residual baseline component using a baseline model; compensation for residual quadratic phase component; refinement of the differential interferogram with improved quadratic phase model. Finally, This technique has been tested with COSMO-SkyMed SAR data and ASAR data respectively for land subsidence derivation of Tianjin.

Based on the comparison between the two results, the following conclusion can be drawn: to begin with, in the case of short temporal baseline and small spatial baseline, a coupe of COSMO interferometry images are more suitable to extract high-precision ground deformation information than a couple of ASAR interferometry images, with the characteristics of high resolution and high coherence. However, based on the COSMO data procession result, there is a big error in the orbit data, which resulted in significant residual stripe phases. Though the complex data processing algorithms can wipe off the phases, at the same time it may lead to new errors caused by the mismatches of the algorithm model with the real situation. The last but not the least, COSMO data are suitable for high-precision information extraction in a relatively small and important area; while ASAR data are fit for regional survey.

A New Method of Near-field Three Dimensional Radar Synthetic Aperture Imaging

Nan-Jing Li, **Chu-Feng Hu**, **and Lin-Xi Zhang**
National Key Laboratory of UAV Specialty Technique, Northwestern Polytechnical University, China

Abstract— A fully 3-D image reconstruction algorithm that quasi-monostatic mode is used and the transmitting antenna works in step frequency was developed. The algorithm is not restricted by far field as the traditional imaging algorithm. Through synthetic aperture processing for radar data, the resolutions of the image and detecting ability of radar are improved. A new back-project method, which can increase accuracy of interpolation, was presented. 3-D image of the objects can be achieved through fast Fourier transform and integrating after interpolation. Numerous imaging results from simulations and experiment were resented. These results show that the algorithm for 3-D image reconstruction based on this back-project method can produce a microwave 3-D image with high resolutions.

The Research of Artificial Corner Reflectors in InSAR

Wu Zhu[1, 2], **Qin Zhang**[1, 2], **Chaoying Zhao**[1, 2], **and Chengsheng Yang**[1, 2]

[1]College of Geology Engineering and Geomatics, Chang'an University, Xi'an 710054, China
[2]Key Laboratory of Western China's Mineral Resources and Geological Engineering
Ministry of Education, Xi'an 710054, China

Abstract— Differential synthetic aperture radar interferometry (DInSAR) had been great development in the last ten years. However, due to loss of time and space coherence as well as atmospheric effects, the application of traditional differential interferometry has been greatly limited. For this reason, some scholars have proposed new technologies that uses some discrete, phase stability target points as the studying object, artificial corner reflector (CR) is one of them. Because CR can artificially control its geometric shape, size, structure and placed position in the SAR image, can show a stable, clear, high amplitude and phase information, can monitor the surface micro-deformation potential in low-coherence region, it has been widely applied and developed in recent years.

The fundamental principle of Corner reflector is: CR are installed in the study area, the radar incident light rays to the CR's two or three mutual perpendicular surfaces. After several reflection, light will ray to rader along the opposite direction of original path. A cross-wire highlight will be generated in the image and we can analysis the highlight's intensity and phase information to extract the surface deformation.

Currently, many institutions have begun to use CR to monitor urban's surface micro-deformation, landslides deformation and have laid a series of CR points. However, they usually can't find the corresponding CR points in the SAR image, particularly in urban where the strong reflection characteristics of the surrounding surface features makes it difficult to accurately identify genuine CR-point. This article is based on the principle that intensity information on the CR point installed before and after the SAR image acquisition has significant change. Taking the three face angle reflector installed in xi'an as example, we detected CR's exact location by registrating the SLC, extracting intensity bias, analysising the deviation, on-site investigation.

Geocoding errors is an important source of error in the application of InSAR technology. The usual method of combinating the ellipsoid equation, slope range equation and Doppler equation to geocode makes the result more or less different from the exact location because of inaccurate orbit data. Therefore, it needs to look for an effective method to correct the result once. As a stable point in SAR image, with the precise GPS observation data, CR can be used as ground control points to correct the geocoded image. In this paper, affine transformation model is applicated and xi'an's geocoded image is corrected using CR points. At the same time, the results before and after correction are compared and found a significantly improvement.

Phase unwrapping is main problem when we need to get the deformation between CRs and there is no an effective way to solve this problem. LAMBED integer ambiguity search method can rapidly and accurately determine the GPS entire week unknowns and can be used to unwrapped the CRs. The text solves the deformation between CRs in xi'an using LAMBED method and compares it with traditional DInSAR results and GPS results.

Inversion of Vegetation Parameters Based on Polarimetric SAR Interferometry

Linxi Zhang[1, 2], **Jie Ren**[2], **Xingzhao Liu**[2], **and Chufeng Hu**[1, 2]

[1]National Key Laboratory of UAV Specialty Technique, Northwestern Polytechnical University
Xi'an, Shaanxi 710072, China
[2]Electronic Information Department, Northwestern Polytechnical University
Xi'an, Shaanxi 710072, China

Abstract— Polarimetric SAR interferometry (PolInSAR) is a well known technique that can be applied to inversion of vegetation parameters. In this paper, a two-layer coherent scattering model composed of a random volume over the ground is established firstly to describe the vegetation parameters, and then the polarization and interference are unified by defining a complex interferometric coherence which can be gained through the model. Finally, the measured SAR data is substituted into the expression of the complex interferometric coherence to come true the inversion of vegetation parameters. In the process of the inversion of vegetation parameters, three-stage method is used. By employing the method, ground topography can be received accurately and other vegetation parameters such as vegetation height and mean extinction coefficient also can be estimated. However, the random model is based on the assumption that volume interferometric coherence is independent of polarization. Under normal circumstances, the propagation of the electromagnetic waves is anisotropic because the extinction coefficients are highly polarization dependent, namely, that volume interferometric coherence is dependent of polarization, so a new vegetation model composed of an oriented volume over the ground needs to be created. For the inversion of the oriented model, three-stage method is still used and the inversion procedure is similar with the random model. The difference between them is the interferometric coherence of random is a line inside the unit circle of the complex coherence plane, while oriented is a triangular region. The simulation results demonstrated that an accurate inversion of the vegetation parameters is still possible.

Detection of Interfaces between Frozen and Melted Sediment Using GPR: A Case Examination on Qinghai-Tibet Railway

Zhen-Wei Guo[1, 2], **Jian-Xin Liu**[1, 2], **Jian-Ping Xiao**[1, 2], **and Xiao-Zhong Tong**[1, 2]

[1]The Institute of Info-physics and Geometrics Engineer, Central South University
Changsha, Hunan 410083, China
[2]Key Laboratory of Non-ferrous Resources and Geological Hazard Detection
Changsha, Hunan 410083, China

Abstract— To survey the frozen earth roadbed of Qinghai-Tibet railway and to treat the hidden trouble of the roadbed are the important approach to steady the roadbed. And it is essential guaranteed to be open to traffic in security. According to the geological data of the typical testing section of Qinghai-Tibet railway, the field experiments are accomplished. Based on the processing results, a significant technology for practical application of ground penetrating radar in detecting frozen roadbed is useful and indispensable.

GPR Data Processing for Permafrost Detection in Qinghai-Tibet Railway

Zhen-Wei Guo[1,2], **Jian-Xin Liu**[1,2], **Jian-Ping Xiao**[1,2], **Xiao-Zhong Tong**[1,2], **Wei Zhang**[1,2], **and Jie Li**[1]

[1]The Institute of Info-physics and Geometrics Engineering, Central South University Changsha 410083, China

[2]Key Laboratory of Non-ferrous Resources and Geological Hazard Detection Changsha, Hunan 410083, China

Abstract— As an advanced technology, Ground-Penetrating Radar (GPR) is a geophysical method based on electromagnetic wave propagation commonly used for nondestructive subsurface imaging, including thruway, glacier, permafrost and pipe. It has also been used as a geophysical method in permafrost research to map subsurface structures and composition. The Qinghai-Tibet Plateau is the world's highest plateau, averaging over 4000 meters above sea level and covering an area of 200,000 square kilometers. The Qinghai-Tibet railway has always been puzzled by permafrost. It is imperative to detect permafrost subgrade fast.

Despite the fact that computer processors are becoming more efficient and GPR software packages are becoming more user friendly, the processing and interpretation of the GPR data from roads, railways and airports is still the most time consuming phase and an interpreter's skills play a key role in the success of a GPR project. GPR data processing can be divided into four phases: (1) preprocessing, (2) data processing, (3) interpretation and visualization and (4) reporting. The processing was divided into several classic steps namely amplitude compensation, filtering, migration, 2D powering for coherent filtering, and display. Permafrost recognition is a significantly indispensable part of data processing for permafrost detection.

Permafrost recognition algorithm was proposed with applying the rolling power spectrum. In the Central South University, we did a test. As a result, it has shown that anomalies have been significantly strengthened. The most important points of this study, related to methodology and processing, are discussed, and finally, a method is proposed using data processing for permafrost detection.

GPR Polarization Simulation with 3D HO FDTD

Jing Li[1], **Zhao-Fa Zeng**[1, 2], **Ling Huang**[1], **and Fengshan Liu**[2]

[1]College of Geoexploration Science and Technology, Jilin University
Changchun 130026, China
[2]Applied Mathematics Research Center, Delaware State University, DE 19901, USA

Abstract— Polarization signal is important in designing GPR data measurement. Its scattering characteristics can be used to discriminate the targets. For the target with different medium properties or orientation, the GPR signal response has a significant difference in different polarization mode. The targets such as metallic, low impedance object and PVC, high impedance objects have different polarization signals while are difficult to discriminate in the traditional GPR acquiring methods. The polarimetric measurement has the potentials to improve the discrimination, reduce the clutter interference and get the better prospecting effect. Meanwhile, the simulation is one of key research issues to understand the radar polarization theoretical. In order to improve simulation accuracy, we use 3D high-order finite difference time domain (HO-FDTD) method to simulate the polarization. It obtains a good application effect. Through the simulation study of GPR polarization measurement, we can provide more accurate and richer theoretical for the practical work.

ACKNOWLEDGMENT

The research work was supported by NSFC (40774055) of China, and a DoD DEPSCoR W911NF-07-1-0422 of USA.

Fine Exploration Based on Dense Frequency Pseudo-random Harmonic Electromagnetic Method

Weibin Luo and Qingchun Li
Department of Geology Engineering and Geomatics, Chang'an University, China

Abstract— In controlled source electromagnetic sounding the exploration depth is determined by frequency of source signal and the earth resistivity. For a fixed resistivity of the uniform half space the lower signal frequency applied and the deeper exploration depth achieved. In current CSEM survey systems the mono frequency square or harmonic signal was adopted at each transmitting. It often took a long time to complete a deep EM sounding. And the vertical resolution of electromagnetic sounding lies on received frequency interval. For improving the vertical resolution a new method of Pseudo-random harmonic electromagnetic sounding is introduced, based on the study of 2^n series Pseudo-random multi-frequency (PRMF) and inverse repeated M sequence pseudorandom multi-frequency signal waveform and spectral features. The bandwidth of PRMF and inverse repeated M sequence pseudorandom multi-frequency signal are controllable, the energy concentrates on several frequencies, which are equally spaced on log scale coordinates. These are ideal excitation sources for electrical exploration such as Induced Polarization method and CSEM sounding. The vertical resolution based on fine signal frequency was analyzed. The designs of dense frequency ratio pseudo-random signal generating, signal transmitting, signal receiving and data proceeding were performed. A novel signal generation cell with GPS synchronization program was designed. The 2^n series pseudo-random multi-frequency signal and invert-repeated m-sequence were generated by hardware using the complex programmable logic device LC4256V-100T from Lattice semiconductor and the tool of hardware description language (VHDL). It can produce different dense frequency waveforms, and has twenty-five frequency options which divided from four dense frequency ratio initial frequencies. The generated 2^n series signal contains up to thirteen frequencies. And the m-signal and invert-repeated m-signal can be generated by up to 32 shift registers. There are up to 104 clock frequencies can be generated and the fine vertical resolution can be achieved. The feasibility of this method is tested and its effectiveness is discussed. It is proved that this method will be an alternatives for design and development of controlled source electromagnetic sounding instruments.

GPR Migration Imaging Algorithm Based on NUFFT

Hao Chen, **Renbiao Wu**, **Jiaxue Liu**, **and Zhiyong Han**
Tianjin Key Laboratory for Advanced Signal Processing, Civil Aviation University of China
Tianjin 300300, China

Abstract— Stolt migration is one of the useful GPR imaging algorithms which has the advantage of fast implementation speed. The datewhich is uniformly distribute in frequency-wavenumber domain, is transformed from frequency-wavenumber domain to wavenumber-wavenumber domain. Then using interpolation method to make sure that the date is uniformly distribute in wavenumber-wavenumber domain. So it will be possibility to use the FFT, which lead efficiencies, to calculate the date. That is the key method of Stolt shift method. Usually, the Linear interpolation and sinc interpolation is used. Interpolation determines the effectiveness of imaging directly, in the practical applications, zero-fill interpolation in time domain is used to improve accuracy but which will increase the computational complexity.

This paper analyzed the root causes of why could not use FFT to calculate the formula for image reconstruction before stolt interpolation. Then introduced the algorithms of computing Fourier transform with unequally spaced data in any of the domain (time or frequency) have been proposed. These algorithms are known as Non-Uniform FFT (NUFFT), NUFFT was first proposed by Dutt and Rokhlin in 1993, Beylkin; Nguyen and Liu; Fessler and Sutton are made great contributions to its development.

In this paper, NUFFT is introduced to realize the fast computing of formula in image reconstruction directly. Both the stolt interpolation and the final range inverse FFT have been substituted by a single NUFFT. This paper describes the detail application of the NUFFT's to the stolt migration algorithm. Compared the new method with the old ones in calculation efficiency and image result. The performance is illustrated with numerical simulations. The simulation of B-scan data of a two-layered medium is generated by the Gprmax 2.0 software. The simulation results show that this method reduce the complexity of the interpolation while ensure the operational speed. at the same time, it use least-square to approximate the function so the energy of the image result is more concentrated. This method achieves good results.

Analysis of MMW Imaging System with Scanning Mirrors and Extended Hemispherical Lens

Zucun Zhang and Wenbin Dou
State Key Laboratory of Millimeter Waves, Southeast University, Nanjing 210096, China

Abstract— Offset parabolic mirror is usually used as energy focusing antenna in multi-beam imaging system. However, due to the characteristics of offset parabolic mirror, the receiving arrays must be arranged on the curved surface, which is a hard work and high-cost. In order to reduce cost and decrease complicity of design and fabrication, the extended hemispherical lens is introduced to an imaging system to construct a small plane array on the extended surface of hemispherical lens. In the present paper, small planar focal plane array (FPA) for MMW imaging application is constructed by bringing an extended hemispherical lens into an imaging system, which is composed of a scanning planar mirror and a focusing parabolic mirror. Firstly, for the imaging system without or with an extended hemispherical lens, the optical path and spot-patterns are calculated and compared. The comparison indicates that the improvement of the focusing performance can be reached by adding an extended hemispherical lens to the imaging system. Secondly, for different incident angles, the contour diagram of electric field in the focal plane of imaging system with extended hemispherical lens is calculated by ray-tracing method and Stratton-Chu vector diffraction integral formula. The numerical results show that the system with extended hemispherical lens has good imaging performance. Our work is very meaningful to design a low-cost and practical system for millimeter-wave imaging.

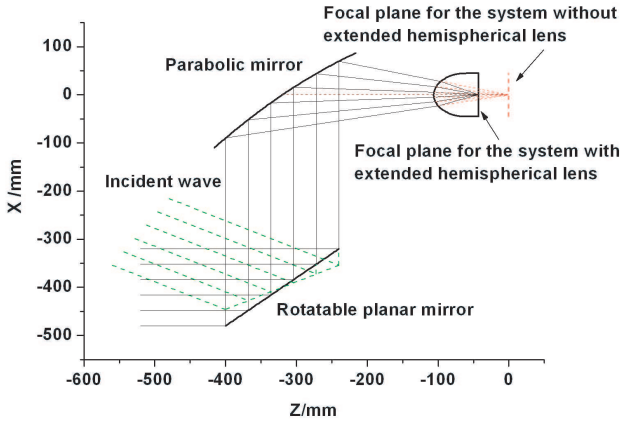

Figure 1: The optical path of the imaging system.

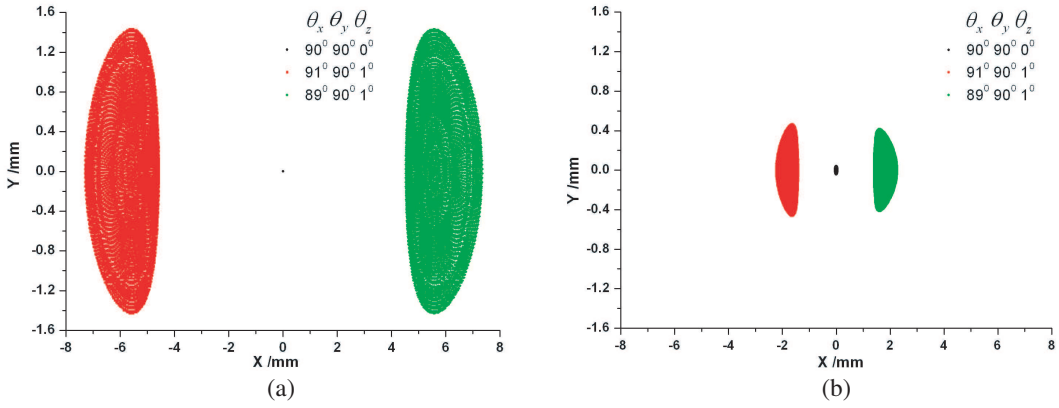

Figure 2: For different incident angles, the spot-patterns on focal plane of the imaging system without or with extended hemispherical lens. (a) Without extended hemispherical lens, (b) with extended hemispherical lens.

Results: Figure 1 shows the optical path of the imaging system with extended hemispherical lens. Incident plane waves enter from the left and are brought to the parabolic mirror by the rotatable planar mirror, and then the waves are focused on to the focal plane of the imaging system. The diameter of incident diaphragm is 160 mm, and the frequency is 100 GHz. The size of the system is only about 400 mm × 600 mm × 160 mm.

In Fig. 3, the diffraction pattern for different incident angles are shown when the planar mirror are kept fixedly. It can be seen clearly that the plane wave for different incident angles has its diffraction pattern in the different position of focal plane. The aberration and the difference of peak value of $|E_x|^2$ are very small and can be tolerated.

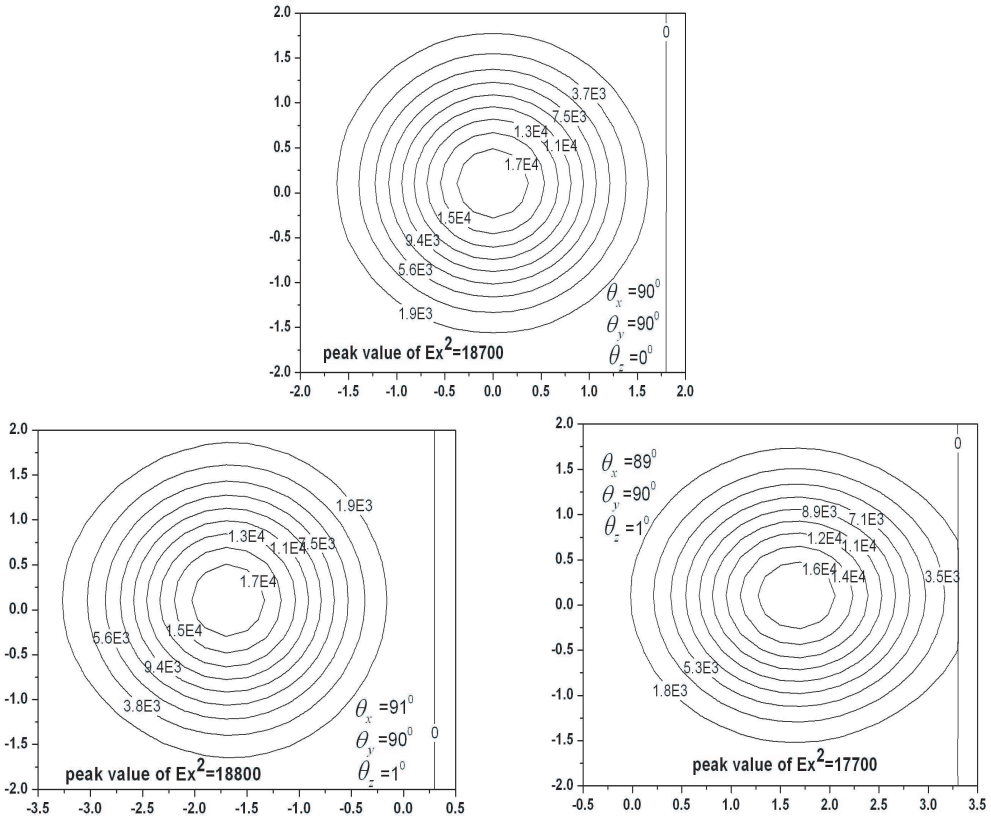

Figure 3: For different incident angles, the diffraction pattern of $|E_x|^2$ for different incident angles.

Simulation for GPR Echoes Based on Non-constant-Q Attenuation Model

Weikun He[1, 2], **Zhigang Su**[1], **Renbiao Wu**[1, 2], **Zhiyong Han**[1], **and Jiaxue Liu**[1]

[1]Tianjin Key Lab for Advanced Signal Processing
Civil Aviation University of China, 300300, China
[2]Electronic and Information Engineering Institute
Tianjin University, 300300, China

Abstract— Ground Penetrating Radar (GPR), as a high-resolution, high-precision and non-destructive detection tool, is widely applied in the quality surveillance for the highways, bridges and runways etc.. The layer media underground belongs to lossy media whose dielectric response is frequency-dependent, so the quality factor (Q) is similarly frequency-dependent which makes it more complicate for the electromagnetic wave to propagate in the layer media. Electromagnetic (EM) wave propagation characteristic in the non-constant-Q layer media and echoes simulation technique are important for the use of the EM wave technology and the data interpretation of the GPR echoes.

Much attention has been attracted to the simulation for GPR echoes propagated in the lossy layer media. The outstanding productions include the method based on the model of the echoes and the method based on the Finite Difference Time Domain (FDTD). For the echo-model-based method, the propagation attenuation is based on the constant-Q model. However, for the lossy media whose quality factor Q isn't constant, but frequency-dependent, the constant-Q model above is invalid for such situations. For the FDTD-based method, more complexity and operation burden are required concerned with the solution to the Maxwell equations iteratively and the setting of the absorbing boundary conditions.

In this paper, we discussed the echoes simulation based on the non-constant-Q attenuation model. Firstly, we studied the Debye diffraction model and the non-constant-Q attenuation model. Then we analyzed the effects of the interface and the inter-layer of the lossy media on the EM wave, and formulated the phase velocity of the EM wave propagated in the lossy media based on the non-constant-Q attenuation model. Finally, the signal model of the GPR echoes and the simulated wave based on the non-constant-Q attenuation model were established. The results were compared and analyzed based on the data obtained by GprMax software which is widely used and is representational for the GPR data simulation. Simulation results demonstrate the echoes obtained by the proposed method can reflect the actual situation and the new method has better performance than that based on the constant-Q attenuation model.

Adaptation in Front of Ground Penetrating Radar (GPR) Antenna by Layered Dielectric Slab and Resistive Loading

Y. Wahyu[1], **R. S. Sianipar**[2], **A. Kurniawan**[3], **Sugihartono**[3], **and A. A. Lestari**[4]

[1]Research Center for Electronics and Telecommunication-LIPI, Indonesia
[2]Radar and Communication Systems (RCS)-Solusi247, Indonesia
[3]School of Electrical Engineering and Informatics, Bandung Institute of Technology, Indonesia
[4]IRCTR, Delft University of Technology-Indonesia Branch, Indonesia

Abstract— One possibility for adaptation in front of the GPR antenna is attached dielectric layered slab between the antenna and ground are illustrated in the Figure 1. The purpose of this approach to create the optimal transition of electromagnetic waves spreading from the antenna into the ground so that the antenna is not sensitive to the presence of soil.

In the GPR antenna systems play an important role, because the general performance of the GPR using impulse radar is determined by the ability of impulse radiating antenna to the ground with the loss and minimum distortion. This means that the impulse GPR antennas must be able to minimize late-time ringing. Resistive loading is used to overcome these internal reflection. Reflections from the medium field boundary can not be avoided in GPR antennas. These reflections lead to a successful energy transmitted into the medium becomes smaller. To minimize this reflection is used dielectric layer transition from the antenna to the medium. By using this dielectric layer is expected amplitude of the signal to the medium is higher.

The proposed GPR antenna is dipole antennas with resistive loading and the dielectric layer. Use no other dipole antenna because a dipole antenna is often used for GPR applications mainly because of its simplicity.

Apart from amplitude, should also be noted the level of ringing. A good antenna has a small ringing level. Therefore, in this simulation is used resistive loading. With resistive loading is expected to wave reflection from the end of the antenna can be reduced. So with the imposition of resistive and dielectric layers are expected to signal that is transmitted to the medium has a low ringing level and also has a high amplitude. Of the overall simulation above can be seen that with the addition of resistive loading can suppress ringing the desired level. The addition the dielectric layer will increase peak to peak main pulse amplitude but will also raise the level of ringing. In terms of input impedance and VSWR, resistive loading can make the resulting input impedance is more flat. The addition of the proposed dielectric layer does not change the form input impedance and VSWR as a whole produced but will shift the graph is approximately 100 MHz to the lower frequencies. Ringing level generated by the linear-profile dielectric layer is not able to meet the high-resolution GPR applications that require ringing level is less than 1% (−40 db).

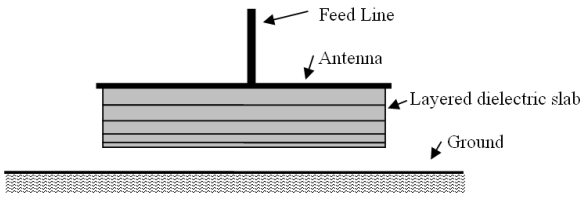

Figure 1: GPR antenna by layered dielectric slab.

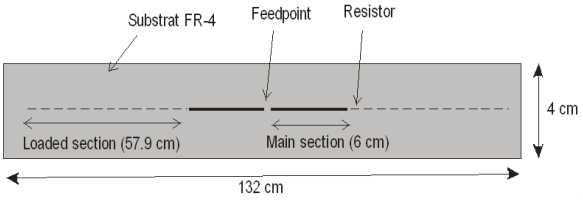

Figure 2: Geometry of dipole by resistive loading.

Consideration of Antenna Pattern Design for FY3 Precipitation Measurement Satellite Dual-frequency Precipitation Radar

Honggang Yin[1] **and Xiaolong Dong**[2]

[1]National Satellite Meteorological Center, China
[2]Center for Space Science and Applied Research CAS, China

Abstract— China suffered from great damage caused by Typhoon almost every year. Hard rain accompanying with Typhoon is one of the primary factors which lead to disaster. Since Typhoon and other tropical cyclone are over sea during much of their life cycle, there is only the spaceborne radar that can measure their three dimensional structure. A prototype of dual-frequency precipitation radar (DPR), which will be the major payload of the FengYun-3 Precipitation Measurement Satellite (FY3 PMS), is being developed in China. This radar will be used to observe Typhoon rain and other types of precipitation, such as stratiform rain, snow and so on. In the case of spaceborne precipitation radar, the rain volume is proximate to the Earth's surface, the backscattered echo of which, especially for the sea surface echo, is much stronger than the rain echo. When rain rate is 0.5 mm/h, for example, typical value of the power ratio of the returned signal from precipitation to the returned signal from sea surface for a precipitation radar with frequency of 13.8 GHz is −35 dB∼−55 dB. The received rain echo may be masked or contaminated by the serious sea clutter through antenna beam. Therefore the sea clutter must be considered for the design of performance parameters for the FY3 DPR. In this paper, the model of sea clutter interference with precipitation measurement of the FY3 DPR is built, the effect of sea clutter on the design of the antenna radiation pattern are analyzed in detail. Based on the analysis of surface clutter, the requirements for antenna beam width and radiation sidelobe level are proposed.

A Millimeter-wave Interferometric Radiometer for Atmosphere Observation from Geostationary Orbit

Ailan Lan, **Shengwei Zhang**, **Hao Liu**, **Jingye Yan**, **and Ji Wu**
Center for Space Science and Applied Research, Chinese Academy of Sciences, China

Abstract— A millimeter wave interferometric radiometer used to detect atmospheric temperature from geostationary orbit is being developed in Center for Sapce Science and Applied Research, CAS. Geostationary meteorological satellite has characteristics of large spatial coverage and timeliness. It can obtain the whole dynamic process of convective weather whose typic life cycle is about 6 hours. On the other hand, the interferometric radiometer uses array antenna to avoid using a large antenna aperture and complicated mechanical scanner in contrast with a real aperture radiometer on a satellite platform. In addition, comparing with visible light and infrared, millimeter wave has the advantage of all-weather and all-day observation. Therefore, using a millimeter wave interferometric radiometer to observe atmospheric temperature from geostationary orbit can improve the detecting ability of meteorological satellite.

In this paper, the objectives of the radiometer are introduced briefly at first. In the second section, the major system parameters and application indices are listed. According to four important performance indices including spatial angular resolution, radiometric sensitivity, aliasing-free field of view and image refresh period, the required number of antennas is estimated. In third section, the design scheme of interferometric radiometer is outlined. The system can be divided into four parts: antenna, mm-wave receiver, wide band quadrature IF receiver and high speed digital system. In this section, the design schemes of the four parts, in particular antenna, are stated in detail. Typical thinned array antenna using in interferometric radiometer, such as Y type and T type, is stationary. However, time-sharing sampling method in this system is used, which can decrease the number of antenna units and improve imaging resolution of the system by shifting the antennas completely or respectively.

Forward Modeling of Direct Current Method Based on ANSYS

Dong-Feng Zhang
Institute of Information Engineering Physics, Central South University, Changsha, Hunan 410083, China

Abstract— In this paper, firstly we have reviewed the developing of numerical methods used in geophysical electric prospecting, and have listed the current state and developing trend of that, then simply have introduced the main characteristics of ANSYS and also mainly have focused on the steps and key problems of using ANSYS to model numerically DC forward problems; Secondly, based on the differential control equations of voltage potential of point current field, we have introduced the boundary value problem and the variational problem (involved in 2 dimension and 3 dimension); based on secondary development of APDL language raised in ANSYS, we have modeled lots of geophysical models, and we have got same perfect results by analyzing the results of numerical modeling; Lastly, we have achieved the proof that is the ANSYS can be used in geophysical electric modeling with high accuracies.

At the end, we have presented the suggestion that ANSYS can be widely used in geophysical forward modeling with valuable applications.

Micro-motion Simulation and Micro-Doppler Extraction

Ning Chao and Huang Jing
National Key Lab. of Target and Environmental Electromagnetic Scattering and Radiation
Beijing 100854, China

Abstract— Micro-motion such vibration and rotation induces Doppler modulation which is called micro-Doppler effect. We simulate micro-motion with a metal cone model and measure it in anechoic chamber by X band radar. The model simulates two kinds of motion, spinning rotation and coning rotation. The measurement of micro-motion model is completed in the anechoic chamber. Two types of data are obtained: data in narrow-band radar and data in wide-band radar. By processing the narrow-band data, micro-motion period could be estimated by several methods. In the paper, some improvement on the autocorrelation algorithm is presented, which will make the algorithm progress faster. Time-Frequency (T-F) transforms are tools to analyze the micro-Doppler modulation. Short time Fourier transform (STFT) is one of T-F transforms. A new method for confirming the dwelling time of STFT is given. The comparison between STFT and Smooth Pseudo Wigner-Ville distribution (SPWVD) is illustrated in the paper, although joint-time-frequency resolution of STFT is not exact enough, STFT still has great advantage of speed and can be used in the case of real time data processing. Hough transform is a technique to feature extract which can be applied in T-F diagram analysis. Some micro-Doppler characteristics are extracted by Hough transform. By processing the wide-band data, a series of one dimension high resolution range profiles (HRRP) along with time could be obtained. Using the methods of T-F transforms and Hough transform, some micro-Doppler characteristics are extracted from HRRP data.

An Integration of Electronic System and Some Solutions to Its Key Point

Yanhong Hao and Jiali Wang
School of Electromechanical Engineering, Xidian University, Xi'an 710071, China

Abstract— With the development of electronic technology, it becomes more and more complex and functional. It tends to an development of PHM system. The paper gives an integration of PHM (Prognostic and Health Management/Monitoring) system as a whole, and an elaborate description of it as well. Because every module of the PHM system is designed for special purpose, it becomes necessary to implement every part concretely, and proper algorithm may be in use. As the uncertainty of data source is one of its key point to PHM technology, the paper presents a BP network data fusion algorithm to reduce this uncertainty. It has voltage test pattern, temperature and energy as its sensors' inputs.

Laser Pulse Scattering from a Moving One Dimensional Rough Surface

M.-J. Wang[1], **Z.-S. Wu**[2], **J.-D. Xu**[3], **and Y.-L. Li**[1]

[1]Institute of E. M. Wave Propagation & Scattering, Xianyang Normal College
Box 103, 712000, China
[2]Science School, Xidian University, Box 273, 710071, China
[3]The Electronic Information Institute, Northwestern Polytechnical University
Xi'an, Shaanxi 710072, China

Abstract— Based on the Kirchhoff's approximation, analytical expressions for pulse scattering mutual coherence function (MCF) from moving rough random surface are presented. It is computed the Double Frequency Scattering Section (DFSS) change with the coherence bandwidth frequency difference and scattering angles in different incident angles incidence on laser (1.06 μm) according to the mean of fluctuating heights and the semi-sphere reflectivity of the plating gild rough polyester moving film surfaces. Some important scattering characteristics of calculations based on the analytical solutions are be discussed in details.

ACKNOWLEDGMENT

This works is supported by the National Natural Science Foundation of China (Grant No. 60801047, 60771038) and the Natural Science Foundation of Shaanxi Province Education Office, China (Grant No. 08Jk480).

Hilbert Transform for Processing of Laser Doppler Microvibration Signals

Ying-Li Wu, **Zhen-Sen Wu**, **Yan-Hui Li**, **and Ping-Zhou Li**
Xidian University, Xi'an, Shaanxi 710071, China

Abstract— Given the laser doppler signal model of the solid target microvibration. When the model of harmonic signal is narrow-band signals, based on Hilbert Transform, the laser doppler vibration instantaneous samples can be conversion into signal spectra samples. By the spectral method, the mean value of the instantaneous frequency per the vibration period can be determined. Further more, the value of frequency can be got by the quadratured procession of the difference samples squence. The amplitude is can be estimated according to relation with frequency deviation of vibration signal. In the end experimental results can be verified according to the measuring method. The results is satisfied.

A Study of Deformation Monitoring Using StaMPS Technique

Huan-Huan Liu[1, 2], **Jian-Ping Chen**[1, 2], **Hong-Li Zhao**[1, 2], **Jing-Hui Fan**[3], **and Xiao-Fang Guo**[3]

[1]School of the Geosciences and Resources, China University of Geosciences (Beijing), Beijing 100083, China
[2]Beijing Land Resources Information Development Research Laboratory, Beijing 100083, China
[3]China Aero Geophysical Survey & Remote Sensing Centre for Land & Resources, Beijing 100083, China

Abstract— Although PSInSAR (permanent scatter InSAR) is possible to avoid many of the limitations of conventional DInSAR by only analyzing pixels, which behave like point scatters and retain some degree of correlation, in almost all its previous algorithms, an initial set of PS pixels using amplitude variation doesn't work very well in non-urban areas, and the approximate temporal model for deformation required to refine PS, estimate and remove nuisance terms, which is complicated and also the aim of study, is usually assumed to be approximately constant in rate, or periodic in nature.

Stanford Method for PS (StaMPS) is a new PS method developed at Stanford University by Andy Hooper et al., which uses spatial correlation of interferogram phase to find a network of stable pixels in almost all terrain without prior knowledge of temporal variations in the deformation. In this paper, StaMPS is applied to monitor the substance in Tianjin area and landslide in Xintan, using ENVISAT ASAR images, SRTM DEM and DEOS precise orbits. 14 SLCs for Tianjin cover from Oct. 2003 to Dec. 2005, and 30 SLCs for Xintan from Aug. 2003 to Dec. 2007. The processes for both of the areas with adjusted methods and parameters can be divided into 2 sections:

In the first section, the master image is chosen as it maximizes the sum correlation of all interferograms and Doris (Delft Object-oriented Radar Interferometric Software) is used to process SLCs from reading parameters and raw data, obtaining precise orbits, coarse and fine coregistration, resampling slave SLCs, interferograms formation, estimating and subtracting the reference phase of the ellipsoid and DEM to geocoding. In coregistration, only master-slave pairs with baseline less than a specified maximum are directly coregistered, while the other slave scenes are coregistered to the 3 nearest slave scenes closer to the master, and the resulting coefficients are estimated by weighted least-squares inversion.

The second section concludes PS identification, PS selection and displacement estimation. An optional initial set of PS candidates is selected, whose amplitude dispersion are lower than a input threshold. Then the PS pixels are refined in an iterative process by estimating its phase variation measure. After that, PS pixels which appear to be persistent only in certain interferograms and seemed to be dominated by scatters in adjacent pixels or deemed too noisy are rejected based on their PS probability, which is calculated by both the amplitude dispersion and phase variation measure. After the selection of PS, the wrapped phase of PS pixels is corrected for spatially-uncorrelated look angle error and unwrapped by a pseudo-3D method. Then spatially-correlated look angle (SCLA) error and master atmosphere and orbit error(AOE) phase is estimated, and the other spatially correlated noise is estimated and removed by low-pass filtering in time and space. The unwrapping accuracy can be further improved by redo phase unwrapping after subtracting SCLA, AOE phase in an interactive way until the unwrapped result becomes stable and reliable.

At last we got relatively satisfactory results showing the distribution and relative values of the deformation in the two areas. As we can see in this paper that by using StaMPS, it is easy to got satisfying result in urban area, and relatively rational results in non-urban area with irregular surface deformation can also be gotten with proper input parameters, the next step is to assess the influences of some crucial input parameters respectively and synthetically. Besides a real 3D phase unwrapping method is needed to be actualized.

Global Land Surface Temperature and IR Spectral Emissivity Monitoring Using Current and Future Satellite Measurements

Daniel K. Zhou
NASA Langley Research Center, Hampton, VA 23681, USA

Abstract— Surface and atmospheric thermodynamic parameters are essential to general atmospheric and Earth science research, climate monitoring, and weather prediction. Surface emissivity and skin temperature retrieved from the current and future operational satellites can and will reveal critical information on the Earth's ecosystem and land surface type properties, which can be utilized as part of long-term monitoring for the Earth's environment and global climate change. Ultraspectral resolution infrared radiances obtained from nadir observations provide atmospheric, surface, and cloud information. The Infrared Atmospheric Sounding Interferometer (IASI) on the MetOp satellite was launched on October 19, 2006. Presented here is the global land surface IR spectral emissivity retrieved from IASI measurements under "clear-sky" conditions. Retrieval methodology is presented and rapidly retrieved surface emissivity spectra are initially evaluated through quality control checks on the retrievals of other impacted atmospheric and surface parameters. Seasonal products of global land emissivity (i.e., monthly mean with a scale of 0.5×0.5 degrees of latitude-longitude), over an annual cycle, are used to demonstrate the capability of current operational satellite instrument in monitoring for the Earth's environment. The NPOESS Cross-track Infrared Sounder (CrIS) on the future NPP and NPOESS satellites will fulfill the observational needs for accurate weather prediction. Since IASI spectral bands cover CrIS bands with a higher spectral resolution and the noise level is equivalent at CrIS spectral resolution, IASI measurements are used to generate proxy data for CrIS. Initial retrieval performance based on these proxy data is presented.

Amazon Forests Did Not Green up during the 2005 Drought

Arindam Samanta[1], **Sangram Ganguly**[1], **Hirofumi Hashimoto**[2], **Sadashiva Devadiga**[3], **Eric Vermote**[4], **Yuri Knyazikhin**[1], **Ramakrishna R. Nemani**[5], **and Ranga B. Myneni**[1]

[1]Department of Geography and Environment, Boston University
Boston, MA 02215, USA
[2]Department of Science and Environmental Policy, California State University
Monterey Bay, Seaside, CA 93955, USA
[3]Science Systems and Applications, Inc., NASA Goddard Space Flight Center
Mail Code 614.5, Greenbelt, MD 20771, USA
[4]Department of Geography, University of Maryland, College Park, MD 20742, USA
[5]Biospheric Science Branch, NASA Ames Research Center
Moffett Field, CA 94035, USA

Abstract— The sensitivity of Amazon rainforests to dry-season droughts remains unresolved with reports of enhanced tree mortality and forest fires, on one hand, and, excessive forest green-up, on the other. Here using the latest and improved version of satellite-derived vegetation greenness data — Collection 5 (C5) Enhanced Vegetation Index (EVI) — we report that the there is no evidence of large-scale greening of the Amazon during the 2005 drought — approximately 11%–12% of these forests display greening, while, 28%–29% show browning or no-change, and for the rest the data are not of sufficient quality to characterize any changes. In addition, independent satellite-derived data on precipitation, surface radiation and aerosols do not substantiate underlying assumptions of the hypothesis of enhanced photosynthetic capacity of intact Amazon forests stimulated by increased light availability during a drought. First, interannual changes in dry-season greenness are unrelated to concurrent changes in light availability. Second, the 2005 drought cannot be used as a surrogate for light availability to these rainforests owing to persistently high aerosols loads in the atmosphere. Third, the spatial extent and magnitude of greening do not change systematically with drought severity. Finally, the changes in vegetation activity of these forests during the drought-stricken dry season of 2005 are not unique in comparison to that observed during dry seasons of non-drought years. Our analysis also demonstrates the critical role of biomass burning aerosols in limiting light availability to water stressed Amazon forests during the dry season of 2005. This will have important implications for the sensitivity of these forests to similar droughts in future.

Compact Dual-band Balanced Handset Antenna for WLAN Application

A. G. Alhaddad[1], **R. A. Abd-Alhameed**[1], **D. Zhou**[1], **C. H. See**[1], **E. A. Elkhazmi**[2], **and P. S. Excell**[3]

[1]Mobile and Satellite Communications Research Centre, University of Bradford, UK
[2]The Higher Institute of Electronics, Bani Walid, Libya
[3]Centre for Applied Internet Research, Glyndwr University, Wrexham, UK

Abstract— Wireless communication has been characterized of the new modern move to make the mobile handsets small and light as possible; without compromising functionality. To miniaturize in line with consumer needs and aspiration and retain multiband functionality, mobile handsets development must be characterized by making all physical components as small as physically possible. The key concerns considered here on the design of antenna systems for small handsets relates to keeping the antenna performance unchanged or improved, even though the antenna size becomes small and reduces the degradation of antenna performance caused by the operator's adjacent effect [1]. A balanced structure is a genuine choice to avoid the aforementioned degradation of the antenna performance when held by users [2].

A built-in planar metal plate antenna for mobile handsets with balanced operation is presented in this paper. The antenna was designed by folding a thin strip planar dipole with extra arm on each monopole. The antenna features balanced operation, is to reduce the current flow on the conducting surface of the handset body. The antenna design model intends to cover 2.4 GHz and the 5.2 GHz WLAN applications.

The proposed dual-band balanced mobile antenna was achieved to generate another resonant frequency by using a two tier process. Firstly, it was started by folding the monopole arm and having a slot inside each monopole with a cut on the bottom side, as shown Figure 1. Secondly, an additional thin-strip arm was inserted into each arm of the planar dipole. This folded element of the proposed antenna was designed to operate at 2.4 GHz with a single arm to generate the second resonant frequency for 5.2 GHz. The dimensions of the antenna geometry were found comparable to the practical handset sizes. Parametric study has been carried out to optimize the impedance matching bandwidth for the proposed antenna in order to achieve the required resonances at 2.4 GHz and 5.2 GHz for WLAN and short range communication systems. The antenna height (h) was considered to be one of the most sensitive parameters to control the impedance bandwidth of the proposed antenna for meeting the design goals. The optimum value of variable h was found to be 4 mm as shown in Figure 2. By modifying the length and location of the additional arm of the proposed antenna, it was able to let the antenna covers the required two frequency bands at acceptable return loss ≤ -10 dB (see Figure 2).

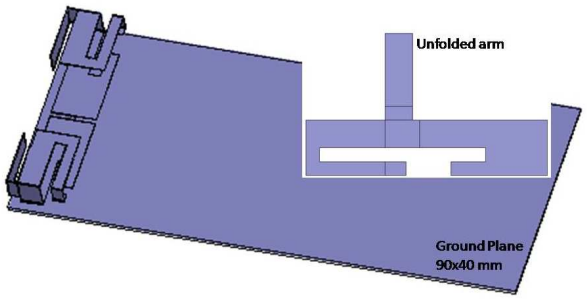

Figure 1: The proposed antenna structure.

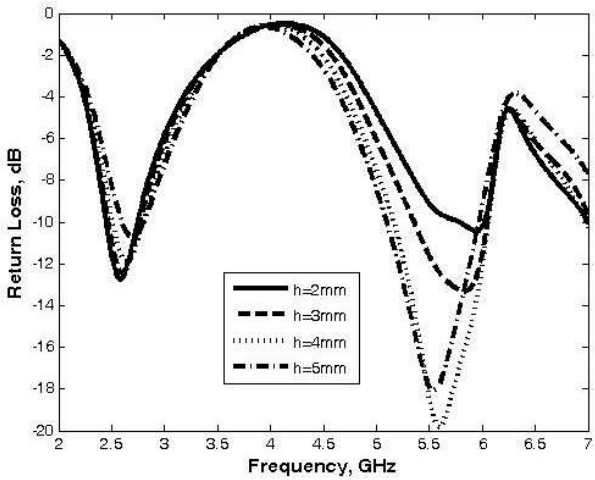

Figure 2: Variation of the parameter h on the effect of return loss.

REFERENCES

1. Morishita, H., H. Furuuchi, and K. Fujimoto, "Performance of balance-fed antenna system for handsets in vicinity of a human head or hand," *IEE Proc. — Microw. Antennas Propag.*, Vol. 149, No. 2, 85–91, April 2002.
2. Abd-Alhameed, R. A., P. S. Excell, K. Khalil, R. Alias, and J. Mustafa, "SAR and radiation performance of balanced and unbalanced mobile antennas using a hybrid formulation," Invited paper, *IEE Proceedings — Science, Measurement and Technology* special issue on Computational Electromagnetics, Vol. 151, No. 6, 440–444, November 2004.

Isolation Enhancement Based on Adaptive Leakage Cancellation

J. Y. Wang[1], **B. Lv**[1], **W. Z. Cui**[2], **W. Ma**[2], **J. T. Huangfu**[1], **and L. X. Ran**[1]

[1]Department of Information and Electronics Engineering, Zhejiang University
Hangzhou 310027, China
[2]Xi'an Institute of Space Radio Technology, Xi'an 710000, China

Abstract— In the direct-conversion architecture, DC-offset may be a big challenge for the system designer, especially when there is some DC information in the received signals. One of the domain origins of DC-offset is the leakage from the transmitter to the receiver, due to the poor isolation between them. Much effort has been taken to cancel this leakage. However, there were always some limitations in the usage of these methods in the past.

In this paper, an adaptive leakage cancellation structure is proposed to improve the isolation performance, with no limitations in the selection of duplexer. The fundamental concept of this structure is to introduce another signal, which has the same amplitude but the opposite phase of the leakage signal. After combined with the signal introduced, the leakage will be cancelled completely in an ideal situation. However, there should be some mismatches in amplitude and phase between the two signals to be combined, which may degrade the performance greatly. This influence has been analyzed in this paper, and a calibration method has also been proposed to improve the performance. The system block is shown in Fig. 1. Both of the variable phase shifter and attenuator are voltage controlled, which can be used to calibrate the mismatches. And a power detector is used to measure the leakage level. The closed-loop architecture is introduced to make the system more adaptive.

An experiment was carried out to improve the isolation of a circulator. And it is believed that, the isolation of a switch and dual antennas can also be improved dramatically by this means.

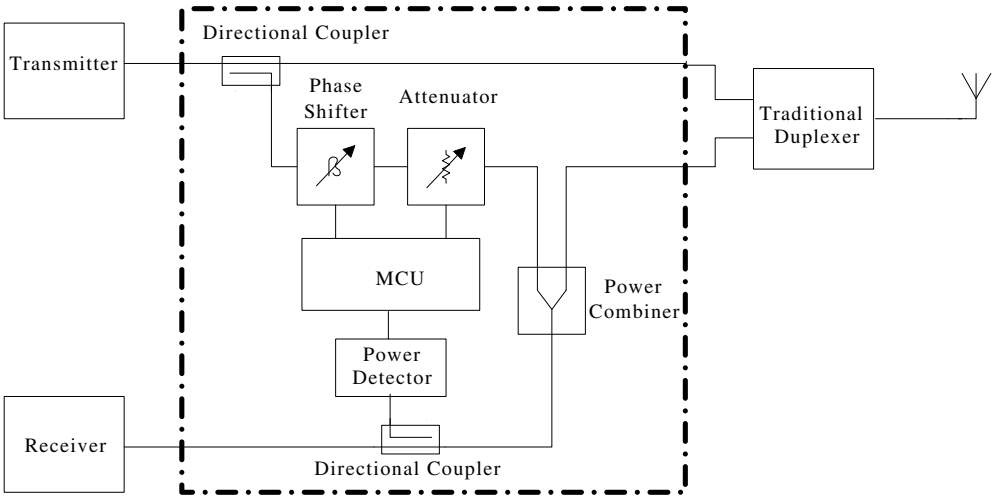

Figure 1: System block of the structure proposed.

Superluminal Phase Velocity in the Dispersive Media

Dexin Ye[1], **Yuhua Wang**[2], **Shan Qiao**[2], **Jiangtao Huangfu**[1], **and Lixin Ran**[1]

[1]Department of Information and Electronic Engineering, Zhejiang University
Hangzhou 310027, China
[2]Department of Information Engineering, Zhejiang University City College
Hangzhou, Zhejiang 310015, China

Abstract— In this paper, we introduce a method to realize superluminal phase velocity of electromagnetic wave which is six thousand times larger than C (C is the speed of light in vacuum) in dispersive uniaxial media.

For the most unartificial media, the phase velocity v_p is always smaller than C (the speed of light in vacuum). In some speical condition, the EM wave can propagate with a larger phase velocity than C such as in the wave guidance. In this case, the phase velocity along the direction of propagation can be superluminal, but the total phase velocity is also smaller than C. So in order to get a real superluminal phase velocity, a kind of media with refractive index smaller than that in vacuum is prerequisite. Theoretical analysis from the k-surface reveals that The EM wave will propagate in plasma media with superluminal phase velocity at a special frequency. So, we design a kind of artificial material called metamaterial instead of plasma media and show by theoretical analysis, simulation and experiments that the phase velocity will be much larger than C at a special frequency.

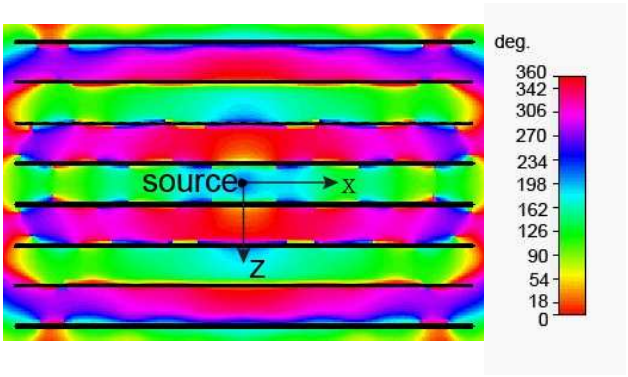

Figure 1: Simulation results of the phase of electric field distribution in the metamaterial slab at the frequency 9.45 GHz.

Microwave Contactless Moisture Measurement for Tobacco

Lingling Jiang, Jiangtao Huangfu, and Lixin Ran
Department of Information and Electronics Engineering, Zhejiang University
Hangzhou 310027, China

Abstract— In the production of tobacco products, the moisture content affects the taste quality greatly, and must be monitored. Chemical moisture sensing is realized on samples collected from the product line and brought into a remote laboratory, which delays the quality control and destroy the product. Thus, a measuring method which is nondestructive and real-time would be more preferable.

Water is found to cause great loss to electromagnetic incident wave. Thus microwave methods are developed to measure the moisture content since 1950s. The method is real-time and cheap. But the microwave measurement is difficult, because the tobacco density varies easily and substantially.

From analysis on observations for tobacco, the density independent technique was invented and developed by previous workers. Based on previous work, here we propose a contactless technique to measure the moisture content of tobacco. Two high directional antennas are used as transceiver systems. The electromagnetic wave was transmitted through air into tobacco material, which is placed on a sheet of high reflected metal, then wave is reflected through air into the receiver. Amplitude and phase of loss factors are measured by transceiver systems. At the same time, we propose algorithm to eliminate the affect of air, and optimal algorithms to accomplish calibration for the density of tobacco.

While the conventional microwave measurement methods needs to form a layer of material of a certain thickness, which implies the contact of the tobacco with some vertical supporting planes, our technique replace it with air and does not need any contact with tobacco, and can be used to bring great improvement to tobacco product lines.

Application of EH4 in the Shihu Gold Deposit of Western Hebei, China

Mingyan Wang[1, 2], **Tagen Dai**[3], **Chaozhuang Xi**[3], **Xiaoming Fu**[3], **and Danyan Huang**[3]

[1]Institute of Mineral Resources of the Chinese Academy of Geological Science, Beijing 100037, China
[2]Department of Mineral Resources, Hunan Non-ferrous Metals Holding Group Co., Ltd
Changsha, Hunan 410015, China
[3]School of Geosciences and Environmental Engineering, Central South University
Changsha, Hunan 410083, China

Abstract— EH4 geophysical systems belong to electromagnetic survey method, the most effective electromagnetic method for metalliferous mineral explorations with high detecting resolution and appropriate depths of penetration. EH4 is widely used in solid minerals, especially in finding concealed ore deposit. In this paper, the author adopt EH4 method to make a synthetic study on Shihu gold deposit in Hebei. The result shows that the geophysical method is quite useful in the exploration of concealed ore deposit.

An Optimized Monopole Microstrip Patch Antenna with Gradual Steps for Ultrawideband Applications

Reza Khalilpour[1], **Javad Nourinia**[2], **and Changiz Ghobadi**[2]

[1]Telecommunication Company of Iran, Iran
[2]Department of Electrical Engineering, Urmia University, Iran

Abstract— In this paper, we propose an optimized ultrawide band antenna for UWB applications. The proposed monopole antenna consists of a patch with complex of gradual increasing and gradual decreasing steps, a single rectangular slot on the patch, and a partial ground plane with special slit with improvement in impedance and good gain bandwidth. Investigations based on experiments and simulations are conducted. The simulation is performed using the commercially available simulation software HFSS 11. The proposed antenna is successfully implemented and the simulated results show reasonable agreement with the measured results. In this design, a 3.2∼14 GHz frequency range for $S_{11} < -10$ dB is obtained. Radiation patterns are also examined.

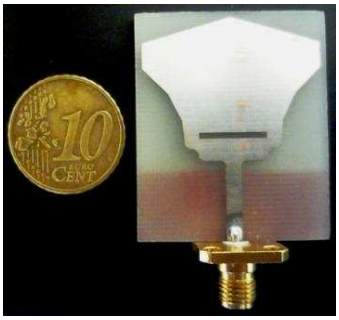

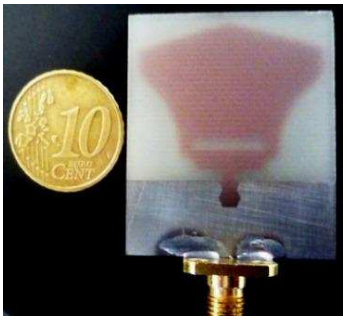

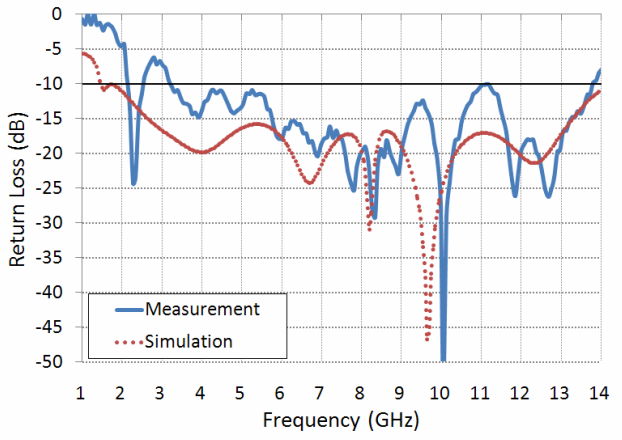

Utilization of Effective Apparent Resistivity in Magnetotelluric Data Processing and Interpretation

Ai-Yong Li, **Jian-Xin Liu**, **Xiao-Zhong Tong**, **Wei Zhang**, **and Chuang-Hua Cao**
School of Info-Physics Geomatics Engineering, Central South University, Changsha 410083, China

Abstract— Effective apparent resistivity is correspondent to the modulus of magnetotelluric response impedance tensor matrix. It is a invariable under the coordinate rotation. Under one dimensional (1-D) condition, It is equal to the normal apparent resistivity ρ_a, when to two dimensional condition, it is the geometry average of apparent resistivity of TE mode (ρ_{TE}) and TM mode (ρ_{TM}), which has the dimensionality reduction property. The parallel moving algorithm can used to do static correction, as effective apparent resistivity curl shape was not affected by the static effect. At the same time, it is irrelative to coordinate rotation, so the inverse deviation can be avoided in the effective apparent resistivity two-dimensional (2-D) inversion, because of the incorrect polarization mode discrimination. So the utilization of effective apparent resistivity in processing and interpretation of the magnetotelluric sounding data was recommended.

Research and Application on Supergain Property of Arrays for Target Detection

Zhanlin Xie and Yingmin Wang
Institute of Acoustic Engineering, Northwestern Polytechnical University, Xi'an, China

Abstract— The method of super gain for a column array and its integrate robust beamforming are presented. The upright super-directive array gain of the column array outperforms a lot over that of a conventional beamforming in isotropic noise fields when the inter-element spacings are less than one-half wavelength. It is the phenomenon of super gain at the top direction to line array. At the horizontal direction, the fact of supergain also exists in the circle array of its cross section. However, in practice, the performance of optimum beamforming algorithms are known to degrade if some of underlying assumptions on the sensor array violated. It is impossible to get the theoretic super gain through optimum disposal. Therefore, the integrate super gain of robust beamforming algorithm (ISBA) is used to improve the robustness of supergain beamforming against random errors. Under the inhibit of beamforming weight vector norm, the column array shows great performance at target search and resist disturbance in two dimensions of orientation and depth.

The Study of Directional Couplers Based on Omni-directional Reflection of Photonic Crystal Optical Waveguide

Zhaohong Wang, **Zichen Liu**, **Bo Ning**, **and Chentao Gu**
Department of Electronic Science and Technology, Xi'an Jiaotong University
Xi'an, Shaanxi 710049, China

Abstract— The one-dimensional photonic crystal structures which was composed of two kinds of periodic dielectric material (such as polystyrene-tellurium periodic film, Silicon- silicon dioxide periodic film), has a wide band range of omni-directional reflector. Therefore, the line defects of one-dimensional photonic crystal, optical waveguides, propagate effectively guided optical wave. In this paper, directional couplers based on one-dimensional photonic crystal waveguides is analyzed by time-domain finite difference method (FDTD), and the relationships between the coupling length and coupling efficiency of directional coupler are obtained. When the directional coupler composed of polystyrene-tellurium was spaced $2a$ (a was the period length, which have the same order of magnitude with wavelength), the coupling length, close to 100% of the energy conversion, was $27a$. When the directional coupler composed of Si-SiO_2 was spaced $2a$, the coupling length, close to 100% of the energy conversion, was $19a$. This greatly reduces the length of the coupling, compared with the published photonic crystal waveguide coupler. And the Si-SiO_2 photonic crystal waveguide has the advantages of being compatible with integrated circuits fabrication. Thus, the photonic crystal waveguides can be expected to realize ultra-dense integrated optical circuit.

ACKNOWLEDGMENT

The research has been partially supported by the National Nature Science Foundation of China (60707011).

Discrete Time Synergetic Control for DC-DC Converter

Qian Wang, **Tao Li**, **and Jiuchao Feng**
School of Electronic and Information, South China University of Technology
Guangzhou 510641, China

Abstract— Digital technology has greatly impacted the design of controller for power electronics with the advent of digital signal processors (DSP) and high-performance processors. The synergetic approach to control theory (SACT) is a novel nonlinear control method that the nonlinearities of system are considered in the control design and a systematic design procedure which yields control laws suitable for digital implementation are offered. Moreover, synergetic control not only gives constant switching frequency operation, but also provides asymptotic stability with respect to the required operating modes, invariance to load variations and robustness to variation of converter parameters. Although the synergetic control is widely utilized in various fields, these synergetic controllers are all continuous-time.

In this paper an alternative discrete-time extension of the SACT design procedure is at first provided, which can not be obtained from its continuous counterpart by means of simple equivalence. The discrete-time extension of the SACT procedure is used to design and implement a SACT controller for buck converters. The performance of the discrete-time SACT controller for this application is compared with that of a conventional Proportional-Integral-Differential (PID) controller through the input voltage step test and the step load test on Simulink. In particular two modified control laws are introduced to avoid transient overshoot, reduce steady-state error and obtain fast transient response. Further, the two controls are evaluated by comparison with the first simple discrete-time synergetic controller.

Novel Optical Signal Processing Using Free Carrier Effect in Silicon

Yukio Iida and Norimitsu Wakama
FSC, and Dept. of Electric and Electron Eng., Faculty of Engineering Science, Kansai University, Japan

Abstract— Computer-generated holograms and digital holography are studied [1, 2]. These combine the digital signal processing on computer and with past holography. On the other hand, The single-mode silicon optical switch with T-shaped SiO_2 optical waveguide as a control gate is proposed [3]. In this report, the optical signal processing using free carrier effect in silicon is studied, and novel optical processing method is proposed.

REFERENCES

1. Matsushima, K., "Computer-generated holograms for three-dimensional surface objects with shade and texture," *Applied Optics*, Vol. 44, 4607–4614, 2005.
2. Matsushima, K., "Formulation of the rotational transformation of wave fields and their application to digital holography," *Applied Optics*, Vol. 47, D110–D116, 2008.
3. Kobayashi, H., Y. Iida, and Y. Omura, "Single-mode silicon optical switch with T-shape SiO_2 waveguide as n control gate," *J. Appl. Phys.*, Vol. 41, 1, No. 4B, 2563–2565, Apr. 2002.

Novel Optical Neuronal Cell and Data Recognition-generation Circuits in RFID Tags

Norimitsu Wakama and Yukio Iida
FSC, and Dept. of Electric and Electron. Eng., Faculty of Engineering Science
Kansai University, Japan

Abstract— The optical neuronal cell composed of silicon structure is studied, and novel cell is proposed.The circuits that recognizes tag call signal and generates the sending data using the analog threshold element with a nonlinear characteristic are also studied.

The research to model animals of the higher orders' nervous systems of the sight by composing the analog threshold element with a nonlinear characteristic in multilayer has been conducted [1, 2]. Recently, there are many reports from two dimension pattern recognition viewpoint though an active research is performed. In addition, single-mode silicon optical switch with T-shaped SiO_2 optical waveguide as a control gate is proposed [3]. In this paper, the neuronal cell composed of silicon waveguide and electronic active elements is studied, and novel neuronal cell is proposed. The electron-hole pairs generated by illumination with short-wavelength light are used here.

On the other hand, RFID (radio frequency identification) technology has fast been noticed and has a great many possible applications [4]. We are proposing the RF recognition system to communicate by using faint radio wave with a little power consumption [5, 6]. In this paper, the circuit that recognizes the tag call signal and the sending data generation circuit by using the analog threshold element with a nonlinear characteristic are studied. It is thought that this is effective to making it to small electric power or more.

REFERENCES

1. Fukushima, K., "Feature extraction by multi-layered network of analog threshold elements," *IECE Trans.*, Vol. 51-C, No. 7, 319–326, 1968.
2. Watanabe, O. and K. Fukushima, "A neural network model of near and far cells," *IEICE Trans.*, Vol. J79-D-11, No. 9, 1404–1413, Sept. 1995.
3. Kobayashi, H., Y. Iida, and Y. Omura, "Single-mode silicon optical switch with T-shape SiO_2 waveguide as N control gate," *Jpn. J. Appl. Phys.*, Vol. 41, Part 1, No. 4B, 2563–2565, Apr. 2002.
4. Finkenzeller, G. K., *RFID Handbook, Radio-frequency Identification Fundamentals and Applications*, John Wiley & Son, Chichester, 1999.
5. Iida, Y., "Proposal of RF recognition system prepared for demand expansion and use of super-regenerative circuit," *Proceedings of 2007 IEICE Society Conference*, B-5-88, Japan, Sept. 2007.
6. Iida, Y., "Novel super regenerative transponder (SRGT) for RFID tags and ASK signals," *PIERS Proceedings*, 551–554, Beijing, China, March 23–27, 2009.

3-D Analysis of Magnetic Flux Density in Modular Toroidal Coil Using Cubic Meshing

M. R. Alizadeh Pahlavani, A. Shiri, and A. Shoulaie
Department of Electrical Engineering, Iran University of Science and Technology (IUST), Tehran, Iran

Abstract— Recent research work in the area of plasma reactors (e.g., Tokamak), Superconductor Magnetic Energy Storage (SMES), and nuclear fusion reactors have studied different coils. Tokamak reactors consist of coils with different structures, such as the modular toroidal, the helical toroidal, the solenoidal, and the poloidal coils as seen in Fig. 1. The capability of modular implementation of the modular toroidal coil (MTC) is one of the main advantages of this coil over the helical toroidal coil. Considering that the MTC has been studied less than other coils, in this paper the MTC is mathematically modeled and analyzed. Since the optimal design of the MTC with different objective functions such as the maximization of the stored magnetic energy, the minimization of the leakage flux, the stabilization of Tokamak reactors, and the elimination of stress requires anaccurate calculation of the inductances of this coil, in this article we first derive the mathematical equations of this coil. The structure of this coil is shown in Fig. 1. As it is observed, this structure is composed of S solenoid coils (SCs) connected in series distributed in the toroidal and the symmetrical form. In this figure, S is assumed to be equal to 8. In this paper, equations for calculation of the 3-D magnetic flux density of the Modular Toroidal Coil (MTC) applicable to Tokamak reactors are presented. These equations are based on the Biot-Savart equation. The numerical analysis of the integrations resulting from these equations is solved using the extended three-point Gaussian algorithm. At the end, the Cubic Meshing approach is employed to present an algorithm to study the three dimensional leakage flux distribution pattern of the coil and to draw the magnetic flux density lines of the MTC. The presented algorithm, due to its simplicity in analysis and ease of implementation of the non-symmetrical and three dimensional objects, is advantageous to the commercial software such as ANSYS, MAXWELL, and FLUX.

In this paper, an appropriate coordinate system is presented to simplify the mathematical equations, the longitudinal components of the rings element of each SC in this coordinate system are introduced, and the relations between the geometrical parameters of the K^{th} SC with the geometrical parameters of the rings located in the same coil are derived. Also, based on the Cubic Meshing approach a new algorithm is presented to compare the magnetic flux density lines of the MTC for $S = 4$ and $S = 8$.

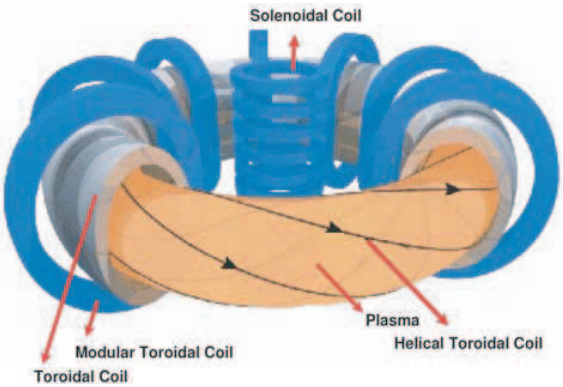

Figure 1: A typical Tokamak reactor.

Electromagnetic Force Distribution on Cylindrical Coils' Body

A. Shiri, M. R. Alizadeh Pahlavani, H. A. Mohammadpour, and A. Shoulaie
Department of Electrical Engineering, Iran University of Science and Technology, Tehran, Iran

Abstract— In this paper, the electromagnetic force distribution on the cylindrical coils' body is evaluated. In designing cylindrical coils in many applications, distribution of the electromagnetic force on the various parts of the coils should be determined. To accomplish this, a method which has recently been developed by authors is employed. The advantage of the proposed method is that just by having the external dimension of the coil and its number of turns, the force on different parts of the coil can be calculated.

Suppose a coil with the turn number of N shown in Figure 1, where r_0 is the inner radius, b is the radial thickness and a is the height of the coil.

As seen in Figure 1, the cross-section of the coil is divided into several segments. In this figure, the coil is divided into $n_r \times n_a$ cells. To calculate the distribution of the force on the different parts of the coil, the force between different filaments (in Figure 1, each filament is specified with two cells in both sides) of the coil is calculated and then added together. The force between filaments j and l is calculated as follows:

$$f = a_z \left(\frac{\mu_0 \, i^2 \, z_{jl} \, k}{2\sqrt{r_j r_l}(1-k^2)} \right) \left[\left(1-k^2\right) K(k) - \left(1 - \frac{1}{2}k^2\right) E(k) \right] \tag{1}$$

In the above equation, r_j and r_l are the radii of the filaments j and l, respectively, z_{jl} is the center to center distance of the two filaments. The current of each filament is supposed to be concentrated on its center, and the current density of the entire coil is supposed to be uniform, and i, which could be calculated using the following equation, is the current of each filament in the coil:

$$i = \frac{NI}{n_r \times n_a} \tag{2}$$

In the above equation, I is the current of the coil.

According to the results obtained, the maximum stress is exerted on the edge parts of the coil at two ends. Thus, it is necessary to sufficiently support those parts of the coil in any application.

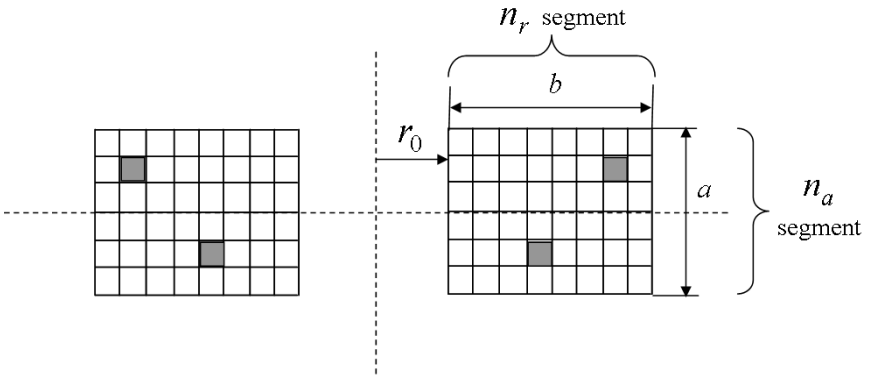

Figure 1: Division of the coil to different meshes to calculate the force distribution.

Magnetic Flux Density Analysis of Helical Toroidal Coil Using Finite Element Approach

M. R. Alizadeh Pahlavani, **A. Shiri**, **H. A. Mohammadpour**, **and A. Shoulaie**
Department of Electrical Engineering, Iran University of Science and Technology (IUST), Tehran, Iran

Abstract— Recent research work in Superconducting Magnetic Energy Storage (SMES) systems, nuclear fusion reactors, and the plasma reactors such as the Tokamak has suggested the use of an advanced coil with a helical toroidal structure. The main reason for this suggestion is the ability to implement special target functions for this coil in comparison with other structures such as the toroidal, the solenoid, and the spherical coils. The structure of this coil is displayed in Figure 1. In this coil, the ratio of the major to the minor radius ($A = R/a$), the number of turns in a ring (N), and the number of rings in a layer (υ) are called aspect ratio, poloidal turns (or the Pitch number), and helical windings, respectively. For example the coil in Figure 1 is composed of five helical windings ($\upsilon = 5$) with nine poloidal turns ($N = 9$). The inductance formulas show that parameters a, R, and N of the helical toroidal coil can be used as design parameters to satisfy special target functions. With respect to the fact that each ring of the coil generates both toroidal and poloidal magnetic fields simultaneously, the coil can be regarded as a combination of coils with toroidal and solenoid fields.

In general, any simulation program that simultaneously solves equations the particle position and its velocity can be called a Particle-in-Cell (PIC) simulation. Inside the plasma community, PIC codes are usually associated with solving the equation of motion of particles with the Newton–Lorenz's force. Usually, the numerical methods based on the PIC simulation are obtained from the solution of partial differential-algebraic equations, for example, by the Fourth-order Runge-Kutta method. Considering the number of the particles which are of order of 10^{10}, the simulations based on PIC methods take long time to solve the above equations. Usually, in order to resolve the time issue in PIC methods, special computers may be employed. On the other hand, this paper used Biot-Savart equation and the mathematical equations of the current path in the conductor of the helical toroidal coil in order to obtain the magnetic flux density components. The numerical integrals resulting from the Biot-Savart equations are solved using the extended three point Gaussian algorithms. This method has the least error among all numerical integration methods. Also, the method used by the authors, contrary to the PIC method, does not need any special computers to solve the equations.

In this paper, analytical equations for calculation of the magnetic flux density components of the Helical Toroidal Coil (HTC) are presented. The numerical analysis of the integrations resulting from these equations is solved using the extended three-point Gaussian algorithm. Comparing the results obtained from the numerical simulation with the particle in cell results confirms the presented equations. At the end, the Finite Element (FE) approach is employed to present an algorithm to study the three dimensional leakage flux distribution pattern of the coil and to draw the magnetic flux density lines of the HTC. The presented algorithm, due to its simplicity in analysis and ease of implementation of the non-symmetrical and three dimensional objects, is advantageous to the commercial software such as ANSYS, MAXWELL, and FLUX.

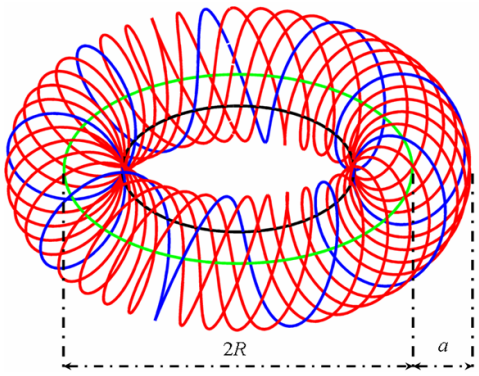

Figure 1: The structure of a monolayer helical toroidal coil with five rings of nine turns.

Session 3P1
Remote Sensing of the Earth, Ocean, and Atmosphere

Numerical Simulations and Analysis of Electromagnetic Scattering from a PEC Target below a Two-layered Dielectric Rough Surfaces: Vertical Polarization

A.-Q. Wang, L.-X. Guo, and C. Chai
School of Science, Xidian University, Xi'an, Shaanxi, China

Abstract— It is significant to study the electromagnetic (EM) scattering from multilayered rough surfaces and the interactions between target and multilayered surfaces in the region of detecting the landmines, pipes, or other buried targets in the soil, and so on. In this paper, to analyze the properties of EM scattering from a target located below a two-layered rough surfaces, the method of moments is introduced and combined with the bi-conjugate gradient method to solve integral equations. A model of two-dimensional perfectly electric conducting (PEC) cylinder and a stack of two one-dimensional rough surfaces separating homogeneous medium is set up. Gaussian rough surface is applied to simulate the realistic rough surface. The incident wave is considered in the vertical polarization. And the tapered wave is used to avoid the artificial edge diffraction due to the finite length of the Monte Carlo simulations. The integral equations of EM scattering from a PEC target located below a two-layered dielectric rough surfaces are provided in this paper. The discrepancies of EM scattering from two-layered rough surfaces only and a target below a two-layered rough surfaces are shown. The bistatic scattering coefficient is calculated. Emphasis is put on discussing the influences of cylinder and surface parameters, such as the radius and altitude of the cylinder, the root mean square (rms) height and correlation length of the Gaussian rough surfaces, the relative permittivity of the mediums, as well as the average height between the two rough surfaces on the bistatic scattering coefficient. It is necessary to note that the work in this paper is just a preliminary research for calculating the EM scattering from a PEC target below a two-layered dielectric rough surface under vertical incidence. The integral equations of this composite model for horizontal case are different from these equations provided in this paper but can be derived similarly.

ACKNOWLEDGMENT

This work was supported by the National Natural Science Foundation of China (Grant No. 60971067) and by the Specialized Research Fund for the Doctoral Program of Higher Education, China (Grant No. 20070701010).

Design and Development of a Ground-based Microwave Radiometer System

Yu Zhang[1, 2], **Jieying He**[1, 2], **and Shengwei Zhang**[1]

[1]Center for Space Science and Applied Research, Chinese Academy of Sciences, Beijing 100190, China
[2]Graduate University of Chinese Academy of Science, Beijing 100190, China

Abstract— This paper presents the design and development of a ground-based microwave radiometer system for the offshore oil platform. It will be used to provide long time series of geophysical parameters such as the sea-surface temperature, the near-surface wind speed and the sea ice type. The ground-based microwave radiometer is a five-frequency, dual-polarized microwave radiometer which is a total power type microwave radiometer based on a heterodyne receiver. It operates at 6.8 GHz, 10.7 GHz, 18.7 GHz, 23.8 GHz and 37 GHz, respectively.

The scanning mode adopts circular scan in a vertical plane. During each period, two-point calibration is performed to calibrate the receiver gain and noise. The antenna beam directs different angles and the blackbody used in calibration to obtain measurement data and calibration data.

The ground-based microwave radiometer system consists of three units: antenna and receiver unit, electronic unit and power supply unit. Antenna and receiver unit collects emission from the atmosphere. It is constructed with several RF components, which include voltage-controlled oscillator, high power amplifier, directional coupler, RF switch, band-pass filter, isolators, detectors and mixers. The received signal is down-converted by the double side band mixer to Intermediate Frequency, and then the IF signals are down-converted to Low Frequency by the detector and integrator. The electronic unit digitizes the LF signal, controls the scanning mechanism and measures physical temperature of the hot target for calibration, and takes charge of communication with a remote computer. The power supply unit performs DC/DC conversion, distributes the DC lines to various sub assemblies and switches.

In paper, the basic principle and technical specifications of microwave radiometer will be briefly introduced, and the block diagram and detail design parameters of the proposed system will be described. The system followed radiometer electronics design and achieved exacting stability and accuracy requirements.

Geophysical Parameter Retrievals from Advanced IR Sounders and Their Applications

Jinlong Li and Jun Li
Cooperative Institute for Meteorological Satellite Studies (CIMSS)
University of Wisconsin-Madison
Madison, WI 53706, USA

Abstract— Hyperspectral infrared sounders on the polar orbiting satellites, such as AIRS (Advanced Infrared Sounder and IASI (Interferometer Atmospheric Sounding Instrument), provide unprecedented global information about atmospheric temperature and moisture profiles as well as surface parameters. Retrieving this information from hyperspectral measurements has great challenges, particularly in handling surface emissivity. Inaccurate surface emissivity will result in the large errors in the retrieval of atmospheric temperature and moisture profiles and surface skin temperature. In this study, we have developed a physically based algorithm to retrieve surface hyperspectral IR emissivity spectrum simultaneously along with the surface skin temperature, temperature and moisture profiles with the reasonable accuracy. The results show that simultaneous retrieval method can improve surface skin temperature as well as temperature and moisture profiles retrievals, especially for the boundary layer moisture. We have applied the algorithm to one month AIRS radiance measurements and derived a global hyperspectral surface IR emissivity product by the composite of clear sky single field of retrievals. The spectral and spatial variations of the derived surface emissivity contain very useful information, which reflect the dramatic differences among the different surface ecosystem types classified in International Geosphere-Biosphere Program (IGBP). The long term hyperspectral IR emissivity database will be very useful in the remote sensing and climate community. The application of the retrieved temperature and moisture profiles in hurricane assimilation will also be demonstrated. The results show that the high spatial resolution temperature and moisture retrievals from advanced IR sounders improved the both hurricane intensity and hurricane path forecasts.

Relationship between Lightning Discharges and Rapid Changes in Cross Polarization Discrimination of the Ka-band Satellite Radio Signal

Yasuyuki Maekawa
Osaka Electro-Communication University, Japan

Abstract— In satellite communication links, degradation of cross-polarization discrimination (XPD) of the radio wave is caused by raindrops and ice crystals along the propagation paths. In thunderstorm events, moreover, rapid changes of XPD and cross-polar phase relative to co-polar phase are frequently observed at time intervals of less than 1 sec. These peculiar phenomena are considered to be related to the change of electric field due to lightning discharges as well as the aero dynamical forces of convective air flows. Up to now, however, detailed mechanisms of the rapid changes of XPD and cross-polar phase are not understood very well.

In this study, statistical distributions of the changes of XPD and cross-polar phase are examined using the Ka-band beacon signal observations of Japan's domestic communication satellites which have been conducted for the past 17 years at 1 sec (partly 0.1 sec) interval in Osaka Electro-Communication University. The occurrence times and amplitudes of these changes is then compared with the lightning locations and times provided by the Kansai Electric Company in Osaka area. Also, the distributions of convective clouds are measured by the X-band weather radar system along the propagation path of the Ka band satellite.

The thunderstorm events are observed more than 70 times from 1990 to 2006, and more than 2500 examples of rapid XPD changes are obtained during these years in our university. Note that most of these XPD changes occurred when appreciable radio wave attenuation was not necessarily measured even in Ka band, suggesting the depolarization is primarily caused by ice crystal in relatively higher part of thunder clouds. At the moment of these rapid changes, about two thirds of the examples indicate the decrease in XPD, which means the increase in depolarization of the propagation medium. Also, about two thirds of the examples show the changing direction of cross-polar phases toward −90 deg, which means the decrease in canting angles of ice crystals that possibly caused the depolarization.

These tendencies seem to be comparatively enhanced in the middle stage of each lightning event, in which the clouds may have massive volume as well as more active convection and electrification. The simultaneous X-band radar observations also reveal wider extent of thunder clouds in this stage with intensive occurrence of lightning strokes. The decrease in XPD, on the other hand, may be related to the canting angles of ice crystals in other places around the lightning as well as those near the lightning, since the difference in their canting angles can induce depolarization cancellation just before a lightning discharge. Thus, the measurements of XPD and cross-polar phase of the satellite signals, combined with the radar observations, are shown to be important to understand the electrification process of thunderclouds and consequently to predict the moment of lightning discharges.

Linearization of NDVI Based on Its Relationship with Vegetation Fraction

Zhangyan Jiang and Alfredo R. Huete
Department of Soil, Water, and Environmental Science, University of Arizona
Tucson, AZ 85721, USA

Abstract— The Normalized Difference Vegetation Index (NDVI) is widely used for global monitoring of land surface vegetation dynamics from space. However, it is well documented that the NDVI approaches saturation asymptotically over highly vegetated areas. In this study, a linearized NDVI (LNDVI) is derived by introducing a linearity-adjustment factor, β, into the NDVI equation to improve the linearity of the relationship with vegetation fraction and mitigate the saturation problem encountered by NDVI. The linearity of the LNDVI was demonstrated using a ground-measured data set and a model-simulated data set. Due to its improved linearity with vegetation fraction, this index would provide more accurate monitoring of vegetation dynamics and estimation of biophysical parameters. Since LNDVI can be calculated based only on NDVI data without knowing input reflectances, it is easy to revisit the historical AVHRR NDVI data and generate LNDVI time series back to 1981.

Derive Atmospheric Soundings from Hyperspectral Infrared Radiances in Cloudy Regions

Jun Li, **Elisabeth Weisz**, **and Jinlong Li**
Cooperative Institute for Meteorological Satellite Studies
University of Wisconsin-Madison
Madison, Wisconsin, USA

Abstract— Hyperspectral InfraRed (IR) Sounders such as the Atmospheric InfraRed Sounder (AIRS) onboard NASA's Earth Observing System (EOS) Aqua platform and the Infrared Atmospheric Sounding Interferometer (IASI) onboard the Europe's METOP-A satellite provide unprecedented global hyperspectral IR radiance measurements. These measurements can be used to retrieve atmospheric temperature and moisture soundings with high vertical resolution and accuracy. The AIRS and IASI radiance measurements have been used in the global Numerical Weather Prediction (NWP) models with a positive impact on weather forecast. However, the current assimilation of AIRS and IASI radiances is limited to clear sky conditions. Development of a radiative transfer model accounting for cloud particle absorption and scattering is critical for atmospheric sounding retrieval and assimilating radiances in cloudy sky conditions. A cloudy radiative transfer model has been developed with one effective cloud layer assumption. The analytical Jacobians (derivative of radiance with respect to a variable) for temperature and trace gas profiles, as well as the cloud parameters (cloud-top pressure, cloud particle radius, cloud optical thickness at 0.55 μm) are also derived and used for physical inverse of the IR radiances for soundings as well as cloud properties in cloudy skies. Sounding retrievals from AIRS and IASI in cloudy skies are evaluated with radiosonde observations and European Centre for Medium-Range Weather Forecasts (ECMWF) analysis, while the cloud properties derived from AIRS and IASI are validated with the Cloud-Aerosol Lidar & Infrared Pathfinder Satellite Observations (CALIPSO) data. The sounding results from optically thin cloudy skies are close to that from clear skies.

Calibration and Temperature Retrieval of Improved Ground-based Atmospheric Microwave Sounder

Jie Ying He[1, 2], **Yu Zhang**[1, 2], **and Sheng Wei Zhang**[1]

[1]Center for Space Science and Applied Research, Chinese Academy of Sciences, Beijing 100190, China
[2]Graduate University of Chinese Academy of Sciences, Beijing 100190, China

Abstract— Calibration and retrieval are two important and critical techniques for ground-based atmospheric microwave sounder. The paper based on an improved ground-based atmospheric microwave sounder prototype which is referring to MP3000 of USA and makes many improvements in receiver, frequency configuration, millimeter antenna, digital control unit, scanning mode and millimeter front-end. Calibration errors are the major source of inaccuracies in radiometric measurements. The standard calibration procedure is to terminate the radiometer inputs with two absolute calibration targets which are assumed to be ideal targets. So adopting proper calibration method will ensure a high sounding resolution. Also, based on the advanced design, calibration unit has significant characters. It uses two calibrated methods like LN2 (22–31 GHz and 51–59 GHz) calibration and sky tipping (tipping curve) calibration (22–31 GHz) to realize relative calibration (internal calibration). Retrievals of regional temperature profiles have an important role in weather forecast, communication, traffic, agriculture and other fields. Assuming the atmospheric temperature profile is known to 2 k (state-of-the-art with present remote sensors) and instrument noise is 1–2 k brightness temperature (achievable with current technology). The paper extracts several clear-air datasets randomly in the available radisonde datasets. It derives atmospheric absorption spectrum from MPM93 model (liebe'93 model) and simulates brightness temperature using radiometric transfer equation. In order to estimate atmospheric temperature profiles from the radiometer data, the algorithm of back-propagation neural network has been used. The retrievals yield good results in the temperature profiles from the surface to nearly 400 hpa. When compared to a linear regression approach, the neural network retrieval yields significantly better results for the retrieval atmospheric levels. So, the prototype of improved ground-based atmospheric microwave sounding meets the requirements and using proper algorithm the retrieval results can be used in many fields.

Investigation of GPS-measured Ionospheric Total Electron Content Variations Generated by HF-heating at Mid-latitudes

V. E. Kunitsyn[1], **A. M. Padokhin**[1], **A. E. Vasiliev**[1], **G. A. Kurbatov**[1], **V. L. Frolov**[2], **and G. P. Komrakov**[2]

[1]M. V. Lomonosov Moscow State University, Russia
[2]Radiophysical Research Institute, N. Novgorod, Russia

Abstract— Numerous investigations of characteristics of artificial turbulence in ionospheric F_2 region carried out by means of powerful HF radiowaves of O-mode showed that near reflection height of radio wave develop ponderomotive parametric, thermal (resonant) parametric and self-focusing instabilities. This causes particularly a significant heating of plasma in this area and generation of artificial electron density irregularities with scales from meters to kilometers. These irregularities significantly influence properties of HF radiowaves propagating through the heated area in ionosphere. Characteristics of such artificial irregularities were studied by different methods: field-aligned scattering of HF radiowaves, radiotomography, etc.

The aim of this work is to present experimental results of the influence of electron density perturbations caused by HF-heating of ionospheric F_2 layer on GNSS navigational signals at mid-latitudes in daytime conditions. The experiments were carried out on the Sura heater near N. Novgorod, Russia using pump wave frequency of 4.3 MHz (during all series of experiments the critical frequency of F_2 layer was greater then heating frequency) and the effective radiated power of about 80 MW. During heating sessions with different time modulation of radiative power ionospheric penetration points for several navigational satellites and GNSS-receiver installed near Sura facility crossed the heated area. For these satellites we investigated variations of total electron content (TEC), proportional to the differential carrier phase of navigational signals. It is shown that for square heating pulses (with periods 1, 6 and 10 minutes) in spectrum of TEC variations appeared perturbations with main heating period. Amplitudes of such perturbations were of order of 0.1 TECU. These TEC oscillations prove the presence of irregularities of electron density field in heated region, caused by such schemes of HF-heating.

ACKNOWLEDGMENT

The work was supported by Russian Foundation for Basic Research (RFBR), grants No. 08-02-00171, 08-05-00676, 07-05-01120.

Fluctuation of Electromagnetic Field Parameters Propagating in Magnetized Plasma with Random Variation of Electron Density and Magnetic Field

G. V. Jandieri[1], **A. Ishimaru**[3], **V. G. Jandieri**[4], **I. B. Shirokov**[1], **Yu. B. Gimpilevich**[1], **A. G. Khantadze**[5], **and N. N. Zhukova**[2]

[1]Physics Department, Georgian Technical University, Tbilisi, Georgia
[2]Institute of Cybernetics, Tbilisi, Georgia
[3]Department of Electrical Engineering, University of Washington, USA
[4]Department of Electrical and Computer Engineering, Kumamoto University, Japan
[5]Physics Department, Tbilisi State University, Tbilisi, Georgia

Abstract— Problem of electromagnetic field fluctuations in magnetized plasma was investigated in [1–4]. Fluctuations of the phase and the angle-of-arrival of scattered radiation caused due to both random electron density and magnetic field fluctuations was studied in the geometrical optics approximation in [3, 4]. In these papers magnetic field was supposed to be fluctuating only in size, but not in direction. Therefore, these results are applicable only for small links, i.e., in the near zone. At arbitrary orientation of the external magnetic field the results should be generalized.

In the present paper using the perturbation method we consider statistical characteristics of scattered and reflected electromagnetic waves by turbulent magnetized plasma layer with electron density and magnetic field fluctuations at arbitrary orientation of an external magnetic field. The obtained results are valid for near and far zones. Anisotropy of magnetic field, which is a random function of the spatial coordinates, leads to the stochastic set of three differential equations for the ordinary and extraordinary waves. Analytical expressions for scattered electric field components, phase and relative amplitude fluctuations are obtained using the perturbation method and the boundary conditions. Correlation functions of these statistical characteristics are analyzed analytically and numerically for the ordinary and extraordinary waves at different orientation of external magnetic field using satellite and remote sensing data. Dumping coefficients of the mean field are computed applying energetic reasons.

REFERENCES

1. Jandieri, G. V., V. G. Gavrilenko, and A. A. Semerikov, "On the effect of absorption on multiple wave-scattering in magnetized turbulent plasma," *Waves in Random Media*, Vol. 9, 427–440, 1999.
2. Jandieri, G. V., V. G. Gavrilenko, A. V. Sorokin, and V. G. Jandieri, "Some properties of the angular power distribution of electromagnetic waves multiply scattered in collisional magnetized plasma," *Plasma Physics Report*, Vol. 31, No. 7, 604–615, 2005.
3. Jandieri, G. V., A. Ishimaru, V. G. Jandieri, A. G. Khantadze, and Z. M. Diasamidze, "Model computations of angular power spectra for anisotropic absorptive turbulent magnetized plasma," *Progress In Electromagnetics Research*, PIER 70, 307–328, 2007.
4. Jandieri, G. V., A. Ishimaru, V. G. Jandieri, A. G. Khantadze, A. I. Gvelesiani, K. V. Kotetishvili, and T. N. Bzhalava, "A note of the angular power spectrum of scattered radiation by anisotropic layer of collisional magnetized turbulent plasma," *International Journal of Microwaves and Optical Technology*, Vol. 3, No. 1, 35–44, 2008.

Recent Advances in Fully Polarimetric Space-SAR Sensor Design and Its Applications to the Remote Sensing of Earth, Ocean and Atmosphere

Wolfgang-Martin Boerner
University of Illinois at Chicago, USA

Abstract— With the un-abating global population increase our natural resources are stressed as never before, and the global day/night monitoring of the terrestrial covers from the mesosphere to the litho-sphere becomes all the more urgent. Microwave radar sensors are ideally suited for space imaging because those are almost weather independent, and microwaves propagate through the atmosphere with little deteriorating effects due to clouds, storms, rain, fog and haze. Globally humidity, haze and cloudiness are increasing at a rather rapid pace, whereas only 20 years ago all of those covered only 48% of the globe, today those have increased to about 62% and within another 20 years may exceed 80% for irreversible reasons. Thus, optical remote sensing from space especially in the tropical and sub-tropical vegetated belts will become rather ineffective, and microwave remote sensing technology must now be advanced strongly and most rapidly hand in hand with digital communications technology because operationally it is more rapidly available especially for disaster mitigation assistance.

The basic radar technologies to do the job are the multimodal Synthetic Aperture Radar (SAR) sensors, first developed for air-borne sensing implemented as for example in 1978 with the first space-borne digital Sea-Sat SAR which enjoyed great popularity and implementation until these days. However, the NASA Sea-Sat L-Band SAR had severe limitations in that it was of fixed wide swath-width at a single arbitrary polarization (HH) and of rather poor 25m resolution. In the meantime, fully polarimetric multimodal high resolution SAR systems at multiple frequencies were introduced first with the multi-band AIRSAR of NASA-JPL culminating in the once-only pair of SIR-C/X-SAR shuttle missions of 1994 April and October, which laid the ground work for true day/night space remote sensing of the terrestrial barren and vegetated land and ocean covers using multi-band polarimetric SAR. Thereafter, NASA suspended further development of the basic need for further advancing airborne and space-borne multimodal SAR imaging techniques except for SRTM shuttle mission of 2000 February; and swiftly the Canadian CCRS, the German DLR and the Japanese NASDA & CRL now JAXA & NICT took over introducing and steadily advancing the Convair-580, the E-SAR and Pi-SAR airborne highly advanced fully polarimetric sensors platforms, respectively.

These separate international multi-modal fully polarimetric and also interferometric SAR developmental efforts culminated in a well coordinated group effort of these three independent teams eventually launching and operating Fully Polarimetric Satellite SAR Sensors at L-Band (ALOS-PALSAR launched by JAXA/Japan in 2006 January), at C-Band (RADARSAT-2 launched by CSA-MDA in 2007 December) and at X-Band (TerraSAR-X launched by DLR-Astrium in 2007 July) with follow-on tandem missions soon to be realized. Thus, international collaboration on advancing day/night global monitoring of the terrestrial covers was demonstrated with the launch of the three fully polarimetric multi-modal SAR Satellites at L-, C-, X-Band, and its tandem satellite-pair updates are forthcoming very swiftly. All of this will be topped by the near-future joint DLR-JPL DESDynI/Tandem-L wide-swath, high-resolution fully polarimetric sensor implementation, which in due time will be enlarged to accommodate next to the L-, C-, X- also P-Band sensors using one and the same reflector, then enabling full assessment also of dense tropical forests which will for example result in curtailing illegal deforestation, there and elsewhere.

In essence, we have created a silent watchful microwave eye in space assisting us in analyzing our biosphere in which we live or in other words microwave remote sensors are becoming the radiologists for providing input to the diagnosticists for assessing the health of the terrestrial covers of our planet *Mother Earth* — the earth, oceans and its atmosphere. Without question, we will continue suffering from natural hazards, which are unavoidable as long life on Earth exists, but the resulting natural disasters are avoidable, and by discovering and assessing the hazards in time, will assist in mitigating the ensuing catastrophes at ground, on oceans and in space due to these new microwave SAR sensors more than ever before for the benefit of sustaining the health of the biosphere in which we reside.

Session 3P2a
EM Scattering Models and Applications

Radar Imaging of Target above the Gaussian Random Rough Surface Using the Accelerated MOM/PO Hybrid Method

Si-Yuan He, **Fang-Shun Deng**, **Jing-Jing Yao**, **and Guo-Qiang Zhu**
School of Electronic Information, Wuhan University, China

Abstract— In this paper, the range profile analysis for a 3D perfectly electric conductor (PEC) target above a 2D PEC Gaussian random rough surface was successfully implemented using the MOM/PO hybrid method accelerated by the matrix decomposition technique. The numerical scattering model of 3D target/rough surface is constructed by considering the target as the MOM region and the rough surface as the PO region where the RWG vector basis function is employed to expand the induced surface currents. Based on the EM numerical simulation, the wide-band backscattered field of the combined model is obtained using a stepped frequency waveform (SFW), which is produced by linearly sampling the desired bandwidth B at specific frequencies. By performing an inverse discrete Fourier transform (IDFT) on the field data in the frequency domain, the time domain response is provided. Accordingly, the 1-D high resolution range profiles (HRRPs) of the target above the random rough surface is achieved, since the time delay of the signal is associated with the position of the scattering center projected on the line of the sight. The range profiles provide information not only about the position but also the scattering strength of the scattering centers along the range direction. The numerical results could be understood and analyzed based on the knowledge of different scattering mechanisms, for example, diffraction and reflection. Compared to the target above a planar surface, the interaction scatterings based on the strong reflection are decreased greatly in the rough surface case because of the rough surface diffuse scattering. Simulated results show that the interaction scattering between the target and the bottom surface leads to a series of equivalent range profiles, especially when the bottom surface is smooth. Range locations of the equivalent range profiles made a good agreement with the predictions made from the ray theory.

Improving the Convergence Properties of Certain Numerical Method for Scattering from Rough Surfaces Using the Second-degree Stochastic Method

Bin Liu and Yang Du
Department of Information Science and Electronics Engineering, Zhejiang University
Hangzhou 310027, China

Abstract— Electromagnetic scattering from rough surfaces is an important issue in remote sensing. Numerical methods are able to provide accurate solution to Maxwell's equations, thus have become popular over the past three decades. Most numerical methods are based on method of moment (MoM), which requires $O(N^3)$ operations, where N is the number of surface unknowns. Direct iterative solvers can reduce the computation complexity to $O(N^2)$, however, it becomes difficult to converge when the rms height and rms slope of rough surface become large. In our previous work, we have developed an efficient and accurate iterative numerical approach to analyze electromagnetic scattering from 1-D dielectric rough surfaces, which is based on a new splitting of the impedance matrix. In this paper, we propose to apply the stochastic second-degree (SSD) method to improve the asymptotic convergence rate of the iterative system, in conjunction with our previous approach. Through extensive numerical experiments, we find that our new method converges when our previous approach fails in large rms slope cases, especially at VV polarization.

Study of the Validity Region of the Extended T-matrix Method for Scattering from Dielectric Cylinders

Wenzhe Yan[1], **Yang Du**[1], **Ziyuan Li**[2], **Erxue Chen**[2], **and Jiancheng Shi**[3]

[1]Department of Information Science and Electronics Engineering, Zhejiang University
Hangzhou 310027, China
[2]Institute of Forest Resources Information Techniques, Chinese Academy of Forestry, Beijing 100091, China
[3]Institute for Computational Earth System Sciences, University of California
Santa Barbara, CA 93106, USA

Abstract— The electromagnetic scattering by canonical physical objects is important in many applications. For the case of dielectric cylinder with finite length, an exact analytical solution is still elusive, and several approximation approaches have been proposed in the literature. One popular approach is the generalized Rayleigh-Gans approximation, where the induced current in the cylinder is approximated by that of infinite length. This method is valid for a needle shaped scatterer with radius much smaller than the wavelength. It should be noted that solutions of such approximate methods in general fail to satisfy the reciprocity theorem. On the other hand, a semi-analytical method called the T-matrix approach, which is based on the extended boundary condition method, is effective in analyzing electromagnetic scattering from finite scatterers. However, in treating scattering from dielectric cylinder of finite length, if any of the parameters including length, equivalent volumetric radius, and relative dielectric constant is adequately large, then the T-matrix approach may suffer from slow convergence or even fail to converge.

To deal with such difficulty, recently we proposed a method based on an extension of the T-matrix approach, where a long cylinder is hypothetically divided into a cluster of identical sub-cylinders, for each the T matrix can be numerically stably calculated. Special care was paid to fulfill the boundary conditions at the hypothetic surface of any two neighboring sub-cylinders. The resultant coupled equations are different from that of multi-scatterer theory. The model results were in good agreement with experiment data available in the literature. However, the validity region of the proposed method was not fully characterized. Now we have developed and validated a method of moment code, and are in a position to carry on the task of characterizing the validity region. The proposed method is found to be applicable to dielectric cylinders of arbitrary length as long as the T matrix is attainable for the elementary sub-cylinder. The conditions for the T matrix to be numerically stably calculated in terms of the equivalent volumetric radius and relative dielectric constant are also empirically obtained.

Channel Capacity Enhancement by Applying 3-D Space-polarization Diversity to MIMO Systems

L. Hai and Y.-R. Zhang
Country College of Electronic Science and Engineering
Nanjing University of Posts and Telecommunications, China

Abstract— Multi-input multi-output (MIMO), one of the important techniques which can improve channel capacity significantly in wireless communications, has two main styles of space-diversity and polarization-diversity, in which the space-diversity systems may attain greater system capacity, yet require adequate spaces for large antenna array and are obviously affected by azimuth angles of antenna array, while the polarization-diversity systems require less spaces, yet have limited ability in improving system capacity because of the conspicuous path-loss of horizontal polarization wave.

One of the main reasons why there are not enough researches on 3-D MIMO channel models is that it is difficult to calculate electromagnetic scattering effects during signal propagation. In this paper, in order to simulate MIMO systems with arbitrary diversity, the electromagnetic scattering effects are abstracted into a set of statistical parameters, based on which a 3-D stochastic physical MIMO channel model, which can be elastically applied to different conditions, is established.

Based on the new model mentioned above, research work on systems with both space-diversity and polarization-diversity is carried out. System capacities under different conditions such as mobile transmit end or receive end, restricted antenna space, and various azimuth angles of antenna array, are calculated and compared with systems of single-diversity.

Simulation results show that systems with both space-diversity and polarization-diversity may gain greater capacity than single-diversity systems, especially than polarization-diversity systems, and that capacity of systems with both space-diversity and polarization-diversity is less affected by azimuth angles of antenna array than space-diversity systems, which results in a much stable system performance. Based on the simulation results, we suggest that with applying space-polarization diversity to MIMO systems, we may attain best system performance by choosing most suitable MIMO antenna styles for various environments, which is especially meaningful for systems with restrict antenna spaces.

Further Study on Electromagnetic Scattering from Multiple Cylinders

Wenzhe Yan[1], **Dawei Liu**[2], **Hong Tat Ewe**[3], **and Yang Du**[1]

[1]Department of Information Science and Electronics Engineering
Zhejiang University, Hangzhou 310058, China
[2]Department of Electrical Engineering, Beihang University
Beijing 100191, China
[3]Tunku Abdul Rahman University, Petaling Jaya 46200, Malaysia

Abstract— In extension to an iterative technique to calculate the electromagnetic scattering from a single dielectric cylinder of finite length, the scattering model of electromagnetic scattering from a cluster of parallel dielectric circular cylinders has been developed. The formulism for multi-cylinder scattering is that the scattered field is taken to be the superposition of scattered fields resulting from the interaction between the incident wave and each scatterer, as well as among the scatterers. It should be noted that when any pair of reasonably long cylinders are close to each other, the circumscribed spheres of cylinders would overlap thus direct application of the conventional multi-scatterer equation is in question. By using division of the elongated cylinders, the volume of the circumscribing spheres is significantly reduced. Meanwhile, since no approximation is introduced in the procedure, this approach is rigorous.

In this paper, we extend the original formalism to a more general form, which can be readily applied to cylinders with arbitrary cross section and arbitrary arrangement of cylinders' positions. Moreover, based on our recently developed code of method of moment (MoM), further applications to more complicated scenes of multiple cylinders will be studied.

Multiyear Analysis of an Inverse Model for Sea Ice Thickness Retrieval

Y. J. Lee[1], **W. K. Lim**[1], **H. T. Ewe**[2], **and H. T. Chuah**[2]

[1]Multimedia University, Malaysia
[2]Universiti Tunku Abdul Rahman, Malaysia

Abstract— The use of remote sensing technology for sea ice parameter retrieval in the polar region has always been a vision for researchers around the world. Such data are important towards the study of global climate change and understanding the effects of changes in the polar region on the world's delicate ecosystem. The implementation of remote sensing technology for data retrieval opens up many different possibilities for researchers such as retrieval of data from inaccessible remote areas within the polar region and long term year round monitoring. In this paper, further details of an inverse microwave scattering model using Radiative Transfer theory developed for the purpose of sea ice thickness retrieval is presented. Utilizing an improved forward model incorporating the Dense Medium Phase and Amplitude Correction Theory and the use of the Levenberg Marquardt Optimization for estimating the sea ice thickness, the model has been applied to retrieve sea ice thickness from actual conditions using ground truth measurement data obtained from Ross Island, Antarctica. While initial simulations using ground truth measurement data from the years 2006 and 2007 have yielded positive results, further investigation into the model is needed to determine the applicability of the model. In order to eliminate the number of uncertain parameters during the retrieval process, a multiyear measurement analysis of ground truth measurements for first year sea ice conducted at Cape Evans from the years 2002 to 2008 are presented. Further testing of the inverse model to retrieve sea ice thickness using ground truth measurement data from the year 2005 is also presented. The multiyear measurement analysis shows that the dielectric constants of the various media found in first year sea ice change very little, but the sea ice volume fraction, thickness and the temperature of the various media can fluctuate depending on the area and time of measurement. The simulation of the inverse model using ground truth measurement data from 2005 also gives a promising result.

Modeling of Microwave Emission from Soil with Vegetation Cover

Luis M. Camacho and Saibun Tjuatja
Wave Scattering Research Center, Department of Electrical Engineering
The University of Texas at Arlington, UTA Box 19016 Arlington, TX 76019-0016, USA

Abstract— Soil moisture is an important factor of the water, energy, and carbon cycles at the interface between the surface of the Earth and atmosphere. Models have been developed to characterize the emission from soil to interpret the observed relations between radiometer observations and soil parameters [1]. However, the emission from soils is in many cases affected by a vegetation layer, which attenuates the soil emission and adds its own contribution to the land surface emission. In order to account for it, models have been developed that incorporate the effect of vegetation on soil emission [2].

In [3], a physical microwave radiometry model is developed for a vegetation canopy based on an iterative solution of the radiative transfer equations. In the model, finite-length dielectric cylinders are used to represent some vegetation components. The scattering amplitude tensors for finite length cylinders are calculated through estimating the inner field with its corresponding inside infinite cylinders having similar radial properties. In [4], a validation of both surface- and volume-current models for electromagnetic scattering from finite-length dielectric cylinders is carried out. These approaches require the length of the cylinder to be much larger than its diameter.

In this study the scattering and emission characteristics for finite-length dielectric cylinders are computed using a numerical approach, namely the FDTD method. In [5], we developed and used a 3D-FDTD algorithm to compute the emissivity of finite-size cylindrical-shape objects, though it can be used for any arbitrary-shape object. A similar approach is used here to attain the scattering properties of the vegetation components under study. The scattering properties of the object are used to generate the phase matrix, which is then integrated into a radiative transfer model. Results from soil emission with vegetation layer modeling for different constituent parameters, frequencies and polarizations will be compared to other models [6] and presented in this paper.

REFERENCES

1. Jackson, T. J. and T. J. Schmugge, "Vegetation effects on the microwave emission of soil," *Remote Sensing Environment*, Vol. 36, 203–212, 1991.
2. Jackson, T. J. and O'neill P. E., "Attenuation of soil microwave emission by corn and soybeans at 1.4 and 5 GHz," *IEEE Transactions on Geoscience and Remote Sensing*, Vol. 28, No. 5, 978–980, September 1990.
3. Karam, M. A., "A physical model for microwave radiometry of vegetation," *IEEE Transactions on Geoscience and Remote Sensing*, Vol. 35, No. 4, 1045–1058, July 1997.
4. De Matthaeis, P. and R. H. Lang, "Comparison of surface and volume currents models for electromagnetic scattering from finite dielectric cylinders," *IEEE Transactions on Antennas and Propagation*, Vol. 57, No. 7, 2216–2220, July 2009.
5. Camacho, L. M., M. Lu, and S. Tjuatja, "Study of emission from finite-size objects using FDTD," *IEEE International Geoscience and Remote Sensing Symposium, 2008*, Vol. 4, IV-1153–IV-1156, July 7–11, 2008.
6. Mo, T., T. J. Choudhury, T. J. Schmugge, J. R. Wang, and T. J. Jackson, "A model for microwave emission from vegetation-covered fields," *Journal of Geophysical Research*, Vol. 87, No. C13, 11229–11237, 1982.

Session 3P2b
Wireless Sensor Network and Applications

Further Results on Performance of Slotted IEEE 802.15.4 with Downlink and Uplink Traffic

Wei Wang and Yang Du
Department of Information Science and Electronics Engineering, Zhejiang University
Hangzhou 310027, China

Abstract— In this work we analyze the performance of slotted IEEE 802.15.4 with both downlink and uplink traffic in the beacon enabled mode. For uplink traffic, the node transfers packet to coordinator with direct transmission while for downlink traffic the coordinator transfers packet to node with indirect transmission. We integrate these two transmission modes in one general analytic framework based on Markov chain model and queueing theory. The impact of some important system parameters and operational configurations on system performance is investigated under both unsaturated and saturated regions. From the analysis we find that coordinator can handle only a small amount of downlink traffic, so the network operating point has to be carefully chosen. Based on the model, we study the normalized throughput, probability of collision and service time of the whole network under different scenarios, and compare them with the results of Network Simulator (NS-2).

An Optimized Ad Hoc MAC Scheduling Algorithm for IEEE 802.15.3

Guangdi Yang, **Fan Wang**, **Rufeng Lin**, **and Yang Du**
Department of Information Science and Electronics Engineering, Zhejiang University
Hangzhou 310027, China

Abstract— In this paper, we propose a new channel aware scheduling algorithm for MPEG-4 traffic in HDR WPAN based on the features of wireless network and the characteristic of MPEG-4 traffic. Compared with different channel aware algorithms applied in HDR WPAN, we demonstrate through simulation that our algorithm is robust and outperforms the others in terms of system throughput under different simulation circumstances. In the simulation, realistic channel and physical layer model were implemented in order to make the results more accurate and convincing. The effects of application aware techniques, including burst transfer eligibility decision (BTED) and frame-decodability aware (FDA) mechanisms, and optimization of scheduling parameter for the proposed algorithm are also studied.

Convergecast of Multi-destinations in Zigbee Tree-based Wireless Sensor Network

P. Juleang[1], **S. Mitatha**[1], **and P. P. Yupapin**[2]

[1]Hybrid Computing Research Laboratory, Faculty of Engineering
King Mongkut's Institute of Technology Ladkrabang, Bangkok 10520, Thailand
[2]Advanced Research Center for Photonics, Faculty of Science
King Mongkut's Institute of Technology Ladkrabang, Bangkok 10520, Thailand

Abstract— Multi-destinations in wireless sensor network have extremely benefited for monitoring system. Then, convergecast is a fundamental operation in wireless sensor network. Existing convergecast solution focused on latency and energy consumption. However, a good design should be complaint to standard. This paper proposes convergecast solution of multi-destinations in Zigbee tree-based wireless sensor network and proves that this solution is simulation. Our solution is optimal convergecast of multi-destination in wireless sensor network and using accompany with network's resource for all destinations. Then, our solution is compliant with the low-power design of IEEE 802.15.4. Simulation results show that the proposed solution can indeed achieve convegecast of multi-destinations.

Conception of Patch Antennas in the GSM and UMTS Band

M. Iftissane[1, 2], **S. Bri**[1, 2], **and L. Bellarbi**[2]

[1]Microwave and Materials Group, ESTM, B. P 3103, Meknès, Morocco
[2]Electrical Engineering Laboratory, ENSET, Rabat, Morocco

Abstract— Of numerous services radio motives develop at present and attract more and more users. The access to these services of only terminal requires the use of compact antennas multi-frequencies and multi-polarizations allowing in particular to disappoint simultaneously the Frequency Modulation, the DVB (Digital Video Broadcasting), the cellular telephony (GSM, UMTS) and the GPS (Global Positioning System). It was to note that the frequencies used by these diverse applications spread out on several octaves and it is thus difficult to conceive a only structure combining the required characteristics allowing the access to these various services. To mitigate this problem certain authors proposed for example compact antennas GSM-GPS presenting interesting characteristics. Other researchers focused their works on the reception by the same antenna of emissions in Digital Audio Broadcasting and in DVB. The properties of materials permittivity, special forms were also run by several investigators for the conception of variants of compact antennas multifrequencies [1–3].

Among antennas developed during these last years which are the object of research works. At present, the reproduction and the variety of the standards of radiomobile communications (GSM, DCS, UMTS, WLAN), Bluetooth, DIGITAL TV), created a very strong need for compact antennas multifrequencies allowing in particular to assure the compatibility of the various standards or to reach numerous services [4, 5]. Indeed, antennas have radiant structures presenting a cover multi-bands and/or wide band. But for the various services, the used frequencies are either very remote, or neighboring according to the standards which we consider.

In front of this constraint, it's thus extremely difficult to imagine a compact structure combining the characteristics allowing to these various services. However, the standards AMPS (Advanced Mobile Phone Service), GSM (Mobile Global System for communication) (880 MHz–960 MHz, DCS (Digital to cellular system) (on 1710–1880 MHz), PCS (Personal Communications Services/System Services/System) (1850–1990 MHz) and UMTS (Universal Mobile Telecommunications System) (1920–2170 MHz) are relatively nearby from the point of view of their characteristics of radiation, band of frequency, power and separately appeal to geometries structures. So, the performances and the reduced dimensions which characterize the printed antennas, these last ones can be integrated with the module of emission or reception on the same substratum and seen the necessity of antennas multibands in the systems of mobile radiocommunications. Our work turned to the conception, the simulation and the realization of some patch antennas multibands by using a software which is based on the moments method.

In this paper, we present the results of simulations of a series of patch antennas and also the experimentales measures by means of an network analyzer. The conception of these patch antennas are realized by software HFSS "Ansoft-High Frequency Structure Simulator" and ADS "Advanced Design System", based themselves essentially on the variation of the shape of the antenna and its conductive material, the nature and the thickness of the substratum to have a structure which resounds in the frequencies used for precices applications. This results is compared of those published in the bibliography [5, 6].

REFERENCES

1. Bri, S., A. Saadi, M. Habibi, A. Hakheli, L. Zenkouar, L. Bellarbi, and A. Mamouni, "Finite difference time domain (FDTD) analysis of new applicators for hyperthermia and evaluation of the SAR distribution in human head near cellular phone," *ANSE-2008*, Vol. 69, No. 2, France, 2008.
2. Eldek, A. A., A. Z. Elsherbini, and C. E. Smith, "Square slot antenna for dual wideband wireless communication systems," *Journal of Electromagnetic Waves and Applications*, Vol. 19, No. 12, 1571–1581, USA, 2005.
3. Almeida, J. F., C. L. Da S. S. Sobrinho, and R. O. Dos Santos, "Analysis by FDTD method of a microstrip antenna with PBG considering the substrate thickness variation," *Journal of Microwave and Optoelectronics*, Vol. 3, No. 3, 41–48, December 2003.

4. Bri, S., K. Elknanai, and A. Nakheli, "Patch antenna at frequency $f = 2.35\,\mathrm{GHz}$ for telecommunications applications," *Progress in Electromagnetics Research Symposium*, Prague, Czech Republic, August 27–30, 2007.
5. Çakir, G. and L. Sevgi, "Design simulation and tests of a low-cost microstrip patch antenna arrays for the wireless communication," *Turk Journal Electrical. Engin.*, Vol. 13, No. 1, 2005.
6. Yang, F., X.-X. Zhang, X. Ye, and Y. Rahmat-Samii, "Wide-band E-shaped patch antennas for wireless communications," *IEEE Trans. Antennas Propagation*, Vol. 49, No. 7, 1094–1100, July 2001.

Session 3P3
Passive Optical Waveguide Theory and Numerical Modelling

Computing 2-D Green's Function for Multi-layer Dielectric Waveguides

Hung-Wen Chang, Chia-Da Chang, and Sin-Yuan Mu
Institute of Electro-optical Engineering and Department of Photonics, National Sun Yat-sen University
Kaohsiung 80424, Taiwan

Abstract— We present two semi-analytical formulations for computing two-dimensional Green's functions (2DGF) in an open unbounded multi-layer dielectric waveguide. Analytic closed-form solution for the 2DGF can be written as an inverse Fourier transformation of the plane-wave solution in the wavenumber domain. However, without an exact inversion, result computed by a numerical integration can not capture the unbounded, slowly decaying radiation field. We show that two-sided radiation fields can be computed using just finite terms of Fourier series or waveguide modes when the waveguide is bounded by a pair of electric/magnetic walls (PECW/PMCW) placed horizontally or vertically. We shall compare the advantages and disadvantage between these two semi-analytical representations and choose one to be an alternate solution to the exact 2-D Greens function of an dielectric slab waveguide.

Computing Leaky Mode Based on Pseudospectral Method

Po-Jui Chiang[1] and Nai-Hsiang Sun[2]

[1]Department of Electronic Engineering, Kaohsiung University of Applied Sciences
415 Chien Kung Road, Sanmin District, Kaohsiung 80778, Taiwan
[2]Department of Electrical Engineering, I-Shou University
1 Sec. 1, Syuecheng Rd., Dashu, Kaohsiung, Taiwan

Abstract— The purpose of this research is to analyze leaky-mode losses for optical fibers using full-vectorial multidomain pseudospectral mode solver in the frequency domain. This method solves a standard eigenvalue problem from the Helmholtz equations for transverse-magnetic components and obtains complex propagation constants of the modes using perfectly matched layers. Some valid and optima parameters of perfectly matched layers are presented. Both the real and the imaginary parts of the complex effective index can be obtained with achieving a high accuracy and fast convergence. The solver is applied to the depressed inner cladding (DIC) single-mode fibers for the assessment of its numerical performance.

Boundary Element Method for Solving Leaky Modes in Photonic Crystal Fiber

Jung-Sheng Chiang, **Jiun-Jie Liau**, **and Jo-Ying Wang**
Department of Electrical Engineering, I-Shou University, Kaohsiung, Taiwan, R.O.C.

Abstract— We report the boundary element method (BEM) in the rigorous vector form to solve the confinement loss of leaky modes for photonic crystal fiber (PCF). The PCF is composed of a single material (generally silica) with multiple air holes periodically arranged around the solid or air core that run along the length of the cladding. In the solid core PCF that we study in here, the guidance mechanism is somewhat similar to the total internal reflection that occurs in conventional fibers. We investigate the confinement losses in PCFs owing to finite numbers of air-holes that can cause the modes to be leaky. An analysis of the confinement losses in PCFs due to the finite numbers of air holes is performed by means of the full-vector BEM. In BEM, the boundaries between regions of different refractive indexes are discretized into linear segments, and then eigenvalue equation for unknowns assigned to segments is obtained by applying Green's theorem. The BEM can be used for calculations of the full complex propagation constant of a PCF. The complex effective index and confinement loss are accurately calculations. We show how the confinement losses from imaginary part of propagation constant varies with hole size, hole shape, the number of rings of holes, and wavelength. In result, the holes are larger, circular, and more holes that confinement losses are smaller. The longer wavelength induces the more than confinement loss.

Cascaded SHG/DFG Coupled Mode Equations Considering the Third-order Susceptibility Effect

Shih-Chiang Lin[1], **Chia-Ming Hu**[2], **Chih-Chun Chen**[1], **and Tsung-Cheng Wu**[1]

[1]Department of Communication Engineering, I-Shou University, Taiwan
[2]Department of Electrical Engineering, I-Shou University, Taiwan

Abstract— A set of four-waves coupled mode equations including pump, second- harmonic of pump, signal and conversion waves had been used to mode a cascaded second-harmonic generation (SHG) and difference-frequency generation (DFG) phenomena. However, such current cascaded SHG/DFG numerical model never considered the intrinsic third-order susceptibility terms because the third-order susceptibility is four orders less than the second-order susceptibility. The cascaded second-order susceptibility can be viewed as equivalent third-order susceptibility. Therefore, for distinguishing the equivalent and intrinsic third-order susceptibility effect in high power situation, the intrinsic third-order susceptibility shall be considered. In this paper, we propose the cascaded SHG/DFG numerical model considering the intrinsic third-order susceptibility terms. The simulation results demonstrate that the difference, for a 0.6 ps and 478 pJ pulse energy case, with and without intrinsic third-order susceptibility are up to 8%.

Radiation Loss at Discontinuities in Dielectric Waveguides Using Perfectly Electric Conductor Approximation Method

Nai-Hsiang Sun, **Chia-Ming Hu**, **and Po-Hao Cheng**
Department of Electrical Engineering, I-Shou University, Taiwan

Abstract— The discontinuities in dielectric waveguides are of great interest since the discontinuities create radiation losses and reduce the efficiency of light transmission between devices. For the design of integrated devices, it is necessary to investigate the radiation loss at the discontinuities in dielectric waveguides. The radiation loss at the junction of two dielectric waveguides has been analyzed in the past by numerous methods. In this paper, the radiation mode is obtained by assuming that the dielectric waveguide is bounded by metallic walls (or perfect electric conductor) positioned far away from the waveguide region. The method is called the perfect electric conductor approximation method (PECAM). We use PECAM to simulate radiation losses of discontinuous interfaces. Moreover, two overlapped integral techniques are proposed to evaluate the discontinuity problem. The transmission, and reflection, and radiation power in a discontinuity interface are evaluated in this paper.

Light Propagation in Micro-optical-lattice Waveguide

Xiaofei Chen, **Yali Qin**, **Hongliang Ren**, **and Fei Liu**
Zhejiang Key Research Lab of Fiber-optic Communication Technology
Colleage of Information Engineering
Zhejiang University of Technology, HangZhou 310023, China

Abstract— Photorefractive crystals play a very important role in all optical communication because of its low-power, high nonlinear index and good modulability, especially bringing convenience in experiment and design for the optical devices. Many observations have been done to study the characteristic of the beam propagation in the optical lattice in the past decades.

In this paper, the evolvement is studied while the light is transmitting across the lattice. The lattice here is much smaller, and can be compared with the wavelength (so called Micro-optical lattice). This design is hoped to have some new good properties: it will not make the light discrete (according to the Floquet-Bloch theory) while it has enough nonlinear to balance the diffusion (according to electro-optic effect) and bring us the solitons. The material in this simulation is SNB:75, and the lattice is produced by two pairs of coherent beam of which the wavelength is 488 nm. The period of the lattice D is 1 μm, the width of the waveguide made by the lattice is 15 μm. The Alternating Direction Implicit Beam Propagation Method (ADI-BPM) is used based on Matlab. And the numerical simulation is done under different conditions by changing the width of the waveguide, value of the space-charge field Esc, and the depth of the lattice. The results show that light propagation in such lattice waveguide have something to do with it: The MOL-waveguide can localize the beam's energy even though the beam's energy is less then the threshold being soliton in the block with other condition being the same . And the most important, it can guide the transmission of the beam so that the light can change its direction. Besides, the beam transmitting in such structure presents a new phenomenon: It compresses energy in x and y direction alternatively with its whole energy maintaining. The light can change its direction under the guidance of MOL waveguide, however, it needs a certain distance before the beam can totally shift its energy to the tilt waveguide perfectly. More characteristics need to be studied about this MOL-waveguide structure.

ACKNOWLEDGMENT

Surported by National Science Foundation.

Numerical Analysis of Dielectric Waveguide Devices Using Coupled Transverse-mode Integral Equation

Yan-Huei Wu[1], **Shih-Min Lu**[1], **Hung-Wen Chang**[1], **and Meng-Huei Sheng**[2]

[1]Department of Photonics, Institute of Electro-optical Engineering
National Sun Yat-sen University, Kaohsiung 80424, Taiwan
[2]Department of Management Information Science
Chia Nan University of Pharmacy & Science, Tainan 71710, Taiwan

Abstract— We apply an in-depth numerical investigation, using our recently proposed coupled transverse-mode integral equation (CTMIE) formulation, to the analysis of general 2-D dielectric passive waveguide devices. The device under study is first approximated by a set of piece-wise constant, 1-D horizontally layered structures called slices. The unknown functions on the interface between slices are the transverse field components which are governed by coupled integral equations. When unknowns are expanded as a linear combination of known basis functions, CTMIE is converted to matrix equations to obtain numerical solutions. We study three waveguide devices in detail to understand the relation between various modeling parameters and target parameters such as accuracy and the convergent rate of the solutions. These cases include a step waveguide junction, a multi-mode interferometer and a quasi-adiabatic tapered waveguide. All results are verified with independent calculations using other proven methods.

Analysis of Scattering Problem at Dielectric Continuity

Nai-Hsiang Sun[1], **Chia-Ming Hu**[1], **Min-Yu Tsai**[1], **and Po-Jui Chiang**[2]

[1]Department of Electrical Engineering, I-Shou University, Taiwan
[2]Department of Electronic Engineering
National Kaohsiung University of Applied Sciences, Taiwan

Abstract— To obtain the radiation loss at the discontinuity junction, radiation modes need to be calculated. Unlike guided modes, radiation modes can not be confined in the waveguide region and have oscillatory solutions in the superstrate and substrate of the waveguide. Radiation modes constitute a continuum of modes and create a continuous spectrum. A single radiation mode has two mathematical difficulties: Power orthogonality and normalization. Since radiation modes have infinite power, the overlap integral of radiation modes in the two regions become very difficult to calculate. In this paper, we analytically derive the overlap integral formula of radiation modes from theoretical method. Then we discretize the continuous spectrum of radiation modes to a discrete set of orthogonal radiation modes. By using the overlap formula, the radiation loss at the discontinuities in dielectric waveguides can be obtained.

A Combined Cavity with Improved Performance under Simultaneous Resonance of Sub-cavities

Chih Jung Wu[1, 2], **Qiang Liu**[1, 3, 4], **Chung Ping Liu**[2], **Jong C. Wang**[2], **and Zhengbiao Ouyang**[1, 3, 4]

[1]THz Technical Research Center, Shenzhen University, Shenzhen 518060, China
[2]Department of Electrical Engineering, Yuan Ze University, Taoyuan 320, Taiwan
[3]Shenzhen Key Lab of Micro-Nano-Photonics Information Technology
Shenzhen 518060, China
[4]College of Electronic Science and Technology, Shenzhen University
Shenzhen 518060, China

Abstract— Signal detection unit is a basic part in electronic, electromagnetic, and optical systems for communications, radars, sensors, etc. It is very important to have high sensitivity for long distance communication, long range radars, biological signal detection, and cosmic signal hunting. Especially, at present, THz signals are usually very weak and how to promote the sensitivity of THz signal detection becomes a key problem for development and application of THz technology.

The idea of combined cavity was presented by the authors in our group a year ago in the hope of promoting the field intensity in a cavity, so that weak signals can be detected. The key point is to make signals to be in double resonance through signal feedback in a combined cavity consisting of two sub-cavities. However, a simple combined cavity would not meet the condition for double resonance. For this we tried to add a piece of dielectric material in the feedback cavity, as shown in Fig. 1, and useful results were obtained. But we are not satisfied with them, and so we now do more studies on the combined cavity for higher sensitivity detection applications. We now add a dielectric rod in the point cavity or increase the volume of the point cavity in the combined system to shift the resonant frequency of the point cavity to be the same as that of the feedback cavity, as shown in Fig. 2. These systems are advantageous over our previous design in that the feedback cavity is uniform and no stray scattering exists in the cavity. We have done investigation on it and found the system can have higher localization field intensity than that in the earlier structure.

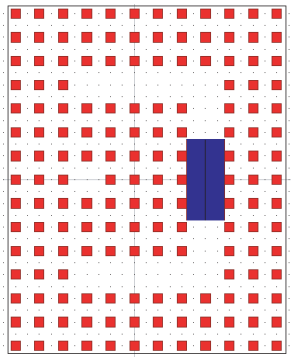

Figure 1: A combined cavity using a dielectric slab in the waveguide resonator to tune the resonance frequency.

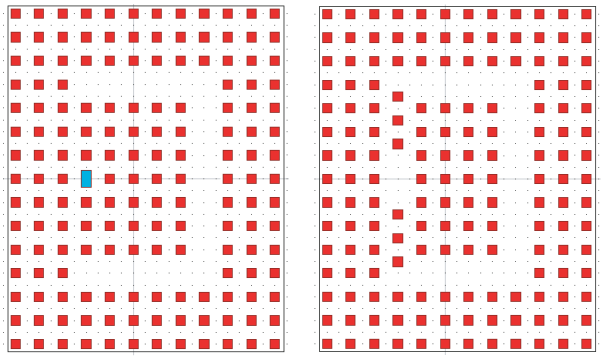

(a) (b)

Figure 2: A combined cavity in which the resonance frequency is tuned by (a) a dielectric slab in the point cavity and (b) increasing the cavity volume.

ACKNOWLEDGMENT

The authors acknowledge the Chinese Natural Science Foundation (Grant No. 60877034), the Guangdong Natural Science Foundation (Key Project No. 8251806001000004), and the Shenzhen Science Bureau (Project No. 200720, 200805).

Coupled Integral-equation Analysis of Crossing Waveguides

Hung-Wen Chang, **Sin-Yuan Mu**, **and Shih-Min Lu**
Institute of Electro-optical Engineering and Department of Photonics
National Sun Yat-sen University, Kaohsiung 80424, Taiwan

Abstract— We present a coupled integral-equation formulations for studying transmission, reflection and crossing coefficients in a crossing waveguide. Even for the simplest case of a microwave crossing waveguide there exist no analytic closed-form solutions due to the fact that fields and waves inside this device are propagating in all four directions. We show that fields in the horizontal/vertical waveguide can be expanded in terms of its waveguide modes. In the crossing region, fields can be written as linear combination of standing wave modes of both waveguides which are completely determined by the fields on the region boundaries. These unknown fields satisfy a coupled integral-equation that connects the waves in the four waveguides with the waves in the overlapped region. This integral equation is then converted to matrix equation to obtain the numerical solutions.

ACKNOWLEDGMENT

The authors are grateful to the support by National Science Council of the Republic of China under the contracts NSC 97-2221-E-110-016 and NSC 98-2221-E-110-012.

Numerical Solutions of Nonlinear Schrödinger Equation by Runge-Kutta Method with Cubic Spline Functions

Sen-Eon Liu and Hung-Wen Chang
Department of Photonics, Institute of Electro-optical Engineering, National Sun Yat-sen University
Kaohsiung 80424, Taiwan

Abstract— The nonlinear Schrödinger equation (NLSE) can be used to study envelope propagation of electromagnetic energy in optical fibers. It has extensively been used for modeling of long-haul optical fiber communication systems. NLSE can not be solved analytically. It is commonly solved by the split-step Fourier method in which the dispersive and nonlinear effects are separately integrated to construct the full solution. The linear term describes dispersion, whereas the nonlinear term describes self-phase modulation (SPM). In this paper, the pulse envelope is first expanded in terms of cubic spline functions. The resulting nonlinear system of ordinary differential equation is then solved by the fourth-order Runge-Kutta method (RK4). This method treats the linear and nonlinear terms simultaneously. It does not require transformation between the temporal and the frequency domains at each step. The performance of fourth-order Runge-Kutta methods with cubic spline functions is compared to conventional split-step Fourier method by modeling the pulse propagation in optical fibers.

ACKNOWLEDGMENT

The authors are grateful to the support by National Science Council of the Republic of China under the contracts NSC 97-2221-E-110-016 and NSC_98_982221-E110012.

Session 3P4
Nonlinear Photonics in Disordered Structures and Metamaterials

Subwavelength Imaging in Disordered Wire Media

David Powell and Yuri Kivshar
Nonlinear Physics Center, Research School of Physics and Engineering, Australian National University
Canberra, ACT 0200, Australia

Abstract— The possibility of reconstructing an image with subwavelength details has been one of the driving forces behind the development of SRR/wire media composite metamaterials. However, several studies have shown (see, e.g., Ref. [1]) that disorder suppresses the left-handed behaviour, which is critical for any type of imaging. Robustness to disorder is essential when scaling a structure down to the scale of THz or optical wavelengths, where precise control of dimensions becomes more difficult.

An alternative structure for sub-wavelength imaging is the thin wire medium operating in the "canalisation regime" [2]. This structure consists of a square lattice of parallel wires oriented along the axis of the lens. This is a much simpler geometry which does not rely on resonant particles. It has also been shown that the structure can operate at higher frequencies where plasmonic effects become significant. However its robustness to disorder has not been studied so far.

In this contribution, we present the analysis of the subwavelength imaging performance of disordered thin wire media in order to understand how its performance may be affected by manufacturing errors. The structure is found to be extremely robust to disorder which keeps the wires parallel. However, we also demonstrate that variation in the orientation of the wires and their longitudinal position may cause more significant degradation in the image quality, which is quantified numerically.

REFERENCES

1. Gorkunov, M. V., S. A. Gredeskul, I. V. Shadrivov, and Y. S. Kivshar, "Effect of microscopic disorder on magnetic properties of metamaterials," *Phys. Rev. E*, Vol. 73, 056605, 2006.
2. Belov, P. A., Y. Hao, and S. Sudhakaran, "Subwavelength microwave imaging using an array of parallel conducting wires as a lens," *Phys. Rev. B*, Vol. 73, 033108, 2006.
3. Powell, D., "The sub-wavelength imaging performance of disordered wire media," *Phys. Lett. A*, Vol. 372, 3919, 2008.

Transmission and Localization of Classical Waves in Weakly Scattering Metamaterials

A. A. Asatryan[1], **S. A. Gredeskul**[2, 3], **L. C. Botten**[1], **M. A. Byrne**[1], **V. D. Freilikher**[4], **I. V. Shadrivov**[3], **R. C. McPhedran**[5], **and Yu. S. Kivshar**[3]

[1]Department of Mathematical Sciences and Center for Ultrahigh-bandwidth Devices for Optical Systems (CUDOS), University of Technology, Sydney, NSW 2007, Australia
[2]Department of Physics, Ben Gurion University of the Negev, Beer-Sheva, 84105, Israel
[3]Nonlinear Physics Center and Center for Ultrahigh-bandwidth Devices for Optical Systems (CUDOS) Australian National University, Canberra, ACT 0200, Australia
[4]Department of Physics, Bar Ilan University, Ramat Gan, 52900, Israel
[5]University of Sydney, Sydney, NSW 2006, Australia

Abstract— We study the transmission and localization of classical waves in one-dimensional disordered structures composed of alternating layers of left- and right-handed materials (mixed stacks) and compare them to the structures composed of different layers of the same material (homogeneous stacks). For weakly scattering layers, we have developed an effective analytical approach and have calculated the transmission length within a wide region of the input parameters. This enables us to describe in a unified way the localized and ballistic regimes as well as the crossover between them. It is shown that if both refractive index and layer thickness are random, in the long-wavelength range, mixed and homogeneous stacks demonstrate different dependencies of the transmission length on the wavelength in localized regime, as well as different structures of ballistic regimes. While in the ultra-long wavelength range normal random dielectric samples transmit light as an effectively uniform medium, the transmission length in mixed stacks is always a strongly fluctuating quantity. In mixed stacks with only refractive-index disorder, the Anderson localization is substantially suppressed, the localization length grows with wavelength much faster, the crossover region becomes essentially wider, and the transmission resonances appear in much longer stacks, than in the general case. Effects of absorption on the one-dimensional transport and localization has also been studied, both analytically and numerically. Specifically, it is shown that the crossover region is particularly sensitive to losses, so that even small absorption suppresses noticeably the oscillations of the transmission length in the frequency domain. All our theoretical predictions are in an excellent agreement with the results of numerical simulations.

Nonlinear and Tunable Metamaterials

Ilya Shadrivov[1], **David Powell**[1], **Michael Lapine**[1, 2], **and Yuri Kivshar**[1]

[1]Nonlinear Physics Center, Research School of Physics and Engineering
Australian National University, Canberra ACT 0200, Australia
[2]Department of Electronics and Electromagnetics, Faculty of Physics
University of Seville, Seville 41015, Spain

Abstract— Metamaterials are prominent for the exceptional opportunities they offer in tailoring macroscopic properties through appropriate choice and arrangement of their structural elements. In this way, it is not only possible to design a metamaterial for a required purpose, but also to implement further adjustment capabilities at the level of assembly. This makes metamaterials different from conventional materials and opens exciting opportunities for multifunctionality via tunability. Tunable metamaterials imply the possibility to continuously change their properties through an external influence or signal with the intrinsic mechanism of tunability. The key means of tuning resonant metamaterials, naturally, lies in affecting the system so as to change the parameters of the resonance. As a consequence, the characteristics of metamaterial can be varied, enabling tunable transmission.

We review the recent experimental results from our Nonlinear Physics Center on tunability and nonlinear response of microstructured metamaterials with negative refractive index. We suggest and design new types of tunable metamaterials exhibiting either nonlinear magnetic or nonlinear electric response at microwave frequencies. By introducing a varactor diode as a nonlinear element within each resonator, we shift the frequency of either magnetic or electric resonance by changing the incident power.

We also propose an efficient approach for tuning the transmission characteristics of metamaterials through a continuous adjustment of the lattice structure and confirm it experimentally in the microwave range. The concept is rather general and applicable to various metamaterials as long as the effective medium description is valid. The demonstrated continuous tuning of a metamaterial response is highly desirable for a number of emerging applications of metamaterials, including sensors, filters, and switches, realizable in a wide frequency range.

Magnetic-resonance Enhanced Second Harmonic Generations in Metamaterials

Shiwei Tang, Hao Xu, and Lei Zhou
Physics Department, Fudan University, Shanghai 200433, China

Abstract— We summarize what we have obtained so far on numerical calculations on second harmonic generations in some optical metamaterials, which are in excellent agreement with the experiments. We find that the stimulated nonlinear signals are strongly enhanced when the incidence wavelength hits the magnetic resonance of the double fishnet structure, which includes the realistic structure (with inclined planes) and the perfect structure (without inclined planes). We study the electric field distributing of realistic fishnet structure and perfect fishnet structure at the frequency of magnetic resonance, and find that the stabilized electric field mainly distributes on the edges and in the middle of the dielectric slab. Then we optimize the angle of the inclined planes, where the SHG signals can be most strongly enhanced. The metamaterials are characteristically different from ordinary molecular media because magnetic resonances of metal nanostructures are intrinsically collective in nature instead of local as in molecular transitions.

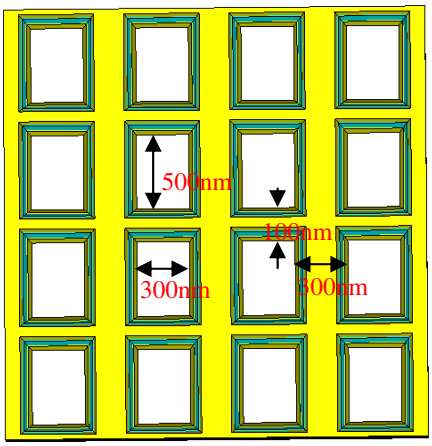

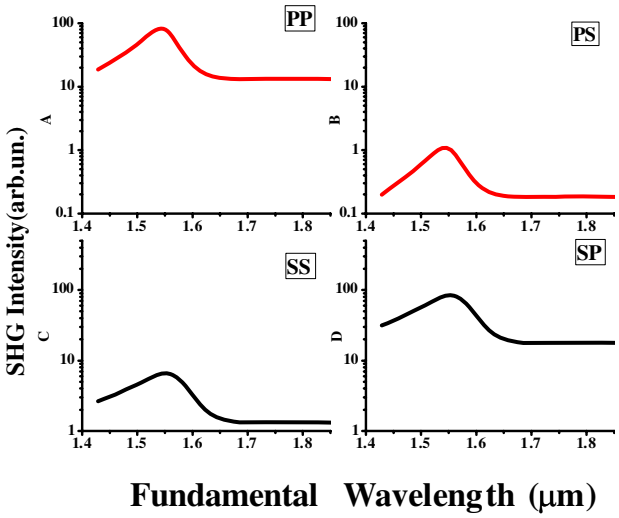

REFERENCES

1. Kim, E., F. Wang, W. Wu, Z. Yu, and Y. R. Shen, "Nonlinear optical spectroscopy of photonic metamaterials," *Phys. Rev. B*, Vol. 78, 113102, 2008.
2. Shen, Y., *Nonlinear Optics*, Wiley, New York, 1973.
3. Krause, D., C. W. Teplin, and C. T. Rogers, "Optical surface second harmonic measurements of isotropic thin-film metals: Gold, silver, copper, aluminum, and tantalum," *J. Appl. Phys.*, Vol. 96, 3626, 2004.

Polarization Effects on Anderson Localization in the Presence of Metamaterials

A. A. Asatryan[1], L. C. Botten[1], M. A. Byrne[1], V. D. Freilikher[2], S. A. Gredeskul[3], I. V. Shadrivov[5], R. C. McPhedran[4], and Y. S. Kivshar[5]

[1]Centre for Ultrahigh-bandwidth Devices for Optical Systems (CUDOS)
Department of Mathematical Sciences, University of Technology
Sydney, NSW 2007, Australia
[2]Department of Physics, Bar-Ilan University, Ramat-Gan 52900, Israel
[3]Department of Physics, Ben Gurion University of the Negev, Beer Sheva 84105, Israel
[4]CUDOS and School of Physics, University of Sydney, NSW 2006, Australia
[5]Nonlinear Physics Centre, Australian National University, ACT 0200, Australia

Abstract— In this work, we will present a comprehensive study of the effects of polarization on Anderson localization in disordered one-dimensional stacks composed either of normal materials, metamaterials, or mixed stacks having alternating layers of normal and metamaterials. Recently, we have shown that the combination of disorder (refractive index disorder) and meta-refraction, can substantially suppress Anderson localisation [1]. The suppression is so strong that it changes the functional behaviour of the localization length at long wavelengths from $\sim\lambda^2$ to $\sim\lambda^6$ at normal incidence. As an illustration of one of the striking polarization effects, we plot in Fig. 1 the dependence of localization length on wavelength for off-axis incidence at $\theta = 30^\circ$ for a mixed stack in which refractive index disorder uniformly distributed in the range [0.75, 1.25] .

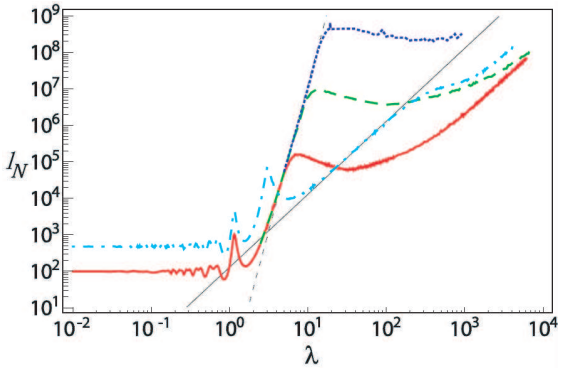

Figure 1: Localization length versus wavelength.

The solid line, dashed line and the dotted line respectively display the localization lengths for the TM (E parallel) polarization calculated for stacks of length 10^5, 10^7 and 10^8 layers in which the electric field is perpendicular to the plane of incidence. The dashed-dotted line is for TE (H parallel) polarization, in which the magnetic field is perpendicular to the plane of incidence, calculated for a stack of length 10^6 layers. While the TE polarized waves are strongly localized at long wavelengths, with the localization length dependence behaving as $\sim\lambda^2$, "E" polarized waves exhibit the same suppression of localization as occurs in the case of normal incidence [1].

In our paper [2], we derived simple and elegant formulae that describe the localization length as a function of wavelength for both mixed stacks and homogenous stacks for normal incidence. We have further shown that with minimal changes, these formulae generalize to the case of off-axis incidence. The presentation will show a number of examples illustrating the effects of polarization on the properties of Anderson localization in the presence of metamaterials.

REFERENCES

1. Asatryan, A. A., L. C. Botten, M. A. Byrne, V. D. Freilikher, S. A. Gredeskul, I. V. Shadrivov, et al., *Phys. Rev. Lett.*, Vol. 99, 193902, 2007.
2. Asatryan, A. A., S. A. Gredeskul, L. C. Botten, M. A. Byrne, V. D. Freilikher, I. V. Shadrivov, R. C. McPhedran, and Y. S. Kivshar, *Phys. Rev. A*, submitted.

Frequency Mixing in Disordered Quadratic Media

W. Wang[1, 2], **K. Kalinowski**[1], **D. Neshev**[1], **Y. Kivshar**[1], **W. Krolikowski**[1], **Y. Kong**[2], **V. Roppo**[3], **C. Cojocaru**[3], **J. Trull**[3], **R. Vilaseca**[3], **and K. Staliunas**[3, 4]

[1]Laser Physics Centre and Nonlinear Physics Centre, Research School of Physics and Engineering
Australian National University, Canberra, Australia
[2]College of Physics Science, Nankai University, Tianjin 300071, China
[3]Departament de Fisica i Enginyeria Nuclear, Universitat Politécnica de Catalunya
Terrassa (Barcelona) 08222, Spain
[4]Institut Catala de Recerca i Estudis Avancats (ICREA), Spain

Abstract— The efficient energy transfer in nonlinear parametric optical processes such as second harmonic generation critically depends on the phase synchronization between the interacting waves. This, the so-called phase matching condition reflects the conservation of linear momentum of light during the wave interaction. In many nonlinear materials, the phase-matching cannot be naturally satisfied because the material dispersion causes the refractive indices of interacting waves to differ. While a number of techniques has been adopted to achieve phase matching, e.g., temperature and angular tuning in birefringent materials, one of the most successful and universal methods is the so-called quasi-phase matching which relies on the spatially periodic poling of ferroelectric crystal. However such periodic structure is only effective for the particular choice of the wavelength of interacting waves. It turns out that broadband operation can be achieved utilizing random ferroelectric domain structures formed naturally in ferroelectric crystals which exhibit multi-domain structure with domains having random distribution of size and orientation. Such a disordered nonlinear medium is equivalent to an effective quasi phase matched system with almost infinite set of reciprocal wave vectors enabling to quasi-phase-match any parametric process, e.g., second harmonic generation or sum-frequency mixing in an ultra-broad frequency range.

In this contribution we present our recent experimental results on second and third harmonic generation in such random nonlinear structures formed in as grown strontium barium niobate crystals. We will consider various types of interaction geometry, discuss properties of the emitted harmonic wave and the possible application of this process in short-pulse monitoring.

Bistability of Localized States in One-dimensional Nonlinear Random Media

I. Shadrivov[1], **K. Bliokh**[2, 5], **Y. Bliokh**[3], **V. Freilikher**[4], **and Y. Kivshar**[1]

[1]Nonlinear Physics Centre, Research School of Physical Sciences and Engineering
Australian National University, Canberra ACT 0200, Australia
[2]Institute of Radio Astronomy, 4 Krasnoznamyonnaya Str., Kharkov 61002, Ukraine
[3]Department of Physics, Technion, Haifa 32000, Israel
[4]Department of Physics, Bar-Ilan University, Ramat-Gan 52900, Israel
[5]Applied Optics Group, Department of Physics, National University of Ireland
Galway, Ireland

Abstract— Wave transmission through a one-dimensional random nonlinear medium has been studied. It has been shown that weak Kerr nonlinearity does not influence the exponentially small transmission at typical (off-resonance) frequencies but affects dramatically the resonant disorder-induced localized modes excited inside the medium. As a result, the optical bistability of the localized states is observed, which is accompanied by a hysteresis loop in the output vs. input power dependence. Numerical modeling shows an excellent agreement with the theoretical predictions based on the concept of a high-Q resonator associated with each localized state. The predicted properties offer a possibility for creating an all-optical switch based on statistically-homogeneous disordered samples without periodicity or regular cavities.

Soliton Propagation through a Disordered Segment: Statistics of the Transmission Delay

Yaroslav Prylepskiy[1, 3], **S. A. Gredeskul**[2], **S. A. Derevyanko**[1], **and A. S. Kovalev**[3]

[1]NCRG, Aston University, Birmingham B4 7ET, UK
[2]Department of Physics, Ben Gurion University of Negev, Beer Sheva, Israel
[3]B. Verkin Institute for Low Temperature Physics and Engineering
NASU, Kharkov 61 103, Ukraine

Abstract— Within the framework one-dimensional self-focusing nonlinear Schrëdinger equation (NLSE) we study the problem of soliton propagation through a segment containing randomly distributed point-like scatterers. The NLSE itself is a ubiquitous nonlinear model appearing in many areas of contemporary physics. It is a one of the main models in the nonlinear fiber optics and the nonlinear fiber arrays. In the condensed matter physics NLSE occurs for example when describing, the nonlinear magnetization dynamics in ferromagnets with the easy-axis type anisotropy. Mathematically the problem consists in considering a perturbed NLSE of the following form:

$$iu_t + u_{xx} + 2|u|^2 u = u \sum_k \varepsilon_k \, \delta(x - x_k), \qquad k = 1, 2, 3, \ldots, \qquad -\infty < x < \infty. \tag{1}$$

Here $u(t, x)$ is the field variable, which can have different physical meaning in dependence on a particular problem, t is supposed to be a time variable (though in deferent contexts it can have meaning of a spatial one), and x is a spatial independent variable. The right hand side of Eq. (1) describes the influence of the point scatterers with (possibly random) intensities ε_k, placed at random positions x_k.

When the concentration of scatterers is small, that is to say the mean distance between scatterers is much larger than the size of a soliton, the transmission of a soliton through a disordered segment can be considered as a sequence of individual events of passing through a single scatterer. After each act of scattering, the transmitted soliton acquires a position shift as well as a change of both energy and velocity (i.e., the scattering is generally inelastic). These changes influence the transmission characteristics of the soliton through the total length of the segment, e.g., the time needed for a soliton to traverse the entire segment (we call it a "transmission time" here). Assuming that the scattering is weak one can postulate that a soliton passing through a single scatterer, experiences only a slight change of its parameters, i.e., it behaves like an effective particle. Based on these assumptions we develop a general method for obtaining the statistical characteristics of the soliton transmission through the segment. This method is applicable in the limit of small concentration of scatterers when the mean distance between the scatterers is much larger than the soliton width. It is shown that if the intensities of individual scatterers are also small and the disordered segment is relatively short, the transmission time delay of a "fast" soliton is mostly determined by the shifts of the soliton center after each act of scattering. On the contrary, for a sufficiently long segment the main contribution to the delay time is due to the shifts of the amplitude and velocity after each scatterer. Corresponding crossover lengths for both cases of "light" and "heavy" solitons are obtained. The method is tantamount to the consideration of a particle transferring via a disordered segment with the given velocity mapping rule after the act of scattering. Finally we calculate the exact probability density function of the soliton transmission time delay for a sufficiently long segment.

Slowing and Stopping Light with Gap-acoustic Solitons

Richard S. Tasgal, **R. Shnaiderman**, **and Y. B. Band**
Departments of Chemistry and Electro-Optics and the Ilse Katz Center for Nano-Science
Ben-Gurion University of the Negev, Beer-Sheva 84105, Israel

Abstract— Gap-acoustic solitons (GASs), which make use of the universal electrostrictive light-sound interaction, offer promising new avenues for slowing light. Optical gap solitons exist inside the frequency region of the band gap created by a Bragg grating. The Bragg grating, which may be considered as a distributed mirror for wavelengths in phase with it, keeps low-intensity light out of the gap. But nonlinearities can distort the optical band structure, and an intense pulse can punch a hole for itself in the band gap, in which it can then reside. The resulting localized structure, called an optical gap soliton, can be stable, with velocities from zero (i.e., stopped light) up to the group-velocity of light in the medium. When one also considers the effects of electrostriction, or the dependence of the index of refraction on the density of the material, optical gap solitons become GASs.

GASs share many of the properties of standard gap-solitons, but they have many interesting properties of their own, especially when their velocities are close to the speed of sound and they interact strongly with the acoustic field [1, 2]. For example, GASs which are moving at supersonic velocities may experience instabilities which leave the GAS whole, but bring the velocity abruptly

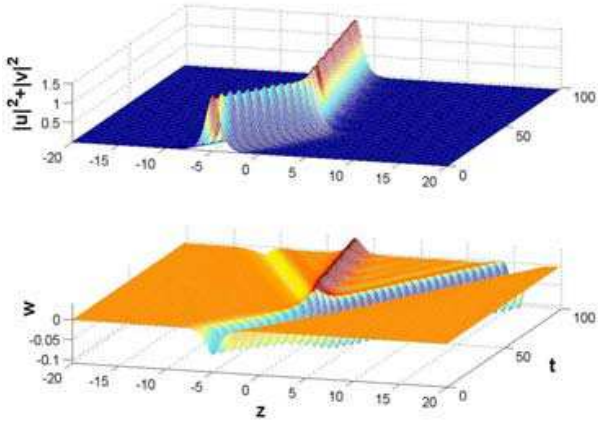

Figure 1.

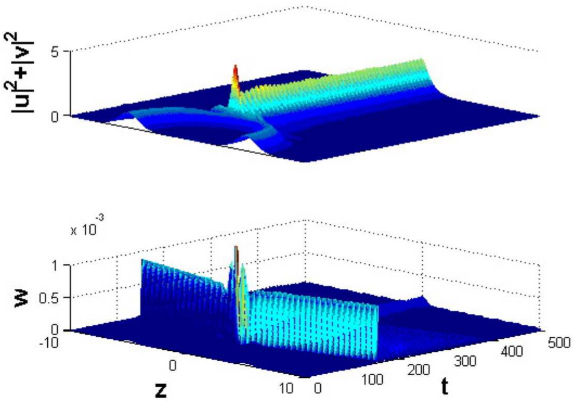

Figure 2.

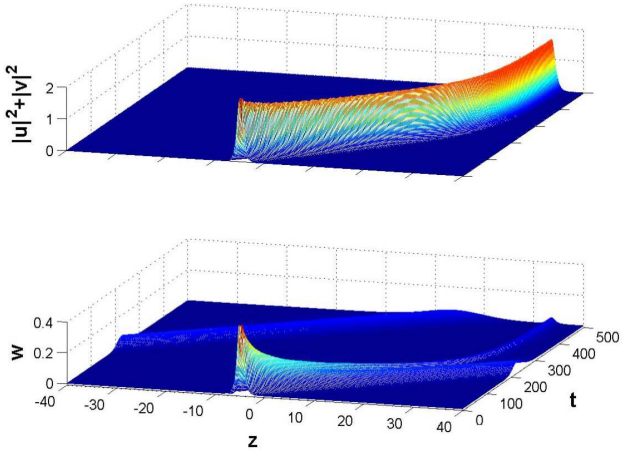

Figure 3.

to close to zero. This is illustrated in Fig. 1, with the light intensity on top and the material density (i.e., acoustic field) below, versus distance in the fiber and time. In the process of stopping, the GAS spins off acoustic waves forward and backward, which balances the decreased GAS momentum. Relatedly, GASs can be made to change velocity by collisions with acoustic pulses. By these effects, the GASs may be stopped and manipulated.

Two moving GASs may collide. In the illustration, Fig. 2, the GASs begin with zero velocity, and accelerate towards each other by a mutual attraction (which depends on the relative phase, and which decreases exponentially with soliton separation). The solitons merge during the collision, emitting energy into the acoustic field. Over a longer time-scale, the remaining excited energy is dissipated into the acoustic field.

Also, phonon damping decelerates GASs, as shown in Fig. 3. The soliton velocity decreases approximately exponentially. During this retardation process, the GAS emits acoustic waves moving in the same direction as the soliton. Using this effect in a recirculating loop, a GAS may be decelerated from a high velocity to low velocity.

In summary: We shall show that acousto-optical interactions of gap-acoustic solitons provides a toolbox by which light may be slowed, and by which slowed and stopped light may be manipulated.

REFERENCES

1. Tasgal, R. S., Y. B. Band, and B. A. Malomed, *Phys. Rev. Lett.*, Vol. 98, 243902, 2007.
2. Tasgal, R. S., R. Shnaiderman, and Y. B. Band, "Gap-acoustic solitons: Slowing and stopping of light," *J. Opt. Soc. Am. B*, (submitted).

Dynamics of Fluctuations in an Optical Laval Nozzle

I. Fouxon, **O. V. Farberovich**, **S. Bar-Ad**, **and V. Fleurov**
Raymond and Beverly Sackler School of Physics and Astronomy, Tel-Aviv University
Tel-Aviv 69978, Israel

Abstract— Using the analogy between the description of coherent light propagation in a medium with Kerr nonlinearity by means of nonlinear Schroedinger equation and that of a dissipationless liquid, we propose an optical analogue of the Laval nozzle. The optical Laval nozzle will allow one to form a transonic flow in which one can observe and study very unusual dynamics of classical and quantum fluctuations, including an analogue of the Hawking radiation of real black holes. Theoretical analysis of this dynamics is supported by numerical calculations, and estimates for a possible experimental realization are presented.

Controlling the Radiation of a Source in One-dimensional Random Media

V. Romanovskii[1], **K. Bliokh**[2, 4], **Y. Bliokh**[3], **and V. Freilikher**[1]

[1]Department of Physics, Bar-Ilan University, Ramat-Gan 52900, Israel
[2]Institute of Radio Astronomy, 4 Krasnoznamyonnaya Str., Kharkov 61002, Ukraine
[3]Department of Physics, Technion, Haifa 32000, Israel
[4]Applied Optics Group, Department of Physics, National University of Ireland, Galway, Ireland

Abstract— The possibility to control the intensity of radiated light, in particular spontaneously emitted, is essential for many applications ranging from lasers and light-emitting diodes, to optical switches, frequency filters, etc. To do this requires a dielectric environment whose response to the electromagnetic radiation can be expeditiously manipulated. Properly tailored one-dimensional random systems provide such an environment, causing the emission to be inhibited or accelerated, or even turned on and off completely. This is due to the existence in such systems of resonances (localized states), which are very narrow, both in space and frequency domain. The resonances are associated with effective high-Q cavities brought about by the interference of multiply scattered random fields. Although the location, effective size, and Q-factor of each cavity are random, they can be retrieved from the measurements of the transmission and reflection, and tuned, for example, by external radiation. We study analytically and numerically the field of a point source in one-dimensional disordered dielectric samples. It has been shown that the radiated intensity is extremely sensitive to the location of the source and to infinitesimal changes in the geometry and refractive index of a small part of the sample. The effect of absorption has also been studied. It appears that losses, if tunable, could provide an additional lever to control the emitted radiation. The results allow the conclusion that random configurations are promising candidates for tunable elements of various optical devices.

Unconventional Metal-insulator Transition in a Quantum Spin Hall Systems

Yshai Avishai[1, 2]

[1]Ben Gurion University of the Negev, Beer Sheva, Israel
[2]Graduate School of Mathematical Science, Komaba Campus, University of Tokyo
Tokyo, Japan

Abstract— Critical behavior of the Anderson metal-insulator transition in a quantum spin Hall system, which is distinguished from the usual symplectic model by its topological property, is studied and elucidated. In sharp contrast with the conventional characteristics of the Anderson transition, the critical exponent ν and the distribution $p(g)$ of the conductance g along the boundary between metal-insulator phases depend on the strength W of the disorder. These physical properties indicate a crossover between conventional symplectic systems and the unconventional ones, and suggest the existence of topological axis in a renormalization-group flow diagram similar to the σ_{xy}-axis in the two parameter flow diagram of the integer quantum Hall system. Level statistics and conductance distribution $p(g)$ for metallic states are studied and indicate that for large g, the metallic phase of the quantum spin Hall system is identical with the conventional symplectic one.

Session 3P5a
Physiological Effects of Static Magnetic Fields

Static Magnetic Field Induced Mechanotransduction in Osteoblastic Cells via Calmodulin-dependent Pathway — An in Vitro Culture Study

Haw-Ming Huang
Graduate Institute of Biomedical Materials and Engineering
Taipei Medical University, Taiwan

Abstract— For years, the effects of static magnetic fields (SMFs) on osteoblastic differentiation are well documented, however the mechanisms of SMFs-indiced signal transduction pathways are still unclear. The purpose of this study was to test the role of calmodulin in the biophysical effects of SMFs on osteoblastic cells. In this study, MG63 cells were exposed to a 0.4 T static magnetic field (SMF). The production of integrin-β1 protein on cell membranes was measured by flow cytometry technique. In addition, the expression of phosphodiesterase RNA in the cytoplasm was monitored by real-time polymerase chain reaction. The differentiation level of the cells was assessed by detecting changes in alkaline phosphatase activity. To test the role of calmodulin in the signal transduction pathway of SMF-induced osteoblastic differentiation, W-7 (calmodulin antagonist) was added in the culture medium during the SMF simulations. Our results showed that when compared to the untreated control group, the alkaline phosphatase activity and phosphodiesterase 1C gene expression of the SMF-exposed cells was significantly greater than that of the controls, with increases of 1.24 fold and 1.3 fold, respectively. However, for the above experiments, addition of W-7 significantly inhibited the SMF induced cellular response. With this regard, we suggest that one possible mechanism by which SMFs affects osteoblastic maturation is through a calmodulin-dependent mechanotransduction pathway.

Static Magnetic Field Interferes with the Physiological Removal of Circulating Apoptotic Lymphocytes

Luciana Dini
Department of Biological and Environmental Science and Technology, University of Salento
via per Monteroni snc, Lecce 73100, Italy

Abstract— During the last 20 years the influence of static magnetic fields (SMFs) on living organisms is becoming a topic of considerable interest due to the substantial evidence of their influence on tissues and cells. In various cellular systems, including cells of the immune system, a number of biological effects have been reported and different mechanisms have been proposed to explain these effects. Although a number of theoretical models have been proposed, the variety of experimental conditions (intensity, frequency and time windows of the fields, differing characteristics of the materials used-cell type, age, treatment) makes contradictory the data present in the literature and the possibility of the replication of the experiments. However, (S)MFs have been reported to perturb distribution of membrane proteins and sugars, receptors, cytoskeleton and trans-membrane fluxes of different ions, especially calcium $[Ca^{++}]i$. In turn, these alterations could interfere with specific physiological activies, like phagocytosis, which are based on receptors, cytoskeleton elements and motor proteins. In a previous work we found that, sinusoidal liver cells quickly recognized and engulfed human lymphocytes exposed for up to 72 h to 6 mT static magnetic fields, by using the same receptors that mediate the clearance of apoptotic cells. Thus, aim of the present work has been to decipher the modifications exerted by the SMF on lymphocytes and/or on the process of phagocytose. We analysed the cell surfaces of normal and apoptotic human lymphocytes in the presence or absence of 6 mT SMF by immunocytochemistry, proteomic, RT-PCR and biochemistry assays. The 2D-PAGE ph 4–7 analysis of cell lysates proteins shows their wide modifications after SMF exposure, that in part overlay those induced by apoptosis. SMF increases, in a time-dependent way, the expression of GD3 and cholesterol on the plasma membrane of normal lymphocytes and prevents GD3 removal on apoptotic-induced cells. The activity of ABCA1 is significantly enhanced in SMF-exposed lymphocytes, with a peak at 48 h of exposure, with respect to not exposed control cells. On the contrary, lipid peroxidation of plasma membrane, observed soon after lymphocytes induction of apoptosis, needs at least 72 h of SMF exposure to get a comparable level. Further studies will clarify if SMF exposure could be used as a novel therapeutic tool to produce "apoptotic dressed cancer cells" and thus promote their elimination.

Studies on the Effect of Static Magnetic Fields on Biological Systems

Arthur D. Rosen
Department of Biological Sciences, Purdue University, West Lafayette, IN 47907, USA

Abstract— In our initial studies on the bioeffects of moderate intensity SMFs we examined the influence of a 120 mT field on the evoked response recorded in visual cortex of mammals, during stimulation of the optic radiation fibers. A significant reduction in the amplitude of the synaptic components of that response was observed during SMF exposure. The most intriguing aspect of this study was the finding that the observed effect developed only after 50 seconds of exposure and persisted for several minutes after the field was turned off. Subsequent studies examined the release of neurotransmitter from the presynaptic membrane during SMF exposure. A decline in neurotransmitter release during exposure was seen, but again only after a delay of up to 50 seconds. In addition, this phenomenon was found to be Ca^{2+} dependent. Utilizing the whole cell patch clamp technique, we examined the effect of a 120 mT SMF on the kinetics of Ca^{2+} currents in cultured GH3 cells. A slowing of channel activation rate without any change in the inactivation rate was noted. This change in channel function was delayed but completely reversible, with return to pre-exposure values within 2 to 3 minutes after the field was turned off. We have proposed that these findings may be explained by the collective diamagnetic properties of membrane phospholipids. Translational movements of these molecules in a SMF, though relatively slow because of intrinsic membrane viscosity, are assumed to impinge on the intramembranous portion of the Ca^{2+} channel, the α_1 subunit. This is the voltage sensitive molecule in the calcium channel complex and is located almost entirely within the membrane where it would be vulnerable to any membrane deformation. Channel inactivation occurs at the intracellular pore formed by the β subunit. Molecular structures in this location would be insensitive to any magnetically induced membrane deformation. All of the bioeffects associated with brief exposures to SMFs were of relatively short duration, with return to baseline function within minutes following termination of exposure. The possibility of a more lasting effect on cellular function was examined during prolonged exposure to a 0.5 T SMF. Growth and size of cultured GH3 cells was examined. Cell proliferation studies employed continuous exposure for periods of 1, 2, or 4 weeks, followed by a 4 week post-exposure period. For the cell size studies, 5 weeks of exposure was followed by a 4 week post-exposure period. Following a 1 week exposure, a transient decline in cell growth was seen. This was not statistically significant but with a 4 week exposure, a statistically significant decline in growth of 51% was seen with return to control levels only after 4 weeks. Cell diameter significantly increased following 3 weeks of exposure with return to control 3 weeks after exposure termination. SMF alteration in membrane Ca^{2+} flux, though relatively small, is cumulative and will eventually be reflected in changes in intracellular Ca^{2+} stores. This, in turn, will result in changes in the actin cytoskeleton. This intracellular structure is not static, but continuously reorganizes in a Ca^{2+} dependent fashion. It has been shown to be essential for a number of cellular processes including cell division following mitosis (cytokinesis). Ca^{2+} dependent changes in the dynamic reorganization of the actin cytoskeleton are suggested as a likely explanation for the effect of SMFs on cell growth and size.

Cellular Perception and Static Magnetic Fields Active Penetration Depth for Pain Magnetotherapy

Pierre Le Chapellier and Badri Matta
Soissons General Hospital, Soissons, France

Abstract— Cellular perception concerns the process by which stimulation induces events through mechanical signaling pathways, according to a sense order whose nature is discussed by epistemology: it is supposed that the signification base at the origin of the cell behavior answers to a "*being-envelope*" whose physical nature can be approached in topological thermodynamics terms. In joined cells with gap-junctions, sense order can be covered by the signaling effect of calcium waves. But as it is related to the cell functional status, it can explain the biphasic response of the cell behavior after exposure to Static Magnetic Fields, SMF.

Four magnetobiological mechanisms solve the "kT *paradox*" about thermal agitation, (whose energy is $4 \cdot 10^{-21}$ J, at 310°K): 1/ Magnetosomes; (endogenous ferromagnetic nanoparticles can have magnetic moments of 2 $10^{-15}\,\mathrm{JT}^{-1}$.) For ionic channels activation, these magnetosomes must operate two other kT independent mechanisms: 2/ Radicals' pair, and 3/ Interference in angular modes of proteins. A fourth mechanism is: 4/ Protons subsystems, (inducing topological evolution in the medium.)

In these mechanisms, the SMF determining parameter is induction B: when comparing clinical trials results about pain relief by SMF, an active induction threshold of 0.5 mT is suggested. With the field decay from the magnet surface, when B is around 0.5 mT, the lateral field gradient, dB/dx, is far under its active threshold, thus secondary.

Therapy must determine the SMF Active Penetration Depth from the skin surface, as compared to the tissue receptors depth. It depends on the magnet characteristics and setting.

Anticonvulsant Effects of Static Magnetic Fields in Animal Seizure Models

Michael J. McLean, **Stefan Engström**, **Qinkun Zhang**, **and Minhua Zhang**
Department of Neurology, Vanderbilt University Medical Center
Nashville, Tennessee, USA

Abstract—

Rationale: We studied the effects of static magnetic fields on audiogenic seizures in genetic and chemically-induced mouse seizure models in an effort to find a novel, non-pharmacological treatment for human epilepsy.

Methods: In three animal models (DBA/2, NMDA and theophylline), pretreatment was accomplished with a water-cooled, static magnetic field (SMF) exposure device built with coils around four ferromagnetic cores in a square array. The coils were wired such that polarity alternated. A constant current power supply energized the coils. All mice were kept in perforated tubes prior to experiments. Different groups of mice served as controls or were treated with SMF for 60 min ($B = 5.27\,\mathrm{mT}$, $\nabla B(\mathrm{perpendicular}) = 0.24\,\mathrm{T/ms}$; values averaged over head volume) before experiments. Black Swiss mice, the fourth model, were exposed to SMF (100–220 mT, 15–40 T/m for 1 h) produced by permanent magnets. In all models, controls were placed in perforated tubes, but were not exposed to SMF (sham). After pretreatment, mice were removed from the tubes and from the SMF and were placed in a closed plexiglass chamber for acoustic stimulation. A speaker in the lid delivered constant white noise at intensities of 70–120 decibels. Untreated seizures evolved from wild running (WR), to loss of righting (LOR) and clonic jerks (CLO) in almost all animals. In some, the seizures were more severe and evolved into tonic hindlimb extension (THE) and death (DEA).

Results: After exposure to $\sim 5\,\mathrm{mT}$ fields for 30 minutes, $\sim 50\%$ of DBA/2 mice exhibited no seizures in response to auditory stimulation, compared to 80–90% of unexposed controls. Also, $\sim 50\%$ of outbred ICR mice survived and had no clonic activity or extensor hindlimb seizures after intra-cerebroventricular injection of NMDA compared to almost all controls. Intraperitoneal injection of theophylline (75 mg/kg) induced audiogenic seizures in outbred ICR mice. SMF pretreatment blocked seizures and death in $\sim 25\%$ of mice compared to comcomitant controls.

Incomplete efficacy of magnetic field pretreatment led us to investigate prophylactic efficacy of pretreatment with a combination of magnetic field exposure and phenytoin in DBA/2 mice. This clinically-used anticonvulsant drug completely suppressed seizure manifestations without significant toxicity in a dose-dependent manner. Mice from one supplier (Charles River Laboratories) required 3–4 fold less phenytoin than was required for protection in mice not exposed to SMF. Mice from a second supplier (Jackson Laboratories) exhibited a different pattern of anticonvulsant response to phenytoin alone, but seizure manifestations not affected by field or phenytoin alone were significantly reduced by pretreatment with a combination of phenytoin and magnetic field.

The hearing threshold (assessed with brainstem auditory responses) of black Swiss mice exposed to SMF (100–220 mT, 15–40 T/m for 1 h) was not different from that in unexposed controls. EEG changes were recorded during audiogenic seizures. Pretreatment with SMF prolonged seizure latency in response to stimulation with white noise of increasing intensity from 74 to 102 dBA (1 min interval between 2 and 4 dBA increments) without significant effects on seizure severity. Gender-related differences were not statistically significant. Stimulation with 10 min sound steps revealed prolongation of latency and reduction of seizure severity in SMF-exposed, but not unexposed, mice. Pretreatment with phenytoin (5 mg/kg) in combination with SMF had significantly greater effects on seizure latency and severity than either pretreatment alone.

Conclusions: These findings demonstrate variable anticonvulsant effects of the SMF studied here and enhancement of the response to phenytoin in combination with exposure to the static magnetic field. It is hoped that these findings will lead to therapeutic trials in human patients with epilepsy. Concomitant treatment with SMF may allow reduction of drug load without sacrificing efficacy; or, efficacy of the highest tolerable drug dose may be potentiated by SMF exposure without increasing systemic side effects.

Analysis of Inhomogeneous Static Magnetic Field-Induced Antinociceptive Activity in Mice

János F. László[1] **and Klára Gyires**[2]
[1]Institute for Research Organization, Hungarian Academy of Sciences
Nádor u. 18, 1051 Budapest, Hungary
[2]Department of Pharmacology and Pharmacotherapy, Semmelweis University, Budapest, Hungary

Abstract— The effect of inhomogeneous static magnetic field (SMF) on visceral pain elicited by the intraperitoneal injection of 0.6% acetic acid (writhing test) was studied in the mouse in an environment, where animals could freely move. Thirty min exposure to SMF (permanent NdFeB N50 grade 10×10 mm cylindrical magnets with alternating poles) following the nociceptive stimulus resulted in a 54% ($p < 0.005$) inhibition of the pain reaction. With the help of several inhomogeneous SMF configurations, where magnets were groupped in partitions and a 2D model of ambulation, motion-induced electric currents, MR-equivalent switching rate and slew rate were estimated. Their contribution to pain inhibition was questionned although some of them exceeded the threshold for peripheral nerve stimulation.

Session 3P5b
Systems and Components, Electromagnetic Compatibility

Radiation Induced Forward Emitter Current Gain Degradation of Lateral and Vertical PNP Power Transistors in Voltage Regulators

Vladimir Vukić[1] and Predrag Osmokrović[2]

[1]Institute of Electrical Engineering "Nikola Tesla", Belgrade, Serbia
[2]Faculty of Electrical Engineering, University of Belgrade, Belgrade, Serbia

Abstract— Voltage regulators "National Semiconductor" LM2940CT5 and "STMicroelectronics" L4940V5 were examined in γ radiation field. It was perceived that voltage regulators LM2940CT5, manufactured by use of conventional monolithic bipolar process with lateral pnp transistors with round emitters, become unfunctional after absorption of low doses of radiation (less then 300 Gy(SiO_2)). The main reason of low total doses circiut failures was not loss of forward emitter current gain, but the degradation of error amplifier circuit. On the other hand, voltage regulators L4940V5, BiCMOS integrated circuits created with implementation of local oxide side isolation process, showed much higher radiation hardness (more then 10 kGy(SiO_2)). Before experiment it was asumed that local oxide may cause creation of parasitic MOSFET, i.e., radiation-induced leakage currents between collector and emitter of serial transistor. However, implementation of isolated collector in integrated circuit made by "HDS^2/P^2 Multipower 20 V" process prevented negative influence of local oxide isolation. Hypothesis was that the main cause of high radiation hardness is small degradation of serial vertical pnp transistor's forward emitter current gain, mainly due to shift of current flow from the surface towards the substrate. Though, detailed examinations pointed on significant reduction of serial transistor's forward emitter current gain, causing the great increase of quiescent current. Yet, the mentioned effect didn't have influence on proper circuit's functioning, even after absorption of very high total doses.

The main reason of high radiation susceptibility of examined vertical serial pnp transistor is implementation of interdigitated emitter, with high perimeter-to-area ratio, applied due to increase of emitter efficiency during the operation with high currents. On the other hand, transistors with round emitters have small perimeter-to-area ratio. This characteristic is very important for operation with high current density, but is also an unfavorable postulate for operation in radiation environment. Experiment showed almost equal influences of emitter geometry and technological process of pnp transistor creation on degradation of power transistor characteristics. Small degradation of maximum output current of voltage regulator L4940V5 suggests that negative feedback reaction caused shift of serial transistor operation point far from the maximum of curve $\beta(I_E)$. In serial transistors operation conditions of high-level carrier injections in emitter area (total circuit's current of 500 mA), when the forward emitter current gain is little affected by the change of base-to-emitter voltage, noticed decline of lateral serial transistor's forward emitter current gain (of voltage regulator LM2940CT5) was some 40%, while the current gain decline of vertical transistor of circuit L4940V5 was about 30%.

Influence of Gamma Radiation on Some Commercial EPROM and EEPROM Components

Boris Loncar[1], **Srboljub Stankovic**[2], **Koviljka Stankovic**[1], **and Bojan Jovanovic**[1]

[1]University of Belgrade, Belgrade, Serbia
[2]VINCA Institute of Nuclear Sciences, Belgrade, Serbia

Abstract— The aim of this work is to examine and investigate comparative analysis the reliability of commercial off the shelf (COTS) Erasable Programmable Read Only Memory (EPROM) and Electrically Erasable Programmable Read Only Memory (EEPROM) components under the influence of gamma radiation. Reliability of programmable memories is of great importance due to their widespread application in electronic devices. When hardness design of these components is not efficient enough, radiation effects can cause their partial damage or complete destruction.

Influence of cobalt-60 gamma radiation was tested on NM27C512 8F85 EPROM and M24128-B W BN 5 T P EEPROM components. Fifty samples were used for both EPROM and EEPROM testing, from which the average results presented in the paper were obtained. All tests were performed at room temperature (25°C). Irradiation of a 50-sample batch was conducted in consecutive steps, corresponding to the increase of total absorbed dose. Dose increment was 20 Gy per irradiation step for EPROMs and 60 Gy for EEPROMs.

EPROM components proved to have better radiation reliability than EEPROMs. Significant faults in EPROM and EEPROM components appeared at 1300 Gy and 1000 Gy, respectively. Changes in EPROMs are reversible, and after erasing and reprogramming, all EPROM components are functional. Reversibility of changes in EPROMs is attributed to partial light-induced annealing of trapped holes during UV erasure. Due to the cumulative radiation effects, first failures of the previously irradiated EPROMs appear at significantly lower doses. On the other hand, EEPROM changes are irreversible. All observed phenomena have a plausible theoretical explanation, based on the interaction of gamma radiation with the oxide layer of memory cell MOS transistors. The influence of gamma radiation is basically manifested through the change of the net gate surface charge density, and consequently of transistor threshold voltage.

Ambiguous Influence of Radiation Effects in Solar Cells

Aleksandra Vasic, **Milos Vujisic**, **Koviljka Stankovic**, **and Bojan Jovanovic**
University of Belgrade, Serbia

Abstract— Regardless of the very high standards in the production of electronic devices, all of them are more or less, prone to the effects of aging even if they are not exposed to extreme (hostile) working conditions. One of the most limiting factors for all kinds of detectors is their noise, such as frequency dependent generation-recombination noise, burst noise and 1/f noise. Common source of noise that is connected to the hostile working conditions is radiation. Photovoltaic (PV) conversion of solar energy is one of the most up-to-date semiconductor technologies that enables application of PV systems for various purposes. Solar cells, the basic elements for photovoltaic conversion of solar energy, are especially susceptible to radiation damage, primarily due to their large surface. The lifetime of the solar cell is restricted by the degree of radiation damage that the cell receives. This is an important factor that affects the performance of the solar cell in practical applications. Introduction of radiation-induced recombination centers reduce the minority carrier lifetime in the base layer of the p-n junction increasing series resistance, and lead to an enormous increase of noise in solar cells. After very high doses of radiation series resistance of the base layer could be so high that most of the power generated by the device is dissipated by its own internal resistance. The aim of this paper is to investigate the influence of radiation on output characteristics of solar cells in connection to their noise level that could lead to better understanding of transport properties, electron-hole pair creation etc.

Influence of Tube Volume on Measurement Uncertainty of GM Counter

Koviljka Stankovic, **Predrag Osmokrovic**, **and Milos Vujisic**
University of Belgrade, Serbia

Abstract— GM counter is used often in radiation detection since it generates strong signal which can be easily detected. Working principal of GM counter is based on ionization interaction of radiation with atoms and molecules of gaseous in counter's tube. Free electrons created as a result of the interaction, present in a counter's tube, become initial electrons, i.e., they start an avalanche process which is detected as a pulse of current. This current pulse is independent on energy imparted in gaseous which is the main difference between GM counter and majority of other radiation detectors. Dependence on incidence radiation energy, tube's orientation and reading system characteristics are labeled in the literacy as the main sources of measurement uncertainty of GM counter. The aim of this paper is to determine influence of counter's tube volume on the measurement uncertainty of GM counter. Therefore, dependence of detecting pulse current formation on counter's tube size will be considered, both in radial and parallel geometry. Initiation and current pulse developing will be treated throughout elementary processes of electrical discharge as Markov processes, while the change of counter's tube volume will be treated throughout space-time enlargement law. Random variable "current pulse in the counter's tube" (i.e., electrical breakdown of the electrode configuration) will be considered statistically and based on it, appropriate theoretical distribution will be determined. Results obtained theoretically will be compared with appropriate experimental results obtained under well controlled laboratory conditions. Parameters varied in the experiment will be ionizing radiation energy and counter's tube orientation on the direction of incidence radiation.

Monte Carlo Simulations of Proton and Ion Beam Irradiation on Titanium Dioxide Memristors

Ćemal Doličanin[1], **Bratislav Iričanin**[2], **Miloš Vujisić**[2], **and Predrag Osmokrovic**[2]

[1]University of Novi Pazar, Serbia
[2]Faculty of Electrical Engineering, University of Belgrade, Serbia

Abstract— The memristor is composed of a titanium dioxide thin film between two platinum electrodes. The oxide layer further consists of an insulating TiO_2 layer and a conducting oxygen deficient TiO_{2-x} layer. Oxygen vacancies in the TiO_{2-x} layer act as mobile positively charged dopants, which can drift in the electric field created by a voltage applied to the device's terminals. The total resitance of the device is determined as a series connection of the highly resistive stoichiometric layer and the conducting oxygen-poor layer. When a voltage is applied, the oxygen vacancies drift, shifting the boundary between the high-resistance and low-resistance layers. The total resistance is thus dependent on charge which has passed through the memristor. Additionally, if the applied voltage is removed, the memristor "remembers" its last state, i.e., the value of total resistance at the moment of voltage suspension. Since memristor resistance is dependent on the distribution of oxygen vacancies, it is to be expected that operation of this device is sensitive to radiation exposure, which could cause displacements of additional oxygen atoms, and thus perturb the distribution of vacancies. The aim of this paper is to investigate effects of titanium dioxide memristor exposure to proton and ion beams. Theoretical discussion of these effects is accompanied by Monte Carlo simulations of particle transport through a multilayered thin-film structure, recently proven to have memristive characteristics. This structure consists of one layer of TiO_2 and one layer of oxygen-deficient TiO_{2-x}, sandwitched between two platinum contacts. It is concluded that radiation response of the memristor depends on the thickness of the conducting oxygen-deficient layer.

Influence of Irradiation on Semiconductor and Gas-filled Diodes for Over-voltage Protection

Radeta Maric[1], **Miladin Jurosevic**[2], **Gvozden Ilic**[1], **and Predrag Osmokrović**[3]

[1]Electric Power Industry of Serbia (EPS), Serbia
[2]Alumina Factory, Birač, Zvornik, Republic of Srpska, Bosnia and Herzegovina
[3]University of Belgrade, Serbia

Abstract— Over-voltage is a rather common occurrence in all electronic circuits, which makes efficient over-voltage protection a primary design requirement. An efficient over-voltage protection has two aspects: protection of integrity (no permanent damage of the protected device) and maintenance of operational functionality (operation reliability in the event of an over-voltage). Both power systems (energy generation, transmission and distribution) and low-voltage (electronic) systems are susceptible to over-voltages. The extent to which an electronic component can withstand a temporary over-voltage without damage is reduced significantly as components are miniaturized. Over-voltage protection components can generally be divided into linear and nonlinear ones. The linear group includes capacitors, coils, resistors, or their combinations as filters. Semiconductor over-voltage diodes (known also as transient voltage suppression diodes) and gas-filled over-voltage diodes (also called gas-filled surge arresters) fall into the group of nonlinear over-voltage protection components. In practice, various hybrid schemes combining the linear and non-linear components are often used. The wide-spread use of semiconductor and gas-filled diodes for non-linear over-voltage protection results in a variety of possible working conditions. It is therefore essential to have a thorough insight into their reliability in exploitation environments which imply exposure to ionizing radiation. The aim of this paper is to investigate the influence of irradiation on over-voltage diode characteristics, by exposing the diodes to Californium-252 combined neutron/gamma radiation field. Irradiation of semiconductor over-voltage diodes causes severe degradation of their protection characteristics. On the other hand, gas-filled over-voltage diodes exhibit a temporal improvement of performance. Results are presented with the accompanying theoretical interpretations of the observed changes in over-voltage diode behavior, based on the interaction of radiation with materials constituting the diodes.

A Shape Display Method Based on Electromagnetic Localization and Actuation

K. Deng[1], **E. T. Enikov**[1], **and P. Marek**[2]
[1]Department of Aerospace and Mechanical Engineering, University of Arizona, USA
[2]Institute of Applied Mechanics and Mechatronics, Slovak University of Technology in Bratislava, Slovakia

Abstract— The need to display graphics to visually impaired people has been growing with the emergence of World Wide Web (WWW). Electronic devices aiming to fulfill this function can be categorized into two groups. One is to use active touch method where the profile of the shape is produced by using a tactile matrix [1, 2] or using the virtual environment through force feedback [3]. These devices, however, either demand a relatively large platform to incorporate a touching interface, or require large driving element to produce enough force to users. The other group of devices is to use passive sensing method where the shape is locally produced to human skin by using spatially discriminated stimulation [4], which is mainly successful for two dimensional graphs. This paper proposes an approach that combines both active and passive tactile method to display three dimensional virtual objects. The proposed device uses an electromagnetic (EM) position detector and a single EM actuator to selectively stimulate human finger based on its location. The working principle is shown by the block diagram in Figure 1. Human brain interacts with the EM actuator as receiving stimulation information and guides the finger to move following its estimate of the reference shape. The real time location of the finger is measured and then compared with coordinates of the reference shape. The comparison results in a decision to engage the actuator and produce vibratory stimulation to the finger at a variable frequency based on

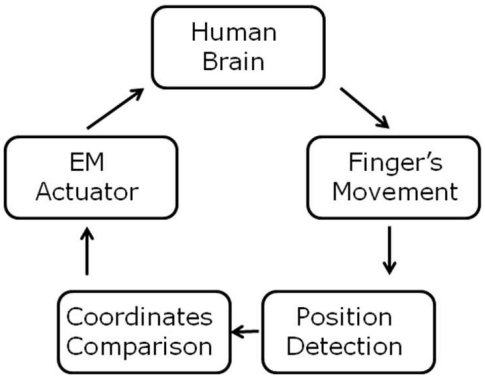

Figure 1: Block diagram of shape display method.

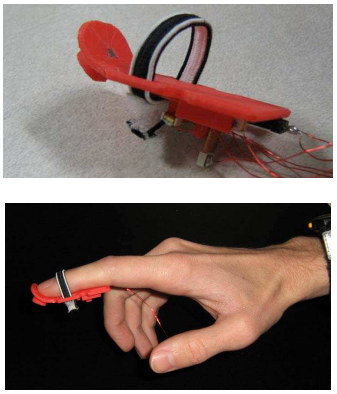

Figure 2: Photograph of the device.

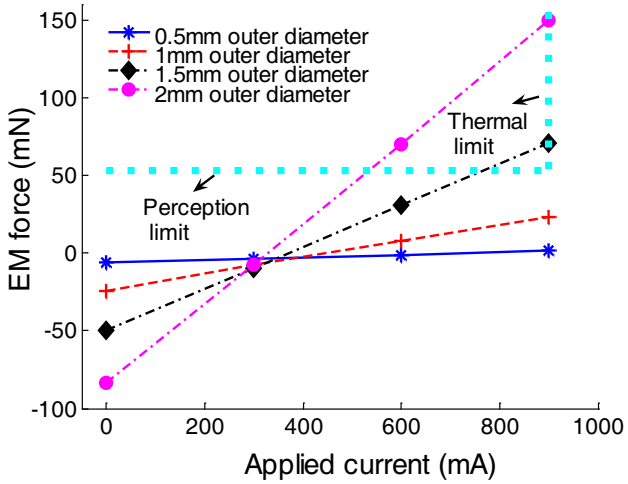

Figure 3: EM force scaling analysis.

the relative location of fingertip to the shape. During iterations of receiving information and modifying the estimates, users may obtain a certainty for an optimal estimation of the shape. The photograph of the device is shown in Figure 2. The experiment participated by three volunteers shows that the perception of small scale or highly curved shapes remains difficult. A device containing array of such actuators is proposed to address this difficulty. The EM force scaling analysis aiming to design a further miniaturized actuator is performed by using finite element software. The results shown in Figure 3 conclude that the actuator with 1.5 mm scale is able to induce tactile stimulation.

REFERENCES

1. Iwata, H. and H. Yano, *Proc. 28th Annual Conf. Comp. Graph and Interactive Tech.*, 469–476, 2001.
2. Kawai, Y. and F. Tomita, *ASSETS'96*, 45–50, 1996.
3. Nikolakis, G. and D. Tzovaras, *SPECOM'2004*, September 2004.
4. Fukuda, T. and H. Morita, *1997 Int. Symp. Micromechatronics and Human Sci.*, 143–148, 1997.

Session 3P6a
Antenna Theory, Radiation, Microstrip and Printed Antennas 2

Coplanar-fed UWB Elliptical Patch Antenna with Notched Band Characteristics

R. A. Sadeghzadeh[1], **M. A. Honarvar**[2], **and A. R. Eskandari**[3]

[1]Dept. of Eng., Khajenasirtoosi University, Tehran, Iran
[2]Islamic Azad University, Najafabad Branch, Isfahan, Iran
[3]Islamic Azad University, East Tehran Branch, Tehran, Iran

Abstract— This paper presents a novel band notched compact size antenna for ultra-wideband (UWB) communication. The antenna consists of a elliptical metal patch and a 50 Ω coplanar waveguide (CPW) transmission line. To achieve wide band characteristic, tapered ground plane is used. By etching two U and inverted U-shaped slots in the metal patch, band-stopped filtering properties are achieved. By attaching two parasitic U-shaped strip to the top layer of antenna stronger notch is obtained. In this case the total length of two strips is equal to the total length of two slots. It was found that the length of slot is corresponding to the notched frequency, so it is convenient for adjusting the length of the slot to control the notched frequency. The notched band width can be tuned slightly through adjusting the width of the slot. Thus a specified notched band can be obtained through tuning the length and width of the slots and the parasitic strips.

Figure 1 shows the configuration of a UWB antenna. The antenna was fabricated on an $h = 1.6$ mm FR4 epoxy substrate with dielectric constant $\varepsilon_r = 4.4$ and loss tangent $\delta = 0.02$. since both the antenna and the feeding are implemented on the same plane, only one layer of substrate with single-sided metallization is used, and the manufacturing of the antenna is very easy and low cost.

The electromagnetic software Ansoft HFSS 10 is employed to perform the design and optimization process. The proposed antenna yields an impedance band width of 3.1–10.5 GHz with VSWR < 2 except the band width of 5–6 GHz for IEEE 802.11a. the stable omni directional patterns in H-plane and symmetric in E-plane are also obtained.

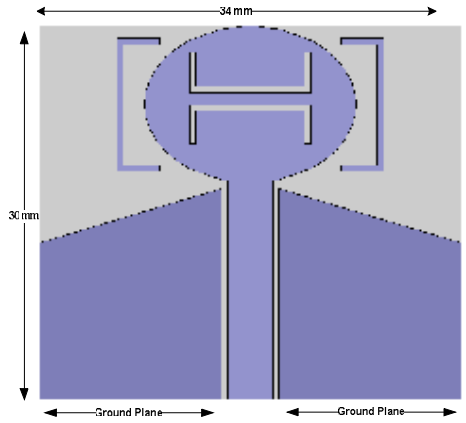

Figure 1: The configuration of proposed antenna.

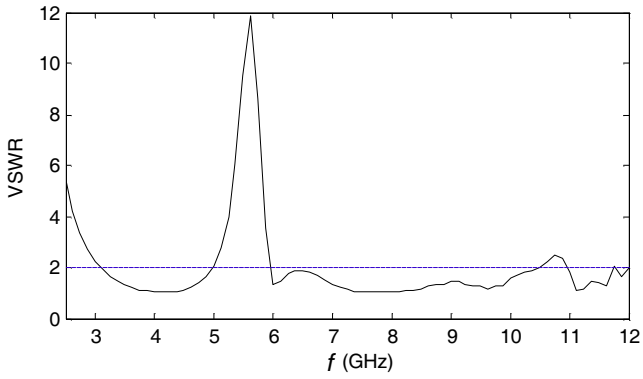

Figure 2: Simulated VSWR of proposed antenna.

Near Field Antenna Investigation and Evaluation for UHF RFID Systems

Zijian Xing, **Ling Wang**, **Changying Wu**, **and Dengshan Huang**
School of Electronics and Information, Northwestern Polytechnical University
Xi'an 710072, China

Abstract— The radio-frequency identification (RFID) technology is of growing interest to commerce, industry, and academia. The reader antenna is an important part and has great influence on the performance of the whole RFID systems. This paper will investigate and evaluate two near field antennas for UHF RFID readers. Near field performance will be focused. Modeling, parameters optimization, and performance of these two near field antenna will be introduced in detail. Furthermore, performance comparison of these two antennas to show the advantages and disadvantages will be given.

These two antennas are both made of PCB board. This kind of antenna is smaller and lighter than some other kinds of antennas, and easily produced. It is suitable for RFID application. The two antennas are both loop structure, which is similar with some other kind of RFID antennas. With the loop structure, the current of loop circuit antenna can be designed to keep consistent, thus the magnetic field distribution around the loop's axis will be concentrated and enhanced, which is easier for tag to receive more energy from reader's antenna. On the other hand, in order to reduce the electrical length and adjust the resonance point of near field antennas, broken loop structure will be a good solution. However, the lumped elements will also have to be exploited and optimized. Since the antenna's operating region is near field, therefore the far field gain of antenna should be low enough to avoid nonessential disturbs, and concentrate more energy in near field. These two antennas investigated and evaluated in this paper are both have lumped resistance to reduce far field gain, and their loop structure also can cause lower far field gain. Another function of resistance is to broaden the bandwidth, because if the antenna loads a matched resistance, it will reduce the quality factor and present a satisfactory impedance matching characteristic in the working band. Both of the antenna have cavity to concentrate the electromagnetism energy in the region of interest. Performance analysis of circuit characteristics and field characteristics shows that both of the antennas are suitable for near field reader antenna of UHF RFID systems.

Design of a Wideband Planar Inverted E Type Antenna

Sinhyung Jeon, **Hyengcheul Choi**, **Seungwoo Kim**, **Oul Cho**, **and Hyeongdong Kim**
Department of Electrical and Computer Engineering, Hanyang University
Haengdang-dong, Seongdong-gu, Seoul, Korea

Abstract— In this paper, a planar inverted E type antenna (PIEA) is proposed to achieve a wide impedance bandwidth. It is possible to realize by simply inserting a capacitance between the feeding line and shorting pin of the PIFA without increasing the antenna size. The additional resonant frequency by a shunt capacitance between the feeding line and shorting pin of the PIFA can be controlled by adjusting the amount of a shunt capacitance. The designed antenna has a very wide impedance bandwidth (VSWR = 2) of 480 MHz (880–1370 MHz) for GSM band. Reasonable agreement between simulated and measured results was obtained and good radiation patterns had been obtained at the desired frequency bands.

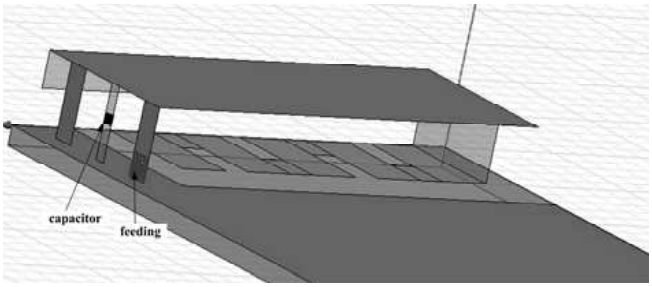

Figure 1: Three-dimensional view of the proposed antenna.

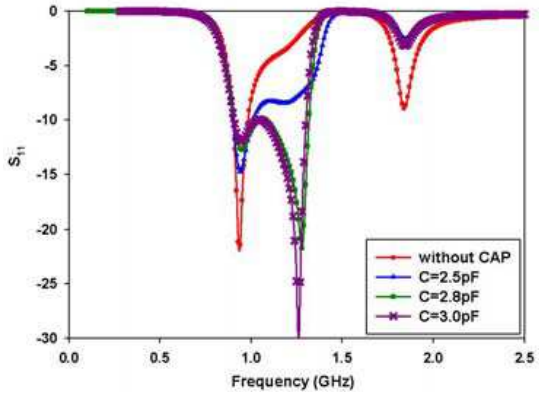

Figure 2: Simulations return loss characteristics.

Session 3P6b
Microstrip, Printed Antenna and Array antennas

Theory of Broadband Planar Traveling-wave Arrays (TWA) with 2-D Elements

Johnson J. H. Wang
Wang Electro-Opto Corporation (WEO), Marietta, Georgia 30067, USA

Abstract— Conventional broadband phased arrays are made of 3-D (three dimensional) elements, such as the Vivaldi type. They suffer from grating lobes in E or H plane at the high end of the operating frequencies, resulting in reduced bandwidth and scan range. The 3-D element structure also makes the array relatively thick, heavy and complex, thus undesirable for transport and incompatible with low-cost planar fabrication processes. To overcome these shortcomings, research on 2-dimensional (2-D) elements for broadband planar phased arrays has recently been carried out. There are now three basic schools of approaches: Current Sheet Antenna (CSA), Fragmented Aperture (FA) array, and the present author's Traveling-Wave Array (TWA) [1; patent pending]. The TWA approach differs by having an inherent ground plane and impedance matching via matched aperture impedance and traveling wave (TW) excitation.

For convenience and rigor, the theory of planar phased array is generally formulated for the case of an infinite array, which is amenable to analysis by Floquet-mode expansion. Fig. 1 shows an example of TWA characterized by a unit cell, *abcd*, for its center element and its immediate vicinity, in an infinite planar periodical array structure. All individual array elements are of similar planar TW structure in similar unit cells. All array elements are strongly coupled or even connected with adjacent elements. The crosssectional view of the array is shown in Fig. 2, in which dielectric superstrate and substrates further facilitate impedance matching. For circular polarization, the element antenna has four feed points in the center.

The hatch lines denote conducting region, and the blank area are non-conducting. As can be seen, the planar structure is close to a selfcomplementary geometry, in which conducting and non-conducting regions are similar and not differentiable. Broadband impedance matching is thus made easy by this pseudo-self-complementary structure, based on Babinet's principle.

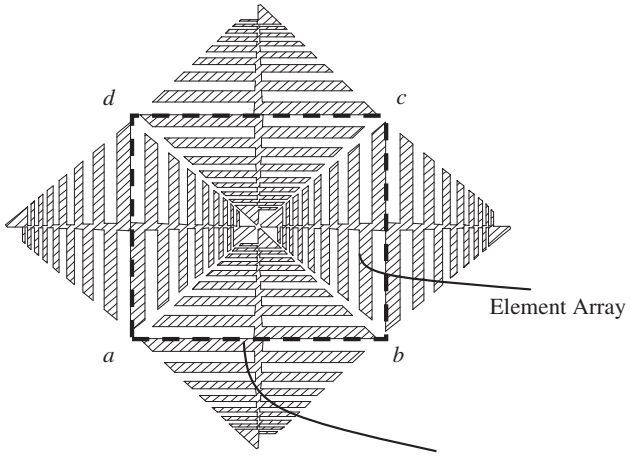

Figure 1: Array center unit cell and its adjacent elements.

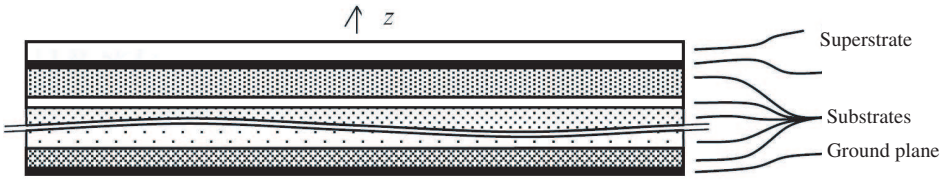

Figure 2: Cross-sectional view of planar array.

The array elements are densely packed, spaced less than 1/2 wavelengths between centers of adjacent elements throughout the entire operating frequencies, to suppress grating lobes; this is a common feature of CSA, FA, and TWA. Strong coupling between adjacent elements reduces discontinuities in phase and amplitude in the source aperture. Different from CSA and FA, in TWA there are an inherent conducting ground plane and a TW structure, which also facilitate propagation of a dominant-mode TW transverse to the broadside axis z in the waveguide structure, as shown in Fig. 2.

The theory above is for the case of a transmit array from the perspectives of radiation, yet applicable to the case of receive as well by way of reciprocity. A theory is also developed independently for the case of receive, from the perspectives of the information sampling theory and electromagnetic scattering theory, leading to results similar to the transmit case yet offering useful and clear insights in key design issues such as impedance matching, gain efficiency, and scan angles.

REFERENCES

1. Wang, J. J. H., "A new planar multioctave broadband traveling-wave beam-scan array antenna," *5th European Workshop on Conformal Antennas*, University of Bristol, UK, Sep. 10–11, 2007.

On the Compound Air-fed Array Antenna with AMC Base

W. X. Zhang and Z. H. Wu
State Key Laboratory on Millimeter Waves, Southeast University, Nanjing, China

Abstract— The Fabry-Perot resonator (F-PR) Antenna succeeds to the property of its optics prototype as spectral device: quite high directivity due to the high reflectivity from covered plate, and very narrow bandwidth of directivity resulted from high-order of resonance between covered and based plates. Any effort to extend the bandwidth must obviously drop the directivity. On the other side, the directivity corresponds to the aperture efficiency, but the gain described by antenna efficiency also depends upon the conductive loss on metal surface and energy leaked by lateral waves from the spacing between finite plates. Thus the contradiction between gain and bandwidth becomes more severe and complicated.

The perfect aperture efficiency (100%) corresponds to an absolute uniform distribution of aperture field. However, the equal magnitude is impossible due to different ray-path attenuation, and also unreasonable for considering side-lobe suppression. A natural tapered magnitude distribution is acceptable. Whatever, the co-phase distribution always benefits for focusing beamwidth and enhancing directivity. In order to perform the phase compensation for different ray-path delay, the cover of dielectric plate printed by quasi-periodic patches with tapered sizes was suggested by the authors, which not only correct the phase difference, but also weaken the frequency sensitivity, as well as in the design of a transmit-array (TA) or reflect-array (RA).

Different from a pure TA or RA which employ only one times refraction or reflection, the multiple reflection and transmission happened in a F-PR. On one side, the first transmitted rays, which illuminated directly by excited radiator, throughout the cover satisfy co-phased condition by means of the tapered FSS on the cover; on the other side, the successive transmitted rays, which corresponding to the contribution of multi reflection between cover and base, are no longer co-phased due to the tapered patches on the cover. In order to correct the different reflection phase from the tapered patches of cover, a artificial magnetic conductive (AMC) surface of grounded FSS or mushroom of patches with inversely tapered sizes is effective and convenient. This structure of tapered cover and inversely tapered base was named as Compound Air-Fed Array (CAFA) antenna by the authors, since it can be considered as a combination of TA and RA.

The CAFA antenna developed as a modified F-PR antenna, had been designed for different targets of maximized directivity, or maximized common bandwidth (for VSWR and gain-drop, even and SLL) in performance, or minimized profile (height) in structure, with the restriction conditions of the other performances; and compared with that of traditional F-PR antenna. The simulated results, designed data, and measured performances of prototypes will be shown in oral presentation.

ACKNOWLEDGMENT

This work was supported by both Natural Science Foundation of China (60671016) and International Cooperated Project of Jiangsu Province (BK 2007601).

A Wideband High-gain Subwavelength Fabry-Perot Cavity Antenna

Kwok L. Chung[1] and Sarawuth Chaimool[2]

[1]Hong Kong Polytechnic University, Hong Kong SAR, China
[2]King Mongkut's University of Technology North Bangkok, Thailand

Abstract— The Fabry-Perot cavity (FPC) antenna is produced based on the phenomenon of multiple reflections of waves between two etalons/mirrors. FPC antenna manifests the cost-effective advantage in minimization of array elements and feed network, and has its wide applications in microwave and millimeter wave regimes. Hence, FPC type antennas received considerable attentions in antenna community over the decades [1, 2]. For the traditional FPC antennas, one or multiple parallel dielectric layers were employed with a metallic (PEC) ground plane as the reflecting mirrors to form a cavity resonator for directivity/gain enhancement. Owing to the resonant nature in PFC type antenna, high directivity can be achieved, however, at the expenses of a high-profile structure (half of the working wavelength, 0.5λ) and a narrow operating bandwidth of a few percent. Recently, with the application of artificial magnetic conductor (AMC) for the replacement of PEC ground plane, the cavity height of a FPC antenna can be reduced from 0.5λ to a quarter working wavelength (0.25λ) while maintaining the antenna's high gain [3]. Meanwhile, with the advent of metamaterial surfaces, Zhou [4] & Ourir [5] took the advantage of the dispersive characteristics from the metasurfaces to produce the metamaterial-based subwavelength cavities.

In this paper, we present a novel design of metamaterial-based subwavelength cavity antenna. The aim of this antenna is expected to be complied with the Hi-Lo-Wi objectives: High gain, Low profile and Wideband. Unlike the complex cavity structures from Zhou & Ourir, in which both the high-impedance surfaces (HIS) and AMC were used as the Partially Reflective Surface (PRS) and the grounded dielectric substrate, respectively. Our antenna uses only a single-layer metasurface, which has been acted as a superstrate and also the PRS for a probe-fed patch antenna. That is, a rectangular patch printed on a grounded FR4 substrate with a metasurface covered on top at a height of 0.065λ. The subwavelength cavity antenna features a wide impedance bandwidth of 7%, a boresight gain of 10.4 dBi at 2.45 GHz with a flat gain bandwidth (> 8 dBi) of 15%. The detailed structure, lateral size, aperture efficiency of this low-profile antenna and comparisons to the previous works by other research teams will be presented and discussed in the conference.

REFERENCES

1. Trentini, G. V., "Partially reflecting sheet array," *IRE Trans. Antennas Propag.*, Vol. 4, 666–671, 1956.
2. Feresidis, A. P. and J. C. Vardaxoglou, "High-gain planar antenna using optimized partially reflective surfaces," *IEE Proc. Microw. Antennas Propag.*, Vol. 148, 345–350, 2001.
3. Feresidis, A. P., G. Goussetis, S. Wang, and Y. C. Vardaxoglou, "Artificial magnetic conductor surfaces and their application to low-profile high-gain planar antennas," *IEEE Trans. Antennas Propagat.*, Vol. 53, 209–215, Jan. 2005.
4. Zhou, L., H. Li, Y. Qin, Z. Wei, and C. T. Chan, "Directive emissions from subwavelength metamaterial-based cavities," *Appl. Phys. Lett.*, Vol. 86, 101101, 2005.
5. Ourir, A., A. de Lustrac, and J.-M. Lourtioz, "All-metamaterial-based subwavelength cavities ($\lambda/60$) for ultrathin directive antennas," *Appl. Phys. Lett.*, Vol. 86, 084103, 2006.

Miniaturization of Rectangular Microstrip Antennas Using Electric-LC Resonators

W. Y. Tam[1] and K. S. Zheng[2]

[1]Department of Electronic and Information Engineering
The Hong Kong Polytechnic University, Hong Kong, China
[2]School of Electronic and Information
Northwestern Polytechnic University, Xi'an, China

Abstract— Rectangular microstrip antennas, due to their inherent capabilities such as low cost, low weight, and low profile, are widely used in wireless communication applications. However, their length cannot be made arbitrarily small, since a rectangular microstrip antenna resonates when its length is a multiple of half wavelength.

With the successful implementation of double-negative (DNG) metamaterials [1] in recent years, several papers have exposed the usefulness of these DNG metamaterials and single-negative (SNG) metamaterials (either negative permittivity or negative permeability) in antenna applications [2, 3]. In [3], it was demonstrated that a rectangular microstrip antenna partially loaded with metamaterial with negative permittivity (ENG) exhibits subwavelength resonance. Therefore, the use of ENG metamaterials can miniaturize microstrip antennas. However, to apply this miniaturization method, we need to develop suitable structures or inclusions to implement the metamaterials. For example, periodically arranged wires have been used to implement negative permittivity but the negative permittivity property does not exhibit when it is inserted between two conducting plates. Therefore, it is not suitable for microstrip antenna applications.

In this paper, the rectangular electric-LC (ELC) resonator [4] is employed to synthesize the ENG metamaterials. The constitutive parameters of the ELC structure were determined by considering an ELC resonator loaded parallel-plate line. The results showed that the effective permittivity of the ELC structure is negative in a certain frequency range, while its effective permeability is positive. Since the substrate of the microstrip antenna includes the ELC structure with negative permittivity below the first normal resonant mode, the antenna can operate in a subwavelength resonance. In our simulation, the resonant length of the subwavelength mode of the microstrip antenna is less than $0.2\lambda_o$.

REFERENCES

1. Smith, D. R., W. J. Padilla, D. C. Vier, S. C. Nemat-Nasser, and S. Schultz, "Composite medium with simultaneously negative permeability and permittivity," *Phys. Rev. Lett.*, Vol. 84, No. 18, 4184–4187, 2000.
2. Ziolkowski, R. W. and A. D. Kipple, "Application of double negative materials to increase the power radiated by electrically small antennas," *IEEE Trans. Antennas Propagat.*, Vol. 51, 2626–2640, 2003.
3. Alù, A., F. Bilotto, N. Engheta, and L. Vegni, "Subwavelength, compact, resonant patch antennas loaded with metamaterials," *IEEE Trans. Antennas Propagat.*, Vol. 55, 13–25, 2007.
4. Schuring, D., J. J. Mock, and D. R. Smith, "Electric-field coupled resonators for negative permittivity metamaterials," *Appl. Phys. Lett.*, Vol. 88, 041109, 2006.

The Design and Simulation of an S-band Circularly Polarized Microstrip Antenna Array

Ying Jiang, **Hongchun Yang**, **and Xiong Wang**
School of Physical Electronics
University of Electronic Science and Technology of China
Chengdu 610054, China

Abstract— It is important to use microstrip antenna in aircraft for stealth and movement. At the resonant frequency 2491.75 MHz, the standing wave ratio of single element antenna is less than 1.5, which meets the project targets and performs well on impedance match. The maximum radiation direction is 0° achieving a maximum gain of 8 dB and the antenna axial ratio is less than 6 dB in $-70° \sim 70°$ cone angle of the space. Based on the principle of rectangle microstrip antenna, the S-band circularly polarized microstrip antenna array is designed according to the quota requirement. By using a software for 3D electro-magnetic field analysis (Ansoft HFSS), the S-band microstrip 2×4 antenna array is simulated and the optimization of the parameters is obtained. The axial ratio of antenna array is better than the requirement by 6 dB. The horizontal 3 dB beam width is larger than 30° and vertical 3 dB beam width is larger than 12°. In the direction of maximum radiation, the gain is close to 17 dB with good directivity which fully meets the design requirements. Based on the simulated results of the antenna array, it was fabricated and tested. in microwave anechoic chamber with E8363B vector network analyzer. The measurement result of the maximum gain of antenna array is about 16 dB, and the main lobe as well as the side lobe conform well with the simulation results of software HFSS. The error of gain is about 1 dB, caused by a variety of factors, such as the accuracy of simulation software, mutual coupling between modules, the accuracy of fabrication, measurement instruments error and so on.

A Design of Reconfigurable Patch Array Antenna with Dual Circular Polarizations

Chung-Hsun Weng, **Hsien-Wen Liu**, **Sheng-Yu Lin**, **and Chang-Fa Yang**
Department of Electrical Engineering, National Taiwan University of Science and Technology
Taipei, Taiwan

Abstract— In this paper, we present a 2×2 microstrip array antenna with dual circular polarizations. To switch the polarization states, the radiating patch is fed by a branch-line coupler and two power dividers. The array antenna can be reconfigured to radiate electromagnetic waves with either the right-handed or left-handed circular polarizations by controlling the branch-line coupler. A prototype is fabricated with a 0.4 mm thick FR4 top layer for radiating elements and a 0.8 mm thick FR4 bottom layer for a feeding network with a 5 mm air gap between the two layers. Simulated and measured results are compared, which show good agreements. Also, the properties of the reconfigurable array antenna with dual circular polarizations and high radiation efficiency are demonstrated.

ACKNOWLEDGMENT

This work was supported in parts by National Science Council of R.O.C. under Grant NSC 97-2221-E-011-024.

Moment-method Analysis of Planar Archimedean Spiral Antenna with Dielectric Superstrate

Yajian Wu, **Huiling Zhao**, **Dan Jiang**, **and Nakun Jing**
Northwestern Polytechnic University, Xi'an, Shanxi 710129, China

Abstract— A planar Archimedean spiral antenna with a dielectric superstrate and substrate is analyzed using curved segment moment method with curved piecewise triangle sub-domain basis and pulse testing functions. The numerical results of input impedance, current distribution and axial ratio of the Archimedean spiral antenna are presented. Numerical results have good agreement with the published results in [1] and commercial software HFSS. Input impedances as a function of arm length is presented. Affection of permittivity and thickness of antenna substrate and superstrate on the input impedance or bandwidth are discussed.

REFERENCES

1. Khamas, S. K., P. L. Starke, and G. G. Cook, "Design of a printed spiral antenna with a dielectric superstrate using an efficient curved segment moment method with optimization using marginal distributions," *IEE Pro. — Microw. Antennas Propag.*, Vol. 151, No. 4, August 2004.

Session 3P7
Modeling and Simulations in Materials Science

Elasticity-stochastic Description on the Adhesion of Elastic Media via Molecular Bond Clusters

Jizeng Wang
College of Civil Engineering and Mechanics, Lanzhou University, Lanzhou, Gansu 730000, China

Abstract— Biological cells actively adhere to extracellular matrix and other cells through a large variety of ligand-receptor bonds. Such adhesion plays a critical role in migration, spreading, differentiation, growth, motility, apoptosis and tissue formation. A quantitative description of initiation, growth and stabilization of focal adhesion from the scale of single molecular bonds to that governed by elastic and viscoelastic deformation will be a critical step toward controlling cell adhesion on substrates. In this description, a key challenge is the stochastic-elasticity modeling that couples the deformations of cell/substrate, the diffusion of individual bonds and the stochastic events of rupture and rebinding of individual bonds. To address this issue, as the first step, we develop an idealized theoretical model on the strength of an adhesive patch of molecular bonds between two dissimilar elastic media subject to an applied tensile load, aimed at a seamless unification of elasticity description of adhesive contact at large scales and statistical description of single bond behaviors at small scales. Steady-state solutions on the normalized pull-off stress, as a function of the stress concentration index α can be obtained by using the coupled elasticity-stochastic theory, indicating that there exists an optimal value of α (proportional to the patch size) beyond which the normalized pull-off stress decreases due to severe stress concentration near the edge of the patch that induces crack-like failure. For very small patch sizes, stochastic behaviors of molecular bonds dominate: the larger the population, the more stable the patch becomes. For large patch size, the elasticity of the system plays an increasingly important role and brings in an upper limit on the adhesion size. This is consistent with experimentally observed upper size limit on FAs in cell-substrate adhesion.

Electromagnetic Elasto-plastic Dynamic Behaviors of Conductive Circular Plate

Yuanwen Gao
Key Laboratory of Mechanics on Western Disaster and Environment
College of Civil Engineering and Mechanics, Lanzhou University
Lanzhou 730000, China

Abstract— Electromagnetic elasto-plastic dynamic response of a conductive circular plate in a magnetic pulse field are studied in this paper, the influence of the strain rate effect is investigated for the electromagnetic elasto-plastic deformation of the conductive plate. Basic governing equations are derived for electromagnetic field (eddy current), the elasto-plastic transient dynamic response and the heat transfer of a conductive circular plate, and then an appropriate numerical code is developed based on the finite element method to quantitatively simulate the magneto-elasto-plastic mechanical behaviors of the conductive circular plate. The Johnson-Cook model is employed to study the strain rate effect and temperature effect on the deformation of the plate. The dynamic response is explained with some characteristic curves of deformation, the eddy current, and the configurations, the temperature of the conductive plate. The numerical results indicate that the strain rate effect has to be considered for the conductive plates, especially for those with high strain rate sensitivity. Comparison of the influence of the temperature effect on the deformation of the plate with that of the strain rate effect shows that the influence of the temperature effect on the deformation of a plate is not significant.

Rearrangement of Martensitic Variants and Mechanical-magneto-thermal Behavior of a Ferromagnetic Shape Memory Alloy Rod

Xingzhe Wang, **Fang Li**, **and Xuebing Han**
Key Laboratory of Mechanics on Western Disasters and Environment, Ministry of Education of China
College of Civil Engineering and Mechanics, Lanzhou University, Lanzhou 730000, China

Abstract— Ferromagnetic shape memory alloys (FSMAs) could be a potential candidates for new generation of actuators and sensors due to their the high energy, large stroke and high bandwidth properties. The FSMAs can be controlled not only by a thermal field and a stress field as the traditional thermoelastic shape memory alloys (like Ni-Ti) have, but also by a magnetic field. It is revealed that the giant reversible field-induced strain is from the rearrangement of martensitic variants of FSMAs. In order to describe the rearrangement mechanism related to the mobility of the twin boundaries, a mechanical-magneto-thermal coupled model is propose in this paper. In the modeling, a general thermodynamic driving forcewhich causes the motion of the twin boundaries, is introduced and derived based on the balance law of energy and the rate of change of entropy at the twin boundary of the coupling system of FSMAs. The whole energy of the system associated with the elastic energy, Zeeman energy and the magneto-crystalline anisotropy energy is considered. The mass fraction is defined as the thermodynamic flux associated with the thermodynamic driving force. An explicit formulation for the mass fraction change between the different martensitic variants, which is the thermodynamic flux conjugate to the thermodynamic driving force, is obtained based on the assumptions of the energy dissipation of system reaching a maximum. The model is used to a 1-D special case of a transverse magnetic field and an axial compression applied to a single crystal FSMA rod for characterizing the martensitic variants revolution and the mechanical-magneto-thermal behaviors. Some results show good agreements with the experimental measurements in literature.

Analysis on Absorption and Thermal Stress of a Functionally Graded-absorbing Infinite Plate in Electromagnetic Fields

Hongyan Tian, **Xingzhe Wang**, **and Youhe Zhou**
Key Laboratory of Mechanics on Western Disasters and Environment
Ministry of Education of China, College of Civil Engineering and Mechanics
Lanzhou University, Lanzhou, Gansu 730000, China

Abstract— High performances and multi-function-absorbing materials and structures are increasingly demanded in various engineering applications where there always associate with the complex environments such as heat, humidity and corrosion. As the good absorbing material candidates, the gradient materials with attractive advantages of great design freedom, easy-to-show broadband, impedance gradient, high-temperature load characteristics are expected. Based on the electromagnetic wave propagation theory and thermo-elasticity, this paper presents a solution to the non-homogeneous problem of graded-absorbing material of infinite plate in electromagnetic wave circumstance. The electromagnetic wave properties, including the absorption and reflection, as well the heat energy of the graded-absorbing material, are analyzed theoretically. And then the transient temperature and thermal stress fields in the graded-absorbing plate are calculated by mean of finite difference method. The effects of material properties of the graded-absorbing plate and the electromagnetic wave irradiation time on the internal temperature field and thermal stress of the graded plate are discussed. The results show that, with the proper material property design on the grade-absorbing plate there are good performance on the lower reflection and high absorption as well the gentle thermal stress distribution. The analysis results are expected to be helpful for designing graded-absorbing material parameters and mechanical parameters.

A Model of Size Effect on Thermal Conductivity for Thin Metallic Films

Wei Luo and Xiaojing Zheng
Key Laboratory of Mechanics on Western Disaster and Environment
Ministry of Education, and Department of Mechanics and Engineering Science
College of Civil Engineering and Mechanics, Lanzhou University, Lanzhou, Gansu 730000, China

Abstract— This study examines the size effect on the thermal conductivity due to the electron scattering in metallic films. Three dominant types of electron scattering mechanisms are considered: the isotropic background scattering, the grain boundary scattering and the external surface scattering; furthermore, the grain boundary scattering consists of two parts: grain boundaries perpendicular to the heat current and grain boundaries parallel to the heat current (parallel to the film surface) which are usually neglected in previous researches. In this study, the external surface scattering and the scattering of grain boundaries parallel to the heat current are considered together as the boundary conditions on the electron-distribution functions by using Hoffman's two-fluid model. And the scattering of grain boundaries perpendicular to the heat current is treated as the potential barriers of suitable widths and heights by solving Schrödinger's equation, and this effect influences the relaxation time with the isotropic background scattering. Additionally, the approximation of local thermal equilibrium in the quasiclassical electron thermal transport need to be modified because of the decrease of film thickness. So, on the basis of the Boltzmann equation in which the modification of the approximation of local thermal equilibrium is accounted for, imposing boundary conditions and considering the effective relaxation time, we propose a model which describes the size effect on thermal conductivity in metallic thin films. The in-plane thermal conductivity of metallic thin films is obtained. The comparison between the theoretical calculations and the experimental results indicates that our model is valid and the grain boundary scattering plays an important role in the electron thermal transport.

Dynamic Analysis for Electrified Cantilever Conductive Thin Plates under Transverse Multi-pulse Magnetic Field

Huijuan Bai and Xiaojing Zheng
Department of Mechanics and Engineering Science, Lanzhou University
Lanzhou, Gansu 730000, China

Abstract— A mathematic model was established for electrified cantilever conductive thin plates under externally transverse multi-pulse magnetic field. The distribution of eddy current induced by the transverse multi-pulse magnetic field would be influenced due to a subsistent inner uniform electric field in the conductive thin plates by adopting finite element numerical method, and also obtained the distribution of temperature field in thin plate from the law of heat conduction. Subsequently the influences of multi-pulse magnetic field and uniform electric field on the in-plane magnetic volume forces and the maximum deformation of thin plate were quantitatively simulated on the basis of electro-magneto-thermo-elastic theory. The simulation results indicate that the dynamic buckling phenomenon is caused by the in-plane magnetic volume compression force arising from the interaction between the eddy current induced by multi-pulse magnetic field and inner uniform electric field. The dynamic buckling phenomenon of cantilever thin plate is determined by the value of maximum magnetic field and impulse parameter, and also the inner uniform electric field.

ACKNOWLEDGMENT

Supported by the Ph.D. Fund of the Ministry of Education of China (No. 20050730016).

A One-dimension Transient Constitutive Model for Giant Magnetostrictive Materials

Tian-Zhong Wang[1, 2], **Le Sun**[1, 2], **and You-He Zhou**[1, 2]

[1]Key Laboratory of Mechanics on Disaster and Environment in Western China, Ministry of Education
Lanzhou University, Lanzhou 730000, China
[2]Department of Mechanics and Engineering Science, College of Civil Engineering and Mechanics
Lanzhou University, Lanzhou 730000, China

Abstract— As a kind of smart or functional materials, the giant magnetostrictive materials has some distinct advantages such as the ability to generate great strain, good magnetomechanical coupling factor, fast response and so on. However, many experiment results for the giant magnetostrictive materials have exhibited that both the magnetization-applied field curve and the magnetostrictive strain-applied field curve have properties of nonlinear magneto-thermomechanical coupling and inherent hysteresis, especially, the shape and the slope of hysteresis loop are sensitive to both the frequency and the amplitude of AC applied magnetic field. Therefore, a general transient constitutive model incorporating nonlinear magneto-thermo-mechanical coupling effect and inherent hysteresis effect is necessary for quantifying complicated properties of the giant magnetostrictive materials and designing corresponding device. Here, a one-dimension transient constitutive model is established on the basis of thermodynamic theory and magnetic domain theory of Jiles and Atherton, which provides an approach for thoroughly and accurately describing the effects of nonlinear magneto-thermo-mechanical coupling and inherent hysteresis for the magnetostrictive materials. The validity and reliability of the model are verified by comparing the predicted results with experimental data. Meanwhile, the performance of the magnetostrictive materials under quasi-static operating conditions and under dynamic operating conditions are numerically simulated and discussed using the transient constitutive model proposed here. The numerical results clearly indicate that the pre-stress, the temperature, the magnetic bias field and the frequency and amplitude of magnetic excitation field have remarkable influence on the performance of the magnetostrictive materials. These essential and important investigations will be significantly benefit to both the theoretical researches and those applications of the materials such as function design when the materials are used as active elements for some smart or intelligent devices.

Crack Problem in a Thin Superconducting Disk

Feng Xue[1, 2] **and You-He Zhou**[1, 2]

[1]Key Laboratory of Mechanics on Disaster and Environment in Western China, Ministry of Education
Lanzhou University, Lanzhou 730000, China
[2]Department of Mechanics and Engineering Science, College of Civil Engineering and Mechanics
Lanzhou University, Lanzhou 730000, China

Abstract— Bulk high-temperature superconductors have now been developed for applications in magnetic bearings, current leads, and flywheel energy storage systems. However, there is a major problem of such bulks, that is mechanical fracturing frequently occurs when a large magnetic field is applying. In this work, the general problem of a central crack in a thin superconducting disk is studied. The dependence of the stress intensity factor on the parameters, including the crack length and the applied field, is investigated. We calculate the body forces by numerical method, solve the magneto-elastic problem and present a simple model in which the effect of the crack on the critical current is taken into account. It is assumed that the crack forms a perfect barrier to the flow of current. The Bean model is considered for the critical state. Based on the complex potential and the boundary collocation methods, the stress intensity factor under the various magnetic field is obtained for a thin superconducting disk containing a central crack. The results show that the crack length and the applied field have significant effects on the fracture behavior of the superconductor. The stress intensity factor will arrive a peak when the magnetic field reduces, there is also a peak for the stress intensity factor as the relative length of the crack is reduced. However, the variation in the stress intensity factor with respect to the relative length of the crack is relatively small. Thus, the results show the times when mechanical fracturing is easy to happen.

Magnetoelastic Model of Magnetizable Media

Ke Jin, **Yong Kou**, **and Xiaojing Zheng**
Department of Mechanics and Engineering Science, Lanzhou University
Lanzhou, Gansu 730000, China

Abstract— The interaction between applied magnetic fields and magnetizable media has always been very complicated, since the distribution of magnetic field and magnetic forces in the media cannot be measured directly. Modeling the magnetic field and magnetic force in the deformable media which can agree to the measured results on the surface of media is very important. Although many works exist in this area, researchers are still puzzled by a number of issues: why are there so many coexistent theoretical models for magnetic force of magnetizable media under a applied magnetic field? How to make a choice? How to calculate the interaction between applied magnetic fields and magnetizable media considering the effect of the magneticelastic coupling? The rationality of magnetoelastic model and validity of calculation are related to whether the model can predict the stability of ferromagnetic structure accurately under the magnetic field in the nuclear industry, high-tech area, etc. In this work, the authors review the various existing magnetic force models by comparing the premises on which the model is based, formulas and results. We also investigate the commonly methods for simulating the magnetoelastic interaction by comparing their numerical results and discussing their scope of application.

ACKNOWLEDGMENT

Supported by the National Science Foundation of China (No. 90405005) and the Ph.D. Fund of the Ministry of Education of China (No. 20050730016).

Theoretical Analysis on Quantum Well at Undoped $GaN/In_xGa_{1-x}N/GaN$ Heterostructure Interface

Shah Mohammad Bahauddin, **Farha Diba Sumana**, **Md. Rubaiyat Hossain**, **Md. Ahsan Uddin**, **and Zahid Hasan Mahmood**
Department of Applied Physics, Electronics & Communication Engineering
University of Dhaka, Bangladesh

Abstract— In our present study, we have analyzed the energy band diagram of undoped $GaN/In_xGa_{1-x}N/GaN$ hetero-structure using 1D Poisson/Schrodinger solver [1]. The hetero-structure consists of 50 nm GaN cap layer with an InGaN layer on 100 nm GaN buffer layer (Fig. 1). The formation of triangular quantum well at the hetero-interface with the existence of 2DEG and 2DHG has been confirmed (Fig. 2) [2]. In Fig. 2, the Fermi level is taken as the reference energy level having 0.0 eV energy. The penetration of Fermi energy by both conduction and valence band indicates the creation of quantum well. It is evident from the figure that the well is formed at InGaN layer. The dependence of sheet carrier density on the alloy composition for different temperature has also been investigated. From Fig. 3, it can be concluded that the density of 2DHG and 2DEG increases with the increase of alloy composition and almost immune to the variation of temperature. Though the density of 2DHG is more dependent to temperature than 2DEG, they remain unaffected at higher alloy composition (Fig. 4). For a given alloy composition the thickness of InGaN layer was varied and corresponding sheet carrier density was observed (Fig. 5). The thickness was taken from 1.0 nm to 50 nm. Again for a fixed InGaN layer thickness, the compositional parameter x was varied and resultant sheet carrier density was also observed (Fig. 6). From the figures, it can be shown that the critical thickness, T^C is decreased with the increase of alloy composition. Thus the relation between the sheet carrier concentrations with the thickness of InGaN layer has been studied and consequently critical thickness for the formation of 2DHG and 2DEG has been found. Table 1 presents a list of critical thickness for different alloy composition at room temperature. Moreover it can be obtained from the figure that the sheet carrier concentration reaches a saturation value after about 50 nm. An important electronic transport property, the low field mobility values for 2DEG has been then investigated for different mole fraction of Indium with corresponding sheet concentrations. Here scattering by two types of phonons are relevant for our study which are acoustic phonon by deformation potential coupling and longitudinal optical phonon. But for higher temperature (≈ 300 K) the mobility is limited by polar optical phonon scattering [3]. Thus we have neglected acoustic phonon scattering as our interest is restricted for operations at room temperature. For InGaN layer, other traditional scattering such as alloy disorder scattering and two structural scattering caused by background impurities and dislocation will also be accounted [3, 4]. In our present work, the temperature dependence of the mobility for LO phonon has been observed (Fig. 7). The figure shows that an average mobility of 4000 $cm^2/V.s$ can be obtained at room temperature though mobility is rapidly decreased at higher temperature.

Table 1: Critical thickness for the formation of 2DEG and 2DHG in different alloy composition* estimated from Figures 5 and 6.

Alloy Composition, x	Critical Thickness for 2DEG T^C_{2DEG} (nm)	Critical Thickness for 2DHG T^C_{2DHG} (nm)
0.1	> 20	> 10
0.2	≈ 10	≈ 5
0.3	> 5	> 2.5
0.5	≈ 2.5	≈ 2
0.7	< 2	1
0.9	< 1	> 0

*Temperature, $T = 300$ K

REFERENCES

1. Tan, I. H., G. L. Snider, L. D. Chang, and E. L. Hu, "A self consistent solution of Schrodinger-Poisson equations using a nonuniform mesh," *J. Appl. Phys.*, Vol. 68, No. 8, 4071–4076, 1990.

2. Upal, T. N., M. A. Uddin, M. Hossain, F. Jahan, and Z. H. Mahmood, "Study of charge density at $In_xGa_{1-x}N$/GaN heterostructure interface," *2nd IEDST'09*, 1–4, June 2009.
3. Wood, C. and D. Jena, *Polarization Effects in Semiconductors: From Ab Initio Theory to Device Applications*, Debdeep Jena, Springer, 2008.
4. Gelmont, B. L., M. Shur, and M. Stroscio, "Polar optical-phonon scattering in three- and two-dimensional electron gases," *J. Appl. Phys.*, Vol. 77, 657, 1995.

Active Vibration Control of a Rotating Laminated Beam with Magnetostrictive Layer

Longfei Li, **Xingzhe Wang**, **and You-He Zhou**
Key Laboratory of Mechanics on Disaster and Environment in Western China, Ministry of Education
College of Civil Engineering and Mechanics, Lanzhou University, Lanzhou 730000, China

Abstract— Rotating machinery is widely used in various engineering application related industries. One typical rotating system is rotating cantilever beam, such as helicopter blades, turbo-engine blades, turbine blades and other elements in engineering industries. Recently, the vibration control of a rotating beam has received much attention due to more practical applications and high performance requirements. Some smart materials, such as piezoelectric material, shape memory alloys and magnetostrictive material, are commonly used as actuators in active vibration control systems. Among those smart materials, the magnetostrictive material has some distinctive advantages such as the ability to generate large forces and the rapidly reaction to external magnetic fields. For the suppression of system vibration, the magnetostrictive material can be easily embedded into host materials, such as glass fiber reinforced plastics (GFRP) and carbon fiber reinforced plastic (CFRP), without effecting the structural integrity significantly. The objective of this work was to present a simulation of vibration suppression of a rotating laminated beam with magnetostrictive layers. In this simulation, the negative velocity feedback control law and the nonlinear constitutive model of the magnetostrictive layer are employed. The numerical results show that the introduced nonlinear constitutive model which can describe the inherent nonlinearities of magnetostrictive material is efficient in vibration suppression. The effects of geometrical and material parameters of the laminated beam and the control parameters of the active vibration control system on the vibration suppression of rotating laminated beam are discussed in detail.

Consistency of Generalized Bruggeman Effective Medium Theory Formula for Dispersive Composites at Microwave Frequencies

Ping Chen and Rui-Xin Wu
Department of Electronic Sciences and Engineering, Nanjing University
Nanjing 210093, China

Abstract— Since the heterogeneous composites are extensively used in different fields, such as electronic devices, aeronautic or aerospace vehicle, new-style sensors, etc., the mixing rules that can exactly describe the effective electromagnetic properties of composites have attracted a persistent interdisciplinary attention. In 1990s, a new mixing rule namely generalized Bruggeman (BG) effective medium theory (G-BG EMT) contributed by Mclachlan et al. was a significant development for this issue, which syncretized the scaling law of percolation theory into the BG formula:

$$f_i \frac{\phi_i^{1/t} - \phi_e^{1/t}}{\phi_i^{1/t} + A\phi_e^{1/t}} + (1 - f_i) \frac{\phi_m^{1/s} - \phi_e^{1/s}}{\phi_m^{1/s} + A\phi_e^{1/s}} = 0 \tag{1}$$

where ϕ_e is the effective electromagnetic parameter of the composite, ϕ_i, ϕ_m are the parameters of filler, i, matrix, m, respectively, f_i is the volume fractions of the constituents, t and s are percolation exponents, and $A = (1 - p_c)/p_c$ where p_c is the percolation threshold. Though the G-BG EMT is phenomenological and has three uncertain fitting parameters in formalism, it has been used to quantitatively analyze the effective properties of numerous composites including the high frequency electromagnetic properties of carbon black composite, metallic magnetic granular composite. It is well known that such composites are dispersive materials at high frequency. Therefore, the doubt about the consistency of fitting parameters in the G-BG formula at different frequency is noticeable.

In this work, the dielectric spectrum and magnetic spectrum of metallic magnetic granular composites at microwave frequencies have been researched in the framework of G-BG EMT. The metallic magnetic composite samples consisting of carbonyl-iron powders (CIPs) and epoxy resin were made with the volume fraction range of CIPs from 10% to 60%. The microwave measurements were performed by an Agilent E8363A vector network analyzer at $1 \sim 10$ GHz and the electromagnetic properties of composites were determined using the transmission/reflection method. We have investigated the dependence of ε and μ on the concentration and the fitting parameters at a series of frequency points. It was found that the G-BG formula yields a good agreement with experiments at various frequencies. The fitting parameters t, s and p_c obtained at different frequency point have been compared and the discrepancy between them is negligible, which suggests the G-BG formula has a good consistency for the dispersive materials at microwave frequencies.

Session 4A1
Microwave Remote Sensing of Land Surface

Optimization for Rotating-scanning Ring Arrays of Synthetic Aperture Radiometer

Weiying Sun, **Hao Liu**, **Zhang Cheng**, **Shengwei Zhang**, **and Ji Wu**
Center for Space Science and Applied Research, Chinese Academy of Sciences
Beijing 100190, China

Abstract— During the past decade, interferometric techniques, inherited from radio astronomy, has been successfully applied to Earth remote sensing. Achieving adequate sensitivity is a critical issue of a synthetic aperture radiometer, which depends largely on the type of an antenna array. To reach the sensitivity of each sampling of visibility function as identical as possible is one of requirements of the optimum antenna array. That is, total integral time of the antenna array distributes as average as possible to each sampling of visibility function.

In this paper, optimization of rotating scan ring arrays is examined on the view of u-v coverage and sensitivity of each sampling point. The relations between the sensitivity and length of baselines and aperture of element antenna are studied. The objective functions and solution space of optimization for rotating scan ring arrays are established, and based on simulated annealing algorithm, the simulation results of rotating scan ring array are presented. The simulation results proved that visibility coverage on u-v plane and equality of sensitivity of each sampling are quite improved.

The methods and results may be used to the similar antenna array design of radiometer, such as millimeter wave radiometer in Geostationary Orbit in the future.

Modeling the Radar-polarimetric Phase Signature over Evaporitic Soils

Ph. Paillou[1], **A. Freeman**[2], **E. Pottier**[3], **and P.-L. Frison**[4]

[1]University of Bordeaux, 2 rue de l'Observatoire, Floirac 33270, France
[2]Jet Propulsion Laboratory, Pasadena, CA, USA
[3]University of Rennes, Rennes, France
[4]University Paris-Est, Marne-la-Vallée, France

Abstract— The presence of water in arid regions is correlated to large evaporitic deposits, with high concentration of salts. Synthetic Aperture Radar observations over such areas show a high variation for both the amplitude and phase of the backscattered signal. This is due to a large dynamic range for both surface roughness and dielectric constant parameters, between the wet and dry season: crystallized salt is rough and presents a low dielectric constant, while salt water surfaces are smooth and conductive. We observed a complete seasonal cycle over the Chott El Jerid evaporitic basin, in South Tunisa, using the C-band SAR on-board RADARSAT-2. One full-polarimetric acquisition was performed every 24 days, from February to September 2009. Besides expected variations in the radar backscattered power, we also observed significant changes in the phase difference between HH and VV polarizations. In order to explain such a phase effect, we considered the phase behavior of the Fresnel reflectivity coefficient when approaching the Brewster angle, for materials with a high loss tangent. Both analytical modeling using IEM and exact modeling using FDTD confirm this hypothesis.

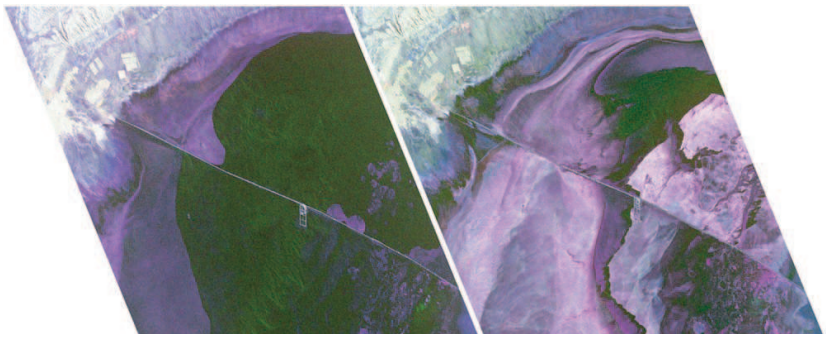

Figure 1: RADARSAT-2 polarimetric SAR scene of the Chott El Jerid, south Tunisia, during the wet season (left) and during the dry season (right).

REFERENCES

1. Lasne, Y., P. Paillou, A. Freeman, T. Farr, K. McDonald, G. Ruffié, J.-M. Malézieux, and B. Chapman, "Study of hypersaline deposits and analysis of their signature in airborne and spaceborne SAR data: Example of Death Valley, California," *IEEE Transactions on Geoscience and Remote Sensing*, Vol. 47, No. 8-1, 2581–2598, 2009.
2. Lasne, Y., P. Paillou, G. Ruffié, C. Serradilla, J.-M. Malézieux, A. Freeman, T. Farr, and K. McDonald, "Effect of salinity on the dielectric properties of geological materials: Implication on soil moisture detection by means of remote sensing," *IEEE Transactions on Geoscience and Remote Sensing*, Vol. 46, No. 6, 1674–1688, 2008.
3. Freeman, A., P. Paillou, Y. Lasne, B. Campbell, K. McDonald, and T. Farr, "Phase differences in longer wavelength polarimetric SAR: Surface or subsurface effects?," *IGARSS'08*, Boston, USA, July 2008.
4. Lasne, Y., P. Paillou, G. Ruffié, and M. Crapeau, "Effect of multiple scattering on the phase signature of wet subsurface structures: Applications to polarimatric L and C-band SAR," *IEEE Transactions on Geoscience and Remote Sensing*, Vol. 43, No. 8, 1716–1726, 2005.
5. Lasne, Y., P. Paillou, T. August-Bernex, G. Ruffié, and G. Grandjean, "A phase signature for detecting subsurface wet structures using polarimetric L-band SAR data," *IEEE Transactions on Geoscience and Remote Sensing*, Vol. 42, No. 8, 1683–1694, 2004.

W-band Dual Polarization Radiometer and Emissivity Measurement Depend on Polarization and Look Angle

Yong-Hoon Kim and Sung-Hyun Kim
School of Information and Mechatronics, Gwangju Institute of Science and Technology
#1 Oryong-dong, Buk-gu, Gwangju 500-712, Korea

Abstract— The radiometer is one of major remote sensing instrument to monitor the sea surface temperature and atmosphere water contents and humidity. But the polarimetric characteristic at millimeter-band is not explained clearly, because limited available polarized radiometer instrument. In this paper, the developed dual (V/H) polarization radiometer in W-band with high radiometric resolution and scanning capability is described and the results of emissivity measurement depend on the V-H polarization, incident angle are presented.

W-band dual polarization radiometer is two channel receivers for H/V polarization and it consist of parabolic cassegrain antenna, OMT, switch for calibration with match load, band pass filter, down converter and high stable local oscillator. For the extraction of Stokes parameter, wideband analog correlator is developed. The measured correlation coefficient of U, V Stokes parameter is 0.92 and 0.96, respectively. The measured brightness temperature of plastic board, rubber sheet and wood board depend on incident angle for V and V Stokes are presented. Using the measured emissivity, characteristic of material (object) like dielectric constant can be estimated.

ACKNOWLEDGMENT

This research was supported by Dual Use Technology Center and BK 21 program at GIST.

A Study of Multipolarized Ka-band Waves Propagation through Trees

Chih-Yuan Chu[1], **Kun-Shan Chen**[1], **and Jiangcheng Shi**[2]

[1]Communication Research Center & Center for Space and Remote Sensing
National Central University, Chung-Li 32001, Taiwan
[2]ICESS, University of California, Santa Barbara, CA 93117, USA

Abstract— The signal attenuation and statistical characteristics of wave propagation in different polarization through tree are investigated by experimental measurements at Ka-band. Two types of tree were selected: needle-leave (pine), broad-leave (ficus). System and free space losses were first calibrated out. To be more precisely, antenna pointing loss was minimized by compass and positioning fine-tuning. Statistically sufficient samples of scattered and attenuated signal at HH, HV, HV, VV polarizations were collected. Statistical analysis was then followed to characterize the received signal. The attenuation due to tree at Ka-band was found to be very large, as expected. Depending on the tree types, the attenuation levels were 9.67 dB/m and 1.51 dB/m through deciduous and evergreen trees, respectively, and 7.24 dB/m for the mixture. The received power, random in nature, follows mostly the Gamma distribution. The needle-leave pinus tree poses much less power loss because of much less leaf area index within the beam volume. On the other hand, broad-leave tree such as Ficus microcarpa in this study posted a very serious power loss for Ka-band signal. The statistical properties of the attenuated signal were also determined. It follows that the Gamma distribution generally fits the measured data best.

Behaviours of Microwave Vegetation Indices Derived from Simulations of the Zeroth and First Radiative Transfer Equation

L. Chai[1, 2, 3], **J. Shi**[1, 3, 4], **L. Zhang**[1, 2], **and L. Jiang**[1, 2]

[1]State Key Laboratory of Remote Sensing Science
Beijing Normal University and Institute of Remote Sensing Applications, Chinese Academy of Sciences
Beijing 100875, China
[2]School of Geography and Remote Sensing Science, Beijing Normal University, Beijing 100875, China
[3]Institute for Computational Earth System Science, University of California
Santa Barbara, CA93106, USA
[4]Institute of Remote Sensing Applications, Chinese Academy of Sciences, Beijing 100101, China

Abstract— The technique for deriving passive microwave vegetation indices (MVIs) has been developed by Shi et al. (2008) for data from the Advanced Microwave Scanning Radiometer (AMSR-E) on the Aqua satellite. In this technique, the quantitative description of MVIs can be derived from the zeroth solution of radiative transfer equation. Then, by using the Advanced Integral Equation Model (AIEM) simulated relationship for emissivity of bare soil surface at different frequencies, MVIs can be described as the v- and h-polarized brightness temperatures under two adjacent AMSR-E frequencies. This technique can minimize the surface emission signal and to maximize the vegetation signal and thus can be used to monitoring the global vegetation status.

In the zeroth solution of radiative transfer equation, the brightness temperature is made up of three parts. They are the direct, upward, self-emitted contribution of the canopy, the direct soil emission attenuated by passage through the canopy and the downward, self-emitted energy that is reflected by the soil surface. It has been proved that the zeroth model can only be used under lower frequency and sparser vegetation covered area. When the frequency becomes higher and the vegetation becomes denser, the zeroth model will lead to larger errors.

Since volume scattering cannot be ignored under higher frequency, we will take one step further to evaluate the behaviours of MVIs derived from simulations of the first solution of radiative transfer model in this study. In the first radiative transfer model, not only the same three parts as in the zeroth radiative transfer model are considered, but also the volume scattering contribution of the canopy is included. Thus, the total brightness temperature is made up of four components: the direct contributions from the canopy temperature profile, the contribution from the lower half space attenuated by the layer, the lower boundary scattering contributions and the volume scattering contribution.

Result shows that the MVIs, respectively derived from simulations of the zeroth and first radiative transfer model, are quite different from each other. This different is mainly caused by the contributions of the ground surface scattering and the canopy volume scattering. Detailed analysis and explanation will be given in the fullpaper. Also, an attempt to improve the MVIs will also be carried out so that they could better describe the vegetation.

Microwave Scattering Model of Vegetated Surfaces for Applications in SMAP Mission

Xiaolan Xu[1], **Leung Tsang**[1], **Shaowu Huang**[1], **and Eni Njoku**[2]

[1]Department of Electrical Engineering, University of Washington
Seattle, WA 98195-2500, USA
[2]Jet Propulsion Laboratory, California Institute of Technology Pasadena, CA 91109, USA

Abstract— In this paper, we present forward model of the microwave backscattering from a vegetated terrain at L band for application in the upcoming SMAP mission. The physical-based forward scattering model is essential to understand the relationship between the vegetated terrain and radar responses. For active microwave remote sensing of bare soil, the radar backscattering cross section is sensitive to the surface roughness and soil moisture. However, the scattering properties of vegetation layer above the soil surface have a significant effect on the backscattering cross section in microwave remote sensing at L band. To include the vegetation effect, we used the discrete scatterer model approach, which required the calculation of individual scatterer. The shapes of the scatterers are cylinders which are used to simulate corn stalks and disks for leaves. Traditionally, the infinite cylinder approximation and Rayleigh approximation are used to calculate the extinction coefficient and scattering cross section. When the size of the scatterers is comparable to the wavelength, such as in corn stalks and in trunks, both approximations are not valid. We use numerical method in this paper. The numerical solutions of Maxwell equations are solved for individual scatterers through discrete dipole approximation (DDA). The comparisons of the results between analytical approximations and DDA are shown. For the layer of vegetation, the distorted Born approximation is applied for the coherent field calculation. The scattering cross section of the vegetation layer and its interaction with the underground soil surface were formulated by using half space Green's Function. The results are expressed explicitly as three scattering mechanisms. A) The double bounce effect as exhibited by rough surface effect on the interface of the vegetation layer and soil is considered by modifying the rough surface reflectivity using the coherent wave as computed by Numerical solution of Maxwell equations of 3 Dimensional simulations (NMM3D) of bare soil scattering, B) The rough surface scattering of the soil was accounted for by NMM3D and C) the direct volume scattering is calculated by DDA. The model predictions are compared with corn field experiment data collected for the SMAP mission.

A Physically Based Parameterized Method to Estimate Cloud Liquid Water over Land Using AMSR-E

Yongqian Wang[1, 2], **Jiancheng Shi**[1], **and Bangsen Tian**[1, 3]

[1]Institute of Remote Sensing Applications, Chinese Academy of Sciences, Beijing 100101, China
[2]Graduate University of Chinese Academy of Sciences, Beijing 100049, China
[3]Center for Earth Observation and Digital Earth of Chinese Academy of Sciences, Beijing 100101, China

Abstract— This paper presents a new scheme that retrieves cloud liquid water (CLW) over land using satellite radiometer measurements without the help of any ancillary data, unlike all existing methods. Surface emission model, Advanced Integral Equation Model (AIEM) and one dimensional atmosphere transfer model (1DRTM) were combined to generate a database. Through analyzing the simulated database, It's found that the ratio of the polarization difference obtained from 36.5 and 89 GHz ($\Delta T_B(36.5)/\Delta T_B(89)$, called PDR_CLW later) is sensitive to CLW. However, PDR_CLW is also sensitive to surface temperature, water vapor, and cloud height. Firstly, Ka band vertical polarization measurements were used to derive the surface temperature (T_s) with a precision which is high enough in the algorithm because most of the surface temperature influences have already been cancelled in PDR_CLW. Secondly, the ratio of the polarization difference between 18.7 and 23.8 GHz ($\Delta T_B(18.7)/\Delta T_B(23.8)$, called PDR_WV later) was used to consider the influence caused by water vapor because 23.8 GHz is most sensitive to water vapor compared to other bands of AMSR-E. At last, considering that 89 GHz is most sensitive to cloud height, an index called HI (Height Index) which has a form $(T_s - T_v(89\,\text{GHz}))/(T_s + T_v(89\,\text{GHz}))$ to remove the influence caused by cloud height was developed. The relationship between PDR_CLW and CLW were regressed and parameterized in terms of PDR_CLW, CLW, PDR_WV, HI and T_s, and all these parameters can be derived using only satellite brightness temperatures. The algorithm was validated using AMSR-E observations over SGP. Firstly, Retrievals in clear sky have an uncertainty on the order of 0.04 mm. Meanwhile CLW data retrieved by five ground based microwave radiometers (MWR) were used to validate the algorithm, with RMS error of 0.11 mm. Comparisons were also made with MODIS CLW retrieval results, and it is well correlated, with RMS error of 0.14 mm.

SMOS First Results

Y. H. Kerr[1], **P. Waldteufel**[2], **F. Cabot**[1], **P. Richaume**[1], **A. Mialon**[1], **S. Delwart**[3], **and J. P. Wigneron**[4]

[1]CESBIO, France
[2]IPSL-SA, France
[3]ESA-ESTEC, The Netherlands
[4]INRA, France

Abstract— It is now well understood that soil moisture and sea surface salinity are required to improve meteorological and climatic predictions. These two quantities are not yet available globally and with an adequate temporal sampling. So as to cover this data gap, it has been recognized that, provided it is possible to accommodate a suitable antenna on board a satellite, L Band radiometry was the most promising way to fulfill this gap. It is within this framework that the European Space Agency (ESA)'s selected the second Earth Explorer Opportunity Mission, namely the Soil Moisture and Ocean Salinity (SMOS) mission. The SMOS mission is a joint program lead by the European Space Agency (ESA) with the Centre National d'Etudes Spatiales (CNES) in France and the Centro para el Desarrollo Teccnologico Industrial (CDTI) in Spain. SMOS carries a single payload, an L band 2D interferometric radiometer in the 1400–1427 MHz protected band. The instrument probes the Earth surface emissivity, which can then be related to the moisture content in the first few centimeters of soil over land, and, after some surface roughness and temperature corrections, spatio temporal aggregation, to the sea surface salinity over oceans. SMOS will achieve an unprecedented maximum spatial resolution of 50 km at L-band (43 km on average over the field of view) providing multiangular-dual polarized (or fully polarized) brightness temperatures over the globe with a revisit time smaller than 3 days so as to retrieve soil moisture and ocean salinity and meeting soil moisture and ocean salinity science objectives. The caveat being that it will have a somewhat reduced sensitivity when compared to conventional radiometers.

The SMOS mission is now ready for launch and awaiting launcher availability The launch date is November 2nd 2009. After a period of 2.5 weeks the instrument will be switched on and data will be collected, processed and analyzed. It is expected thus to show the first results during this meeting.

Analysis of Electromagnetic Scattering by Random Rough Soil Surfaces at L Band Using Numerical Solutions of Maxwell Equations of 3 Dimensional Simulations (NMM3D)

Shaowu Huang[1], **Leung Tsang**[1], **Eni Njoku**[2], **and Kuan Shan Chen**[3]

[1]Department of Electrical Engineering, University of Washington
Seattle, WA 98195-2500, USA
[2]Jet Propulsion Laboratory, California Institute of Technology
Pasadena, CA 91109, USA
[3]Center for Space and Remote Sensing Research, National Central University
Chung-Li, 32054, Taiwan

Abstract— The study of microwave scattering by soil surfaces is an important problem in remote sensing of soil moisture for both bare soil surfaces and vegetated surfaces. The soil backscattering and emissivities are studied in this paper in relation to the upcoming SMAP satellite mission.

We used NMM3D (Numerical Maxwell Model of 3-dimensional simulations) to calculate the backscattering and emissivities of soil surfaces using Gaussian random rough surfaces with exponential correlation functions. In 3D simulations, the rough surface height $f(x, y)$ vary on both horizontal directions. In the past, numerical simulations were largely limited to 2D simulations with the rough surface height $f(x)$ only varying in one horizontal direction. There were very few results of 3D cases. In this paper, close to 200 cases were computed by varying rms height, correlation lengths and soil permittivity. Method of Moments (MoM) with Rao-Wilton-Glisson (RWG) basis functions are used to form the dense matrix equations. The solutions are accelerated by the Sparse Matrix Canonical Grid (SMCG) method and are implemented on parallel computing. For each case, 15 realizations of rough surface profiles are generated, and 30 solutions are simulated for horizontal and vertical polarizations combined. The energy conservations are checked and are obeyed to within 0.01. The backscattering coefficients and emissivities are compared with empirical models and analytical models, including Dubois formula, Small Perturbation Method (SPM), Kirchhoff Approximation (KA), Advanced Integral Equation Model (AIEM), and Modified Advanced Integral Equation Model (MAIEM). Comparisons with experimental measurements are also made and are found to be in good agreement. Interpolation tables are made up based on the computed cases. This data cube can be directly applied to L-band passive and active microwave remote sensing of soil moisture, such as in the upcoming SMAP mission.

Comparison of Algorithms for Retrieving Soil Moisture from High Resolution ASAR Images

C. Notarnicola[1], **S. Paloscia**[2], **S. Pettinato**[2], **G. Preziosa**[3], **E. Santi**[2], **and Bartolomeo Ventura**[4]

[1]Institute for Applied Remote Sensing, Eurac Research, Viale Druso, 1, I-39100 Bolzano, Italy
[2]CNR-IFAC, Florence, Italy
[3]Politecnico di Bari, Bari, Italy
[4]Università di Bari, Bari, Italy

Abstract— In the last years, with the increasing number of space-borne sensors, the estimation of bio-geophysical surface parameters from remotely sensed data has arisen a growing interest of the remote sensing community. In this research field, one of the most challenging problems is related to the estimation of soil moisture content from microwave active sensors (Synthetic Aperture Radar, SAR).

Soil moisture affects numerous environmental variables, relative to surface climatology, hydrology and ecology. Variations of soil moisture have a strong effect on surface energy balance, regional runoff and vegetation productivity. Furthermore, it is a key variable for early warning for risks such as droughts, flooding, and fire.

This paper exploits the use of two different inversion techniques, one based on a Neural Network approach and the other on a Bayesian procedure to retrieve soil moisture from high resolution ASAR images.

The two methodologies have been tested on two areas which show different surface and environmental characteristics and seasonal conditions. The first one, the Scrivia basin is a flat agricultural area close to Alessandria, in northern Italy. It is a flat alluvial plain measuring about 300 km^2 and situated close to the confluence of the Scrivia and Po rivers. This area is characterized by large, homogeneous agricultural fields of wheat, alfalfa, fodder crops, corn, and sugarbeet. The second test area is placed in the outskirts of Matera town, Southern Italy, and is characterized by long period of drought and high vulnerability to fire. The area is mainly covered by agricultural fields devoted to wheat cultivation.

A series of ENVISAT/ASAR images and ground data was acquired, in the past four years in order to monitor the areas under different seasonal conditions. Simultaneously with the satellite passes, ground campaigns were carried in selected foelds of the two areas. At least 4–6 measurements of SMC, surface roughness and vegetation parameters were carried out for each field, depending on its dimensions. The volumetric soil moisture (SMC, in cm^3/cm^3) was measured by using a Time Domain Reflectometer (TDR) calibrated with a number of gravimetric samples. The soil layer investigated was of the order of 10–20 cm, depending on the soil density. Soil surface roughness was measured by using a 120 cm long needle profilometer, with a sampling of 0.4 cm. Measurements were gathered along and across the field rows. Both the Standard Deviation of the Heights (s, in cm) and the correlation length (lc, in cm) were extracted from the measured profile by means of a digital autocorrelation procedure. The vegetation parameters measured included plant height (in cm), density (plants/m^2), leaf number and dimensions (in cm), and fresh biomass (in kg/m^2).

Both ground and backscattering (σ^2) data were averaged field by field (at least 200 pixels each). The main aim of this analysis is to cross-compare the two methodologies in different types of test areas and verify if they retrieve the same spatial and temporal soil moisture features by indicating what can be expected for different soil and environmental conditions in terms of accuracy, range of applicability, and method advantages and disadvantages. Furthermore, the algorithms are also compared in terms of processing times. A further analysis is to verify the feasibility to individuate some soil characteristics and field features where the results of the two methodologies during the time of observation converge with the highest accuracy. These stable points have been proved to be suitable in order to infer information over the whole basin.

Session 4A2
EMC and EM protection

TDIE-TDPO Hybrid Formulation Using the Laguerre Polynomials for Scattering from Three-Dimensional Perfectly Conducting Bodies

Ming-Da Zhu[1], **Xi-Lang Zhou**[1], **and Wen-Yan Yin**[2, 1]

[1]Center for Microwave and RF Technologies (CMRFT), Shanghai Jiao Tong University
Shanghai 200240, China
[2]Center for Optical and EM Research (COER), Zhejiang University, Hangzhou 310058, China

Abstract— In this paper, an efficient and stable hybrid method based on TDIE and time-domain physical optics (TDPO) is proposed to investigate scattering characteristics of arbitrary 3-D structures. In our methodology, planar triangular patches are used to model the surface with the spatial basis functions of RWG basis functions implemented, while the temporal basis functions of weighted Laguerre polynomials are also employed. However, the customary marching-on-in-time (MOT) scheme is not utilized here, as MOT scheme suffers from the occurrence of late-time instabilities in the form of exponentially increasing oscillation. We know that a new method called the marching-on-in-order (MOO) has been proposed more recently to solve the TDIE efficiently. It uses the weighted Laguerre polynomials as temporal basis and testing functions. Due to the properties of the weighted Laguerre polynomials, the temporal variables can be completely eliminated from all the computations and the time derivatives can be handled analytically. This also eliminates the need of temporal interpolation, and therefore, much stable results can be obtained even for late time. Although the MOO method is always stable, it still suffers from high computational complexity. One remedy is to employ hybridizations of integral and optical methods in time domain. We solve TDIE-TDPO hybrid equations by expressing the transient behavior in terms of weighted Laguerre polynomials. The object surface is partitioned into two regions: TDIE region S^{IE} and TDPO region S^{PO}. In the TDIE region, currents are updated by solving a time-domain electric field integral equation (TD-EFIE) by MOO. In the TDPO region, PO currents are obtained according to the incident fields as well as the fields radiated by all currents in the TDIE regions. In order to avoid solving of a matrix equation for obtaining the coefficients of the bases in S^{PO}, we adopt the projection procedure presented by Jakobus and Landstorfer. Normally, the cost of analyzing scattering using a classical MOO scheme for N_D orders from an object whose surface current is discretized in terms of N_S spatial unknowns scales as $O(N_D^2 N_S^2)$. The proposed TDIE-TDPO hybrid method reduces CPU and memory requirements to $O(N_D^2 N_S^{\mathrm{IE}} N_S^{\mathrm{PO}})$ and $O((N_S^{\mathrm{IE}})^2)$, respectively, where N_S^{IE} and N_S^{PO} are the spatial unknowns in the two regions.

In contrast with the results obtained by TD-EFIE using MOO scheme, it is shown that our method can get very good accuracy and efficiency for analyzing the scattering of complex structures.

Transient Responses Analysis of Ultra-wideband Filters Illuminated by High-power Electromagnetic Pulses (EMP)

Zheng Jiang[1], **Jian Wang**[2], **and Wen-Yan Yin**[1, 2]

[1]Center for Optical and EM Research (COER), Zhejiang University, Hangzhou 310058, China
[2]Center for Microwave and RF Technologies (CMRFT), Shanghai Jiao Tong University
Shanghai 200240, China

Abstract— It is well known that intentional or unintentional electromagnetic interference can impact on microwave circuits or systems to make them improper functionality. In this paper, we use a modified FDTD method to analyze the transient response of some ultra-wideband (UWB) filters with a switch diode enclosed and illuminated by a high-power electromagnetic pulse (EMP), respectively.

Our attention is focused on evaluating EMP interference effects on the input/output ports which can be further characterised by S-patameters. We compute some induced voltage terms firstly excited by the external fields, then the S-parameters interference at the input/output ports can be calculated. In our simulation, the S-parameters of the UWB filters illuminated by an external pulse with an arbitrary incident direction or polarization state is detected. The two different types of UWB filters are disturbed by the external EMP seriously, especially for S_{11}, about arising 2–3 dB between 3 GHz and 11 GHz. Furthermore, statistical analysis of parasitic studies are performed to discribe the degree of failure effects disturbed by the external EMP. To measure the interference of the device by external EMP clearly, the breakdown failure error of $S_{i,j}$ (BFES) is defined in this paper. The mean-BFES varying with the two different kinds of pulses, such as the fast and UWB double-exponential pulses, is carried out to obtain the relation between them to know the susceptibility of S-parameters. The statistical analysis provides a new procedure for a confidence determination of the interference behavior parameters.

In contrast with the results obtained by HFSS and measurement, it is shown that our code can show very good agreements and is performed to demonstrate the EMP interference effect on the S-parameters of the reconfigurable UWB bandpass and the compact UWB filters.

Research on New Technology on Protection of Electronic Systems from High Power Electromagnetic Pulse

Zhonghao Lu, **Chunxiao Jian**, **Shuanglin Wan**, **and Peiguo Liu**
School of Electronic Science and Engineering, NUDT, Changsha 410073, China

Abstract— The definition of high power microwave (HMP) weapon and its damage to people and other weapons is discussed first. Recent progress and perspectives of the research on the new technology on protection of electronic systems from high power electromagnetic pulse (EMP) damage are expatiated in the form of new structure and material. The hypothesis is proved by computer simulation at last.

Multi-physics Simulation and Analysis for High-power EMP Effects on Micro/Nanoelectronics Devices

Xiao-Peng Wang[1], **Ming Yi**[2], **and Wen-Yan Yin**[1, 2]

[1]Center for Optical and EM Research (COER), Zhejiang University, Hangzhou 310058, China
[2]Center for Microwave and RF Technologies (CMRFT), Shanghai Jiao Tong University
Shanghai 200240, China

Abstract— More recently, intentional electromagnetic interference (IEMI) has drawn some special attentions in the EMC community, which means that intentional malicious generation of electromagnetic energy introduces noise or signals into electrical and electronic systems, thus disrupting, confusing, or damaging these systems for terrorist or criminal purposes. Such an IEMI can be generated by a high-power microwave (HPM) source and even a high-power ultra-wide band pulse (HP-UWBP) antenna.

In this paper, our attention will be focused on multi-physics simulation and analysis for transient electro-thermal and electro-thermo-mechanical responses of some typical micro/nanoelectronics devices and interconnects under the impact of a high-power electromagnetic pulse (HP-EMP) for different waveform parameters, respectively. The mathematical methodology is mainly based on hybrid time-domain finite element method (TD-FEM), which has been successfully implemented in our previous studies of electro-thermal and thermo-mechanical responses of 3-D interconnects and wire bondings. As the temperature-dependences of most material parameters involved are considered, such as the electrical conductivity, thermal conductivity, thermal expansion coefficient, and Young's modulus of the structures, the developed TD-FEM algorithm can capture transient electro-thermal as well as electro-thermo-mechanical responses of various micro/nanoelectronics devices and interconnects accurately.

A Novel Hybrid Method for Solving the Response of Non-uniform Transmission Line Network

Yujian Qin, **Peiguo Liu**, **and Jianguo He**
School of Electronic Science and Engineering, NUDT, China

Abstract— In the analysis of transmission line networks on complex systems, the most appropriate method is BLT equation. However, BLT equation is inapplicable in non-uniform circumstances. In practice, non-uniform transmission lines are unavoidable. Therefore, methods in time domain are appropriate rather than methods in frequency domain, such as Finite Difference Time Domain (FDTD). But FDTD is more time-consuming than BLT equation.

If a method could calculate the responses of large-scale transmission line networks rapidly, and could handle the non-uniform lines, simultaneously; the practical analysis requirement can be satisfied primely. Based on that, we combine the advantages of BLT equation and FDTD method, propose a BLT-FDTD hybrid method. While maintaining the precision, this method could maximize the computational efficiency.

The process of BLT-FDTD hybrid method is: (1) Calculating the S parameters of non-uniform parts by FDTD; (2) Treat them as the junctions in BLT equation, and solve the whole network.

The proposed method overcomes the inapplicability of the methods in frequency domain and avoids the high computational cost of the methods in time domain. It has the capability for solving complex transmission line networks.

Solving Method for Electromagnetic Pulse Propagation Based on Combination of EMT and TDIE

Gaosheng Li, **Yujian Qin**, **Peiguo Liu**, **and Jianguo He**
College of Electronic Science and Engineering, National University of Defense Technology
Changsha 410073, China

Abstract— A solving method for propagation and coupling of Electromagnetic Pulse (EMP) is provided. The idea is to combine the theory of Electromagnetic Topology (EMT) and the method of Time Domain Integral Equation (TDIE). The former offers methodology and the latter carries out the computations, which can improve the efficiency of analysis and the size of area that can be computed. By this way, the difficulty of direct computation of complex electronics system can be conquered, and virtues of time domain computing can be used adequately. Situations of computing of electromagnetic problems nowadays as well as requirement of precise computing in the area of electromagnetic compatibility and electromagnetic protection are introduced Principal ideas of EMT for analyzing and solving problems are introduced, after which the four main steps of using EMT to find solutions of propagation and coupling of EMP are summarized. Method to combine EMT and TDIE is put forward, together with the advantages of TDIE for analyzing EMP. Finally, to improve computing efficiency of TDIE, relative speeding algorithms are expatiated, including Plane Wave Time Domain (PWTD), Time Domain Adaptive Integral Method (TD-AIM) and other mixed algorithms such as Physical Optics-TDIE (PO-TDIE) and Uniform Geometrical Theory of Diffraction-TDIE (UTD-TDIE).

Session 4A3
Optics, Fiber, Lasers and Optical Sensors

Phase Control in the Ramsey Resonance Cavity with 2 Ring Cavities at both Ends by Inserting Loop Antenna Using Varactor in Series in the Rings for Cesium Beam Frequency Standard

Koji Nakagiri and Yusuke Kawano
Kinki University, Kinokawa City, Wakayama 649-6493, Japan

Abstract— A vertical cesium beam experimental frequency standard is under construction. It aims at an accuracy of around 7×10^{-15} or less by adopting new techniques such as 4-pole electromagnets for energy selection and beam focus including velocity selection, and a Ramsey resonance cavity in which the microwave phase of interactions with the cesium beam may be controlled by changing the cesium beam velocity electrically by the magnet and measuring the cavity frequency shift, because the cavity phase and Doppler frequency shifts are proportional to the cesium beam velocity.

The investigation on phase control of ring cavities has been conducted, to which the microwave is supplied through a single-U type waveguide which has a E-plane T-couple in the center and is connected with the E-plane T-couple of ring cavity at both ends. We inserted a single or double loop antenna using the varactor (variable capacitance tip diode) in series to the H-plane of ring type cavities to control the phase of the microwave and the cesium beam interaction region in the ring cavities, respectively. The phase of ring cavity is measured by using a loop antenna. The positions of antenna are separately placed $1/4\lambda_g$ away from a E-plane T-couple of the ring cavity, in right or left direction. The varactor loop antenna is connected in series with a coaxial semi-rigid cable of variable length, which is shorted at the end.

The frequency center of resonance in ring cavity is influenced by the varactor loop antenna in the same ring cavity more than that in another ring cavity. This unbalance makes the difference between the both ring cavities by the voltage supply to the varactors, respectively.

The phase difference about 2 degrees between the both detection antennas were typically obtained by the voltage change of 10 V in the case of double loop varactor antenna. In the case of single loop varactor antenna the phase change will be less than 1 degree due to the small frequency change between the both ring cavities. But the small power change and distortion of resonance curve between the cavities at both ends is better for the phase control of frequency standard.

Study of Sapphire Loaded H-Maser in Shanghai Observatory

Ke Dai[1, 2], **Wei Qun Zhang**[1], **Yan Jun Zhang**[1], **and Wen Ming Wang**[1, 2]

[1]Shanghai Astronomical Observatory, Chinese Academy of Sciences, Shanghai 200030, China
[2]Graduate School of Chinese Academy of Science, Beijing 100049, China

Abstract— Sapphire loaded cavity for active H-maser was designed to minimize the mass and volume of the traditional active H-maser. The ability of sapphire loaded cavity to achieve self-oscillation was calculated. Then we made the experiment for sapphire loaded cavity in traditional H-maser as bed. The signal was found with oscillation power of −102 dBm while the beam flux is about 1 mA. For the temperature coefficient of sapphire loaded cavity is too high, the way to compensate the temperature-coefficient was studied. The region of "zero temperature coefficient point" was discussed.

Improvements on Phase-Shifted Distributed-Coupling-Coefficient Distributed Feedback Laser Structures for Single Longitudinal Mode Operation

J. Boavida[1], **C. Fernandes**[1], **and J. Morgado**[1, 2]

[1]Instituto de Telecomunicacoes, Portugal
[2]Portuguese Air Force Academy, Portugal

Abstract— Optical communication systems (OCS) have earned great attention from the scientific community, due to the increasing demand for high-bit rate data links. An OCS depends heavily on the performance of the light emitter, usually a Distributed Feedback (DFB) laser. However, not every DFB laser structure is considered an efficient device, creating the need to optimize, as much as possible, these structures. This paper presents optimized Phase-Shifted (PS) Distributed-Coupling-Coefficient (DCC) DFB laser structures specially designed for single longitudinal mode operation in the OCS context. The optimization and analysis process is divided into two stages: near and above threshold.

Near threshold, the purpose is simultaneously the maximization of the normalized mode selectivity (S) and the minimization of the electric field flatness (F). These figures of merit are given, respectively, by $S = (\alpha L) - (\alpha_{th} L)$ and $F = \frac{1}{L}\int_0^L [I(z) - \bar{I}]^2 dz$, where $(\alpha_{th} L)$ is the normalized threshold gain, (αL) is the normalized gain of the main side mode, and $I(z)$ is the normalized electric field intensity at an arbitrary position z, inside the L-length laser cavity. In order to evaluate these figures of merit, a simulation model was built using the transfer matrix method, which is based on the coupled wave equations.

Above threshold, the power emission spectrum is assessed, as well as the Side Mode Suppression Ratio ($SMSR$). Besides, the wavelength stability with current injection is also assessed. This model takes into account the undesired effects of the spatial hole burning, which deteriorate the laser performance with increasing biasing current.

The structure achieved after optimization contains a single phase-shift, and has a coupling coefficient profile that includes three distinct values, which is designated as a 1PS-3DCC-DFB structure. For the 1PS-3DCC-DFB, $S \approx 2.34$, $F \approx 0.021$ and $SMSR \geq 49$ dB are achieved, as well as a tight wavelength stability, which clearly outperforms similar laser structures proposed elsewhere, harder to manufacture.

This analysis shows that, if this structure was manufactured, it could be extremely useful to attain an exceptional light emitter in the OCS context.

On the Performance of DFB Laser Structures Specially Designed for Directly-Modulated Optical Communication Systems

J. Boavida[1], **C. Fernandes**[1], **and J. Morgado**[1, 2]

[1]Instituto de Telecomunicacoes, Portugal
[2]Portuguese Air Force Academy, Portugal

Abstract— Nowadays, directly-modulated (DM) distributed-feedback (DFB) lasers are playing an important role as transmitter sources in high bit rate optical-communication-systems (OCS) due to its low cost operation, small size, low dynamic voltage and high optical output power, when compared with other transmitters using external modulation schemes. In this context, it is very important to develop a suitable design for DM-DFB lasers in order to achieve a stable single-longitudinal-mode (SLM) operation with high power efficiency and ensuring the best emitted wavelength stability ($\frac{\Delta\lambda}{\lambda}$) to avoid pulse transmission dispersion. Accordingly, it is crucial to minimize the impact of spatial-hole-burning (SHB) effect on DM-DFB lasers operation. Such effect is straightforwardly responsible for the degradation of both the side-mode-suppression-ratio (SMSR) and the wavelength stability.

In this paper, we propose two very easily manufacturable distributed-coupling-coefficient (DCC)-DFB optimized laser structures with asymmetric facet configuration — with a high-reflectivity (HR) facet and an anti-reflection (AR) facet — in order to channel all the output power to the AR facet. The difference between these two structures lies on the DCC profile design, which is considerably more sophisticated for the second structure, enhancing the mode selectivity. The proposed structures both present, simultaneously, high power efficiency ($\geq 0.32\,\mathrm{W{\cdot}A^{-1}}$), tight wavelength tolerance ($\approx 0.15\,\mathrm{nm}$), a good SHB immunity ($\mathrm{SMSR} \geq 41\,\mathrm{dB}$ and $\frac{\Delta\lambda}{\lambda} \leq 1.3 \times 10^{-5}$) and high yield ($> 50\%$) that is the probability of the modal selectivity exceeding a preset value.

The proposed lasers fulfill all the requirements concerning the usage of DM-DFB lasers in the OCS context. Similar performances have been recently reported but at the expense of laser structures demanding a much more intricate fabrication process than the ones associated with the laser structures proposed in this paper.

Reduction of Four-wave-mixing Noises by Unequally-spaced Allocations with Dual Base Units in FDM Optical Fiber Transmission Systems

Toru Nakamura and Takahiro Numai
Department of Electrical and Electronic Engineering, Ritsumeikan University
1-1-1 Noji-Higashi, Kusatsu, Shiga 525-8577, Japan

Abstract— Transmission characteristics in frequency-division-multiplexing (FDM) optical fiber transmission systems with low-dispersion optical fibers such as dispersion-shifted fibers (DSFs) are limited by four-wave mixing (FWM). In recent years, several FWM suppression techniques such as optical multiplexers and demultiplexers with the combination of delay lines, modified return-to-zero (RZ) signals, hybrid wavelength-/time-division multiplexing (WDM/TDM) technique, arrangement of polarization allocations of channels, separation between signal frequencies and the zero-dispersion frequency, combination of frequency/polarization allocations and separation of signal frequencies from the zero-dispersion frequency, the hybrid amplitude-/frequency-shift keying (ASK/FSK) modulation with prechirped pulses, and unequal channel spacing have been reported.

Characteristics of FWM are also closely related to frequency allocations and modulation formats. From the viewpoint of frequency allocations, unequally-spaced (US) allocations, repeated US (RUS) allocations, and modified RUSs such as equally-spaced RUS (ERUS) and unequally-spaced RUS (URUS) allocations have been demonstrated to overcome the problems in equally-spaced (ES) allocation. It was found that RUS, ERUS, and URUS have lower FWM light intensities with channel frequencies than ES and narrower total bandwidths than US. From the viewpoint of modulation formats, FWM noises have been analyzed for non-return-to-zero (NRZ), random RZ, differential phase-shift keying (DPSK), and bit-phase arranged RZ (BARZ) in ES, RUS, ERUS, and URUS, and it has been revealed that FWM noises are lowest in URUS with BARZ.

In this paper, to reduce FWM noises further, US with dual base units, which have different frequency spacings, is proposed. It is found that the allowed input optical power is improved by 4.7 dB than URUS in an FDM lightwave transmission system with intensity modulation/direct detection. In our calculations, it is assumed that an oscillation wavelength for a light source is 1550 nm. A DSF is assumed to have the derivative dispersion coefficient $\mathrm{d}D_\mathrm{c}/\mathrm{d}\lambda$ of 0.07 ps/km/nm^2, the fiber length L of 80 km, and the decay rate α of 0.2 dB/km. The base unit and the channel spaces are common in all frequency allocations which are studied in this paper, and the frequency separations are the same as those in to make the pulse delay and pulse broadening as small as possible.

ACKNOWLEDGMENT

This research was partially supported by the Japan Society for Science, Grant-in-Aid for Scientific Research (C) 20560379, 2009.

Reduction of Four-wave-mixing Noises by FSK Modulation with Dual Deviation Frequencies in FDM Optical Fiber Transmission Systems

Takuya Tamo and Takahiro Numai
Department of Electrical and Electronic Engineering, Ritsumeikan University
1-1-1 Noji-Higashi, Kusatsu, Shiga 525-8577, Japan

Abstract— Transmission characteristics in frequency-division-multiplexing (FDM) optical fiber transmission systems with low-dispersion optical fibers such as dispersion-shifted fibers (DSFs) are limited by four-wave mixing (FWM). In recent years, several FWM suppression techniques such as optical multiplexers and demultiplexers with the combination of delay lines, modified return-to-zero (RZ) signals, hybrid wavelength-/time-division multiplexing (WDM/TDM) technique, arrangement of polarization allocations of channels, separation between signal frequencies and the zero-dispersion frequency, combination of frequency/polarization allocations and separation of signal frequencies from the zero-dispersion frequency, the hybrid amplitude-/frequency-shift keying (ASK/FSK) modulation with prechirped pulses, and unequal channel spacing have been reported.

Characteristics of FWM are also closely related to frequency allocations and modulation formats. From the viewpoint of frequency allocations, unequally-spaced (US) allocations, repeated US (RUS) allocations, and modified RUSs such as equally-spaced RUS (ERUS) and unequally-spaced RUS (URUS) allocations have been demonstrated to overcome the problems in equally-spaced (ES) allocation. It was found that RUS, ERUS, and URUS have lower FWM light intensities with channel frequencies than ES and narrower total bandwidths than US. From the viewpoint of modulation formats, FWM noises have been analyzed for non-return-to-zero (NRZ), random RZ, differential phase-shift keying (DPSK), and bit-phase arranged RZ (BARZ) in ES, RUS, ERUS, and URUS, and it has been revealed that FWM noises are lowest in URUS with BARZ.

In this paper, to reduce FWM noises further, FSK modulation with dual deviation frequencies is proposed. It is found that the crosstalk is improved by 4.9 dB, and the power penalty is improved by 2.5 dB than FSK modulation with a single deviation frequency in an FDM lightwave transmission system with FSK modulation/direct detection. In our calculations, it is assumed that an oscillation wavelength for a light source is 1550 nm. A DSF is assumed to have the derivative dispersion coefficient $\mathrm{d}D_\mathrm{c}/\mathrm{d}\lambda$ of 0.07 ps/km/nm^2, the fiber length L of 80 km, and the decay rate α of 0.2 dB/km. The base unit and the channel spaces are common in all frequency allocations which are studied in this paper, and the frequency separations are the same as those in to make the pulse delay and pulse broadening as small as possible.

ACKNOWLEDGMENT

This research was partially supported by the Japan Society for Science, Grant-in-Aid for Scientific Research (C) 20560379, 2009.

Fabrication of Separately Formed Electro-spun Fibers

Hirohisa Tamagawa
Department of Human and Information Systems, Faculty of Engineering, Gifu University, Japan

Abstract— Electrospining has been known as a strong tool for the fabrication of fine polymer fibers. However, the extraction of single electro-spun fiber is a tough task. Electro-spun fibers are inevitably stick together or entangled one another during their spinning process. They cannot be separately formed. The author of this paper found that simply placing a paper mesh between the syringe needle and counter electrode of electrospinning unit, the straight fibers were separately formed between the paper mesh and counter electrode. As an ingredient of electro-spun fiber, polynorbornen was employed. Polynorbornen was dissolved into THF, and the mixture of polynorobornen-THF was electro-spun into short fine fibers. The resulting fibers were separately formed, and those fibers were extracted individually without their sticking or entangling. The formation process of such fibers of polynorobornen was investigated. Fiber formation process was captured by the high speed camera. It elucidated that the fiber was quite slim and waved vehemently in the early stage of its electro-spun process, but it gradually grew fat and its dynamic wavy motion calmed down, resulting in a bit fat straight and rigid short fiber. Using this simple technique employing a paper mesh, the composite fibers fabrication was attempted, which consisted of polymer and metal powder. As the ingredients of composite fiber, polyvinylacetate and copper powder were employed. Poyvinylacetate was dissolved into THF, and subsequently copper powder was mixed with this polyvinylacetate-THF mixture. This composite ingredient underwent the electrospinning process employing a paper mesh. Finally, the composite fibers were separately formed successfully and extracted easily.

Performance Improvement of Phase Modulation with Interferometric Detection through Low-biasing

Lan Liu, **Shilie Zheng**, **Xianmin Zhang**, **Xiaofeng Jin**, **and Hao Chi**
Department of Information Science & Electronic Engineering, Zhejiang University, Hangzhou 310027, China

Abstract— Phase modulation (PM) offers many advantages in analog-photonic link. The most important one is that PM needn't bias circuitry, which may not only reduce the complication of transmitting end, but also avoid the problems caused by bias-voltage drift. Moreover, PM provides linear conversion of input voltage to optical phase. However, suitable detection through PM to intensity modulation (IM) conversion is needed in the phase modulated system. In this paper, PM-to-IM is realized via interferometric detection, whose performance is improved through tuning the laser wavelength while not complicating the system configuration.

In our interferometric detection scheme, a Mach-Zehnder interferometer (MZI) composing of two couplers and two fiber arms with different length is used. The theory of PM-to-IM through this interferometric detection is fully investigated, including the link gain, NF, SFDR and IP_3, OIP_3 (the input and output RF signal power, respectively, when the third-order intermodulation output equals to the fundamental output). It is said that the link gain, noise figure (NF) and spur-free dynamic range (SFDR) are related with the input optical power, laser frequency, input RF signal frequency, link loss, and the differential delay τ between the two arms of the MZI. If τ is fixed, NF can be improved through tuning the laser wavelength. Both the theory calculation and simulation results show that there is an optimum wavelength for NF, which can be seen in Fig. 1. The curve a is with input optical power of 0.1 W and curve b is with input optical power of 1 W. Besides, the expression for the effective half-wave voltage of phase modulator with MZI is also developed, which only affects the value of NF, but not SFDR.

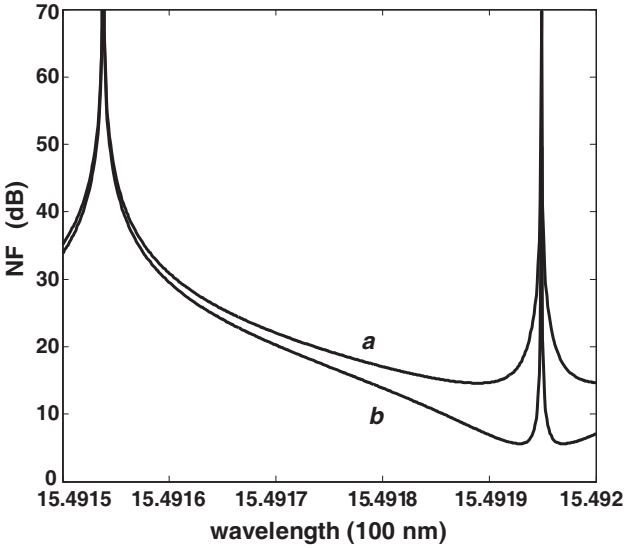

Figure 1: The simulation results of NF with respected to wavelength.

Profile Measurement for Micro-optical Component Using Lensless Fourier Digital Holography

Yunxin Wang, **Dayong Wang**, **Yan Li**, **Jie Zhao**, **Yizhuo Zhang**, **Yuhong Wan**, **and Zhuqing Jiang**
College of Applied Sciences, Beijing University of Technology, Beijing 100124, China

Abstract— Three-dimensional (3D) profile measurement for micro-optical component has attracted remarkable attention recently for its wide application in many filed such as optical imaging, transmission and communication. Digital holography (DH) has become a research focus in 3D profile reconstruction discipline in view of its high resolution, non-invasion, non-contact, and full wave field mode. In this contribution, digital holography imaging method based on off-axis lensless Fourier transform (LFT) is presented for 3D profile detection of micro-optical component. Since the phase is proportional to the height of transparent object under the condition of constant refractive index, the quantitative 3D profile can be acquired with the combination of phase and amplitude. Firstly, the LFT holography configuration is designed, and the amplitude and phase of the whole wave field are reconstructed from only a single recorded hologram by Fresnel reconstruction method. Then phase compensation is adopted to remove the quadric phase aberration, and the accurate phase information is extracted in use of the least-squares phase-unwrapping algorithm. Finally, the performance of LFT holography imaging is validated with two kinds of micro-lens array, one is the spherical micro-lens array with 3.07 μm height and 860.70 μm half width, and another one is cylindrical micro-lens arrays with 2.77 μm height and 166.90 μm half width. Properties like lens height, radius of curvature (ROC), and surface roughness of micro-lens arrays are measured by LFT holography configuration. In order to verify the feasibility and effectiveness of the developed method, we acquire and compare the profile parameters of the aforementioned micro-lens arrays using the stylus profilometer. The results indicate that the profile parameters obtained above are in good agreement, which demonstrates that LFT holography method provides an effective tool for 3D profile detection, and has wide application perspective in quality evaluation and machining guidance for micro-optical component.

A Novel Data Transmission Security via a Noisy Channel Using a Microring Resonator System

T. Threepak[1], **S. Mitatha**[1], **and P. P Yupapin**[2]

[1]Hibrid Computing Research Laboratory, Faculty of Engineering
King Mongkut's Institute of Technology Ladkrabang, Bangkok, Thailand
[2]Advance Research Center for Photonics, Department of Applied Physics
King Mongkut's Institute of Technology Ladkrabang, Bangkok, Thailand

Abstract— A novel verification and encryption methods using microring resonator is presented. By using the proposed system, the confidentiality and integrity of information in optical communication can be formed. In this paper, chaostic noise sophisticates irreversible and unpredictable in nonlinear microring resonator that is used as the encrypted function. In our successfully simulation results, the microring resonator and add/drop filter are uses to generate the message authentication code for maintaining data integrity. Additionally, the noisy signals/channels created by the microring resonator are combined with the encoded information to protect the man-in-the-middle attacks (decipher). By using the extremely small processing device, the propose design can be easily applied to secure any form of communication in wireless network, mobile communication network and military applications with low power consumption and very high-speed procedures.

Ferroelectric Properties of $BiFeO_3$ Thin Film Grown on $LaNiO_3$ Buffered Si (100) Substrate via Pulsed Laser Deposition

Feng Yan[1], **Li Lu**[1], **Man On Lai**[1], **and Tiejun Zhu**[2]

[1]Department of Mechanical Engineering, National University of Singapore
9, Engineering Drive 1, 117576, Singapore
[2]Department of Materials Science and Engineering, Zhejiang University
Hangzhou 310027, China

Abstract— Ferroelectric properties of multiferroic $BiFeO_3$ (BFO) thin films have been grown on a $LaNiO_3$ conductive layer buffered Si (100) substrate via pulsed laser deposition method. The crystalline structure and surface morphology of the film were characterized by X-ray diffraction studies and atomic force microscopy, which confirmed the strong (100) texture growth, the surface roughness, RMS $\approx$ 7.832 nm, and the polarization direction is close to $\langle 100 \rangle$. The BFO film showed a well saturated ferroelectric hysteresis loops with a remanent polarization of 55 mC/cm^2, and coercive field of approximately 180 kV/cm The dielectric property was obtained in a frequency range of 100 $\sim$ 1 MHz. The ferroelectric domain structure and piezoresponse behavior in the BFO thin film were also studies by piezoelectric force microscopy.

Session 4A4a
Metamaterial and Electromagnetic Cloak

An Experimental Design for Reversed Cherenkov Radiation in a Double-negative-metamaterial-loaded Waveguide

Zhaoyun Duan[1], **Xutong Mao**[1], **Jucheng Lu**[1], **Yanyu Wei**[1], **Yubin Gong**[1], **Wenxiang Wang**[1], **Bae-Ian Wu**[2], **and Min Chen**[3]

[1]Vacuum Electronics National Laboratory, School of Physical Electronics
University of Electronic Science and Technology of China, Chengdu 610054, China
[2]Research Laboratory of Electronics, Massachusetts Institute of Technology, Cambridge, MA 02139, USA
[3]Department of Physics, Massachusetts Institute of Technology, Cambridge, MA 02139, USA

Abstract— We have proposed an experimental design for verifying the reverse Cherenkov radiation (RCR) in a circular waveguide partially filled by double-negative metamaterials. These media are composed of different materials such as the metallic strips for the SRRs and rods/dielectric materials for holding the strips, and can be characterized by simultaneously negative permittivity and permeability tensors at a frequency of ∼10.8 GHz. We have been designing such a structure with some small slots that it is suitable for quasi-TM mode. Thus, the electromagnetic waves at a frequency of 10.8 GHz can effectively interact with an electron beam and the RCR can be produced and detected by an antenna. Currently, the related work on the manufacture, assembling, and measurement is underway.

ACKNOWLEDGMENT

This work was supported by National Natural Science Foundation of China (Grant Nos. 60971031, 60601007, and 60532010) and Sichuan Youth Foundation.

Electromagnetic Detection of a Perfect Transformation-based Invisibility Cloak

Baile Zhang and Bae-Ian Wu
Research Laboratory of Electronics, Massachusetts Institute of Technology, Cambridge, MA 02139, USA

Abstract— The most attractive prediction of transformation optics might be the possibility of perfect invisibility cloaking, where the cloak mimics the coordinate transformation, squeezing the originally flat electromagnetic (EM) space and guiding light smoothly along curved trajectories around a hidden object. Perfect cloaking is believed to be undetectable because a perfect cloak is equivalent to a curved but empty EM space. Although the first cloak models can achieve invisibility only in a very narrow frequency band, efforts to extend the bandwidth are currently proceeding. The possibility of realizing invisibility cloaking has great significance on both theoretical and practical levels and has attracted a lot of attention from scientific community. However, the other side of this issue — how to detect a perfect invisibility cloak or a curved EM space — has not been solved in previous studies.

It is the purpose of this paper to develop a method to detect a perfect invisibility cloak electromagnetically, no matter what frequency band it works in. Our results demonstrate the asymmetry of coordinate transformation: Though this transformation of EM space can completely control the motion of photons, it is not directly applicable to the motion of charges. It can be argued that, a photon, which perceives only the EM space, does not know that the EM space is curved, since there is no other reference for it to make judgement. However, one should notice that when the space for Maxwell's equations (EM space) is squeezed, the space for Newton's laws of motion (mechanical space) is still flat. Before the coordinate transformation, they share the same physical space, but after transformation, they are separated. In other words, at the same physical location, the curved EM space and the flat mechanical space overlap. If one chooses the flat mechanical space as the reference, the bending of EM space is perceivable.

The only bridge from the flat mechanical space to the curved EM space is the charge attached to a particle. Thus a fast moving charged particle moving in both spaces can perceive the bending of EM space because of the reference function of the flat mechanical space. A broadband radiation will be generated in this process, making the cloak visible. The whole radiation process is explained by comparing the motion of the charged particle in both EM and mechanical spaces. Detailed calculation is based on an extension of Frank and Tamm's theory on Cerenkov radiation, together with dyadic Green functions.

Non-magnetic Cylindrical Cloak with Optimized Homogeneous Isotropic Layers

Zhenzhong Yu, Yijun Feng, and Xiaofei Xu
Department of Electronic Science and Engineering, Nanjing University, Nanjing 210093, China

Abstract— Electromagnetic invisibility cloaks designed through transformations optics usually require anisotropic and inhomogeneous media [1]. Such idea has been demonstrated experimentally at microwave frequencies using inhomogeneous structured metamaterial with different unit cells of split ring resonators, which is difficult to fabricated and not easy to extend to optical range [2]. To solve this problem, we have proposed cloak with concentric layered structure of alternating homogeneous isotropic materials [3]. Based on the effective medium theory, such structure could have better cloaking performance as increasing the number of layers. Recently optimized cloaks with only limited number of layers have been proposed [4, 5], however these proposals still need layers of anisotropic metamaterial which is difficult to achieve for an optical cloak.

In this presentation, we will demonstrate that our proposed cloak with concentric layered structure of alternating homogeneous isotropic materials can be optimized to significantly reduce the number of layers. With optimized design of the permittivity or the thickness of the alternating layers through genetic algorithm, we could achieve non-magnetic cylindrical cloak with only six or less layers of homogeneous isotropic dielectrics. Meanwhile, the values of permittivity parameters can be constrained to a proper range, which can be realized through normal materials. The performance of our optimized design has been verified through both rigorous analysis and full-wave electromagnetic simulation based on the finite element method (Fig. 1). The proposed cloaking structure could be possibly realized by nano-structured normal materials, therefore may lead to a practical path to an experimental demonstration of electromagnetic cloaking in the optical range.

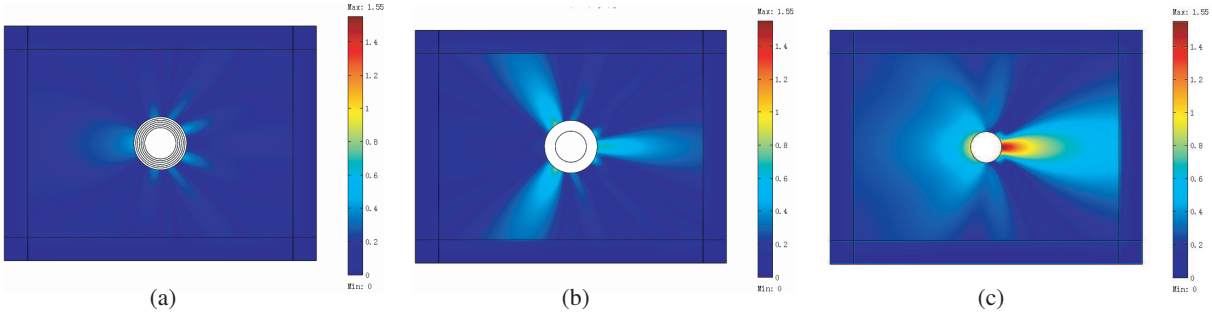

(a) (b) (c)

Figure 1: Comparison of the electromagnetic scattering fields from (a) optimized cylindrical cloak with only six layers, (b) cylindrical cloak designed with the reduced set of linear transformation and (c) a bare conducting cylinder without cloak.

ACKNOWLEDGMENT

Supported by the National Basic Research Program of China (2004CB719800), and the National Nature Science Foundation (60671002, 60801001).

REFERENCES

1. Pendry, J. B., D. Schurig, and D. R. Smith, *Science*, Vol. 312, 1780–1782, 2006.
2. Schurig, D., et al., *Science*, Vol. 314, 977–980, 2006.
3. Huang, Y., Y. Feng, and T. Jiang, *Opt. Express*, Vol. 15, 11133, 2007.
4. Popa, B. I. and S. A. Cummer, *Phys. Rev. A*, Vol. 79, 023806, 2009.
5. Xi, S., H. S. Chen, B. Zhang, B. I. Wu, and J. A. Kong, *Phys. Rev. B*, Vol. 79, 155122, 2009.

Transient Investigation of Super-lens Realized by Transmission Line Metamaterials

Junming Zhao and Yijun Feng
Department of Electronic Science and Engineering, Nanjing University, Nanjing 210093, China

Abstract— One of the intriguing properties of metamaterials is their ability to construct super-lens to achieve image resolution that overcomes the diffraction limit of conventional imaging systems [1]. Extensive studies, both theoretical and experimental, have been endeavored on the properties of super-lens, however most of them are focused on the stabilized image pattern under a given frequency. Recently, it is noticed by theoretical analysis that the transient phenomena or the relaxation mechanisms play important roles in the set-up of sub-diffraction images by the super-lens [2, 3]. Therefore, further transient exploration through experimental verification or simulation on realistic super-lens system is required.

In this presentation, we report the transient investigation of the planar super-lens system realized by compensated bilayer of transmission line metamaterials. The sub-diffraction imaging properties of this compensated bilayer super-lens have been verified under the stabilized situation in our earlier work [4]. Here we demonstrate the transient analysis of the set-up of the image through the super-lens when a gauss-pulse modulated signal is applied as the source signal. Through microwave circuit simulations on this realistic super-lens, we find that when increasing the thickness of the super-lens, much delay time is required to set-up the image to reach its maximum value, and the maximum value is decreased. Meanwhile, when increasing the gauss pulse width, it takes much time to set-up the image, but the maximum value is increased. We believe that these transient properties could be helpful to understand the mechanism of the super-lens, and be useful in the application of super-lens to real optical system.

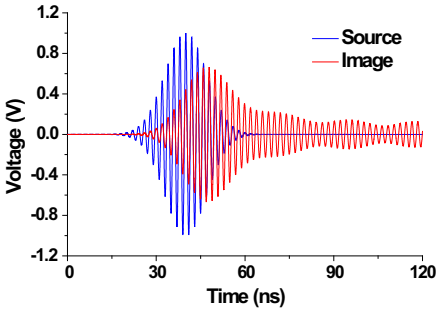

Figure 1: Transient waveform of the source and image signals in a realistic super-lens system designed by transmission line metamaterials.

ACKNOWLEDGMENT

Supported by the National Basic Research Program of China (2004CB719800), and the National Nature Science Foundation (60671002, 60801001).

REFERENCES

1. Pendry, J. B., *Phys. Rev. Lett.*, Vol. 85, 3966, 2000.
2. Zhou, L. and C. T. Chan, *Appl. Phys. Lett.*, Vol. 86, 101104, 2005.
3. Jiang, X., W. Han, P. Yao, and W. Li, *Appl. Phys. Lett.*, Vol. 89, 221102, 2006.
4. Feng, Y., J. Zhao, X. Teng, Y. Chen, and T. Jiang, *Phys. Rev. B*, Vol. 75, 155107, 2007.

A Novel Broadband Metamaterial Resonator with Negative Permittivity

J. Zhang and Z. R. Hu
Microwave and Communication Systems Group, School of Electrical and Engineering
Faculty of Engineering and Physical Sciences, University of Manchester, UK

Abstract— Metamaterials has led to considerable interests in the electromagnetism area in the first decade of 21st century. This is due to some of its unique electromagnetic features that may provide solutions for solving current technological limitations. It is well known that the properties of a metamaterial are usually determined from the geometrical structure and material parameters rather than composition. One of the problems of resonant types of metamaterials is that they usually have narrow operating bandwidth. In this paper, a novel metamaterial resonator with desired broadband negative permittivity was proposed. The unit cell resonator is composed of three metal rings on top of a dielectric substrate, as shown in Fig. 1. The size of the unit cell is of 3.333 mm × 3.333 mm. These rings are copper with 0.25 mm width and the outside radiuses are 0.5 mm, 1 mm and 1.5 mm respectively. The substrate is FR4 with 0.203 mm thickness. The novel structure presented here exhibits a strong negative permittivity response at 21 GHz to 32 GHz bands, as shown in Fig. 2. The unit cell resonator was simulated using two floquet ports on master and slave boundaries conditions by Ansoft HFSS (High Frequency Structural Simulator). The effective permittivity and permeability of this metamaterial was extracted from simulated S-parameters S_{11} and S_{21}. The full wave simulated results show that the medium constructed of a single layer of these resonators can provide negative permittivity in rather broad bandwidth, which is from 21 GHz to 32 GHz in this case. Its fractional bandwidth is of 42%, which is about twice larger than that reported in "Electric-field-coupled resonators for negative permittivity metamaterials" [1].

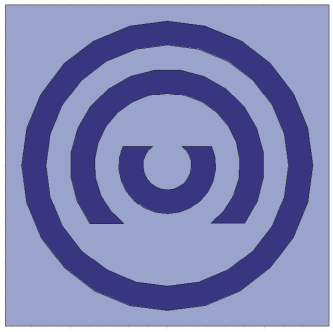

Figure 1: Structure of the unit cell resonator.

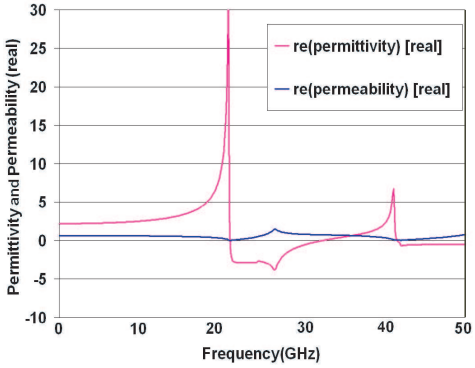

Figure 2: The real parts of the permittivity and permeability of the novel structure.

REFERENCES

1. Schurig, D., J. J. Mock, and D. R. Smith, "Electric-field-coupled resonators for negative permittivity metamaterials," *Appl. Phys. Lett.*, Vol. 88, 041109, 2006.

Study of Cherenkov Radiation in Matematerials

Sheng Xi[1, 4], **Hongsheng Chen**[1], **Binzheng Zhang**[4], **Bae-Ian Wu**[2], **and Min Chen**[3]

[1]The Electromagnetics Academy at Zhejiang University, Zhejiang University, Hangzhou 310027, China
[2]Research Laboratory of Electronics, Massachusetts Institute of Technology, Cambridge, MA 02139, USA
[3]Department of Physics, Massachusetts Institute of Technology, Cambridge, Massachusetts 02139, USA
[4]Thayer School of Engineering, Dartmouth College, Hanover, NH 03755, USA

Abstract— The properties of Cherenkov Radiation (CR) in a medium due to a fast moving charged particle are determined by the intrinsic dispersion relation of the host medium. In conventional materials, CR can be observed only when the speed of the particle is larger than the phase velocity of the waves in the host medium, and a forward propagating cone is formed. However, CR is reversed in an isotropic left-handed material (LHM) due to the unusual dispersion properties of electromagnetic waves in LHMs. That is to say CR is in the backward direction, which enables the design of new types of applications of CR. For both conventional materials and LHMs, the dispersion relations are closed circles or ellipses. In this paper, we firstly make a review on the recent progress in the CR in metamaterials. We then investigate some new CR phenomena in metamterials with more complicated constitutive parameters.

Session 4A4b
Micro/Nanomanufacturing of Metamaterials and Photonic Structures

Fabrication of THz Meta-foil by Means of Microlithography and Metal Deposition

L. K. Jian[1], **H. O. Moser**[1, 2], **S. M. P. Kalaiselvi**[1], **S. Virasawmy**[1], **S. M. Maniam**[1], **M. Bahou**[1], **S. P. Heussler**[1], **Shahrain bin Mahmood**[1], **H. S. Chen**[3, 4], **X. X. Cheng**[4], **and B. I. Wu**[3, 4]

[1]Singapore Synchrotron Light Source (SSLS), National University of Singapore (NUS)
5 Research Link, 117603, Singapore
[2]Department of Physics, National University of Singapore
2 Science Drive 3, 117542, Singapore
[3]Research Laboratory of Electronics, Massachusetts Institute of Technology
Cambridge, Massachusetts 02139, USA
[4]The Electromagnetics Academy at Zhejiang University, Zhejiang University
Hangzhou 310058, China

Abstract— Present-day metamaterials are usually fabricated by including dielectrics as a structural material, either as a substrate or a matrix, which might substantially restrict their usefulness and applicability due to the electric, mechanical, and thermal properties of substrates or matrices as well as their sensitivity to humidity and radiation degradation. In previous work [1], metamaterial bi-layer chips which consisted of S-shape string-like microstructures held by a frame without any substrate or matrix, were fabricated and studied by means of simulation and experiment. The meta-foil, our latest achievement [2], has two significant improvements: first, S-shape string-like microstructures are positioned up-right to facilitate magnetic field coupling to the structure under normal incidence; second, it is self-supporting (free-standing and matrix-free), locally stiff, but globally flexible.

In this presentation, we describe the fabrication method of THz meta-foils with a detailed discussion of the process which combines multiple-level microlithography with precise multiple-layer alignment, metal deposition with accurate thickness control and sacrificial-release technique, to get an all-metal metamaterial in which the individual Au S-strings are connected by transverse Au rods thus creating the all-metal space-grid as mentioned above. As it looks like a foil, we baptize it "meta-foil". Meta-foils can be tailor-made to virtually any shape required by a specific application. They can be bent and wrapped around objects to hide and shield them from electromagnetic radiation.

REFERENCES

1. Moser, H. O., J. A. Kong, L. K. Jian, H. S. Chen, G. Liu, M. Bahou, S. M. P. Kalaiselvi, S. M. Maniam, X. X. Cheng, B. I. Wu, P. D. Gu, A. Chen, S. P. Heussler, S. bin Mahmood, and L. Wen, "Free-standing THz electromagnetic metamaterials," *Opt. Express*, Vol. 16, No. 18, 13773–13780, 2008.
2. Moser, H. O., L. K. Jian, H. S. Chen, M. Bahou, S. M. P. Kalaiselvi, S. Virasawmy, S. M. Maniam, X. X. Cheng, S. P. Heussler, S. bin Mahmood, and B.-I. Wu, "All-metal self-supported THz metamaterial — The meta-foil," *Opt. Express*, 2009 (submitted).

Properties of Meta-foils

H. O. Moser[1, 2], L. K. Jian[1], M. Bahou[1], S. M. P. Kalaiselvi[1], S. Virasawmy[1], K. Banas[1], A. Banas[1], S. M. Maniam[1], S. P. Heussler[1], H. S. Chen[3, 4], X. X. Cheng[4], and B. I. Wu[3, 4]

[1]Singapore Synchrotron Light Source (SSLS), National University of Singapore (NUS)
5 Research Link, 117603, Singapore
[2]Department of Physics, National University of Singapore
2 Science Drive 3, 117542, Singapore
[3]The Electromagnetics Academy at Zhejiang University, Zhejiang University
Hangzhou 310058, China
[4]Research Laboratory of Electronics, Massachusetts Institute of Technology
Cambridge, Massachusetts 02139, USA

Abstract— The meta-foil is a purely metallic space-grid that features S-strings interconnected by metal lines. Such structures support the typical resonances of S-strings. The importance of meta-foils rests on the fact that it consists of metal only and is no longer influenced by any supporting or embedding dielectrics. It can be tailored and shaped according to the application and can be used at higher temperatures. We discuss properties of the meta-foil as they are dependent on the geometry. The coupling of an electromagnetic wave to the meta-foil is maximized for normal incidence. The resonance spectra exhibit the typical magnetic and electric peaks of which the first is left-handed and the second right-handed. Both experiments and simulation show that the useful angular range of incidence around normal is rather broad which eases applications for tilting around the z and y axes in a reference frame where z points along the S-string, y is transverse to the strings, and x is normal to the plane of the meta-foil and indicates normal incidence. The amplitude of the left-handed peak grows with decreasing density of interconnecting lines. The spectra are insensitive to mechanical bending and to heating. When the meta-foil is exposed to dielectrics, the resonance peaks will shift and decrease which makes them potential sensors for dielectric materials. While the first-generation meta-foils have a constant geometry across the whole foil, introduction of an index-gradient will enable the implementation of more sophisticated optical functions like deflecting, focusing, and imaging which might have implications for THz imaging and infrared microscopy.

Metamaterials via Ferroelectrics and Liquid Crystal Technologies

Fuli Zhang[1, 2], **Qian Zhao**[3], **Lei Kang**[4], **Ji Zhou**[4], **and Didier Lippens**[1]

[1]Institut d'Electronique de Microélectronique et de Nanotechnologie, CNRS 8520
Université des Sciences et Technologies de Lille, 59652 Villeneuve d'Ascq Cedex, France
[2]Department of Applied Physics, Northwestern Polytechnical University, Xi'an 710072, China
[3]State Key Lab of Tribology, Department of Precision Instruments and Mechanology
Tsinghua University, Beijing 100084, China
[4]State Key Lab of New Ceramics and Fine Processing, Department of Materials Science and Engineering
Tsinghua University, Beijing 100084, China

Abstract— We report on the various possibilities afforded by the Ferroelectrics and Liquid Crystal (LC) technologies for the fabrication of isotropic and anisotropic tunable metamaterials, aimed at operating at microwave and sub-millimeter-wave frequency ranges.

Bulk BST Ferroelectrics technologies were investigated for the design of isotropic metamaterials. Their singular properties notably the achievement of negative values of the permeability are obtained by the so-called magnetic Mie resonance. In short, displacement currents, induced by the incident magnetic field, give rise to current loop within the BST inclusions (rods, cubes or spheres) which form the basic cell of a periodic medium [1]. It results from this a resonant magnetic moment. The corresponding artificial permeability shows a Lorentz-type dispersion characteristic with negative values of μ_{eff} between the resonant and the magnetic plasma frequencies. In order to operate in the long wavelength regime, extremely high values of the permittivity were used (ε_{reff} between 200 and 1000). For cubes with $\varepsilon_{reff} = 850$, we recently show that the EM properties are isotropic but with an unexpected sensitivity to the polarization for oblique incidence [2]. On this basis, it was shown that an artificial magnetic conductor can be designed with potential applications in directive antennas. For rods or rectangular shaped patterns, the targeted application is the fabrication of a transparency cloak [3] by inducing the radial permeability gradients, derived from transformation optics [4], either by changing the rod size or the filling factor. The experimental demonstrations were carried out at microwaves. However, it is believed that the high dielectric constant and hence the artificial magnetism can be preserved up to the sub-millimeter frequency range where dielectric relaxation takes place [5].

The tunability of uniaxial metamaterial was addressed on the basis either of the omega-type [6, 7] or the Transmission Line (TL) approach. Both configurations, which are resonant in essence, show however a relatively broad band of operation with the prospect to tune the dispersion characteristics by the voltage control of the BST films permittivity (here the permittivity value are of the order of 300) or by the orientation of LC molecules which exhibit birefringence effects. For the latter, the orientation was controlled by a dc magnetic field. For the TL approach, special attention was given to the tunability of *balanced* composite Left and Right Handed dispersion characteristics with a transmission window between 8 and 32 GHz [8]. For the SRR technology, an experimental demonstration around 10 GHz of the tunability of the resonance frequencies by LC was reported for a magnetic single negative media [9]. The tunability concept was subsequently extended to the transmission characteristics of a double negative media by means of an omega type pattern [10].

REFERENCES

1. Zhao, Q., J. Zhou, F. Zhang, and D. Lippens, *Materials Today*, 2009 (Invited Review, in press).
2. Zhang, F., Q. Zhao, L. Kang, J. Zhou, and D. Lippens, *Phys. Rev. B*, (to be published).
3. Gaillot, D. P., C. Croënne, and D. Lippens, *Opt. Express*, Vol. 16, 3986, 2008.
4. Gaillot, D. P., C. Croënne, F. Zhang, and D. Lippens, *New J. Phys.*, Vol. 10, 115039, 2008.
5. Houzet, G., G. Velu, L. Burgnies, J.-C. Carru, and D. Lippens, *Appl. Phys. Lett.*, Vol. 93, 053507, 2008.
6. Zhang, F., G. Houzet, É. Lheurette, D. Lippens, M. Chaubet, and X. Zhao, *J. Appl. Phys.*, Vol. 103, 084312, 2008.
7. Zhang, F., S. Potet, J. Carbonell, É. Lheurette, O. Vanbésien, X. Zhao, and D. Lippens, *IEEE Trans. Microwave Theory Tech.*, Vol. 56, 2566, 2008.
8. Marteau, A., G. Velu, G. Houzet, L. Burgnies, É. Lheurette, J.-C. Carru, and D. Lippens, *App. Phys. Lett.*, Vol. 94, 023507, 2009.

9. Zhang, F., Q. Zhao, L. Kang, X. Zhao, J. Zhou, and D. Lippens, *Appl. Phys. Lett.*, Vol. 92, 193104, 2008.
10. Zhang, F., L. Kang, Q. Zhao, J. Zhou, X. Zhao, and D. Lippens, *Opt. Express*, Vol. 17, 4360, 2009.

Metamaterial-based Optical Components for the Terahertz (THz) Technology

O. Paul[1], **P. Weis**[1], **B. Reinhard**[1], **R. Beigang**[1, 2], **and M. Rahm**[1, 2]

[1]Department of Physics and Research Center OPTIMAS, University of Kaiserslautern Kaiserslautern 67663, Germany
[2]Fraunhofer Institute for Physical Measurement Techniques IPM, Freiburg 79110, Germany

Abstract— Metamaterials provide a complete tool set for the design of functional components that allow a precise control of electromagnetic fields. The possibility to tailor optical components with a specific functionality in a pre-defined frequency range opens new pathways for the development of innovative and adaptive optics for the THz technology. In this context, we designed, fabricated and experimentally investigated various metamaterial-based structures for the well-aimed manipulation of THz radiation. We present an active, voltage-controlled and polarization-independent modulator that can achieve modulation frequencies of up to 100 kHz and a quasi-steady-state modulation depth of 59%. The metamaterial consisted of gold crosses fabricated on n-doped gallium arsenide (GaAs). Furthermore, we demonstrate flexible, free-standing, large-area metamaterial membranes as functional passive THz components with low intrinsic loss. We report two types of metamaterial-based spectral band-pass filters with a peak amplitude transmittance of 80% and support the observations by a very intuitive model based on the mechanism of trapped mode excitation. As a further example, we demonstrate thin quarter- and half wave plates with high transmission in the terahertz regime. The wave plates are based on cut-wire-pair metamaterials with refractive indices of opposite signs for incident waves with orthogonal field polarizations. A maximum figure of merit of 23 (FOM) was observed around a frequency of 1.3 THz for a refractive index of $n = -1.7$. This corresponds to the one of the highest FOMs reported at THz frequencies. Further examples for metamaterial-based functional THz components will be presented and discussed.

Optical Metamaterials and Photonic Crystals: Aspects of Large-scale Micro- and Nanofabrication

R. Geiss[1], **C. Helgert**[1], **H. Hartung**[1], **E.-B. Kley**[1], **C. Rockstuhl**[2], **F. Schrempel**[1, 4], **F. Lederer**[2], **A. Tünnermann**[1, 3], **W. Wesch**[4], **and T. Pertsch**[1]

[1]Institute of Applied Physics, Friedrich-Schiller-Universität Jena, Germany
[2]Institute of Condensed Matter Theory and Solid State Optics
Friedrich-Schiller-Universität Jena, Germany
[3]Fraunhofer Institute for Applied Optics and Precision Engineering, Jena 07745, Germany
[4]Institute of Solid State Physics, Friedrich-Schiller-Universität Jena, Germany

Abstract— Electron beam lithography (EBL) has been applied to the fabrication of micro- and nanoscale photonic structures such as planar metamaterials and photonic crystals. The traditional shortcoming of EBL, that is, showing inherently a comparatively low writing-speed, can be overcome by the usage of a variable-shaped beam pattern generator and chemically amplified e-beam resists. This approach effectively increases the fabrication speed of state-of-the-art optical metamaterials and photonic microstructures. Hand in hand with comprehensive nanopattern-transfer technologies such as lift-off techniques, ion-beam and ion-beam-enhanced etching methods we are able to provide a powerful tool enabling the realization of various types of complex optical micro- and nanostructures on large scale. In this contribution we will present our most recent experimental results and discuss some important aspects concerning fabrication methods and optical measurements. Particular emphasis shall be put on optical metamaterials and photonic crystals.

As for optical metamaterials, we show a negative-index behavior obtained independent of the polarization state of normally incident light [1] and consider the transition from a periodic to an amorphous metamaterial [2]. For photonic crystals we demonstrate the structuring of lithium niobate by means of ion beam enhanced etching [3]. This technique allows for the fabrication of freestanding ultrathin membranes patterned with photonic crystal structures [4, 5]. On the basis of these examples we firmly believe that our fabrication technology yields great potential toward the fabrication of large-area optical metamaterials and photonic crystals at the benefit of an appreciable throughput.

REFERENCES

1. Helgert, C., C. Menzel, C. Rockstuhl, E. Pshenay-Severin, E.-B. Kley, A. Chipouline, A. Tünnermann, F. Lederer, and T. Pertsch, "Polarization-independent negative-index metamaterial in the near-infrared," *Opt. Lett.*, Vol. 34, 704–706, 2009.
2. Helgert, C., C. Rockstuhl, C. Etrich, C. Menzel, E.-B. Kley, A. Tünnermann, F. Lederer, and T. Pertsch, "Effective properties of amorphous metamaterials," *Phys. Rev. B*, Vol. 78, 233107, 2009.
3. Gischkat, T., H. Hartung, F. Schrempel, E.-B. Kley, A. Tünnermann, and W. Wesch, "Patterning of $LiNbO_3$ by means of ion irradiation using the electronic energy deposition and wet etching," *Microelectron. Eng.*, Vol. 86, 910–912, 2009.
4. Schrempel, F., T. Gischkat, H. Hartung, T. Höche, E.-B. Kley, A. Tünnermann, and W. Wesch, "Ultrathin membranes in x-cut lithium niobate," *Opt. Lett.*, Vol. 34, 1426–1428, 2009.
5. Hartung, H., R. Geiss, T. Gischkat, F. Schrempel, R. Iliew, T. Pertsch, F. Lederer, W. Wesch, E.-B. Kley, and A. Tünnermann, "Photonic crystals in lithium niobate by ion-beam enhanced etching," *IEEE/LEOS Winter Topicals Meeting Series*, Vol. 1, 64–65, 2009.

Session 4A5
Novel Mathematical Methods in Electromagnetics

Maxwell Equation in Electromagnetic and Gravitational Fields

Zi-Hua Weng
School of Physics and Mechanical & Electrical Engineering, Xiamen University
Xiamen 361005, China

Abstract— The validity of Maxwell equation is being doubted all the time in the case for coexistence of gravitational field and electromagnetic field. And this validity remains as puzzling as ever. The existing theories do not explain why Maxwell equation keeps unchanged, and then do not offer compelling reason for this special situation. The paper attempts to find out why Maxwell equation remains the same in most cases, even in the gravitational field.

The electromagnetic theory can be rephrased with the quaternion, which was invented by W. R. Hamilton in 1843. The algebra of quaternions was first used by J. C. Maxwell to represent field equations and properties of electromagnetic field in 1861. Dividing the quaternion into the scalar and vector, O. Heaviside recast Maxwell equation in terms of vector terminology in 1884, thereby reduced the original twenty equations down to the four differential equations.

The algebra of quaternions can be used to rephrase the gravitational theory. In 1687, I. Newton published the mechanical theory to describe the three laws of motion and the universal gravitation. In 1812, S. D. Poisson reformulated Newton's law of gravitation in terms of the scalar potential. Two quaternions can be combined together to become one octonion. The latter can be used to rephrase the gravitational field and electromagnetic field simultaneously.

With the quaternions, we find Maxwell equation is the same as that in classical electromagnetic theory, and Newton's law of gravitation is identical with that in classical gravitational theory. By the algebra of octonions, the results claim that the related conclusions can be spread to the case for coexistence of electromagnetic field and gravitational field. And Maxwell equation will remain the same, even in the gravitational field, except for the direction of displacement current.

ACKNOWLEDGMENT

The author is grateful for the financial support from the National Natural Science Foundation of China under grant number 60677039.

Electromagnetic Stresses and Torques on Rotating Media

Robin W. Tucker
Lancaster University, Lancaster, UK

Abstract— This paper offers a conceptually straightforward method for the calculation of stresses and torques in moving polarisable media based on the notion of a differential drive form derived from the total stress-energy momentum tensor of an interacting system and its property of being closed in spacetimes with symmetry. After an outline of the notation required to exploit the powerful exterior calculus of differential forms, a discussion of the relation between Killing isometries and conservation laws for smooth and distributional drive forms is given. Instantaneous forces and torques on isolated spacetime domains and regions with interfaces are defined, based on manifestly covariant equations of motion. The theory is applied to the calculation of the force and torque on a rotating polarisable and magnetisable disc in an electromagnetic wave and the results put into the context of the Abraham-Minkowski debate on the appropriate description of electromagnetic momenta in a material medium.

Study on Description of Electromagnetic Wave

Yelin Xu
Institute of Biophysics, Chinese Academy of Sciences, Beijing 100101, China

Abstract— Classic electromagnetic wave theory describes electromagnetic wave as electricity producing magnetism and magnetism producing electricity... The author calls this theory ring-ring theory. Ring-ring theory regards that both magnetic line ring and electric line ring are fixed and immovable; electromagnetic wave has longitudinal component; electricity and magnetism have different phase; electricity and magnetism have different energy... All these above imply that ring-ring theory is completely opposite to experimental results. The author points out that the electric line ring in ring-ring theory corresponds to the coil of a transformer, magnetic line ring corresponds to the iron-core of the transformer. Therefore, ring-ring theory is the connection chart of many transformers rather than the description of electromagnetic wave. Consequently, it is reasonable for us to calculate ring-ring theory by using the method to calculate a transformer. The result of the calculation is: for the electromagnetic wave described by ring-ring theory, whenever it walks one wave length, its intensity decays from the original 100% to 2%.

The author suggests we seek a new description of electromagnetic wave according to Maxwell Equation. When we observe carefully the mathematical solution of Maxwell Equation, we find an interesting phenomenon: the electricity and magnetism in the solution of Maxwell Equation are exactly the same as that in Faraday Induction Rule. Therefore, the author assumes that the electricity and magnetism in Maxwell Equation's solution are just the electricity and magnetism in Faraday Generator Rule. Electromagnetic wave becomes quite simple under this assumption: the antenna is an independent wire, the alternating current in the wire does work and radiate magnetic line ring. Magnetic line ring has momentum! Based on conservation of momentum, surely it can keep going farther and farther. Transversely-moving magnetic line cuts space to produce electric line, this is just the electricity and magnetism of electromagnetic wave. This description of electromagnetic wave is completely consistent with experimental results.

The new description of electromagnetic wave brings us new knowledge: electromagnetic wave has the function of continuously adjusting its velocity automatically, that is, if the magnetic line goes too fast, it will induct out too many electric lines, then its load will become heavy, as a result, the magnetic line will slow down; otherwise the process is contrary. When the speed of electromagnetic wave is light velocity c, its state becomes stable.

Mutual Inductance Calculations Using Bessel Functions for Non Coaxial Coils with an Explicitly Finite Number of Turns

John T. Conway
University of Agder, Grimstad, Norway

Abstract— In some recent papers [1, 2] noncoaxial inductance calculations were presented for various coils based on a Bessel function formulation. The core equation of the method [1] is an integral for the mutual inductance of two discrete circular turns which involves a product of three Bessel functions and an exponential factor:

$$M_{21} = \mu_0 \, \pi \, R_1 \, R_2 \int_0^\infty J_0(sp) J_1(s \, R_2) \, J_1(s \, R_1) \exp\left(-s \, |z_2 - z_1|\right) ds. \tag{1}$$

In this equation, R_1 and R_2 are the turn radii, z_1 and z_2 are the axial coordinates of the turns, p is the perpendicular distance between the axes of the two turns and μ_0 is the magnetic permeability. This integral can be evaluated numerically for $z_2 \neq z_1$ and analytically in terms of Legendre functions or elliptic integrals when $z_2 = z_1$ or $p = 0$.

The various geometric parameters in Equation (1) appear as separate factors, and this allows (1) to be integrated both axially and radially over the windings of two coils [1, 2] in the usual approximation where the discrete turns of the coil are considered to be smeared out over the coil windings. This approximation is also made in finite element calculations of inductance. Nevertheless, coils do consist of a finite number of discrete turns, and in some practical cases the number of turns is not large.

The infinite integral above is relatively slow to evaluate numerically and it is therefore an undesirable option to evaluate the discrete contributions of each pair of turns using (1) and then sum them. For coaxial cases (1) can be replaced with a well known formula in terms of complete elliptic integrals and the contributions from each pair of turns explicitly summed, but no such formula exists yet for the coaxial case. However, for two coils consisting regularly spaced turns, the exponential factors in (1) can be analytically summed as geometric series to give a single Bessel integral for the mutual inductance of two single layer coils, regardless of the number of turns. Multiple layer coils can then be evaluated as a greatly reduced number of terms.

The paper will describe the method above in detail, and provide numerical results for pairs of specific discrete coils. The relationship between the discrete formulation and the smeared out approximation will be investigated as the number of turns is increased.

REFERENCES

1. Conway, J. T., "Inductance calculations for noncoaxial coils using bessel functions," *IEEE Trans. Magnetics*, Vol. 43, No. 3, 1023–1034, 2007.
2. Conway, J. T., "Inductance calculations for coils of rectangular cross section using bessel and struve functions," to be published in *IEEE Trans. Magnetics*.

On 3D Potential Field Solutions for Atmospheric Charge Distributions

G. C. Dijkhuis
Convectron NV, Rotterdam, The Netherlands

Abstract— Charge on dust particles and aerosols endows atmospheric electricity with a degree of freedom not included in conventional plasma and MHD theory for ionized gases. Significant space charge is manifest in thundercloud electrification and lightning discharge, with stratospheric analogues seen as blue jets, sprites and elves forming at ionospheric altitudes. Enigmatic properties of ball lightning also involve atmospheric space charge distributions. For these phenomena H. Kikuchi formulates electro-hydrodynamic theory featuring field line reconnection at critical ionization velocities in electric cusps [1]. We obtain static cusps as charged eigenstate solutions of the 3D Poisson equation from hyper-complex quaternion potentials.

We present 3D potential field solutions from 4D quaternion functions regularized by twelve symmetry conditions on their sixteen partial derivatives, moments and eigenvalue equations. Our real matrix format extends Cauchy-Riemann conditions for complex planes into quaternion space as regularization scheme [2]. We find inductive proofs for smooth closure in complex planes extendable to standard polynomial and cyclometric functions in quaternion space. The real coefficients in their series expansions also admit quaternion versions of the Laurent series. We plot equipotential surfaces in parametric form, and likewise the field lines as intersection of two complementary sets of field surfaces.

We construct quaternion potentials from three complex sub-planes by Joukowski transformations combining uniform field at infinity with dipolar sources at the origin. The planar map plots an orthogonal iso-line network with cusps and branch points located at zeroes of the unit circle shown in Fig. 1(a). This circle serves as branched field line or iso-potential in two con-jugate solutions with field sources directed either anti-parallel along the X-axis, or parallel along the Y-axis.

Our quaternion map replaces imaginary units by elementary matrices that copy Hamilton's product rules and give non-zero determinants needed for division algebra [2]. Our regularization scheme secures non-zero Jacobian determinants needed for smooth inverse functions and parametric plots. Fig. 1(b) plots the the 3D Joukowski potential as symmetric surfaces with cusps on the X-axis at zeroes of the unit sphere, and lined by ribbons for the field surfaces. Field lines on the sphere branch out and reunite as meridians do on opposite poles. Field lines are orthogonal to equipotential surfaces, but field surfaces and their eigenvectors lack right angles needed for conjugate field solutions. By Poisson's equation we find the charge density as laplacian of the Joukowski potential in quaternion space.

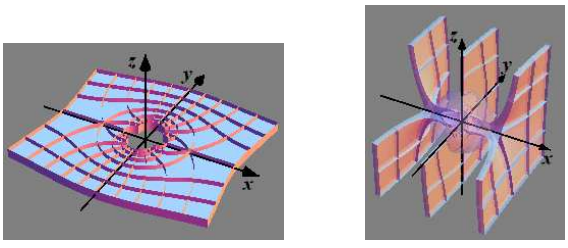

(a) (b)

Figure 1: Joukowski map plots electric cusps (a) in complex plane, (b) from quaternion potential.

REFERENCES

1. Kikuchi, H., *Electrohydrodynamics in Dusty and Dirty Plasmas*, Kluwer Academic Publishers, Dordrecht, 2001.
2. Dijkhuis, G. C., "Ball lightning as thermodynamic limit of the periodic system," *The Atmosphere and Iono-sphere: Dynamics, Processing and Monitoring*, Eds. V. Bychkov, G. Golubkov, A. Nikitin, Springer Verlag, in press.

Spectral Theory of Beam Scatterings for Object Imaging Using Scanning Millimeter Wave Radar Sensor

Yasumitsu Miyazaki
Department of Media Informatics, Aichi University of Technology
50-2 Manori, Nishihasama-cho, Gamagori 443-0047, Japan

Abstract— Shape image recognition system of objects using millimeter electromagnetic waves has excellent characteristics for object sensing and detection, comparing with optical shape recognition system, because physical properties of transparent and reflecting material consisting objects for millimeter electromagnetic waves have very different properties compared with optical characteristics. In case that target objects are buried in optical lossy media with large attenuation of optical waves and, invisible and optical large attenuation structures are located between optical incident generator and sensing target, optical sensing and detection system for object shape recognition can not be applied. Object imaging system using millimeter waves may be very excellent system for object recognition in case of large optical attenuation media. Optical and X-ray computer tomographies have been rapidly developed and recently, ultra-sonic CT has been also well accomplished. Millimeter wave CT has not been so much discussed. In this paper, beam scattering theory of object imaging using scanning millimeter wave radar is studied for object shape recognition and millimeter wave computer tomography.

Gaussian beam waves with temporal Gaussian impulse radiated from millimeter wave antenna incident to complicated targets are considered. Spatial and temporal spectral functions are introduced using transverse wave number spectrum for the spatial space and angular frequencies for time domain. Spatial spectral functions are expressed for incident and scattering electromagnetic fields. Asymptotic expressions concerned with Hermite-Gaussian eigenfunctions are derived for the incident Gaussian beam, and reflected and scattered waves, using beam waist and beam spot size.

Scattered and transmitted waves are discussed using eigenfunction orthogonalities, satisfying boundary conditions on complicated target shape for spectral functions of incident, reflected and transmitted waves. Based on temporal and spatial characteristics of millimeter wave scattering, image recognition of object targets using scanning millimeter wave radars of scanning millimeter wave radars of synthetic aperture type are shown with computer image processing.

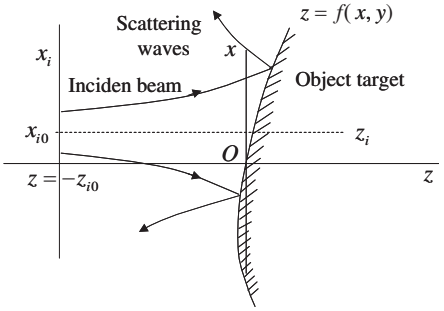

Figure 1: Object imaging and beam scattering.

REFERENCES

1. Miyazaki, Y. and Y. Akao, "Reflection and mode conversion of beam wave through a curved interface between dielectrics and thick dielectric lens," *Trans. of IECE, Japan*, Vol. 51-B, No. 1, 25–31, 1968.
2. Miyazaki, Y., "Space-time impulse responses of electromagnetic backscatterings of beam waves for sensing," *Proc. of OFSET 2000*, 361–364, 2000.
3. Miyazaki, Y., "Electromagnetic scattering and filtering in random media for image sensing," *PIERS Proceedings*, 689–697, Cambridge, USA, July 2–6, 2008.

FDTD Parallel Computing of Electromagnetic Wave Scattering by Clouds for Microwave Remote Sensing of Weather Satellite

Yasumitsu Miyazaki[1], **Nobuo Goto**[2], **and Koichi Takahashi**[1]

[1]Department of Media Informatics, Aichi University of Technology
50-2 Manori, Nishihasama-cho, Gamagori 443-0047, Japan
[2]Institute of Technology and Science, The University of Tokushima
2-1 Minamijosanjima-cho, Tokushima 770-8506, Japan

Abstract— The spaceborne remote sensing is very important for direct measurement of weather environment in wide area and is effective for safety system of ITS and disaster prevention system to disasters caused by strong rainfalls. In this paper, we consider cloud observation system using satellite remote sensing and analyze the electromagnetic scattering by statistically distributed clouds in rain region. The satellite antenna is very high over earth surface and moves on two dimensional plane. Clouds of rain region can be evaluated by SAR system.

The space resolution of the microwave remote sensing using the Synthetic Aperture Radar (SAR) is about 5–10 meters, and a resolution of about 1 meter in the case of optical sensor has so far been obtained. In this study, characteristics of electromagnetic wave scattering from clouds in various conditions are analyzed, as a purpose to improve the space resolution of the microwave remote sensing using weather satellite.

We analyzed electromagnetic backscattering from clouds using weather satellite by numerical method of FDTD. The incident field from an antenna is calculated from the wave equations using Green's function. The scattering field by clouds is calculated using FDTD method. And, the far field for received field of signals at satellite position is calculated using the surface equivalent electric and magnetic currents derived by FDTD method. The characteristics of electromagnetic backscattering for microwave remote sensing are analyzed by FDTD and analytical method.

The model is three dimensional, for the case of clouds near the earth surface. In this model, the electromagnetic backscattering at satellite position has been analyzed with respect to various parameters of clouds. Gaussian pulse is transmitted from the satellite antenna. In case of normal incidence and moving satellite, received electric field at satellite position has been calculated. SAR images have been reconstructed from the received electric field, the objects of clouds and the ground has been imaged. In clouds region, complex dielectric constant ε^* and complex refractive index n_r^* are given by $\varepsilon^* = \varepsilon + \sigma/(j\omega) = n_r^{*2}\varepsilon_0$, $n_r^* = n_1 - jn_2$.

For the analysis of microwave scattering by clouds and rains, the analysis region including clouds and raindrops is much larger than the wavelength. Parallel computation of FDTD using grid computer is applied to get scattering field. To perform parallel processing using grid computer, the total analysis space is divided into subdomains.

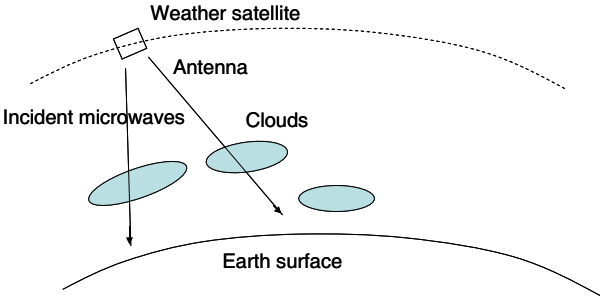

Figure 1: Weather satellite and microwave scattering.

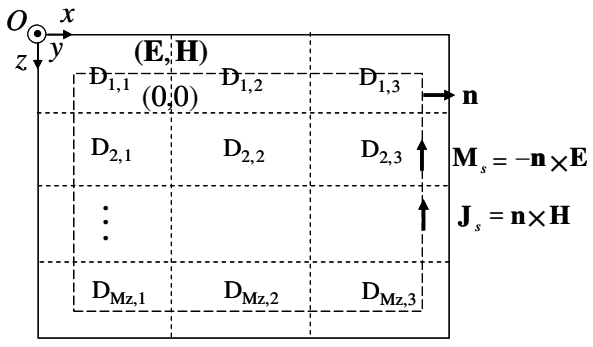

Figure 2: Parallel computation and subdomains.

REFERENCES

1. Miyazaki, Y. and T. Kawakami, "Electromagnetic backscattering of microwaves by objects on random groud surfaces in satellite remote sensing," *Proc. of CJMW2000*, 217–220, 2000.

2. Miyazaki, Y., T. Kawakami, and K. Takahashi, "Electromagnetic backscattering of radiation wave of satellite antenna due to objects of random ground surface," *Proc. of ISAP2000*, Vol. 2, 863–866, 2000.
3. Sonoda, J. and Y. Miyazaki, "Analysis of electromagnetic scattering using FDTD method and near to far field transformation for satellite remote sensor," *Technical Paper of IEE Japan*, EMT-00-102, 19–24, 2000.
4. Rodriguez, G., Y. Miyazaki, and N. Goto, "Matrix-based FDTD parallel algorithm for big areas and its applications to high-speed wireless communications," *IEEE Trans. Antennas & Propagat.*, Vol. 54, No. 3, 785–796, 2006.

THz Applications for the Engineering Approach to Modelling Frequency Dispersion within Normal Metals at Room Temperature

Stepan Lucyszyn and Yun Zhou
Imperial College London, UK

Abstract— When compared to the over-simplified classical skin-effect model, used to derive equations for circuit parameters (e.g., surface impedance, the attenuation constant of transmission lines and Q-factor of resonant structures), the more accurate classical relaxation-effect modelling approach for THz structures at room temperature [1] can be rather cumbersome. This paper will give derivations for such parameters using the concepts of kinetic surface inductance and complex skin depth. For the first time, it will be shown that the complex classical relaxation-effect model can reduce down to forms that are identical to those corresponding to the simple classical skin-effect model.

Kinetic inductance is created from the inertial mass of mobile charge carriers within an alternating electric field and is normally associated with superconductors. With normal metals at room temperature, the phenomenological scattering relaxation time for the free electrons (i.e., mean time between collisions, τ) is too short to make the associated kinetic reactance significant when compared to ohmic resistance. However, the effective classical skin-effect surface inductance (i.e., internal magnetic inductance associated with the energy stored in the external magnetic field) decreases as a function of $(\omega\tau)^{-0.5}$, where $\omega = 2\pi f$ is the angular frequency and f is the frequency of the driving electromagnetic field. In contrast, it will be shown that the effective classical relaxation-effect surface inductance has as additional kinetic surface inductance term that increases as a function of $(\omega\tau)^{+0.5}$. As a result, the kinetic surface reactance will dominate the classical skin-effect surface resistance above $\omega = 1/\tau$, as shown in Fig. 1.

Equations for surface impedance, the attenuation constant of metal-pipe rectangular waveguides and the Q-factor of resonant cavities, all at THz frequencies, were previously given for accurate calculations at THz operating frequencies [1]. For example, for an air-filled rectangular waveguide cavity, we previously quoted (without any formal proof), for the general case of a metal with $\mu_r \neq 1$ and $\omega\tau > 0$, the closed-form expression for unloaded Q-factor as follows [1]:

$$Q_u(\omega_o) = \frac{\lambda_I(\omega_I)}{8\mu_r \Im\{\delta_c(\omega_o)\}} \left(\frac{\omega_I}{\omega_o}\right) \left\{ \frac{2b\left(a^2+d^2\right)^{\frac{3}{2}}}{\left[2b\left(a^3+d^3\right)+ad\left(a^2+d^2\right)\right]} \right\} \tag{1}$$

where complex skin depth is given by: $\delta_u(\omega_o) \equiv \delta_c'(\omega_o) - j\delta_c''(\omega_o) = \frac{1}{\gamma_s(\omega_o)}$.

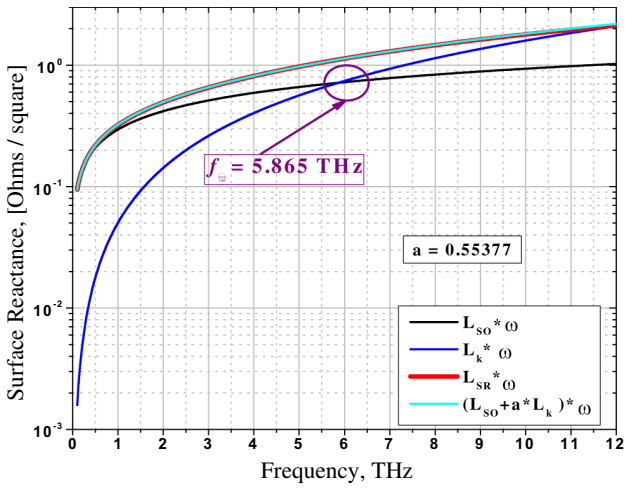

Figure 1: Surface reactance for different models.

Equation (1) will be derived from first-principles using the new concept of complex skin depth, and also extended for the more general case of a lossy dielectric-filled cavity. Moreover, similar techniques will be employed to derive accurate expressions for surface impedance and the attenuation constant of THz metal-pipe rectangular waveguides operating at room temperature.

REFERENCES

1. Zhou, Y. and S. Lucyszyn, "HFSS^{TM} modelling anomalies with THz metal-pipe rectangular waveguide structures at room temperature," *PIERS Online*, Vol. 5, No. 3, 201–211, 2009.

Session 4A6a
Biological Effects of Electromagnetic Fields

Evaluation of Wireless Electromagnetic Interference Due to the Interaction between Cellular Phones and Medical Devices within Hospital Environments

Hsing-Yi Chen and Cheng-Yi Chou
Department of Communications Engineering, Yuan Ze University
No. 135, Yuan-Tung Road, Nei-Li, Chung-Li, Taoyuan Shian, Taiwan

Abstract— The FDTD method was used to calculate the electric fields emitted from cellular phones. Cellular phones were modeled by a quarter-wavelength monopole antenna mounted on a rectangular box with equivalent material in the interior of the rectangular box and a dielectric coating in the exterior of the rectangular box. Measurements of the electric fields emitted from cellular phones were also performed by using a Narda Model SRM-3000 high frequency selective radiation meter with an isotropic E-field probe. From measurement and simulation results, electric fields emitted from cellular phones are in the range of 0.02∼39.0 V/m for separation distances of 0∼3 meters between handsets and test points. It is found that field strengths emitted from cellular phones may meet the recommended EMI immunity level of 3 V/m set by the IEC for medical equipment keeping a separation distance of more than 1 meter from cellular phones. An interference threshold separation distance of 3 meters is proposed for evaluating the interaction between cellular phones and medical devices.

Sensing of Human Micro-vibration Transmitted Along Solid Using Pico-Tesla Magneto-impedance Sensor (pT-MI Sensor)

K. Mohri[1, 2], Y. Nakamura[3], T. Uchiyama[4], Y. Mohri[5], Yu. Mohri[6], and Y. Inden[7]

[1]Nagoya Industrial Science Research Institute (NISRI), Nagoya 464-0819, Japan
[2]Aichi Micro Intelligent Co., Tokai 476-8666, Japan
[3]Yamazaki Mazak Optonics Co., Minokamo 505-0037, Japan
[4]Graduate School of Eng., Nagoya University, Nagoya 464-8603, Japan
[5]Graduate School of Eng., Meijo University, Nagoya 468-8502, Japan
[6]Graduate School of Arts, Meijo University, Nagoya 468-8502, Japan
[7]Graduate School of Med., Nagoya University, Nagoya 466-8550, Japan

Abstract— The micro-vibration is the human skin mechanical vibration with few micro-meter amplitude and frequencies of $0.1 \sim 40$ Hz and its time series reflects the brain consciousness such as sleepiness degree [1]. Therefore, sensitive and simple sensing method for the micro-vibration is strongly required for realization of new diagnosis for the central nervous system (CNS) diseases and blood circulation activities. We constructed an extremely sensitive magnetic sensor showing one pico-Tesla (pT) resolution using a single amorphous wire & CMOS IC magneto-impedance sensor with a selective dc negative feedback circuitry ("pT-MI sensor"), in which dc disturbance magnetic fields such as the geomagnetic field of around 50 μT in maximum is cancelled. Micro-vibration creating a pT-MI sensor head rotation with more than 1.8 micro degree is detected in the geomagnetic field (around 100 μT change for 180° rotation) by applying a micro-vibration stress directly or indirectly via a solid to the sensor head. Advantageous of the pT-MI sensor type micro-vibration sensor is a high sensitivity even for ultra-low frequency range of $0.1 \sim 20$ Hz comparing with conventional piezo-electric acceleration sensors.

Various human micro-vibrations such as for the back of the head (mechano-encephalogram), the spinal-cord, the heart beat and following blood flow pulsation, and muscle tremors are stably detected.

REFERENCES

1. Rohracher, H., "Parmanente rhythmische mikrobegungen des warmbluter-organismus ("Mikrovibration")," *Naturwissenschaften*, Vol. 49, No. 7, 145–150, 1962.

Numerical Modelling for Evaluation of Biological Effects Due to High Frequency Radiations in Indoor Environment

M. Cacciola, G. Megali, D. Pellicanò, M. Versaci, and F. C. Morabito
Department Via Graziella Feo di Vito, DIMET, University "Mediterranea" of Reggio Calabria
I-89100 Reggio Calabria, Italy

Abstract— Wireless personal communication is a rapidly expanding sector, particularly in the field of wireless local area networks. In an indoor wireless network system, the user of the mobile terminal can find himself in close proximity to the radiating antenna. It is, therefore, important to consider possible health hazards due to this type of exposure. This paper presents an approach to estimate and evaluate the main characteristics, i.e., Specific Absorption Rate and temperature rise, related to human exposure to electromagnetic energy generated by common wireless devices such as Access Point or Hot-Spot Wireless. The assessment is done numerically using two different approaches, respectively Wireless Insite package and Finite Element Method. The general goal is to provide an efficient and sufficiently accurate method to assess human head exposure to electromagnetic fields at a frequency of 2.45 GHz and for different types of exposure conditions.

Introduction: In the last recent years, wireless personal communications have registered a rapidly expansion in particularly in the field of wireless local area networks (WLANs). The existing applications of WLANs are unlicensed spread spectrum systems operating at the Industrial Scientific Medical (ISM) frequency (2.45 GHz) and the Unlicensed National Information Infrastructure (U-NII) (5.5 GHz) [1]. Although this sector has given numerously advantages to common people, the steadily increasing use of these new technologies may result in greater radio-frequency (RF) exposure in homes and work places. Health agencies and the public have expressed their concern about cumulative exposure and have requested further information [2]. In this paper we focus our attention in the risks of human head exposure to such devices evaluating some important parameters like Specific Absorption Rate (SAR) and superficial temperature increasing. Our goal is to verify if actual standards in wireless devices respect the Institute of Electrical and Electronic Engineers (IEEE) and European Committee for Electrotechnical Standardization (CENELEC) standards. In order to evaluate the energy absorption in human head has been used a two-step procedure. In the first step Wireless Insite has been used to calculate electromagnetic (EM) field generated by the access point inside the indoor scenario. Different type of indoor scenarios and different kind of wireless antennas have been considered to provide a such wide variety of results. Results obtained by ray-tracing approach give the EM field in a volume space with the presence of a human head. In second-step this volume space as been re-created with a Finite Element code with the presence of a human head. Maxwell and bio-heat equations have been respectively exploited the evaluation of two different parameters: SAR and temperature increase on human head surface. The goal was principally to verify that the SAR results follow international standards of the International Commission on Non-Ionozing Radiation Protection (ICNRIP). In post-processing phase, plotting of slice of SAR in human head let us to verify also how much radiations penetrate inside the head and, from surface to inner parts, which tissues absorb most part of radiation. Surface plot of temperature, instead, shows the corresponding increase of temperature in those part. Final results and their analysis will be presented in the final version of the paper.

REFERENCES

1. Bernardi, P., M. Cavagnaro, and S. Pisa, "Assessment of the potential risk for humans exposed to millimeter-wave wireless LANs: The power absorbed in the eye," *Wireless Networks*, Vol. 3, No. 6, 511–517, 1997.
2. Kuhn, S., U. Lott, A. Kramer, and N. Kuster, "Assessment methods for demonstrating compliance with safety limits of wireless devices used in home and office environments," *IEEE Transaction on Electromagnetic Compatibility*, Vol. 49, No. 3, 519–525, 2007.

ADI-PSTD Simulation of Light Scattered from Biological Tissues Using Optical Phase Conjugation Refocusing

Hong-Xing Zheng
Tianjin University of Technology and Education, China

Abstract— Optical wavelengths are beneficial for medical diagnosis purposes but in general don't penetrate deep into biological tissues. Recently, an approach is by utilizing the optical phase conjugation (OPC) of a phase conjugate mirror (PCM) [1]. By inverting the phase of the light field, the OPC phenomenon causes light to propagate in reversed directions, back-trace its previous trajectories, and refocus at where it originated. Experimental effort to realize the OPC phenomenon of a PCM has been reported in [2], showing that the scattering effect caused by scattering media can be undone by the OPC phenomenon. One of the interesting phenomena is that the OPC refocused light cross-sectional width is observed to be approximately the same regardless of the thickness of the scattering medium. The OPC phenomenon enables undoing the light scattering effect which is the dominating factor causing biological tissues to be opaque. Undoing the scattering effect enables light to be guided deeper into human body. This can potentially enable new treatment or diagnosis applications using optical techniques. To realize such applications, it is important to understand the optical characteristics of OPC for thick scattering medium. However, the factors that affect the cross-sectional width of the OPC refocused light need to be resolved in order to utilize the OPC phenomenon. The Pseudospectral time-domain (PSTD) technique is capable of rigorously simulating light scattering problems of macroscopic dimensions [3]. To analyze the OPC phenomenon for scattering media of various thicknesses, the alternating- direction-implicit (ADI) technique used in PSTD technique is implemented. Based on Maxwell's equations, the PSTD method is a grid-based technique capable of simulating light scattering by arbitrary geometries. In this paper, the OPC refocused phenomenon where the light intensity decreases with increasing thickness of the scattering medium is simulated and analyzed. Numerical results show that the OPC refocused intensity decrease is a consequence of scattering rather than absorption effect of the turbid medium. Furthermore, the simulation results show that the cross-sectional width of the OPC refocused light pulse is insensitive to the optical thickness of the scattering medium, even for scattering medium as thick as 6 times the transport mean free path.

ACKNOWLEDGMENT

This work was supported by the Young Scholar Scheme of the Tianjin University of Technology and Education (Project No. 05010).

REFERENCES

1. Yaqoob, Z., D. Psaltis, M. S. Feld, and C. Yang, "Optical phase conjugation for turbidity suppression in biological samples," *Nature Photonics*, Vol. 2, 110–115, 2008.
2. Vellekoop, I. M. and A. P. Mosk, "Focusing coherent light through opaque strongly scattering media," *Optics Letters*, Vol. 32, 2309–2311, 2007.
3. Liu, Q. H., "The PSTD algorithm: A time-domain method requiring only two cells per wavelength," *Microwave and Optical Technology Letters*, Vol. 15, 158–165, 1997.

Session 4A6b
Applicators for Medical and Industrial Applications of EM Field

Waveguide-based Applicators for Local Microwave Thermotherapy: Feasibility Study of Matrix Array Treatment

Barbora Vrbova and Jan Vrba
Department of Electromagnetic Field, Faculty of Electrical Engineering
Czech Technical University in Prague, Technicka 2, 166 27 Prague 6, Czech Republic

Abstract— Thermotherapy is a method based on the differences in behavior of healthy and tumors tissue under enhanced temperatures. The major advantage of this method is the fact that it is not limited by the total dose of radiation as in chemotherapy or radiotherapy. However, one of the disadvantages is generation of blisters and particularly the limitation of the area of effective treatment.

Technical purpose of this article is the design, realization and testing of microwave applicators which is a basic part of thermotherapeutical system. The focus is on two kinds of applicators for local thermotherapy — the stripline applicator with TEM mode and the microwave waveguide applicator with TE_{10} mode in two simulation programs — SEMCAD X EM Field simulator and CST MICROWAVE STUDIO program.

Due to the impedance matching the applicators were tuned to suitable levels of the reflection coefficient S_{11}. The stripline applicator has been tuned to the value of $S_{11} = -32.3\,\mathrm{dB}$ in the SEMCAD X program, which is equal to the value of VSWR = 1.05 at frequency 434 MHz. The microwave waveguide applicator has been tuned to the value of $s_{11} = -26.92\,\mathrm{dB}$ in the CST program, which is equal to the value of VSWR = 1.095. In general we are trying to keep value of VSWR under level of 2 by aid of impedance matching. The depth of penetration is 3 cm under the surface of agar phantom, which is mimicking the biological tissue, has been determined by these simulations.

Multiple applicators can be used for enlarging the area of irradiation. The matrix composition of 4 applicators of the same kind has been studied and will be described in details in full paper.

When using the matrix composition of 4 applicators located closely together the SAR distribution created 2 maxima on the central vertical line on planar phantom. On the cylindrical phantom which represents the hand, 4 applicators of the same kind has been used. When locating the applicators on the cylindrical phantom with their electrical intensity vectors in parallel with the longitudinal axis of the phantom, the SAR distribution has a rounded shape, which is about half the diameter smaller than the phantom.

The given applicators have been tuned to suitable level of S_{11} parameter. The stripline applicator reached the value of $S_{11} = -33.4\,\mathrm{dB}$ which is equal to VSWR = 1.04 and the waveguide applicator has been tuned to the value of $S_{11} = -23.23\,\mathrm{dB}$ which represents the value of VSWR = 1.148.

The applicators have been tested by thermovision and their effective depth of heating has been reached up to 3 cm under the tissue's surface. The applicators are therefore suitable for treating tumors which are located not very deep under the biological tissue surface.

ACKNOWLEDGMENT

This research is supported by Grant Agency of the Czech Republic, project: "Non-standard application of physical fields — analogy, modeling, verification and simulation" (102/08/H081) and the SEMCAD software was provided for SEMCAD X Student Research Award 2009 competition by Schmid & Partner Engineering AG (SPEAG).

Comparisson and Verification of Dosimetry Results Obtained by Two Different Numerical Methods of the Whole-body Exposure Chamber

Lukas Visek and Jan Vrba
Dept. of Electromagnetic Field, Czech Technical University
Technicka 2, 166 27 Prague, Czech Republic

Abstract— The rapidly increasing use of sophisticated devices emitting microwave electromagnetic field, mobile phones in particular, has raised public concern about possible harmful health impacts. The whole-body exposure system for unrestrained animals was designed in order to analyze the influence of electromagnetic field. The setup operating at 900 MHz was designed with respect to induced uniform field, external radiation elimination, accurate absorbed power determination, sufficient space for mice, even mice exposure and costs. The major advantage of the system is the capability of measurement the whole-body averaged Specific Absorption Rate (SAR) which is performed by analysis of measured scatter parameters.

The setup basic properties such as electromagnetic field distribution and impedance matching were optimized and verified by 3D simulator of EM field based on the finite-difference-time-domain method.

Dosimetry is an inherent task for exposure setups. In general, dosimetry indicates quantifying the SAR, or the temperature rise caused by the SAR, in a biological body. It generally is difficult to measure the SAR directly in a living biological body, and therefore dosimetry efforts are forced to rely on computer simulations.

An anatomically based biological model is essential for numerical dosimetry. Therefore, the anatomical mouse model has been developed from computed tomography (CT) scans.

The main aim of this work is to assure if the dosimetry results reached by computer simulations can be used for exact determination of absorbed power in the biological tissue. The whole-body exposure chamber with anatomical mouse model was simulated by different numerical methods e.g., finite-difference-time-domain method (FDTD) and Finite Integration Technique (FIT) and its dosimetry results were compared and verified by computed SAR values.

ACKNOWLEDGMENT

This research is supported by Grant Agency of the Czech Republic, project: "Non-standard application of physical fields — analogy, modeling, verification and simulation" (102/08/H081).

Microwave Intracavitary Applicators for Thermotherapy in Urology an Cardiology

J. Vrba, **K. Novotna**, **and B. Vrbova**
Dept. of EM Field, Czech Technical University, Technická 2, 16627 Prague, Czech Rep.

Abstract— Paper deals with new results in the field of intracavitary microwave applicators used for Benign Prostatic Hyperplasia (BPH) treatment.

Costs and risks associated with clasical BPH treatment (TURP and open surgery) have promoted the development of minimally invasive methods. Microwave thermotherapy, varying forms of laser treatment, transurethral needle ablation, etc. have all been developed in the 1990s. The underlying principle behind these methods is to coagulate prostatic adenomatous tissue by means of heat. Of all the available minimal invasive treatment modalities, transurethral microwave is one of the most wide spread at present [1].

We have investigated basic types of microwave intracavitary applicators suitable for BPH treatment, i.e., monopole, dipole and a helical coil structures. These applicators are designed to work at 915 MHz. In the conference contribution we would like to discuss it's effective heating depth, based on the comparison of the theoretical and experimental results. Basic mechanisms and parameters influencing (limiting) heating effective depth are described and explained in Ref. [2–4].

The basic type of intracavitary applicator is a monopole applicator. The construction of this applicator is very simple, but numerically modelled (calculated by software product SEMCAD) and measured "Specific Absorption Rate" ("SAR") distribution along the applicator is more complicated. During measurements of SAR along the applicator we have found, that typically there is not only a one main "SAR" maximum (first from the right side), but also a second and/or higher order maximas can be created, being produced by outside back wave propagating along the coaxial cable. To eliminate this second maximum and optimise the focusing of "SAR" in predetermined area of biological tissue needs to use the helical coil antenna structure. After coil radius and length optimisation we have obtained very good results of "SAR" distribution.

As a novel results of our work we could mention that various microwave applicators for prostate cancer or BPH treatment have been developed and evaluated. Theoretical analysis of effective heating depth of these applicators and its experimental evaluation will be given.

ACKNOWLEDGMENT

This research is supported by the research program MSM6840770012 "Transdisciplinary Research in the Area of Biomedical Engineering II" of the CTU in Prague, sponsored by the Ministry of Education, Youth and Sports of the Czech Republic.

REFERENCES

1. De la Rosette, J., F. D'Ancona, and F. Debruyne, "Current status of thermotherapy of the prostate," *J. Urol.*, Vol. 157, 430–438, 1997.
2. Vrba, J., C. Franconi, and M. Lapes, "Theoretical limits for the penetration depth of the intracavitary applicators," *International Journal of Hyperthermia*, Vol. 12., No. 6., 737–742, 1996.
3. Vrba, J., M. Lapes, and L. Oppl, "Technical aspects of microwave thermotherapy," *Bioelectrochemistry and Bioenergetics*, Vol. 48, 305–309, 1999.
4. Bolmsjö, M., L. Wagrell, A. Hallin, T. Eliasson, B. E. Erlandsson, and A. Mattiasson, "The heat is on — but how? A comparison of TUMT devices," *Br. J. Urol.*, Vol. 78, 564–572, 1996.

Evanescent Mode Waveguide Applicators for Microwave Thermotherapy

Jan Vrba[1], **Paolo Togni**[1], **Jan Vrba**[2], **and David Vrba**[1]

[1]Dept. of EM Field, Czech Technical University in Prague, Prague, Czech Republic
[2]Inst. of EM Field Theory, RWTH Aachen University, Aachen, Germany

Abstract— In this contribution we would like to describe our new results dealing with evanescent mode waveguide hyperthermia applicators, typically used for cancer treatment. We have developped theoretical basis of this technology and designed & evaluated different versions of these applicators working below waveguide cut-off frequency.

In our contribution we would like to discuss what happens, when the frequency f of hyperthermia apparatus is either very different (i.e., much higher or lower) from the cut-off frequency f_c or very near (even equal) to the cut-off frequency f_c of the used waveguide applicator. This special case of our interest can happen when either the hyperthermia apparatus is tunable in broader frequency range or the cut-off frequency f_c of the applicator is changed by different dielectric parameters of various types of biological tissues.

There is a substantial difference between the two ways of the waveguide applicator excitation (i.e., above or under the cut-off frequency f_c) and in the propagation and "behaviour" of the EM field inside such applicator also. Basic differences would be explained during the presentation.

For the following discussion we have chosen the case of the rectangular applicator with a flange. But similar results is possible to obtain for other important cases like e.g., rectangular applicators without flange or for the family of circular applicators.

Waveguide flange is in our approach considered as an electric wall, dashed line going into the biological tissue determines the magnetic wall of our model. The distance between these walls determines the cut-off frequency f_c of the applicator aperture. Of course, f_c is influenced by the tissue permittivity also.

The results we would like to describe in our contribution are interesting from theoretical point of view of the knowledges about the general properties of the waveguide applicators. And are very important also for the treatment — Our results demonstrate very substantial changes of SAR distribution in the treated biological tissue. If f is going to f_c then so called hot spots complicating the treatment can arise.

ACKNOWLEDGMENT

This research is supported by the research program MSM6840770012 "Transdisciplinary Research in the Area of Biomedical Engineering II" of the CTU in Prague, sponsored by the Ministry of Education, Youth and Sports of the Czech Republic.

Prospective Medical Imaging and Diagnostics Based on Microwave Technology

Jan Vrba[1], **Ladislav Oppl**[1], **Jaroslav Vorlíček**[1], **David Vrba**[1], **and Jan Vrba**[2]

[1]Dept. of EM Field, Czech Technical University in Prague, Prague, Czech Republic
[2]Chair of EM Theory, RWTH Aachen University, Kopernikusstraβe 16, 52074 Aachen, Germany

Abstract— Future trends in medical applications of microwave technique and technology can be seen in development of new diagnostic and imaging methods based on high frequency EM field. A significant importance for the future can be identified for the following methods: Microwave tomography, Microwave radiometry, Measurement of complex permittivity, Imaging in the Terahertz waves band and Microwave diagnostic radars.

Interactions of EM field with biological systems are utilised in the area of therapy (oncology, physiotherapy, urology atp.) from late seventieth of last century. Wideutilization of microwave thermotherapy can be observed in the countries of EU, USA and Japan. Our activities in microwave thermotherapy in former Czechoslovakia started in the year 1981. Since 1990 we are member of ESHO (European Society for Hyprthermia Oncology), which co-operates with NAHS (North American Hyperthermia Society) and ASHO (Asian Society of Hyperthermia Oncology).

Recent trends in microwave medical applications are to study the possibilities to develop new diagnostics based on EM field resp. on microwace technique. A significant importance for the future can be identified for the next methods:

- Magnetic resonance,
- Microwave tomography,
- Microwave radiometry,
- Measurement of complex permittivity,
- Imaging with terahertz waves,
- Microwave diagnostic radar.

We will not talk here about magnetic resonance, as it is just well known and broadly used application of EM field in medical diagnostics. We will focus here on other above mentioned methods (excluding microwave diagnostics radars).

ACKNOWLEDGMENT

This research is supported by Grant Agency of the Czech Republic, project: "Microwave Imaging for Biomedical Applications" (102/05/0959) and by the research program MSM6840770012 "Transdisciplinary Research in the Area of Biomedical Engineering II" of the CTU in Prague, sponsored by the Ministry of Education, Youth and Sports of the Czech Republic.

REFERENCES

1. Vrba, J., *Medical Applications of Microwaves*, 1st Edition, 168, Issued by CTU, Prague, 2003, ISBN 80-01-02705-8.
2. Semenov, S. Y., et al., "Three-dimensional microwave tomography, initial experimental imaging of animals," *IEEE Transactions on BME*, Vol. 49, No. 1, 55–63, Jan. 2002.
3. Gabriel, S., R. W. Lau, and C. Gabriel, "The dielectric properties of biological tissue — II. Measurements in the frequency range 10 Hz to 20 GHz," *Phys. Med. Biol.*, Vol. 41, 2251–2269, 1996.

Session 4A7
Matter, Signals and Waves

The Absorption Capability Measurements of the Free Space Absorbers

L. Nowosielski, **M. Wnuk**, **R. Kubacki**, **and R. Przesmycki**
Faculty of Electronics, Military University of Technology, 2 Gen. S. Kaliski str., 00-908 Warsaw, Poland

Abstract— The aim of this work is to present the procedure for absorption measurements of absorbing materials. In presented procedure as the electromagnetic wave absorption measure among other was used RCS (Radar Cross Section) parameter. RCS describes the extend to which an absorbing material reflects an incident electromagnetic wave. It is a measure of strength of the electromagnetic wave backscattered from a absorbing material for a given incident power. The presented measurement procedure requires a double face flat steel panel, where one is used as reflector material (reference) and the other is coated with absorbing material. The panel is fixed on a support, which is positioned in front of the receiving and transmitting antennas. With this method is necessary to make two separate measurements of the signal level reflected by the plate with and without absorbing material. The advantage of this methodology is that it allows the evaluation of the absorption in the angle axis by rotating the transmitting and receiving antennas. In the paper the methodology, detailed description of laboratory stand and laboratory stand calibrating procedure were presented.

The absorption of broadband absorber constructed as flat, pyramidalshaped and impregnated with a magnetic material was successfully evaluated using described method in the frequency range of (2–4) GHz. The measurements were carried out in the anechoic chamber located at Laboratory of Electromagnetic Compatibility, Faculty of Electronics, Military University of Technology in Poland. In this paper the measurements results and discussion on the results are presented too.

Electric and Magnetic Properties of Powdered Ferrite Materials

Roman Kubacki, **Marian Wnuk**,
Leszek Nowosielski, **and Rafał Przesmycki**
Military University of Technology
2, Gen. S. Kaliski Str., 00-908 Warsaw, Poland

Abstract— Nowadays absorbing materials, which are widely employed in microwave technology, should be composed of conducting and also magnetic materials. For such materials it is possible to reduce the reflectivity and significantly increase the absorption of the shielding materials. Taking into account that effective absorbers must operate in wide frequency range and have not only a solid but also a flexible form, there is a need to develop numerical simulation of the final properties of absorbers. It is possible to predict final properties however, electric and magnetic data of each component should be determined.

The electromagnetic properties of isotropic substances can be determined macroscopically by scalar material properties in term of relative complex permittivity (ε) and permeability (μ):

$$\begin{aligned} \varepsilon &= \varepsilon' - j\varepsilon'' \\ \mu &= \mu' - j\mu'' \end{aligned}$$

where: ε', μ' are the electric and magnetic constants and ε'', μ'' are the electric and magnetic loss factors.

The method described in the paper allows to measure complex relative permittivity ε and permeability μ of non solid (mainly powdered) substrate in wide band of frequency. The technique of measurement has been based on method developed for coaxial transmission line where substance under test is inserted into coaxial line between two walls. Values of permittivity and permeability of measured powder were calculated from scattering parameters of measured sample. Because of the symmetrical and reciprocal network the scattering matrix satisfies the following condition: $S_{ik} = S_{ki}$.

Analytical method which allows to extract electromagnetic data of measured powder substrate from measured data of whole sample has been derived on the base of scattering parameters describing two-port networks. To receive mathematical formulas which allow to extract scattering parameters of networks representing the powder material the graph method of calculation has been introduced. The graph method has been derived from the theory of power flow in the network branches. The formulas of the sample (substrate under test and 2 walls) are functions of scattering parameters of substrate under test (S_{11}, S_{21}) and a wall (E_{11}, E_{21})

$$\begin{aligned} SW_{11} &= E_{11} + E_{21}\frac{\left(1 - E_{11}S_{11}\right)S_{11} + E_{11}S_{21}^2}{\left(1 - E_{11}S_{11}\right)^2 - E_{11}^2S_{21}^2} \\ SW_{21} &= \frac{E_{21}^2S_{21}}{\left(1 - E_{11}S_{11}\right)^2 - E_{11}S_{21}} \end{aligned}$$

where: SW_{11} and SW_{21} — scattering parameters of whole sample.

As a magnetic material the Yiitrium Garnet YIG class ferrite was used for measurements. Samples for measurements were prepared in solid state and also in powder forms. Values of permittivity and permeability of slid state ferrite and of powder received from this material were measured in frequency range from 0.2 GHz till 1.2 GHz. Obtained data allows to verify Landau and Lifshits equations to simulate the air-mixture properties from solid state material properties. In the work, the verification was done for material having not only electric but also magnetic properties.

REFERENCES

1. Baker-Jarvis, J., "Transmission/reflection and short-circuit line permittivity measurements," NIST Technical Note, 2005.
2. Krupka, J. and R. G. Geyer, "Complex permeability of demagnetized microwave ferrites near and above gyromagnetic resonance," *IEEE Trans. Magnetics*, Vol. 32, No. 3, 1924–1933, 1996.
3. Kubacki, R., J. Sobiech, and K. Wardak, "The comparison of dielectric properties of young and mature animal tissues in microwaves," *Przeglad Elektrotechniczny*, Vol. 5, 43–45, 2006.

4. Nelson, S. O., "Density-permittivity relationships for powdered and granular materials," *IEEE Trans. Instrum. Meas.*, Vol. 54, No. 5, 2033–2040, 2005.
5. Wiatr, W., R. Frender, and M. browski, "Characterization of microwave absorbing materials using a wideband T/R measurement technique," *Conference Proceedings on International Conference on Microwaves, Radar and Wireless Communications*, Vol. 2, 475–478, Wroclaw, Poland, 2008.

Influence of Parameters of Dielectric in Aperture-coupled Stacked Patch Antenna on the Bandwidth

Jarosław Bugaj, **Marian Wnuk**, **and Leszek Nowosielski**
Faculty of Electronics, Military University of Technology, 2 Gen. S. Kaliski str., Warsaw 00-908, Poland

Abstract— Millimeter wave printed antennas can take many forms, including microstrip patch elements and variety of proximity coupled printed radiators. The microstripline-fed printed slot and the aperture coupled patch are examples of this latter type and may be useful in certain planar array applications. The present paper described a method of analysis that can be applied to these geometries, as well as related configurations. The theory is describes, and impedance result for to the microstripline-fed printed slot antenna and the aperture-coupled microstrip patch are given. The method is based on the reciprocity theorem and uses the exact Green's functions for dielectric slab, and moment method solutions for the unknown antenna current.

The paper presents a model of the antenna on which the simulation was conducted on the impact parameter on bandwidth. Phenomena setting in the aperture-coupled stacked microstrip antennas were introduced. Presented are parameters the optimized model. Examining the influence of the changes of thickness and the permittivity of the individual layers of dielectric in multilayer antenna on the bandwidth is the object of the work. The influence of the changes of the value of these parameters of individual layers on the bandwidth was talked over. At the end shows the influence of the thickness of the antenna on antenna's bandwidth. Paper shows the analysis of multilayer microstrip antennas process is very complex and time consuming. Knowledge of the impact of changes in the permeability and thickness of the dielectric layer to predict changes in parameters of the antenna under the influence of different factors such as temperature, etc. Analysis of the antenna was made by using IE3D — Zeland Software.

Multi-element Antenna on Dielectric Layer with Circular Polarization

Marek Bugaj, **Marian Wnuk**, **and Roman Kubacki**
Military University of Technology, 00-908 Warsaw, 2 gen. S. Kaliski str., Poland

Abstract— One of the methods to increase resistance of radiocommunication systems to interference is use of radiating systems with circular polarization. Particularly important is application of such antennas in devices and systems of manoeuvring objects, such as aircrafts and missiles, because this eliminates the effect of object location on the correct structure of information transfer. Currently one of the most innovative fields of antenna engineering are antennas on dielectric base — microstrip antennas.

Circular polarization can be obtained in antennas on dielectric base when inducing in them two perpendicular vibration types with phase difference of $\pi/2$, or its uneven multiple. For this purpose one may use square or round patches with their stimulation by two perpendicular inductors providing phase shift of $K \cdot \pi/2$ where $K = (2n-1)$, and n is positive integer. Circular polarization can also be obtained by delivering single-point power supply to the patch, to which an interrupting element has been inserted, destroying patch symmetry against the point of power supply.

An antenna with circular polarization may be presented as a system of 3 main cascade connected parts (Fig. 1):

- supply network, passage from the concentric line to the strip line (h),
- matching circuit (c),
- antenna element (a).

Circular polarization field is created as a result of delivering signal of the same amplitude with 90° phase offset to two antenna inputs. In the general case, this can be two radiating elements respectively powered with shifted phase signals. In the theoretical model of the antenna in the power supply part each component is represented by **S** matrix parameter which can be directly measured, whereas in the radiating part the antenna is characterized by radiation field components in planes of perpendicular lines that can be linked with **S** matrix parameters.

Dispersion matrix of this system is described in the function of **S** matrix of different components, where the two first elements have non-complicated **S** matrix, but difficulties arise with the description of the radiating element (antenna).

In the proposed antenna's solution, the sequential circulation technique has been used. At the same time one aimed at maximizing the antenna's working band. It was assumed that the structure will produce circular polarization, in a middle frequency of the antenna's working band, its ellipticity understood as polarization ellipse semi-axis ratio will approach one.

The proposed antenna solution has a number of potential applications. Improvement in directivity can be obtained by series, or parallel connection of such antennas into a larger network. Applications should be sought in the field of communication, radio navigation etc.

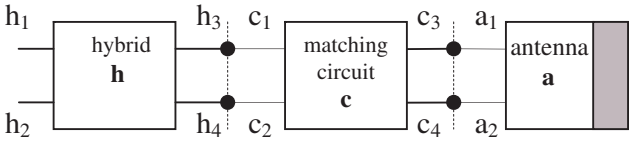

Figure 1: Model of antenna with circular polarization in the form of four terminal network cascade.

REFERENCES

1. Yano, Y. T. and A. Ishimaru, "A theoretical study of the input impedance of a circular microstrip antenna," *IEEE Trans. on Antenna and Propag.*, Vol. 29, No. 1, 77–83, Jan. 1981.
2. Wnuk, M., G. Różański, and M. Bugaj, "The analysis of microstrip antennas with utilization the FDTD method," *CMEM Computational Methods and Experimental Measurements*, WIT press, Southampton Boston, UK, 2005.
3. Wnuk, M. and M. Bugaj, "Aperture-coupled microstrip antennas," *MIKON XV-International Conference on Microwaves Radar and Wireless Communications*, Kraków, May 2006.

The Expanded Uncertainty for Radio Frequency Immunity Testing

Rafał Przesmycki, **Leszek Nowosielski**, **Marian Wnuk**, **and Roman Kubacki**
Faculty of Electronics, Military University of Technology, 2 Gen. S. Kaliski str., Warsaw 00-908, Poland

Abstract— EMC testing is a process of taking measurement. Whenever the electromagnetic field strength is measured the result is never an exactly correct value. The reported value will inevitably differ from the true value by some amount, hopefully small.

For any given electromagnetic field strength measurement method, there are usually several sources of measurement uncertainty, although only one or two may dominate. Each individual source has to be analysed. A values to each of these sources have to be assigned and then summed using an appropriate manner to give the total measurement uncertainty.

This paper concerns the problems of electromagnetic compatibility for RF (radio frequency) immunity testing according the EN 61000-4-3 standard. The measurement uncertainty budget calculation techniques recommended in standardising documents are barely described and very often they are not adapted to the specific needs of tests performed within the scope of EMC (Electromagnetic Compatibility). For that reason, authors of the paper attempt to develop recommended techniques. The authors focused attention on presentation of the measurement uncertainty budget calculation algorithm. The information related to measurement uncertainty of RF signal test level setting during the RF immunity test in an anechoic chamber are presented. The example of uncertainty budget for laboratory stand used by accredited EMC laboratory for RF immunity testing of information technology equipment is precisely described too.

The methodology shown in this paper will be useful for the EMC laboratory workers during the new test procedure preparation process.

Audio Hash Function Used for Digital Rights Management

Zbigniew Piotrowski and Piotr Gajewski
Military University of Technology, 2 gen. S. Kaliski str., Warsaw 00-908, Poland

Abstract— A hash function in everyday cryptology is used to verify the integrity of digital transmission, verify digital signature etc. It is worth to notice that cryptographic hash function is its extreme fragility taking into consideration changing bit order sequence or even the small piece of a bit stream. Hash function should be easily computable function that maps every sequence to another bit sequence with dedicated length.

Using digital signal processing for digital rights management purposes the audio hashing is used mainly because of its specific algorithm is robust for intentional or unintentional bit sequence changing of the information source. Using audio hash function it does not matter if a few audio samples were changed or not because the audio intelligibility and quality does not change.

In this paper the new audio hashing algorithm for Digital Rights Management is presented. Robust hash extraction algorithm is described using block scheme as well as mathematical formulas. Spectral representation is computed by performing a Fast Fourier Transform on every frame. The windowing function acts main role in audio preprocessing stage. Basic metrics of the audio signal in time domain are computed. At the plots and figures the efficiency of described algorithm is shown. There is also the proposal of the DRM audio system using data hiding technology together with the audio hash function to indentify the original host signal from forged one. The main DRM system scheme is presented on dedicated plot.

REFERENCES

1. Haitsma, J., T. Kalker, and J. Oostveen, "Robust audio hashing for content identification," *Proces. of the International Workshop on Content-based Multimedia Indexing*, Brescia, Italy, October 2001.
2. Hurley, N. J., F. Balado, E. P. McCarthy, and G. C. M. Silvestre, "Performance of philips audio fingerprinting under additive noise," Austrian Computer Society (OCG), 2007.
3. Balado, F., N. Hurley, E. McCarthy, and G. Silvestre, "Performance analysis of robust audio hashing," *IEEE Trans. on Information Forensics and Security*, Vol. 2, 1556–6013, June 2007.
4. Piotrowski, Z. and P. Gajewski, "Acoustic watermark server effectiveness," *Computational Methods and Experimental Measurements XIV, CMEM XIV*, 251–258, WIT Press, Southampton, Boston, 2009.
5. Piotrowski, Z. and P. Gajewski, "Voice spoofing as an impersonation attack and the way of protection," *Journal of Information Assurance and Security*, Vol. 2, No. 3, 223–225, Dynamic Publishers, Inc., USA, September 2007.

Multi-spectral Optoelectronic Sensor Employing Cavity Enhanced Absorption Spectroscopy

Jacek Wojtas, **Zbigniew Bielecki**, **Janusz Mikołajczyk**,
Mirosław Nowakowski, **and Beata Rutecka**
Institute of Optoelectronics, Military University of Technology
2 Kaliskiego Str., Warsaw 00-908, Poland

Abstract— In the paper, a multi-spectral optoelectronic sensor basing on cavity enhanced absorption spectroscopy (CEAS) is presented. There is applied a special photoreceiver. The photoreceiver is characterized by wide range of the detected wavelengths. The optical signal from many laser sources can be measured using the photoreceiver. Thanks to this, in one cavity, a value of absorption coefficient at a few different wavelengths can be determined parallel.

In the CEAS technique a beam of the laser radiation is injected under a very small angle related to the optical axis of the cavity. The radiation is reflected inside the optical cavity, similarly as inside a multipass cell. Through to this, dense structure modes are received. All systems operating on the basis of CEAS method can work with weak modes structure. That is why, they are of low sensitivity to instabilities. The CEAS sensors can obtain sensitivity of about $10^{-9}\,\mathrm{cm}^{-1}$.

The multi-spectral sensor requires properly designed and optimized optical system and photoreceiver. Typical CEAS system, designed for the measurement of the trace gases concentration, consists of a pulse radiation source, optical cavity, photoreceiver, and a signal processing system. In the experimental setup two lasers and two optical lanes are used. The setup makes it possible to detect a trace concentration of two gases at the same time. Using the special constructed photoreceiver the optical signals from two lasers are registered. The photoreceiver works with telecommunication techniques, well-known as time division multiplexing. Every laser will be assigned to the suitable channel — the strictly determined temporary window. In this window, the signal from the exits of the optical cavity is registered. The presented setup is of greatest interest with respect to the possible applications. For example, it can be used in ambience monitoring, luggage monitoring in ports, on airports, entry points, as well as in strategic objects and rooms also in undertakings connected with the counteraction to terrorist attacks.

REFERENCES

1. Bielecki, Z., W. Kolosowski, G. Rozanski, and J. Wojtas, "Nitrogen dioxide detection using optoelectronic sensor," *Computational Methods and Experimental Measurements XIII*, 809–818, WIT Press, 2007.
2. Berden, G., R. Peeters, and G. Meijer, "Cavity ring-down spectroscopy: Experimental schemes and applications," *International Reviews in Physical Chemistry*, Vol. 19, No. 4. 565–607, 2000.
3. Engel, G. S., E. J. Moyer, F. N. Ketusch, and J. G. Anderson, "Innovations in cavity enhanced laser absorption spectroscopy: Using in situ measurements to probe the mechanisms driving climate change," *Earth Science Technology Conference, Laser Sensor Technologies*, Jun. 2003.
4. Kasyutich, V. L., C. S. E. Bale, C. E. Canosa-Mas, C. Pfrang, S. Vaughan, and R. P. Wayne, "Cavity-enhanced absorption: Detection of nitrogen dioxide and iodine monoxide using a violet laser diode," *Applied Physics B*, Vol. 76, No. 6, 691–698, 2003.
5. Courtillot, I., J. Morville, V. Motto-Ros, and D. Romanini, "Sub-ppb NO_2 detection by optical feedback cavity-enhanced absorption spectroscopy with a blue diode laser," *Applied Physics B*, Vol. 85, 407–412, 2006.
6. Wojtas, J., A. Czyzewski, T. Stacewicz, and Z. Bielecki, "Sensitive detection of NO_2 with cavity enhanced spectroscopy," *Optica Applicata*, Vol. 36, 2006.
7. Merienne, M. F., A. Jenouvrier, and B. Coquart, "The NO_2 absorption spectrum. I: Absorption cross-sections at ambient temperature in the 300–500 nm region," *J. Atmos. Chem.*, Vol. 20, No. 3, 281–297, 1995.
8. Bielecki, Z., M. Leszczyńki, K. Holz, L. Marona, J. Mikołjczyk, M. Nowakowski, P. Perlin, B. Rutecka, T. Stacewicz, and J. Wojtas, "Sub-ppb NO_x detection by CEAS system with blue and IR diode laser," *Computational Methods and Experimental Measurements XIV*, 809–818, WIT Press, 2009.

9. Diodes, A. L., "Datasheet of the HL6312G/13G," *Hitachi*, ODE-208-190H (Z), Rev. 8, Jan. 2003.
10. Wojtas, J. and Z. Bielecki, "Signal processing system in the cavity enhanced spectroscopy," *Opto.-Electron. Rev.*, Vol. 16, No. 4, 44–51, 2008.
11. Bielecki, Z. and A. Rogalski, *Optical Signals Detection*, Scientific-Technical Publishing House, Warsaw, Polish, 2001.

Free Space Optics Second Generation versus Shorter Wavelengths

M. Nowakowski, Z. Bielecki, J. Mikołajczyk, J. Wojtas, and M. Gutowska
Institute of Optoelectronics, Military University of Technology
2 Kaliskiego Str., 00-908 Warsaw, Poland

Abstract— Free-Space Optics (FSO) is a proven, reliable technology for last mile telecommunications applications, used worldwide for both enterprise network building-to-building connections and for wireless access to more traditional land line communications networks. The link range amounts to c.a. few hundred meters. It is primarily affected by fog and low clouds. In the paper 10 μm FSO performance compared to shorter wavelengths (e.g., 850 nm and 1.5 μm) are presented. The choice of the wavelength range applied to optical communication is mainly formed by atmosphere features (absorption, scattering, reflection and background radiation) and parameters of available optical elements, radiation sources and detectors with preamps. In the system quantum cascade laser and an HgCdTe heterostructural photodiode operating at the wavelength of 10 μm were applied. The Quantum Cascade Laser Module LM-03-D of Cascade Technologies firm was used in our transmitter. The laser system generates radiation pulses the length of which reached the value of 0.02–10 μs, frequency up to $1.2 \cdot 10^6$ Hz, and peak power of 100 mW. The radiation intensity was registered by the PVI-2TE-10.6 type photodetector. The designed system was prepared for distance range operation about of 1 km. The experimental results and simulation data demonstrate that the system could be used for example in light fog or rainfall rate of 100 mm/hr. The FSO system is promising and effective communication link.

REFERENCES

1. Juarez, J. C., "Free-space optical communications for next-generation military networks," *IEEE Communications Magazine*, 46–51, November 2006.
2. Kinkade, K., "Free-space optics builds invisible bridges," *Laser Focus World*, No. 12, 2003.
3. Manor, H. and A. Argon, "Performance of an optical wireless communication system as a function of wavelength," *Applied Optics*, Vol. 42, No. 21, July 1, 2003.
4. Capasso, F., et al., "Quantum cascade lasers: Ultrahigh-speed operation, optical wireless communication, narrow linewidth, and far-infrared emission," *IEEE Journal of Quantum Electronics*, Vol. 38, No. 6, June 2002.
5. Achour, M., "Free-space optics wavelength selection: 10 μm versus shorter wavelengths," http://www.ulmtech.com.
6. Faist, J., "Continuous-wave, room temperature quantum cascade lasers," *OPN*, 32–36, May 2006.
7. Maulini, R., A. Mohan, M. Giovannini, J. Faist, and E. Gini, "External cavity quantum-cascade laser tunable from 8.2 to 10.4 μm using a gain element with a heterogeneous cascade," *Appl. Phys. Lett.*, Vol. 88, 2006.
8. Hofstetter, D., M. Beck, T. Aellen, and S. Blust, "High frequency modulation of a quantum cascade lasers using a monolithically integrated intracavity modulator," *IEEE Photonics Techn. Letters*, Vol. 15, No. 8, 1044–1046, 2003.
9. www.alpeslasers.ch/.
10. Piotrowski, A., W. Gawron, K. Klos, J. Pawluczyk, J. Piotrowski, P. Madejczyk, and A. Rogalski, "Improvements in MOCVD growth of $Hg_{1-x}Cd_xTe$ heterostructures for uncooled infrared photodetectors," *Proc. SPIE*, Vol. 5957, 116, 2005.
11. Bielecki, Z., W. Kołosowski, J. Mikołajczyk, M. Nowakowski, E. Sędek, and J. Wojtas, "Free-space optical communications using quantum cascade laser, *MIKON 2008, Conf. Proc.* Vol. 2, 295–298, 2008.
12. Bielecki, Z., W. Kołosowski, and J. Mikołajczyk, "Free-space optical data link using quantum cascade laser," *PIERS Proceedings*, 108–111, Cambridge, USA, July 2–6, 2008.
13. Mikołajczyk, J., Z. Bielecki, M. Nowakowski, and J. Wojtas, "Second generation FSO for communications systems," *IRS2 Conference Proc.*, 313–316, 2008.

Infrared Detection Module for Free Space Optics

Marcin Ratajczyk[1], **Ryszard Paliwoda**[1], **Maciej Rzeczkowski**[1], **Waldemar Gawron**[2], **Jarosław Pawluczyk**[1], **and Józef Piotrowski**[1]

[1]VIGO System S.A., 05-850 Ozarow Mazowiecki, 129/133 Poznanska str., Poland
[2]Institute of Applied Physics, Military University of Technology, 2 Kaliskiego Str., Warsaw 00-908, Poland

Abstract— Free space optics (FSO) communication in LWIR range is less sensitive to atmosphere features. VIGO System S.A. — company from Poland — develops high performance detector module optimized for LWIR range. We present new detection module dedicated to open space optical communication optimized for 10 µm.

Module specification:

- Detector: PVI-2TE-10 photodiode with immersion lens, thermoelectrically cooled.
- Operating temperature range: $-30 \ldots +60°C$.
- Detector temperature stabilization precision: 0.01°C.
- Detector time constant: < 1 ns.
- Preamplifier bandwidth: 100 MHz.
- Input current noise: $5\,\mathrm{pA}/\sqrt{\mathrm{Hz}}$.
- Detector capacity < 5 pF.

Detection module is based on PVI-2TE-10 HgCdTe photodiode, thermoelectrically cooled by two stage Peltier cooler. It is optimized for long wavelength — 10 µm. TEC controller stabilizes detector temperature with high precision in wide ambient temperature range. Immersion lens enables optimization of the detector physical dimensions, decreasing detector capacity and time constant.

Module parameters enables maximum transmission speed 100 Mb/s. Low bit error rate requires correct transmission with low and high signal level. Detector and preamplifier have wide linear working range, noise optimization provides module high detectivity. DC reverse bias increases dynamic resistance and improves frequency response.

REFERENCES

1. Juarez, J. C., "Free-space optical communications for next-generation military networks," *IEEE Communications Magazine*, 46–51, November 2006.
2. Kinkade, K., "Free-space optics builds invisible bridges," *Laser Focus World*, No. 12, 2003.
3. Piotrowski, J. and A. Piotrowski, "Uncooled infrared photodetectors in Poland," *Proc. SPIE*, Vol. 5957, 117–128, 2005.
4. Piotrowski, J. and A. Rogalski, *High-operating-temperature Infrared Photodetectors*, Ed. SPIE, Bellingham, ISBN: 9780819465351, 2007.
5. Piotrowski, J., "Hg1 xCdxTe infrared photodetectors," *Infrared Photodetectors*, 391–494, SPIE, Bellingham, 1995.
6. Piotrowski, A., K. Kłos, W. Gawron, J. Pawluczyk, Z. Orman, and J. Piotrowski, "Uncooled or minimally cooled 10 µm photodetectors with subnanosecond response time," *Proc. SPIE*, 6542, 2007.
7. Achour, M., "Free-space optics wavelength selection: 10 µm versus shorter wavelengths," http://www.ulmtech.com.
8. Piotrowski, A., W. Gawron, K. Klos, J. Pawluczyk, J. Piotrowski, P. Madejczyk, and A. Rogalski, "Improvements in MOCVD growth of Hg1-xCdxTe heterostructures for uncooled infrared photodetectors," *Proc. SPIE*, Vol. 5957, 108–116, 2005.
9. Frendinandow, E. and T. Mitsev, "Link range of free space laser communication system," *Microwave Review*, 41–42, December 2003.

Session 4AP
Poster Session 3

Long-term Data Record of Vegetation Leaf Area Index from Multiple Satellite-borne Sensors: Evaluation and Validation

Sangram Ganguly[1], **Arindam Samanta**[1], **Mitchell A. Schull**[1], **Cristina Milesi**[2], **Ramakrishna R. Nemani**[3], **Yuri Knyazikhin**[1], **and Ranga B. Myneni**[1]

[1]Department of Geography and Environment, Boston University
Boston, MA 02215, USA
[2]NASA Ames Research Center, University Corporation Monterey, California, USA
[3]Biospheric Science Branch, NASA Ames Research Center, Moffett Field
CA 94035, USA

Abstract— The evaluation of a new global monthly leaf area index (LAI) data set for the period July 1981 to December 2006 derived from AVHRR Normalized Difference Vegetation Index (NDVI) data is described. The theoretical principle in retrieving LAI from NDVI is based on a physical algorithm rooted on the radiative transfer theory of canopy spectral invariants. Establishing the consistency and validity of the long-term coarse resolution LAI product is a challenging task. First, a detailed implementation of the LAI retrieval algorithm from AVHRR NDVI in a global scale is performed. Second, we evaluate the consistency of our dataset with respect to the MODIS LAI product, which is taken as a benchmark for tuning the performance of our retrieval algorithm. The results indicate qualitative agreement of the AVHRR LAI dataset with the MODIS Collection 5 (C5) LAI data set for the overlapping time period, 2000–2003, covering a global — to a regional — and to a pixel-scale. On a global scale, considering all biomes (land cover types), the AVHRR LAI values can explain 97.5% ($R^2 = 0.975$) variability in MODIS C5 LAI and, on average the AVHRR LAI values will be in error (RMSE = 0.187) in their estimation by 0.18 LAI, compared to the MODIS C5 LAI. The regional and local scale comparison also testifies to a high degree of correspondence between the AVHRR and MODIS LAI within an error of 0.5 LAI units. The LAI dataset is also compared with CYCLOPES LAI for the period 2000–2003 over a selective BELMANIP benchmark network of sites representative of different biomes. The inter-comparison indicates reasonable agreement in most of the biomes, with a systematic underestimation in the AVHRR LAI (< 0.5 RMSE), which also justifies the theoretical constraints in scaling LAI retrievals. Third, we perform a validation of our dataset with field measurements of LAI and high resolution LAI maps obtained via the ORNL DAAC Mercury system. Comparison with plot scale field measurements (covering 22 sites and 44 measurements) over homogeneous vegetation patches indicated a 7% underestimation when all major vegetation types are taken into account. The error in mean values of LAI obtained from distributions of AVHRR LAI and high resolution LAI maps for different biomes is within 0.5 LAI for six out of the ten selected sites. Finally, to establish the robustness of the LAI dataset for the earlier period, 1980s–1990s, we compare the temporal trends in LAI with the existing, well established, temporal trends in vegetation growth vis-à-vis trends in climate variables like land surface temperature in the northern hemisphere and precipitation in the semi-arid tropics. We also isolate well correlated modes of variability between temperature, precipitation and greenness, and assess their relationship to largescale circulation anomalies associated with the El Niño-Southern Oscillation (ENSO) and the Arctic Oscillation (AO) using canonical correlation analysis (CCA). Inter-comparison with different datasets, establishing and validating long term trends with known fluctuations in climate variables, and instituting field level comparison studies corroborates the confidence in utilizing the physically derived AVHRR LAI dataset for long term vegetation monitoring and large scale modeling studies.

Real Time Atmosphere Sensing from Singular Ground-based GPS Station

Qing-Lin Zhu[1], **Zhen-Sen Wu**[1], **Zhen-Wei Zhao**[2], **and Le-Ke Lin**[2]

[1]School of Science, Xidian University, Xi'an 710071, China
[2]China Research Institute of Radio Wave Propagation, Qingdao 266107, China

Abstract— In recent years, Global Positioning System has become a powerful tool in a number of applications such as geophysics and remote sensing. The GPS signal progation delay in the atmosphere at slant path is a very important parameter in monitoring the state the atmosphere and of benefit in near real time weather forecasting. The values of troposphere slant delay at very low elevation might proof to be useful for meteorological applications, correction of refractivity and nearby real time numerical weather prediction, since the delay values are much higher near the horizon than in zenith direction and involve more information related to the troposphere. So the investigation of developing the troposphere slant delay is important. In the past, the delay is only available from radiosonde data. However, since the radiosonde is usually available every 12 hours in a day and also a rather expensive instrument, it is not an efficient instrument for real time climatologic applications. In the paper, a method of real time monitoring atmosphere from singular ground-based GPS observations at low elevation angles ($< 5^\circ$) is presented. Compared to the radiosonde, the GPS method has several advantages, such as its high efficiency, low cost, high accuracy and all-weather operability. Several day observations from shantou GPS station are disposed and analyzed. Through comparison with radiosondes, it is found that results from GPS agree well with those from radiosondes and related coefficients between two results are above 0.99. It is feasible to real time monitoring atmosphere from singular ground-based GPS station. GPS is likely promoted to be potential of being used for monitoring the troposphere instead of radiosonde, for instance the reconstruction of refractivity profiles.

Experimental Study of Relationship between Sea Clutter and Wave Height in Littoral Environment

Yu-Shi Zhang[1, 2], **Zhen-Sen Wu**[1], **and Hui-Ming Li**[2]

[1]School of Science, Xidian University, Xi'an, Shaanxi 710071, China
[2]China Reserch Institute of Radiowave Propagation, Qingdao, Shandong 266107, China

Abstract— In littoral environment, the sea surface is different from that in the open sea. Due to the existence of local wind or swell, the sea surface is difficult to reach a state of equilibrium (or is called fully developed sea). In many cases, wind direction is inconsistency with wave direction, and the relationship between wind speed and wave height is not agree with equilibrium sea surface sate. Sea clutter, namely, the radar backscatter echo from the sea surface, is completely different from fully developed sea and often leads to larger radar false alarm rate. The representative semi-empirical sea clutter models (the GIT model, the TSC model, the HYB model) are not ideal applicability in these environments. So it is necessary to model sea clutter in littoral environment. In order to develop a really meaningful sea clutter model, relationship between sea clutter and parameters of sea conditions need to be studied. The wave height is a major influencing factor among these parameters of sea conditions. In this paper, experimental data used to study the relationship between sea clutter and wave height. These data sets were collected by using L-band step frequency radar of China Research Institute of Radiowave Propagation in Qingdao City, Shandong Province. Firstly, the effects of wave height factor in these representative sea clutter models are compared and analyzed. Secondly, through the analysis of multiple sets of real recorded data, combined with the marine environment parameters, the availability of wave height factor is studied. Lastly, the parameters of relationship of wave height and sea clutter are obtained. These work play an important role in establishment of sea clutter in littoral environment.

D-InSAR Atmospheric Delay Correction by MODIS and GPS — A Case of Xi'an

Cheng-Sheng Yang, **Qin Zhang**, **Chao-Ying Zhao**, **and Wu Zhu**
Institute of Geological Engineering and Surveying, Chang'an University, Xi'an 710054, China

Abstract— Repeat track Interferometric Synthetic Aperture Radar (InSAR) has been widely used in the Earth surface topography and surface deformation monitoring, which has become one of indispensable space-to-earth observation technologies. However, the atmospheric effect, especially atmospheric water vapor content changing in time and space cause the radar signal delay, is one of the main error sources, and it is difficult to eliminate. The atmospheric effect has become a major constraint factors to improve accuracy of InSAR. So the atmospheric effect has greatly limited the application of differential InSAR in the slow and small magnitude surface deformation area.

Thus, it must be considered, analyzed and to eliminate the impact of atmospheric delay in high precision differential InSAR monitoring. Moderate Resolution Imaging Spectroradiometer (MODIS), as an important sensor of National Aeronautics and Space Administration (NASA) Earth Observing System (EOS), can provide the worldwide atmospheric water vapor products under the clear sky conditions. Especially, Terra satellite, which carried the MODIS sensor, has the same near-polar sun-synchronous orbit as ERS-2 and Envisat, and they also pass the same area nearly the same time that it is possible to correct atmospheric delay phase in differential InSAR results by MODIS data. However, the MODIS Precipitable Water Vapor value has a bias with the actual value, leaded by the measurement error in MODIS near-infrared sun reflected radiation channel. On the other hand, the Global Positioning System (GPS) have been able to obtain Precipitable Water Vapor value (PWV) with a high precision under all-weather. Therefore, we can make use of GPS data to correct MODIS Precipitable water vapor product, which can improve the accuracy of atmospheric correction in differential InSAR results.

This paper collected two Envisat data, acquired June 18, 2005 and April 29, 2006, MODIS data and terms GPS data. After analyzing the MODIS PWV correction model, this paper did an atmospheric delay correction experiment using MODIS data. The main research content is as follows:

1, studying the conversion factor between PWV with the zenith wet delay ZWD, considering the variation of season and latitude;
2, studying the correction model of MODIS PWV using seven terms GPS data from 2006.6 to 2009.6 and ground meteorological data in Xi'an;
3, doing an atmospheric delay correction experiment using MODIS and Envisat SAR data.

Simulation of Beam Filling Effect on Spaceborne Precipitation Radar Rainfall Retrieval

Honggang Yin[1], **Ailan Lan**[2], **and Hu Yang**[1]

[1]National Satellite Meteorological Center, China
[2]Center for Space Science and Applied Research CAS, China

Abstract— Global precipitation measurement is essential not only for the climate modeling and weather forecasting but also for the research of the global change. Since the earth surface is mostly covered by sea water, it is necessary to observe this important atmospheric variable from space. It is more attractive to use spaceborne radar to measure precipitation than to use passive techniques, because it is able to provide the most overall detection of rainfall field that can be thought currently. The Precipitation Radar (PR) aboard the Tropical Rainfall Measuring Mission (TRMM) satellite is the first-ever spaceborne instrument. A spaceborne radar like the Dual-frequency Precipitation Radar (DPR) on the Global Precipitation Measurement (GPM) core satellite, which will be installed on the FengYun-3 Precipitation Measurement Satellite (FY3 PMS), is also being developed in China. The parameters measured by all these spaceborne radars are the radar reflectivity factor and the path integrated attenuation (PIA), and they are usually assumed to be uniform within the antenna beam in order to estimate rain rate quantitatively. It means that the rainfall is uniformly spread within a range of a few kilometers, because the instantaneous fields of view of these spaceborne precipitation radar are about 5 km. Such an assumption may be valid for widespread stratiform rain. While in most cases of convective rain, the footprint size of spaceborne radar is larger than the rain cell size, then the reflectivity and the PIA are not accurate due to nonuniform beam filling. As a result, the retrieved rain rate is also biased. In this paper, beam filling effects on spaceborne precipitation radar are investigated theoretically according to whether rain attenuation can be neglected. And then data from the Airborne Rain Mapping Radar (ARMAR) are used to simulate observations of spaceborne precipitation radar with different beam width.

Comparison of ASAR IM Data and ASAR WS Data in Investigating Co-seismic Deformation of Yutian Earthquake

Xi'ai Cui[1], **Qiming Zeng**[1, 2], **Cunren Liang**[1], **and Jian Jiao**[1]

[1]Institute of Remote Sensing and GIS, Peking University, Beijing 100871, China
[2]Key Lab of Spatial Information Integration and Applications of Beijing Municipal Peking University, Beijing 100871, China

Abstract— An Ms7.3 earthquake occurred in Yutian (Mar. 21, 2008 local time in China), which is located in Xinjiang Province, several hundred kilometers north of the convergent India-Eurasia plate boundary. Up to 2,200 houses were damaged or flattened and four houses collapsed. The earthquake cost great direct economic losses. In our research, we use Differential Interferometric Synthetic Aperture Radar (D-InSAR) technology to study the co-seismic deformation of the Yutian earthquake and get IM/IM interferogram and WS/WS interferogram. The IM/IM interferogram has fair fringes, showing the deformation clearly in two dimensions. And in the IM/IM interferogram we can find that 105 km width of the IM mode data is not enough to cover the northwestern region of the fault. Due to the limited coverage of IM mode data we can not get the complete co-seismic deformation field. The 405 km width of the WS mode data can overcome this shortcoming. And in the displacement result using the WS data, we can clearly observe that the northwestern region falls and the southeastern region rises. The maximum falling amount is 54 cm and the maximum rising amount is 65 cm. Both the IM/IM interferogram and the WS/WS interferogram can provide useful information about this specific earthquake for the seismological researchers. By comparing the two modes (IM and WS) in investigating co-seismic deformation of the earthquake, we can get more reliable conclusion about Yutian Earthquake.

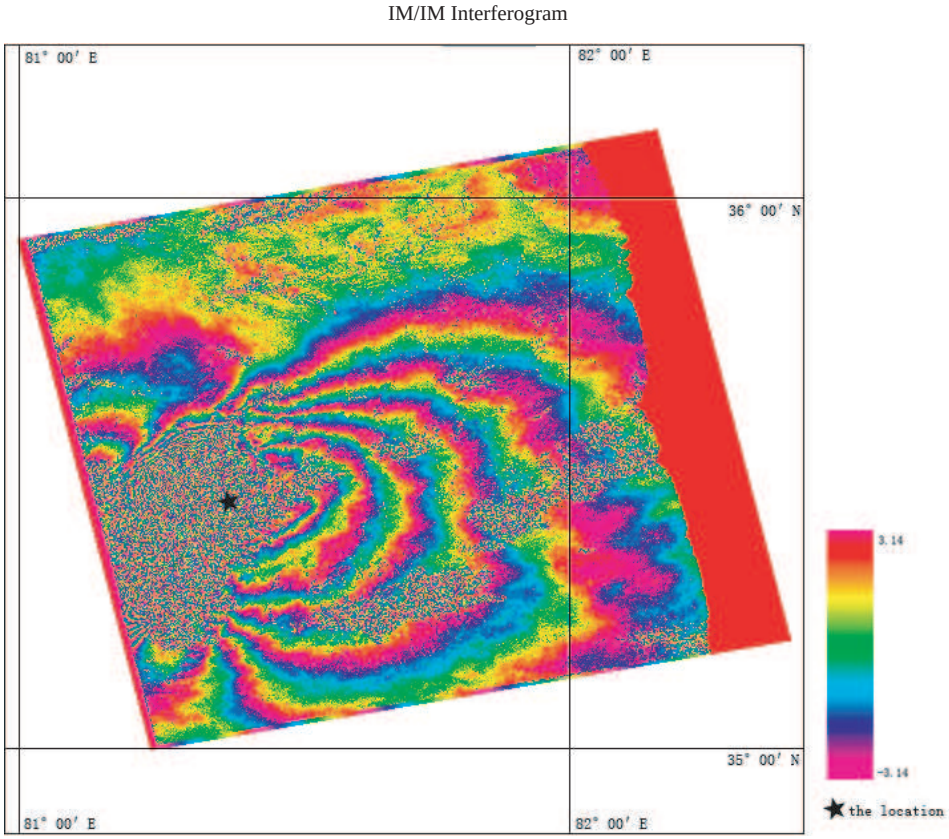

Figure 1: Interferogram of the Image Mode data track 155. (Master: 20080222, Slave: 20080502; Vertical Baseline: −28.2 m).

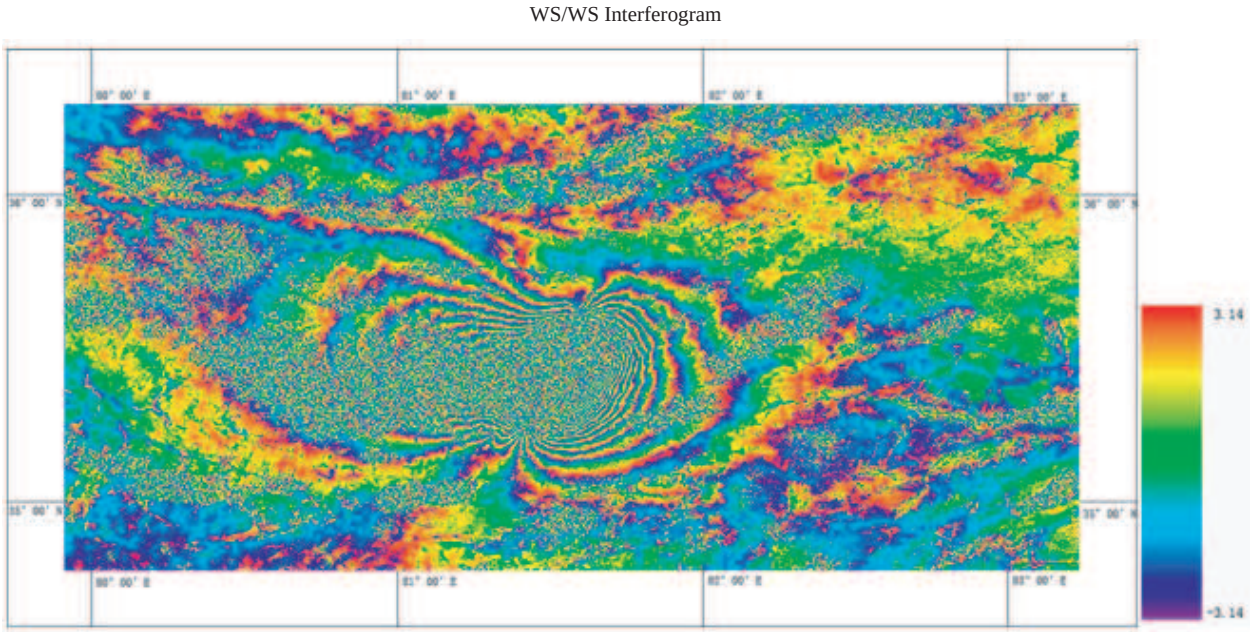

Figure 2: Interferogram of the Wide Swatch data. (Master: 20071129, Slave: 20080417; Vertical Baseline: 182.5 m).

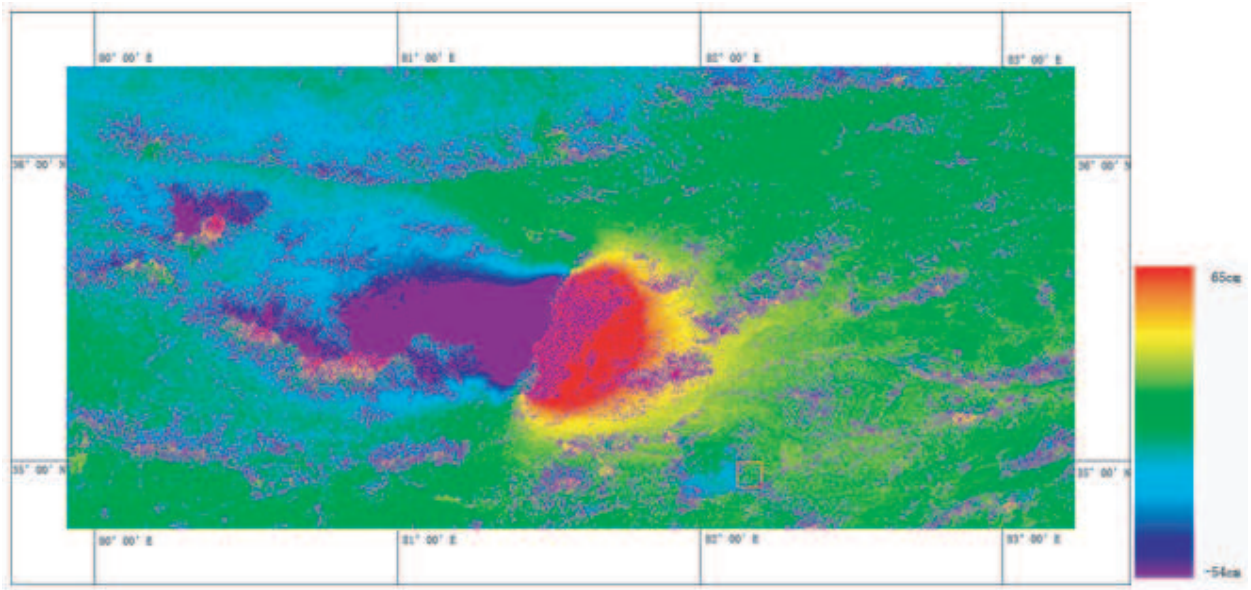

Figure 3: Displacement of Yutian using WS data. (Negative value stands for falling; Positive value stands for rising).

Field Campaigns by Multi-frequency and Multi-polarized Synthetic Aperture Radars in the Coastal Area of South Korea

Chan-Su Yang[1], **Kazuo Ouchi**[2], **and Kazuki Nakamura**[3]

[1]Ocean Satellite Research Group, Korea Ocean Research and Development Institute
Sa2-dong 1270, Sangnuk-gu, Ansan, Gyeonggi-do 426-744, Korea
[2]Department of Information Science, School of Electrical and Computer Engineering
National Defense Academy, 1-10-20, Hashirimizu, Yokosuka 239-8686, Japan
[3]GEO Grid Research Group, Information Technology Research Center
National Institute of Advanced Industrial Science and Technology (AIST)
Central 2, Umezono1-1-1, Tsukuba, Ibaraki 305-8568, Japan

Abstract— Synthetic aperture radar (SAR) is a powerful sensor for ship and oil detection, and intertidal zone and land use monitoring, etc. because of its ability to penetrate cloud cover and day-and-night observation capability, and a substantial number of papers have been reported on this issue. When using spaceborne SARs, the main problem is long repeat cycles, some of which are over 40 days. Use of multiple identical SARs such as COSMO-SkyMed and SAR-Rupe series is a solution. Another way is to use multiple available SAR sensors. In this study, three different SARs can be combined L-band ALOS-PALSAR (Advanced Land Observing Satellite — Phased Array L-band SAR), C-band ENVISAT ASAR (Advanced SAR), and X-band TerraSAR-X which were obtained at 13:23 h, 13:46 h, and 21:43 h on June 3, 2009, respectively, over the west coastal area of South Korea. There are a high volume of ship traffic, intertidal zones, and various land uses such as land reclamation, vegetation area, and paddy fields. The PALSAR and TerraSAR-X sensors can control the polarization directions of both transmitted and received microwave signals. Therefore, it is possible to observe in HH, HV, VH and VV modes. This paper also provides preliminary results of comparative evaluation of multi-frequency and multi-polarized SAR backscatter to the targets: ship, intertidal zone, and paddy field.

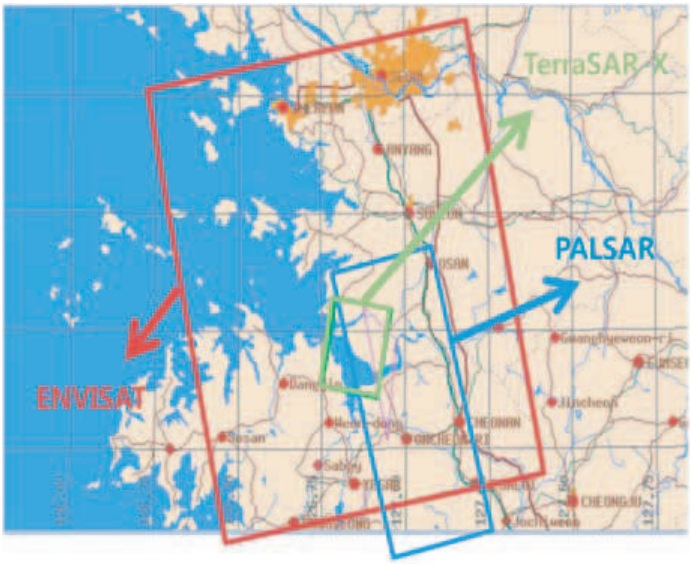

Figure 1: Multi-frequency observation using ENVISAT ASAR (C-Band), ALOS PALSAR (L-Band), and TerraSAR-X (X-Band) at 13:23 h, 13:46 h, and 21:43 h on June 3, 2009, respectively over the west coastal area of South Korea.

Interpretation of First-year Sea Ice Parameters by Multi-frequency and Multi-polarized Synthetic Aperture Radars in Kongsfjorden, Svalbard: Recent Results from the Spring 2009 Measurement

Chan-Su Yang[1], **Kazuo Ouchi**[2], **and Kazuki Nakamura**[3]

[1]Ocean Satellite Research Group, Korea Ocean Research and Development Institute
Sa2-dong 1270, Sangnuk-gu, Ansan, Gyeonggi-do 426-744, Korea
[2]Department of Information Science, School of Electrical and Computer Engineering
National Defense Academy, 1-10-20, Hashirimizu, Yokosuka 239-8686, Japan
[3]GEO Grid Research Group, Information Technology Research Center
National Institute of Advanced Industrial Science and Technology (AIST)
Central 2, Umezono1-1-1, Tsukuba, Ibaraki 305-8568, Japan

Abstract— Large regions of the Polar Oceans are covered by sea ice. The ice has a profound impact on the exchange of heat, momentum, and matter between the ocean and the atmosphere, on the solar albedo of the ocean, and on deep ocean circulation. Information about sea ice conditions are needed for ship navigation, fisheries, or oil and gas's exploration, in geo and biophysical studies, and in climate research. Remote sensing by Synthetic aperture radar (SAR) is the most important method of observing sea ice on a regional scale independent of cloud cover and daylight conditions. In Arctic Ocean, its repeat cycle is less than half day, and when multiple satellites used, the SAR observation would be possible in two or three hours.

Sea ice is a complex, polycrystalline composite of pure ice with random brine, air pockets and snow layers. Its backscatter depends on many physical parameters, such as surface roughness, salinity, air, crystal structure, snow cover and others. Two major mechanisms: (1) surface scattering and (2) volume scattering are taken into consideration in describing the dependence of the backscatter coefficient on several sea ice properties. The penetration depth of radar waves into the sea ice is determined by its complex dielectric constant. When it is large, there is little transmission into the material, and thus little or no volume scattering can take place. The complex dielectric constant of sea ice strongly depends on the distribution of liquid brine and air pockets within the sea.

Fast ice in Kongsfjorden of Svalbard consists solely of seasonal ice, i.e., ice that melts completely in summer. Each autumn and winter, new fast ice forms. Sea ice formed during the current winter contains typically from 6 to 10 psu salinity, enough to limit the penetration of C-band radar waves into the ice to a few centimeters [1]. Therefore, the backscatter from first-year ice is dominated by surface scattering. In this study, three different SARs were used L-band ALOS-PALSAR (Advanced Land Observing Satellite — Phased Array L-band SAR), C-band ENVISAT ASAR (Advanced SAR), and X-band TerraSAR-X over Kongsfjorden of Svalbard. In this study, methods of sea ice monitoring using synthetic aperture radar are addressed. The influence of sea ice properties such as surface roughness or volume structure on the observed radar signatures is explained, also considering environmental effects.

REFERENCES

1. Shokr, M., "Field observations and model calculations of dielectric properties of Arctic sea ice in the microwave C-band," *IEEE Transactions on Geoscience and Remote Sensing*, Vol. 36, No. 2, 463–478, 1998.

Design of Electrometric Amplifier for Aspiration Condenser Measurement

Z. Roubal and M. Steinbauer
Faculty of Electrical Engineering and Communication, Brno University of Technology
Kolejní 2906/4, Brno 612 00, Czech Republic

Abstract— It was confirmed that concentration light air ions have positive influence on the human health. When measuring concentration of light air ions using aspiration condenser, we meet with problems related to measurement of very low current of order 10^{-12} A. In this paper will be analyze possible sources of error, caused by noise, thermoelectric voltage, real properties of used OZ and leakage current. Taking it into account, some equivalent circuit models will be introduced. Based on these models, a new electrometric amplifier will be designed with minimalised systematic error and this design will be verified.

REFERENCES

1. Charry, J. M. and R. Kavet, *Air Ions: Physical and Biological Aspects*, CRC Press, Inc., Boca Raton, Florida, 1987.
2. Tammet, H. F., *The Aspiration Method for Determination of Atmospheric-Ion Spectra*, IPST, Jerusalem, 1970.
3. Tardif, A. "Remarks on the construction and design of a solid-state photometer for astronomy," *International Amateur-Professional Photoelectric Photometry Communication*, No. 12, 41–59, 1983.
4. Burkhardt, W., M. Iacopini, and P. Maranesi, "Picoammeter for ion chamber spans six decades without range switching," *IEEE Transactions on Nuclear Science*, Vol. 30, No. 1, 311–313, 1983.
5. Vojtek, T., T. Skoupil, P. Fiala, and K. Bartušek, "Accuracy of air ion field measurement," *PIERS Online*, Vol. 2, No. 4, 412–415, 2006.
6. Steinbauer, M., P. Fiala, K. Bartušek, and Z. Szabó, "Experiments with accuracy of air ion field measurement," *PIERS Proceedings*, 1062–1066, Hangzhou, China, March 24–28, 2008.

Calculation of Angstrom Coefficient of Nano-size Particles in Liquid Environment

Gholamreza Shayeganrad[1], **Leila Mashhadi**[2], **and Tahereh Ghanbarirad**[1]

[1]Islamic Azad University, Karaj Branch, Karaj, Iran
[2]Physics Department, Amirkabir University of Technology, Tehran, Iran

Abstract— One of the optical properties of nano-size particles in the liquid environment is the optical thickness. Optical thickness is measure of amount direct light reaching a detector that respond to a single wavelength of light. It is affected by absorption and scattering. The portion of optical thickness due to nanoparticles is called nanoparticles optical thickness or nanoparticles optical depth, τ. In this work we have shown that τ can be related to percent transmission of direct light. Moreover, the Angstrom coefficient is defined which express the wavelength dependence of extinction coefficient, $\propto$. The obtained values of $\propto$ can be used in principle to evaluate particle size and determine the size distribution of the particles.

Electromagnetic Properties of Surface Waves on Multilayer Absorbing Coated Plane

H. Y. Yao
Temasek Laboratories, National University of Singapore, Singapore

Abstract— Zenneck investigated surface waves guided by a plane interface between two different materials in 1907, which was named as Zenneck wave. This kind of electromagnetic wave is an inhomogeneous plane wave, which has characteristics of an exponential decay over the wavefront with increase of distance from the interface and having a propagation constant along the interface. Since then, many theoretical studies about surface waves on various material interfaces have been made, such as, dielectric coated plane/cylinder and corrugated plane/cylinder. Moreover, applications in different areas have been discussed, which are (a) transmission system; (b) surface-wave aerials; (c) frequency selective surface (FSS); (d) electromagnetic compatibility (EMC). In this paper, our objectives are to investigate the characteristics of surface waves, and then to design the proper structure to perform the efficient transformation from space waves to surface waves. This is to explore the application of backscattered power reduction.

A structure of multilayered absorbing materials supported by a perfect conducting plane, which is illuminated by a plane wave, is analyzed by using the transmission-line theory (TLT) in this paper. The dispersion equation is derived from the equivalent transmission-line circuit for propagation along the normal direction of the surface. Subsequently, propagation constant, constant phase/amplitude fronts and the reflection coefficient are obtained. Finally, the constitutive parameters of the materials and geometric parameters of the structure are designed to obtain high launching efficiency for surface waves by applying the optimization algorithm (Evolutionary Algorithm). We give a two-layer structure as an example. The corresponding numerical results are presented. It is shown that the effective transformation from space waves to surface waves is possible, which leads to great reduction in reflection coefficient. The numerical results elucidate the potential for reducing the backscattered power.

Application of Genetic Algorithm for of a Partially Immersed Non-uniform Conductivity Cylinder

Wei Chien[1], **Hua-Pin Chen**[2], **Chi-Hsien Sun**[3], **Chien-Ching Chiu**[3], **and Yi Sun**[4]

[1]Electronic Engineering Department, De Lin Institute of Technology
Tu-Cheng, Taiwan, R.O.C.
[2]Department of Electronic Engineering and Institute of Electronic Engineering
Ming Chi University of Technology, Taiwan, R.O.C.
[3]Electrical Engineering Department, Tamkang University
Tamsui, Taiwan, R.O.C.
[4]School of Electrical Engineering, Beijing Jiaotong University, Beijing, China

Abstract— We consider the inverse problem of determining both the shape and the conductivity of a partially immersed non-uniform conductivity cylinder from knowledge of the far-field pattern of TM waves by solving the ill posed nonlinear equation. Based on the boundary condition and the measured scattered field, a set of nonlinear integral equations is derived and the imaging problem is reformulated into an optimization problem. The genetic algorithm is then employed to find out the global extreme solution of the object function. As a result, the shape and the conductivity of the conductor can be obtained. Numerical results are given to demonstrate that even in the presence of noise, good reconstruction has been obtained.

An Iteration Method for Solving the Asymptotic Equation of Optically Thick Layers

Guangyuan Zhao[1] and Xianming Sun[2]

[1]School of Computer Science and Technology
Shandong University of Technology, ZiBo, Shandong 255049, China
[2]School of Electrical and Electronic Engineering
Shandong University of Technology, ZiBo, Shandong 255049, China

Abstract— The radiation inside and emerging from a plane-parallel homogeneous atmosphere with a general law of single scattering and with arbitrary optical thickness can be calculated using various computational schemes. However, the solution of these methods becomes increasingly difficult as optical thickness increases. Consequently, it is very important that simple asymptotic expressions for the quantities characterizing the radiation field may be found for particles layers of large optical thickness. The asymptotic relations have been derived by various authors using different methods. The relations show that the reflected intensity can be expressed in especially simple functional forms.

In spite of the advantages of the asymptotic theory, it is difficult to apply them directly for the calculation of the reflection functions of particle layers. This is because they include two unknown function, i.e., escape function and reflection function of semi-infinite layer, and three unknown constants. Van De Hulst suggested using an asymptotic fitting method whereby computational results from the doubling method are fit to known general forms of the asymptotic equations. Nakajima and King derived matrix equation for computing the functions and constants that appeared in the asymptotic expressions by using discrete ordinates method of radiative transfer.

In this paper, we use an iterative method to solve the Ambartsumian's nonlinear integral equation, suggested by Mishchenko et al., by expanding the phase function in a Legendre polynomial series. The diffusion pattern and the diffusion exponent are obtained by solving a characteristic equation with a combination of the normalization condition of diffusion pattern and the so-called Sobolev-Van De Hulst relation. After these have been determined, escape function is obtained by iteration of an integral equation for it. This is a simple and accurate technique for computing the functions and constants included in the asymptotic expression. The formulation for computation of the asymptotic expression is summarized in Section 2. Comparisons of the accuracy of this method with asymptotic fitting and discrete ordinates methods are presented in Section 3, followed by a conclusion presented in Section 4.

Depolarization and Polarization of Light Scattering by Dustlike Tropospheric Aerosols

Xianming Sun and Haihua Wang
School of Electrical and Electronic Engineering
Shandong University of Technology, ZiBo, Shandong 255049, China

Abstract— Tropospheric aerosols are thought to cause a significant direct and indirect climate forcing, but the magnitude of this forcing remains highly uncertain because of poor knowledge of global aerosol characteristics and temporal changes [1]. Microphotographs of naturally occurring dustlike aerosols show a highly variable shapes and a great variability of the particle aspect ratio (ratio of the largest to the smallest particle dimensions), and laboratory and in situ measurements for natural sand and dust particles show that in most case, phase function are relatively smooth and featureless, especially at side-scattering angles [2]. However, any particle shape, either spherical or nonspherical, produces its own, shape-specific scattering parttern. Two well know examples are provided by halos produced by single or aggregated hexagonal particles and by rainbows produced by spheres [3, 4]. So, it makes questionable the ability of spherical or a single nonspherical shape to represent scattering properties of the natural sand and dust aerosols, but our calculation show that the phase function of the natural dust particles can be adequately modeled using a wide aspect-ratio distribution of spheroidal gains, although natural dust particles are, of course, not perfect spheroids.

On the other hand, in order to retrieve the aerosol properties, most current and proposed satellite remote sensing of tropospheric aerosols relies upon radiance measurement that are interpreted using algorithms that determine best fits to precalculated scattered sunlight for one or more "standard" aerosol models, but this can pose a severe uniqueness problems [5]. Experience and theory have demonstrated that the measurements of polarization as well as the radiance can resolve such uniqueness problem [5], and the measurements of the linear and circular depolarization ratios at the backscattering direction are also a powerful remote sensing technique for characterizing the microphysics of aerosol particles. Unfortunately, the arrangement of source of light and detector usually precludes laboratory measurement at scattering angle close to 0° and 180°. This makes experimental determinations of phase matrix and depolarization ratios in the backscattering direction (180°) very difficult and greatly enhances the importance of accurate theoretical calculation.

Based on these two questions, we modeled the dustlike aerosols using shape distributions of polydisperse, randomly oriented spheroids with refractive indices and size distributions representative of naturally occurring dust aerosols, and we evaluated the depolarization and polarization characteristics of light scattering by dustlike aerosols using the **T**-matrix method.

Error Analysis of Using Henyey-Greensterin in Monte Carlo Radiative Transfer Simulations

Guangyuan Zhao[1] and Xianming Sun[2]

[1]School of Computer Science and Technology
Shandong University of Technology, ZiBo, Shandong 255049, China
[2]School of Electrical and Electronic Engineering
Shandong University of Technology, ZiBo, Shandong 255049, China

Abstract— When studying multiple scattering in planetary atmospheres using Monte Carlo methods, the real phase functions should be simulated using the statistical method to define the new photon direction after each scattering event. However, the angular characteristics of the atmosphere particles, even if the particles are assumed spherical, can not be approximated with sufficient accuracy by asymptotic expressions based on geometrical optics or Green's function approximations.

Usually we model the phase function using the Henyey-Greenstein or modified Henyey-Greenstein with as precise a value of asymmetry factor g as possible. But even in this case, these functions are sometimes a poor approximation of real phase function. Instead of using these phase function, we propose to simulate real phase function directly. Though this means an increase in calculation time, this will improve the computation accuracy.

This paper is organized as following, in Section 2, we introduce the computation of different phase function, for example, the Mie phase function for spherical atmosphere particles, the phase function of hexagonal ice crystal evaluated by geometrical optics method, and the spheroidal phase function calculated by T-matrix method. In Section 3, we give the Monte Carlo simulations of Henyey-Greenstein and other real functions, and compare each of them. Section 4 provides the simulated results in Monte Carto multiple scattering, and we will analyze the errors and the reasons.

2-D Image Reconstruction from Microwave Scattering Data

Jie Li and Jiadong Xu
School of Electronics and Information, Northwestern Polytechnical University, Xi'an, China

Abstract— Microwave imaging has found many applications in the nondestructive testing, geophysical exploration, and biomedical imaging. The microwave imaging based on the diffraction tomography is relatively straightforward to implement and usually efficient in computation due to the linearization of the problem.

The interpolation methods and the conversion of coordinate have been studied in this paper. According to the Fourier Diffraction Theorem, the object function may be recovered by inverse Fourier transform. The conversion between samples in frequency domain over circular arcs and samples over a rectangular lattice is necessity for the convenience of inverse FFT. Three interpolation methods, the nearest-neighbor, bilinear, and bi-sinc interpolation, are chosen to balance imaging accuracy and efficiency. Although the conversion from rectangular lattices to polar-like coordinate has been discussed in some proposed paper, but the relationship of interpolation methods and the conversion method is seldom presented. The transformations between rectangular and polar-like coordinates are presented according to different methods. In order to get more accurate result, the samples should be much denser, which means a larger $M \times N$ number and longer time in calculating interpolated values. That is the reason we choose the bi-sinc method, which is based on the 1-D sinc interpolation, to save computation time in interpolating values from truncated data.

In this paper a 2-D lossless cylindrical object is imaged use different interpolation methods. It is concluded that the nearest neighbor interpolation is more convenient in the rectangular coordinate, whereas the bilinear and bi-sinc interpolation methods are better in polar-like coordinate. The bi-sinc interpolation method is a good balance between time and accuracy. It consumes less time and gets more accurate image.

Surface Plasmon Resonance Absorption in a Multilayered Bigrating

T. Suyama[1], **Y. Zhang**[2], **Y. Okuno**[1], **Z. Luo**[1], **and T. Matsuda**[3]

[1]Graduate School of Science and Technology, Kumamoto University, Japan
[2]Department of Physics and Electronic Information, Wenzhou University, China
[3]Kumamoto National College of Technology, Japan

Abstract— Metal film grating has an interesting property known as the resonance absorption [1], which causes partial or total absorption of incident light energy. The absorption is associated with the excitation of surface plasmons on a grating surface: An incident light couples with surface plasmons via an evanescent spectral order generated by the grating [2]. The resonance absorption in metal film grating has been the subject of many theoretical and experimental investigation in connection with chemical sensing [3], surface enhanced phenomena such as second-harmonic generation and Ramman scattering [4], and photonic band gaps [5]. Most of studies on the resonance absorption have mainly dealt with a thin metal film grating whose surfaces are periodic in one direction [6, 7]. Doubly periodic metal film grating, i.e., periodic in two directions, also causes the plasmon resonance absorption as well as singly periodic grating [8]. The absorption in a doubly periodic metal grating has been of considerable interest since we can expect more complex behaviors in the absorption phenomena [9] by virtue of the presence of double periodicity and multilayer structure. In this paper we investigate the resonance absorption of a multilayered bigrating, which consists of dielectric and metallic thin-films corrugated periodically in two directions. We describe a numerical algorithm based on Yasuura's method [10] for analyzing diffraction of a plane wave by a multilayered bigrating. Using the algorithm we numerically examine characteristics of the resonance absorption in the multilayered bigrating.

REFERENCES

1. Raeter, H., "Surface plasmon and roughness," *Surface Polaritons*, 331–403, V. M. Argranovich and D. L. Mills (eds.), North-Holland, New York, 1982.
2. Nevièr, M., "The homogenous problem," *Electromagnetic Theory of Gratings*, 123–157, R. Petit (ed.), Springer-Verlag, Berlin, 1980.
3. DeGrandpre, M. D. and L. W. Burgess, "Thin film planar waveguide sensor for liquid phase absorbance measurement," *Anal. Chem.*, Vol. 62, 2012–2017, 1990.
4. Nevièr, M., R. Reinisch, and D. Maystrel, "Surface enhanced second-harmonic generation at a silver grating: A numerical study," *Phys. Rev. B*, Vol. 32, No. 6, 3634–3641, 1994.
5. Barnes, W. L., T. W. Preist, S. C. Kitson, J. R. Sambles, N. P. K. Cotter, and D. J. Nash, "Photonic gaps in the dispersion of surface plasmons on gratings," *Phys. Rev. B*, Vol. 51, 11164–11167, 1995.
6. Chen, Z., I. R. Hooper, and J. R. Sambles, "Strongly coupled surface plasmons on thin shallow metallic gratings," *Phys. Rev. B*, Vol. 77, 161405, 2008.
7. Okuno, Y. and T. Suyama, "Numerical analysis of surface plasmons excited on a thin metal grating," *Journal of Zhejiang University — Science A*, Vol. 7, No. 1, 55–70, 2006.
8. Inagaki, T., J. P. Goudonnet, J. W. Little, and E. T. Arakawa, "Photoacoustic study of plasmon-resonance absorption in a bigrating," *J. Opt Soc. Am. B*, Vol. 2, No. 3, 433–439, 1985.
9. Matsuda, T., D. Zhou, and Y. Okuno, "Numerical analysis of plasmon resonance absorption in bisinusoidal metal gratings," *J. Opt Soc. Am. A*, Vol. 19, No. 4, 695–701, 2002.
10. Yasuura, K., "A view of numerical methods in diffraction problems," *Progress in Radio Science 1966–1969*, 257–270, W. V. Tilson and M. Sauzade (eds.), URSI, Brussels, 1971.

A Low-frequency RCS Measurement System in an Anechoic Chamber

C. F. Hu[1, 2], J. D. Xu[1], N. J. Li[2], and L. X. Zhang[2]

[1]Electronic Engineering Department, Northwestern Polytechnic University, China
[2]National Key Laboratory of UAV Specialty Technique, Northwestern Polytechnic University, China

Abstract— A practical RCS measurement system on low-frequency (VHF/UHF) is constructed in an anechoic chamber. Stepped-frequency signal generated by a network analyzer is transmitted by a log-periodic dipole antenna (LPDA). Another LPDA close to the transmitting antenna is applied to receive echoes. The rotation velocity of support and the interval of sample are controlled by a centre computer. With the revolving stage rotating, a trigger signal is sent to the network analyzer and the measurement begins. Many kinds of DSP techniques are employed to remove unwanted signals. Firstly, the frequency-domain data of background are subtracted from that of targets. Then high resolution time-domain response is got by inverse fast Fourier transform (IFFT), which reflects scattering distribution of the whole chamber. The energy of target area can be chosen by a time-domain gating which removes the coupling between antennas and other clutters. For expanding effective bandwidth, a low side lobe window function is adding to the frequency-domain data before gating. After scaling at the Rayleigh region of metal sphere, the accurate low-frequency RCS can be obtained. Experimental results show that the valid data waved less than ± 1 dB can be got over UHF band for a metal sphere with 15 cm diameter, and the precision of ± 2 dB is obtained on parts of VHF band.

Analytical Solutions of TD Scattering Fields from Parabolic Reflector Antenna Illuminated by Plane Waves and Gaussian Beams

Shih-Chung Tuan[1] and Hsi-Tseng Chou[2]

[1]Department of Communication Engineering, Oriental Institute of Technology
Taipei, Taiwan
[2]Department of Communication Engineering, Yuan Ze University
Chung-Li, Taiwan

Abstract— The increasing interests in the use of ultra-wideband or short pulse antennas for the target identification and remote sensing applications have driven the efforts to obtain direct time domain (TD) solutions in the electromagnetic (EM) analysis. This paper develops an Analytic Analysis of Transient Scattering from a parabolic reflector antenna illuminated by an Incident Plane Wave and electromagnetic (EM) fields of a general astigmatic Gaussian Beam (GB) respectively. The time domain transient analysis of Time Domain Physical Optical (TDPO) for parabolic reflector antenna illuminated by plane wave and TDPO with analytic time transform (ATT) for parabolic reflector antenna illuminated by Gaussian Beam (GB) are presented. It is obtained by analytically inverting, in closed-form, the corresponding frequency-domain (FD) solution based on physical optics (PO) integral, and coincidently can be decomposed in terms of reflection and diffraction effects as usually described in high-frequency asymptotic solutions. The ATT allows complex formulations with complex time variations in TD, and is thus able to treat the complex propagation phases resulted from a GB illumination on the reflector.

THz Bessel Beams Generated by BOEs

Yanzhong Yu
School of Science, Quanzhou Normal University
Quanzhou, Fujian 362000, China

Abstract— Bessel beams, which are one family of diffraction-free beams, were discovered for the first time by Durnin and co-worker in 1987. In the cylindrical coordinates system an ideal Bessel beam can be given by:

$$E_n(\rho, \phi, z) = E_0 J_n(k_\perp \rho) \exp(ik_z z) \exp(in\phi)$$

where E_0 is a constant, J_n denotes the nth-order Bessel function of the first kind, $\rho^2 = x^2 + y^2$, $k_\perp^2 + k_z^2 = (2\pi/\lambda)^2$, $k_\perp$ and k_z are the radial and longitudinal wave numbers, respectively, λ is a wavelength in free space. The central spot of the zero-order Bessel beam (denoted by J_0) is always bright; whereas that of all the higher-order Bessel beams (denoted by J_n, n is an integer and ≥ 1) is always dark on axis surrounded by concentric rings whose peak intensities decrease as ρ^{-1}. Since perfect Bessel beams own lots of novel characteristics and therefore have many promising applications, such as imaging, alignment and measurement, the study of generation and applications of these beams has been widely carried out in various fields, including optics, acoustics and the relevant science of physics. Numerous methods for generating Bessel beams have been presented and demonstrated, one of which is using binary optical elements (BOEs), whose diffractive fields are calculated by scalar diffraction theory, to convert an incident beam into Bessel light beam.

In view of the high diffraction efficiencies of BOEs, they are thus used to create Bessel beams at THz frequencies in our design. The conventional design approaches, based on scalar theory, are no longer suitable, as the feature sizes of BOEs used are on the order of or smaller than the submillimeter wavelengths. Accordingly, the rigorous electromagnetic analysis method, such as MOM, FEM and FDTD, should be employed to calculate the fields diffracted by BOEs. However, it is known that the full three-dimensional (3-D) analysis demands excessive computational memory and time. So the optimization design method is typically classified as computationally intensive and becomes an intractable problem. Two measures are applied to conquer this difficulty in our design, that is, a body-of-revolution finite-difference time-domain (BOR-FDTD) method and a microgenetic algorithm (MGA). Simulation results demonstrate that the designed BOEs can not only produce arbitrary order Bessel beams, also have higher diffraction efficiencies when compared with amplitude holograms.

Creation of Approximate Bessel Beams by Use of a Fractal Conical Lens

Yanzhong Yu
School of Science, Quanzhou Normal University, Quanzhou, Fujian 362000, China

Abstract— In 1987, Bessel beams were introduced by Durnin and co-workers in optics for the first time. Ideal Bessel beams own many novel properties, such as long depth of fields, propagation invariant and reconstruction, and therefore have lots of potential applications. Ideal Bessel beams extend infinitely in the radial direction and contain infinite energy, and therefore physically generated Bessel beams are only an approximation to the ideal. Numerous approaches for producing Bessel beams have been suggested, among of which using axicon is the simplest and most effective method.

An axicon, which was first introduced in 1954 by McLeod, is a specialized type of lens and has a figure of revolution. Generally speaking, axicons can be divided into three main types, i.e., refractive axicons (conical lenses), reflective axicons (conical mirrors), and diffractive axicons (circular diffraction gratings). An axicon images a point source into a focal line along the optic axis, and this line can be approximated by a Bessel-type (nondiffracting) beam that has extremely narrow intensity profile and yet possesses a very large depth of field. These properties of an axicon have many potential applications in imaging, alignment, laser machining, etc., and the number of axicon applications has also increased significantly in the last few years. Accordingly, much interest has been provoked in design and analysis of axicons. Recently many novel axicons, such as fractal conical lenses, Fresnel axicons, and fractal axicons, have been proposed and investigated. However, all of these axicons are analysed by scalar approximate theory in optics. But at our interesting band, i.e., mm- and sub mm-wavelengths, it is known that the scalar-based analysis method is usually not suitable for calculating the fields diffracted by an axicon. Therefore, the present work applies 2-D FDTD method in conjunction with Stratton-Chu formulas to analyze the fields diffracted by a fractal conical lens. The analysis results and conclusions are given.

Ku-band Balanced Resistive FET Mixer with Very Low IMD3

R. A. Sadeghzadeh[1], **A. R. Eskandari**[2], **and M. A. Honarvar**[3]

[1]Department Electrical Engineering, Khajenasirtoosi University, Tehran, Iran
[2]Islamic Azad University, East Tehran Branch, Tehran, Iran
[3]Islamic Azad University, Najafabad Branch, Isfahan, Iran

Abstract— The most commonly used mixers in microwave systems employ Schottky-barrier diodes as the mixing elements. The active elements such as FETs which is used for fabrication of microwave mixers, not only can improve the conversion loss but also causes appearing conversion gain. Disadvantages of active mixers in comparison with Schottky-barrier mixers, are instability and more complicated bias circuits. Simplicity of bias circuits, is obtained by using the resistive region of FET, furthermore it decreases probability of instability. On the other hand, because of the very weak nonlinearity of channel resistance, the mixer generates very low intermodulation products and results in high 1-dB compression point.

Table 1: Table of the comparison between simulation and measurement.

(f RF = 14 GHz , f LO = 12 GHz , P LO = 10 dBm)

	Simulation	Measurement
conversion loss	6.3 dB	7.8 dB
IMD3	43 dBc	48.5 dBc
LO/RF isolation	20.3 dB	45 dB
IP3	16.7 dBm	19.8 dBm

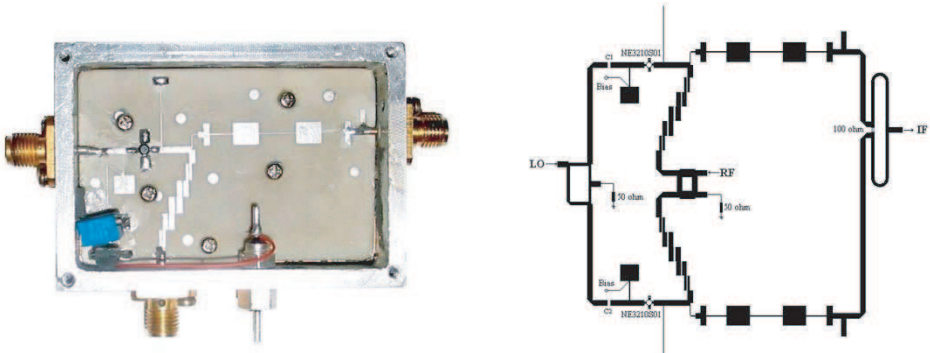

(a) (b)

Figure 1: (a) Picture of fabricated single mixer, (b) circuit layout of balanced mixer.

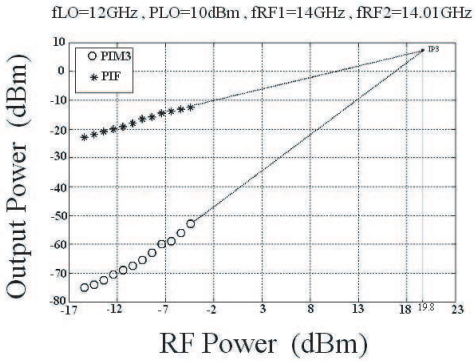

Figure 2: Measured IF power and IMD3 power and showing IP3.

In this paper, a single resistive mixer with MESFET has been designed and fabricated. Input and output frequency of the mixer is in Ku-band and L-band respectively. Then the mixer was simulated in various characteristics such as conversion loss, port-to-port isolation, return loss, P1 dB, intermodulation, the level of spurious responses, sensitivity LO power variation and noise figure were obtained. For improvement of some parameters, balanced mixer structure was proposed and it was accomplished with design of suitable hybrids and combination them with single mixer. At the end, one of types was selected for fabrication and it was tested after fabrication. Analysis has accomplished by Harmonic-Balance method, using Microwave-Office software.

Good agreement between mixer's simulation and experimental results was demonstrated. The IMD3 characteristic of the fabricated resistive mixer is 48.5 dBc with −10 dBm RF power. The measured conversion loss is 7.8 dB with 10 dBm LO power. 45 dB isolation is measured for LO/RF isolation and 19.8 dBm IP3 is obtained.

Efficient Computer Aided Design of Compact Multi-coupled Stripline Resonators Filters

Jorge A. Ruiz-Cruz[1], **Pedro Crespo-Valero**[2], **and Juan R. Mosig**[3]

[1]Escuela Politécnica Superior, Universidad Autónoma de Madrid, Madrid 28049, Spain
[2]Schmid & Partner Engineering AG (SPEAG), CH-8004 Zurich, Switzerland
[3]Laboratory of Electromagnetics and Acoustics, École Polytechnique Fédérale de Lausanne
CH-1015 Lausanne, Switzerland

Abstract— Compact resonator structures are of great practical interest as filtering devices in microwave systems. Different configurations have been proposed in the literature in order to achieve demanding figures of merit as quality factor and ease of integration. A representative group corresponds to the stripline filters, which can be used, for instance, in combline or interdigital structures. These configurations can synthesize complex filtering functions within a very compact shielded device, that can be manufactured in diverse attractive technologies including Low Temperature Co-fired Ceramics (LTCC).

Although this type of filters have been used for many years, new approaches have been recently proposed to further reduce its size, as the coupled-stripline resonators in [1]. This paper proposes a Computer Aided Design (CAD) tool to address efficiently their design. Subsequently, it also investigates alternative topologies for achieving compact stripline filters with very selective transfer functions.

The electromagnetic model has been formulated using an ad-hoc Electric Field Integral Equation. The advantage of this technique lies in the definition of a Green's Function that already provides a quasi-analytic model of the homogenous medium within the metallic shield, thus reducing the unknowns of the numerical problem to the currents over the striplines. In order to have an efficient CAD, special care has been taken in the formulation of the transmission line model, the coupling integrals and the series acceleration arising in this technique [2].

We believe that this method offers a good trade-off between accuracy, efficiency and generality, since it still leaves enough degrees of freedom for the design (e.g., shape/size/location of the stripline resonators and the dimensions of the shielding). These features have been exploited in the optimization of classical structures and to address the design of new topologies using multi-layer stripline resonators with cross-couplings.

REFERENCES

1. Zhang et al., "Miniature broadband bandpass filters using double-layer coupled stripline resonators," *IEEE TMTT*, Vol. 54, 3370–3377, Aug. 2006.
2. Crespo-Valero et al., "On the coupling integrals arising in the method of moments formulation of laterally bounded structures," *IEEE TMTT*, Vol. 56, 2885–2891, Dec. 2008.

Ultra-compact MMIC Chip Set Employing InGaP/GaAs HBT for Ku-band Receiver System

Young-Bae Park, Bo-Ra Jung, Jang-Hyeon Jeong, Jeong-Gab Ju, Suk-Youb Kang, and Young Yun
Department of Radio Communication Engineering, Korea Maritime University, Republic of Korea

Abstract— In this work, a highly integrated downconverter MMIC employing heterojunction bipolar transistor (HBT) was developed for application to Ku-band system. Especially, spiral inductor structures were used for a suppression of LO and its second harmonic leakage signals. Especially, owing to the optimally designed on-chip spiral inductor filters, the downconverter MMIC showed a highly suppressed LO leakage power of −35 dBm and second harmonic LO leakage power of −53 dBm without external filters. The RF and IF frequency of downconverter MMIC were designed 12 and 1 GHz, respectively, with a LO frequency of 11 GHz. Figure 1 shows

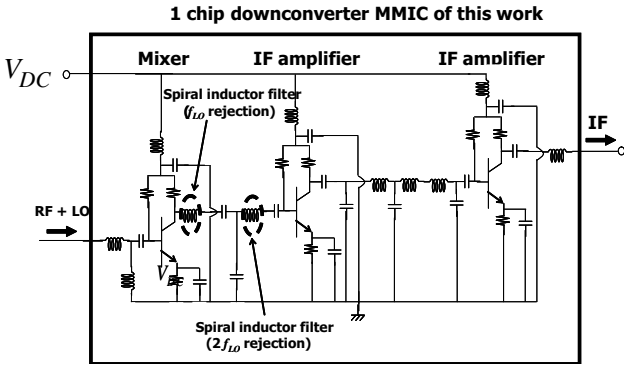

Figure 1: Schematic of downconveter MMIC.

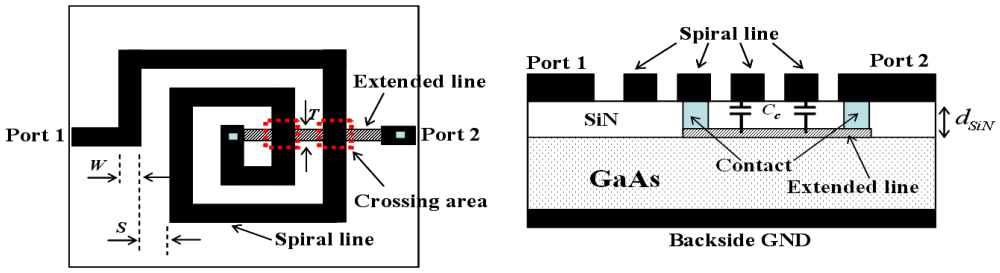

Figure 2: Structure of spiral inductor.

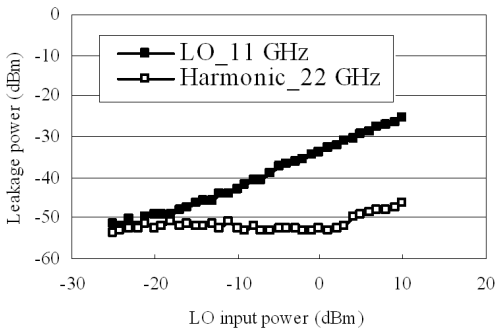

Figure 3: Measured LO and its 2th harmonic leakage power at IF output.

a schematic circuit of the downconverter MMIC proposed in this work. As shown in this figure, a base-pumping mixer was employed using HBT, and the mixed RF and LO signals were applied to the base of the HBT of first stage mixer. For a suppression of leakage signals for LO and its second harmonic, spiral inductor filter, which can be integrated on MMIC due to its small size, was realized using the self-resonance characteristic of spiral inductor. Figures 2(a) and 2(b) show the top and side view of the structure of spiral inductor, respectively. The spiral line is directly connected to port 1, and extended line is connected to port 2 through contact. In order to induce a parasitic capacitance, SiN film was placed between spiral and extended line, and a parasitic capacitance C_c occurs between the spiral and extended line (C_c is shown in Figure 2(b)), which plays a very important role for the self-resonance characteristic of spiral inductor. Figure 3 shows LO and its second harmonic leakage power at IF output, and their frequencies correspond to 11 and 22 GHz, respectively. The leakage powers for LO and its second harmonic signals were suppressed to a great extent by using the optimally designed spiral inductors. Concretely, at a LO power of -1 dBm, LO and its second harmonic leakage power are -35 and -53 dBm, respectively. Considering that a LO leakage power of less than -25 dBm is required for a normal operation of commercial DBS system including external IF filter.

A Study on RF LTCC Coupler Reliability Assessment

Soon-Mi Hwang and No-Chang Park
Korea Electronics Technology Institute (KETI), Korea

Abstract— As the component for dividing and sampling the high frequency signal of high frequency coupler, it is used in the mobile communication repeaters and transmitter-receivers. The present thesis developed the standards for the reliability evaluation of the domestic LTCC coupler that holds outstanding technical expertise and analyzed the results through actual examinations.

The development for the reliability evaluation was based on the IEC 60068 to reference the standards of domestic and foreign advanced companies and reflected upon the opinions of experts through working group conferences for its preparation.

For the reliability certification, the performed test is largely divided into the quality test and the failure rate test. The items of evaluating the capabilities of the subject parts and the environment were included within the quality test and the item of evaluating the failure rate was included within the failure rate test. Within the quality test, only the evaluation of whether the subject part satisfies the quality related capability conditions (capability and environment related) are accomplished and the failure rate test guarantees the fixed reliability standards for the product's failure rate.

The items of the developed capability test are 5 items of degree of isolation, coupling, insertion loss, input/output impedance and standing wave ratio with the items of the environment test to be a total of 8 items of high temperature and high humidity test, high temperature test, soldering test, surge test, temperature cycle test, low temperature test, sine wave vibration test and shock test. The main failure mode and failure mechanism of the LTCC coupler is the random failure form of changes in the interior balance and lines according to the sudden high temperatures and temperature changes. Accordingly, the failure rate was determined as the reliability evaluation scale to postulate the failure distribution as exponential distribution. The time of examination and the sample size was determined by referencing the KS C 6032.

In accordance to the developed reliability standards, the ideal LTCC coupler model was selected for the capability test, environment test were performed on the 5 samples per item. No failures existed after the capability and environment test. The failure rate test performed the securing tests within the 90% reliability standards for the M standard 1.0×10^{-5}/h of the developed dimensions on the 154 samples but no failures existed.

A Study on Global Positioning System Module Made by Domestic Products and Foreign Advanced Products

Soon-Mi Hwang, **Chul-Hee Kim**, **Kwan-Hun Lee**, **and Byeong-Suk Song**
Korea Electronics Technology Institute (KETI), Korea

Abstract— The present thesis accurately compared and evaluated the quality standards and the reliability standards amongst the domestic global positioning system module and the advanced products to confirm the technical position of the domestic product.

The comparative evaluation item and method followed the RS C 0051 'Automobile Application Global Positioning System Module, 2003' that is the reliability evaluation standards and performed the failure rate examinations for the capability examination and the reliability confirmation.

The sample used in the evaluation was selected as the products similar in capability and usage. Moreover, for the accurate comparison, products of each type from 2 domestic companies and 2 foreign companies were selected.

As a result of the capability test, the domestic products displayed greater capabilities in the majority of the items in comparison to the foreign products and as a result of the failure rate exam, both the domestic and foreign products did not satisfy the failure rate standard (reliability standard 70%) of 5.0×10^{-5}/h within the presented environment. After the failure rate test, failure occurred in 3 domestic products and 3 foreign products and all 6 products revealed the occurrence of not being able to receive the satellite data. As a result of an analysis, it was the damage of Flash IC caused by the electrical overstress.

Although it is difficult to conclude the supremacy of reliability and quality of domestic and foreign products merely with the evaluation processed within the comparative evaluation, it will be possible to verify that the domestic products hold the technical standards of equal or higher in comparison to the products of technically advanced countries with the results of the comparative evaluation.

A Novel 4 Way Ka-band Power Divider/Combiner Based on Fin-line

Yi-Hong Zhou, **Jia-Yin Li**, **and Hai-Yang Wang**
High Power Radiation Laboratory, University of Electronic Science and Technology of China
Chengdu 610054, China

Abstract— In this paper, a resonant four-way divider/combiner based on fin-line is presented. This divider/combiner is composed of four units coupling power from fin-line to microstrip lines. Coupling is achieved through the microstrip probe on the top side of the base board with the fin-line on the bottom side of the base board. The advantages of this divider/combiner are ease of fabraction, efficient heat sinking of MMIC, as well as its potential for high power-combining efficiency. Experments on the four-way passive divider/combiner back-to-back design demonstrates a minimum overall instertion loss of 1.1 dB at 35.1 GHz, and the insterting loss in 34.4–35.4 GHz is less than 1.5 dB.

A X-band Duplexer Based on 3-D SICC Using LTCC Technology

Jian Gu, **Yong Fan**, **and Dakui Wu**
Extreme High Frequency Key Laboratory, UESTC, Chengdu, Sichuan 610054, China

Abstract— In this paper, two compact X-band band pass filters (BPFs) with low loss and narrow-band using low temperature co-fired ceramic (LTCC) technology are proposed, and then they are used to constitute the duplexer. The filters and duplexer are based on the substrate integrated circular cavity (SICC) resonators and fed by transmission lines. The duplexer exhibits low loss (IL $<$ 2.39 dB for the first channel and IL $<$ 2.65 dB for the second channel), high isolation (better than 51 dB for the first channel and 61 dB for the second channel), and narrow-band ($\sim$ 4.1% and $\sim$ 3.7% for two filters respectively).

Introduction: A compact LTCC duplexer for X-Band narrow-band applications based on two multilayer SICC BPFs is developed. The merits of this novel SICC duplexer are as such: it is with compact size and simply structure, its insertion loss is very low and isolation is very high. Such kind of duplexer is suitable to be used in 3D LTCC RF and microwave front end modules.

Design of the SICC BPF and Duplexer: Two five-pole BPFs based on Chebyshev low-pass prototype filter are developed for 3-dB insertion loss, 0.1 dB in-band ripple, and their fractional bandwidths are designed to be 4.1% ($\sim$ 440 MHz) and 3.7% ($\sim$ 440 MHz) respectively. The filter based on multilayer SICC presented in this paper is much smaller than the other two filters based on planar SICC and multilayer rectangular SIW. It is larger than the filter based on LTCC folded SIW, but compared with the latter one, its structure is much simpler.

The TM_{010} mode is selected here as the operating mode in SICC. The field distribution of TM_{010} mode in SICC is axisymmetrical, so it has high flexibility in adjusting the position and angle of the input/output ports of the BPFs and duplexer. The designed duplexer has small size, and the size including whole pad is 18 mm $\times$ 10 mm $\times$ 1.78 mm.

Simulation Results: The first channel filter of duplexer exhibits an insertion loss 1.01 dB, and a 3-dB bandwidth of approximately 440 MHz ($\sim$ 4.1%) at the center frequency of 10.86 GHz. For the second channel filter, the insertion loss is 0.99 dB at the center frequency 11.75 GHz, and a 3-dB bandwidth is approximately 440MHz ($\sim$ 3.7%).

As for the insertion loss of the duplexer for two channels BPFs, the first channel exhibits an insertion loss $<$ 2.39 dB, the second channel exhibits an insertion loss $<$ 2.65 dB. The isolation is better than 51 dB across the first channel and it is better than 61 dB across the second channel. It is found that the microstrip lines of input/output ports can rotate around the center of the SICC resonator, and the performances of BPFs and duplexer based on SICC structure will not be greatly influenced when we change the angles between the input and output ports in the designing.

Conclusion: Advantages of this LTCC duplexer structure are low insertion loss, high isolation, very compact size and simple structure. It's suitable to be used in compact front end modules for microwave and millimeter-wave applications.

The Solution and Simulation for the Stability of Active Receiving Antennas

Jing Li, **Lei Xing**, **Qian Xu**, **Jun Ding**, **and Chenjiang Guo**
School of Electronic and Information, Northwestern Polytechnical University, Xi'an 710129, China

Abstract— The stability of active receiving antenna is analyzed in this paper. The microstrip antenna with fast changing input impedance will lead to the instability of Low Noise Amplifier (LNA) easily. By analyzing the S-parameters of amplifier and 3 dB lange coupler, the stability condition of the balanced amplifier is derived. The results validate that the instability problem of the active receiving antenna can be solved by balanced amplifier efficiently. Finally, an active receiving patch antenna with lange coupler and high electron mobility transistor FHX35LG is designed. The simulation results are obtained by ADS simulation software of Agilent Company. Compared with antenna without lange coupler, the optimized antenna works in unconditional stability situation and the stability of active receiving antenna is improved greatly (Stability factor is always greater than 1 in working frequency band).

Improved Design of a Compact Ultra-wideband Microwave Bandpass Filter Using a EBG Structure

Haiyan Chen, **Haipeng Lu**, **and Longjiang Deng**
State Key Laboratory of Electronic Thin Film Integrated Device
University of Electronic Science and Technology of China, Chengdu 610054, China

Abstract— A compact ultra-wideband microwave bandpass filter (BPF) is presented using a electromagnetic band-gap (EBG) structure for the microwave application. As EBG structure, two linear arrays of metallic vias are used to generate shunt inductors, and the two resonators with a novel stepped-impedance resonator (SIR) structure are coupling to create a ultra-wide passband. Its characteristics are analyzed in terms of transmission line mode to exhibit the prosperities of ultra-wideband passband. The presented filter was fabricated and measured. Experimental results are presented and compared to obtained from a finite element method (FEM) approach, and demonstrated the super-wideband properties from 2.12 to 5.41 GHz (−3 dB bandwidth), which is fractional bandwidth (FBW) of 87% at the center frequency 3.76 GHz. The filter also exhibits a stiff slope response at the lower passband edge.

Tuned Periodical Structures in THz Band Applied in Safety Applications

Pavel Fiala, **Radim Kadlec**, **and Petr Drexler**
Brno, FEEC BUT, UTEE, Kolejní 2906/4, Brno 612 00, Czech Republic

Abstract— The aim of this paper is to present the particulars of new research in the special structures used for THz applications, particularly safety and security scenario. The practical application is focused on impedance matching of the basic THz structure for the wave transformation and research of periodical homogenous metamaterials and periodical structures. The element produced by nanotechnology was numerically modeled and the analysis of obtained results was used for the subsequent change of design. The final design was prepared for the visible spectrum and near infrared wavelength applications. According to the interpretation of the results, the basic design was prepared for experimental fabrication of the first prototype of these nanostructure elements. Application of the metamaterial structures is focused to scenario of increase of safety VIP person on security program, like a sniper problems.

ACKNOWLEDGMENT

The research described in the paper was financially supported by FRV (a fund of university development) by research plan No. MSM 0021630513 ELCOM, No. MSM 0021630516 and grant GACR No. 102/09/0314.

REFERENCES

1. Caloz, C. and T. Itoh, "Application of the transmission line theory of left-handed (LH) materials to the realization of a microstrip 'LH line'," *Antennas and Propagation Society International Symposium, 2002, IEEE*, Vol. 2, June 16–21, 2002.
2. Lai, A., C. Caloz, and T. Itoh, "Composite right/left-handed transmission line metamaterials," *IEEE Microwave Magazine*, 2004.
3. Baccarelli, P., et al., "Fundamental modal properties of surface waves on metamaterial grounded slabs," *IEEE Trans. on MTT*, Vol. 53, No. 4, April 2005.
4. Zhang, J. J., J. T. Huangfu, Y. Luo, H. S. Chen, J. A. Kong, and B.-I. Wu, "Cloak changing with background," *PIERS Proceedings*, 765–769, Hangzhou, China, March 24–28, 2008.
5. Cai, X. and G. Hu, "Electromagnetic absorption by metamaterial grating system," *PIERS Proceedings*, 770–774, Hangzhou, China, March 24–28, 2008.
6. Kim, S., J. Jin, Y.-J. Kim, I.-Y. Park, Y. Kim, and S.-W. Kim, "Highharmonic generation by resonant plasmon field enhancement," *Nature*, Vol. 453, 757–760, June 5, 2008.
7. Wu, R.-X., "Design negative index materials with ferrites," *Progress In Electromagnetics Research Symposium Abstracts*, Beijing, China, March 26–30, 2007.
8. Ahward, I. S. and B. T. Cunningham, "Honey I shrunk the world," *IEEE Nanotechnology Magazine*, Vol. 1, No. 2, USA, December 2007.
9. Lu, T. and S. Xu, "A novel super wideband compact filter based on dual-layer left-handed materials for millimeter-wave applications," *Progress In Electromagnetics Research Symposium Abstracts*, Beijing, China, March 26–30, 2007.
10. Zhang, J., H. Chen, L. Ran, Y. Luo, and J. A. Kong, "Two-dimensional cross embedded metamaterials," *PIERS Proceedings*, 294–298, Beijing, China, March 26–30, 2007.

The Application of a Novel Snake-like Gap Slanted DGS Structure in Microstrip Filter Design

Bin Dong, **Quanyuan Feng**, **and Lei Hou**
Institute of Microelectronics, Southwest Jiaotong University, Chengdu 610031, China

Abstract— By modifying the gap shape and dumbbell position of the traditional dumbbell DGS structure, a new snake-like slanted DGS structure was introduced and more steep frequency characteristics and lower resonant frequency point can be achieved, moreover, several decibels of attenuation can be obtained at the resonant frequency. At last the new DGS structure was introduced into design of microstrip filters, result shows good practicality and effectiveness.

Millimetre Wave Beam Combiner Designed by a GA and the HFSS

Yanzhong Yu[1] and Mei Lin[2]

[1]School of Science, Quanzhou Normal University, Quanzhou 362000, China
[2]Department of Electronic Engineering, Jiangxi Polytechnic College, Pingxiang 337055, China

Abstract— The Polarization Beam Combiner is a high performance quasioptical component that combines two orthogonal polarization Gaussian beams into a single one. There are many practical applications. For example, a compact, millimeter wave high power radar can be obtained by combining the output of many corrugated horns. Currently, there are many technical schemes for constructing a beam combiner are proposed, such as diffractive optical element (DOE), frequency selective surface (FSS), and photonic crystal. Because grids consisting of a number of parallel metallic wires are one of the earliest and simplest quasioptical components, they are thus used to make a high power beam combiner at millimeter wavelength in our design. Approximate expressions for wire grids reflection or transmission coefficients are well known theoretically, but they are only suitable for thin wires, that is, the radius of the round wires is usually less than one percent of the wavelength of the incident radiation. For example, in our design, assuming that the incident wavelength of $\lambda = 10\,\text{mm}$, to satisfy above requirement, the radius a of the round wires is demanded that $a \leq 0.1\,\text{mm}$. Such wire is so thin that it can not bear high power and is therefore unfit to construct a high power beam combiner. To bear high power, in our design we demand that $a \geq 0.5\,\text{mm}$, under $\lambda = 10\,\text{mm}$. Therefore, under this condition, we should not apply approximate expressions to calculate reflection or transmission power of wire grids. Nevertheless, Ansoft HFSS is an excellent software package for calculating the electromagnetic behaviour of a structure, and can hence accomplish these tasks. Moreover, in order to improve the performance of a beam combiner, a GA is introduced. The design process and results are presented in the paper.

Computer Aided Design of Depressed Collector for TWTs Using a New Numerical Methodology

Jianqiang Lai, **Yubin Gong**, **Hairong Yin**, **Yanyu Wei**, **and Wenxiang Wang**
National Key Laboratory of High Power Vacuum Electronics, School of Physical Electronics
University of Electronic Science and Technology of China, Chengdu 610054, China

Abstract— We employed a new numerical methodology-virtual boundary element method for trajectory simulation in multistage depressed collector (MSDC) for traveling wave tubes (TWTs). During the theoretical analysis, the core idea of the virtual boundary element method is extracted: expanding the real boundary as virtual boundary and setting virtual field sources on virtual boundary, the virtual field source distributed along the virtual could substitute for the real source or physical quantity that can be regarded as field source on the real boundary [1]. The basic equations for VBE method and the numerical solution are deduced. The shape of virtual boundary, the distance between the virtual and real boundaries and the discretization number of virtual boundary which are close related to the calculation precision are discussed and they are consolidated by the analysis and calculation for a model of two parallel plates. The discrepancy between VBE method and other developed methods such as finite difference method, finite element method and boundary element method are analyzed. The VBE method maintained the advantages of these methods but eliminate most of the disadvantages. Theoretical analysis demonstrates that VBE method is a rigorous method however the complex boundary may make it approximate in practical calculation.

A new computer aided design (CAD) codes-CCAD is developed utilizing VBE method to design and analyze the MSDC system for high efficiency TWTs. A four-stage two-dimensional axis symmetric depressed collector is designed. Its simulation results are compared with EGUN [2], good agreement indicated the viability of VBE method. Theory and numerical calculation of VBE method demonstrate that the advantages mainly lie in fast calculation and precise solution. Theoretical analysis and simulation results demonstrate the validity of VBE method applying in MSDC systems. The potential extension of VBE method applies to three-dimensional collector would be of great interest to the CAD community.

REFERENCES

1. Zhang, Y. M., H. C. Sun, and J. X. Yang, "Theoretical analysis for virtual boundary element method," *Chinese J. of Comput. Mechs.*, Vol. 17, No. 1, 56–62, Feb. 2000.
2. Herrmannsfeldt, W. B., "EGUN-An electron optics and gun design program," SLAC-331, Stanford, CA, Oct. 1988.

Study on Circularly Polarized Traveling Wave Tube

Xiong Xu, **Yan-Yu Wei**, **Wen-Xing Liu**, **Jian-Ping Wei**,
Wen-Xiang Wang, **and Yu-Bin Gong**
National Key Laboratory of High Power Vacuum Electronics
University of Electronic Science and Technology of China
Chengdu 610054, China

Abstract— An interesting vacuum microwave power amplifier, named circularly polarized traveling wave tube (CPTWT), is introduced. Different from traditional O-type traveling wave tube, it works on the interaction between circularly polarized electromagnetic wave and electron beam transverse wave [1, 2]. Therefore, it is supposed to have high efficiency and good linearity of phase frequency characteristics so that can be used to improve the performances of many microwave systems such as radar, satellite communication and electronic countermeasure (ECM).

Till now, a number of theoretical and experimental studies have been carried out at Lomonosov Moscow State University [1]. However, there are still a lot of problems. So it is worth while understanding the essence of interaction in depth with some modern advanced professional simulation software.

In this paper, firstly, the basic principle of circularly polarized traveling wave tube is briefly described. The structure of circularly polarized electromagnetic wave is presented, which can excite the electron beam transverse wave. Then, the picture of action of electron beam transverse wave is illustrated. Secondly, a special slow wave structure, called spiral twinned comb, which circularly polarized electromagnetic wave can propagate through, is mentioned. And its high frequency characteristics are studied by simulation with HFSS. Finally, the process of interaction is showed with our partial-in-cell software CHIPIC 3.0. And we can see electron beam is rotated with the center axis. The phenomenon is accord with the results of the above theoretical analysis. Thus, it indicates that circularly polarized traveling wave tube may have excellent characteristics. In conclusion, circularly polarized traveling wave tube is a promising device.

REFERENCES

1. Vanke, V. A., "Transverse electron-beam waves for microwave electronics," *Physics-Uspekhi*, Vol. 48, No. 9, 917–937, 2005.
2. Chernin, D., T. M. Antonsen, Jr., B. Levush, et al., "A comparison of linearity and efficiency in conventional and transverse TWT amplifiers," *IEEE Trans. Electron Devices*, Vol. 54, No. 2, 194–201, 2007.

A Ka-band Power Amplifier Based on Double-probe Microstrip to Waveguide Transition

Yi-Hong Zhou, **Jia-Yin Li**, **Bo Zhao**, **and Hai-Yang Wang**
School of Physical Electronics, University of Electronic Science and Technology of China
Chengdu, Sichuan 610054, China

Abstract— In this paper, a Ka-band power amplifier based on double-probe microstrip to waveguide transition is presented. The advantages of this power-combining/dividing structure are its low profile, ease of fabrication, as well as its potential for high power-combining efficiency. In addition, efficient heat sinking of monolithic microwave integrated circuit (MMIC) devices is achieved. In contrast with the traditional waveguide T combiner, the double-probe structure doubles the number of the combining way of this combiner. The measured results demonstrate a power-combining efficiency higher than 72% in 33–37 GH band, especially higher than 80% in 34.5–35 GHz band.

A 3.5 GHz High-efficiency CMOS RF Power Amplifier with Adaptive Bias

Yi-Chen Chen and Jeng-Rern Yang
Microwave Laboratory, Department of Communication Engineering, Yuan Ze University
No. 135, Yuan-Dong Rd., Jhong Li City, Taoyuan County 320, Taiwan, R.O.C.

Abstract— This paper proposes a High-Efficiency 3.5 GHz CMOS power amplifier by using an improved linearizer as an adaptive bias control circuit. The proposed design is simulated by TSMC 0.18 µm RF CMOS process. At 1-dB compression point ($P_{1\,\mathrm{dB}}$), the power amplifier exhibits 25.5 dBm of output power with a high power-added-efficiency (PAE) of 39% and sufficient gain (25.5 dB) at a supply voltage of 3.3 V. At the output power 6-dB back-off from $P_{1\,\mathrm{dB}}$, the PAE remains at 15%. The proposed structure improves PAE by 5% ∼ 6% more than the resistor bias.

Figure 1 shows a schematic of the power amplifier with adaptive bias. The proposed structure improves the PAE of 5 ∼ 6% than the resistor bias, as Figure 2 illustrates. Figure 3 presents the simulation results of the proposed power amplifier, which indicating an output power of 25 dBm, PAE of 39%, and linear gain of 25 dB using a 3.3 V supply. Figure 4 is the circuit layout of the proposed power amplifier.

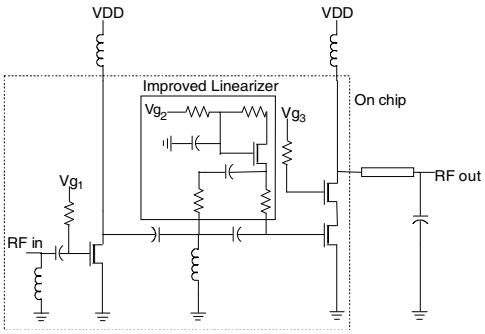

Figure 1: Schematic of the proposed power amplifier.

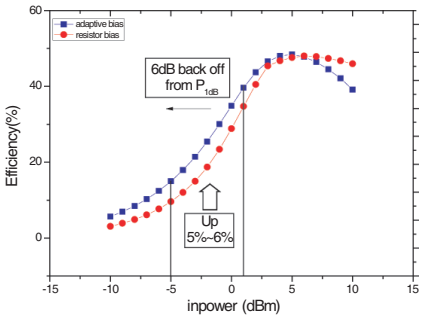

Figure 2: Simulation result of PAE compare to the result using diode linearizer.

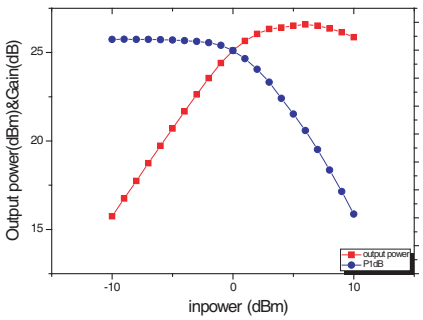

Figure 3: Simulation results of linear gain and output power.

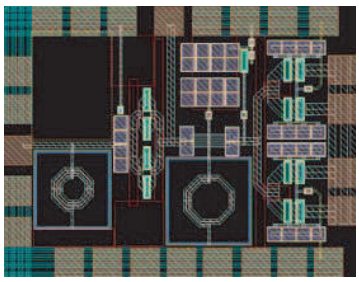

Figure 4: Layout of the proposed PA (1 mm × 0.75 mm).

ACKNOWLEDGMENT

The authors would like to thank the Chip Implementation Center (CIC) of the National Science Council, Taiwan, R.O.C., for supporting the TSMC CMOS process.

REFERENCES

1. Huang, C.-C. and W.-C. Lin, "A compact high-efficiency CMOS power amplifier with built-in linearizer," *Microwave and Wireless Components Letters, IEEE*, Vol. 19, No. 9, 587–589, Sept. 2009.

A Novel Four-way Ka-band Power Divider/Combiner Based on Finline

Yi-Hong Zhou, **Jia-Yin Li**, **and Hai-Yang Wang**
School of Physical Electronics, University of Electronic Science and Technology of China
Chengdu 610054, China

Abstract— In this paper, a resonant four-way divider/combiner based on fin-line is presented. This divider/combiner is composed of four units coupling power from finline to microstrip lines. Coupling is achieved through the microstrip probe on the top side of the dielectric substrate with the finline on the bottom side. The advantages of this divider/combiner are ease of fabraction, efficient heat sinking of MMIC, as well as its potential for high power-combining efficiency. Experiments on the four-way passive divider/combiner back-to-back design demonstrate a minimum overall insertion loss of 0.96 dB at 35.2 GHz, and the inserting loss in 34–36 GHz band is less than 1.8 dB.

The Design a LNA of 3.1∼10.6 GHz UWB Receive System

Chao-Hsu Chen and Jeng-Rern Yang
Microwave Laboratory, Department of Communication Engineering, Yuan Ze University
No. 135 Yuan-Dong Rd., Jhong LI City, Taoyuan County 320, Taiwan, R.O.C.

Abstract— The TSMC 0.18 µm CMOS Process is used to design a 3.1 GHz∼10.6 GHz Low Noise Amplifier for UWB system. The circuit adopts the Current Reuse structure and resistive feedback technology. The results demonstrate the following performances of the design: the total power consumption is 10.55 mW under 1.8 V supply voltage, the forward gain is 10.98 for 3.1∼10.6 GHz wideband frequency, the gain flatness is less than ±0.46 dB in band, the noise figure is 2.91∼3.59 dB, and the P1dB is −19∼−16 dBm. The chip area is 0.78 mm*0.82 mm. This Paper contribution are low NF and gain flatness.

Main Content: The circuit framework designed in this study, as shown in Figure 1, is based on using a current re-use framework and electrical impedance and capacitance return to achieve a UWB low-noise amplifier. This circuit adjusts the parameters of L_1, C_1, and R_2 and selecting M_1 in an appropriate width and bias to achieve good input impedance in 3.1∼10.6 GHz channels and to obtain a minimized noise index. Good impedance matching is obtained through adjusting the RLC harmonic vibration circuit. In addition, L_3 can to raise the high-frequency gain of M_2; a good gain flatness can be obtained in the operating frequency range in this way.

Simulation Results: As the design of this circuit was applied to a UWB (3.1∼10.6 GHz) receiver system, simulation results are for the 3.1∼10.6 GHz range. The simulation results reveals below.

S_{11} was less than −7.3 dB. S_{22} was less than −9.9 dB. The gain within 3.1∼10.6 GHz is approximately 10.98 ± 0.46 dB. The NF was 2.91∼3.59 dB. The P1dB was −19 dBm. The IIP3 was −12 dBm when the input signal frequency was 3.1 GHz.

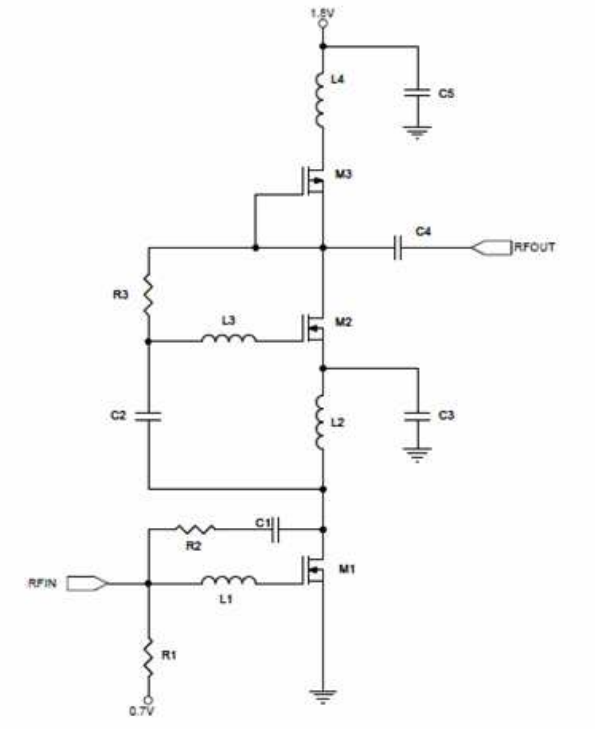

Figure 1: Circuit framework design.

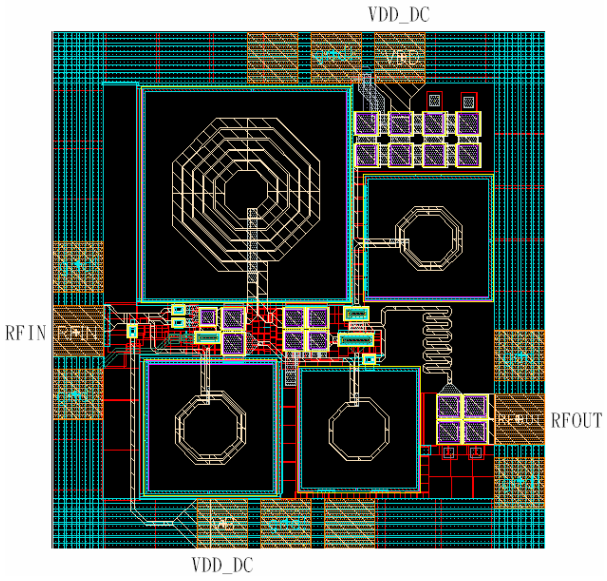

Figure 2: Overall circuit layout diagram.

Design of Fully Integrated RF Power Amplifier for WLAN Applications

Cheng-Tang Liu and Jeng-Rern Yang
Microwave Laboratory, Department of Communication Engineering, Yuan Ze University
No. 135, Yuan-Dong Rd., Jhongli City, Taoyuan Country 320, Taiwan, R.O.C.

Abstract— To meet the demands of wireless networks for the new generation and the future requirements of wireless communication, we present the design of a fully integrated RF power amplifier for WLAN applications in 0.18-µm CMOS technology. The proposed inductor improves the current density, increases the Q factor, and reforms the output-matching network to reduce the chip area. The power amplifier draws 0.846 W with a chip size 1.38 mm^2.

The schematic of the fully integrated RF power amplifier (PA) with the proposed inductor (L3) is shown in Fig. 1. L3 plays an important role in this circuit design: it functions not only as a choke for the DC network but also as an output-matching element in the circuit. We compared the inductor's Q factor with that of the TSMC module using an Agilent ADS simulator in Fig. 2, and could clearly see that the proposed inductor is effective in increasing the Q factor. Furthermore, we set up the width of line to improve the current density. The simulation results of the PA are illustrated in Figs. 3 and 4. Operated with a 3.6-V supply, the characteristics of the output power were as follows: P1 dB = 22.2 dBm, linear gain = 20.1 dB, and power added efficiency (PAE) = 21.2%. Fig. 5 presents the layout.

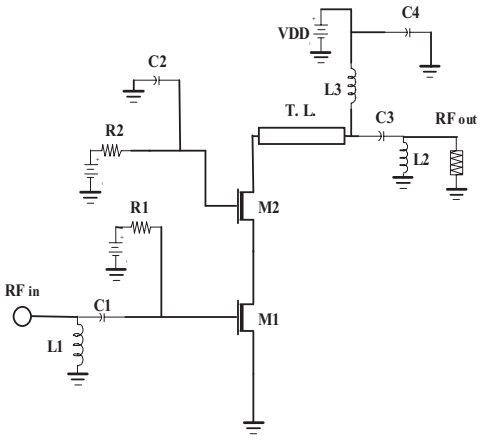

Figure 1: Schematic of PA.

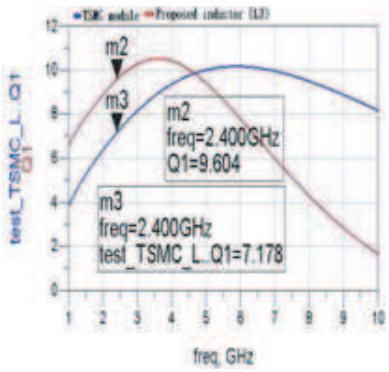

Figure 2: Comparison of Q factor between the inductor and TSMC module.

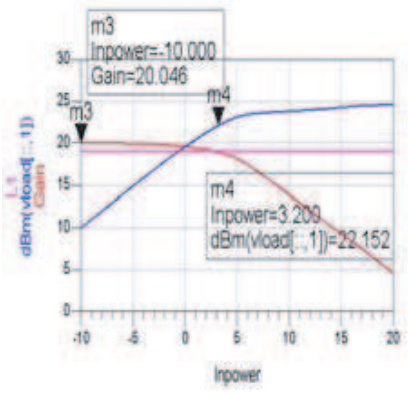

Figure 3: Simulation result of linear gain and output power.

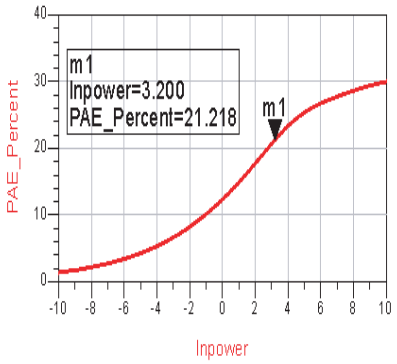

Figure 4: Simulation result of PAE.

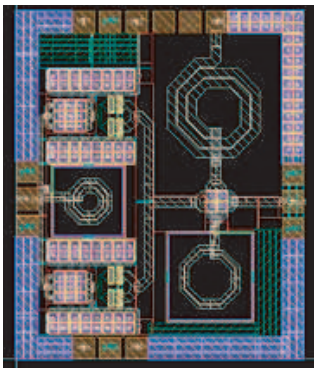

Figure 5: Layout of the proposed PA ($1.08 \times 1.28\,\mathrm{mm}^2$).

ACKNOWLEDGMENT

The authors would like to thank the Chip Implementation Center (CIC) of the National Science Council, Taiwan, R.O.C., for supporting the TSMC 0.18-μm 1P6M CMOS process.

REFERENCES

1. Oh, H.-S., C.-S. Kim, H.-K. Yu, and C.-K. Kim, "A fully-integrated +23-dBm CMOS triple cascode linear power amplifier with inner-parallel power control scheme," *Radio Frequency Integrated Circuits (RFIC) Symposium*, June 2006.
2. Yang, L.-Y., H.-S. Chen, and Y.-J. E. Chen, "A 2.4 GHz fully integrated cascode-cascade CMOS doherty power amplifier," *IEEE Microwave and Wireless Components Letters*, Vol. 18, No. 3, 197–199, March 2008.

The Analysis and Design of High Power Millimeter Wave Pulse Detector for 2 mm Frequency Band

Guangqiang Wang[1], **Jianguo Wang**[2,3], **Xingzhou Wang**[2], **and Ruyu Fan**[1,2]

[1]Department of Engineering Physics, Tsinghua University, Beijing 100084, China
[2]Northwest Institute of Nuclear Technology, Xi'an 710024, China
[3]School of Electronics and Information Engineering, Xi'an Jiaotong University, Xi'an 710049, China

Abstract— The semiconductor detector, so-called resistive sensor, for high power millimeter wave pulse measurement has been designed in a frequency range 113–173 GHz for the first time. Two separate semiconductors shorted with very thin metal on top are placed in the center of the wide wall of the waveguide. Based on hot-carrier effect in semiconductors the detector converts the millimeter wave pulse to the dc voltage pulse when the high power pulse propagates through it. This paper analyzes the principle of the detector theoretically and derives the sensitivity of the detector in the warm-electron region at first. From the experss of the sensitivity the output voltage of the detector is found to be in proportion to the input power of the pulse under linear approximation. After choosing the n-type Si as the sensing semiconductor within a waveguide segment (waveguide window $1.651 \times 0.8225\,\mathrm{mm}^2$), the structural parameters of the detector are caculated and optimized to make the frequency response flat over the waveguide frequency band. A three-dimensional finite difference time domain (FDTD) method is used here. The results show that, while the biased voltage on the seneing element is 10V, the sentivity of the optimized detector is about $6\,\mathrm{V/kW^{-1}}$ with a fluctuation less than 27% in the frequency range 113-173GHz, especially less than 9.8% in the frequency range 130–160 GHz, and the voltage standing wave ratio (VSWR) caused by the inserted semiconductors is about 1.2. Finally, compared with the diode detectors in 2 mm frequency band, the designed semiconductor detector has more flatter frequency response, smaller VSWR, and can measure 1.5 kW pulse power directly with an output singal of the order of a few tens of volts, which leads to less attenuation used in the power measurements and good performances in high electromagnetic interference environments. The designed detector is being fabricated and will be used in our 0.14 THz high power pulse generation test soon.

Interference Suppression in DC-DC Switch Converter By H∞ Controller

Yanhua Xian[1, 2] **and Jiuchao Feng**[1]

[1]School of Electronic and Information Engineering, South China University of Technology
Guangzhou 510641, China
[2]College of Electronic Engineering, Guangxi Normal University
Guilin 541004, China

Abstract— Switch converter is core of power supply, and its effectivity and stability is key factors in practical application. For the stability problem of power supply, the effect of input voltage and load resistor has been paid much attention, while external noise is not considered frequently.

In this paper, based on H∞ control theory, a new control strategy for DC-DC switch converter is proposed and realized, which takes into account perturbations of input voltage and output current, and external noise. In this approach, the interference is feedback to form H∞ controller to weaken the impact of interference.

The proposed H∞ controller is designed by using solving a pair of Riccati equations of system, and is an asymptotically stable controller. The controller guarantees closed loop stability and minimizing the infinity norm of the transfer function of the controlled system.

As an example, a H∞ controller for boost converter (DC-DC) operating in continuous conduction mode is derived in detail. The controlled system is formed by two parts. One is the boost model, which is averaged and linearized. Another is weight functions, which are chosen for reducing the stationary tracking error. Those are given by using robust control toolbox in Matlab platform.

Simulations are executed in frequency and time domain. The results demonstrate the controlled system with a big phase margin, perfect tracking of the desired output voltage and high immunity to aforementioned perturbations.

Volume Phase Holographic Grating Fabricated in Trans-4-Stilbenemethanol Doped PMMA

Z. F. Zhang[1], **X. M. Tao**[1], **G. F. Wang**[1], **and J. M. Yu**[2]

[1]The Hong Kong Polytechnic University, Hong Kong, China
[2]Fountain Set Limited, Hong Kong, China

Abstract— Volume phase holographic (VPH) gratings have been intensively studied and successfully applied in astronomy in recent years because they have higher diffraction efficiency, lower scattered light and other advantages over traditional surface relief gratings (SRG) such as easy handling, high line density and tenability [1]. Besides liquid systems which are traditionally used for writing VPH gratings, different kinds of polymer systems, such as amorphous polymer [2] and photochromic polymers [3], have been developed to write VPH gratings and to expand their applications areas. In this paper, we report VPH fabricated in trans-4-stilbenemethanol (trans-SBM) doped PMMA host-guest system. To suppress SRG formation when the film of trans-SBM doped PMMA was sandwiched between two glass slides and irradiated in the interference field of 325 nm He/Cd laser. Decreased refractive index was found in this system due to trans-cis photoisomerization of SBM molecules in PMMA upon UV irradiation. Bragg diffraction of VPH was observed immediately after the film was placed in the interference field, implying that trans-cis photoisomerization of SBM molecules were not inhibited in the solid polymer system. By adjusting the intersecting angle of two beams, the period of VPH was tuned to as low as 350 nm. However, the change of refractive index was small because of low doping concentration. The diffraction efficiency is less than 1% for 532 nm light. It was found that zero order diffraction of phase mask had influence on the period of VPH. When the intersecting angle of two interfere metric beams equals to the diffraction angle of phase mask, the period of VPH doubles if the zero order diffraction light is not blocked.

Efforts are being taken to write VPH in single mode polymer optical fibers with trans-SBM doped PMMA as the core, and this kind of VPH gratings are essentially fiber Bragg grating (FBG), which have great application potential in fiber sensor technology and CWDM system.

REFERENCES

1. Barden, S. C., J. A. Arns, and W. S. Colburn, "Astronomical applications of volume-phase holographic gratings," *18th Congress of the International Commission for Optics*, 52–53, San Francisco, USA, August 1999.
2. Zilker, S. J., T. Bieringer, D. Haarer, R. S. Stein, J. W. van Egmond, and S. G. Kostromine, "Holographic data storage in amorphous polymers," *Adv. Mater*, Vol. 10, No. 11, 855–859, 1998.
3. Bianco, A., C. Bertarelli, P. Conconi, E. Molinari, C. Quaglia, G. Toso, and F. M. Zerbi, "New developments in photochromic materials for volume phase holographic gratings," *Optomechanical Technologies for Astronomy*, 62733V, Orlando, USA, May 2006.

Optimization of Broadband Antireflection Coating for Solar Cell Applications by Genetic Algoritms

Ming-Jer Jeng[1], **Yun-Hsih Chou**[2], **Jun-Yi Dong**[1], **and Liann-Be Chang**[1]

[1]Department of Electronic Engineering, Chang Gung University, Taiwan, R.O.C.
[2]Department of Electronic Engineering, St. John's University, Taiwan, R.O.C.

Abstract— Antireflection (AR) coating has been widely used in solar cell devices to reduce the undesirable reflection from the surfaces of solar cell devices. In this paper, a triple junction solar cell was fabricated and the optimized thickness of antireflection coating was determined by genetic algorithm. It is found that the solar cells with an anti-reflection coating layer have an efficiency improvement of 5%. The solar cells with one antireflection coating layer of SiO_2 material in the thickness range of 80 nm $\sim$ 125 nm will have the efficiency variation of 1%. The optimizing thickness of one antireflection coating (SiO_2) is about 100 nm for a triple junction solar cell with the top surface of InGaP layer. Genetic algorithm mainly includes three processes: reproduction, crossover and mutation. However, before preceding these processes, we have to encode every parameter into a finite bit string (i.e., one string represents one parameter). In addition, randomly pick up a certain amount of individual base on the need of the question as an initial population. Decode the initial population and define a fitness function according to the purpose of the question to evaluate the adaptability and behavior of every individual and find out if this individual should be survived or not. Then reproduce the best one according to its fitness function value. After reproduction, base on the crossover probability of the newly produced population, randomly pick up two individual of the population and exchange part of the bit value of certain strings of one population enhance the production of a new production. Then pick up the best string from the information exchange pool to become a real value after decoding. Thus evolution of one generation after another, liked the natural development in the biological field, until the qualified optimization is found. The characteristic matrix for each layer with index n and thickness d is used to calculate the effective admittance Y. The reflectivity is given from the effective admittance. Take the sum of the square difference between the calculated reflectivity and the desired zero reflectivity at various wavelengths across the visible region as a fitness function. The calculating optimization thickness of an antireflection coating with one SiO_2 layer on the top surface of InGaP layer is about 100 nm for the lowest reflectivity. It is consistent to the experimental observation very well. The calculation of multiple antireflection coating is still under progress.

Analysis of Optical Properties of a High-temperature Superconducting Film Operating in Near Zero-permittivity Region

Heng-Tung Hsu[1] and Chien-Jang Wu[2]

[1]Department of Communication Engineering, Yuan Ze University, Chungli 320, Taiwan
[2]Institute of Electro-Optical Science and Technology, National Taiwan Normal University
Taipei 116, Taiwan

Abstract— The optical properties of a high-temperature superconductor in the near-zero-permittivity operation range are theoretically investigated. Investigations are performed through the calculations of optical reflectance over three model structures. Firstly, the calculated wavelength-dependent reflectance for a bulk superconductor occupying half-space shows that the threshold wavelength is strongly influenced by the angle of incidence and the polarization of wave. Secondly, the reflectance response in a single superconducting slab has a peak at the threshold wavelength for the transverse magnetic (TM) wave whereas the shape of the peak is very sensitive to the angle of incidence. Finally, the reflectance is calculated for a superconductor-dielectric bilayer structure. The results illustrate that the dielectric substrate has a pronounced effect on the reflectance response for both transverse magnetic and transverse electric (TE) waves.

Investigation of Detector Responsivity in the "Water Window" Wavelength Range

J. Mikołajczyk, **Z. Bielecki**, **M. Nowakowski**, **and J. Wojtas**
Institute of Optoelectronics, Military University of Technology, 2 Kaliskiego Str., Warsaw 00-908, Poland

Abstract— The paper presents a laboratory setup for investigation of spatial non-uniformity of detector responsivity [1]. The spectrum is of great interest in biology. In the so-called water-window region, where water is rather transparent and microscopic observation of living objects is possible [2].

The lab setup consists of a radiation source, a metrology chamber, and a scanning mechanism. In the source, the gas puff target is irradiated with the radiation generated by Nd:YAG laser [3]. The spectrum of source emission depends on the used gas. For the generation of water window spectrum, the N_2 or Ar can be used. The investigations show that N_2 gas spectrum is characterized by a single strong emission line at the wavelength of 2.88 nm. In the case of Ar gas, the spectrum is widen in the wavelength range of 2–4.5 nm [4].

The preliminary investigations of the source showed that the efficiency and stability depend on conditions of plasma generation. The measured stability of the source radiation influences the accuracy of detector testing procedure. For this reason, a special metrology chamber with optical beam splitter was constructed. The setup makes it possible to control radiation level using monitor detector.

The main elements of the splitter are two Cr/Ti multilayer mirrors produced at the Fraunhofer Institute for Applied Optics (Jena, Germany) [5]. The mirrors are characterized by reflectance of above 20% for incidence angle of 70° and wavelength of (2.85 ± 0.03) nm. The beam is separated into the two chamber flanges. In the flanges, the monitor detector and tested detector (photodiode, CCD etc.) are mounted. As the monitor instrument, a AXUV-100HYB1 amplifier with calibrated silicon photodiode is applied [6].

The scanning procedure is carried out using a holder with a pinhole, XYZ translation stage, and a movement driver [7] The whole investigation mechanism is automated by special prepared software.

REFERENCES

1. Durak, M., et al., "Spatial non-uniformity measurements of large area silicon photodiodes," *Turk. J. Phys.*, Vol. 26, 375–379, 2002.
2. Majima, T., "Soft X-ray imaging of living cells in water: Flash contact soft X-ray microscope," *Trends in Analytical Chemistry*, Vol. 23, No. 7, 520–525, 2004.
3. Fiedorowicz, H., et al., "Compact laser plasma EUV source based on a gas puff target for metrology applications," *Journal of Alloys and Compounds*, Vol. 401, 99–103, 2005.
4. Fiedorowicz, H., et al., "Investigation of soft X-ray emission from a gas puff target irradiated with a Nd:YAG laser," *Optics Communications*, Vol. 163, No. 1–3, 103–114, 1999.
5. Uspenskii, Y., et al., "Optimal design of multilayer mirrors for water-window microscope optics," *Optical Review*, Vol. 14, No. 1, 64–73, 2007.
6. Fonck, R. J., et al. "Low noise photodiode detector for optical fluctuation diagnostics," *Rev. of Sci. Instr.*, Vol. 63, 4924–4926, 1992.
7. Mikolajczyk, J., et al., "System for calibration of EUV detectors," *Photonics Letters of Poland*, Vol. 1, No. 2, 70–72, 2009.

The Novel Active Mode-locking 402.5 MHz Repetition Rate Pico-second Laser Based on PLL Structure

Yan Zhou[1, 2]

[1]The Department of Electronic Information Engineering, Beihang University, Beijing, China
[2]The Department of Electronic Engineering, University of California-Santa Cruz, Santa Cruz, USA

Abstract— The novel active mode-locking Pico-second Laser (PSL) system with 402.5 MHz repetition rate based on Phase Locked Loops (PLL) has been present in this paper. The complete PSL system configuration was been introduced, while suitable PLL structure has been used to get phase noise and jitters' decreasing. At the same time, the better pulse output feature been got. Agreement of the theoretical and experimental results confirms the applicability of this 402.5 MHz repetition rate Pico-second Laser system design.

Disorder Effect on Energy Gap of GeSn

H.-Z. Lin[1], **T.-Y. Lin**[1], **K.-J. Su**[1], **J.-S. Guo**[1], **H.-C. Chang**[1], **H. H. Cheng**[2], **and K.-M. Hung**[1]

[1]Department of Electronics Engineering, National Kaohsiung University of Applied Sciences
Kaohsiung, Taiwan
[2]CCMS, National Taiwan University, Taipei, Taiwan

Abstract— Direct gap in GeSn alloys has attracted a significant amount of attention in recent years according to the promise in the applications of light-emitting device and solar cell. The appearance of a direct gap for the range of Sn mole fraction x is controversial in the recent reports [1–4]. In this work, we show that the ambiguity may result from the effect of disorder configuration.

In this study, the density functional theory with the DMOL and CASTEP codes is applied to calculate the lattice constant and band structure of bulk GeSn alloys, respectively. A supper cell including 64 atoms with a mixed-atom (quasi-disorder) configuration is used in the calculations.

Direct and indirect gap energies as a function of x, as shown in Fig. 1, reveals that the direct gap occurs at $x > 0.09$ for an extreme quasi-disorder configuration, formation of a tin cluster. However, Fig. 2 shows that the direct gap never occurs for an order configuration.

This work shows that the disorder configuration dominates the energy gap in bulk GeSn alloys. The direct gap occurs as $x > 0.09$, which is well agreement with the experimental result reported in the near recent [1].

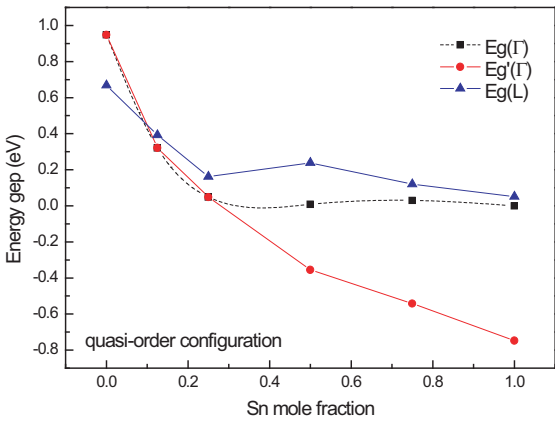

Figure 1.

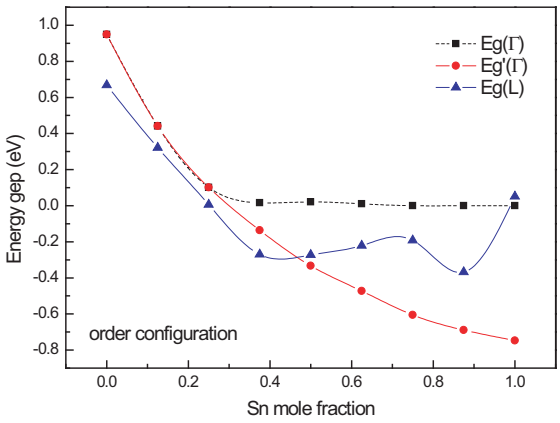

Figure 2.

REFERENCES

1. Perez Ladron de Guevara, H., et al., *Appl. Phys. Lett.*, Vol. 91, 161909, 2007.
2. Yin, W.-J., et al., *Phys. Rev. B*, Vol. 78, 161203R, 2008.
3. Moontragoon, P., et al., *Semicond. Sci. Technol.*, Vol. 22, 742, 2007.
4. Mäder, K. A., et al., *Solid State Commun.*, Vol. 69, 1123, 1989.

Charge-induced Deformation in Heavily-doped Si

N.-C. Hsieh[1], **K.-J. Su**[1], **C.-H. Chang**[1], **H. H. Cheng**[2], **and K.-M. Hung**[1]

[1]Department of Electronics Engineering, National Kaohsiung University of Applied Sciences
Kaohsiung, Taiwan
[2]CCMS, National Taiwan University, Taipei, Taiwan

Abstract— Ultra-heavy and ultra-shallow doping in silicon channel is one of the key technologies in new generation fabrication of nano-scale metal-oxide-semiconductor field-effect transistors (NSMOS) [1]. However, it is well known that a fraction of dopants will be precipitated into a cluster as the dopant density is greater than the solubility of Si matrix. In this work, we show that the electric charges in doped Si strongly affect the volume of the dopant clusters. This charge-induced deformation will affect the characteristics, including effective mass and fundamental gap, of carriers in the conducting channel of NSMOS.

In this study, the density functional theory with the CASTEP code is applied to calculate the bond length of doped Si. A supper cell including 62 Si atoms and two phosphorous atoms is used in the calculations. The structure with and without charges in the system is fully relaxed to minimize the total energy. The calculated results of the bond lengths are shown in the following figure for (a) positive charging, (b) neutral charging and (c) negative charging. For positive charging, the bond length decreases as increasing the charging density, while in opposite charging it increases.

The charge-induced deformation in ultra-shallow doped Si is observed. This effect is significant in new generation fabrication of NSMOS.

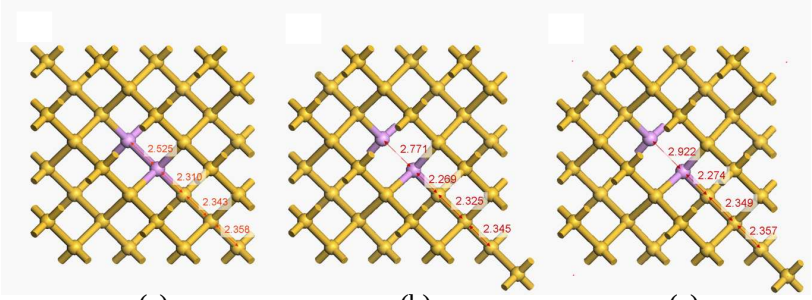

(a) (b) (c)

REFERENCES

1. Khanna, V. K., *Physics Reports*, Vol. 398, 67, 2004.

Implantable Antenna for Biotelemetry with Medical Devices

Ho-Jun Lee, Jin-Sup Kim, and Se-Hwan Choi
Convergence Communication Components Research Center
Korea Electronics Technology Institute, R. O. Korea

Abstract— In this paper, we proposed a novel design of dual band microstirp antenna for implantable biometry in the Medical Implant Communication Services band (MICS band; 400 MHz, 2.4 GHz). The proposed antenna configuration is shown in Figure 1(a). The proposed antenna has a simple structure. This antenna has a coplanar waveguide (CPW) fed that is optimized the 50 Ω impedance matching by positioning feed line and slot width. Antennas in this paper are simulated by using the Ansoft simulation software high-frequency structure simulator (HFSS) for achieving the broad bandwidth of 40 MHz (Low Band: 380 ∼ 420 MHz) and 300 MHz (High Band: 2.2 ∼ 2.5 GHz) at return loss of 10 dB in the MICS band. Figure 1(b) shows its measured return losses compared with its simulated results. Figure 1(C) shows a photograph of the fabricated antenna. We manufactured the antenna based on the results of optimized simulation results and measured characteristics of the suggested antenna in the anechoic chamber. Details of the proposed antenna designs are described, and typical experimental results are presented and discussed.

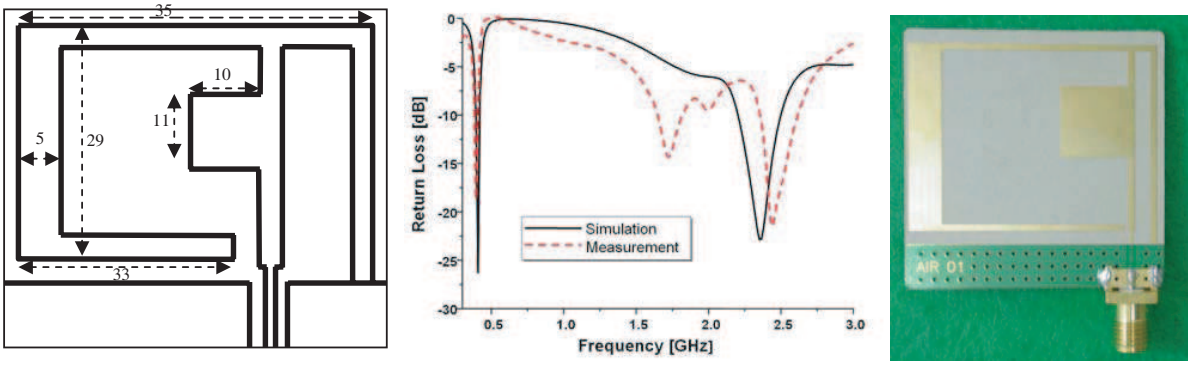

(a) (b) (c)

Figure 1: Proposed antenna. (a) Proposed antenna configuration. (b) Measured and simulated results of return loss. (c) Photograph of the fabricated antenna.

REFERENCES

1. Jaehoon, K. and Y. Rahmat-Samii, "Implanted antennas inside a human body: Simulations, designs, and characterizations," *IEEE Trans. Microw. Theory Tech.*, Vol. 52, No. 8, 1934–1943, 2004.
2. Soontornpipit, P., C. M. Furse, and C. C. You, "Design of implantable microstrip antenna for communication with medical implants," *IEEE Trans. Microw. Theory Tech.*, Vol. 52, No. 8, 1944–1951, 2004.

Static Magnetic Field Synergizes with Paramagnetic Nanoparticles to Induce Cellular Toxicity in Normal Hepatocytes

Kwon-Seok Chae
Kyungpook National University, Korea

Abstract— Recently, there have been many reports which showed MRI contrasting agents such as paramagnetic nanoparticles have not shown notable cellular toxicity. All of those studies have examined cellular toxicity not of the static magnetic field from MRI operation but of paramagnetic nanoparticles themselves. Here, we show that both static magnetic field and Resovist, a paramagnetic nanoparticle, a well-known clinically used liver-specific MRI contrasting agent, induce remarkable cellular toxicity in mouse hepatocytes cells, NCTC 1469. The cellular toxicity was determined by the WST-1 assay for the effect of the magnetic field and a luciferase assay for Resovist or Resovist along with the magnetic field. The intensity of the magnetic field (~ 0.4 Tesla) and the concentration of the Resovist proportionally increased the cellular toxicity and they synergized in the induction of the effect *in vitro*. The synergistic cellular toxicity was accompanied by the aggregation of the paramagnetic nanoparticles and the extent of which was dependent on both the intensity of the magnetic field and the concentration of the Resovist. In contrast to previous studies, these results strongly suggest that Resovist and presumably similar kind of paramagnetic nanoparticles used for contrasting agent, might induce detrimental cellular effect under a strong static magnetic field. A variety of following investigation including *in vivo* study is required.

Measurement of Electropotentials on Interface of Solid-liquid Phase

Miloslav Steinbauer[1], **Zdeněk Roubal**[1], **and Dominik Heger**[2]

[1]Faculty of Electrical Engineering and Communication, Brno University of Technology
Kolejní 2906/4, Brno 612 00, Czech Republic
[2]Faculty of Science, Department of Chemistry, Masaryk University
Kamenice 5/A8, Brno 625 00, Czech Republic

Abstract— On interface of solid-liquid phases of water solutions some electric potential occurs during freezing process, caused by separation of ions from solid phase. Whenever freezing is often used for preservation of biological samples, the influence of electric field induced by this process to biological samples is the subject of investigation. For this purpose we need some facility and measurement device to measure this potential. In this paper, we will discus some aspect of described phenomenon and the design of laboratory measuring facility and electrometer will be introduced. First problem lie in measurement of low potential from source with very high inner impedance. Because the solid phase (ice) is bad conductor, the reference electrode is situated out from vessel with freezed medium and has only capacitive connection to the inner platinum electrode. The next problem is in cooling system for controlled freezing, when temperature as low as 170 K has to be reaches.

Investigation of Artificial Dress Embedded with Nano-magnetic Particles

Ya-Hui Chan[1], **Sheng-Wei Feng**[2], **Hsin-Ta Wang**[1], **Keng-Liang Ou**[3], **Che-Tong Lin**[2], **and Haw-Ming Huang**[3]

[1]School of Organic and Polymeric, National Taipei University of Technology
Taipei, Taiwan
[2]School of Dentistry, Taipei Medical University, Taipei, Taiwan
[3]Graduate Institute of Biomedical Materials and Engineering
Taipei Medical University, Taipei, Taiwan

Abstract— In the treatment of extensively burned patients, grafting of devitalized tissue is the major source of skin replacement. However, patients with large total body surface area bums cannot be completely grafted. Artificial skin replacement and wound dressing offer effective treatment for burn and wound care in the treatment of patients with large surface area bums. Accordingly, development of a functional and cheap artificial dressing has become an urgent goal for emergency medicine. Many researches have proved that magnetic stimulation can promote wound healing. However, artificial dressing combined with static magnetic field is still unavailable. With this regard, the aim of this study is to develop a novel magnetic dressing material. The Fe_3O_4 nano-particles were prepared by the chemical-precipitation method, and the diameter of there particles were analyzed using Transmission electron microscopy. After mixing the Fe_3O_4 nano-particles and poly-lactic acid (PLLA) solution with a concentration of 3 g/3 g (Fe_3O_4/PLLA), nanofiber membrane was manufactured via electrospinning technique. Our results showed that the diameter of the Fe_3O_4 nanoparticles concentrated at 2–8 nm (84.2%). After magnetizing the new-developed PLLA-Fe_3O_4 membrane, we found the residual magnetic intensity was 0.28 ± 0.06 G, and there exists an approximate linear relationship between the magnetic intensity and membrane thickness ($R = 0.82$, $p < 0.05$). The results of cell viability tests and cell morphology observations demonstrated that our PLLA-Fe_3O_4 membrane has excellent biological compatibility. These results serve as a reference for future animal studies.

Static Magnetic Field Reduced Disseminated Intravascular Coagulation in the LPS-induced Mice

Wei-Yi Lai[1], **Che-Tong Lin**[2], **Sheng-Yang Lee**[2], **and Haw-Ming Huang**[1]

[1]Graduate Institute of Biomedical Materials and Engineering, Taipei Medical University, Taiwan
[2]School of Dentistry, Taipei Medical University, Taiwan

Abstract— Disseminated intravascular coagulation (DIC) is a complex systemic thrombohemorrhagic disorder involving intravascular coagulation and hemorrhage. Previous study has demonstrated that static magnetic field (SMF) is effective in attenuating lipopolysaccharide (LPS)-induced DIC. The aim of this study is to investigate the mechanisms that SMF affects LPS-challenged mice. In this study, BALB/cByNarl mice were chosen as tested subjects. The tested animal were challenged with high-dose endotoxin (LPS) and exposed to a static magnetic field (0.4 T). The survival rates of the mice were monitored and changes of body temperatures of the tested mice were recorded. In addition, liver and kidney biopsy were performed to explain the mechanism of SMF effects on DIC. Our results showed that SMF significantly increases ($p < 0.05$) the survival rate of LPS-challenged mice, with a ratio of 1.5 fold. In addition, after 6 hours of LPS injection, the average body temperature of SMF exposed mice was 1.07°C lower than that of unexposed animal. Results from our tissue biopsy demonstrated that SMF exposure reduces the damage of liver and kidney in the LPS-challenged mice. According to our results, it is reasonable to suggest that the mortality-reductive effects of SMF on LPS-challenged mice should be related to the increase in temperature-controlled capability of the DIC mice.

Inference of SMF on Red-blood-cells Cryopreservation

Chun-Yen Lin[1], **Po-Chieh Yang**[2], **Sheng-Yang Lee**[1], **Che-Tong Lin**[1], **and Haw-Ming Huang**[2]

[1]School of Dentistry, Taipei Medical University, Taiwan
[2]Graduate Institute of Biomedical Materials and Engineering
Taipei Medical University, Taiwan

Abstract— The development of regenerative and reparative medicine, based mainly on biologic cell therapy and cell tissue banking technology, requires more and new approaches in low-temperature storage. An efficient storage technology must have a good cell recovery rate and preserve cell functions. A novel cooling device, coupling with 0.4 T static magnetic field (SMF), for low-temperature storage was developed in this study. To test the performance of the device, human red blood cells (RBC) mixed with 10% glycerol, were set in our cooling device. Then the device was put into a -25°C temperature-controlled refrigerator. The cooling-rate of the RBC samples was controlled to 1°C/min. After freezing and thawing, cell morphology was observed by optical microscopy. Blood cells counter and the percentage of hemolysis were performed to monitor RBC recovery rate. Our results showed that SMF exposure has no effect on the morphology of RBC. However, freezing RBC with SMF results in less hemolysis and greater recovery rate, compared with control group. The recovery rates of SMF-exposed RBC are 8.89% and 7.04% greater than the control group after one and three days-low temperature storage, respectively. Based on our limited results, we suggest that SMF can increase the resistance of cryo-injury of freezing RBC. Although more investigations were needed to improve SMF cryo-protection, it is reasonable to suggest that SMF can be a useful tool for low-temperature storage.

Magnetic Resonance Imaging (MRI) Safety of Implants: Estimating Specific Absorption Rate (SAR) at Design-simplified Stents of Different Lengths Placed Inside a Virtual Phantom Model Using a Generic RF Body Coil at a MR Frequency of 63.9 MHz

Mark J. Pawlenka and Gregor Schaefers
Testing Laboratory for Magnetic Resonance Safety & Compatibility, MR:comp GmbH
Gelsenkirchen, Germany

Abstract—

Objective: In respect of imaging quality and patient safety, temperature rises and SAR distributions, which are caused by interaction of the applied electromagnetic fields during MR exams, are of high interest for implants in MR tomography, too. High local SAR values are equivalent to high local temperature increases. For developing support for radio frequency (RF) induced heating experiments, SAR values were virtually investigated at design-simplified stents with different lengths inside a virtual human torso shaped phantom model to determine whether such complex elongated thin structures can be electromagnetically simulated with current computer technology.

Methods: 5 design simplified stent models with different lengths (50–250 mm), but equal inner diameter (8 mm) and same material properties as well as same strut structure and thickness (0.8 mm) were modeled with SPEAG simulation software SEMCAD X. The stents were positioned at half 'gel depth' inside a virtual body phantom with geometrical dimensions described in ASTM standard F2182-02a [1] for experimental testing of RF induced heating of implants. The virtual phantom was filled with a medium ('gel') having an averaged conductivity of 0.47 S/m and dielectric property ($\varepsilon_r = 81$) of human tissue. The phantom was exposed to the electromagnetic environment generated by a virtual generic birdcage coil for investigating how the stent length and the imaging frequency affect the SAR distribution in the surrounding of the stents. The longitudinal axes of the stents were oriented parallel to the vector of the static main magnetic field B_0 and the electrical field. All stent and phantom configurations were investigated at the frequency (63.9 MHz) equivalent to a 1.5 Tesla MR system. The impact of different stent lengths on the local SAR values and distribution at Larmour frequency with its maximum SAR values at about half wave length is well-known. The simulation results and the theoretical results were compared.

Results: The results showed that each conductive loop of structure of a stents leads to higher local SAR values in the surrounding of the stent having a maximum effect for the stent lengths at half a wavelength in the specific conductive medium. However, the highest local SAR spatially occurred at the ends of the stents Fig. 1.

The SAR is highly localized and its magnitude depends strongly on the stent length and on the frequency of the electromagnetic field in the specific conductive environment. Design-dependent

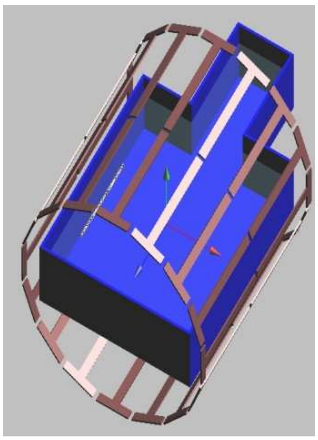

Figure 1: Simulation setup.

Figure 2: Exemplary 1 gram avg. SAR distribution (linear scaling), design-simplified 200 mm stent structure.

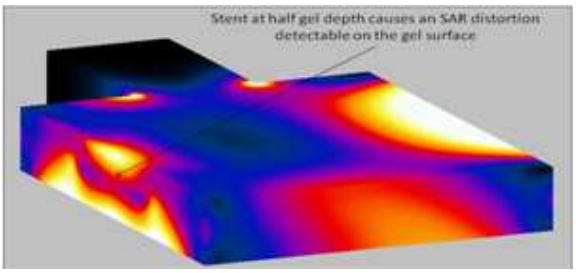

Figure 3: 1 gram averaged SAR surface field view (250 mm stent).

effects, which could impact the RF induced heating, were not considered in this study because of design-simplified stent models.

Conclusion: The relationship of RF induced heating is a multi-parameter dependent issue and basically related to parameters like the dimension of a conductive structure, the electromagnetic properties of the surrounding medium/tissue as well as the electromagnetic environment of the MR system. The numerical investigation is very helpful in depicting the local SAR distribution at implants before performing experiments. Validation of numerical results and further research is necessary to establish computer modeling as a standard tool to support in RF heating testing of implants.

REFERENCES

1. ASTM F2182-02a, "Standard test method for measurement of radio frequency induced heating near passive implants during magnetic resonance imaging," 2002, www.astm.org.

Accurate Evaluation of RF Coil-tissue Interactions Using a Hybrid FDTD-MoM Method

Wenlong Xu[1], **Feng Liu**[2], **Ling Xia**[3], **and Stuart Crozier**[2]

[1]Department of Biomedical Engineering, China Jiliang University, China
[2]School of Information Technology and Electrical Engineering, The University of Queensland, Australia
[3]Department of Biomedical Engineering, Zhejiang University, China

Abstract— A comprehensive consideration of loading effects is essential to the design/analysis of high-frequency MRI radio frequency (RF) coils. In this study, a hybrid finite difference time domain (FDTD)-method of moments (MoM) simulation method is implemented for the accurate evaluation of RF coil-tissue interaction. Using this approach, the RF coil is modelled using the MoM algorithm, and the biological load is handled with the FDTD algorithm. Effective communication between these two approaches is realized through a Huygence equivalent surface. The algorithm has been successfully validated and applied to a loaded coil study and the simulation demonstrated the potential of the hybrid algorithm for high frequency RF coil designs.

In the algorithm, the complex coil/tissue interactions have been explicitly accounted for, and in particular, this method does not make any compromise for RF coil modelling (simplified current/voltage source, staircase assumption, etc), and it enables us to consider more sophisticated coil structures and particularly the mutual coupling between coil-coil & coil-load in an accurate way, which is important for high field RF technology.

Choice of Suitable Wavelets for MR Image Processing

Karel Bartusek[1] and Eva Gescheidtova[2]

[1]Institute of Scientific Instruments, Academy of Sciences of the Czech Republic v.v.i
Kralovopolska 147, Brno 612 00, Czech Republic
[2]Faculty of Electrical Engineering and Communication, Brno University of Technology
Kolejni 2906/4, Brno 612 00, Czech Republic

Abstract— Magnetic nuclear resonance is used in particular as a diagnostic imaging method. Images of selected parts of organs must be of sufficient quality for doctors to be able to not miss any details and to make reliable diagnoses. The detected images are often of low contras and resolution. They are mainly subjected to noise, whose level depends, among other things, on the level of the signal being detected, local proton density, voxel size, bandwidth, system design, quality of RF coil, and detection parameters. Noise is in the same frequency band as the image spectral components that carry the details. Suppressing noise without knowing its properties must be a compromise between the desired smoothing and improvement of SNR on the one hand and a loss of details on the other hand. If the filtering method is applied to remove noise from MR images, a correct choice of individual filtering parameters is important.

Classical linear filtering methods (Fourier and Wiener filtering) remove noise from useful signal by suppressing the chosen frequency bands without distinguishing its usefulness. They are not suitable in suppressing broadband noise and they do not adapt to the noise level in useful signal, which results in insufficient efficiency in modern digital signal processing and thus new solutions have to be looked for. One of the new solutions consists in using wavelet non-linear methods, which make use of the thresholding techniques and are able to better suppress wideband noise, to partially distinguish useful signal from noise and which adapt to the useful signal in any of its segments and at any level of decay. The result of filtering is influenced by the wavelet choice and decay level. Finding optimum decay levels and threshold magnitudes for the individual images being processed is a matter of extensive experiments.

The basis of wavelet transform is the application of a wavelet, a signal limited in time, to a part or to the whole of the signal being processed. This is the main difference in comparison with the other transforms, where harmonic signals of infinite length were used.

The basic wavelet is also referred to as the mother wavelet because further wavelets of the same shape but extended (compressed) and shifted are derived from it via changing the scale and shifting along the time axis. The mother wavelet must have zero mean value. It can have a non-zero mean value only on a finite time interval, which is fulfilled in the case of wavelets with compact carrier. An important property that the wavelet function bases should possess is orthogonality. Today there are over 400 types of wavelet in use, whose properties more or less meet the requirements of the task to be solved.

Rules for the selection of a suitable wavelet can be can be summed up in the following recommendations: complex wavelets detect oscillations well but are not suitable for the detection of isolated singularities; pure real wavelets with few oscillations detect well the peaks and singularities in the signal; asymmetrical wavelets are suitable for the detection of changes in the gradient; symmetrical wavelets do not cause any phase shift between the peak, singularity and oscillation in the signal and the respective manifestation in wavelet coefficients; to detect amplitude and phase simultaneously the complex wavelet must be used.

In the paper, the selection is described of wavelets suitable for improving the quality of MR images of temporomandibular joint and their evaluation according to three criteria: increased SNR, steepness of the change in signal intensity in the image, and the change in contrast.

Criteria for Wavelet Selection in MR Image Filtering

Eva Gescheidtova[1] and Karel Bartusek[2]

[1]Faculty of Electrical Engineering and Communication, Brno University of Technology
Kolejni 2906/4, Brno 612 00, Czech Republic
[2]Institute of Scientific Instruments, Academy of Sciences of the Czech Republic v.v.i
Kralovopolska 147, Brno 612 00, Czech Republic

Abstract— In the early 1980s, transformations were reported that describe in a novel way a suitable combination of time and frequency information about signals, in other words transformations that are more local than the Short Time Fourier Transform (STFT). A marked advance in methods for selecting the useful signal from non-stationary signals degraded by additive noise (MR signal) came with the definition of *lossless wavelet transforms*, e.g., transforms based on the Daubechies, and the Haar, Shannon wavelets. The discrete implementation of wavelet transform is closely connected with digital filtering via filter banks, where the wavelet can be the pulse characteristic of a suitable FIR digital filter of the type of high-pass filter. These short-time signals can better adapt to real signals than infinitely long cosine and sine curves used, for example, in the Fourier transforms. In combination with digital filter banks with perfect signal reconstruction the wavelets define the pulse characteristics of reconstruction filters. Using the wavelet transform, a marked suppression of wideband noise can be obtained via adapting individual parts of the system during filtering to the level of useful signal and distinguishing it from noise.

The introduction of wavelet transform provided an efficient tool for processing not only MR signals but also MR images. For a successful processing of images it is important to select the many currently used types of wavelet. An inappropriate choice of the wavelet can lead to the loss of important information contained in the image or, on the contrary, filtering can be less efficient.

When removing noise from signals, a common criterion for wavelet selection is the SNR, defined as a ratio of the spectral power densities of useful signal and the noise contained in the signal. SNR can also be accepted as the main criterion in image filtering but here its formulation is, for the time being, not unique. The calculation of SNR in images has come to be interpreted as a ratio of signal root mean square and noise root mean square

$$\mathrm{SNR} = 20 \log \frac{\mathrm{RMS}_{\mathrm{Signal}}}{\mathrm{RMS}_{\mathrm{Noise}}}.$$

Further but not so current criteria for the selection of suitable wavelets are the steepness of change in signal intensity in the image at the site of step change, and the change in contrast during filtering.

In the paper, the above given criteria are described and their importance in the selection of wavelets suitable for MR image processing is evaluated.

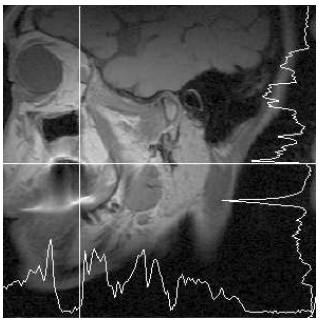

Figure 1: Signal intensity in the image being processed.

Diffusion Characteristics of Accumulators Electrode Materials

P. Marcon[1, 2], **P. Drexler**[1], **and K. Bartusek**[2]
[1]Department of Theoretical and Experimental Electrical Engineering
Brno University of Technology, Kolejni 2906/4, Brno 612 00, Czech Republic
[2]Institute of Scientific Instruments, Academy of Sciences of the Czech Republic
Kralovopolska 147, Brno 612 64, Czech Republic

Abstract— This contribution deals with a study of relaxation measurement and diffusion constants accumulator electrode materials using nuclear magnetic resonance method. Magnetic resonance phenomenon is applied to increase of particles energy in the RF pulse with Larmor frequency. The RF pulse added energy to the electrode material which is in the magnetic field B_0. A FID up to 90° RF pulse absorption line we obtain transverse T_2^* and it will be sufficient to acquire relaxation time T_2. Further we can use a spin echo method for relaxation time measurement that use the 90° RF pulse and next series of 180° RF pulses. The T_2 relaxation time is directly acquired from measured values (inhomogeneous will be eliminated).

The spin echo method was used for the measuring of diffusion material constant with the gradient field. The basic saturation recovery method uses the 90° RF pulses and inversion recovery method works with repeated sequences of RF pulses ($180° - \tau - 90°$). There were used both methods for the longitudinal relaxation time T_1 measurement. It was tested another measurement methods for acquire T_1, for example method which can use the different flip angles sequences of the RF pulses.

The methods which use the different flip angles sequences were developed and tested for measurement of accumulator electrode materials characteristics.

ACKNOWLEDGMENT

The research described in the paper was financially supported by FRVŠ (a fund of university development) by research plan No. MSM 0021630513 ELCOM, No. MSM 0021630516 and grant Czech ministry of industry and trade MPO No. FR-TI1/001, GACR 102/09/0314.

REFERENCES

1. Rychnovský, J. and K. Bartušek, *Experimental Verification of Glass Foam Characteristics Used a Labour Insulation for 129Xe MR Tomographs Chamber*, Elektrorevue [online]. 8. 12. 2004, http://www.elektrorevue.cz/clanky/04062/index.html.
2. Haacke, E. M., R. W. Brown, M. L. Thompson, and R. Venkatesan, *Magnetic Resonance Imaging: Physical Principles and Sequence*, John Wiley, 1999.
3. Patyal, B. R., J. H. Gao, R. F. Williams, J. Roby, B. Saam, B. A. Rockwell, R. J. Thomas, D. J. Stolarski, and P. T. Fox, "Longitudinal relaxation and diffusion measurements using magnetic resonance signals from laser-hyperpolarized 129Xe nuclei," *Journal of Magnetic Resonance*, Vol. 126, 58–65, 1997.

Measurement of X-ray Radiation in Airplanes and the Related Methods of Protection

M. Al-Khaddour and R. Kubasek
Department of Theoretical and Experimental Electrical Engineering, Brno University of Technology
Kolejni 2906/4, Brno 612 00, Czech Republic

Abstract— The source of radiation, control and identify the forms of radiation disintegration and its interaction with particles (α, β, δ) and their effect of radiation on living cells is very important to protect of radiation risks to humans and we need to know how the ionizing radiation is measured. What amount of radiation in the plane and features images of X-ray film and photography to identify alleged conservative medical imaging and screens, films, photographs and film release of solid and clear technical specifications of the augmentation sensitive screens for medical imaging — Photography (dimensions Movies) and X cassette of Medical Diagnostic X-sensitive clip Radio Cassette logical and dose mammography systems in (the movie) which radiates spherical ionizing radiation when dealing with materials and products.

REFERENCES

1. The publication about specifications of X-ray radiation, Syrian Arabian Republic Standards Organization (SASMO), Ministry of Industry, Syria.
2. The publication about specifications of X-ray radiation, The Saudi Arabian Standards Organization (SASO).
3. L'Annunziata, M. and M. Baradei, *Handbook of Radioactivity Analysis*, 58, Academic Press, 2003.
4. Burattini, E. and A. Ballerna, ""Preface". Biomedical applications of synchrotron radiation," *Proceedings of the 128th Course*, IOS Press, the International School of Physics, Enrico Fermi, Varenna, Italy, July 12–22, 1994.

Computation of SAR Distribution in a Human Exposed to Mobile Phone Electromagnetic Fields

Luan Ahma, **Mimoza Ibrani**, **and Enver Hamiti**
Faculty of Electrical and Computer Engineering, University of Prishtina, Kosovo

Abstract— Even though mobile phone is considered by many as fundamental of their lifestyle, exposure to cellular mobile communication electromagnetic fields has raised individual and public concern regarding possible adverse effects to people exposed to such radiation. The most important dosimetric parameter used to assess human exposure to RF electromagnetic fields is SAR (Specific Absorption Rate).

Since SAR, time rate of RF energy absorbed per unit mass of body biological tissue depends from dielectric properties of biological tissues and rms of induced electric field, dielectric properties of human body tissues are addressed. At mobile communication frequencies biological tissues may be considered as dielectric with looses.

Even though lately there have been many studies showing that dielectric properties of biological tissues are also age dependent, in paper SAR is calculated for human of middle age, no gender or age distinction.

Analyzing penetration depth at RF we can say that most critical organs are external biological tissues while comparing permittivity of body biological tissues can be concluded that on eyes, gallbladder, and body liquids will have stronger induced flux for same exposure conditions.

Thus human eyes are among most sensitive organs as they are external and have big values of relative permittivity. Of course, this has to be considered if we place phone near eyes.

Radiation from mobile phone on talk position mostly covers human head. Moreover the transmitted power is not such a big so we cannot expect big values of induced SAR in other parts of body.

In order to assess human exposure to mobile phone GSM electromagnetic field we have run simulations with SEMCAD (FDTD code) for model: human head + mobile phone.

As model for human head is used SAM (Specific Anthropomorphic Mannequin) phantom while mobile phone is modeled as perfectly conducting box with monopole antenna.

Obtained result of Spatial Peak SAR averaged over 1 g of body tissues is 2.1 mW/g for typical transmitting power of mobile phone 250 mW.

Visually and graphically SAR distribution at different position in human head are shown in figures. As noticed Peak SAR appears near human ear.

Effects of Heliogeomagnetic Disturbances on Haemorheological Parameters of Human

Yu. Ya. Varakin[1], **V. G. Ionova**[1], **G. V. Gornostaeva**[1], **E. A. Sazanova**[2, 3], **and N. P. Sergeenko**[2]

[1]Scientific Center of Neurology RAMS, Moscow, Russia
[2]Pushkov Institute of Terrestrial Magnetism, Ionosphere and Radio Wave Propagation RAS Troitsk, Moscow, Russia
[3]Clinical Hospital of Russian Academy of Sciences, Troitsk, Moscow, Russia

Abstract— The changes of the rheological characteristics of blood at the healthy people and in the patients with cerebrovascular pathology during 23 geomagnetic disturbances were studied. The analysis of dynamics of haemorheological parameters of both human groups has shown that the most of parameters are beginning statistically authentically to fall outside the normal limits already prior the beginning of the magnetic disturbance, others — per day of a beginning of disturbance. This fact specifies at an increase of fibrinogen concentration and the variability of functional platelets activity and of markedly enhanced red cells (RBC) aggregation in conditions of geomagnetic disturbance and allows to assume presence of direct influences of an environmental physical processes of haemorheological functions. The deterioration of RBC-deformability and the activation of platelets is observed in the patients with cerebrovascular pathology. The analysis of the data has resulted in occurrence of a hypothesis about appearance of instability at platelet-vascular part of haemostasis under influence of variation of electromagnetic field in during of magnetospheric disturbances.

Such effect can be caused as direct and indirect action of an electrmagnetic field of the Earth on the cells of blood. Haemoglobin of erythrocytes includes atoms of iron, having a deflection of the magnetic moment. In the cells, which had their erythrocytes membrane under influence of an electrmagnetic field, had diminution of electrical mobility that can influence the dynamics of physiological process of aggregation-disaggregation of red cells in a stream of blood.

Another channel of influence of geomagnetic disturbances on rheological property of blood can be connected with the action of electrmagnetic fields through synchronization of rhythms of electromagnetic cells oscillations in central nervous system. From the entire spectrum of an electrmagnetic field apparent on the surface of the Earth, biologically effective factor is in a range of ultra low frequencies from 0,0001 up to 100 Γ?. The biorhythms of the brain, such as an alpha, beta, delta, tetra and gamma rhythms are characteristic for the man in this range. At the development of the resonant phenomena there is a stressful reaction that conducts to increase of concentration of catecholamines in the blood and activation of red cells and platelet aggregation.

Improvement of the Confidence Interval Level of Multi-frequency Microwave Radiometer System for Measuring Deep Brain Temperature in New Born Infants

T. Sugiura[1], **N. Umehara**[1], **S. Mizushina**[2], **and H. Hirata**[1]

[1]Research Institute of Electronics, Shizuoka University, 3-5-1 Johoku, Hamamatsu 432-8011, Japan
[2]Hamamatsu Science Promotion Financial Group, 3-5-1 Johoku, Hamamatsu 432-8561, Japan

Abstract— Although cooling the brain of newborn baby can reduce neuro-developmental impairment after a hypoxic-ischemic insult, clinical trials are currently hindered by the difficulty in measuring brain temperature non-invasively as well as continuously. MRI and MR spectroscopy methods have been used to measure temperature changes in the brain, however, these require access to complex equipment and they are not suitable for routine measurements repeated over a prolonged period of time. As one of the possible alternative methods for non-invasive temperature sensing and monitoring that is completely passive and inherently safe is microwave radiometry (MWR). The first temperature measurement study for an agar-phantom by MWR have been reported in PIERS 2006 especially on the temperature resolutions of five microwave receivers as well as the temperature sensing accuracy at 5 cm depth from the surface. Then temperature resolutions were 0.280, 0.321, 0.155, 0.113 and 0.122°C for 1.2, 1.65, 2.3, 3.0, and 3.6 GHz receivers, respectively. Using these resolutions, the confidence interval level at 5 cm depth was simulated to be 1.6°C. Because the clinical requirement is 1°C, further improvements of MWR system were essential for a successful hypothermia treatment. We have done a couple of actions to reduce background noise and obtained better temperature resolutions of 0.103, 0.129, 0.138, 0.105 and 0.111 for each receiver. This improvement results in better confidence interval level of 0.70°C at 5 cm depth from the surface. This paper describes the feasibility of MWR system for clinical hypothermic treatment.

Validity of Inverse Coupler to Improve Temperature Resolution of One-band Microwave Radiometer for Non-invasive Brain Temperature Monitoring

H. Hirata[1], **T. Ishii**[1], **Y. Okita**[2], **and T. Sugiura**[1]

[1]Research Institute of Electronics, Shizuoka University
3-5-1 Johoku, Hamamatsu 432-8011, Japan
[2]Graduate School of Science and Technology, Shizuoka University
3-5-1 Johoku, Hamamatsu 432-8011, Japan

Abstract— In this study, we present a design for one-band microwave radiometer aimed at prolonged monitoring of deep brain temperature and suitable for use during hypothermic neural rescue therapy. Clinical requirement of confidence interval level of temperature estimation at 5 cm depth from head surface is about 1°C. This requirement is a tough goal because the microwave radiometer measures average power of noise coming from inside the brain and indistinguishable from the noise generated by a warm resistor (background) or by receiver electronics. Though the structure of radiometer is almost the same as that of a radio-telescope and the radiometer noise in the radio-telescope is usually minimized by cooling the receiver to cryogenic temperatures, the present microwave radiometer needs to operate in a room temperature as might be expected. In order to reduce the background noise, an inverse coupler was inserted at the input to the receiver and the temperature resolution was compared with that without the coupler by measuring the noise power of water. Thus obtained confidence interval was improved from 0.654°C to 0.233°C (64% amelioration) though further actions are fundamental to the practical implementation of the technique.

Influence of Effective Mode Area on Stimulated Brillouin Scattering Slow Light in Optical Fibers

Shang-Lin Hou, **Zhong-Yi Wang**, **Suo-Ping Li**, **and Jing-Li Lei**
School of Science, Lanzhou University of Technology
Lanzhou 730050, China

Abstract— The stimulated Brillouin scattering (SBS) in fibers to produce tunable delays has been extensively studied for its advantages [1, 2]. Since SBS slow light was first demonstrated experimentally by Kwang Yong Song et al. [3], great progress has been made on how to obtain longer pulse delay and control the pulse distortion experimentally. Some theoretical researches of SBS slow light, which provides an insight into the SBS slow light process were implemented by numerical methods [4]. Further research towards successful exploring an ideal optical fiber will make it possible to realize slow light devices with a much high efficiency.

In this work, the SBS model was described and the stimulated Brillouin scattering coupled equations were solved numerically, we present our numerical simulation results in analyzing the effect of effective mode area on time delay and pulse broadening within the gain range of $0 \sim 16$. Both regimes of small signal and gain saturation were considered. We expect our research will be useful for designing this kind of optical device.

Characterization of InP Based SAGCM Avalanche Photodetector for Single Photon Fiber Optic Communications

Wen-Jeng Ho, **Jheng-Jie Liou**, **and Cheng-Ju Chen**
Institute of Electro-Optical Engineering, National Taipei University of Technology
1, Sec. 3, Chung-Hsiao E. Rd., Taipei 106, Taiwan

Abstract— This paper presents the characterization of InP-based separate absorption, grading, charge, and multiplication (SAGCM) avalanche photo-detectors (APDs) for single photon fiber optic communications. Recently, single photon communications, i.e., quantum key distribution (QKD), have received much interest due to their confirmed security. InP-based avalanche photodiodes operating in Geiger-mode at low temperature as single-photon avalanche detectors (SPADs) have emerged as a key component for 1550 nm QKD system application. However, SPADs for single photon detection are demanded to have a high single-photon detection efficiency (SPDE, η_{det}) and a low dark count probability (P_{dc}). For quantum key distribution, single-photon detection efficiency is proportional to bit rate. The ratio of P_{dc} to η_{det} is a factor of quantum bit-error rate of a detector (QBER_{det}), which a low QBER_{det} was required for single photon fiber optic communications. In this work, we report the fabricated SPAD from our laboratory on performance characterization of dark current (I_d), dark count probability (P_{dc}), single-photon detection efficiency (η_{det}), noise equivalent power (NEP), afterpulsing effect, and quantum bit-error rate of a detector (QBER_{det}).

The fabricated InP based single photon avalanche detector was grown by metal-organic vapor phase epitaxy (MOVPE) on an n-type (100) InP substrate. The epitaxial layer structure was separate InGaAs-absorption, InGaAsP-grading, InP-charge, and InP/InAlAs hetro-multiplication (SAGCM). The p-n junction was achieved by Zn diffusion through a 90-μm diameter widow in SiNx layer, creating a p^+-InP region in the n-InP/InAlAs multiplication layer. P and N electrode contacts were AuZn and AuGeNi deposited on the front-side and back-side of the substrate, respectively. We packaged an APD chip in a TO-46 pig-tail module. The module then was placed with an impedance-matching circuit-board into a temperature controlled vacuum chamber for device performance testing. The dark current of SPAD at 90% of the breakdown voltage ($0.9\,V_{\mathrm{BR}}$) was 37.8 pA and 18.8 nA at 200 K and 300 K, respectively. Under -40°C and gate repetition frequency of 10 KHz with pulse width of 2 ns, the performance of $P_{dc} = 0.02$, $\eta_{det} = 12.5\%$, NEP $= 5 \times 10^{-14}$ W/(Hz)$^{1/2}$, $P_{dc}/\eta_{det} = 0.16$ were simultaneously achieved. In addition, we also report on the generation source of dark current and dark count in InP based SAGCM SPAD at temperature range from 200 K to 300 K using activation energy (E_a) analysis. Both the dark current and the dark count exhibited activation energy of 0.24 eV in temperature below 240 K.

In summary, we have fabricated InP based SAGCM SPAD for single photon fiber optic communications. The SPAD performance of dark current (I_d), dark count probability (P_{dc}), single-photon detection efficiency (η_{det}), noise equivalent power (NEP), afterpulsing effect, and quantum bit-error rate of a detector (QBER_{det}) are reported. Both the dark current and the dark count exhibited the activation energy of 0.24 eV in lower temperature and showing the dominant generation source was band-to-band tunneling or the field-enhanced band-traps-band tunneling.

ACKNOWLEDGMENT

The authors would like to thank the financial support from the National Science Council under Grant NSC-97-2221-E-027-008-MY2.

Design of a Novel Voltage Sensor Based on Fiber Bragg Grating with Electro-optic Crystal Material Cladding

Shang-Lin Hou, **Bo Chen**, **Zhong-Yi Wang**, **Yan-Jun Liu**, **and Jing-Li Lei**
School of Science, Lanzhou University of Technology, Lanzhou 730050, China

Abstract— Influence of electric field running along the fiber Bragg gratings on the reflectivity and Bragg wavelength of the fiber with cladding made of uniaxial anisotropic and electro-optic crystal material whose optical axis is parallel to the axis of fiber was investigated. The calculated results indicate that the electric field has a strong impact on the reflectivity and Bragg wavelength of this kind of fiber, especially when the parameter K_{cl}, i.e., the ratio of the extraordinary to the ordinary ray refractive index changed by the electric field, varied from 1.00 to 1.01. These studies provide an important basis for designing new voltage sensors and studying some characteristics of electro-optic crystal. A novel voltage sensor based on fiber Bragg grating with $LiNbO_3$ electro-optic crystal material cladding was designed.

Numerical Simulation of the HPM Breakdown on Dielectric Surface Including Outgassing

Libing Cai[1] **and Jianguo Wang**[1, 2]

[1]Northwest Institute of Nuclear Technology, P. O. Box 69-12, Xi'an 710024, China
[2]School of Electronic and Information Engineering, Xi'an Jiaotong University, Xi'an 710049, China

Abstract— With the development of HPM (High Power Microwave), plasma breakdown at dielectric windows has become an important challenge with the advent of GW power level sources. This paper presents the electrostatic PIC-MCC method for simulating the breakdown of dielectric surface illuminated by high-power microwaves, and establishes the physical model of HPM dielectric surface breakdown including outgassing. The process of the breakdown is simulated including field emission, mutipactor, outgassing and gas collision ionization.

The temporal evolution of the number of electrons and the breakdown delay time are also shown in this paper. The temporal evolution of the number of electrons is characterized by three-phase development. Phase one comprises a fast several nanoseconds buildup of a saturated secondary electron avalanche. Phase two is associated with a slow increase of electrons number, with a duration on the order of 10 ns, the number increases by about ten times. The final phase three is characterized again by a fast nanoseconds electrons number rise up.

This paper investigates the influence of outgassing to the breakdown by simulating the process of breakdown with different electron-stimulated desorption efficiency. The results show that when the electron-stimulated desorption efficiency is less than 0.1, the breakdown doesn't occur for a 50-ns HPM pulse because the formation of the gas layer on the dielectric surface is too slow. When the electron-stimulated desorption efficiency is greater than 0.1, the breakdown occurs and the breakdown delay time is shorter with the gas desorption rate increase. In addition, we verify the rationality of our simulation by comparing our simulation result to the experimental results of the DC dielectric surface breakdown.

Multi-branch Waveguide Bender by Using Embedded Optical Transformations

Jianhong Lv, **Lei Wan**, **Baorong Yan**, **Linghua Kong**,
Zhaoquan Chen, **Minghai Liu**, **and Xiwei Hu**
College of Electrical and Electronic Engineering, Huazhong University of Science and Technology, China

Abstract— Transformation optics has attracted much attention in the past three years, as it opens up many possibilities and methods to control the electromagnetic (EM) fields, and helps to construct many complex devices, such as invisible cloak, field rotator, concentrator, beam shifter and splitter, and so on.

Recently, many groups studied the waveguide bender based on the finite embedded optical transformation technique, and it can bend the EM wave to arbitrary desired directions. In this paper, we extend their work to multi-branch case by employing the same principle of coordinate transformation. With this multi-branch bender, the EM wave can be simultaneously bended to different directions with desired angles in a waveguide or in the free space without any reflections. Furthermore, in the process of obtaining the relative permittivity and permeability tensors of the medium of each branch in the transformed space, we find that if we obtain the constitutive parameters tensors of one branch, the constitutive parameter tensors of other branches can be easily obtained only by replacing some given constants. Then, in order to investigate the performance of this multi-branches waveguide bender, numerical simulations based on the finite element method were carried out, and the results verify our design very well.

Lastly, without loss of generality, we discuss the case that two bend branches are crossed to each other, and get the modified constitutive parameter tensors. From the numerical simulated results, we find that it can also bend the EM wave to the desired directions, though the EM wave in two branches interfering to each other. The results in this paper may be useful in designing waveguide bender and other devices.

A Planar and Polarization Insensitive Perfect Metamaterial Absorber

Lei Lu[1], **Shaobo Qu**[1], **Zhuo Xu**[2], **Jiafu Wang**[1], **Hua Ma**[1], **Xinhua Wang**[1], **and Chao Gu**[1]

[1]College of Science, Air Force Engineering University, Xi'an, Shaanxi 710051, China
[2]Electronic Materials Research Laboratory, Key Laboratory of the Ministry of Education
Xi'an Jiaotong University, Xi'an, Shaanxi 710049, China

Abstract— A planar and polarization independent perfect metamaterial absorber was proposed in this paper. As simulated, the plane wave was nearly perfect absorbed at 9.9 GHz, with a 98.2% absorption. We fabricated and tested the sample of the metamaterial absorber, the absorptivity was only 81.9% at 11.2 GHz. For the metamaterial absorber was composed of highly symmetric two-layered structures, it was independent to the polarizations of normal incidence.

A Wideband Three-dimensional Metamaterial Absorber

Lei Lu[1], **Shaobo Qu**[1], **Zhuo Xu**[2], **Jiafu Wang**[1], **Hua Ma**[1], **Xinhua Wang**[1], **and Chao Gu**[1]

[1]College of Science, Air Force Engineering University, Xi'an, Shaanxi 710051, China
[2]Electronic Materials Research Laboratory, Key Laboratory of the Ministry of Education
Xi'an Jiaotong University, Xi'an, Shaanxi 710049, China

Abstract— In this paper, a wideband three-dimensional metamaterial absorber was presented. The structure of the metamaterial absorber was rotationally symmetrical, so it was polarization-insensitive. A 98.4% absorptivity was achieved at 14 GHz, and the 50% absorbance bandwidth is 16.7% in simulation. Another passband appeared at the left side of the absorbing passband, this may be useful for some application, such as communication.

Modeling and Simulation of Large-scale Rectangular Surface-wave Plasma Source

Chaohui Lan, **Wendou Wang**, **Qiang Wang**, **Long Xie**, **Jihao Jiang**, **and Caihua Wei**
Institute of Fluid Physics, CAEP, Mianyang 621900, China

Abstract— Surface-wave plasma (SWP) source can produce high-density and large-scale uniform plasma through microwave without the use of external electrodes or magnets. In recent years, SWP source has been developed to be a competitive processing tool for ultra-large-scale integrated (ULSI) circuit devices, flat panel displays etc. To date, significant progress has been made in this field, however, some problems like the antenna-surface wave coupling mechanism and the optimum design of the slot antenna have not been satisfactorily resolved yet. In this paper, a self-consistent and three-dimensional model of argon discharge in a large-scale rectangular SWP source is presented, which is based on the finite-difference time-domain (FDTD) approximation to Maxwell's equations self-consistently coupled with a time-stepping fluid diffusion model for plasma evolution. The spontaneous outspread of plasma towards quartz edge under the drive of surface wave can be simulated by this model, and the final steady states of electron density and electron temperature distributions can be obtained. The numerical simulation results reveal the electromagnetic wave distributions in the whole device and confirm the existence of the surface wave. The results also show that the electron density has a characteristic profile such that the peak is located several centimeters from quartz boundary, while the electron temperature monotonously increases toward the boundary. The tendencies and the orders of magnitudes of the results show good agreement with existing experiment data. The code been developed can not only be used to the analysis of the electromagnetic fields and the plasma parameters in the whole device, but also be a useful tool for computer-aided optimization of the SWP source design.

Property of Subwavelength Resonator with DNG Metamaterials by FDTD Method

Kui-Song Zheng, **Chang-Ying Wu**, **Jia-Dong Xu**, **and Gao Wei**
School of Electronics and Information, Northwestern Polytechnical University, Chang'an Campus
Xi'an, Shaanxi 710129, China

Abstract— In this paper, a subwavelength resonator loaded with metamaterials has been investigated both analytically and numerically. Based on constructive equations of DNG materials modeled by Drude model, the updated equations in the DNG materials are deduced and determined with the FDTD scheme. In the one-dimensional case, a subwavelength cavity with metamaterials of negative permeability is proposed. Numerical results show that the resonator with MNG materials has two resonances: one is a normal resonance; the other one is a subwavelength resonance. The proposed subwavelength resonator overcomes the diffractive limitation. By analyzing the numerical results, the physical dimensions of the subwavlength cavity with operating in the subwavelength frequency can reduce to 0.083 times the operating wavelength in comparison to 0.5 times the operating wavelength for the conventional resonator. A new avenue has supplied for manufacturing the subwavelength resonator.

Experimental Verification of Anisotropic Three-dimensional Left-handed Metamaterial Composed of Jerusalem Crosses

Jiafu Wang[1], **Shaobo Qu**[1], **Hua Ma**[1], **Song Xia**[2], **Yiming Yang**[1], **Lei Lu**[1], **Xiang Wu**[1], **Zhuo Xu**[2], **and Qian Wang**[3]

[1]College of Science, Air Force Engineering University, Xi'an, Shaanxi 710051, China
[2]Electronic Materials Research Laboratory, Key Laboratory of the Ministry of Education Xi'an Jiaotong University, Xi'an, Shaanxi 710049, China
[3]College of Environment and Planning, Liaocheng University, Liaocheng, Shandong 252000, China

Abstract— An anisotropic three-dimensional (3D) left-handed metamaterial (LHM) was proposed in this paper. The LHM is composed of unit cells with metallic Jerusalem crosses etched correspondingly on both sides of dielectric substrates. 3D left-handed property is realized by the couplings between neighboring metallic Jerusalem crosses. The LHM was fabricated and experimentally measured. The results show that the LHM always exhibits left-handed bands for incident plane waves along x, y, and z directions. Because of the symmetry of the unit cell, left-handed properties of the proposed 3D LHM in x and y directions are the same but are different from that in z direction. This verifies the validity of the proposed anisotropic 3D LHM.

Application of Optimization Algorithm to Designing Absorber Composed of RHM and LHM

Dan Lv[1, 2], **C. M. Tong**[1, 2], **and Y. Geng**[3]

[1]25 Letter Box, China
[2]State Key Lab. of Millimeter Waves, China
[3]Satellite Control Center, China

Abstract— The permittivity and permeability of left-handed materials (LHM) both are negative. When electromagnetic wave is propagating in these materials, electric field, magnetic field and wave vector conform to the left-hand screw rule. It means that the direction of phase velocity is contrary to the direction of group velocity. In this paper, the reflection characteristics of an absorber composed of right-handed materials (RHM) and LHM are analyzed by transmission line model. Particle swarm optimization (PSO) has been applied to optimization design broadly since it was presented because it is simpler than other intelligent optimization algorithms. But sometimes PSO is not applicable for some complex problems. By using simulated annealing (SA) algorithm, if the fitness value of new state is worse than the fitness value of current state, there is some probability of accepting the new state. It means that the current state may be worse than previous state. So SA can help the optimization avoid being trapped in the local optima. Thus a hybrid algorithm based on improved PSO and SA algorithm is derived to optimize the parameters of the absorber. With the optimal permittivity, permeability and thickness of LHM and optimal thickness of RHM, the least reflectivity will be attained. Then the reflectivity is also computed when one parameter is changeable and the other parameters are unchangeable. The results show the relationship between reflectivity and frequency with a fixed parameter.

The Transmission Properties of Electromagnetic Wave in Three-dimensional Plasma Photonic Crystals

J.-W. Xu and J.-M. Shi
State Key Laboratory of Pulsed Power Laser Technology
Key Laboratory of Infrared and Low Temperature Plasma of Anhui Province
Electronic Engineering Institute, Hefei 230037, China

Abstract— The transmission properties of electromagnetic wave in three-dimensional plasma photonic crystals (PPCs) are studied by the Finite Difference Time Domain (FDTD) method in this paper. The results were presented that the plasma frequency, plasma collision frequency, layer number, and ratio of radius to crystal lattice constant can influence the transmissivity in the face-centered cubic (fcc) and face-centered tetragonal (fct) lattice woodpile structure PPCs.

The Non-constancy of Speed of Light in Vacuum for Different Galilean Reference Systems (Revisited)

Namik Yener
Technical Education Faculty, Umuttepe Campus, Kocaeli University
Izmit 41380, Kocaeli, Turkey

Abstract— It was established by the author in a previous article that the postulate of the constancy of speed of light of Special Relativity Theory is false for an electromagnetic system that consisted of a rest frame (denoted by K) constituted by a simple medium with loss (medium (I)), and a frame (denoted by K') in uniform rectilinear motion with respect to the first, wherein a perfectly conducting medium (medium (II)) fills the half space such that the interface of the two media is an infinite plane, perpendicular to the direction of motion of K'. In that system a plane wave was assumed to impinge on the boundary of the two media. In this paper we consider the same electromagnetic system but we add a point charge in uniform motion parallel to one of the rectangular axes perpendicular to the direction of motion of K'. Now it is this charge that is the source for the fields. However we find that the relationship that was found in the above mentioned article and that was the basis for arguing the falsity of the Special Relativity Theory does not change in the present system as well. The said relationship is an algebraic relationship between the relative speed of K' with respect to K, frequency measured from K', the constitutive parameters of medium (I) and the speed of light c in vacuum for reference system K. It is also remarked that, the falsity of Special Relativity Theory rises not only because of dependence of c on the frequency in this algebraic relationship, but also because of its dependence on the relative speed of K' with respect to K, which implies dependence of c on the reference systems.

Non-constancy of Speed of Light in Vacuum for Different Galilean Reference Systems in Case of an Impulsive Plane Wave

Namik Yener
Technical Education Faculty, Umuttepe Campus, Kocaeli University, Izmit 41380, Kocaeli, Turkey

Abstract— Previous work which negates Special Relativity Theory and which was carried out only for a monochromatic plane wave is extended to an impulsive plane wave. The media considered consist in a linear dispersive medium with absorption (the Lorentz medium) that fills the space $x > -x_0$, where $x_0 > 0$ holds with free space to exist for $x < -x_0$ (medium (I)) and a simple but lossy medium (II) initially filling the half space $x > 0$. Medium (I) has frequency dependent conductance and dielectric permittivity in distinction from the original work for the monochromatic wave. Inertial frames K and K' are attached to medium (I) and (II), and the above description of these two media are true when they are observed from K and K' respectively. K and K' have coincident origins in space and time initially, and at $t = t' = 0$, K' starts a uniform rectilinear motion with respect to K. An impulsive in time plane wave is assumed to impinge on the plane $x = -x_0$, at the time t_0, when $-x_0$ and t_0 are both measured from K. Complex phase invariance principle is applied to the resulting elementary plane waves whose superposition yields the impulse response of the system. Transformation relations for the wave numbers and frequencies for incident and reflected waves for the interface of medium (I) and (II), are obtained using a 'modified Lorentz transformation' which incorporates different speeds of light in vacuum c and c' for K and K', as was done for the monochromatic plane wave case. Next using the dispersion relations for the incident and reflected waves an algebraic relation is derived between constitutive parameters of the Lorentz medium, the frequency, c and the relative speed of K' with respect to K. This result implies that the speed of light in vacuum c is dependent on the reference frame, a violation of the basic assumption of Special Relativity Theory.

Non-constancy of Speed of Light in Vacuum for Different Galilean Reference Systems and Momentum and Energy of a Particle

Namik Yener
Technical Education Faculty, Umuttepe Campus, Kocaeli University, Izmit 41380, Kocaeli, Turkey

Abstract— The conservation of energy and momentum of a particle is investigated under a 'modified Lorentz transformation' which is a transformation law that emerges as compulsory after considering two lossy media to which inertial frames K and K' are attached. This emergence is an outcome of the failure of Special Relativity Theory to account for the mentioned loss in one of the media, as proved by the author in reported preceding work. This 'modified Lorentz transformation' incorporates different speeds of light in vacuum c and c' for K and K'. The velocity addition law under this transformation is given. Dependence of the relativistic expressions of momentum and energy for a particle which are relegated to their nonrelativistic values in the limiting case, on the magnitude of velocity is sought for. To this end collision and scattering of two identical particles are considered. A small scattering angle θ' is assumed in a glancing collision of the two particles, and the demanded dependences on the magnitude of the velocity of the particle are derived. This is achieved by considering a Taylor expansion of the conservation of energy equation around the point $\theta' = 0$. The results dictate a covariant but not invariant relation between the energy of a particle and its mass. This is due to the assumption of existence of different speeds of light in vacuum c and c' for frames K and K'. This development is identical with an existing one in the literature, but here the principle of constancy of speed of light is put aside on the basis of the falsity of Special Relativity Theory that was established previously.

Numberical Methods for Three-dimensional Electromagnetic Invisible Cloaks with Irregular Boundary Shapes

Xinhua Wang[1], **Shaobo Qu**[1, 2], **Song Xia**[2], **Binke Wang**[1], **Zhuo Xu**[2], **Hua Ma**[1], **Jiafu Wang**[1], **Chao Gu**[1], **Xiang Wu**[1], **Lei Lu**[1], **and Hang Zhou**[1]

[1]College of Science, Air Force Engineering University, Xi'an 710051, China
[2]Electronic Materials Research Laboratory, Key Laboratory of Ministry of Education
Xi'an Jiaotong University, Xi'an 710049, China

Abstract— The coordinate transformation theory is used to design invisible cloaks including the electromagnetic wave and the acoustic wave ones. By solving Laplace's equation that describes how the coordinates transform, three-dimensional (3-D) electromagnetic (EM) invisible cloaks with irregular boundary shapes can be designed provided the boundary conditions of the cloaks can be determined by the corresponding transformation. This design process is efficiency to design complicated and practical structures. Full wave simulations based on finite element method verified the designed 3-D EM invisible cloaks. The constitutive material parameters of the EM invisible cloaks can be calculated according to the coordinate transformation theory.

Accurate Determination of Refraction Points on the Interfaces of Multi-layer Media

Zhiyong Han, **Weikun He**, **Hao Chen**, **and Renbiao Wu**
Tianjin Key Lab for Advanced Signal Processing, Civil Aviation University of China
Tianjin 300300, China

Abstract— Ground penetrating radar (GPR) is a newly developed geophysics method in the detection and recognition of subsurface targetsDelay and Sum (DAS) imaging method based on time-domain focusing of pulse-echo radar data is commonly applied in imaging technique. For multi-media, DAS needs to determine refraction points on the interfaces of different media which is critical to SAR imaging. Because of time consuming or inaccuracy, there is not a perfect algorithm to solve this problem. In this paperone algorithm for the determination of refraction points of multi-media is presented which is proved to be much efficient and accurate.

For a two-layer media model as shown in Figure 1, according to Snell's law, the horizon range x_i is determined by

$$x_i = x_a + h_1 \tan\theta + h_2\sqrt{\varepsilon_1}\frac{\sin\theta}{\sqrt{\varepsilon_2 - \varepsilon_1 \sin^2\theta}} \tag{1}$$

where (x_a, h_1) is the location of the source, h_2 is the depth of the focal point: ε_1, ε_2 are the dielectric coefficients of the two layers, respectively, θ denotes the incident angle.

Increase θ from 0 to $\frac{\pi}{2}$, when the deference between the x_i getting from Equation (1) and the actual location of refraction point is limited in the thresholdwe can get the accurate refraction point which is represented by θ. This method also can be used in the multi-media.

Compared with fourth-order equations and engineering algorithmthe method introduced above simplifies the computational process and increases the accuracy of the calculation of refraction points on the interfaces of multi-media.

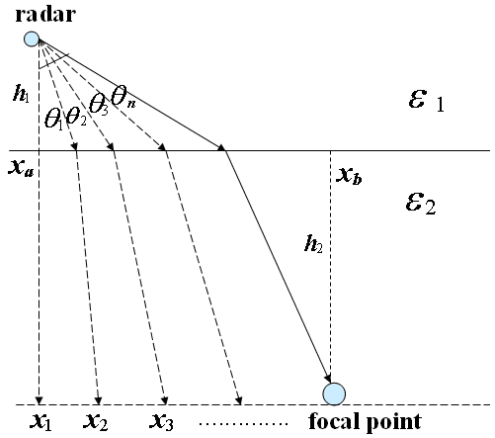

Figure 1: Model of two-layer media refraction.

The Stress of Multilayers of W/Si, WSi_2/Si and Single Layer Coatings of W, WSi_2, Si

Qiushi Huang, **Jingtao Zhu**, **Jing Xu**, **Xiaoqiang Wang**, **and Zhanshan Wang**
Institute of Precision Optical Engineering, Department of Physics
Tongji University, Shanghai 200092, China

Abstract— A series of W, WSi_2, Si thin films and W/Si, WSi_2/Si periodic multilayers were fabricated using DC magnetron sputtering. Surface profiles before and after deposition were measured with a stylus profiler and the stress values were calculated. The results indicate that W thin film shows relatively large compressive stress, while W/Si multilayers show tensile stress. For both WSi_2 thin films and WSi_2/Si multilayers, the stress keep compressive without a sharp change, they have the most stable stress state.

Millimeter-wave Signals Generated by Using Up-conversion for Radio-on-fiber System

C. C. Weng[1], **W. S. Tsai**[1], **Y. F. Lin**[1], **and H. H. Lu**[2]

[1]Department of Electrical Engineering, Ming Chi University of Technology
84 Gungjuan Rd., Taishan, Taipei 24301, Taiwan, R.O.C.
[2]Department of Electro-Optical Engineering, National Taipei University of Technology
1, Sec. 3, Chung-hsiao E. Rd., Taipei 10608, Taiwan, R.O.C.

Abstract— Recently, the microwave frequency of millimeter-wave band in 30 $\sim$ 300 GHz is most popular. We would like to generate tens of thousands of millimeter-wave frequency in traditional electronics. Because of four-wave mixing (FWM) phenomenon within semiconductor optical amplifier (SOA). We could achieve needs of millimeter-wave signal. The use of millimeter-wave signals generated a wide bandwidth, simple system architecture and lower cost, etc. The millimeter-wave is also suitable for short-range transmission, broadcast and broadband internet signal in the future.

In this letter, we proposed simple up-conversion system architecture, make the use of SOA to achieve the frequency multiplication for nonlinear effects of FWM. We will feed 7.5 GHz signal into the mach-zehnder modulation (MZM) modulation to generate double sideband (DSB) signal, as well as adjust the DC bias to eliminate central wavelength. Signal will be amplified by using erbium doped fiber amplifier (EDFA). The signal was filtered by the optical band pass filter (OBF), then generate a FWM efficiency for the SOA. We can product the new signal and detect by photo diode (PD), generate doubled frequency, tripled frequency even to quadruple frequency multiplications, it means that 15 GHz, 22.5 GHz and 30 GHz signal can achieve. Finally this millimeter-wave is filtered out by using the OBF. The high-frequency signals depend on the input RF signal frequency that is more flexible. Comparing to traditional high-frequency signal generator system, this system is simple and lower cost.

SVM-based Approach for Buried Object Detection

Qing He Zhang[1] and Jing-Jing Yao[2]

[1]School of Science, Three Gorges University, Yichang, Hubei 443002, China
[2]School of Electronics Information, Wuhan University, Wuhan 430079, China

Abstract— In this paper, a new method for the buried object detection is proposed. The center position and dielectric properties of 2-D buried object are estimated by means of a regression technique based on the use of support vector machines (SVMs). The proposed method, after a proper training procedure, is able to reconstruct the center position and dielectric properties of buried object inside a given investigation domain. Numerical results are provided for the validation of the approach.

Session 4P1a
Remote Sensing of Water Cycle Related Components

Estimation on Snow Water Equivalent Using High-frequency SAR Observations

Jinyang Du[1] **and Jiancheng Shi**[2]

[1]Institute of Remote Sensing Applications, Chinese Academy of Sciences
P. O. Box 9718, Beijing 100101, China
[2]Institute for Computational Earth System Science, University of California
Santa Barbara, USA

Abstract— High-frequency SAR, with its high sensitivity to snowpack properties and fine spatial resolutions, has become one of the most promising techniques for estimating snow water equivalent (SWE). Future high-frequency SAR systems, especially a dual band, high-frequency (X- and Ku-Band) SAR system for the on-going mission Cold Regions Hydrology High-resolution Observatory ($CoReH_2O$), will enable an accurate description of the characteristics of the cycle of snow.

In this study, a method for estimating SWE for high frequency SAR observations was described. The method was developed based on the following steps: (1) Generating a snow scattering database for X and Ku-band SAR observations using theoretical models; (2) estimating snow volume scattering component from the total SAR signals by using decomposition techniques; (3) estimating SWE based on the analysis of the relationships between different frequencies. To validate the SWE inversion technique, simulated database and Ground-Based Synthetic Aperture Radar (GBSAR) measurements obtained from SARALPS-2007 field experiment were used. The estimated SWE is found to be well correlated with simulated/measured SWE with an acceptable accuracy.

Bistatic Measurements of Soil Moisture by Using GNSS Signals: An Experimental Campaign

M. Brogioni[1], **M. Caparrini**[2], **A. Egido**[2], **E. Farres**[2], **E. Motte**[2], **N. Floury**[3], **L. Guerriero**[4], **S. Paloscia**[1], **P. Pampaloni**[4], **S. Pettinato**[4], **N. Pierdicca**[4], **and E. Santi**[1]

[1]IFAC-CNR, Florence, Italy
[2]STARLAB, Barcelona, Spain
[3]ESA/ESTEC, Noordwijk, The Netherlands
[4]CeTeM, Florence, Italy

Abstract— The use of microwave radar and radiometer in estimating soil moisture and vegetation parameters of land has shown a good potential. However, both experimental activities and theoretical results seem to indicate that important limitations to the actual use of monostatic radar exist. They are: in soil moisture applications the simultaneous disturbing effects of soil roughness and vegetation cover; in vegetation monitoring, the early saturation of its response with respect to plant biomass. As far as radiometric measurements are concerned, the ground resolution required in many applications remains a challenging issue.

Global Navigation Satellite System are another possible source for bistatic radar observations of the Earth's surface. Indeed, preliminary investigations have demonstrated the capability of GPS scatterometers to sense small changes in surface reflectivity. Nevertheless, in order to obtain precise soil moisture estimates there are several phenomena that need to be taken into consideration, mainly the effects of diffuse scattering over the soil surface due to surface roughness and vegetation canopy.

In order to investigate the potentialities of GNSS signals for quantitative land bio-geophysical parameters remote sensing, and their future possible applications from spaceborne platforms a project has been promoted and funded by ESA. As a part of this project, an experimental campaign was carried on an agricultural area located in Italy close to Florence along the Pesa River. Bare soil was first worked with several types of surface roughness, then half of the area was seeded with sunflowers.

A GNSS instrument was installed on a hydraulic platform, at a height of 20 meter above soil. The instrument features an up-looking GPS L1 RHCP antenna, for the reception of the direct signal, and two down-looking LHCP and RHCP antennas for the reception of the two polarization components of the reflected signal. Both down-looking antennas share a common receiving channel, therefore the operative antenna is selected at each time by a radio-frequency switch. In addition to the GPS Antenna sections, two logical separated sections comprise the instrument: the Radio Frequency and the Digital Signal Processing section. The former comprises the calibration chain, which is a main part in the scatterometric instrument design, and the GPS front-ends, where the signal is down-converted to intermediate frequency, and digitized in a successive stage. In the Digital Signal Processing section the digitized signal is parallelized and sent to the instrument's software receiver, where the correlation of the signal with the clean replica is performed in order to finally produce the complex waveforms. The instruments records direct and reflected complex waveforms, and time series of the waveforms peaks from which the basic soil bio-geophysical observables are obtained.

Ground truth data, collected on the area at the same time as the GNSS measurements, comprised the most significant vegetation and soil parameters (plant density, leaf and stalk dimensions, number of leaves per plant, plant water content and moisture, volumetric and gravimetric soil moisture, surface height standard deviation and correlation length). Soil moisture of the first (10 cm) soil layer was continuously measured (24 h/day) using 6 FDR (Frequency Domain Reflection) probes. Additional measurements were carried out with a portable TDR probe once a week. Gravimetric soil moisture was also measured collecting and weighting samples of soil before and after drying. These measurements were used for checking the calibration of FDR/TDR probes. Some meteorological parameters (i.e., air temperature, humidity, rainfall, etc.) were also measured on site. Vegetation parameters were measured by using conventional methods. Surface roughness measurements were obtained by using needle and laser profilometers. Soil temperature was monitored with a thermal infrared sensors and a PT 100 probe placed 10 cm below surface.

The campaign lasted from early March to early September 2009 and made it possible to collect a significant amount of data in various surface and meteorological conditions. Comparison of

GNSS and ground truth data will provide the opportunity to estimate the sensitivity of GNSS signal to soil and vegetation conditions, and to perform a first estimate of the potentialities of the method in agricultural and hydrological applications.

A Study on Estimation of Soil Moisture with a Combined L-band Radar and Radiometer Measurements

Jiancheng Shi, **K. S. Chen**, **L. Tsang**, **D. Entekhabi**, **E. Njoku**, **T. Jackson**, **and P. O'Neill**
ICESS, University of California, Santa Barbara, USA

Abstract— Soil moisture is a key parameter in numerous environmental studies, including hydrology, meteorology, and agriculture. It plays an important role in the interactions between the land surface and the atmosphere, as well as the partitioning of precipitation into runoff and ground water storage. Therefore, the spatial and temporal dynamics of soil moisture are important parameters for various processes in the soil-vegetation-atmosphere-interface. The Hydrosphere State Mission (Hydros) with both Active/Passive L-band instruments has been approved by NASA for monitoring global soil moisture and freeze/thraw. The Hydros instrument combines radar and radiometer subsystems. The radar operates with VV, HH, and HV transmit-receive polarizations, and uses separate transmit frequencies for the H (1.26 GHz) and V (1.29 GHz) polarizations. The radiometer operates with V, H and U (third Stokes parameter) polarizations at 1.41 GHz.

In attempt to use the active or passive microwave remote sensors for estimation of soil moisture, we are mainly facing two common problems: effects of surface roughness and vegetation cover. Natural variability and the complexity of the vegetation canopy and surface roughness significantly affect the sensitivity of backscattering and brightness temperature to soil moisture. Backscattering and brightness temperature signals from vegetated areas is a function of water content and its spatial distribution as determined by vegetation structure and underlying surface conditions including surface roughness parameters and dielectric properties. Due to the limited observations from either passive or active measurements alone, an ill condition, the number of measurements and equations are less than the number of unknowns, is expected. It results in the uncertainties in estimation of soil moisture.

In this study, we develop a combined active/passive technique to estimate surface soil moisture with the focus on the short vegetated surfaces. We first simulated a database for both active and passive signals under Hydros's sensor configurations using the radiative transfer model with a wide range of conditions for surface soil moisture, roughness and vegetation properties that we considered as the random orientated disks and cylinders. Using this database, we developed 1) the techniques to estimate surface backscattering and emission components and 2) the technique to estimate soil moisture with the estimated surface backscattering and emission components. We will demonstrate these techniques with the model simulated data and its validation with the airborne PALS image data from the soil moisture SGP'99 and SMEX'02 experiments.

Improvement of Bare Surface Soil Moisture Estimation with L-band Multi-polarization Radar Data

Ruijing Sun[1], **J. C. Shi**[1, 2], **T. Jackson**[3], **K. S. Chen**[4], **and Y. Oh**[5]

[1]Institute for Remote Sensing Applications, CAS, Beijing, China
[2]ICESS, University of California, Santa Barbara, CA 93106, USA
[3]USDA ARS, Beltsville, MD 20705, USA
[4]CSRSR, National Central University, Chung-Li, Taiwan
[5]Hongik University, Seoul, Korea

Abstract— Soil moisture is a key parameter in numerous environmental studies, including hydrology, meteorology, and agriculture. The spatial and temporal dynamics of soil moisture are important parameters for various processes in the soil-vegetation-atmosphere-interface. The Soil Moisture Active and Passive Mission (SMAP) with both Active/Passive L-band instruments will be launched by NASA in 2013 for global mapping of soil moisture and freeze/thaw status. It will provide the first quick repeat (3-days) capability of the multi-polarization (VV, HH, and HV) measurements with the constant incidence angle and the moderate resolution (1–3 km).

During past years, investigations have demonstrated the capability of active microwave instruments on soil moisture mapping. It is well known that radar backscattering is controlled by surface dielectric and roughness properties. The later is described by the surface height probability distribution function and surface correlation function (Ogilvy, 1991). The height probability distribution function of random rough surfaces is usually assumed as Gaussian function. The commonly used surface correlation functions are either Gaussian or exponential correlation functions. They represent two extreme cases: the purely single scale random rough surfaces and the multi-scale random rough surfaces. However, the actual correlation functions from field measurements are very complicated and often range between them. How to reduce the effects of the surface correlation function has become one of the major problems in soil moisture retrieval algorithm development. This study investigates the techniques to estimate surface soil moisture of bare surfaces under SMAP radar sensor configuration: L-band (1.26 GHz), multi-polarization (VV, HH, and HV), and 40° incidence radar measurements.

We first established a model simulated data-base using the AIEM model (Wu, et al., 2001) with the random rough surface assumption to simulate the wide range of soil moisture and roughness conditions for co-polarized signals and the Oh's semi-empirical model to the depolarization factor VH/VV of the surface backscattering, then, the cross-polarized signals can be obtained using AIEM simulated VV polarization signals.

We then describe a simple backscattering model that consists of the two functions: a dielectric function and a roughness function.

$$\sigma^s_{pq} = Sr_{pq} \cdot R_{pq} \tag{1}$$

Sr_{pq} is the roughness parameter that depending on the polarization, incidence angle, surface RMS height, correlation length, and the correlation function form. It represents an overall effect of the surface roughness. R_{pq} represents the surface reflectivity.

Due to the radar cross-polarization measurements are extreme sensitive to the present of vegetation cover, our focus in this study is only for the co-polarization measurements. Through analyses of the model simulated data-base, we developed a technique to estimate surface soil moisture under SMAP radar sensor configuration using the co-polarization measurements. In the algorithm development, the most difficult problem or the uncertainty that reduces the accuracy on soil moisture estimation is how to describe the relationship between the surface roughness parameters Sr_{pq} at different polarizations in order to reduce the number of unknowns. Therefore, we first developed a technique to estimate the surface roughness index parameter. This can be done based on the relationship between R_{vv} and R_{hh}, from which the dielectric property effect on radar measurements can be cancelled out. As expected, these surface roughness index parameters are found to vary greatly for the same surface rms height and correlation length when with the different correlation functions. Through analyses, however, we find that the relative differences between Sr_{vv} and Sr_{hh} have only the limited affect by the correlation functions and can be estimated from the surface roughness index parameters. In this way, the relationship between Sr_{vv} and Sr_{hh} can be described with the certain level of the accuracy. This significant finding

makes it possible to develop a soil moisture retrieval algorithm for using the dual co-polarization measurements from SMAP. We will demonstrate this algorithm development in details and its validation with the field experimental data.

Monitoring Air and Surface Temperature Evolution in Antarctica by Means of Microwave Remote Sensing

M. Brogioni, G. Macelloni, S. Pettinato, and E. Santi
Istituto di Fisica Applicata, Consiglio Nazionale delle Ricerche, Firenze, Italy

Abstract— In the last decades there has been a growing interest in the study of natural phenomena due to the climate global changes and the intensification of natural disasters. The scientific community, through the international organizations and the research institutes, started to study and analyze the impact of the mankind on the environment since the end of the last century. Although some groups (mainly bound to the oil lobbies) claims that the results of the studies were controversial, the Intergovernmental Panel on Climate Changes, IPCC, found that there was evidence that the greenhouse gasses produced by human activities has led to the climate changes and global warming. Among all the themes investigated by the researchers, a special attention have been paid to the cryosphere because it represents a major indicator of the global warming. Many glaciers, the Greenland ice sheet, permafrost and frozen ground, snow cover and Arctic sea ice are exhibiting dramatic changes which alter the ecosystems and consequently the human life. In particular the Earth climate is affected by the polar ice caps which contain more than the 95% of fresh water on Earth and directly influence the gas and particle fluxes, energy surface exchange, clouds, precipitation, hydrological conditions, atmospheric and ocean dynamics. In this scenario, Antarctica plays a fundamental role on the global climate due to its extension, surface temperatures and quantity of ice (the mean ice thickness is 1500 meters). Despite its high importance on the environment, Antarctica is the most unexplored and undersampled area of the Earth due to the extremely conditions which let almost impossible the human life and consequently its monitoring. The latter problem can be partially overcome by the use of remote sensing techniques, which rely mainly on the satellite measured data.

Up to now, only the surface temperature of snow can be estimated on wide areas such the Antarctic Plateau, but no estimates of the sub-surface temperature are available, so far. The measurement of the temperature of the deep snow layers is carried out only in few sites by means of local probes. The use of microwave passive satellite instruments data (collected by AMSR-E or alternatively SSM/I and Windsat sensors) will make it possible to realize sub-surface snow temperature maps, which could be useful to determine the spatial and temporal trends of the energy contained in the snowpack and therefore the evolution of the global warming. Thus this work aimed at investigating the evolution of the Antarctica surface and sub-surface temperatures by means of microwave passive remote sensing data because they are almost insensitive to the clouds coverage and can penetrate the snow surface. In fact, several analyses and experiments carried out in 2005-06 on a small area (about 100 km × 100 km) surrounding the Dome-C Station on the Antarctic Plateau showed that the snow surface and subsurface temperatures down to 2 meters can be estimated from the brightness temperatures at 19 and 37 GHz of the AMSR-E radiometer, with an error lower than 2%.

The aim of this work is to estimate the sub-superficial snow temperature of a large area in the Antarctic Plateau by using empirical relationships. The data used are brightness temperature images at 10, 19 and 37 GHz collected by the SSM/I and AMSR-E sensors since 1997, air temperature data measured by the Dome-C Automatic Weather Station since 1984, and snow temperature profiles measured at Concordia Station from Jan. 2005 until Dec. 2008. Remote sensing data at 19 and 37 GHz are found to be strongly correlated to local measurements taken respectively 50 cm and 100 cm below the snow surface, with a determination coefficients of the linear regressions are higher than 0.9. These regressions, which are developed by using data collected from Jan. 2005 until Dec. 2008, are used to estimate the sub-superficial snow temperature of the Dome C site since 1997 (when no ground measurements were available). The obtained regressions are used to spatially extend the snow temperature estimation over an area of $100 \times 100\,\mathrm{km}^2$. The extent of this area is established by increasing the distance from the central pixel until the difference between its 10 GHz brightness temperature and the average value of a surrounding annular zone remained below 1 K. This analysis is performed by using all the AMSR-E images collected from 2003 until 2008 along three orbits slightly misaligned.

Finally, given the strong relationships between snow and brightness temperatures, the data are analyzed in order to investigate possible effects of the climate changes in the Dome C area at decadal scale. The results show significant increases of the air (about 0.6°C) and brightness temperature at 19 and 37 GHz (about 0.7 K) since 1996. Instead, the trend computed for the air temperature only in the period 1984–1995 shows no significant variation.

ACKNOWLEDGMENT

The activity of Marco Brogioni was supported by a Post-Doctoral fellowship of the AXA Research Fund.

Session 4P1b
Synthetic Aperture Radars: Systems and Applications

Development of Novel CP-SAR Sensor onboard an Unmanned Aerial Vehicle Platform

P. Rizki Akbar, **J. T. Sri Sumantyo**, **and H. Kuze**
Center for Environmental Remote Sensing, Chiba University
1-33, Yayoi, Inage, Chiba 263-8522, Japan

Abstract— Synthetic Aperture Radar (SAR) systems currently developed and operated onboard spaceborne platforms, are based on linearly polarized microwave radiation. Such linearly polarized SAR systems are in general very sensitive to Faraday rotation in the ionosphere and platform posture, both of which will increase system noise superposed on the resulting backscattering signature. In order to improve the situation, we are developing a Circularly Polarized Synthetic Aperture Radar (CP-SAR) in Microwave Remote Sensing Laboratory, Chiba University, Japan. In this paper, we describe the possibility of implementing a smaller antenna using the new CP-SAR technique than with conventional linear polarization SAR systems. Furthermore, our theoretical results show that a simpler, faster and more accurate signal processing is offered by this CP-SAR system. These features contribute to the realization of a compact CP-SAR sensor, which is suitable for a small and low cost platform yielding a real time SAR image data. As a preliminary stage of the development of this Earth-observing sensor, we will make use of a small airborne platform, called an Unmanned Aerial Vehicle (UAV) for testing CP-SAR capabilities. The system will be operated at 1.27 GHz (L-Band), and the experience and knowledge will be very useful to realize a CP-SAR sensor onboard a small satellite platform as the target stage of the CP-SAR sensor development. The satellite realization and launch is planned to be in the year of 2014. Thus, this research will be a pioneer work for airborne and spaceborne SAR sensors conducted in Japan on the university level.

Electronically Tunable Current Mode Second Order High Pass Filter with Variable Central Frequency f_0

G. N. Shinde[1] and D. D. Mulajkar[2]

[1]Indira Gandhi (SR) College, Nanded, Maharashtra 431603, India
[2]Dnyanasadhana College, Thane, Maharashtra 400604, India

Abstract— At present there is a growing interest in designing capacitor-less, resistor-less current mode active only filters using only active elements such as Operational amplifier [OA], Operational transconductance amplifiers [OTAs]. Current mode filters have many advantages compared with their voltage mode counterparts. Current mode filters have large dynamic range, higher bandwidth, greater linearity, simple circuitry, low power consumption etc.

A novel single-input current-mode active-R filter using two operational amplifiers (OAs) and resistors is presented. The circuit is fully programmable and implements high pass (HP) functions. The availability of currents at high impedances facilitates cascadibility feature. The filter performance factors center frequency (ω_0), bandwidth (ω_0/Q), quality factor (Q) and gain (G) are electronically tunable. The SPICE simulation results are included to confirm the workability of the proposed circuit.

This circuit can realize quadratic transfer function. Paper includes theoretical frequency response of second order high pass filter for cut off frequency 50 K with variable Q. The circuit is suitable for high frequency operation and monolithic integration. The proposed second order high pass filter works ideal for $Q = 10$ and central frequency from 1 kHz to 50 kHz. The gain roll-off is 40 dB/decade. The designed filter has passive sensitivities less than unity magnitude and active sensitivities half in magnitude.

A SAR Superresolution Method Based on 2D Linear Prediction Extrapolation

Ping Zhang and Zhen Li
Center for Earth Observation and Digital Earth, Chinese Academy of Sciences
Kedian Tower F14, No. 9 Beiyitiao Road, Zhongguancun Haidian District, Beijing 100190, China

Abstract— Conventional radar imaging methods based on Fourier transform provide good resolution as long as the backscattered data is available over a large bandwidth and a sufficient aspect region. Wider transmitted bandwidth achieves higher range resolution. Either a higher centre frequency or wider aspect angle variation will improve azimuth resolution. But in many practical applications only limited frequency and limited aspect region are available. This leads to radar images with limited resolution. The paper provides an efficient bandwidth extrapolation algorithm to reach a higher resolution in SAR (Synthetic Aperture Radar) imaging based on 2D linear prediction algorithm.

In this paper, we present a SAR bandwidth extrapolation method to improve SAR image resolution based on two-dimensional linear prediction extrapolation. The method uses the SLC SAR image signal model as the prior information to estimate the 2D AR (AutoRegression) parameters.

On the basis of the SAR imaging theory, the signal model of SAR imagery is analyzed to be feasible by using data extrapolation methods to improve the SAR image resolution. Generally, SAR systems use linear FM signal as transmitted signal. After imaging processing, SAR image can be represented to be an expression of targets location in slant range, azimuth direction, transmitted signal bandwidth and Doppler bandwidth in azimuth, supporting by a rectangle domain in phase history domain. The SAR image in phase history domain is a band-pass function with a main frequency support domain. Thus, the problem of superresolution SAR imaging is transformed to solve the efficient bandwidth extrapolation.

The 2D AR parameters are estimated using the data of efficient bandwidth. According to the 2D AR linear prediction model, the lap-to-lap approach is used for the extrapolation of the efficient bandwidth to obtain a large dimension frequency domain spectrum, i.e., the bandwidth of the SAR image is increased. The lap-to-lap approach can use more data of the efficient bandwidth. Then the new data in the frequency domain can be transformed to the time domain and better resolution can be achieved.

Long Term Continuously DInSAR for Volume Change Estimation of Land Deformation

Josaphat Tetuko Sri Sumantyo
Center for Environmental Remote Sensing, Chiba University
1-33, Yayoi, Inage, Chiba 263-8522, Japan

Abstract— In this research, a technique to estimate the volume change by using Differential Interferometric Synthetic Aperture Radar (DInSAR) is proposed to retrieve the volume change of long-term continuously land deformation (uplift or subsidence). This technique is employed to investigate subsidence of Bandung city, Indonesia to demonstrate the capability of this technique by assessing two Japanese L band Spaceborne SARs (JERS-1 SAR and ALOS PALSAR) in continuously periods of 1993–1997 and 2007–2008. This result shows the subsidence occurred concentrating seriously at industrial complexes and settlements of Bandung area, especially at Cimahi, Dayeuhkolot, and Baleendah districs. Statistics and ground survey data shows increasing large scale of flood volume and wrecking infrastructures nowadays. The analysis result of ALOS PALSAR by using this technique also shows new subsidence areas at industrial and settlement areas of Majasari, Majalaya, Cilampeni and Rancaekek districts. These results are confirmed by using statistical data of 1991–2008 published by The Indonesian Statistics Bureau (BPS), two campaigns of ground surveys to compiling the recent condition of buildings and other infrastructures, population, number of industries, ground water level data and analysis of geological formation of this area. This research shows a strong capability of this technique to investigate the volume change caused by land deformation, especially subsidence.

Extraction of Typhoon-damaged Forests from High-resolution Polarimetric SAR Images

Haipeng Wang[1] and Kazuo Ouchi[2]

[1]Key Laboratory of Wave Scattering and Remote Sensing Information (MoE), Fudan University
Shanghai 200433, China
[2]Department of Information Science, National Defense Academy
Hashirimizu 1-10-20, Yokosuka 239-8686, Japan

Abstract— The purpose of this study is to extract the forests destroyed by typhoons and to quantitatively estimate the damage levels by using high-resolution polarimetric synthetic aperture radar (SAR) data. The study area is located in Tomakomai, Hokkaido, Japan. The typhoon "Songda" (Japanese typhoon number 18) attacked the area in September, 8th, 2004 and caused heavy damage over 50% in many stands. The forests map showing damaged stands from ground survey is available for comparison.

Two sets of SAR images selected in this study are L-band fully polarimetric airborne Pi-SAR data over Tomakomai forests with $3\,\mathrm{m} \times 3\,\mathrm{m}$ resolution (4-look in azimuth direction). One set was acquired before the typhoon damage in November, 7th, 2002 and the other after the damage in November, 3rd, 2004. Both data sets were acquired in similar conditions, such as the look direction and incidence angle (difference $< 0.5^\circ$ at the study area).

Amplitude images were first analyzed. It was found that the values of RCS (Radar Cross Section) averaged over the whole image after the typhoon damage changed by $-0.94\,\mathrm{dB}$, $0.1\,\mathrm{dB}$, and $1.28\,\mathrm{dB}$ at HH-, HV-, and VV-polarization respectively in comparison with those before the damage.

To fully utilize the data, a model of the linear combination of the cross- and co-polarization changes was developed to estimate damage levels. Similar analytical approaches were also applied to the three-component decomposition analysis. The changes in RCS of double-, volume- and surface-scattering mechanisms after the damage were respectively $27.5\,\mathrm{dB}$, $-0.20\,\mathrm{dB}$ and $-20.3\,\mathrm{dB}$. Finally, by comparing with the ground survey data, the accuracies of 64.1% and 77.7% were obtained for amplitude and decomposition data respectively. Thus, the experimental results do not appear in very good agreement with those observed from ground. There could be two reasons for this discrepancy. The first is that the ground-observation is subjective and does not specify damage areas within each stand, so that the ground-observation map shows "average damage" of each stand. The second is that fallen trees were still there when Pi-SAR observation was made. Half-fallen trees can be regarded as standing trees by Pi-SAR, but they were categorized as fallen trees by ground-observation. Nevertheless, Pi-SAR has finer spatial resolution than the ground-observation map, and therefore, its data have potential to estimate damaged areas of forests caused by typhoons.

ACKNOWLEDGMENT

This project is supported in part by the National Science Foundation of China under Grants 40901201.

Ship Detection Experiments by Multiple Synthetic Aperture Radars

Chan-Su Yang[1], **Seong-In Hwang**[2], **Shunsuke Taniguchi**[2], **and Kazuo Ouchi**[2]

[1]Ocean Satellite Research Group, Korea Ocean Research and Development Institute
Sa2-dong 1270, Sangnuk-gu, Ansan, Gyeonggi-do 426-744, Korea
[2]Department of Information Science, School of Electrical and Computer Engineering
National Defense Academy, 1-10-20, Hashirimizu, Yokosuka 239-8686, Japan

Abstract— Synthetic aperture radar (SAR) is a powerful sensor for ship detection because of its ability to penetrate cloud cover and day-and-night observation capability, and a substantial number of papers have been reported on this issue. In recent years, the technique has attracted much attention since increasing numbers of illegally operating ships such as piracy and fishery have become an international problem. When using spaceborne SARs, the main problem is long repeat cycles, some of which are over 40 days. Use of multiple identical SARs such as COSMO-SkyMed and SAR-Rupe series is a solution. Another way is to use multiple available SAR sensors.

The purpose of the present study is to examine the ability of extracting and identifying ships using multiple spaceborne SAR sensors, including L-band ALOS-PALSAR (Advanced Land Observing Satellite — Phased Array L-band SAR), C-band ENVISAT ASAR (Advanced SAR), and X-band TerraSAR-X. The study area is the mouth of Tokyo Bay, Japan. We also used the data simultaneously acquired by the X-band ground-based radar with AIS (Automatic Identification System), and also some optical data both from space and ground. Several different algorithms were used to test their performances. These algorithms were amplitude thresholding, CFAR (Constant False Alarm Rate), MLCC (Multi-Look Cross-Correlation), and MLCC-CFAR, i.e., CFAR applied to MLCC processed coherence images. The MLCC and MLCC-CFAR algorithms were applied only to the PALSAR data as other raw data were not available.

All algorithms showed their characteristics, and TerraSAR-X had higher accuracy than the others for estimating the size of ships for the obvious reason of higher spatial resolution. Polarimetric analyses of PALSAR data did not perform well because of low spatial resolution, although the technique has a potential of ship identification if the resolution is higher. The newly developed MLCC-CFAR applied to PALSAR data showed substantial improvement in FAR (False Alarm Rate) by 30% and SNR (Signal to Noise Ratio) by 12% in comparison with MLCC. These algorithms are described and results are illustrated to show their characteristics and the ability of each SAR sensors.

Deriving Ocean Surface Drift Using Multiple SAR Sensors

Ming-Kuang Hsu[1] and Antony K. Liu[2]

[1]Technology and Science Institute of Northern Taiwan, Taipei, Taiwan
[2]NASA Goddard Space Flight Center, Greenbelt, Maryland, USA

Abstract— Tracking and monitoring ocean features which have short coherent time periods from sequential satellite images requires that the images have both very high spatial resolutions and temporal sampling intervals. Satellite images from a single sensor in a polar-orbiting satellite usually can not meet the requirement since high spatial resolution of the sensor may result in relatively long temporal sampling intervals and vice versa, such as the Synthetic Aperture Radar (SAR). This paper presents a new multi-sensor approach to overcome the long temporal sampling intervals associated with a single SAR sensor while taking advantage of high spatial resolutions of SAR images for the application of ocean feature tracking. Currently, there are two SAR sensors on different satellites, the European Remote Sensing Satellite-2 (ERS-2) and the ENVIronment SATellite (ENVISAT), having acquisition time offset around 28 minutes with almost the exactly same path. That is, ERS-2 is following ENVISAT with a 28-minutes delay, which is a good time-scale for ocean mesosclae feature tracking. The pairs of SAR images from ERS-2 and ENVISAT collected on April 27, 2005 have been chosen to track ocean surface features by using wavelet analysis. As demonstrated in the case studies, this technique is robust and capable to derive ocean surface drift near an oil slick and around a big eddy in the South China Sea (SCS).

Session 4P2
Satellite Land Products, Validation, and Applications

An Angular-dependent Single Channel Algorithm for Land Surface Temperature Retrieval from the HJ-1B/IRS Thermal Infrared Data

Qinhuo Liu, H. Li, and B. Zhong
State Key Laboratory of Remote Sensing Science
Institute of Remote Sensing Applications, Chinese Academy of Sciences
Beijing 100101, China

Abstract— The two Chinese satellites HJ-1A and HJ-1B were launched by one rocket on September 6, 2008. There are two sensors onboard HJ-1B: one is a CCD camera with 720 km swath, 30 m resolution for 4 visible and near-infrared bands; another one is an infrared scanner(IRS) with 720 km swath, 150 m resolution for 3 near/mid infrared bands and 300 m resolution for one thermal infrared channel. This paper proposes an angular-dependent single channel algorithm for retrieving land surface temperature form the HJ-1B/IRS thermal infrared data. The algorithm takes into account the angular dependence of the atmospheric correction due to the increase of the atmospheric optical path with angle which involves construction of the empirical relationships between the atmospheric parameters and atmospheric water vapor content. The method for estimating the atmospheric parameters, the land surface emissivity and simplification of Planck function are discussed in details. The proposed algorithm requires inputs such as at-sensor radiance, the view angle, the emissivities and the approximate water vapor content (which may provided by the MODIS product MOD07). The sensitivity analysis using the NCEP atmospheric profiles and the simulated data shows that the root mean square error (RMSE) is about of 1.5 K with water vapor content is lower than 3 g/cm^2. The comparison analysis indicates that the HJ-1B/IRS LST is basically consistent with the MODIS LST product with a reasonable accuracy.

A Spatial Representativeness Analysis Model for Satellite LST Validation

Ming Chen[1], **Yunyue Yu**[2], **Dan Tarply**[3], **and Jeffrey L. Privette**[4]

[1]I. M. Systems Group, Inc. Camp Springs, MD 20746, USA
[2]Center for Satellite Applications and Research, NOAA/NESDIS, Camp Springs, MD 20746, USA
[3]Short & Associates, Camp Springs, MD 20746, USA
[4]National Climate Data Center, NOAA/NESDIS, Asheville, NC 28801, USA

Abstract— Satellite LST validation is usually performed with reference to ground-based observations. Satellite LST and ground-based LST both have observation errors although ground-based LST is often taken as "truth". Since satellite pixel LST is mean values of limited area, it may also involve representativeness error which is due to sub-pixel heterogeneity and improper handling of such sub-pixel variations in the LST retrieval algorithm. In spite of the difficulty to quantify representativeness error, sub-pixel heterogeneity is usually unavoidable. To establish proper representativeness analysis model is thus not only necessary for satellite validation at specific sample pixels/locations, but also crucial for the improvement of algorithm capacity in handling sub-pixel heterogeneity, and consequently the general improvement of global LST product. After all, the satellite LST validation at specific sample locations are not just for those samples, but for the validation over all the possible satellite covered area.

A representativeness analysis model will be shown in this presentation to characterize the expected "true" differences between ground observations of LST, such as made at SURFRAD or CRN stations, and LST estimates from virtual coarser satellite pixels synthesized from higher-resolution satellite observations. The synthetic satellite pixels will retain sufficient sub-pixel information so that they may be taken as the "true" proxy of the real coarser satellite imagers such as AVHRR, MODIS, VIIRS or ABI. The higher-resolution data sets used for model development are clear-sky ASTER imager scenes coincident with selected SURFRAD and CRN stations. The analysis results at five selected SURFRAD sites will be shown in this presentation.

Monitoring Snow Cover with Multisensor Automated Snow Mapping System at NOAA/NESDIS

Peter Romanov
Cooperative Institute for Climate Studies (CICS), University of Maryland, College Park, USA

Abstract— Snow cover is an important element of the Earth's climate system. Information on the snow cover extent and spatial distribution is highly important for the numerical weather prediction, hydrological analysis and climate change studies. Owing to a short revisit time, global coverage and operational availability of data from meteorological satellites, satellite observations are seen as a primary tool for continental to global scale monitoring of snow cover for meteorological and climatological applications.

An automated multisensor snow and ice mapping system has been developed at NOAA/NESDIS to provide routine operational monitoring of the global snow cover. The technique is based on combined observations in the visible, middle infrared, infrared and microwave spectral bands made from polar orbiting and geostationary meteorological satellites. The primary product is a global snow and ice cover map generated at a spatial resolution of 4 km. Synergy of satellite observations in the visible/infrared and in the microwave allows for generating continuous (gap-free) maps of snow cover distribution on a daily basis. To assess the accuracy of the product we routinely compare it with surface observations of snow depth and with snow cover maps drawn interactively by NOAA analysts.

In the talk we give a brief description of the developed snow detection and mapping algorithms and of the technique to combine snow retrievals from different satellite sensors. The results of snow cover monitoring during four years of system operation will be presented.

Satellite Data Utilization over Land in NCEP Data Assimilation System

Weizhong Zheng[1], **Michael Ek**[1], **Helin Wei**[1], **Jesse Meng**[1], **John Derber**[1], **Xubin Zeng**[2], **and Zhuo Wang**[2]

[1]NOAA/NCEP/EMC, USA
[2]University of Arizona, USA

Abstract— Satellite observed brightness temperature (Tb) in various spectral channels is assimilated through the JCSDA Community Radiative Transfer Model (CRTM) on the NCEP Gridpoint Statistical Interpolation (GSI). Land surface skin temperature (LST) predicted by the NCEP operational Forecast System (GFS) is a critical factor in determining Tb simulation for satellite surface sensitive channels. The amount of satellite data assimilated over land in the current operational GSI is far less than over ocean. One of the chief reasons is the much larger cold bias in GFS predicted LST over desert and arid regions during daytime in the warm season. The large cold bias of LST results in large errors in CRTM simulated satellite brightness temperatures over land and rejection of satellite data in GSI, especially for surface sensitive satellite channels.

Investigation in GFS testing has revealed a major cause of cold daytime LST bias is in the treatment for roughness length for heat (Zot) in the physics of surface turbulent heat transfer. In this study, alternate vegetation-based formulations of momentum and thermal roughness lengths developed by Zeng et al. are tested. The result shows that new formulations substantially reduce the large GFS daytime LST cold biases over desert and arid regions in the warm season. With improvement of LST, there is a reduction in the large biases of calculated brightness temperatures found for infrared and microwave satellite sensors in window or near window channels, so that much more satellite data can be used in the GSI data assimilation system. In desert or bare soil regions, unreasonable surface emissivity for microwave sensors in CRTM are corrected (Yan and Weng, 2009), and the new emissivity model together with improved LST via changes in surface roughness lengths give smaller biases and root-mean-square errors in calculated brightness temperatures.

Construction of a Global Database of Surface Reflectance and Emissivity at a Sub km Resolution

L. Gonzalez[1], **F.-M. Bréon**[2], **and X. Briottet**[3]

[1]LOA UFR de Physique, Université des Sciences et Technologies de Lille
F-59655 Villeneuve d'Ascq Cedex, France
[2]LSCE-Orme, point courrier 129, CEA-Orme des Merisiers, F-91191 Gif-sur-Yvette Cedex, France
[3]ONERA/DOTA, 2 Avenue E. Belin, BP 74025, F-31055 Toulouse, France

Abstract— The MODIS instruments have been flying onboard the Terra and Aqua platforms and acquire Earth observation data since early 2000 and mid 2002. Data processing allows the monitoring of the land cover dynamic. Here, a data processing scheme is described to generate Earth reflectance and emissivity time series at a sub-kilometer spatial resolution and with a period of 8 days. The data processing allows the identification of artifacts generated by clouds, aerosols or other unwanted effects that corrupt the time series. In addition, a bidirectional reflectance model, depending on the surface cover type, is applied to i) normalize the reflectance to a constant viewing geometry and ii) compute a land surface albedo.

A web-service tool has also been developed for an easy analysis of the reflectance images and their time-evolution. It is expected that the database and the tool will help researchers to identify and quantify the anthropogenic impact on the Earth surface cover, and the impact of naturally-induced disturbances such as fires, floods or droughts.

Evaluation of MODIS VI Products Using the AERONET-based Surface Reflectance Validation Network Dataset

Zhangyan Jiang[1], **Alfredo R. Huete**[1], **Yujie Wang**[2], **and Alexei Lyapustin**[2]

[1]Department of Soil, Water, and Environmental Science, University of Arizona, Tucson, AZ 85721, USA
[2]GEST Center, University of Maryland Baltimore County, Catonsville, MD 21228, USA

Abstract— The MODIS vegetation index (VI) products (MOD13) have been widely used in many terrestrial science applications that aim to monitor ad characterize the Earth's vegetation dynamic from space. The quality and reliability of the MODIS VI products are vital to these studies. Therefore, there is a need to assess the quality of the MODIS VI products. In this study, the AERONET-based Surface Reflectance Validation Network (ASRVN) dataset, which is designed as a validation tool for the moderate resolution ($\sim$ 1 km) global surface reflectance products from the EOS sensors, is used as a reference to evaluate the quality of the MODIS 1 km, 16-day composite VI products. Our results show that the positive bias of the MODIS red reflectance compared with the ASRVN reflectance is responsible for the bias in the MODIS NDVI and EVI2. The negative bias of the MODIS blue reflectance cancels out the effects of the positive red bias on the MODIS EVI, resulting in insignificant bias in EVI. The overall mean absolute differences between the 16-day composite MODIS VIs and nadir-adjusted ASRVN VIs are 0.025 for NDVI, 0.016 for EVI and EVI2. MOD13 EVI and NDVI temporal profiles match ASRVN VI profiles even during higher AOT periods, indicating that MODIS VI products are not significantly affected by aerosol. The results suggest the good quality of the MODIS VI products.

Land Surface Products from the Advanced Baseline Imager of U.S. GOES-R Satellite Mission

Yunyue Yu, **Mitchell D. Goldberg**, **and Ivan Csiszar**
Center for Satellite Applications and Research, NOAA/NESDIS
5200 Auth Rd., Camp Springs, MD 20746-4304, USA

Abstract— The Land team of the GOES-R Algorithm Working Group (AWG) has been working on algorithm development and evaluation for the GOES-R land surface products since late 2005. There are six land surface products that are currently under development: two baseline products and four option 2 products. The baseline products are land surface temperature (LST) and fire/hot spot characterization (FIRE); the option 2 products are normalized difference vegetation index (NDVI), green vegetation fraction (GVF), land surface albedo, and land surface flood/standing water. All the products will be based on the advanced baseline imager (ABI) which is a significantly enhanced and improved version of the current U.S. GOES Imagers and will be onboard the GOES-R satellite. Currently, the land team of GOES-R AWG has finalized techniques needed for developing the LST, FIRE, and NDVI products. A so-called eighty percent readiness package of these algorithms have been delivered in summer 2009, and the one-hundred percent readiness deliveries are schedule in summer 2010. The deliveries include the algorithm theoretical bases document (ATBD) for each product, software design and implementation code, description documents, test datasets and test reports, and evaluation results. For the option 2 algorithms, the eighty percent readiness deliveries and the one-hundred percent readiness deliveries are scheduled in summer 2010 and 2011, respectively. Meanwhile, the land team of GOES-R AWG is planning solid validation procedures for all the land surface products. This paper will present activities and accomplishments of the land team for developing, testing and validating algorithms of the above GOES-R land surface products.

Session 4P3
Optical and Quantum Tweezers for Atom/Molecile Trapping and Transportation

The Cold Atoms Upward Transportation

Xuanhui Lu, **Kaikai Huang**, **Xian Zhang**, **Lei Sun**, **Zhouxiang Xu**, **and Hao Xu**
Department of Physics, Zhejiang University
Zheda Rd. 38#, Hangzhou 310027, China

Abstract— To build an atom interferometer on measuring the earth gravity, we have developed a series of atom cooling, trapping and controlling systems.

In a ultra-high vacuum chamber, we applied a magnetic-optical trap (MOT), cooled the 87Rb atoms to the Doppler limit of ∼150 μK and trapped them in the center area of the MOT. After the MOT, we shut down the magnetic coil, compensated the earth magnetic field, and detuned the upward propagating beams to some frequency difference with the downward propagating beams, to get the cold atoms launched to a different height. Meanwhile, by elegantly detuning the laser frequency and sweeping the laser intensity, we've broken through the Doppler limit and achieved the polarization gradient cooling, cooled the atoms at about 10 μK.

A New Concept of Cold Atom Using Fast Optical Tweezers

B. Jakgoljun, **K. Srinuanjan**, **S. Kamoldilok**, **and P. P. Yupapin**
Advanced Research Center for Photonics, Faculty of Science
King Mongkut's Institute of Technology Ladkrabang, Bangkok 10520, Thailand

Abstract— We propose a new concept of a cold atom generation using a tiny optical device system. A system consists of a multi-stage nonlinear mirroring system incorporating an add/drop filter, which the storage unit can be formed the fast tweezers and the cold atom concept presented. In operation, the optical tweezers can be generated by using a Gaussian pulse input into the mirroring system, where the amplified and tuned optical tweezers using a light pulse propagating within an add/drop filter. By using the suitable parameters such as ring radii, effective areas, coupling coefficients and refractive indices, an atom/particle can be trapped by the specific optical tweezers and propagating within a storage ring. Results obtained have shown that the fast tweezers time is approached the negligible value, where the terms of time independent motion of atom/particle can be performed by using the fast tweezers, and the cold atom concept is obtained. In application, such a technique can be used to form the similar manner for molecule, DNA, photon, or Ion, where the memory unit of them can be formed, which will be available for a hybrid memory or computer in the near future.

Novel Nanoscale Signal Processing and Networking via a Wavelength Router

P. Youplao[1], **S. Mitatha**[1], **and P. P. Yupapin**[2]

[1]Hybrid Computing Research Laboratory, Faculty of Engineering
King Mongkut's Institute of Technology Ladkrabang, Bangkok 10520, Thailand
[2]Advanced Research Center for Photonics, Faculty of Science
King Mongkut's Institute of Technology Ladkrabang, Bangkok 10520, Thailand

Abstract— This paper presents the very fascinating simulation results of light pulse traveling within a ring resonator system that have shown the unexpected results with various applications. The design system consists of a nonlinear microring/nanoring resonator system incorporating an add/drop filter. The proposed fabricated material used is **InGaAsP/InP**, which can provide the required output behaviors. Three different forms of input light pulses are Gaussian pulse, dark and bright soliton, whereas the suitable simulation parameters are input power, pulse width, ring radii and the material refractive indices. Three different forms of the results have been interpreted, whereas the dominants behaviors are such as Gaussian soliton, multisoliton and tunable dark soliton are described, and the potential applications for new laser sources, new communication bands, dynamic optical tweezers, high frequency source and imaging resolution using THz technology are described. The use of the proposed system incorporating a nanoscale communication and networking via wavelength router is also discussed.

Novel Molecular Networking via a Simultaneous Optical Wireless Up-down Link Systems

P. Udomariyasap[1], **S. Noppanakeepong**[1], **S. Mitatha**[2], **and P. P. Yupapin**[3]

[1]Department of Telecommunication Engineering, Faculty of Engineering
King Mongkut's Institute of Technology Ladkrabang, Bangkok 10520, Thailand
[2]Hybrid Computing Research Laboratory, Faculty of Engineering
King Mongkut's Institute of Technology Ladkrabang, Bangkok 10520, Thailand
[3]Advanced Research Center for Photonics, Faculty of Science
King Mongkut's Institute of Technology Ladkrabang, Bangkok 10520, Thailand

Abstract— In this paper, the interesting results of THz carrier frequency generation using the small device system for high frequency generation. Simulation results obtained using a Gaussian beam propagating within the nonlinear device system, which is required to use in the THz regime. A generated system consists of a micro and nano rings that can be integrated into a signal system, which can be employed to generate the large bandwidth of high frequency bands by a Gaussian pulse propagating within the ring resonator system incorporating an add/drop filter. The multiplexed transporters are generated and multiplexed via add/drop filter, which can be used for high capacity molecular signal processing and communication system. By controlling the ring parameters, add/drop filter to increase input add port, the appropriate output power can be obtained, which can be modified to be suitable for nano-scale communication applications. Moreover, the very wide band of wavelength can be simultaneously generated and controlled for various applications. We found that the generated output power with the THz frequency carrier regime can be achieved.In this paper, the interesting results of THz carrier frequency generation using the small device system for high frequency generation. Simulation results obtained using a Gaussian beam propagating within the nonlinear device system, which is required to use in the THz regime. A generated system consists of a micro and nano rings that can be integrated into a signal system, which can be employed to generate the large bandwidth of high frequency bands by a Gaussian pulse propagating within the ring resonator system incorporating an add/drop filter. The multiplexed transporters are generated and multiplexed via add/drop filter, which can be used for high capacity molecular signal processing and communication system. By controlling the ring parameters, add/drop filter to increase input add port, the appropriate output power can be obtained, which can be modified to be suitable for nano-scale communication applications. Moreover, the very wide band of wavelength can be simultaneously generated and controlled for various applications. We found that the generated output power with the THz frequency carrier regime can be achieved.

Quantum Parallel Processing Manipulation Using Gaussian Pulses via an Optical Multiplexer

P. Pongwongtragull[1], **S. Suchat**[2], **S. Mitatha**[3], **and P. P. Yupapin**[1]

[1]Advanced Research Center for Photonics, Faculty of Science
King Mongkut's Institute of Technology Ladkrabang, Bangkon 10520, Thailand
[2]Faculty of Science and Technology, Phranakhon Rajabhat University, Bangkok 10220, Thailand
[3]Department of Computer Engineering, Faculty of Engineering
King Mongkut's Institute of Technology Ladkrabang, Bangkok 10520, Thailand

Abstract— We propose a new system of quantum signal and parallel processing using Gaussian pulses propagating within a nonlinear ring resonator system. To increase the channel capacity and security, the multiplexer is operated incorporating a quantum processing unit via an optical multiplexer. The transmitted part can be used to generate the high capacity packet of quantum codes within the series of micro ring resonators. The received part can be used to detect the quantum bits (qubits) via the optical link, which can be obtained via the end quantum processor. The reference states can be recognized by using the cloning unit, which is operated by the add/drop filter. Two add-drops that are in two parts can be used to be Alice and Bob, respectively, in quantum communication. Results obtained have shown that the multiplexed wavelengths can be formed by using the multiple operating systems, which is allowed the filtering at the end users (Bob). In application, the embedded system within the computer processing unit is available for quantum computer. Furthermore, such a concept is also available for hybrid communications, for instance, wire/wireless, satellite, which will be discussed in details.

Molecular Transporters Generations Based on Ant Colony Algorithm for Molecular and Storage Applications

T. Taengtang[1, 2], **K. Praitoonwattanakit**[1], **and P. P. Yupapin**[2]

[1]Faculty of Engineering, King Mongkut's Institute of Technology Ladkrabang
Bangkok 10520, Thailand
[2]Advance Research Center for Photonics, Faculty of Science
King Mongkut's of Institute of Technology Ladkrabang
Bangkok 10520, Thailand

Abstract— We propose a new method of molecular transporters generations based on ant colony algorithm for molecular classification and storage applications. The transportation network of molecules via multi tweezers inside the close system can be manipulated in the same way of ant colony algorithm relationship. In the proposed method, we assign each of ants represents an individual tweezer. By using ant colony system, the random codes can be used to communicate between ants inside swarm with pheromone being formed the random network. The quantum state of transporters (individual ant) with different states and wavelengths can be represented by the pheromone. In application, this proposal can be an alternative random networking which may be use for communication security, where the fast multiple access may be plausible.

Multi-photons Trapping Stability within a Fiber Bragg Grating for Quantum Sensor Use

H. M. Hairi[1], **T. Saktioto**[1, 2], **S. Nafisah**[1], **M. Fadhali**[3], **Rabia Qindeel**[1], **P. P. Yupapin**[4], **and J. Ali**[1]

[1]Advanced Photonics and Science Institute, Universiti Teknologi Malaysia, Malaysia
[2]University of Riau, Pekanbaru, Riau 28293, Indonesia
[3]Ibb University, Yemen
[4]Advanced Research Center for Photonics, Faculty of Science
King Mongkut's Institute of Technology Ladkrabang, Bangkok 10520, Thailand

Abstract— We propose an interesting result of the trapped multi photons distribution within a fiber Bragg grating. The trapped photons are confined by the potential well, which introduce the motion of photons in a fiber Bragg grating affected by multi perturbations. The external perturbations are defined as series of nonlinear parametric in terms of potential energy. This investigation is developed by using the nonlinear couple mode equations and under Bragg resonance condition where the initial frequency of the light, ω_0 is the same value as the Bragg frequency, ω_B. The results show that the higher perturbation series represents the potential well is much indifferent of equilibrium. In applications, the perturbation can cause the trapped photons instability which introduces the escape photons from the potential well. The applications such as entangled photon source and quantum sensors can be performed.

Novel Multi Channels — Multi Layers Atom Transportation and Quantum Security Using Dynamic Tweezer for Communication Link

C. Vongchumyen[1], **S. Mitatha**[1], **and P. P. Yupapin**[2]

[1]Hybrid Computing Research Laboratory, Department of Computer Engineering, Faculty of Engineering
King Mongkut's Institute of Technology Ladkrabang, Bangkok 10520, Thailand
[2]Advanced Research Center for Photonics, Physics Division, Faculty of Science
King Mongkut's Institute of Technology Ladkrabang, Bangkok 10520, Thailand

Abstract— We propose a novel system of multi molecules transportation that can be used to form the hybrid data communication security using quantum-molecular technique in communication link. Furthermore, it can be formed multi channels — multi layers communication link by using the transportation of atoms/molecules via dynamic tweezers. The system consists of two parts. Firstly, the generated dynamic tweezers can be used to collect atoms and transport via wavelength router. Secondly, the transporters (trapped atoms) are moderated by the microwave signals and formed the transmission link. The modulated signals are transmitted via the microwave communication link. The received signals still have some trapped atoms which can be detected/demodulated and recovered. Furthermore, quantum security can be obtained by using quantum processing unit to detect atom polarization, where the atomic states can be identified. If the communication has been trapped, the modulated atoms may be lost, and they cannot be detected by the un-required receivers, which are implied that the security system has been broken.

Generalized DNA Codes via Nonlinear Micro Ring Resonator for Signal Security Use

W. Chatsri[1], **W. Sririth**[1, 2], **S. Mitatha**[1], **O. Pingern**[3], **and P. P. Yupapin**[4]

[1]Department of Computer Engineering, Faculty of Engineering
King Mongkut's Institute of Technology Ladkrabang, Bangkok 10520, Thailand
[2]Faculty of Engineering, Chiangrai College, Chiangrai 57000, Thailand
[3]Faculty of Science, Ramkhamhaeng University, Bangkok 10400, Thailand
[4]Advanced Research Center for Photonics, Faculty of Science
King Mongkut's Institute of Technology Ladkrabang, Bangkok 10520, Thailand

Abstract— We propose a new design of a security scheme by using the nonlinear behaviors of light pulses in a micro ring resonator for signal security application. The randomly DNA codes can be performed and modulated by the generated carrier within the ring system. The DNA codes can be generated and formed by the logical pulses "A" or "T" or "C" or "G" by using the signal quantizing method, which can be randomly coded by controlling the specific optical input coupling power, i.e., coupling coefficient and ring radii. Simulation results when the ring radius used is 10.0 μm, $A_{eff} = 25\,\mu m^2$, and the other selected parameters are closed to the practical device values that are presented and discussed. The security concept provided by DNA codes can be generated using the random control of coupling powers. For instance, the controlled input power used is between 2.0 and 3.5 mW, whereas the quantizing threshold powers and the traveling roundtrips are 0.3–0.4 mW and 8,000–10,000, respectively. In application, the required information data can be secured in the transmission lines in the public networks.

Perfume Distribution Using Molecular Networking via an Optical Wireless Link

X. Louangvilay[1], **M. Tassakorn**[2], **S. Mitatha**[1], **and P. P. Yupapin**[2]

[1]Hybrid Computing Research Laboratory, Faculty of Engineering
King Mongkut's Institute of Technology Ladkrabang, Bangkok 10520, Thailand
[2]Advanced Research Center for Photonics, Faculty of Science
King Mongkut's Institute of Technology Ladkrabang, Bangkok 10520, Thailand

Abstract— We propose a new system of a molecular-quantum networking using the optical tweezers, whereas the transportation of molecules via wavelength router and network can be performed. In addition, the molecule transportation states can be identified by using the quantum states of the transporters, which can be formed in the network. The proposed fabricated material used is **InGaAsP/InP**, which can provide the required output signals. The design system consists of a nonlinear microring/nanoring resonator system incorporating an add/drop filter and a wavelength router. The transporter can be formed by the dark soliton, the optical transporter is tuned and amplified by the bright soliton and transmitted into the network. In applications, the use of the proposed system incorporating a nanoscale communication and networking via wavelength router is available for long distance link.

Multi Transporters Generation for High Density Molecule Transportation via Optical Communication

S. Thongmee[1], **S. Pipatsart**[2], **and P. P. Yupapin**[2]

[1]Department of Electronics Technology, Faculty of Science
Ramkhamhaeng University, Bangkok 10240, Thailand
[2]Advanced Research Center for Photonics, Faculty of Science
King Mongkut's Institute of Technology Ladkrabang, Bangkok 10520, Thailand

Abstract— We propose a novel system of a quantum-molecular cryptography using the optical tweezers, whereas the transportation of molecules in the communication system can be performed. The molecule transportation states can be identified by using a single photon state of the transporter, which can be formed in the transmission line. The proposed fabricated material used is **InGaAsP/InP**, which can provide the required output signals. The design system consists of a nonlinear microring/nanoring resonator system incorporating an add/drop filter and a quantum signal processor. The transporter can be formed by the dark soliton, where the optical transporter is tuned and attenuated to be a single photon by the bright soliton control and transmitted into the link. In applications, the use of the proposed system incorporating a quantum processor can be performed the secured molecular communication.

Multi Quantum-molecular Transportation via Multi Wavelength Layers in a Wavelength Router

S. Chaiyasoonthorn[1] and P. P. Yupapin[2]

[1]Department of Electronics Technology, Faculty of Science
Ramkhamhaeng University, Bangkok 10240, Thailand
[2]Advanced Research Center for Photonics, Faculty of Science
King Mongkut's Institute of Technology Ladkrabang, Bangkok 10520, Thailand

Abstract— We propose a new system of a multi molecular transporters generation for hybrid signal processing and networking applications. The transportation of molecules via multi tweezers in the wavelength layer and network can be performed. The design system consists of a nonlinear microring/nanoring resonator system incorporating an add/drop filter and a wavelength router. The multi transporters with different wavelengths can be generated and formed by the multi optical tweezers. The multiplexed transporters can be use for high capacity molecular signal processing and communication in the hybrid networks. In applications, the use of the proposed system incorporating a nanoscale communication and networking via the multi wavelength layer and routers is available for high density molecule transportation and long distance link.

Molecule Transportation via Hybrid MUX/DEMUX System

N. Sangwaranatee[1], **P. Chaiyachate**[2], **S. Mitatha**[3], **and P. P. Yupapin**[2]

[1]Faculty of Science and Technology, Rajamangala University of Technology Krungthep, Thailand
[2]Advanced Research Center for Photonics, Faculty of Science
King Mongkut's Institute of Technology, Ladkrabang, Bangkok 10520, Thailand
[3]Department of Computer Engineering, Faculty of Engineering
King Mongkut's Institute of Technology, Ladkrabang, Bangkok 10520, Thailand

Abstract— We propose a novel system of a hybrid quantum-molecular multiplexing using the dynamic optical tweezers, whereas the high density molecule transportation in the communication system can be performed. The molecule transportation states can be identified by using a single photon state of the transporters, which can be formed in the transmission lines. The proposed fabricated material used is **InGaAsP/InP**, which can provide the required output signals. The transmitted part can be used to generate the high density molecules within the series of micro ring resonators. The received part can be used to detect the quantum states via the optical link, which can be obtained via the end quantum processor. The reference states can be recognized by using the cloning unit, which is operated by the add/drop filter. Two add-drops that are in two parts can be used to be confirmed between Alice and Bob, respectively, in quantum communication. Results obtained have shown that the multiplexed tweezers can be formed by using the multiple operating systems, which is allowed the filtering at the end users (Bob). In addition, the transporters can be formed by the dark soliton, where the optical transporter is tuned and attenuated to be a single photon by the bright soliton controlled and transmitted into the link. In application, the use of the proposed system incorporating a quantum processor can be performed the secured molecular communication.

Session 4P4
Theory and Application of Biisotropic and Anisotropic Metamaterials

Lateral Shift of an Electromagnetic Wave Reflected from the Chiral Metamaterial

L. Gao[1], **W. T. Dong**[1], **and C. W. Qiu**[2]

[1]Department of Physics, Soochow University, Suzhou 215006, China
[2]Department of Electrical and Computer Engineering, National University of Singapore
Kent Ridge, Singapore 119620, Republic of Singapore

Abstract— Applying Artmann's formula to the TE-polarized incident waves, we investigate the Goos-Hanchen (GH) shift of electromagnetic waves from semi-infinite chiral metamaterials or chiral metameterial slab. GH shifts are observed for both perpendicular and parallel components of the reflected field near the respective critical angles. For semi-infinite chiral metamateials, it is found that positive and negative shifts can be attained when the incident angle is larger than the first critical angle, whereas if the angle of incidence exceeds the second critical angle, only positive shifts can be observed. On the other hand, the GH shifts near the angle of the pseudo-Brewster dip of the reflection from a slab of chiral metamaterial can be greatly enhanced. Moreover, the GH shifts depend not only on the slab thickness and the incident angle, but also on the constitutive parameters of the chiral medium. In particular, when the incident angle is close to the critical angle of total reflection for LCP wave, significant enhancement of the GH shifts can be obtained. Finally, the validity of the stationary-phase analysis is demonstrated by numerical simulations of a Gaussian-shaped beam.

REFERENCES

1. Hoppe, D. J. and Y. Rahmat-Samii, "Gaussian beam reflection at a dielectric-chiral interface," *Journal of Electromagnetic Waves and Applications*, Vol. 6, 603–624, 1992.
2. Dong, W. T., L. Gao, and C. W. Qiu, "Goos-Hänchen shift at the surface of chiral negative refractive media," *Progress In Electromganetics Research*, PIER 90, 255–268, 2009.
3. Dong, W. T., L. Gao, and C. W. Qiu, *Opt. Express*, revised, 2009.

Electromagnetic Field Energy in Metamaterial Media with Strong Dispersion and Finite Loss

Pi-Gang Luan
Department of Optics and Photonics, National Central University, Jhongli 320, Taiwan

Abstract— Up to now most metamaterials are artificial structures consisting of conducting elements such as wires, split-ring resonators (SRR), or metallic thin films, and usually using their resonance properties to achieve unusual physical phenomena such like negative refraction. This implies that metamaterials are dispersive media in general and have finite loss. When the loss effect is negligible, the formula for calculating the energy density stored in the dispersive media can be obtained via analyzing an adiabatic electromagnetic process, and we refer this formula as classical formula [1, 2]. However, when nonzero absorption is present, one has to develop different methods such as equivalent circuit (EC) method [3] or electrodynamic (ED) method [4, 5] to evaluate the energy density. There are several papers concerning the energy density problems of the wire-SRR metamaterial system using EC and ED approaches [3, 4], but their results are inconsistent, which seems to imply that only one of the two approaches are reliable. Besides, it is surprising that some of these results do not recover the result of the classical formula in the lossless limit. In this paper, we explain why these previous results should be corrected and how to correct them. We will also show that the inconsistency between the EC and ED approaches are only apparent and we can indeed obtain consistent results if we carefully analyzing the mechanism of the loss. This new formula developed by us gives classical result when the loss effect is negligible. Our study reveals that a careful analysis of the power loss mechanism is essential before using the ED method. In addition to the wire-SRR medium, we also discuss how to use our energy density formula to calculate the energy stored in the metal-dielectric thin films medium or some simple chiral media with single resonance.

REFERENCES

1. Brillouin, L., *Wave Propagation and Group Velocity*, Academic Press, 1960.
2. Landau, L. D. and E. M. Lifshitz, *Electrodynamics of Continuous Media*, 2nd Edition, Pergamon Press, 1984.
3. Tretyakov, S. A., "Electromagnetic field energy density in artificial microwave materials with strong dispersion and loss," *Phys. Lett. A*, Vol. 343, 231, 2005.
4. Boardman, A. D. and K. Marinov, "Electromagnetic energy in a dispersive metamaterial," *Phys. Rev. B*, Vol. 73, 165110, 2006.
5. Ruppin, R., "Electromagnetic energy density in a dispersive and absorptive materialm," *Phys. Lett. A*, Vol. 299, 309, 2002.

The Metamaterials: The New Electronic Aggregate Composite Materials and Their Applications

Alain Priou and Habiba Ouslimani
Energy, Mechanics and Electromagnetic Labs (LEME), University Paris West
50 rue de Sèvres, 92410 Ville d'Avray, France

Abstract— In the permittivity and permeability and refractive index diagram (ε and μ diagram) three quadrant parts are well known. They are related to existing materials being either isotropic, bi-isotropic or anisotropic and bi-anisotropic media. They corresponds to either $\varepsilon > 0$ and $\mu > 0$, or $\varepsilon > 0$ and $\mu < 0$ and or $\varepsilon < 0$ and $\mu > 0$. All those media can be found in the nature and are described by constitutive relations associated with the Maxwell equations as mentioned in the book of J. A. Kong [1]. In early 1968, in his pioneering works, Vesalago [2] mentioned media with $\varepsilon < 0$ and $\mu < 0$ and solved the Maxwell equations showing very interesting new properties for these new materials, called the Metamaterials. In the $\varepsilon < 0$ and $\mu < 0$ quadrant part, it is shown that those materials can be only made by man. It was the opening of new researches and new applications are can merged from these studies.

In TEM waveguide we can change over the equation of the field theory associated with the Maxwell equations to those of the circuit theory of the Telegraphist equations and vice versa [3]. Starting from this point, it could be possible to design negative index materials using electronic circuits having equivalent negative values in some certain conditions. The use of rods and split rings has shown to have such negative index media behaviors in specific frequency bands. Composite materials can be designed and realized by association of circuit elements in series, in parallel or in more complex manner. And metamaterials-like electronic circuit composite materials can be realized.

During the presentation, we will introduce this possibility to create circuit elements having negative index behaviors in microwave range. We will make comparison with composite materials made of loading dielectric or metallic particles with those made of circuit elements associated in series or in parallel or else. We will show the applications we can realize with this electronic composite materials made by metamaterial structures and association of metamaterial structures for the application of radôme, antennas and antenna arrays with their new properties. We will present, also, the perspectives for having new impedance sheets and materials made of such metamaterials distributed on period manner or in random distribution or by using metamaterial nanostructures.

REFERENCES

1. Kong, J. A., *Electromagnetic Wave Theory*, EMW, Cambridge, 2000.
2. Veselago, V. G., "The electrodynamics of substances with simultaneously negative values for permittivity and permeability," *Soviet Physics, Uspekhi*, Vol. 10, 509–514, 1968.
3. Von Hippel, A. R., *Dielectric and Waves*, John Wiley & Sons, New York, 1954.

Hermite-Gaussian Beam Scattering by a Chiral-coating Conducting Sphere

Qiong-Kun Yuan, **Zhen-Sen Wu**, **Hai-Ying Li**, **and Zheng-Jun Li**
School of Science, Xidian University, Xi'an, Shaanxi 710071, China

Abstract— The scattering characteristics of chiral media have attracted much attention due to many associated interesting phenomena in optical and electromagnetic activities and their potential applications in various fields. On the other hand, there has been increasing interest in the scattering problem from a Gaussian beam. In this paper, an analytical solution to the scattering of a Hermite-Gaussian beam by a chiral-coating conducting sphere is proposed. The incident Hermite-Gaussian beam is expanded with the spherical vector wave functions and the beam shape coefficients are obtained by the complex source point method. The electromagnetic fields in the chiral layer are expressed in terms of the first and second kinds of spherical vector wave functions with two different eigenvalues. Applying the boundary conditions on each interface among the conducting sphere, chiral medium and free space, the expansion coefficients for the internal and the scattered fields are determined. As numerical examples, the radar cross sections for the far scattered fields in multi-mode Hermite-Gaussian beam are calculated. The effects of the chirality, the nonreciprocity and the thickness of the chiral coating on the field distributions are examined. The dependence of the scattering properties on the beam width, beam waist center positioning and the mode of the beam are also analyzed. Our results for a Hermite-Gaussian beam incidence can be reduced to those for a plane wave and the chiral coating can be reduced to an isotropic one. The analysis in this paper is useful in the areas of target stealth, radar detection and microwave device fabrication.

Three-Dimensional Scattering by an Infinite Homogeneous Gyrotropic Elliptic Cylinder

Shi-Chun Mao and Zhen-Sen Wu
School of Science, Xidian University, Xi'an 710071, China

Abstract— Solutions to the problem of two-dimensional scattering by objects of elliptic cylinders or cylindrical configurations of elliptic shapes have been investigated theoretically in many papers. However, to our knowledge, three-dimensional scattering by an infinite homogeneous gyrotropic elliptic cylinder has not yet been discussed.

A solution to the problem of three-dimensional scattering by an infinite homogeneous gyrotropic elliptic cylinder for an obliquely incident plane wave of an arbitrary linear polarization is proposed. Based on the source-free Maxwell's equations in gyrotropic media, the axial components of the electromagnetic fields inside a gyrotropic elliptic cylinder are represented as two coupled integrals of suitable eigenfunctions in elliptic coordinates in terms of Mathieu functions, while the transverse components of the fields can be determined by the axial components. Different from many other harmonics, the elliptic cylinder harmonics or Mathieu functions inside the anisotropic media are nonorthogonal with those outside. Consequently, scattering by a gyrotropic elliptic cylinder is different from scattering by a sphere or a circular cylinder because of the nonorthogonality properties of Mathieu functions at the interface between two different media. In order to obtain numerical results, the Galerkin's method is applied to the boundary conditions at the interface between the anisotropic and the free space regions. A matrix inversion is required for the computation of unknown expansion coefficients of the scattered and internal fields. Numerical results are presented, discussed and compared with available data for the sake of validating the numerical scheme.

A General Method for Designing Transformation Materials of Arbitrary Configuration

Zheng Chang[1], **Jin Hu**[2], **Xiaoming Zhou**[1], **and Gengkai Hu**[1]

[1]School of Aerospace Engineering, Beijing Institute of Technology, Beijing 100081, China
[2]School of Information and Electronics, Beijing Institute of Technology, Beijing 100081, China

Abstract— Based on the transformation optics, a general approach is proposed to design electromagnetic devices of arbitrary configurations. Transformation optics is a theory of inverse problem, deriving the material parameters from the prescribed coordinate transformation characterized by the Jacobin (transformation) matrix. The proposed method comes from an alternative explanation of the Jacobin matrix. When we consider the coordinate transformation as the deformation from a flat grid to a distorted one, the Jacobin matrix is the deformation tensor in continuum mechanics. With a partial differential equation (PDE) governing the deformation of grids, this idea introduces a new way to the design of arbitrary transformation materials. For ordinary transformation optics, devices with irregular boundaries are very hard to design, since the irregular boundary is hardly translated to a mathematical expression. Many researchers approximate this problem by splitting an irregular boundary into many regular lines or curves. However by introducing a PDE, for example the Laplace's equation, the proposed method can easily manipulate materials with irregular boundaries. It is further shown that the design and verification of transformation materials of arbitrary shapes can be well performed by a two-step model in the finite-element package, COMSOL Multiphysics. Moreover, one has the flexibility in choosing the PDE to govern the deformation of coordinate grids. The PDE solutions only reflect the distributions of material parameters, but don't change the prescribed functionality. If the Poisson's equation is employed, instead of Laplace's one, the source function will become a controllable parameter to tune the distribution of permittivity and permeability for easy realization in practice. However, the improper choose of PDE may bring more difficulty in practical realization, for example the Helmholtz equation. When the propagation constant in Helmholtz equation is a large real value, the designed device may involve many singular regions, where material parameters approach infinity. All of above ideas and explanations can be demonstrated by simulation results.

Experimental Study on Electromagnetic Beam Bender

Q. B. Deng[1], J. Hu[2], Z. Chang[1], X. M. Zhou[1], and G. K. Hu[1]

[1]School of Aerospace Engineering, Beijing Institute of Technology, Beijing 100081, China
[2]School of Information and Electronics, Beijing Institute of Technology, Beijing 100081, China

Abstract— Electromagnetic beam bender designed with transformation optics receives much attention recently. A bender can change the propagating direction of an incoming wave. There are no cut-off frequency and mode restrictions for waves under bended, in contrary to conventional metallic waveguides. Waves travel in the transformation bender, just like in the free space. Many works have contributed to the design of beam benders and simplification of their material parameters. In this work, we systematically study the beam bender based on the deformation perspective of transformation optics. The deformation transformation optics (DTO) tells that coordinate transformation is equivalent to the deformation of coordinate grids, therefore material parameters can be determined uniquely according to the grid deformation. When different combinations of principle stretches in three perpendicular directions are considered, all existing results can be recovered, showing the powerfulness of DTO. For further study, we study in experiment the beam benders by two strategies. One sample is fabricated with the metamaterial technology, where split ring resonators (SRR) are employed to realize the anisotropic and inhomogeneous magnetic constants of the bender. Both simulation and experimental results show the bending function, as expected. However, the sample can only operate in a narrow frequency band, as arises from the limitation of artificial resonances of metamaterials. The second strategy comes from a successful simplification of material parameters and suggests that there exists a dielectric bender for TM waves. We then propose an idea of fabricating the bender by drilling sub-wavelength holes in a dielectric plate. By tuning the radius and distribution of small holes, one can control the wave propagation in the bender. Experimental result shows well its functionality. Compared with the first sample, the second one is non-dispersive, meaning that it can work in a very wide band, just below a specific frequency determined by the sub-wavelength microstructures, and easier to make of course.

Scattering of Two Uniaxial Anisotropic Spheres to Plane Wave

Zheng-Jun Li, **Zhen-Sen Wu**, **and Hai-Ying Li**
School of Science, Xidian University, Xi'an 710071, China

Abstract— Based on the scattering of a uniaxial anisotropic sphere to plane wave, the generation multi-sphere Mie theory (GMM) is extended from the scattering of isotropic spheres to the scattering of anisotropic spheres. Then we investigate the simplest scattering problem that the scattering of two uniaxial anisotropic spheres with arbitrary configuration to plane waves and the principal axes of the two anisotropic spheres are all parallel with the incident wave direction. The incident and scattered fields are expanded in terms of the spherical vector wave functions (SVWFs) and the expanded forms of the internal field in terms of the SVWFs are also derived using the fourier-integral method. Utilizing the addition theorem of the SVWFs, the scattered field at one of the sphere coordinate system can be transferred into the incident field at another sphere coordinate system. Then like as general Mie theory, the equations on the scattering coefficients is derived according the continuous tangential boundary conditions. Through solving the equations set, the analytical solution on the plane wave scattering from two uniaxial anisotropic spheres are obtained. The scattering characteristic of the plane wave scattering from two uniaxial anisotropic spheres is analyzed by the analytically method and the numerical method with the commercial software CST. The two results with regard to the angular distribution of the radar cross section (RCS) with different distances of the two spheres center are compared with each other and are in good agreeable with each other. The work in this paper provides some theory tools and stated base for further research on the scattering of many uniaxial anisotropic spheres to plane waves or Gaussian Beams.

Plasmonic Nanoparticles as Terahertz Oscillators

Xiaobing Cai and Gengkai Hu
School of Aerospace Engineering, Beijing Institute of Technology
Beijing 100081, China

Abstract— In a highly nonuniform radiation field of hertz dipole induced by polarized laser lights, the gradient force exerted on a metamaterial nanoparticle is extremely large when the laser is excited near Fröhlich frequency. The force always tends to pull the nanoparticle back to the central position of the radiation field where the electric field is maximal. According to this mechanism, a nanoparticle oscillator and a rotational oscillator of a spheroidal nanoparticle are proposed with operating frequency up to terahertz.

Session 4P5
High Frequency Properties of Materials and Their Applications

Microwave Absorption Properties of Cobalt Nanowires Fabricated by Pulse Electrodeposition

Wenbing Chen, **Mangui Han**, **and Longjiang Deng**
State Key Laboratory of Electronic Thin Films and Integrated Devices
University of Science and Technology of China, Chengdu 610054, China

Abstract— In this work, cobalt nanowires with a preferred growth orientation have been fabricated by a pulse electrodeposition method and the dynamic permittivity and permeability spectra of the nanowire/paraffin composite samples were measured in the range of 0.5∼18 GHz. The imaginary part of the permeability spectra for the nanowire/paraffin composite samples exhibit a strong absorption peak at 6.1 GHz and two minor peaks at above 10 GHz. It is determined that the peak at 6.1 GHz is attributed to the natural resonance mechanism and the other two peaks are caused by eddy current effect. By proposing an anisotropy constant that integrates the effect of magnetocrystalline anisotropy and magnetostatic interaction among nanowires, we have fitted the permeability spectra attributed to natural resonance using the LLG equation. Calculation based on the Kittel equation substantiates our explanation. The electromagnetic wave reflection loss values of the nanowire/paraffin composite samples are lower than −20 dB when the thickness of the nanowire/paraffin composite is adjusted, suggesting that the cobalt nanowire composites can find application as microwave absorbers.

A Comparative Study of the Field Dependence of the Properties of Colloidal Suspensions of Nanoparticles and of Magnetic Microspheres

P. C. Fannin[1], **C. N. Marin**[2], **C. Couper**[1], **I. Malaescu**[2], **and N. Stefu**[2]

[1]Department of Electronic and Electrical Engineering, Trinity College, Dublin 2, Ireland
[2]Faculty of Physics, West University of Timisoara, B-dul V. Parvan, No. 4, Timisoara 300223, Romania

Abstract— Field and frequency-dependent, complex susceptibility, $\chi(\omega, H) = \chi'(\omega, H) - i\chi''(H, \omega)$, measurements is a proven method for the investigation of the dynamic properties of colloidal suspensions [1]. In particular, polarised measurements have been used to investigate many properties, including, relaxation mechanisms and the presence or absence of aggregates in samples. Furthermore, important information on the hysteresis and isotropic properties of samples can also be obtained through the use of polarised measurements.

In this presentation examples of the determination of the above mentioned properties of colloidal suspensions of nanoparticles and of magnetic spheres will be presented and discussed.

REFERENCES

1. Fannin, P. C., B. K. P. Scaife, and S. W. Charles, "The measurement of the frequency dependent susceptibility of magnetic colloids," *J. Magn. and Magn. Mater.*, Vol. 72, 95–108, 1988.

Microwave Susceptibility Dispersion Spectra of Nanodot Arrays with Perpendicular Anisotropy

Wenbing Chen and Mangui Han
State Key Laboratory of Electronic Thin Films and Integrated Devices
University of Electronic Science and Technology of China, Chengdu 610054, China

Abstract— In this work, we have studied that the remnant magnetization states of nanodots and the microwave susceptibility spectra associated with different domain states by employing the micromagnetic simulation approach. The micromagnetic simulations are performed using the public domain 3D OOMMF by solving the Landau-Lifshitz-Gilbert (LLG) equation as a function of time. The material parameters in OOMMF for cobalt are taken: saturation magnetization $M_s = 14 \times 10^5\,\mathrm{A/m}$, exchange stiffness constant $A = 30 \times 10^{-12}\,\mathrm{J/m}$, anisotropy constant $K_1 = 5.2 \times 10^5\,\mathrm{J/m^3}$. The direction of the anisotropy constant is set to be along the length direction of the nanodots to ensure perpendicular anisotropy. The gyromagnetic ratio γ is set to be $2.21 \times 10^5\,\mathrm{mA^{-1}S^{-1}}$ and the damping constant α is set to be 0.015. A cubic cell size of $5 \times 5 \times 5\,\mathrm{nm^3}$ is taken. The field-dependent behavior of a single isolated cylindrical nanodot with height of 50 nm and its corresponding 3×3 periodic arrays is simulated. For the purpose of comparison, the diameter of these nanodots is fixed to be 100 nm and the adjacent interdot distance (d) is varied from 10 nm to 60 nm. The simulation results demonstrate that the stable magnetization state for a single isolated nanodot with diameter of 100 nm and height of 50 nm is flowering state. In contrast, the nanodots in the arrays exhibit a variety of domain states as the interdot distance varies. For instance, the domain state for the nanodot at the center of the array transforms from stripe-domain to bubble state, to multi-domain state with the co-occurrence of bubble state and stripe-domain, to flowering state as d increases. In the meantime, the susceptibility spectra of the nanodot arrays are closely related to their domain state. A comparison between the domain states and related susceptibility spectra allows us to divide the resonance peaks of the susceptibility spectra into four categories: the ones associated with flowering state, the ones ascribed to stripe-domain state, the ones caused by the bubble state, and the ones attributed to the interaction between different domain states. Since magnetostatic interaction between nanodots is the prime variable brought about by the change of d, it should account for the evolution of domain states and their corresponding susceptibility spectra as a function of d.

Tunable Microwave Metamaterials Based on Frequency Select Surface Controlled by PIN Diodes

Mangui Han
State Key Laboratory of Electronic Thin Films and Integrated Devices
University of Electronic Science and Technology of China, Chengdu 610054, China

Abstract— In this paper, three different types of frequency select surfaces (FSS) based on the periodic PIN diodes have been designed and fabricated to construct tunable microwave metamaterials, below which low loss spacing materials backed by metal boards have been used. HFSS software has been employed to construct the reflectivity simulation models and the accuracy of simulations also has been verified. We have simulated the effects of bias conditions of PIN diodes, the thickness of spacer, the FSS dielectric layer and the spacer materials on the behaviors of microwave reflectivity. A variety of parameters have been optimized so that the microwave absorbers show good tunable behaviors within a certain bandwidth. Based on the optimization results, the microwave metamaterials have been experimentally fabricated. The experimental reflectivity results show that the simulations and experiments agree well. By controlling the bias voltages of diodes to turn them "on" and "off", the metamaterials show a single reflectivity peak with a value less than −10 dB within a frequency range of 4 GHz–14 GHz, the reflectivity peak position also can be tuned between 6.2 GHz and 11.8 GHz. The transmission line equivalent circuits are used to explain the tunable behaviors of these microwave metamaterials.

Oxides as Terahertz Optical Materials

Qi-Ye Wen, Huai-Wu Zhang, and Qing-Hui Yang
State Key Laboratory of Electronic Films and Integrated Devices
University of Electronic Science and Technology of China, Chengdu 610054, China

Abstract— Due to recent advances in femtosecond lasers and optical materials, the THz radiation band from 0.1 to 10 THz is now routinely accessible. THz-time domain spectrometer (THz-TDS) has been employed to study the optical properties of a wide variety of materials such as chemical mixture, polymer, explosives, semiconductor and dielectric materials, etc. In this report, we investigate the time-domain spectrum in THz band of NiO and CeO_2 polycrystals fabricated by solid-state reaction. Both the absorption coefficient and the refraction index were calculated by FFT. According to the relation of optical constants, the dielectric constant, absorption coefficient, and even refraction index were calculated as a function of frequency. The results indicate that all these properties of the oxides in the high frequency of THz are quite different from the microwave regime.

The results of Fe doped CeO_2 are quite interesting and which update the physics of THz spectroscopy. Our results show that the pure CeO_2 only has a small dielectric constant (ε) of 4, while a small amount of Fe (0.9%) doping into CeO_2 promotes the densification and induces a large ε of 23. From the THz spectroscopy, it is found that for undoped CeO_2 both the power absorption and the index of refraction increase with frequency, while for Fe doped CeO_2 we measure a remarkable transparency together with a flat index curve. The absorption coefficient of Fe doped CeO_2 was less than $0.35\,\mathrm{cm}^{-1}$ ranging from 0.2 to 1.8 THz, rendering it a potential THz optical material. These results disclose the effect of dielectric constant of oxide on its properties at high-frequency band.

Thickness Effects on Microwave Magnetic Properties of FeCoBSi Films Deposited on Flexible Substrate

Haipeng Lu, **Jing Yang**, **and Longjiang Deng**
State Key Laboratory of Electronic Thin Films and Integrated Devices
University of Electronic Science and Technology of China
Chengdu 610054, China

Abstract— Nowadays, more and more new applications such as flexible EMI suppressors require flectional samples which under a suitable form [1]. This was the motivation for the experimental study of thin films deposited on thin flexible substrates. Iron-based films are known with high saturation magnetization. Alloying iron with cobalt, boron and silicon may result in the materials with high saturation magnetization and appropriate anisotropy or resistivity. Such films may have high permeability at frequencies of several GHz. The paper deals with FeCoBSi films of different thickness based on flexible mylar substrates, aiming at the structure and microwave properties of the films.

$Fe_{66}Co_{17}B_{16}Si_1$ thin films were produced on flexible 11.5 μm thick mylar substrates by DC magnetron sputtering. The microstructure of the thin films was examined using X-ray diffractometry (XRD) with Cu Kα radiation, and the electrical resistivity of the samples is determined by a standard four-point method. The permeability has been measured from 500 MHz up to 18 GHz using a coaxial technique described elsewhere [2]. The technique implies winding a film into a roll sample that adapts to the geometry of the coaxial line cavity.

FeCoBSi films prepared on thin flexible substrates are showed as an amorphous structure. Amorphous structure is beneficial to obtaining lower coercivity and larger permeability. For the laminates filled with FeCoBSi film, increasing the film thickness leads to an increase in the level for the real part and imaginary part of the permeability of the laminates. It is attributed to the increasing metal volume fraction. From the magnetic spectra of FeCoBSi films with a range of thickness, the general trend is that the ferromagnetic resonances shift toward the low frequencies with the increasing thickness. When the thickness was more than 1 μm, the values of both permeability and resonance frequency decreased significantly. The results may be attributed to the increase of eddy current loss. But we also noticed that the values of permeability increased with an increasing thickness of the films when the thickness was less than 1 μm. It is worthy of attention because the phenomenon is inconsistent with most reports. This unusual result may be due to the various microstructures, stress, defects, etc. The electric properties, including sheet resistance and resistivity for the films with various thicknesses, have also been investigated in this paper.

REFERENCES

1. Valls, O., D. Damiani, et al., "High frequency permeability of fecov thin films deposited on thin flexible substrates," *Digests of the Intermag Conference*, FD07, 2002.
2. Acher, O., J. L. Vermeulen, et al., "Permeability measurement on ferromagnetic thin films from 50 MHz up to 18 GHz," *J. Magn. Magn. Mater.*, Vol. 136, 269, 1994.

Effect of the Very Thin Dielectric Film on the Transmission Properties of the FSS

Xinyu Hou, **Wenming Tian**, **and Yongxing Che**
State Key Laboratory of Electronic Thin Films and Integrated Devices
School of Microelectronics and Solid-State Electronics
University of Electronic Science and Technology of China
Chengdu 610054, China

Abstract— This paper investigates the influential rule of the thickness and dielectric constant of glue-film material to the resonant frequency of one-layer FSS in fabrication. Firstly, ring loop and four-legged loaded elements of one-layer FSS is designed and calculated. The results show that the resonant frequency (f_0) bounds when the dielectric thickness is $1/4\lambda$ and $3/4\lambda$ for both structures. Then glue-film material is added bellow and above conducting FSS. The results show that the f_0 changes when the glue-film's thickness and dielectric constant varies and bounds at some values. This illuminates that the thickness and dielectric constant of glue-film material is paramount factor for the f_0 of one-layer FSS in practical fabrication.

Microwave Multi-resonant Magnetic Pattern and EM Wave Absorption Application

Peiheng Zhou, **Haipeng Lu**, **Huibin Zhang**, **Haoran Xu**, **and Longjiang Deng**
State Key Laboratory of Electronic Thin Films & Integrated Devices
University of Electronic Science and Technology of China
Chengdu 610054, People's Republic of China

Abstract— Microwave multi-resonance is currently one of the very attractive research areas in electromagnetic materials. It has led to important fundamental discoveries, the non-uniform precession excitation and resonances overlapping effect, which promise the wideband and high frequency applications, especially for EM wave absorption. In our work, magnetic thin-film patterns with microwave multi-resonance are fabricated and designed to absorbing EM wave. The final absorber is a multilayer sheet with improved absorption comparing with traditional absorbers. The microwave behavior of thin-film pattern is studied from the view point of non-uniform precession in micromagnetism. It is found that magnetization orientation affects the spin wave modes excited, in another word the resonances. Finally, the rule of pattern design for absorption purpose is introduced.

High Frequency Characteristics and Electrical Properties of Multilayer FeCoHfO/AlO_x Films

Yu-Ming Kuo[1], **Shandong Li**[2], **Jenq-Gong Duh**[1], **and Su-Yueh Tsai**[3]

[1]Department of Material Science and Engineering, National Tsing Hua University
Hsinchu 30013, Taiwan, R.O.C.
[2]Department of Physics, Fujian Normal University, Fuzhou 35007, China
[3]Precision Instrument Center, National Tsing Hua University, Hsinchu 30013, Taiwan, R.O.C.

Abstract— The soft magnetic thin films provide favorable alternatives in reduction of the device dimensions and in the development of electromagnetic high-frequency devices. For the high frequency application in mobile communication technology, the operated frequency is over 3 GHz. Hence the ferromagnetic resonance frequency (f_{res}) of magnetic films must be over 3 GHz. In this study, FeCoHfO is chosen as the appropriate material systems for this application. It is well known that FeCo alloys have the high magnetization saturation. Doping Hf in magnetic materials can reduce the FeCo grain size. However, the eddy current loss is one of the main dissipation factors at high frequency range. Inserting an insulator (e.g., AlO_x) layer into ferromagnetic layers is a good way to exhibits high resistivity and to reduce the eddy current loss.

Nanocrystalline (FeCoHfO/AlO_x)$_n$ multilayered films were developed using dc reactive magnetron sputtering. The multilayered structure was the FeCoHfO ferromagnetic layer with total thickness of 1.2 μm separated by AlO_x interlayers with 10 nm in thickness. The FeCoHfO/AlO_x multilayered films were post-magnetically annealed for 3 hours along hard axis. A significant reduction of hard axis anisotropic field was observed when the number of multilayer reached five. With this optimum conditions of [FeCoHfO (400 nm)/AlO_x (10 nm)]$_3$, favorable soft magnetic properties (easy axis coercivity: 4.4 Oe and effective anisotropy field: 110 Oe) and high frequency characteristics (permeability $\sim$ 100 at 100 MHz and ferromagnetic resonance frequency over 3 GHz) and high electrical resistivity $\rho \sim 1074$ μΩcm were obtained. The variation of film microstructure and the induced stress due to the introduction of oxide spacers in the multilayer feature were probed and discussed. The insertion of amorphous AlO_x might play an important part in absorbing the film stress, which would induce the decrease of anisotropic field. Besides, inserting the amorphous AlO_x layer into FeCoHfO layers is a good way to increase resistivity. It is demonstrated that the FeCoHfO/AlO_x multilayered films are promising for practical applications as a high-frequency ferromagnetic material.

A Novel Method to Solve the Complex Transcendental Equation for the Permittivity Determination in Short-circuited Line

Changying Wu, **Jianzhou Li**, **Gao Wei**, **and Jiadong Xu**
School of Electronic Information, Northwestern Polytechnical University
Xi'an 710129, China

Abstract— The precise permittivity determination of dielectric materials has been a very important task for ever-increasing microwave and millimeter-wave applications. For these reasons, various microwave techniques, each with its unique advantage and constraints, are introduced to characterize the electrical properties of materials. Owing to its relative simplicity, broad frequency coverage and higher accuracy, short-circuited line method, a type of non-resonant method, is widely utilized for characterization of materials. However, obtaining the electrical permittivity from the experimental measurements requires solving a transcendental equation of the form $(\tanh z)/z = c$ on the complex plane, where c is obtained experimentally. In solving these transcendental equations, iterative numerical methods are employed, of which the more commonly used is the Nowton-Raphson method. However, the main problem is that the transcendental equation has many roots, and it is difficult for its solution to converge to the correct value unless a very good initial guess is provided using some extra approach.

In this presentation, a mathematical procedure was proposed which combines contour integral method, full label triangles method, and simplex method for solving the transcendental equation on the complex plane which arises in the short-circuited line method. Although this equation possesses infinite solutions, only one of them is physical. Before deciding which of the solutions is the physical one it is better to find all possible permittivity in the given range. In our procedure, a formula of contour integral is used to determine the root number of the transcendental equation in the given range after the singularities are eliminated. And the equation is solved by simplex method from the initial values found by full label triangles method. The main advantage of this procedure is that all roots can be solved only one time. The inherent ambiguity in the transcendental equation is avoided with the aid of measurement results at adjacent frequency. By using this procedure, a precise characterization of the complex permittivity is possible, thus overcoming some limitations of previous methods. Simulation and measurement of reference material have been carried out to validate the method.

Adaptor Calibration Using a Matched Load and an Adjustable Shorter without Specified Phases

Changying Wu, **Kuisong Zheng**, **Gao Wei**, **and Jiadong Xu**
School of Electronic Information, Northwestern Polytechnical University, Xi'an 710129, China

Abstract— The vector network analyzer (VNA) has been widely applied in the measurement of microwave devices with wide frequency bandwidths. Particularly, the measurement of the complex reflection coefficients of waveguide devices is its important applications. Due to connecting the devices to be measured to the VNA with a coaxial-to-waveguide adaptor, the systemic error caused by the defect of the coaxial-to-waveguide adaptor will be introduced. For solving the problem, the calibration of the coaxial-to-waveguide adaptor is needed by connecting a series of known standard components to the measurement system. Subsequently, the systemic error can be obtained by analyzing the measurement results of the known standard components. The traditional calibration method uses three standard components, i.e., a load, a short circuit, and an offset short with known phase. However, with the traditional calibration method, the exact location of the short plane is difficult to be determined at the range of millimeter wave frequencies.

In this paper, a novel calibration procedure using a matched load and an adjustable shorter with several unspecified phases is proposed to reduce the systemic error caused by the adaptor. The advantage of this method is only to define one shorter plane as reference plane. During the calibration process, the position of the piston is unnecessary to be recorded. More offset shorts are used; more accurate de-embedding effect can be get. The proposed calibration method is especially fitted to the system calibration at the range of millimeter wave frequencies, where the accuracy of the system calibration is very sensitive to the position of standard short plane. The measured results show that the module of corrected S_{11} of a shorter is less than 0.1 dB with linear phase delay and the corrected S_{11} of a matched load is below -40 dB. The results are much more accurate than the raw readings, 1.3 dB and -15 dB respectively, before the adaptor calibration. It is also shown that the technique is resistant to the error of the adjustable shorter position and is easy to implement.

Session 4P6a
Integrated RF Passives

A Highly Miniaturized Broadband on-chip Impedance Transformer Employing Periodically Arrayed Ground Structure on Silicon RFIC

Jeong-Gab Ju, **Young-Bae Park**, **Bo-Ra Jung**,
Jang-Hyeon Jung, **Suk-Youb Kang**, **and Young Yun**
Department of Radio Sciences and Engineering, Korea Maritime University, Korea

Abstract— In this work, using a coplanar waveguide employing Periodically Arrayed Ground Structure (PAGS) on silicon RFIC, a highly miniaturized and broadband on-chip impedance transformer was developed for application to low impedance matching in broadband. Its size was 0.01 mm^2 on silicon substrate, which was 6.99% of the one fabricated by conventional coplanar waveguide . The transformer showed a good RF performance from 1 to 40 GHz.

Figure 1 shows a top view and corresponds to a cross-sectional view of the coplanar waveguide employing PAGS. As shown in Fig. 1, PAGS exists at the interface between the SiO_2 film and the silicon substrate, and it was electrically connected to top-side ground planes (GND planes) through the contacts. Therefore, PAGS was grounded through GND planes. As is well known, a conventional coplanar waveguide without PAGS has only a periodical capacitance C_a per unit length, while the coplanar waveguide employing PAGS has an additional capacitance, C_b as well as C_a, owing to PAGS. As shown in Fig. 1, C_b is a capacitance between the line and PAGS. From this figure, we can see that the coplanar waveguide with PAGS exhibits much lower characteristic impedance (Z_0) and shorter guided-wavelength (λ_g) than conventional one, because Z_0 and λ_g are inversely proportional to the periodical capacitance, in other words, $Z_0 = (L/C)^{0.5}$ and $\lambda_g = 1/\left[f \cdot (LC)^{0.5}\right]$.

Using the PAGS structure, a highly miniaturized and on-chip impedance transformer was developed for RFIC applications. Fig. 2 shows a photography of the impedance transformer. Measured return loss S_{11} and insertion loss S_{21} are shown in Fig. 3. The return and insertion loss are −45 and −1.3 dB, respectively, at a centre frequency of 21 GHz. We can observe return loss values better than −11.5 dB from 1 to 40 GHz, and insertion loss values better than −1.93 dB in the above frequency range, which mainly originate from a high conductivity of silicon substrate.

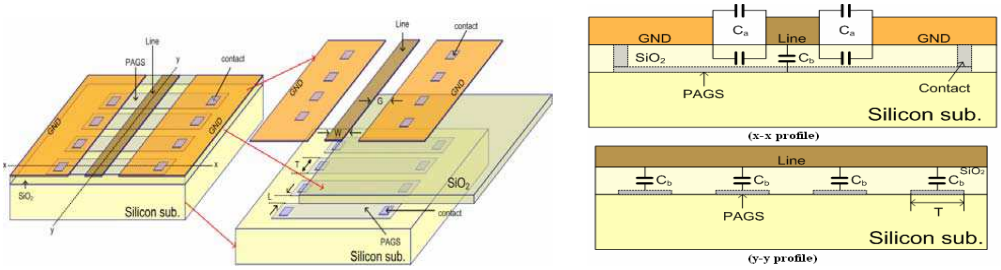

Figure 1: Structure of coplanar waveguide employing PAGS.

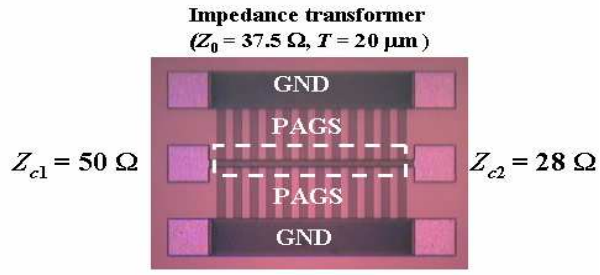

Figure 2: A photography of the impedance transformer.

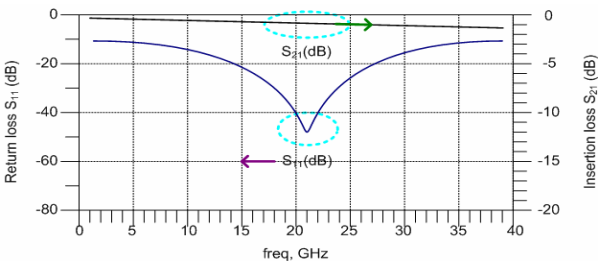

Figure 3: Measured return and insertion loss.

Highly Miniaturized On-chip 90° Hybrid Coupler Employing Transmission Line with Periodic Structure

Bo-Ra Jung, Young-Bae Park, Suk-Youb Kang, Jang-Hyeon Jung, Jeong-Gab Ju, and Young Yun
Department Radio Communication Engineering, Korea Maritime University, Republic of Korea

Abstract— In this paper, we propose a highly miniaturized on-chip 90° hybrid coupler on silicon radio frequency integrated circuit (RFIC), which was fabricated by a coplanar line employing periodically arrayed grounded-strip structure (PAGS).

Figure 1 shows, a structure of the coplanar waveguide employing PAGS, and Fig. 2 corresponds to a cross-sectional view according to X-X and Y-Y direction of Fig. 1. As shown in Fig. 1, PAGS exists at the interface between $Si0_2$ film and silicon substrate, and it was electrically connected to top-side ground planes though the contacts. As is well known, conventional coplanar waveguide without PAGS has only a periodical capacitance C_a (C_a is shown in Fig. 2) per a unit length, while the coplanar waveguide employing PAGS has additional capacitance C_b as well as C_a due to PAGS. From this figure, we can see that the coplanar line with PAGS exhibits much lower characteristic impedance (Z_0) and shorter guided-wavelength (λ_g) than conventional one, because Z_0 and λ_g are inversely proportional to the periodical capacitance, in other words, $Z_0 = (L/C)^{0.5}$ and $\lambda_g = 1/\left[f \cdot (LC)^{0.5}\right]$. Fig. 3 shows a photograph of 90° hybrid coupler. Its size was $0.46 \times 0.55\,\mathrm{mm}^2$, which is 37% of conventional one fabricated by conventional coplanar waveguide without PAGS. Measured power division, isolation and phase division characteristics are shown in Fig. 4. We can observe good power division characteristic from 41.75 to 50 GHz. Concretely, S_{21} and S_{31} exhibit a value of -5.7 dB at 46 GHz. In a frequency range of 41.75–50 GHz, S_{21} and S_{31} show a value of -5.9 ± 0.5 and -5.5 ± 0.5 dB, respectively. Isolation characteristic (S_{41}) shows a value of -18.1 dB at 46 GHz, and a value of $-13 \sim -18.1$ dB in a frequency range of 41.75–50 GHz. The phase division shows a value of 90.1° at 46 GHz, and a value of 90 ± 4.8° in a frequency range of 41.75–50 GHz.

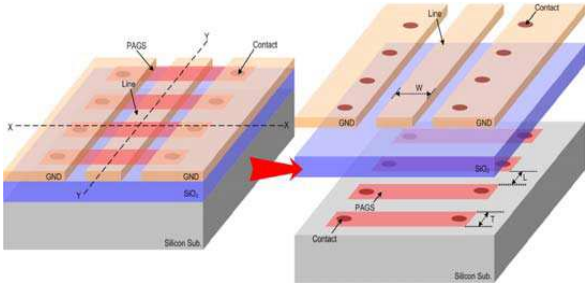

Figure 1: A structure of the coplanar waveguide employing PAGS.

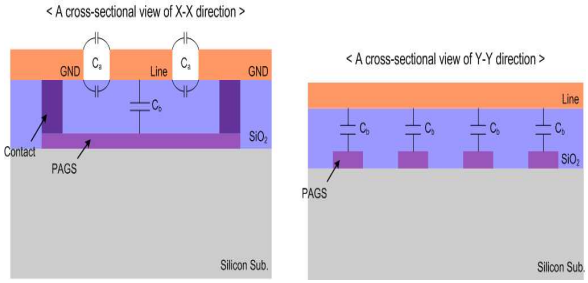

Figure 2: A cross-sectional view of X-X and Y-Y direction.

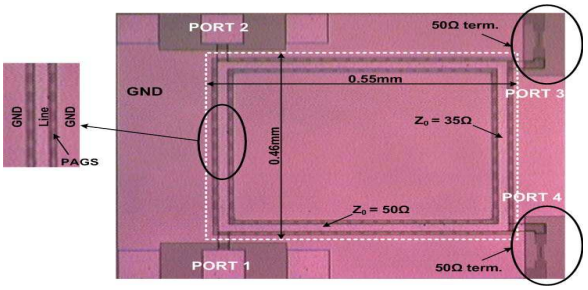

Figure 3: A photograph of the chip 90° hybrid coupler employing PAGS.

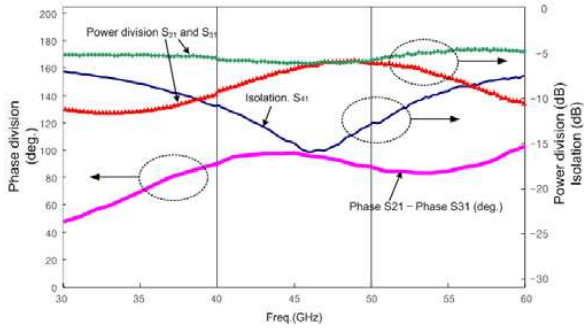

Figure 4: Measured RF characteristics.

An Artificial-transmission-line-based Miniaturized Doubly Balanced Ring Mixer

C. H. Lai, Y. T. Cheng, and T. G. Ma
Department of Electrical Engineering, National Taiwan University of Science and Technology
Taipei, Taiwan, R.O.C.

Abstract— The microwave mixer is one of the core components in the RF front end. The doubly balanced mixer, which utilizes two pairs of diodes in either a ring or star configuration, is a good candidate for achieving improved performances. In this paper, a miniaturized doubly balanced ring mixer using coupled artificial transmission lines is presented and investigated. The proposed miniaturized mixer is composed of two novel Marchand baluns and four diodes in a ring configuration. The Marchand balun, the most critical part in a doubly balanced mixer, consists of two sections of coupled artificial transmission lines and an additional artificial line for phase compensation. By replacing the conventional coupled lines with the miniaturized coupled artificial lines, the proposed Marchand balun features a very compact size but comparable operating bandwidth when comparing with its conventional counterpart. The doubly balanced ring mixer is fabricated on a six-layered printed circuit board. The Marchand baluns are designed at metal layers M3 and M4 while all diodes are mounted on the top layer, i.e., metal layer M1. The two baluns are separately connected to the RF and LO ports. The four diodes are arranged in a ring configuration with the nodes being interleaved connected to the baluns for signal mixing. The output ports of the RF balun, on the other hand, are combined together by an air bridge for retrieving the IF signal. The size of the proposed ring mixer is merely 16.7 by 16 mm^2. As the RF frequency varies from 1.1 to 3 GHz, the ring mixer exhibits a conversion loss of less than 11 dB. The isolations between all three ports remain pretty good for frequencies up to 4.5 GHz. The 1-dB compression power is 5 dBm. A photograph of the fabricated sample is shown in Fig. 1.

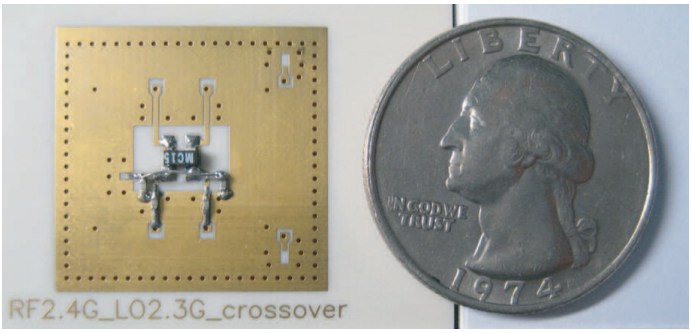

Figure 1: Photograph of the miniaturized doubly balanced ring mixer.

Balanced Dual-band Bandpass Filter Design Using Coupled Stepped-impedance Resonators

Chao-Hsing Hsu, **Yu-Chieh Hung**, **and Jung-Ming Kuo**
Department of Electronic Engineering, Chienkuo Technology University
No. 1 Chieh Shou N. Rd., Changhua, Taiwan

Abstract— A novel dual-band microstrip balanced bandpass filter is proposed based on the coupled half-wavelength ($\lambda/2$) stepped-impedance resonators (SIRs). By properly adjusting the ratio of both impedances in each SIR, the dual-band central frequencies could be obtained. A parallel coupled half-wavelength SIR is inserted between I/O ports, which make the differential-mode signal coupled to output port and the common-mode signal filtered out. A perfect balanced bandpass filter has to possess the performance to pass the desired differential-mode signal and suppress the common-mode signal. The proposed dual-band balanced bandpass filter can make the differential-mode signal pass in the 2.45 GHz and 5.25 GHz two bands and the common-mode signal suppressed below −20 dB. Its common-mode stopband could be extended beyond 6.5 GHz so that good CMRR values can be derived in these two bands. Two single-band filters combined together could be come a dual-band filter, but its circuit area and cost will be increased in this kind of method. So, it is very important to design a dual-band filter in a sole structure. In recent years, the handset and wireless LAN have fast developed, which offers the convenient and omnipresent wireless communication service. The dual-band function increased the communication quality reliability. Therefore, a dual-band balanced bandpass filter has become a key element in RF circuit. In this paper, a third-order balanced bandpass filter is designed to possess a narrow-band response in the differential-mode operation with the center frequency at f_0^d and f_1^d. In order to obtain the gaps between adjacent resonators, the differential-mode coupling coefficients M_{ab}^{dd} must be calculated. Besides, in order to obtain the length ratio α_i, the differential-mode I/O external quality factors Q_e^{dd} must be calculated. The corresponding element values of the low-pass prototype are g_1, g_2. To determine the physical dimensions of the dual-band balanced filter, the differential-mode coupling coefficients M_{ab}^{dd} and I/O external quality factors Q_e^{dd} can be calculated as follows:

$$\alpha_i = \frac{L_{i1}}{L_{i1} + L_{i2}} \tag{1}$$

$$M_{ab}^{dd} = \frac{FBW}{\sqrt{g_1 g_2}} \tag{2}$$

$$Q_e^{dd} = \frac{g_0 g_1}{FBW} \tag{3}$$

Session 4P6b
Microwave and Millimeter Wave Circuits and Devices

Experimental Study of a Longitudinal Magnetic Filter

C. Polyon, S. Photharin, and K. Wiangnon
Department of Physics, Faculty of Science, Ubon Ratchathani University
Ubon Ratchathani, Thailand

Abstract— The purpose of this work was to set up a magnetic filtration in laboratory scale. Theoretical discussions for a longitudinal magnetic filtration are described. A magnetic filter was designed and built to capture magnetic-particle samples (paramagnetic, diamagnetic or ferromagnetic materials) in fluid flowing in the direction of a uniform external magnetic field from 0 to 105.4 mT. The samples, Fe powder with diameter less than 75 μm suspending in a PVC-pipe flowing at a constant velocity of 1.7 mm/s, were captured by a bed of spherical collectors (85 pieces with diameter 3.455 mm for each), ferromagnetic materials. In order to obtain the filter performance, efficiencies of both the filter and the collectors were discussed relative to the previous magnetic field range. The experimental results show good agreement with the theoretical calculation from related reports.

A Novel Type Phase Shifter Using Rat Race Hybrid

Jan-Dong Tseng, Chien-Wen Ting, and Chien-Hua Su
Department of Electronic Engineering, National Chin-Yi University of Technology
35, Lane 215, Sec. 1, Chung-Shan Road, Taiping, Taichung 411, Taiwan, R.O.C.

Abstract— Phase shifters are widely used in phase array radar systems [1, 2] for radiation beam steering on searching and tracking, and modern wireless communication system's base station antennas for adjusting the radiation coverage to improve the service quality. Phase shifter circuit can be simply made by different transmission lines and switches. In 1965, J. F. White used high power PIN diodes and transmission lines created L/S bands phase shifter circuit [3]. Y. C. Cheah, F. J. Paoloni proposed a variable attenuators and phase shifters also using PIN diodes in 1984 [4]. R. E. Neidert, C. M. Krowne in 1985 proposed a voltage-controlled phase shifter [5]. C. Lian, S. A. Rosenau, W.-K. Zhang, C.-C. Chang, C. W. Domier and N. C. Luhmann used lumped element in phase shifter design in 2000 [6].

In this paper, we proposed a novel type phase shifter using rat-race hybrid with one additional quarter-wavelength transmission line for phase compensation and two varactors as phase controlling elements. The circuit has been simulated by Microwave Office and IE3D and fabricated in FR-4 substrate. The simulated and measured results are in good agreement within the frequency of interest.

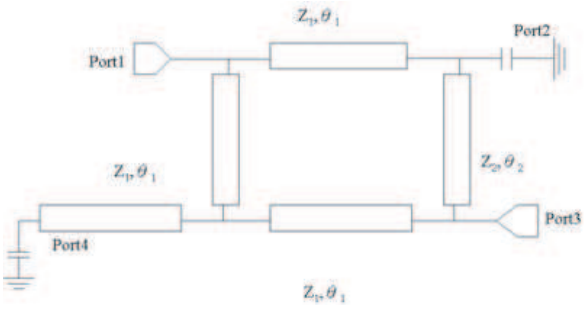

Figure 1: Schematic diagram of the circuit.

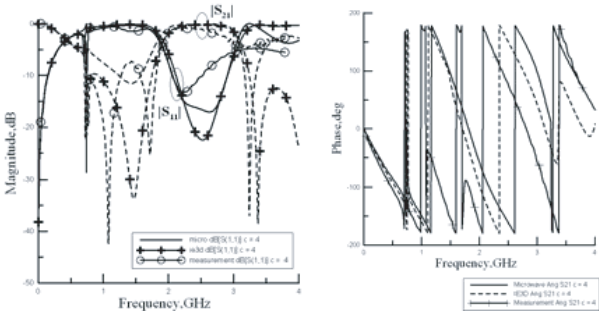

Figure 2: The simulated and measured results (f = 2.45 GHz).

REFERENCES

1. Mailloux, R. J., "Antenna array architecture," *Proc. IEEE*, Vol. 80, No. 1, 163–172, January 1992.
2. Hansen, R. C., "Array pattern control and synthesis," *Proc. IEEE*, Vol. 80, No. 1, 141–151, January 1992.
3. White, J. F., "High power, p-i-n diode controlled microwave transmission phase shifters," *IEEE Transactions on Microwave Theory and Techniques*, Vol. 13, 233–242, March 1965.
4. Cheah, Y. C. and F. J. Paoloni, "Design of a microwave pin diode complex weight circuit," *Electronic Letters*, Vol. 20, 822–824, September 1984.
5. Neidert, R. E. and C. M. Krowne, "Votage variable microwave phase shifter," *Electronic Letters*, Vol. 21, 636–638, July 1985.
6. Lian, C., S. A. Rosenau, W.-K. Zhang, C.-C. Chang, C. W. Domier, and N. C. Luhman, "Advances in solid-state array technology for microwave and millimeter-wave applications," *The 2nd International Conference on ICMMT 2000 Microwave and Millimeter Wave Technology*, No. 9, 10–15, September 2000.

Design of a Class F Power Amplifier

Tian He[1] **and Uma Balaji**[2]

[1]California State University Chico, Chico, CA 95926, USA
[2]Farmingdale State College, Farmingdale, NY 11735, USA

Abstract— The Class F amplifier is a reduced angle amplifier with load harmonic modulation control to shape the drain voltage in a way that it does not or rarely does coincide with drain current, thus greatly reducing the power dissipated by the device, and hence further increasing the efficiency without having to drive the amplifier into compression.

Design of a Class F amplifier involves matching network design at the fundamental frequency, and load harmonic tuning network design up to certain order harmonics. The optimum load and source impedances at the fundamental frequency are usually obtained by load pulling and source pulling. However, since the transistor is a bilateral device, changing the load impedance could affect the source side and vice versa. This makes the pulling an iterative back and forth process. In this paper, a new method utilizing an EDA tool is proposed as an alternative means of obtaining the optimum impedances. First, the transistor transfer characteristic is obtained, based on which a voltage source with certain values is connected to the transistor gate. This ensures that the load pull performed later on gives the correct optimum load impedance. Next, load pull analysis is performed. Once the optimum load impedance is obtained, source pull analysis is performed to obtain the optimum source impedance.

Although source pulling as an empirical method is convenient, it is beneficial to analyze the problem of input matching mathematically. In this paper, several issues on input matching are investigated. Most noticeably, the notion that maximum power transfer guarantees maximum gate voltage given a certain amount of input power is mathematically proved. The result turns out to give a factor that should be considered when choosing the transistor.

Finally, a Class F power amplifier at 2.5 GHz is designed with the GaN HEMT device CGH40010 provided by Cree, Inc. The harmonic modulation is up to 3rd order. It is tested to have 15.7 dB gain with 75.75% power added efficiency, at an input level of 25 dBm. Various practical design issues are discussed, including transmission line junctions, capacitors and load harmonic modulation.

Numerical Simulation and Primary Experiment of High Power Terahertz Backward Wave Oscillator

Xiaoze Li[1], **Changjiang Tong**[1], **Guangqiang Wang**[2], **Jianguo Wang**[1, 3], **and Xingzhou Wang**[1]

[1]Northwest Institute of Nuclear Technology, Xi'an 710024, China
[2]Department of Engineering Physics, Tsinghua University, Beijing 100084, China
[3]School of Electronics and Information Engineering, Xi'an Jiaotong University, Xi'an 710049, China

Abstract— Microwave vacuum electron devices (MVED) are capable of handling more power in a smaller interaction volume than the solid-state devices. An over-mode high power terahertz backward wave oscillator (BWO) is proposed. The slow wave structure (SWS) is constructed as follow: a series of equidistant annular slots are cut in the inner wall of a cylindrical waveguide. The parameters of this structure are optimized by using 2.5D UNIPIC code. The experiment is based on compact power accelerator CKP-1000 with 180–230 kV output voltage and can work with a pulse repetitive frequency up to 100 Hz. The foilless diode produces annular electron beam and drives the BWO. The impedance of the diode is between 50–200 Ω and change with not only the shape of diode but also with the guiding magnetic field and the working voltage. The generate annular electron beam is guided by pulse magnet which consists of one coil and can generates magnetic field up to 5 Tesla. Under the condition of the electron beam with the voltage of 200 kV, the current of 1100 A, the inner radius of 2 mm , the outer radius of 2.5 mm, and magnetic field of 2 Tesla, a 1.5 ns Terahertz signal is generated. The power is measured with 2 mm detector and is about 0.443 kW. The frequency is scaled with cut-off method and is between 0.115–0.150 THz. This accords with the simulation results.

A Study on Equivalent Circuit of Short Wavelength Microstrip Line Employing PPGM on GaAs MMIC

Jang-Hyeon Jung, **Bo-Ra Jung**, **Young-Bae Park**, **Se-Ho Kim**, **Jeong-Gab Ju**, **Suk-Youb Kang**, **Dong-Woo Kang**, **Mi-Jung Kim**, **Byeong-Su Lim**, **Cheol-Hee Do**, **and Young Yun**
Department of Radio Sciences and Engineering, Korea Maritime University, Korea

Abstract— In this work, we propose the short wavelength microstrip line employing PPGM (Periodically Perforated Ground Metal), and its equivalent circuit was thoroughly studied for application to circuit design.

Figure 1 shows the structure of the microstrip line employing PPGM, and its cross-sectional view according to Y-Y direction. As shown in Fig. 1, PPGM was inserted at the interface between SiN film and GaAs substrate, and it was electrically connected to backside GND metal through the via-holes. As is well known, conventional microstrip line without PPGM has only a periodical capacitance C_a (C_a is shown in Fig. 1) per a unit length, while the microstrip line employing PPGM has additional capacitance C_b as well as C_a due to PPGM. Therefore, as shown in Table 1, the microstrip line with PPGM exhibits much shorter guided-wavelength (λ_g) than conventional one, because λ_g is inversely proportional to the periodical capacitance, in other words, $\lambda_g = 1/\left[f \cdot (LC)^{0.5}\right]$. Above results indicate that highly miniaturized passive circuits can be realized by using the microstrip line employing PPGM.

Equivalent circuit for single cell of the microstrip line employing PPGM is shown in Fig. 2. The

Table 1: Measured wavelength (λ_g) for the microstrip line employing PPGM and conventional one at 20 GHz.

Microstrip line employing PPGM	2.2 mm
Conventional microstrip line	5.6 mm

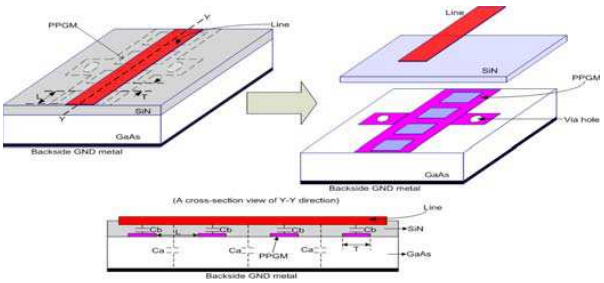

Figure 1: Structure of microstrip line employing PPGM.

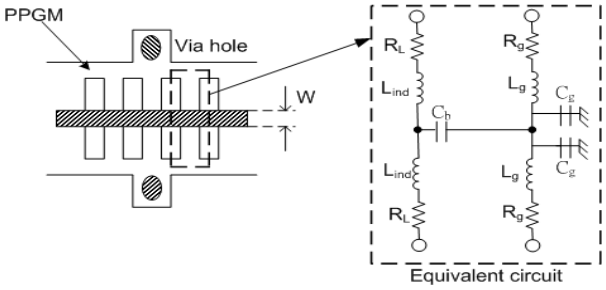

Figure 2: An equivalent circuit for a unit cell of the micriostrip line employing PPGM.

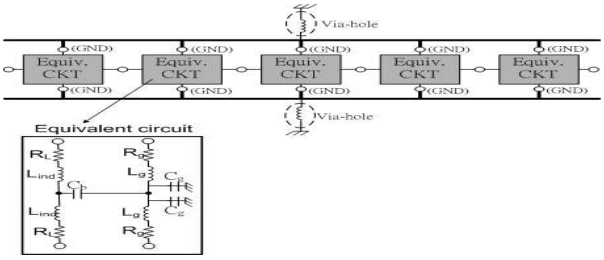

Figure 3: The equivalent circuit for microstrip line structure employing PPGM.

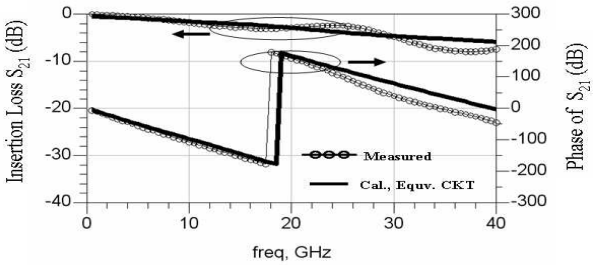

Figure 4: Measured and calculated insertion loss S_{21} for microstrip line employing PPGM.

lumped parameters were expressed by following equations,

$$L_{ind} = \left[0.0267 - \left(\frac{T}{W}\right) \times 0.776 + \left(\frac{T}{W}\right)^2 \times 0.0533\right] (\text{nH})$$

$$C_b = \left[0.0933 + \left(\frac{T}{d_i}\right) \times 6 \times 10^{-4} - \left(\frac{T}{d_i}\right)^2 \times 1.33 \times 10^{-6}\right] (\text{pF})$$

where, W, T and d_i are top line width, width of periodic metal strip and the thickness of SiN (See Fig. 1). The whole equivalent circuit is shown in Fig. 3. As shown in this figure, a number of the equivalent circuits of unit section are connected to each other, and via-hole was expressed as lumped inductor. Fig. 4 shows measured and calculated insertion loss S_{21} for microstrip line employing PPGM. For the calculation result, equivalent circuit of Fig. 3 and above closed form equations were used. As shown in this figure, we can observe a fairly good agreement between calculated and measured results.

A Design of the LTCC Balanced-to-Unbalanced Bandpass Filters

Yujie Zhao, **Yali Qin**, **and Shuwei Yang**
Zhejiang Key Research Lab of Fiber-optic Communication Technology, China

Abstract— Recently, the demand for compact and low-cost passive components is increased with the rapid development of wireless communication technologies. And the balanced-to-unbalanced bandpass filters which transform an unbalanced signal to two signals with the same magnitude and the reverse phase are important in a communication system.

In this paper, by using multilayer configuration which provided by LTCC (Low Temperature Co-fired Ceramic) technology, a design method of the balun bandpass filter is presented. The balun bandpass filter is composed of a 2-port filter and a 3-port balun with an unbalanced input and two balanced outputs. We utilize a second order filter using quarter-wave-length SIR (Stepped Impedance Resonators) to reduce the size of resonator. In order to improve the suppression performance at the stopband, two transmission zeros is introduced into the proposed filter, one below the passband and the other above the passband. There is magnetic and electric coupling between the resonators. When the magnetic coupling is in the ascendant, the pole is above the pass band. Then, a lumped capacitance between the two resonators is added to produce the pole below the pass band. The design method for the balun is based on three quarter-wave-length transmission lines, and each line is implemented as a spiral line for size reduction. By using the high-frequency simulation software, a balun bandpass filter realized in 9 layers is designed, whose center frequency is 2.45 GHz. Its insertion loss is less than 4 dB and size is 2.1 mm × 1.25 mm × 0.9 mm, which is widely used for wireless communication systems such as bluetooth and WLAN system. It has lower insertion loss and smaller size than the balun filter manufactured on PCB (Printed Circuit Board).

ACKNOWLEDGMENT

Surported by the Shen Zhen Shun Luo Electronic Limited Company.

Author Index